兰州理工大学

科研成果汇总

学　　号：	221081101002
研 究 生：	张磐
导　　师：	王志文　教授
研究方向：	信息物理系统
论文题目：	基于通信调度策略的 2-D 系统滤波问题研究
学　　科：	控制理论与控制工程
学　　院：	电气工程与信息工程学院
入学时间：	2022 年 9 月

目录

图书馆　　文献检索报告

兰州理工大学图书馆 LUTLIB

机构：兰州理工大学

姓名：张磐　[221081101002]

著者要求对其在国内外学术出版物所发表的科技论著被以下数据库收录情况进行查证。

检索范围：

- 科学引文索引（Science Citation Index Expanded）：1900年-2025年

检索结果：

检索类型	数据库	年份范围	总篇数	第一作者篇数	第二作者篇数
SCI-E 收录	SCI-EXPANDED	2024 - 2025	6	3	3

End

委托人声明：

　　本人委托兰州理工大学图书馆查询论著被指定检索工具收录情况，经核对检索结果，附件中所列文献均为本人论著，特此声明。

作　　者（签字）：张磐

完成人（签字）：安宗玉

完　成　日　期：2025年3月24日

完成单位（盖章）：兰州理工大学图书馆信息咨询与学科服务部

（本检索报告仅限校内使用）

图书馆

文献检索报告
SCI-E 收录

报告编号：**R2025-0239 SCI-E 收录**

| 数据库：科学引文索引 (Science Citation Index Expanded) | 作者姓名：张攀 | 检索人员： |
| 时间范围：2024年至2025年 | 作者单位：兰州理工大学 | 检索日期：2025年3月24日 |

检索结果：被 SCI-E 收录文献 6 篇

| #	作者	地址	标题	来源出版物	文献类型	入藏号
1	Zhu, CQ; **Zhang, P**; Wang, ZW	[Zhu, Chaoqun; Zhang, Pan; Wang, Zhiwen] Lanzhou Univ Technol, Coll Elect & Informat Engn, Lanzhou, Peoples R China.; [Wang, Zhiwen] Lanzhou Univ Technol, Coll Elect & Informat Engn, Lanzhou 730050, Peoples R China.	Set-membership filtering for two-dimensional shift-varying systems with stochastic communication protocol and uniform quantization	*TRANSACTIONS OF THE INSTITUTE OF MEASUREMENT AND CONTROL* 2024, 46 (3): 538-554.	J Article	WOS:0010 218952000 01
2	Zhu, CQ; **Zhang, P**; Lu, ZB; Yang, B; Wang, ZW	[Zhu, Chaoqun; Zhang, Pan; Yang, Bin; Wang, Zhiwen] Lanzhou Univ Technol, Coll Elect & Informat Engn, Lanzhou, Peoples R China.; [Lu, Zibao] Anhui Normal Univ, Sch Phys & Elect Informat, Wuhu, Peoples R China.; [Wang, Zhiwen] Lanzhou Univ Technol, Coll Elect & Informat Engn, Lanzhou 730050, Peoples R China.	Recursive filtering for time-varying systems with mixed time-delays subject to stochastic communication protocol and dynamic quantization effects	*PROCEEDINGS OF THE INSTITUTION OF MECHANICAL ENGINEERS PART I-JOURNAL OF SYSTEMS AND CONTROL ENGINEERING* 2024, 238 (1): 112-129.	J Article	WOS:0010 221003000 01
3	**Zhang, P**; Zhu, CQ; Yang, B; Wang, ZW; Hao, ML	[Zhang, Pan; Zhu, Chaoqun; Yang, Bin; Wang, Zhiwen; Hao, Menglu] Lanzhou Univ Technol, Coll Elect & Informat Engn, Lanzhou 730050, Peoples R China.	Event-Triggered Ultimately Bounded Filtering for Two-Dimensional Discrete-Time Systems under Hybrid Cyber Attacks	*JOURNAL OF THE FRANKLIN INSTITUTE-ENGINEERING AND APPLIED MATHEMATICS* 2024, 361 (2): 683-711.	J Article	WOS:0011 684046000 01
4	**Zhang, P**; Zhu, CQ; Yang, B; Wang, ZW; Lv, JQ	[Zhang, Pan; Zhu, Chaoqun; Yang, Bin; Wang, Zhiwen; Lv, Jiaqi] Lanzhou Univ Technol, Coll Elect & Informat Engn, Lanzhou 730050, Peoples R China.	Asynchronous filtering for two-dimensional Markovian jump systems with time delays under stochastic communication protocol and hybrid cyber attacks	*TRANSACTIONS OF THE INSTITUTE OF MEASUREMENT AND CONTROL* 2025, 47 (1): 129-149.	J Article	WOS:0012 048745000 01
5	**Zhang, P**; Zhu, CQ; Wang, ZW; Yang, B	[Zhang, Pan; Zhu, Chaoqun; Wang, Zhiwen; Yang, Bin] Lanzhou Univ Technol, Coll Elect & Informat Engn, Lanzhou 730050, Peoples R China.	Recursive set-membership filtering for two-dimensional shift-varying systems with FlexRay protocol and hybrid cyber attacks	*ASIAN JOURNAL OF CONTROL* 2025, 27 (2): 797-816.	J Article	WOS:0013 030405000 01
6	Zhang, BH; **Zhang, P**; Wang, ZW; Lv, JQ; Miao, W	[Zhang, Bohan; Zhang, Pan; Wang, Zhiwen; Lv, Jiaqi] Lanzhou Univ Technol, Coll Elect & Informat Engn, Lanzhou	ADIMPL: a dynamic, real-time and robustness attack detection model for industrial cyber-physical systems based	*APPLIED INTELLIGENCE* 2025, 55 (6): 491.	J Article	WOS:0014 349122000 03

730050, Peoples R China.; [Miao, Wei] GS Univ Intelligent Transportat Syst & Control Tec., Lanzhou 730050, Peoples R China.	on improved meta pseudo labels		
		合计	6
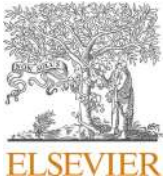
Event-Triggered Ultimately Bounded Filtering for Two-Dimensional Discrete-Time Systems under Hybrid Cyber Attacks

Pan Zhang, Chaoqun Zhu, Bin Yang, Zhiwen Wang [*], Menglu Hao

College of Electrical and Information Engineering, Lanzhou University of Technology, Lanzhou 730050, China

A R T I C L E   I N F O

A B S T R A C T

This paper investigates the design problem of event-triggered ultimately bounded filter for two-dimensional discrete systems with time-varying delays subject to hybrid cyber-attacks. A bi-directional time-sequence event-triggered transmission scheme is developed under hybrid cyber-attacks to lighten the load of network bandwidth while preserving a satisfactory filtering performance. The impact of hybrid cyber-attacks, which occur in random patterns, on the filtering performance is also taken into account. In such a framework, an augmented system model accounting for the simultaneous presence of hybrid cyber-attacks and event-triggered transmission mechanism is established with respect to two-dimensional shift-varying discrete systems with time-varying delays. On the basis of the augmented model, sufficient conditions ensuring dynamic filtering error systems exponentially ultimately bounded in the mean-square sense are obtained in virtue of Lyapunov stability theory and the linear matrix inequality technique. Then, the asymptotic upper bound of the dynamic filtering error can be specifically quantified in terms of noise variance and cyber-attacks intensity. Furthermore, criteria for simultaneously designing the weighting matrix of event-triggered scheme and the filter gain matrix are derived by minimizing the asymptotic upper bound of filtering error. Finally, the validity of proposed ultimately bounded filtering algorithm is demonstrated by utilizing an example of the industrial heating exchange process.

1. Introduction

In recent decades, two-dimensional (2-D) systems have attracted increasing attention due to their ability to accurately characterize many practical systems, which are extensively used in various fields, such as multi-variable network implementation, seismic detection data processing, power transmission lines, X-ray image enhancement, and so on [1–4]. Accordingly, the 2-D systems theory becomes one of the most promising branches in the control science field. Generally speaking, three kinds of state space models have evolved from 2-D systems, including the Roesser model [5], the Fornasini and Marchesini (FM) model [6,7], and the Kurek model [8]. On the other hand, due to the integration of network communication technology and control theory, the investigation of control theory has gradually changed from the traditional point-to-point control to distributed and networked control, and the control science of

networked systems has emerged [9–13]. In this context, the research results related to networked Roesser and FM-based models are frequently reported due to their profound implications in practical engineering [14–19]. For example, the stability analysis issues in network-based 2-D Roesser and FM model are discussed in [14–16], and the design of control and filtering algorithms is proposed for 2-D Roesser and FM systems in [17–19].

The filtering problem is another research hotspot in control and signal processing communities. With the rapid development of filtering technology, several well-known filtering methods have been developed according to different performance requirements, including but not limited to the recursive filtering [20,21], the H_∞ filtering [22,23], the set-membership filtering [24,25], and the ultimately bounded filtering [26,27]. In general, the typical recursive schemes are commonly used to solve the state estimation problem, namely, classical Kalman filtering [28], extended Kalman filtering [29], unscented Kalman filtering [30], cubature Kalman filtering [31] and Tobit Kalman filtering [32]. The recursive filtering method is always recognized as the most reliable approach for systems with Gaussian noises. The H_∞ filtering approach usually guarantees a given disturbance attenuation level for the filtering error subject to bounded noise. The set-membership filtering method has been developed by limiting all the error vectors and unknown-but-bounded noises that fall into a given set of ellipsoids. The ultimately bounded filtering is capable of effectively dealing with the stochastic abrupt changes, which can well quantify the effect of the norm-bounded noise on the steady-state filtering performance. In engineering practice, a substantial body of dynamic systems often exposed to stochastic abrupt changes, (e.g., stochastic occurrence of failure and recovery, subsystem changes and changes in the interconnection of subsystems, abrupt changes in the external environment, malicious attacks, etc.). In light of this, the ultimate boundedness of the networked systems has aroused intense research interest by the academic community [33,34]. Despite much literature on the ultimate boundedness filtering problem for one-dimensional (1-D) systems, very few results are concerning the ultimate boundedness filtering of 2-D systems subject to impulsive abrupt changes, where the main challenges may be (1) to develop complex Lyapunov functions based on bidirectional evolutionary features, and on this basis to analyze the exponentially ultimately boundedness in mean-square sense for the filtering error systems, the upper bound of filtering error intimately associated with impulsive abrupt changes, as well as the decay rate of filtering error systems; (2) Constructing matrices in the framework of 2-D systems to perform congruent transformation and obtain the required linear matrix inequalities without decreasing conservatism. Therefore, how to derive sufficient conditions guaranteeing the ultimate boundedness of filtering error for 2-D systems with stochastic impulsive abrupt changes is the main motivation for us to undertake this investigation.

Along with the accelerated development of communication technology and control science, the issue of information security has gained unprecedented attention. In the network-based scenario, there are generally three kinds of cyber-attacks that are under extensive investigation, namely, Denial of Service (DoS), False Data Injection (FDI), and Replay attacks. Up to date, scholars have produced fruitful results on this research frontier hotspot [35–37]. Furthermore, it should be highlighted that adversaries prefer to maximize the attack effect through the pattern of multi-source collaborative cyber-attacks, and the security issues of hybrid cyber-attacks pattern have recently attracted a great deal of research attention [28-30,38-40]. On the other hand, for networked systems in the age of the information and data explosion, reducing the transmission and computational burden of communication networks under the premise of guaranteeing system control performance is another frontier of research. Event-triggered transmission mechanism has been appreciated by scholars as a tool to effectively schedule network resources. In contrast to the time-triggered mechanism that transmits data at each sampling instant, the event-triggered mechanism determines whether the data is authorized to be transmitted or not by preset triggering conditions. Generally speaking, the event-triggered mechanism mainly including static event-triggered mechanism [41], dynamic event-triggered mechanism [42], adaptive event-triggered mechanism [43], furthermore, the problem of event-triggered security control and filtering based on information security and network resource scheduling has attracted strong attention in recent years [44–47]. It is worth noting that, compared to 1-D systems that evolve in only one dimension, the dynamic behavior of 2-D systems has both vertical and horizontal evolutionary directions, which also confirms that 2-D systems are more susceptible to network traffic jams due to data redundancy. Consequently, it is of more practical significance to investigate event-triggered security filtering for 2-D systems. Nevertheless, most of the results of event-triggered security filtering are generated around 1-D systems, and establishing a reasonable bi-directional independent sequence of triggering instants and cyber-attacks parameters are the main difficulty for 2-D systems. Compared with 1-D systems with event-triggered security filtering, the research on the event-triggered security filtering based on 2-D systems is as yet in the initial stage, and the related research results are still very scattered. It is essential that most of the design methods for event-triggered security filter based on 1-D systems are no longer be directly available for 2-D systems.

In response to the aforementioned discussion, we are dedicated to the investigation of event-triggered ultimately bounded filtering for a class of 2-D systems described by Roesser model under hybrid cyber-attacks. The innovations of this paper are summarized as follows: 1) For the first time, a descriptive model of shift-varying 2-D systems subject to the event-triggered transmissions and hybrid cyber-attacks is provided, and both scheduling mechanism and hybrid cyber-attacks models are developed in bidirectional indexes. 2) Based on the results of 1), the decay rate and the asymptotic upper bound of the dynamic filtering error system are derived, and the upper bound can be specifically quantified in terms of noise variance and hybrid cyber-attacks intensity. 3) The explicit filter gain matrices can be easily obtained by solving the problem of minimizing the asymptotic upper bound on the filtering error, which are subject to a set of linear matrix inequalities.

The rest of this paper is organized as follows. In Section 2, the problem description and preliminaries are presented. In Section 3, an ultimately bounded filtering algorithm is proposed for 2-D systems with the impacts of the hybrid cyber-attacks and the event-triggered scheduling. Section 4 uses a practical example to illustrate the effectiveness and superiority of the proposed filter. Finally, the paper is concluded, and future research directions are discussed in Section 5.

Notation: The notation used throughout the paper is fairly standard. denotes the n-dimensional Euclidean space and $P > 0 (P \geq 0)$

means that it is real symmetric and positive definite (semi-definite). G^T and G^{-1} represent the transpose and the inverse of the matrix G, respectively. $diag\{\rho_1, \cdots, \rho_n\}$ stands for a diagonal matrix with the indicated elements on the diagonal and zeros are located elsewhere. $\| A \|$ refers to the norm of a matrix A defined by $\| A \| = \sqrt{A^T A}$. $\mathbb{N}$ denotes the set of natural numbers. the n-dimensional identity matrix is denoted by I_n.

2. Problem Description and Preliminaries

Considering the following 2-D discrete nonlinear systems with time-varying delays described by Roesser model [13]:

$$\begin{cases} \mathscr{X}(i,j) = A_1(i,j)\boldsymbol{x}(i,j) + A_2(i,j)\boldsymbol{x}_\tau(i,j) + B(i,j)\boldsymbol{g}(\boldsymbol{x}(i,j)) + E(i,j)\boldsymbol{\omega}(i,j) \\ \mathscr{Y}(i,j) = C(i,j)\boldsymbol{x}(i,j) + D(i,j)\boldsymbol{\omega}(i,j) \\ \mathscr{Z}(i,j) = H(i,j)\boldsymbol{x}(i,j) \end{cases} \quad , \quad (i,j \in \mathbb{N}) \tag{1}$$

where

$$\mathscr{X}(i,j) = \begin{bmatrix} \boldsymbol{x}^h(i+1,j) \\ \boldsymbol{x}^v(i,j+1) \end{bmatrix}, \boldsymbol{x}(i,j) = \begin{bmatrix} \boldsymbol{x}^h(i,j) \\ \boldsymbol{x}^v(i,j) \end{bmatrix}, \boldsymbol{x}_\tau(i,j) = \begin{bmatrix} \boldsymbol{x}^h(i-\tau_h(i,j),j) \\ \boldsymbol{x}^v(i,j-\tau_v(i,j)) \end{bmatrix}, \boldsymbol{g}(\boldsymbol{x}(i,j)) = \begin{bmatrix} \boldsymbol{g}^h(\boldsymbol{x}_h(i,j)) \\ \boldsymbol{g}^v(\boldsymbol{x}_v(i,j)) \end{bmatrix},$$

$\boldsymbol{x}^h(i,j) \in R^{n_h}$ and $\boldsymbol{x}^v(i,j) \in R^{n_v}$ represent the horizontal and vertical components of the state vector, respectively. $\mathscr{Y}(i,j) \in R^{n_y}$ and $\mathscr{Z}(i,j) \in R^{n_z}$ are the output signal directly measured and the controlled output, respectively. $\boldsymbol{\omega}(i,j) \in R^{n_\omega}$ is a Gaussian white noise process with zero mean and variance of $W = \mathscr{W}\mathscr{W}^T \geq 0$, which denotes the process noise with bounded energy. $\boldsymbol{g}(\boldsymbol{x}(i,j)) \in R^{n_h+n_v}$ is known smooth nonlinear functions and to be defined later. $A_1(i,j), A_2(i,j), B(i,j), E(i,j), C(i,j), D(i,j)$ and $H(i,j)$ are time-varying constant matrices with appropriate dimensions.

In addition, $\tau_h(i,j)$ and $\tau_v(i,j)$ are the positive integers that characterize time-varying delays occurring in the horizontal and vertical dimensions, and satisfying the following bounded conditions:

$$1 \leq \underline{\tau} \leq \tau_h(i,j) \leq \overline{\tau}, 1 \leq \underline{\tau} \leq \tau_v(i,j) \leq \overline{\tau},$$

where $\underline{\tau}$ and $\overline{\tau}$ are given positive integers. Assume that the initial states are irrelevant to other variables and the following relationships are satisfied:

$$\begin{cases} \boldsymbol{x}_h(i,j) = \psi(i,j), \forall 0 \leq j \leq k_1, i \in [-\overline{\tau} \quad 0] \\ \boldsymbol{x}_v(i,j) = \Gamma(i,j), \forall 0 \leq i \leq k_2, j \in [-\overline{\tau} \quad 0] \\ \boldsymbol{x}_h(i,j) = 0, \forall j > k_1, i \in [-\overline{\tau} \quad 0] \\ \boldsymbol{x}_v(i,j) = 0, \forall i > k_2, j \in [-\overline{\tau} \quad 0] \end{cases}, \tag{2}$$

where $\psi(i,j)$ and $\Gamma(i,j)$ are given vectors, k_1 and k_2 are two sufficiently large positive integers.

Assumption 1.   It is assumed that $\zeta_1, \varsigma_1, \zeta_2$ and ς_2 are arbitrary vectors with appropriate dimensions, and the nonlinear functions $\boldsymbol{g}^h(\cdot)$ and $\boldsymbol{g}^v(\cdot)$ are defined as follows:

$$\left[\boldsymbol{g}^h(\zeta_1) - \boldsymbol{g}^h(\varsigma_1) - G_1^h(\zeta_1 - \varsigma_1) \right]^T \left[\boldsymbol{g}^h(\zeta_1) - \boldsymbol{g}^h(\varsigma_1) - G_2^h(\zeta_1 - \varsigma_1) \right] \leq 0, \boldsymbol{g}^h(0) = 0, \boldsymbol{g}^h(0) = 0, \tag{3}$$

$$\left[\boldsymbol{g}^v(\zeta_2) - \boldsymbol{g}^v(\varsigma_2) - G_1^v(\zeta_2 - \varsigma_2) \right]^T \left[\boldsymbol{g}^v(\zeta_2) - \boldsymbol{g}^v(\varsigma_2) - G_2^v(\zeta_2 - \varsigma_2) \right] \leq 0, \boldsymbol{g}^v(0) = 0, \tag{4}$$

where G_1^h, G_2^h, G_1^v and G_2^v are known constant matrices with appropriate dimensions and satisfy conditions $G_2^h \geq G_1^h$ and $G_2^v \geq G_1^v$.

To facilitate subsequent development, we reconstruct the following nonlinear functions $\boldsymbol{g}^h(\zeta_1)$ and $\boldsymbol{g}^v(\zeta_2)$ subject to **Assumption 1**:

$$\boldsymbol{g}^h(\zeta_1) \overset{\Delta}{=} \widehat{\boldsymbol{g}}^h(\zeta_1) + G_1^h\zeta_1, \boldsymbol{g}^v(\zeta_1) \overset{\Delta}{=} \widehat{\boldsymbol{g}}^v(\zeta_1) + G_1^v\zeta_1,$$

where $\widehat{\boldsymbol{g}}^h(\zeta_1)$ and $\widehat{\boldsymbol{g}}^h(\zeta_1)$ belong to sets Ω_1 and Ω_2, respectively. We define

$$\Omega_1 \overset{\Delta}{=} \left\{ \widehat{\boldsymbol{g}}^h(\zeta_1) \Big| (\widehat{\boldsymbol{g}}^h(\zeta_1))^T (\widehat{\boldsymbol{g}}^h(\zeta_1) - G^h\zeta_1) \leq 0 \right\}, \tag{5}$$

$$\Omega_2 \overset{\Delta}{=} \left\{ \widehat{\boldsymbol{g}}^v(\zeta_2) \Big| (\widehat{\boldsymbol{g}}^v(\zeta_2))^T (\widehat{\boldsymbol{g}}^v(\zeta_2) - G^v\zeta_2) \leq 0 \right\}, \tag{6}$$

and $G^h \overset{\Delta}{=} G_2^h - G_1^h, G^v \overset{\Delta}{=} G_2^v - G_1^v$.

Remark 1.   As shown in Fig. 2, the evolution of the 2-D systems depends on the changes in horizontal and vertical components, and

the update priorities of the horizontal or vertical components represent the evolutionary feature of the 2-D systems. More specifically, the state information of 1-D systems contains all the information about the past instant (global information), while the state information of 2-D systems only contains local information, which is the main difference between these two types of dynamic systems. It is worth noting that a prevalent general principle is that 2-D systems are more sophisticated to be analyzed and synthesized than 1-D systems owing to their complicated characteristics of bi-directional evolution.

A. Event-triggered mechanism

As shown in Fig. 1, in order to conserve limited network resources and relieve communication pressure, it is necessary to take specific measures to reasonably schedule the data transmission process of shared communication networks. The event-triggered mechanism has attracted widespread attention as an effective means of distributing communication resources, which motivates us to propose an event-based transmission mechanism with bi-directional indicators in the framework of 2-D shift-varying systems. For subsequent development, an order associated with horizontal and vertical directions is first defined:

$$(i,j)\langle(\widetilde{i},\widetilde{j}) \Leftrightarrow \{(i,j)|i=\widetilde{i}, j<\widetilde{j}\} \cup \{(i,j)|i<\widetilde{i}, j=\widetilde{j}\}, (i_1,j_1)=(i_2,j_2) \Leftrightarrow i=i_2 \quad and \quad j=j_2.$$

In addition, we introduce a monotonically increasing sequence of event triggering that (i_0,j_0) and (i_k,j_k) represent the initial triggering instant and the k-th triggering instant respectively, and satisfy the condition as follows:

$$(0,0)=(i_0,j_0)<(i_1,j_1)<\cdots<(i_k,j_k)<\cdots, k\in[1\infty)$$

The following event-based decision rules are implemented to update the triggering time, so that some unnecessary data transmission can be eliminated as a way to alleviate the communication pressure. As a result, the measured output can only be transmitted to the remote filter through the shared communication network after the following conditions are satisfied:

$$(i_{k+1}, j_{k+1}) = \inf\{(i,j)|(i,j)>(i_k,j_k), l(i,j)>0\}, \tag{7}$$

where $l(i,j) = r^T(i,j)\Phi_{(ij)}r(i,j) - \sigma\mathscr{Y}^T(i,j)\Phi_{(ij)}\mathscr{Y}(i,j)$, $r(i,j) = \mathscr{Y}(i_k,j_k) - \mathscr{Y}(i,j)$, $\sigma\in[01)$ represents the threshold parameter, $\Phi_{(ij)}$ is a positive definite symmetric matrix and represents the weight matrix of the event triggering sequence at shift instant (i,j), $\mathscr{Y}(i_k,j_k)$ denotes the measured output that is released at the k-th triggering instant.

Then, the latest measured output signal scheduled by the event-triggered mechanism (7) can be described as:

$$\mathscr{Y}(i_k,j_k) = \begin{bmatrix} \mathscr{Y}_1^T(i_k,j_k) & \mathscr{Y}_2^T(i_k,j_k) & \cdots & \mathscr{Y}_{n_y}^T(i_k,j_k) \end{bmatrix}^T,$$

where $\mathscr{Y}_m^T(i_k,j_k)$ $(1\leq m\leq n_y)$ denotes the latest measurement output of the m-th sensor node before the network transmission.
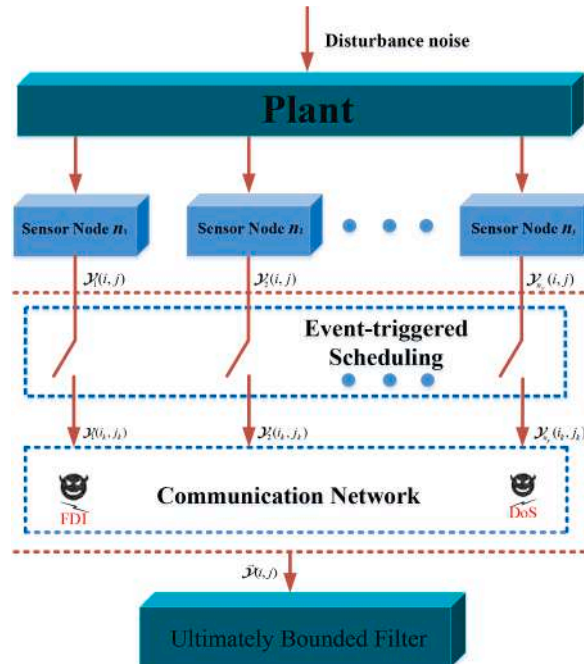

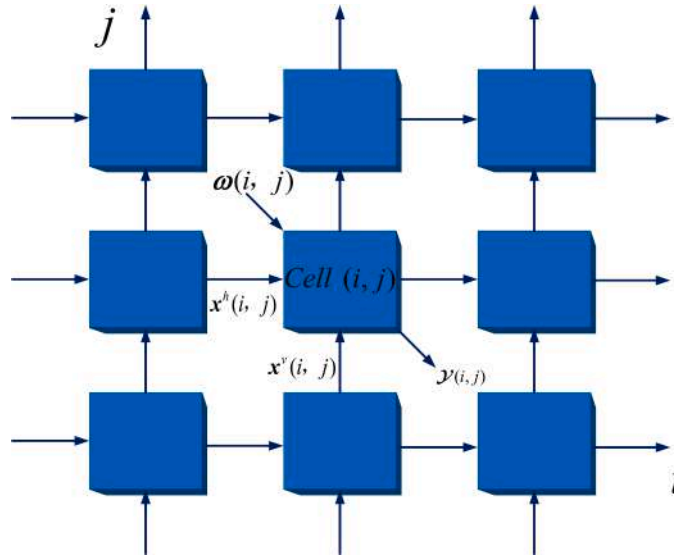**Fig. 1.** Ultimately bounded filtering problem for 2-D Roesser model.

Fig. 2. The structure diagram of 2-D Roesser model.

Remark 2. According to equation (7), event triggering relies on the measurement output error $r(i,j)$ and the trigger threshold. If equation (7) is true, it indicates that the current observation $\mathscr{Y}(i,j)$ contains key information that should be updated for utilization in the filter to guarantee excellent filtering performance while preserving network resources. Obviously, the smaller the threshold, the more frequently the data transmission is triggered, and in particular, when the threshold $\sigma = 0$, the event-triggered mechanism degrades to the traditional time-triggered mechanism. In addition, more frequent event-triggered transmission means that the filter receives more information, resulting in better filtering performance, while the high frequency of information transmission also increases the burden on the network.

B. Hybrid cyber-attacks model

In this section, the stochastic model of hybrid cyber-attacks is introduced. As previously mentioned, in order to maximize attacks damage, the adversaries often implement the hybrid cyber-attacks strategy that includes both DoS attacks and FDI attacks. It is assumed that the attackers have adequate resources and knowledge to enforce a successful attack, and the characteristics of hybrid cyber-attacks will be provided in detail thereafter.

Firstly, FDI attacks are considered, which usually degrade the filtering performance by utilizing malicious data information to tamper with normal data information. We take the binary-valued stochastic variable $\vartheta(i,j) \in \{0,1\}$ as the indicator of FDI attacks. $\vartheta(i, j) = 1$ indicates that the FDI attacks utilize false data information to distort normal data information successfully, while $\vartheta(i,j) = 0$ denotes that the FDI attacks fail to tamper with data information. It is assumed that the binary-valued stochastic variable $\vartheta(i,j)$ is governed by an independent and identically distributed Bernoulli process, and the occurrence probability of stochastic variable $\vartheta(i,j)$ is given as follows:

$$\Pr\{\vartheta(i,j) = 1\} = \overline{\vartheta}, \Pr\{\vartheta(i,j) = 0\} = 1 - \overline{\vartheta}.$$

Then, in light of (7), for $(i_k,j_k) \leq (i,j) < (i_{k+1},j_{k+1})$, the measurement output impacted by FDI attacks can be described as follows:

$$\widetilde{\mathscr{Y}}(i,j) = \mathscr{Y}(i_k,j_k) + \vartheta(i,j)\mathscr{G}(i,j), \tag{8}$$

where $\mathscr{G}(i,j) = \begin{bmatrix} \mathscr{G}_1^T(i,j) & \mathscr{G}_2^T(i,j) & \cdots & \mathscr{G}_{n_y}^T(i,j) \end{bmatrix}^T$ represents the false data signals injected into the communication network by the adversaries, and can be generated a form as follows:

$$\mathscr{G}(i,j) = -\mathscr{Y}(i_k,j_k) + \boldsymbol{v}(i,j),$$

where $\boldsymbol{v}(i,j)$ denotes the arbitrary bounded energy single, which satisfies the norm-bounded condition $\| \boldsymbol{v}(i,j) \| \leq \overline{\boldsymbol{v}}$.

Subsequently, we consider DoS attacks in the communication network, which block the normal transmission of measurement channels, and assume that the occurrence probability of DoS attacks is managed by another Bernoulli stochastic process. We take another binary-valued stochastic variable $\xi(i,j) \in \{0,1\}$ as the indicator of DoS attacks. Similarly, $\xi(i,j) = 0$ represents that the DoS attacks occur during the signal transmission, while $\xi(i,j) = 1$ expresses that the DoS attacks failed to block the network channels. The following probability distribution is defined to describe whether DoS attacks occur successfully:

$$\Pr\{\xi(i,j) = 1\} = \overline{\xi}, \Pr\{\xi(i,j) = 0\} = 1 - \overline{\xi}.$$

Consequently, the latest measurement output after collaborative FDI and DoS attacks can be expressed as

$$\overrightarrow{\mathscr{V}}(i,j) = \xi(i,j)\mathscr{Y}(i_k,j_k) + \xi(i,j)\vartheta(i,j)\mathscr{G}(i,j). \tag{9}$$

Remark 3. In practical engineering, it is very difficult for the attacker and the defender to obtain the real-time attack situation due to equipment and communication capacity limitations. In this sense, the cyber-attacks occurring in a stochastic manner obeying a sequence of probability distributions with certain statistical properties have become one of the most popular modeling approaches. Based on the established measurement outputs subject to collaborative DoS and FDI attacks (9), it can be found that when the stochastic variables $\xi(i,j)$ and $\vartheta(i,j)$ take different values representing different kinds of attacks on the measurement output. When $\xi(i,j) = 0$ and $\vartheta(i,j) = 0$, the measurement output is affected only by DoS attacks; When $\xi(i,j) = 0$ and $\vartheta(i,j) = 1$, the measurement output is affected by both DoS and FDI attacks; When $\xi(i,j) = 1$ and $\vartheta(i,j) = 0$, the measurement output is not affected by cyber attacks; When $\xi(i,j) = 1$ and $\vartheta(i,j) = 1$, the measurement output is only affected by FDI attacks. Considering that the random variables $\xi(i,j)$ and $\vartheta(i,j)$ are independent of each other, the probability of simultaneous attacks is $\overline{\xi}(1 - \overline{\vartheta})$. In addition, the stochastic model of DoS attacks mainly reflects the data transmission jamming problem, and another queuing DoS model, which mainly transformsin to time-delays, is also worth paying attention. The investigation of queuing DoS attacks based on 2-D systems is one of the future research directions.

C. Problem formulation

The ultimately bounded filtering problem will be addressed for 2-D discrete systems (1) subject to the event-triggered mechanism and hybrid cyber-attacks. For $(i_k,j_k) \leq (i,j) < (i_{k+1},j_{k+1})$, the following form of filter is developed:

$$\begin{cases} \widehat{\mathscr{X}}(i,j) = A_1(i,j)\widehat{\mathbf{x}}(i,j) + A_2(i,j)\widehat{\mathbf{x}}_\tau(i,j) + B(i,j)\mathbf{g}(\widehat{\mathbf{x}}(i,j)) + L(i,j)\left(\overrightarrow{\mathscr{V}}(i,j) - C(i,j)\widehat{\mathbf{x}}(i,j)\right) \\ \widehat{\mathscr{Z}}(i,j) = H(i,j)\widehat{\mathbf{x}}(i,j) \end{cases}, \tag{10}$$

where $\widehat{\mathscr{X}}(i,j) \in R^{n_h+n_v}$, $\widehat{\mathbf{x}}(i,j) \in R^{n_h+n_v}$ and $\widehat{\mathbf{x}}_\tau(i,j) \in R^{n_h+n_v}$ are the estimation of state vector $\mathscr{X}(i,j)$, $\mathbf{x}(i,j)$ and $\mathbf{x}_\tau(i,j)$. $\widehat{\mathscr{Z}}(i,j)$ is the estimation of the controlled output $\mathscr{Z}(i,j)$. $L(i,j) \in R^{(n_h+n_v)\times n_y}$ is the filtering gain to be determined later. The initial state of filter is set as $\widehat{\mathbf{x}}^h(i,j) \triangleq 0$ for $i \leq 0, j \in \mathbb{N}$ and $\widehat{\mathbf{x}}^v(i,j) \triangleq 0$ for $i \in \mathbb{N}, j \leq 0$.

Moreover, according to (7)-(9), for $(i_k,j_k) \leq (i,j) < (i_{k+1},j_{k+1})$, the latest measurement output $\overrightarrow{\mathscr{V}}(i,j)$ with the event-triggered mechanism and hybrid cyber-attacks can be derived as:

$$\begin{aligned} \overrightarrow{\mathscr{V}}(i,j) &= \xi(i,j)((1 - \vartheta(i,j))(\mathbf{r}(i,j) + \mathscr{Y}(i,j)) + \vartheta(i,j)\mathbf{v}(i,j)) \\ &= \xi(i,j)(1 - \vartheta(i,j))(\mathbf{r}(i,j) + C(i,j)\mathbf{x}(i,j) + D(i,j)\boldsymbol{\omega}(i,j)) + \xi(i,j)\vartheta(i,j)\mathbf{v}(i,j). \end{aligned} \tag{11}$$

Define the filtering error and controlled output error as $\mathbf{e}(i,j) = \mathbf{x}(i,j) - \widehat{\mathbf{x}}(i,j)$ and $\widetilde{\mathscr{Z}}(i,j) = \mathscr{Z}(i,j) - \widehat{\mathscr{Z}}(i,j)$, respectively, then we construct the following augmented variables:

$$\iota(i,j) = \begin{bmatrix} \iota^h(i+1,j) \\ \iota^v(i,j+1) \end{bmatrix}, \iota(i,j) = \begin{bmatrix} \iota^h(i,j) \\ \iota^v(i,j) \end{bmatrix}, \iota_\tau(i,j) = \begin{bmatrix} \iota^h(i - \tau^h(i,j),j) \\ \iota^v(i,j - \tau^v(i,j)) \end{bmatrix}, \iota^h(i,j) = \begin{bmatrix} \mathbf{x}^h(i,j) \\ \mathbf{e}^h(i,j) \end{bmatrix},$$

$$\iota^v(i,j) = \begin{bmatrix} \mathbf{x}^v(i,j) \\ \mathbf{e}^v(i,j) \end{bmatrix}, \widehat{\widetilde{\mathscr{Z}}}(i,j) = \begin{bmatrix} \mathscr{Z}(i,j) \\ \widetilde{\mathscr{Z}}(i,j) \end{bmatrix}, \iota^h(i+1,j) = \begin{bmatrix} \mathbf{x}^h(i+1,j) \\ \mathbf{e}^h(i+1,j) \end{bmatrix}, \iota^v(i,j+1) = \begin{bmatrix} \mathbf{x}^v(i,j+1) \\ \mathbf{e}^v(i,j+1) \end{bmatrix},$$

$$\iota^h(i - \tau_h(i,j),j) = \begin{bmatrix} \mathbf{x}^h(i - \tau_h(i,j),j) \\ \mathbf{e}^h(i - \tau_h(i,j),j) \end{bmatrix}, \iota^v(i,j - \tau_v(i,j)) = \begin{bmatrix} \mathbf{x}^v(i,j - \tau_v(i,j)) \\ \mathbf{e}^v(i,j - \tau_v(i,j)) \end{bmatrix}, \overline{\mathbf{g}}(\iota(i,j)) = \begin{bmatrix} \overline{\mathbf{g}}^h(\iota^h(i,j)) \\ \overline{\mathbf{g}}^v(\iota^v(i,j)) \end{bmatrix},$$

$$\overline{\mathbf{g}}^h(\iota^h(i,j)) = \begin{bmatrix} \widehat{\mathbf{g}}^h(\mathbf{x}^h(i,j)) \\ \widetilde{\mathbf{g}}^h(\mathbf{e}^h(i,j)) \end{bmatrix}, \overline{\mathbf{g}}^v(\iota^v(i,j)) = \begin{bmatrix} \widehat{\mathbf{g}}^v(\mathbf{x}^v(i,j)) \\ \widetilde{\mathbf{g}}^v(\mathbf{e}^v(i,j)) \end{bmatrix}, \widetilde{\mathbf{g}}^h(\mathbf{e}^h(i,j)) = \widehat{\mathbf{g}}^h(\mathbf{x}^h(i,j)) - \widehat{\mathbf{g}}^h(\widehat{\mathbf{x}}^h(i,j)),$$

$$\widetilde{\mathbf{g}}^v(\mathbf{e}^v(i,j)) = \widehat{\mathbf{g}}^v(\mathbf{x}^v(i,j)) - \widehat{\mathbf{g}}^v(\widehat{\mathbf{x}}^v(i,j)), \mathbf{g}^h(\zeta_1) = \widehat{\mathbf{g}}^h(\zeta_1) + G_1^h\zeta_1, \mathbf{g}^v(\zeta_1) = \widehat{\mathbf{g}}^v(\zeta_1) + G_1^v\zeta_1,$$

hence, by considering (1), (10) and (11), the dynamic filtering error systems can be constructed as follows:

$$\begin{cases} \iota(i,j) = (\widetilde{A}_1(i,j) + \widetilde{B}(i,j)\widetilde{M})\eta(i,j) + \widetilde{A}_2(i,j)\iota_\tau(i,j) + \widetilde{B}(i,j)\overline{\mathbf{g}}(\iota(i,j)) \\ \qquad\qquad + \widetilde{E}(i,j)\boldsymbol{\omega}(i,j) + \widetilde{O}(i,j)\mathbf{v}(i,j) + \widetilde{R}(i,j)\mathbf{r}(i,j) \\ \mathscr{Y}(i,j) = \widetilde{C}(i,j)\iota(i,j) + D\boldsymbol{\omega}(i,j) \\ \widetilde{\mathscr{Z}}(i,j) = \widetilde{H}(i,j)\iota(i,j) \end{cases}, \tag{12}$$

where $\widetilde{A}_1(i,j) = \Omega^T \overline{A}_1(i,j)\Omega, \widetilde{A}_2(i,j) = \Omega^T \overline{A}_2(i,j)\Omega, \widetilde{B}(i,j) = \Omega^T \overline{B}(i,j)\Omega, \widetilde{M} = \Omega^T M\Omega, \widetilde{E}(i,j) = \Omega^T \overline{E}(i,j), \widetilde{O}(i,j) = \Omega^T \overline{O}(i,j), \widetilde{R}(i,j) = \Omega^T \overline{R}(i,j),$
$\widetilde{H}(i,j) = \overline{H}(i,j)\Omega, \widetilde{C}(i,j) = \overline{C}(i,j)\Omega,$

$$\overline{A}_1(i,j) = \begin{bmatrix} A_1(i,j) & 0 \\ L(i,j)(1-\xi(i,j))(1-\vartheta(i,j))C(i,j) & A_1(i,j) - L(i,j)C(i,j) \end{bmatrix}, \overline{A}_2(i,j) = \begin{bmatrix} A_2(i,j) & 0 \\ 0 & A_2(i,j) \end{bmatrix},$$

$$\Omega = \begin{bmatrix} I_{n_h} & 0 & 0 & 0 \\ 0 & 0 & I_{n_v} & 0 \\ 0 & I_{n_h} & 0 & 0 \\ 0 & 0 & 0 & I_{n_v} \end{bmatrix}, M = diag\{G_1^h, G_1^v, G_1^h, G_1^v\}, \overline{B}(i,j) = \begin{bmatrix} B(i,j) & 0 \\ 0 & B(i,j) \end{bmatrix},$$

$$\overline{E}(i,j) = \begin{bmatrix} E(i,j) \\ E(i,j) - L(i,j)\xi(i,j)(1-\vartheta(i,j))D(i,j) \end{bmatrix}, \overline{O}(i,j) = \begin{bmatrix} 0 \\ -L(i,j)\xi(i,j)\vartheta(i,j) \end{bmatrix},$$

$$\overline{R}(i,j) = \begin{bmatrix} 0 \\ -L(i,j)\xi(i,j)(1-\vartheta(i,j)) \end{bmatrix}, \overline{H}(i,j) = [0 \quad H(i,j)], \overline{C}(i,j) = [C(i,j) \quad 0].$$

Furthermore, taking into account the relationship between stochastic variables $\vartheta(i,j)$, $\xi(i,j)$ and probabilities $\overline{\vartheta}$, $\overline{\xi}$, the dynamic filtering error systems (12) can be rewritten as follows:

$$\begin{cases} \iota(i,j) = \left(\widehat{\mathscr{A}}_1(i,j) + \boldsymbol{\varpi}_1(i,j)\breve{\mathscr{A}}_1(i,j) + \widetilde{B}(i,j)\widetilde{M}\right)\iota(i,j) + \widetilde{A}_2(i,j)\iota_\tau(i,j) + \widetilde{B}(i,j)\overline{\mathbf{g}}(\iota(i,j)) \\ \qquad + \left(\widehat{\mathscr{E}}(i,j) + \boldsymbol{\varpi}_1(i,j)\breve{\mathscr{E}}(i,j)\right)\boldsymbol{\omega}(i,j) + \left(\widehat{\mathscr{O}}(i,j) + \boldsymbol{\varpi}_2(i,j)\breve{\mathscr{O}}(i,j)\right)\boldsymbol{v}(i,j) + \left(\widehat{\mathscr{R}}(i,j) + \boldsymbol{\varpi}_1(i,j)\breve{\mathscr{R}}(i,j)\right)\mathbf{r}(i,j) \\ \mathscr{Y}(i,j) = \widetilde{C}(i,j)\iota(i,j) + D\boldsymbol{\omega}(i,j) \\ \widetilde{\mathscr{Z}}(i,j) = \widetilde{H}(i,j)\iota(i,j) \end{cases} \tag{13}$$

where $\widehat{\mathscr{A}}_1(i,j) = \Omega^T \widehat{A}_1(i,j)\Omega, \breve{\mathscr{A}}_1(i,j) = \Omega^T \breve{A}_1(i,j)\Omega, \widehat{\mathscr{E}}(i,j) = \Omega^T \widehat{E}(i,j), \breve{\mathscr{E}}(i,j) = \Omega^T \breve{E}(i,j) \widehat{\mathscr{O}}(i,j) = \Omega^T \widehat{O}(i,j), \breve{\mathscr{O}}(i,j) = \Omega^T \breve{O}(i,j), \widehat{\mathscr{R}}(i,j) = \Omega^T \widehat{R}(i,j), \breve{\mathscr{R}}(i,j) = \Omega^T \breve{R}(i,j), \widehat{A}_1(i,j) = \begin{bmatrix} A_1(i,j) & 0 \\ L(i,j)(1-\overline{\xi}(1-\overline{\vartheta}))C(i,j) & A_1(i,j) - L(i,j)C(i,j) \end{bmatrix}, \breve{A}_1(i,j) = \begin{bmatrix} 0 & 0 \\ -L(i,j)C(i,j) & 0 \end{bmatrix}, \widehat{E}(i,j) = \begin{bmatrix} E(i,j) \\ E(i,j) - L(i,j)(1-\overline{\xi}(1-\overline{\vartheta}))D(i,j) \end{bmatrix}, \breve{E}(i,j) = \begin{bmatrix} 0 & 0 \\ -L(i,j)D(i,j) & 0 \end{bmatrix}, \widehat{O}(i,j) = \begin{bmatrix} 0 \\ -L(i,j)\overline{\xi}\overline{\vartheta} \end{bmatrix}, \widehat{R}(i,j) = \begin{bmatrix} 0 \\ -L(i,j)\overline{\xi}(1-\overline{\vartheta}) \end{bmatrix}, \breve{R}(i,j) = \breve{O}(i,j) = \begin{bmatrix} 0 \\ -L(i,j) \end{bmatrix}, \boldsymbol{\varpi}_1(i,j) = \xi(i,j)(1-\vartheta(i,j)) - \overline{\xi}(1-\overline{\vartheta}), \boldsymbol{\varpi}_2(i,j) = \xi(i,j)\vartheta(i,j) - \overline{\xi}(1-\overline{\vartheta}).$

Additionally, in order to accelerate the presentation of subsequent results, the several statistical properties regarding the stochastic sequences of DoS and FDI attacks are given as follows:

$$E\{\boldsymbol{\varpi}_1^2(i,j)\} = \overline{\varsigma}_1^2, E\{\boldsymbol{\varpi}_2^2(i,j)\} = \overline{\varsigma}_2^2, E\{\boldsymbol{\varpi}_1(i,j)\boldsymbol{\varpi}_2(i,j)\} = \overline{\varsigma}_{12}^2.$$

Definition 1. [17] The dynamic filtering error systems (13) is said to be exponentially ultimately bounded in mean-square sense for given nonnegative integers a and $b(a \geq b)$, if there exist positive constants $\beta \in [01)$, $\alpha > 0$, and $\pi > 0$, such that

$$E\left\{\sum_{i+j=a} \| \iota(i,j) \|^2\right\} \leq \alpha\beta^{a-b}\sum_{i+j=b} \| \iota(i,j) \|_{\mathscr{M}}^2 + \pi, \quad (a > b)$$

where

$$\sum_{i+j=b} \| \iota(i,j) \|_{\mathscr{M}}^2 \overset{\Delta}{=} \sup_{\substack{-\overline{\tau} \leq \theta \leq 0 \\ -\overline{\tau} \leq s \leq 0}} \sum_{i+j=b} \left\{\| \iota^h(i+\theta,j) \|^2 + \| \iota^v(i,j+s) \|^2\right\},$$

then, β and π are referred to as the decay rate of dynamic filtering error systems (13), and the asymptotic upper bound of $E\left\{\sum_{i+j=a} \| \iota(i,j) \|^2\right\}$, respectively.

3. Main Results

Theorem 1. For the dynamic filtering error systems (13) under the event-triggered mechanism (7) and hybrid cyber-attacks (9), and given scalars $\overline{\tau}, \underline{\tau}, \rho$ as well as filtering gains $L(i,j) \in R^{(n_h+n_v) \times n_y}$, if there exist positive definite symmetric matrices $P(i,j) = diag\{P^h(i,j), P^v(i,j)\} \in R^{(2n_h+2n_v) \times (2n_h+2n_v)}, S_1(i,j) = diag\{S_1^h(i,j), S_1^v(i,j)\} \in R^{(2n_h+2n_v) \times (2n_h+2n_v)}, S_2(i,j) = diag\{S_2^h(i,j), S_2^v(i,j)\} \in R^{(2n_h+2n_v) \times (2n_h+2n_v)}$ and $S_3 = diag\{S_3^h(i,j), S_3^v(i,j)\} \in R^{(2n_h+2n_v) \times (2n_h+2n_v)}$, positive scalars $\gamma_1(i,j)$ and $\gamma_2(i,j)$, such that the following inequalities hold:

$$\Pi = \begin{bmatrix} \Pi_{11} & \Pi_{12} \\ * & \Pi_{22} \end{bmatrix} \leq 0, \tag{14}$$

$$S_2^h(i,j) \geq S_3^h(i,j), \quad S_2^v(i,j) \geq S_3^v(i,j), \tag{15}$$

$$(1+\overline{\tau})S_1(i,j) + \overline{\tau}S_2(i,j) - \underline{\tau}S_3(i,j) \leq \rho(S_2(i,j) - S_3(i,j)), \tag{16}$$

where

$$\Pi_{11} = \begin{bmatrix} \overline{S}(i,j) - \left(1 - \dfrac{1}{\rho}\right)P(i,j) + \sigma\gamma_1(i,j)\widetilde{C}^T(i,j)\Phi_{(i,j)}\widetilde{C}(i,j) & 0 & \widetilde{\mathscr{F}}^T & 0 & 0 \\ * & -S_1(i,j) & 0 & 0 & 0 \\ * & * & -2I_{2n_x+2n_v} & 0 & 0 \\ * & * & * & -\gamma_1(i,j)\Phi_{(i,j)} & 0 \\ * & * & * & * & -\gamma_2(i,j)I_{n_y} \end{bmatrix},$$

$$\Pi_{12} = \begin{bmatrix} \left(\widehat{\mathscr{A}}_1(i,j) + \widetilde{B}(i,j)\widetilde{M}\right)^T & \overline{\varsigma}_1\breve{\mathscr{A}}_1^T(i,j) & \overline{\varsigma}_{12}\breve{\mathscr{A}}_1^T(i,j) & 0 & 0 \\ \widetilde{A}_2^T(i,j) & 0 & 0 & 0 & 0 \\ \widetilde{B}^T(i,j) & 0 & 0 & 0 & 0 \\ \widehat{\mathscr{R}}(i,j) & \overline{\varsigma}_1\breve{\mathscr{R}}^T(i,j) & 0 & \overline{\varsigma}_{12}\breve{\mathscr{R}}^T(i,j) & 0 \\ \widehat{\mathscr{O}}^T(i,j) & 0 & 0 & 0 & \sqrt{(\overline{\varsigma}_2^2 + 2\overline{\varsigma}_{12}^2)}\breve{\mathscr{O}}^T(i,j) \end{bmatrix},$$

$$\Pi_{22} = I_5 \otimes -P^{-1}(i,j), \overline{S} = \left(1 + \overline{\tau} - \underline{\tau}\right)S_1(i,j) + \left(\overline{\tau}S_2(i,j) - \underline{\tau}S_3(i,j)\right), \widetilde{\mathscr{F}} = \Omega^T\widehat{M}\Omega, \widehat{M} = diag\{G^h, G^v, G^h, G^v\},$$

$$\delta = tr\left\{ \mathscr{W}^T \left(\widehat{\mathscr{E}}^T(i,j)P(i,j)\widehat{\mathscr{E}}(i,j) + \overline{\varsigma}_1^2\breve{\mathscr{E}}^T(i,j)P(i,j)\breve{\mathscr{E}}(i,j) + \sigma\gamma_1(i,j)D^T(i,j)\Phi_{(i,j)}D(i,j) \right) \mathscr{W} \right\} + \gamma_2(i,j)\overline{v}^2,$$

$$\varsigma_1 = \lambda_{\min}(P(i,j)), \varrho = 1 - \dfrac{1}{\rho},$$

then, the dynamic filtering error systems (13) satisfying $E\left\{ \sum_{i+j=K} \| \iota(i,j) \|^2 \right\} \leq \dfrac{\varsigma_2}{\varsigma_1}\varrho^{K-S} \sum_{i+j=S} \| \iota(i,j) \|_{\mathscr{M}}^2 + \dfrac{1-\varrho^{K-S}}{\varsigma_1(1-\varrho)}\delta(i,j)$ $(K > \max\{k_1,k_2\} > S)$, and is said to be exponentially ultimately bounded in mean-square sense with asymptotic upper bound $\dfrac{\delta(i,j)}{\varsigma_1(1-\varrho)}$, and the decay rate is less than ϱ.

Proof. The proof is provided in Appendix A.

Remark 4. It is noticed that the dynamic filtering error systems (13) involves both process noise and false data injection, and the stability and dynamic behavior of the filtering error systems are affected by both of them. Therefore, in this paper, we mainly concerned with the boundedness problem of the filtering error system, which is more reflective of the evolutionary characteristics of the system compared to the stability alone (From inequality (47), it can be seen that in the absence of noise and FDI attacks, the conclusion that the exponentially ultimately bounded in mean-square sense of the filtering error systems will degrade to exponentially stable in mean-square sense). Furthermore, in order to avoid that the asymptotic upper bound are too large and out of practical significance, we attempt to obtain the minimum upper bound of the dynamic filter error systems.

Remark 5. In Theorem 1, we have derived sufficient conditions to ensure that the ultimately bounded of the dynamic filtering error systems (13). From inequality (16), we can obtain that parameter ρ is larger than τ_m, and it is easy to obtain the lower bound of the decay rate is $1 - \dfrac{1}{\tau_m}$. In addition, as an important index to evaluate the convergence of the system, the decay rate should be considered in the practical engineering. In what follows, we will endeavor to derive sufficient conditions that the filtering gain matrix to minimize the upper bound of the control output error $\| \widetilde{z}(i,j)\|^2$ for a given decay rate.

Until now, sufficient conditions guaranteeing the dynamic filtering error systems (13) to be exponentially ultimately bounded in mean-square sense are provided. In what follows, we are going to derive the filtering gain by minimizing the controlled output error and present the filtering gain in explicit form.

Theorem 2. For the dynamic filtering error systems (13) under the event-triggered mechanism (7) and hybrid cyber-attacks (9), and given positive scalars $\overline{\tau}, \underline{\tau}, \rho$ as well as the filter gains $L(i,j) \in R^{(n_h+n_v)\times n_y}$, if there exist positive definite symmetric matrices $\overline{P}(i,j) = diag\{\overline{P}^h(i, j), \overline{P}^v(i, j)\} \in R^{(2n_h+2n_v)\times(2n_h+2n_v)}$, $S_1(i, j) = diag\{S_1^h(i, j), S_1^v(i, j)\} \in R^{(2n_h+2n_v)\times(2n_h+2n_v)}$, $S_2(i, j) = diag\{S_2^h(i, j), S_2^v(i, j)\} \in R^{(2n_h+2n_v)\times(2n_h+2n_v)}$, $S_3(i,j) = diag\{S_3^h(i,j), S_3^v(i,j)\} \in R^{(2n_h+2n_v)\times(2n_h+2n_v)}$, $Q(i,j) \in R^{(2n_h+2n_v)\times(2n_h+2n_v)}$, and positive scalars $\gamma_1(i,j)$ as well

as $\gamma_2(i,j)$, such that the following inequalities hold:

$$\Theta = \begin{bmatrix} \Theta_{11} & \Theta_{12} \\ * & \Theta_{22} \end{bmatrix} \leq 0, \tag{17}$$

$$S_2^h(i,j) \geq S_3^h(i,j), S_2^v(i,j) \geq S_3^v(i,j), \tag{18}$$

$$(1+\overline{\tau})S_1(i,j) + \overline{\tau}S_2(i,j) - \underline{\tau}S_3(i,j) \leq \rho(S_2(i,j) - S_3(i,j)), \tag{19}$$

$$\begin{bmatrix} -Q(i,j) & \Omega^T \\ * & -\overline{P}(i,j) \end{bmatrix} \leq 0, \tag{20}$$

$$2I_{2n_h+2n_v} - \Omega^T\overline{P}(i,j)\Omega \geq \widetilde{H}^T(i,j)\widetilde{H}(i,j), \tag{21}$$

where

$$\Theta_{11} = \begin{bmatrix} \Theta_{11}^1 & 0 & \widehat{M}^T\Omega & 0 & 0 \\ * & -\overline{S}_1(i,j) & 0 & 0 & 0 \\ * & * & -2I_{2n_x+2n_v} & 0 & 0 \\ * & * & * & -\gamma_1(i,j)\Phi_{(i,j)} & 0 \\ * & * & * & * & -\gamma_2(i,j)I_{n_y} \end{bmatrix}, \widehat{M} = diag\{G^h, G^v, G^h, G^v\},$$

$$\Theta_{11}^1 = \left(1+\overline{\tau}-\underline{\tau}\right)\overline{S}_1(i,j) + \left(\overline{\tau}\overline{S}_2(i,j) - \underline{\tau}\overline{S}_3(i,j)\right) + \sigma\gamma_1(i,j)\Omega\widetilde{C}^T(i,j)\Phi_{(i,j)}\widetilde{C}(i,j)\Omega^T + \left(1-\frac{1}{\rho}\right)\overline{P}(i,j) - 2\left(1-\frac{1}{\rho}\right)I_{2n_h+2n_v},$$

$$\Theta_{12} = \begin{bmatrix} \widehat{A}_1^T(i,j) + M^T\overline{B}^T(i,j) & \overline{\varsigma}_1\breve{A}_1^T(i,j) & \overline{\varsigma}_{12}\breve{A}_1^T(i,j) & 0 & 0 \\ \overline{A}_2^T(i,j) & 0 & 0 & 0 & 0 \\ \Omega^T\overline{B}^T(i,j) & 0 & 0 & 0 & 0 \\ \widehat{\mathscr{R}}^T(i,j)\Omega^T & \overline{\varsigma}_1\breve{\mathscr{R}}^T(i,j)\Omega^T & 0 & \overline{\varsigma}_{12}\breve{\mathscr{R}}^T(i,j)\Omega^T & 0 \\ \widehat{\mathscr{O}}^T(i,j)\Omega^T & 0 & 0 & 0 & \sqrt{(\overline{\varsigma}_2^2+2\overline{\varsigma}_{12}^2)}\breve{\mathscr{O}}^T(i,j)\Omega^T \end{bmatrix},$$

$$\Theta_{22} = I_5 \otimes -\overline{P}(i,j), \overline{S}_1 = \begin{bmatrix} \overline{I}_{n_h}S_1^h(i,j)\overline{I}_{n_h} + \overline{I}_{n_v}S_1^v(i,j)\overline{I}_{n_v} & \overline{I}_{n_h}S_1^h(i,j)\widetilde{I}_{n_h} + \overline{I}_{n_v}S_1^v(i,j)\widetilde{I}_{n_v} \\ * & \widetilde{I}_{n_h}S_1^h(i,j)\widetilde{I}_{n_h} + \widetilde{I}_{n_v}S_1^v(i,j)\widetilde{I}_{n_v} \end{bmatrix},$$

$$\overline{S}_2 = \begin{bmatrix} \overline{I}_{n_h}S_2^h(i,j)\overline{I}_{n_h} + \overline{I}_{n_v}S_2^v(i,j)\overline{I}_{n_v} & \overline{I}_{n_h}S_2^h(i,j)\widetilde{I}_{n_h} + \overline{I}_{n_v}S_2^v(i,j)\widetilde{I}_{n_v} \\ * & \widetilde{I}_{n_h}S_2^h(i,j)\widetilde{I}_{n_h} + \widetilde{I}_{n_v}S_2^v(i,j)\widetilde{I}_{n_v} \end{bmatrix}, \overline{I}_{n_v} = \begin{bmatrix} 0 & 0 \\ I_{n_v} & 0 \end{bmatrix}, \widetilde{I}_{n_v} = \begin{bmatrix} 0 & 0 \\ 0 & I_{n_v} \end{bmatrix},$$

$$\overline{S}_3 = \begin{bmatrix} \overline{I}_{n_h}S_3^h(i,j)\overline{I}_{n_h} + \overline{I}_{n_v}S_3^v(i,j)\overline{I}_{n_v} & \overline{I}_{n_h}S_3^h(i,j)\widetilde{I}_{n_h} + \overline{I}_{n_v}S_3^v(i,j)\widetilde{I}_{n_v} \\ * & \widetilde{I}_{n_h}S_3^h(i,j)\widetilde{I}_{n_h} + \widetilde{I}_{n_v}S_3^v(i,j)\widetilde{I}_{n_v} \end{bmatrix}, \overline{I}_{n_h} = \begin{bmatrix} I_{n_h} & 0 \\ 0 & 0 \end{bmatrix}, \widetilde{I}_{n_h} = \begin{bmatrix} 0 & I_{n_h} \\ 0 & 0 \end{bmatrix},$$

and other parameters are defined in Theorem 1. Then, the dynamic filtering error systems (13) is exponentially ultimately bounded in mean-square sense. Moreover, the minimum upper bound of controlled output error $\|\widetilde{z}(i,j)\|^2$ is obtained by solving the following optimization problem:

$$\min\widehat{\delta}(i,j) = \left\{tr\left\{\mathscr{W}^T\left(\widehat{\mathscr{E}}^T(i,j)Q(i,j)\widehat{\mathscr{E}}(i,j) + \overline{\varsigma}_1^2\breve{\mathscr{E}}^T(i,j)Q(i,j)\breve{\mathscr{E}}(i,j) + \sigma\gamma_1(i,j)\widetilde{D}^T(i,j)\Phi_{(i,j)}\widetilde{D}(i,j)\right)\mathscr{W}\right\} + \gamma_2(i,j)\overline{v}^2\right\}$$

s.t. (17)-(21).

Proof.　The proof is provided in Appendix B.

Remark 6.　Theorem 2 presents a filter design method that guarantees the exponentially ultimately bounded in mean-square sense of filtering error systems, and the upper bound of the controlled output error is minimized by solving an optimization problem. The previous research on 2-D systems filtering methods (including set-membership filtering and H$_\infty$ filtering) mainly focuses on the stability of the filtering error systems, and neglects the quantitative analysis of the impact of noise and abrupt changes on the filtering performance. The filtering algorithms proposed in this paper can more intuitively demonstrate the dynamic behavior of the filtering

error systems, including the decay rate and the upper bound of the filtering error, and the upper bound is only related to the noise and the abrupt changes, which is more instructive in the practical engineering compared with the simple stability analysis. In addition, it should be further noted that the solutions of the filtering gain matrices are performed online, and thus alleviating the computational burden to a greater extent (by utilizing dynamic event-triggered strategy or self-triggered mechanism) while ensuring the filtering performance is one of the future research directions.

Remark 7. The main results established in Theorem 1 and Theorem 2 simultaneously consider bidirectional evolutionary characterizations of 2-D systems, nonlinear function constraints, upper and lower bound on the time-varying delays, event-triggered mechanism, cyber-attacks parameters and boundary on noise. The novelties are summarized in the following aspects: 1) For the first time, a schematic model of 2-D systems with event-triggered transmissions and hybrid cyber-attacks is available, in which the scheduling mechanism and hybrid cyber-attacks are modeled in a bidirectional indexed scheme. 2) The decay rate and the asymptotic upper bound of the dynamic filtering error are inferred, and the upper bound can be specifically quantified in terms of noise variance and hybrid cyber-attacks intensity. 3) The explicit filter gain matrices can be easily obtained by solving the problem of minimizing the asymptotic upper bound on the filtering error, which is subject to a set of linear matrix inequalities.

Now, we will generalize above obtained results to more universal 2-D Roesser model, which mainly include nonlinear Roesser 2-D model without time-delays and linear Roesser 2-D model with time-delays.

Case 1: The following 2-D discrete systems with time-varying delays characterized by the Roesser model is considered:

$$
\begin{cases}
\mathscr{X}(i,j) = A_1(i,j)\boldsymbol{x}(i,j) + A_2(i,j)\boldsymbol{x}_\tau(i,j) + E(i,j)\boldsymbol{\omega}(i,j) \\
\mathscr{Y}(i,j) = C(i,j)\boldsymbol{x}(i,j) + D(i,j)\boldsymbol{\omega}(i,j) \\
\mathscr{Z}(i,j) = H(i,j)\boldsymbol{x}(i,j)
\end{cases}
. \tag{22}
$$

Then, we adopt the following filter structure:

$$
\begin{cases}
\widehat{\mathscr{X}}(i,j) = A_1(i,j)\widehat{\boldsymbol{x}}(i,j) + A_2(i,j)\widehat{\boldsymbol{x}}_\tau(i,j) + L(i,j)\left(\widehat{\mathscr{Y}}(i,j) - C(i,j)\widehat{\boldsymbol{x}}(i,j) \right) \\
\widehat{\mathscr{Z}}(i,j) = H(i,j)\widehat{\boldsymbol{x}}(i,j)
\end{cases}
.
$$

Similarly, from (22) the dynamic filtering error systems can be reconstructed into the following form:

$$
\begin{aligned}
\iota(i,j) ={}& \left(\mathscr{A}_1(i,j) + \boldsymbol{\varpi}_1(i,j)\breve{\mathscr{A}}_1(i,j) \right)\iota(i,j) + \widetilde{A}_2(i,j)\iota_\tau(i,j) + \left(\widehat{\mathscr{E}}(i,j) + \boldsymbol{\varpi}_1(i,j)\breve{\mathscr{E}}(i,j) \right)\boldsymbol{\omega}(i,j) \\
&+ \left(\widehat{\mathscr{O}}(i,j) + \boldsymbol{\varpi}_2(i,j)\breve{\mathscr{O}}(i,j) \right)\boldsymbol{v}(i,j) + \left(\widehat{\mathscr{R}}(i,j) + \boldsymbol{\varpi}_1(i,j)\breve{\mathscr{R}}(i,j) \right)\boldsymbol{r}(i,j).
\end{aligned} \tag{23}
$$

In what follows, it is easy to obtain corollary 1 based on the results of Theorem 1 and Theorem 2.

Corollary 1. For dynamic filtering error systems (23) under the event-triggered mechanism (7) and hybrid cyber-attacks (9), and given positive scalars $\overline{\tau}$, $\underline{\tau}$, as well as the filtering gains $L(i,j) \in R^{(n_h+n_v)\times n_y}$, if there exist positive definite symmetric matrices $\overline{P}(i,j) = diag\{\overline{P}^h(i,\ j),\ \overline{P}^v(i,\ j)\} \in R^{(2n_h+2n_v)\times(2n_h+2n_v)}$, $S_1(i,\ j) = diag\{S_1^h(i,\ j),\ S_1^v(i,\ j)\} \in R^{(2n_h+2n_v)\times(2n_h+2n_v)}$, $S_2(i,\ j) = diag\{S_2^h(i,\ j),\ S_2^v(i,\ j)\} \in R^{(2n_h+2n_v)\times(2n_h+2n_v)}$, $S_3(i,j) = diag\{S_3^h(i,j), S_3^v(i,j)\} \in R^{(2n_h+2n_v)\times(2n_h+2n_v)}$, $Q(i,j) \in R^{(2n_h+2n_v)\times(2n_h+2n_v)}$, positive scalars ρ, $\gamma_1(i,j)$ and $\gamma_2(i,j)$, such that the following inequalities hold:

$$
\Theta = \begin{bmatrix} \Theta_{11} & \Theta_{12} \\ * & \Theta_{22} \end{bmatrix} \le 0, \tag{24}
$$

$$
S_2^h(i,j) \ge S_3^h(i,j), S_2^v(i,j) \ge S_3^v(i,j), \tag{25}
$$

$$
(1+\overline{\tau})S_1(i,j) + \overline{\tau}S_2(i,j) - \underline{\tau}S_3(i,j) \le \rho(S_2(i,j) - S_3(i,j)), \tag{26}
$$

$$
\begin{bmatrix} -Q(i,j) & \Omega^T \\ * & -\overline{P}(i,j) \end{bmatrix} \le 0, \tag{27}
$$

$$
2I_{2n_h+2n_v} - \Omega^T\overline{P}(i,j)\Omega \ge \widetilde{H}^T(i,j)\widetilde{H}(i,j), \tag{28}
$$

where

$$\Theta_{11} = \begin{bmatrix} \Theta_{11}^1 & 0 & 0 & 0 \\ * & -\overline{S}_1(i,j) & 0 & 0 \\ * & * & -\gamma_1(i,j)\Phi_{(i,j)} & 0 \\ * & * & * & -\gamma_2(i,j)I_{n_y} \end{bmatrix},$$

$$\Theta_{12} = \begin{bmatrix} \widehat{A}_1^T(i,j) + M^T\overline{B}^T(i,j) & \overline{\varsigma}_1\breve{A}_1^T(i,j) & \overline{\varsigma}_{12}\breve{A}_1^T(i,j) & 0 & 0 \\ \overline{A}_2^T(i,j) & 0 & 0 & 0 & 0 \\ \widehat{\mathscr{R}}(i,j)\Omega^T & \overline{\varsigma}_1\breve{\mathscr{R}}^T(i,j)\Omega^T & 0 & \overline{\varsigma}_{12}\breve{\mathscr{R}}^T(i,j)\Omega^T & 0 \\ \widehat{\mathscr{O}}^T(i,j)\Omega^T & 0 & 0 & 0 & \sqrt{(\overline{\varsigma}_2^2 + 2\overline{\varsigma}_{12}^2)}\breve{\mathscr{O}}^T(i,j)\Omega^T \end{bmatrix},$$

$$\Theta_{22} = I_5 \otimes -\overline{P}(i,j),$$

$$\Theta_{11}^1 = \left(1 + \overline{\tau} - \underline{\tau}\right)\overline{S}_1(i,j) + \left(\overline{\tau}\overline{S}_2(i,j) - \underline{\tau}\overline{S}_3(i,j)\right) + \sigma\gamma_1(i,j)\Omega\widetilde{C}^T(i,j)\Phi_{(i,j)}\widetilde{C}(i,j)\Omega^T + \left(1 - \frac{1}{\rho}\right)\overline{P}(i,j) - 2\left(1 - \frac{1}{\rho}\right)I_{2n_h + 2n_v},$$

$$\overline{S}_1 = \begin{bmatrix} \overline{I}_{n_h}S_1^h(i,j)\overline{I}_{n_h} + \overline{I}_{n_v}S_1^v(i,j)\overline{I}_{n_v} & \overline{I}_{n_h}S_1^h(i,j)\widetilde{I}_{n_h} + \overline{I}_{n_v}S_1^v(i,j)\widetilde{I}_{n_v} \\ * & \widetilde{I}_{n_h}S_1^h(i,j)\widetilde{I}_{n_h} + \widetilde{I}_{n_v}S_1^v(i,j)\widetilde{I}_{n_v} \end{bmatrix}, \overline{I}_{n_v} = \begin{bmatrix} 0 & 0 \\ I_{n_v} & 0 \end{bmatrix}, \widetilde{I}_{n_v} = \begin{bmatrix} 0 & 0 \\ 0 & I_{n_v} \end{bmatrix},$$

$$\overline{S}_2 = \begin{bmatrix} \overline{I}_{n_h}S_2^h(i,j)\overline{I}_{n_h} + \overline{I}_{n_v}S_2^v(i,j)\overline{I}_{n_v} & \overline{I}_{n_h}S_2^h(i,j)\widetilde{I}_{n_h} + \overline{I}_{n_v}S_2^v(i,j)\widetilde{I}_{n_v} \\ * & \widetilde{I}_{n_h}S_2^h(i,j)\widetilde{I}_{n_h} + \widetilde{I}_{n_v}S_2^v(i,j)\widetilde{I}_{n_v} \end{bmatrix}, \overline{I}_{n_h} = \begin{bmatrix} I_{n_h} & 0 \\ 0 & 0 \end{bmatrix}, \widetilde{I}_{n_h} = \begin{bmatrix} 0 & I_{n_h} \\ 0 & 0 \end{bmatrix},$$

$$\overline{S}_3 = \begin{bmatrix} \overline{I}_{n_h}S_3^h(i,j)\overline{I}_{n_h} + \overline{I}_{n_v}S_3^v(i,j)\overline{I}_{n_v} & \overline{I}_{n_h}S_3^h(i,j)\widetilde{I}_{n_h} + \overline{I}_{n_v}S_3^v(i,j)\widetilde{I}_{n_v} \\ * & \widetilde{I}_{n_h}S_3^h(i,j)\widetilde{I}_{n_h} + \widetilde{I}_{n_v}S_3^v(i,j)\widetilde{I}_{n_v} \end{bmatrix},$$

and other parameters are defined in Theorem 1. Then, the dynamic filtering error systems (23) is exponentially ultimately bounded in mean-square sense. Moreover, the minimum upper bound of controlled output error $\|\widetilde{\mathscr{Z}}(i,j)\|^2$ is obtained by solving the following optimization problem:

$$\min\widehat{\delta}(i,j) = \left\{ tr\left\{ \mathscr{W}^T\left(\widehat{\mathscr{E}}^T(i,j)Q(i,j)\widehat{\mathscr{E}}(i,j) + \overline{\varsigma}_1^2\breve{\mathscr{E}}^T(i,j)Q(i,j)\breve{\mathscr{E}}(i,j) + \sigma\gamma_1(i,j)\widetilde{D}^T(i,j)\Phi_{(i,j)}\widetilde{D}(i,j)\right)\mathscr{W}\right\} + \gamma_2(i,j)\overline{v}^2 \right\}$$

s.t. (24)-(28).

Case 2: The following 2-D discrete nonlinear systems characterized by the Roesser model is considered:

$$\begin{cases} \mathscr{X}(i,j) = A_1(i,j)\boldsymbol{x}(i,j) + B(i,j)\boldsymbol{g}(\boldsymbol{x}(i,j)) + E(i,j)\boldsymbol{\omega}(i,j) \\ \mathscr{Y}(i,j) = C(i,j)\boldsymbol{x}(i,j) + D(i,j)\boldsymbol{\omega}(i,j) \\ \mathscr{Z}(i,j) = H(i,j)\boldsymbol{x}(i,j) \end{cases}. \tag{29}$$

Furthermore, the following filter form is employed:

$$\begin{cases} \widehat{\mathscr{X}}(i,j) = A_1(i,j)\widehat{\boldsymbol{x}}(i,j) + B(i,j)\boldsymbol{g}(\widehat{\boldsymbol{x}}(i,j)) + L(i,j)\left(\widehat{\mathscr{Y}}(i,j) - C(i,j)\widehat{\boldsymbol{x}}(i,j)\right) \\ \widehat{\mathscr{Z}}(i,j) = H(i,j)\widehat{\boldsymbol{x}}(i,j) \end{cases}.$$

Similarly, the dynamic filtering error systems based on (29) can be reconstructed into the following form:

$$\begin{aligned} \iota(i,j) &= \left(\widehat{\mathscr{A}}_1(i,j) + \boldsymbol{\varpi}_1(i,j)\breve{\mathscr{A}}_1(i,j) + \widetilde{B}(i,j)\widetilde{M}\right)\iota(i,j) + \widetilde{B}(i,j)\overline{\boldsymbol{g}}(\iota(i,j)) + \left(\widehat{\mathscr{E}}(i,j) + \boldsymbol{\varpi}_1(i,j)\breve{\mathscr{E}}(i,j)\right)\boldsymbol{\omega}(i,j) \\ &\quad + \boldsymbol{\varpi}_2(i,j)\breve{\mathscr{O}}(i,j))\boldsymbol{v}(i,j) + \left(\widehat{\mathscr{R}}(i,j) + \boldsymbol{\varpi}_1(i,j)\breve{\mathscr{R}}(i,j)\right)\boldsymbol{r}(i,j), \end{aligned} \tag{30}$$

then, it is straightforward to obtain corollary 2 based on the results of Theorem 1 and Theorem 2.

Corollary 2. For dynamic filtering error systems (30) under the event-triggered mechanism (7) and hybrid cyber-attacks (9), and the filtering gains $L(i,j) \in R^{(n_h+n_v)\times n_y}$, if there exist positive definite symmetric matrix $\overline{P}(i,j) = diag\{\overline{P}^h(i,j), \overline{P}^v(i,j)\} \in R^{(2n_h+2n_v)\times(2n_h+2n_v)}$, $Q(i,j) \in R^{(2n_h+2n_v)\times(2n_h+2n_v)}$, positive scalars ρ, $\gamma_1(i,j)$ as well as $\gamma_2(i,j)$, such that the following inequalities hold:

$$\Theta = \begin{bmatrix} \Theta_{11} & \Theta_{12} \\ * & \Theta_{22} \end{bmatrix} \le 0, \tag{31}$$

$$\begin{bmatrix} -Q(i,j) & \Omega^T \\ * & -\overline{P}(i,j) \end{bmatrix} \le 0, \tag{32}$$

$$2I_{2n_h+2n_v} - \Omega^T \overline{P}(i,j)\Omega \ge \widetilde{H}^T(i,j)\widetilde{H}(i,j), \tag{33}$$

where

$$\Theta_{11} = \begin{bmatrix} \Theta_{11}^1 & \widetilde{M}^T\Omega & 0 & 0 \\ * & -2I_{2n_h+2n_v} & 0 & 0 \\ * & * & -\gamma_1(i,j)\Phi_{(i,j)} & 0 \\ * & * & * & -\gamma_2(i,j)I_{n_y} \end{bmatrix},$$

$$\Theta_{12} = \begin{bmatrix} \widehat{A}_1^T(i,j) + M^T\overline{B}^T(i,j) & \overline{\varsigma}_1\breve{A}_1^T(i,j) & \overline{\varsigma}_{12}\breve{A}_1^T(i,j) & 0 & 0 \\ \Omega^T\overline{B}^T(i,j) & 0 & 0 & 0 & 0 \\ \widehat{\mathscr{R}}(i,j)\Omega^T & \overline{\varsigma}_1\breve{\mathscr{R}}^T(i,j)\Omega^T & 0 & \overline{\varsigma}_{12}\breve{\mathscr{R}}^T(i,j)\Omega^T & 0 \\ \widehat{\mathscr{O}}^T(i,j)\Omega^T & 0 & 0 & 0 & \sqrt{(\overline{\varsigma}_2^2 + 2\overline{\varsigma}_{12}^2)}\breve{\mathscr{O}}^T(i,j)\Omega^T \end{bmatrix},$$

$$\Theta_{22} = I_5 \otimes -\overline{P}(i,j), \Theta_{11}^1 = \boldsymbol{\sigma}\gamma_1(i,j)\Omega\widetilde{C}^T(i,j)\Phi_{(i,j)}\widetilde{C}(i,j)\Omega^T + \left(1 - \frac{1}{\rho}\right)\overline{P}(i,j) - 2\left(1 - \frac{1}{\rho}\right)I_{2n_h+2n_v},$$

and other parameters are defined in Theorem 1. Then, the dynamic filtering error systems (30) is exponentially ultimately bounded in mean-square sense. Moreover, the minimum upper bound of controlled output error $\|\widetilde{\mathscr{Z}}(i,j)\|^2$ is obtained by solving the following optimization problem:

$$\min\widehat{\delta}(i,j) = \left\{ tr\left\{ \mathscr{W}^T\left(\widehat{\mathscr{E}}^T(i,j)Q(i,j)\widehat{\mathscr{E}}(i,j) + \overline{\varsigma}_1^2\breve{\mathscr{E}}^T(i,j)Q(i,j)\breve{\mathscr{E}}(i,j) + \boldsymbol{\sigma}\gamma_1(i,j)\widetilde{D}^T(i,j)\Phi_{(i,j)}\widetilde{D}(i,j)\right)\mathscr{W}\right\} + \gamma_2(i,j)\overline{v}^2\right\}$$
$$s.t.(31) - (33).$$

4. Numerical Simulations

We consider an industrial heating exchange process satisfying the following partial differential equation with time-delays, which structure diagram is shown in Fig. 3.

$$\frac{\partial\hbar(x,t)}{\partial x} + \frac{\partial\hbar(x,t)}{\partial t} = -a_0\hbar(x,t) - a_1\hbar(x, t - \tau(t)), \tag{34}$$

where $\hbar(x,t)$ is the temperature function associated with both the space dimension $x \in [0 \quad X]$ and the time dimension $t \in [0 \quad T]$, and $\tau(t) > 0$ denotes time-varying delays. In addition, from a practical engineering perspective, the structural model of the heating exchange process often appears time-varying properties due to the limitations of the chemical reactor components. Thus, the parameters a_0 and a_1 with time-varying characteristics are used to represent the exchange coefficients in the heating exchange process.

Define $\hbar(i,j) = \hbar(i\Delta x, j\Delta t), r(i,j) = r(i\Delta x, j\Delta t)$, then one has

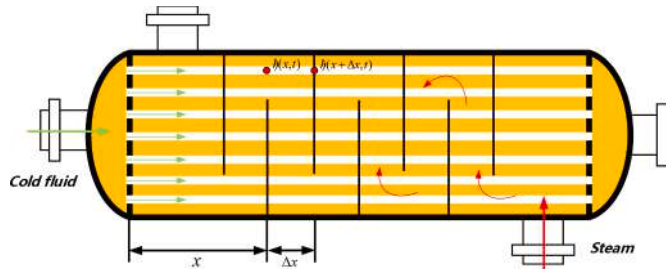**Fig. 3.** The heating exchange process.

$$\frac{\partial \hbar(x,t)}{\partial x} \approx \frac{\hbar(i\Delta x, j\Delta t) - \hbar((i-1)\Delta x, j\Delta t)}{\Delta x}, \frac{\partial \hbar(x,t)}{\partial t} \approx \frac{\hbar(i\Delta x, j\Delta t) - \hbar(i\Delta x, (j-1)\Delta t)}{\Delta t} \hbar(x,t) \approx \hbar(i,j).$$

Furthermore, equation (34) can be approximately rewritten in the following form:

$$\hbar(i,j+1) = \left(1 - \frac{\Delta t}{\Delta x} - a_0 \Delta t\right) \hbar(i,j) + \frac{\Delta t}{\Delta x} \hbar(i-1,j) - a_1 \Delta t \hbar(i, j - \tau(j)). \tag{35}$$

We denote $x^h(i,j) = \hbar(i-1,j), x^v(i,j) = \hbar(i,j)$, then, the equivalent Roesser model can be derived from the original partial differential equation (35) as follows:

$$\begin{bmatrix} x^h(i+1,j) \\ x^v(i,j+1) \end{bmatrix} = \begin{bmatrix} 0 & 1 \\ \frac{\Delta t}{\Delta x} & 1 - \frac{\Delta t}{\Delta x} - a_0 \Delta t \end{bmatrix} \begin{bmatrix} x^h(i,j) \\ x^v(i,j) \end{bmatrix} + \begin{bmatrix} 0 & 0 \\ 0 & -a_1 \Delta t \end{bmatrix} \begin{bmatrix} x^h((i - \tau(i),j)) \\ x^v((i, j - \tau(j))) \end{bmatrix}.$$

Subsequently, according to the literature [19], we adopt the following parameters:

$$\Delta t = 0.1, \quad \Delta x = 0.4, \quad a_0 = \sin(i+j) - 4, \quad a_1 = 3\cos(i+j),$$

then, the mathematical model of the industrial heating exchange process can be described by 2-D systems with the following parameters:

$$A_1(i,j) = \begin{bmatrix} 0 & 1 \\ 0.25 & 0.35 - 0.1\sin(i+j) \end{bmatrix}, A_2(i,j) = \begin{bmatrix} 0 & 0 \\ 0 & -0.3\cos(i+j) \end{bmatrix}, B(i,j) = \begin{bmatrix} 0.2 & -0.05 \\ -0.2 + 0.1\tanh(i+j) & 0.16 \end{bmatrix},$$

$$E(i,j) = \begin{bmatrix} -0.4 + 0.1\sin(0.2i+j) \\ 0.15 \end{bmatrix}, C(i,j) = \begin{bmatrix} 0.35 + 0.1\cos(j) & 0.2 \\ 0.2 & 0.35 \end{bmatrix}, D(i,j) = \begin{bmatrix} 0.3 \\ 0.2 - 0.1\tanh(i+j) \end{bmatrix},$$

$$H(i,j) = \begin{bmatrix} 0.65 & -0.12 \end{bmatrix}.$$

Additionally, we take the initial state of systems as $x(i,j) = 2.2\sin(i)\cos(j+1)$ for $i \leq 0$ and $j \in [0 \quad 50]$, as well as $x(i,j) = 2.3\sin(i+1)\cos(j)$ for $i \in [0 \quad 50]$ and $j \leq 0$. The decay rate ρ, threshold parameter σ and weight matrix $\Phi_{(ij)}$ are set as 50, 0.3 and $1.2I$. The external disturbance $\omega(i,j)$ is assumed to be the Gaussian white noise process with the variance $W = 0.5I$. Then, suppose that the hybrid cyber-attacks are implemented in the interval $i,j \in [20 \quad 40]$, and the corresponding probabilities are $\bar{\vartheta} = 0.3$ and $\bar{\xi} = 0.65$, respectively. Moreover, the false data function is chosen as:

$$v(i,j) = \begin{cases} [0.3\sin(0.45(i+j)) \quad 0.25\cos(0.3(i+j))]^T i,j \in [20 \quad 40] \\ 0 \, otherwise \end{cases}.$$

In this example, the nonlinear function is taken as

$$g(x(i,j)) = \begin{bmatrix} 0.4\sin(-x^h(i,j)) + 0.2x^h(i,j) \\ -0.4\sin(x^v(i,j)) + 0.2x^v(i,j) \end{bmatrix}.$$

Considering that the $\sin(\cdot)$ function is an odd function and the value domain belongs to $[-1 \quad 1]$, it is straightforward to confirm that the parameters $G_1^h = G_1^v = -0.3$ and $G_1^h = G_2^h = 0.2$, which satisfy Assumption 1.

Then, by applying Theorem 2 and in virtue of the LMI toolbox of MATLAB, the part of feasible solutions and filtering gain matrices can be obtained and listed as Tables 1 and 2:

The simulation results are shown in Fig. 4–Fig. 9. Fig. 4 and Fig. 5 depict the event-triggered instants and the hybrid cyber-attacks case, respectively. Fig. 4 indicates that the employed event-triggered strategy arranges the measurement output to be released at certain instants, effectively relieving the communication pressure of the network. Fig. 4 shows hybrid cyber-attacks occurring on interval $i,j \in [20 \quad 40]$, where the blue dots indicate DoS attacks instant and the red asterisks indicate FDI attacks instant. Fig. 6 and Fig. 7 are concerning the trajectories of the state $x(i,j)$ and its estimate $\hat{x}(i,j)$. Fig. 8 and Fig. 9 show the trajectories of the dynamic filtering error $e^h(i,j)$ and the dynamic filtering error $e^v(i,j)$, respectively. It can be seen from Fig. 8-11 that filtering error fluctuates in the finite horizon $i,j \in [0 \quad 40]$ due to external disturbance and hybrid cyber-attacks. In order to more intuitively illustrate the superior

Table 1

Part of the feasible solution $\bar{P}(i,j)$.

$\bar{P}(1,1) = \begin{bmatrix} 1.3193 & 0.0005 & 0 & 0 \\ 0.0005 & 1.7234 & 0 & 0 \\ 0 & 0 & 1.4273 & 0.1837 \\ 0 & 0 & 0.1837 & 1.6637 \end{bmatrix}$		$\bar{P}(1,2) = \begin{bmatrix} 1.2418 & 0.0010 & 0 & 0 \\ 0.0010 & 1.8171 & 0 & 0 \\ 0 & 0 & 1.7706 & 0.1213 \\ 0 & 0 & 0.1213 & 1.4912 \end{bmatrix}$	...
...		...	...
$\bar{P}(50,1) = \begin{bmatrix} 1.5174 & 0.0209 & 0 & 0 \\ 0.0209 & 1.4313 & 0 & 0 \\ 0 & 0 & 1.5663 & 0.0965 \\ 0 & 0 & 0.0965 & 1.0648 \end{bmatrix}$		$\bar{P}(50,2) = \begin{bmatrix} 1.3795 & 0.1148 & 0 & 0 \\ 0.1148 & 1.7200 & 0 & 0 \\ 0 & 0 & 1.3218 & 0.1513 \\ 0 & 0 & 0.1513 & 1.5962 \end{bmatrix}$	

Table 2
Part of the filter gains $L(i,j)$.

$$L(1,1) = \begin{bmatrix} 0.8331 & 0.0122 \\ -0.0177 & 0.9302 \end{bmatrix} \qquad L(1,2) = \begin{bmatrix} 0.7885 & 0.1019 \\ -0.0169 & 0.7860 \end{bmatrix} \qquad \cdots$$

$$\cdots \qquad\qquad\qquad\qquad\qquad \cdots \qquad\qquad\qquad\qquad\qquad \cdots$$

$$L(2,1) = \begin{bmatrix} 0.9101 & 0.0112 \\ -0.0164 & 0.7851 \end{bmatrix} \qquad L(2,2) = \begin{bmatrix} 0.8435 & 0.0139 \\ -0.0174 & 0.7682 \end{bmatrix} \qquad \cdots$$

$$L(50,1) = \begin{bmatrix} 0.8220 & 0.0122 \\ -0.0175 & 0.8192 \end{bmatrix} \qquad L(50,2) = \begin{bmatrix} 0.8012 & 0.0122 \\ -0.0164 & 0.7986 \end{bmatrix} \qquad \cdots$$
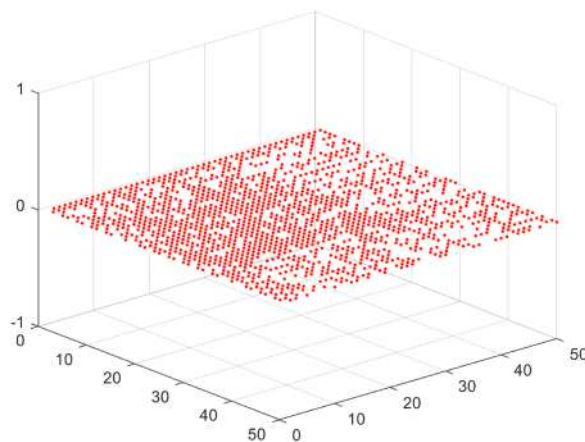
Fig. 4. The event-triggered instants.
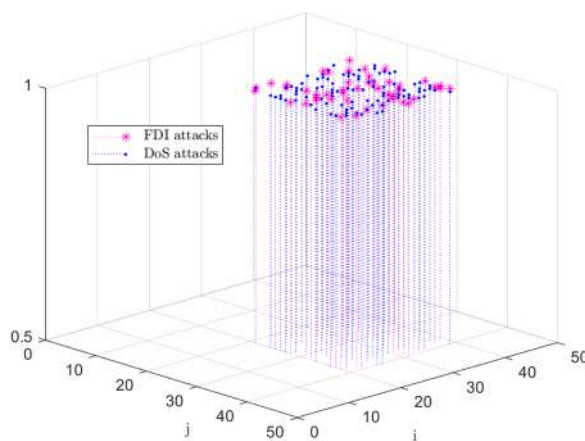
Fig. 5. The hybrid cyber-attacks case.

performance of proposed filter, we limit the vertical component j and horizontal component i to evolve independently from 8 to 9. The comparison of the system state with the estimated state are shown in Fig. 10–Fig. 11. Fig. 6-Fig. 11 exhibit that the estimation of proposed filtering algorithm can effectively follow the actual state of systems, and the proposed filtering algorithm has excellent estimated performance.

In addition, in order to facilitate the comparison of the filtering algorithm proposed in this paper with the existing H_∞ filtering algorithms of [18], we introduce the mean square error of the state estimation in the horizontal and vertical directions as $MSE_h(i,j)$ and $MSE_v(i,j)$, respectively, where $MSE_h(i,j) = \frac{1}{T_1^2}\sum_{j=1}^{T_1}\sum_{i=1}^{T_1}(x^h(i,j) - \hat{x}^h(i,j))^2 \, (T_1 = 50)$ and $MSE_v(i,j) = \frac{1}{T_1^2}\sum_{j=1}^{T_1}\sum_{i=1}^{T_1}(x^v(i,j) - \hat{x}^v(i,j))^2 \, (T_1 = 50)$. Under the same initial conditions described above, we performed simulation verification and the results are shown in Fig. 12–Fig. 15. The estimation error trajectory $e^h(i,j)$ in the horizontal direction and the estimation error $e^v(i,j)$ in the vertical direction under both algorithms are presented in Fig. 11 and Fig. 12, respectively. The trajectories of $MSE_h(i,j)$ and $MSE_v(i,j)$ under the above two filtering design strategies are shown in Fig. 13 and Fig. 14. Fig. 12- Fig. 15 demonstrate that the proposed ultimately bounded filtering algorithm has smaller mean square error and better tracking performance compared with the robust filtering algorithm of [18].
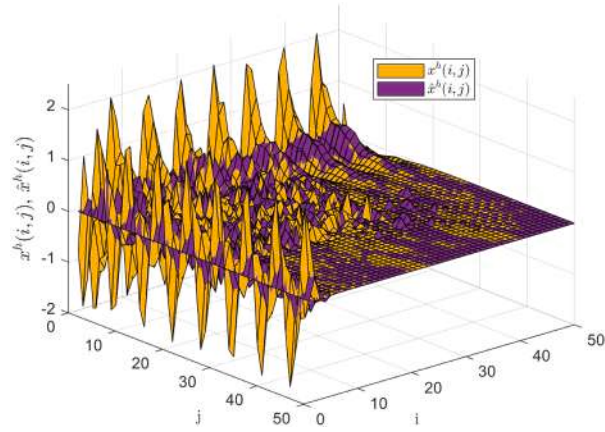
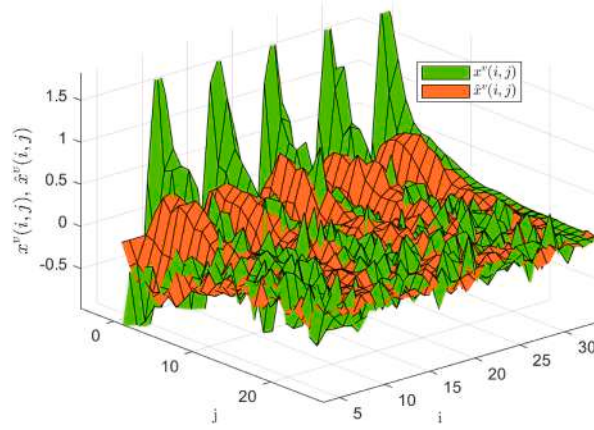**Fig. 6.** The trajectory of the state $x^h(i,j)$ and $\hat{x}^h(i,j)$.

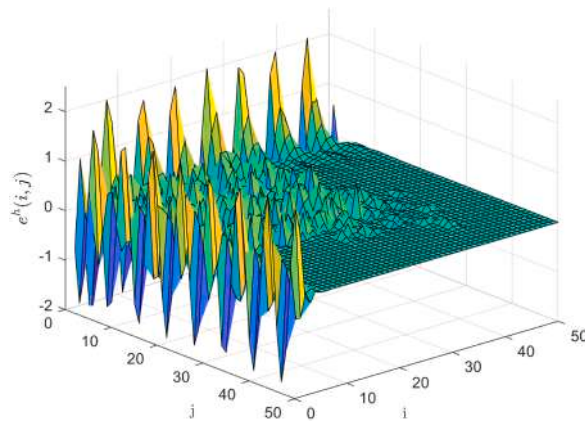**Fig. 7.** The trajectory of the state $x^v(i,j)$ and $\hat{x}^v(i,j)$.

Fig. 8. The trajectory of the dynamic filtering error $e^h(i,j)$.

Finally, we will discuss the effect of decay rate ϱ, the external disturbance variance W and the event-triggered threshold σ on the average value of controlled output error $\frac{1}{T^2}\sum_{i=0}^{T}\sum_{j=0}^{T}\|\widetilde{\mathscr{Z}}(i,j)\|^2$ and the average value of upper bound $\frac{1}{T^2}\sum_{i=0}^{T}\sum_{j=0}^{T}\widehat{\delta}(i,j)$ in the interval $i,\,j\in[0\quad30]$, respectively. $\frac{1}{T^2}\sum_{i=0}^{T}\sum_{j=0}^{T}\|\widetilde{\mathscr{Z}}(i,j)\|^2$ $(T=30,W=0.5I,\sigma=0.3,\varrho=0.90)$ and $\frac{1}{T^2}\sum_{i=0}^{T}\sum_{j=0}^{T}\widehat{\delta}(i,j)(T=30,$ $W=0.5I,\sigma=0.3,\varrho=0.90)$ are shown in Fig. 16 and Fig. 17, respectively. It can be seen from Fig. 16. that the average value of the
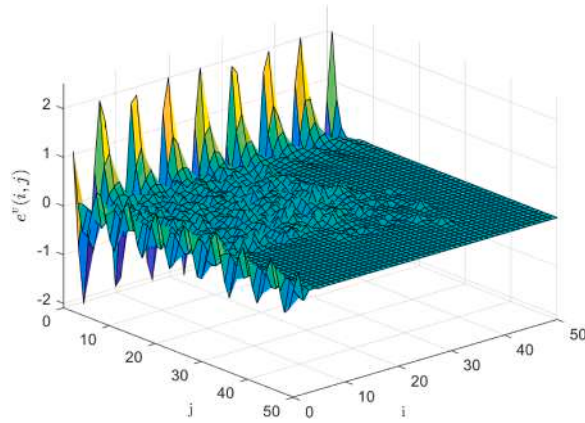
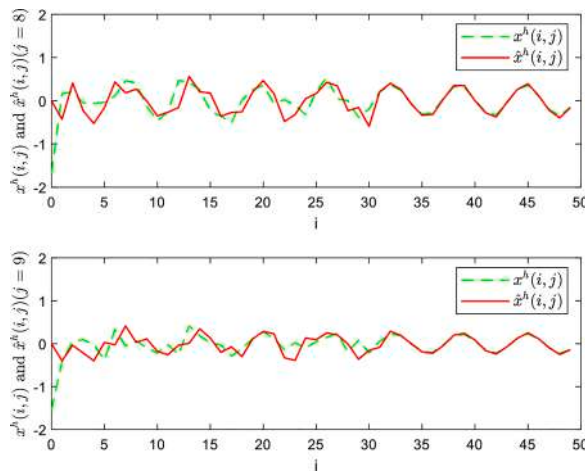**Fig. 9.** The trajectory of the dynamic filtering error $e^v(i,j)$.

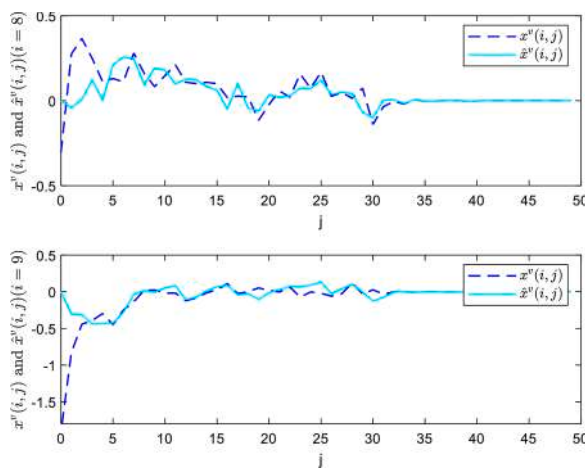**Fig. 10.** The state $x^h(i,j)$ and its estimate $\hat{x}^h(i,j)$ on $j = 8, 9$.

Fig. 11. The state $x^v(i,j)$ and its estimate $\hat{x}^v(i,j)$ on $i = 8, 9$.

dynamic output estimation error eventually converges to a certain determined value, which is mainly due to the presence of external disturbance and hybrid attacks in the interval $i, j \in [0 \quad 30]$. In other words, if there are not external disturbance and hybrid cyber-
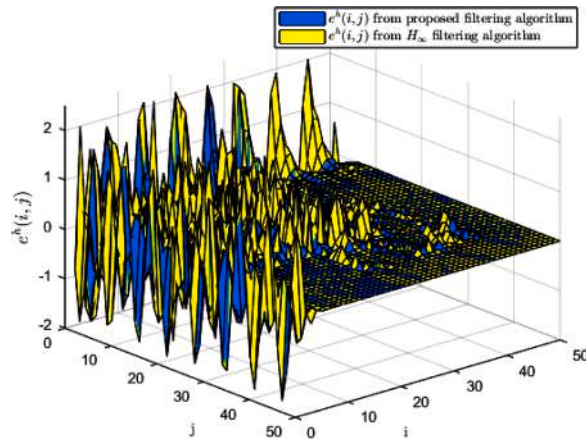
Fig. 12. The trajectories of $e^h(i,j)$ under the proposed filtering and H$_\infty$ robust filtering algorithm.
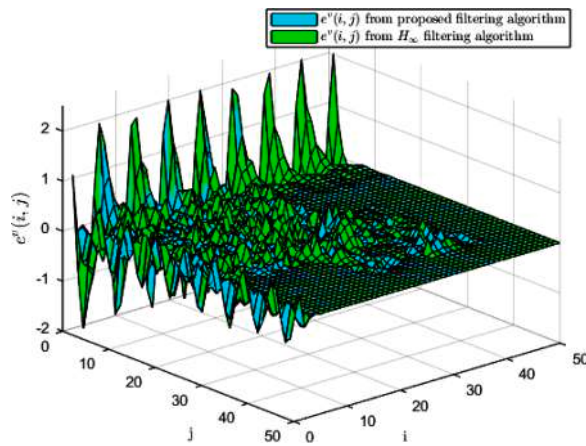

Fig. 13. The trajectories of $e^v(i,j)$ under the proposed filtering and H$_\infty$ robust filtering algorithm.
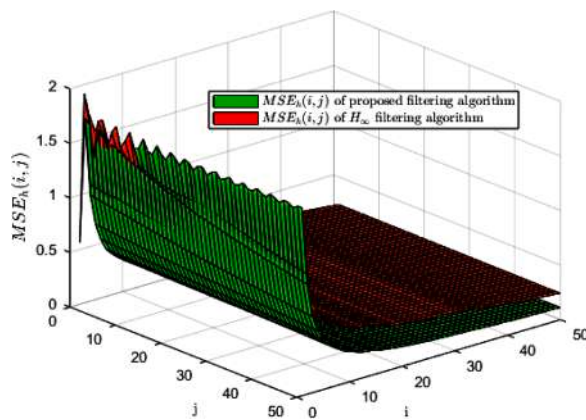

Fig. 14. The $MSE_h(i,j)$ under the proposed filtering and H$_\infty$ robust filtering algorithm.

attacks, the result obtained in this paper would have converged from being exponentially ultimately bounded to being exponentially stable in mean-square sense. It also can be seen from Fig. 17 that the average value of upper bound eventually evolves to the determined value. In addition, we provide the average value of controlled output error and the average value of upper bound with different valve of W, ϱ and σ, as detailed in Table 3 and 4. It is can be seen from Table 3 that $\frac{1}{T^2}\sum_{i=0}^{T}\sum_{j=0}^{T}\|\widetilde{\mathcal{Z}}(i,j)\|^2$ and
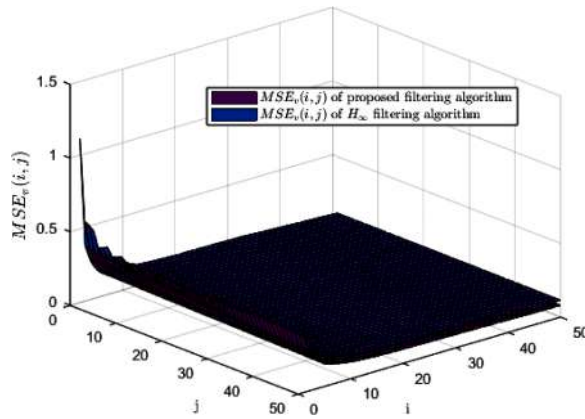
Fig. 15. The $MSE_v(i,j)$ under the proposed filtering and H_∞ robust filtering algorithm.
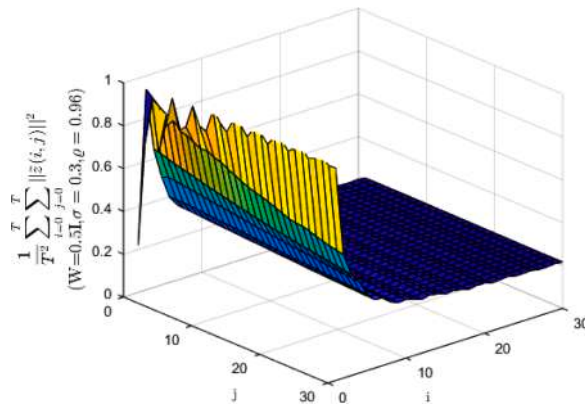

Fig. 16. The average value of controlled output error $\frac{1}{T^2}\sum_{i=0}^{T}\sum_{j=0}^{T}\|\widetilde{\mathscr{Z}}(i,j)\|^2$.
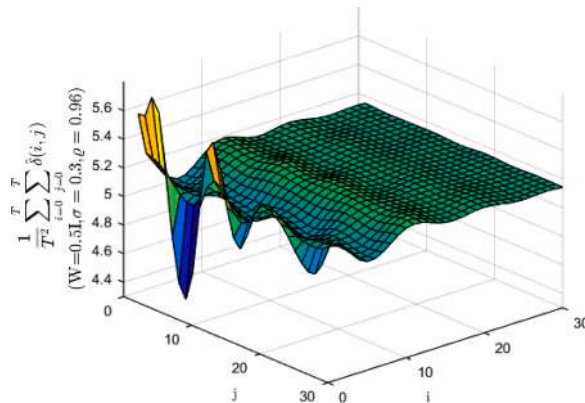

Fig. 17. The average value of upper bound $\frac{1}{T^2}\sum_{i=0}^{T}\sum_{j=0}^{T}\widehat{\delta}(i,j)$.

$\frac{1}{T^2}\sum_{i=0}^{T}\sum_{j=0}^{T}\widehat{\delta}(i,j)(T=30)$ also increase with the increasing of the external disturbance variance W or the decay rate ϱ, which consistent with theoretical results obtained in Theorems 1 and 2 that if the decay rate ϱ increases, the controlled output error $\|\widetilde{z}(i,j)\|^2$ will converge quicker and the upper bound $\widehat{\delta}(i,j)$ will also increase. Furthermore, Table 4 illustrates the influence of the threshold σ on the filtering performance, and it can be seen that $\frac{1}{T^2}\sum_{i=0}^{T}\sum_{j=0}^{T}\|\widetilde{\mathscr{Z}}(i,j)\|^2$ and $\frac{1}{T^2}\sum_{i=0}^{T}\sum_{j=0}^{T}\widehat{\delta}(i,j)(T=30)$ will increase as the σ increases (the more harsh triggering condition). The above simulation results demonstrate that the developed filtering algorithm is effective under the event-triggered mechanism and hybrid cyber-attacks.

Table 3
The average value of the controlled output error and upper bound with different W and ϱ ($T = 30, \sigma = 0.3$).

	$W = 0.5I$	$W = 0.7I$	$W = 0.9I$	$W = 1.1I$
$\frac{1}{T^2}\sum_{i=0}^{T}\sum_{j=0}^{T}\|\widetilde{\mathcal{Z}}(i,j)\|^2(\varrho = 0.96)$	0.2180	0.2405	0.3193	0.3897
$\frac{1}{T^2}\sum_{i=0}^{T}\sum_{j=0}^{T}\widehat{\delta}(i,j)(\varrho = 0.96)$	5.1217	6.0502	7.1963	8.3142
$\frac{1}{T^2}\sum_{i=0}^{T}\sum_{j=0}^{T}\|\widetilde{\mathcal{Z}}(i,j)\|^2(\varrho = 0.94)$	0.1959	0.2363	0.2819	0.3620
$\frac{1}{T^2}\sum_{i=0}^{T}\sum_{j=0}^{T}\widehat{\delta}(i,j)(\varrho = 0.94)$	4.1217	5.3184	6.2821	7.5421
$\frac{1}{T^2}\sum_{i=0}^{T}\sum_{j=0}^{T}\|\widetilde{\mathcal{Z}}(i,j)\|^2(\varrho = 0.92)$	0.1735	0.2128	0.2781	0.3324
$\frac{1}{T^2}\sum_{i=0}^{T}\sum_{j=0}^{T}\widehat{\delta}(i,j)(\varrho = 0.92)$	3.3821	4.3153	5.5416	6.4752
$\frac{1}{T^2}\sum_{i=0}^{T}\sum_{j=0}^{T}\|\widetilde{\mathcal{Z}}(i,j)\|^2(\varrho = 0.90)$	0.1674	0.2113	0.2645	0.3198
$\frac{1}{T^2}\sum_{i=0}^{T}\sum_{j=0}^{T}\widehat{\delta}(i,j)(\varrho = 0.90)$	3.0422	3.5761	4.6001	5.6985

Table 4
The average value of the controlled output error and upper bound with different σ and ϱ ($T = 30$, $W = 0.5I$).

	$\sigma = 0.3$	$\sigma = 0.4$	$\sigma = 0.5$	$\sigma = 0.6$
$\frac{1}{T^2}\sum_{i=0}^{T}\sum_{j=0}^{T}\|\widetilde{\mathcal{Z}}(i,j)\|^2(\varrho = 0.96)$	0.2180	0.3245	0.4086	0.4951
$\frac{1}{T^2}\sum_{i=0}^{T}\sum_{j=0}^{T}\widehat{\delta}(i,j)(\varrho = 0.96)$	5.1217	6.3174	7.3014	8.8814
$\frac{1}{T^2}\sum_{i=0}^{T}\sum_{j=0}^{T}\|\widetilde{\mathcal{Z}}(i,j)\|^2(\varrho = 0.94)$	0.1959	0.2883	0.3406	0.4199
$\frac{1}{T^2}\sum_{i=0}^{T}\sum_{j=0}^{T}\widehat{\delta}(i,j)(\varrho = 0.94)$	4.1217	5.9451	6.8821	7.8234
$\frac{1}{T^2}\sum_{i=0}^{T}\sum_{j=0}^{T}\|\widetilde{\mathcal{Z}}(i,j)\|^2(\varrho = 0.92)$	0.1735	0.2528	0.3142	0.3736
$\frac{1}{T^2}\sum_{i=0}^{T}\sum_{j=0}^{T}\widehat{\delta}(i,j)(\varrho = 0.92)$	3.3821	4.7236	6.1147	7.0425
$\frac{1}{T^2}\sum_{i=0}^{T}\sum_{j=0}^{T}\|\widetilde{\mathcal{Z}}(i,j)\|^2(\varrho = 0.90)$	0.1674	0.2113	0.2645	0.3198
$\frac{1}{T^2}\sum_{i=0}^{T}\sum_{j=0}^{T}\widehat{\delta}(i,j)(\varrho = 0.90)$	3.0422	3.5844	5.5424	6.2776

5. Conclusions

This paper has investigated the design problem of ultimately bounded filter for 2-D discrete nonlinear systems with time-varying delays limited by the event-triggered mechanism and the hybrid cyber-attacks. On account of the limited bandwidth of the communication network, a bi-directional time-sequence event-triggered transmission protocol is introduced, which is based on the principle of utilizing predefined triggering conditions to determine whether the current data is transmitted. Besides, the impact of hybrid cyber-attacks, which occur in stochastic patterns, on the filtering performance is also discussed. In such a framework, an augmented model of 2-D systems described by Roesser model is developed under the concerted influence of event-triggered mechanism and hybrid cyber-attacks. Then, sufficient conditions are derived to guarantee that the dynamic filtering error systems satisfy exponentially ultimately bounded in mean-square sense. Furthermore, the filtering gains ensuring the desired decay rate of the dynamic filtering error systems can be obtained by minimizing the asymptotic upper bound of the controlled output error. Finally, the effectiveness of the proposed ultimately bounded filtering algorithm is verified by a simulation example. It is worth noting that this investigation is a preliminary attempt to combine the event-triggered mechanism and the ultimately bounded filtering technique for 2-D systems, and the proposed method has certain application potential for long-distance transmission systems described by 2-D systems. In addition, considering that the calculation of filter gains in this paper is carried out online, it is one of the future development directions that utilizing other event triggering mechanisms (e.g., dynamic event-triggered, self-triggered, periodic-triggered) to alleviate the pressure of network communication to a greater extent as well as reducing the computational complexity for the filtering problem of 2-D systems.

Declaration of Conflicting Interests

The authors declare that there is no competing financial interest or personal relationship that could have appeared to influence the work reported in this paper.

Acknowledgments

Appendix A. The Proof of Theorem 1

Proof. First of all, we consider the exponentially bounded performance of dynamic filtering error systems (13) under bounded initial conditions. Choose the following Lyapunov energy-like function:

$$V(i,j) = V^h(i,j) + V^v(i,j) = \sum_{q=1}^{4} V_q(i,j), \tag{36a}$$

$$V_q(i,j) = V_q^h(i,j) + V_q^v(i,j), \tag{36b}$$

$$V^+(i,j) = V^h(i+1,j) + V^v(i,j+1) = \sum_{q=1}^{4} V_q^h(i+1,j) + \sum_{q=1}^{4} V_q^v(i,j+1), \tag{36c}$$

with $V_1^h(i,j) = (\iota^h(i,j))^T P^h(i,j)\iota^h(i,j)$, $V_2^h(i,j) = \sum_{\theta=-\tau^h(i,j)}^{-1}(\iota^h(i+\theta,j))^T S_1^h(i,j)(\iota(i+\theta,j))$, $V_3^h(i,j) = \sum_{\theta=1-\overline{\tau}}^{-\tau}\sum_{s=\theta}^{-1}(\iota^h(i+s,j))^T S_1^h(i,j)(\iota^h(i+s,j))$, $V_4^h(i,j) = \sum_{\theta=-\overline{\tau}}^{-1}\sum_{s=\theta}^{-1}(\iota^h(i+s,j))^T S_2^h(i,j)(\iota^h(i+s,j)) - \sum_{\theta=-\underline{\tau}}^{-1}\sum_{s=\theta}^{-1}(\iota^h(i+s,j))^T S_3^h(i,j)(\iota^h(i+s,j))$, $V_1^v(i,j) = (\iota^v(i,j))^T P^v(i,j)\iota^v(i,j)$,

$V_2^v(i,j) = \sum_{\theta=-\tau^v(i,j)}^{-1}(\iota^v(i,j+\theta))^T S_1^v(i,j)(\iota^v(i,j+\theta))$, $V_3^v(i,j) = \sum_{\theta=1-\overline{\tau}}^{-\tau}\sum_{s=\theta}^{-1}(\iota^v(i,j+s))^T S_1^v(i,j)(\iota^v(i,j+s))$,

$$V_4^v(i,j) = \sum_{\theta=-\overline{\tau}}^{-1}\sum_{s=\theta}^{-1}(\iota^v(i,j+s))^T S_2^v(i,j)(\iota^v(i,j+s)) - \sum_{\theta=-\underline{\tau}}^{-1}\sum_{s=\theta}^{-1}(\iota^v(i,j+s))^T S_3^v(i,j)(\iota^v(i,j+s)),$$

where $P^h(i,j) \in R^{2n_h \times 2n_h}$, $S_1^h(i,j) \in R^{2n_h \times 2n_h}$, $S_2^h(i,j) \in R^{2n_h \times 2n_h}$, $S_3^h(i,j) \in R^{2n_h \times 2n_h}$, $P^v(i,j) \in R^{2n_v \times 2n_v}$, $S_1^v(i,j) \in R^{2n_v \times 2n_v}$, $S_2^v(i,j) \in R^{2n_v \times 2n_v}$,

$S_3^v(i,j) \in R^{2n_v \times 2n_v}$, $P(i,j) = \begin{bmatrix} P^h(i,j) & 0 \\ 0 & P^v(i,j) \end{bmatrix} \in R^{(2n_h+2n_v)\times(2n_h+2n_v)}$, $S_1(i,j) = \begin{bmatrix} S_1^h(i,j) & 0 \\ 0 & S_1^v(i,j) \end{bmatrix} \in R^{(2n_h+2n_v)\times(2n_h+2n_v)}$, $S_2(i,j) =$

$\begin{bmatrix} S_2^h(i,j) & 0 \\ 0 & S_2^v(i,j) \end{bmatrix} \in R^{(2n_h+2n_v)\times(2n_h+2n_v)}$, $S_3(i,j) = \begin{bmatrix} S_3^h(i,j) & 0 \\ 0 & S_3^v(i,j) \end{bmatrix} \in R^{(2n_h+2n_v)\times(2n_h+2n_v)}$.

In what follows, we consider the following index:

$$J(i,j) \overset{\Delta}{=} E\{V^+(i,j) - V(i,j)|\partial(i,j)\} = E\left\{ \sum_{q=1}^{4}\Delta V_q^h(i,j) + \sum_{q=1}^{4}\Delta V_q^v(i,j)|\partial(i,j) \right\}, \tag{37}$$

where $\partial(i,j) \overset{\Delta}{=} \{\eta(i,j),\eta(i,j-1),...,\eta(i,j-\overline{\tau}),\eta(i-1,j),\eta(i-2,j),...,\eta(i-\overline{\tau},j)\}$, $\Delta V_q^h(i,j) = V_q^h(i+1,j) - V_q^h(i,j)$, $\Delta V_q^v(i,j) = V_q^v(i,j+1) - V_q^v(i,j)$.

Then, the mathematical expectation of the difference will be derived along the dynamic filtering error systems (13). Considering (34), which yields

$$E\{\Delta V_1^h(i,j)\} = E\left\{ (\iota^h(i+1,j))^T P^h(i,j)\iota^h(i+1,j) - (\iota^h(i,j))^T P^h(i,j)\iota^h(i,j)|\partial(i,j) \right\}, \tag{38}$$

$$E\{\Delta V_2^h(i,j)\}$$
$$= E\left\{ \sum_{\theta=-\tau^h(i+1,j)}^{-1}(\iota^h(i+\theta+1,j))^T S_1^h(i,j)\iota^h(i+\theta+1,j) - \sum_{\theta=-\tau^h(i,j)}^{-1}(\iota^h(i+\theta,j))^T S_1^h(i,j)\iota^h(i+\theta,j)|\partial(i,j) \right\}$$
$$= (\iota^h(i,j))^T S_1^h(i,j)\iota^h(i,j) - (\iota^h(i-\tau^h(i,j),j))^T S_1^h(i,j)\iota^h(i-\tau^h(i,j),j)$$
$$+ \sum_{\theta=1-\tau^h(i+1,j)}^{-1}(\iota^h(i+\theta,j))^T S_1^h(i,j)\iota^h(i+\theta,j) - \sum_{\theta=1-\tau^h(i,j)}^{-1}(\iota^h(i+\theta,j))^T S_1^h(i,j)\iota^h(i+\theta,j), \tag{39}$$
$$\leq (\iota^h(i,j))^T S_1^h(i,j)\iota(i,j) - (\iota^h(i-\tau^h(i,j),j))^T S_1^h(i,j)\iota^h(i-\tau^h(i,j),j) + \sum_{\theta=1-\overline{\tau}}^{-\underline{\tau}}(\iota^h(i+\theta,j))^T S_1^h(i,j)\iota^h(i+\theta,j),$$

$$E\{\Delta V_3^h(i,j)\}$$

$$= E\left\{\left(\sum_{\theta=1-\bar{\tau}}^{-\underline{\tau}}\sum_{s=\theta}^{-1}\left(\iota^h(i+s+1,j)\right)^T S_1^h(i,j)\iota^h(i+s+1,j) - \sum_{\theta=1-\bar{\tau}}^{-\underline{\tau}}\sum_{s=\theta}^{-1}\left(\iota^h(i+s,j)\right)^T S_1^h(i,j)\iota^h(i+s,j)\right)|\partial(i,j)\right\}$$

$$= \sum_{\theta=1-\bar{\tau}}^{-\underline{\tau}}\left(\iota^h(i,j)\right)^T S_1^h(i,j)\iota^h(i,j) - \left(\iota^h(i+\theta,j)\right)^T S_1^h(i,j)\iota^h(i+\theta,j)$$

$$= \left(\bar{\tau}-\underline{\tau}\right)\left(\iota^h(i,j)\right)^T S_1^h(i,j)\iota(i,j) - \sum_{\theta=1-\bar{\tau}}^{-\underline{\tau}}\left(\iota^h(i+\theta,j)\right)^T S_1^h(i,j)\iota^h(i+\theta,j), \tag{40}$$

$$E\{\Delta V_4^h(i,j)\}$$

$$= E\left\{\left(\sum_{\theta=-\bar{\tau}}^{-1}\sum_{s=\theta}^{-1}\left(\iota^h(i+s+1,j)\right)^T S_2^h(i,j)\left(\iota^h(i+s+1,j)\right) - \sum_{\theta=-\underline{\tau}}^{-1}\sum_{s=\theta}^{-1}\left(\iota^h(i+s+1,j)\right)^T S_3^h(i,j)\left(\iota^h(i+s+1,j)\right)\right)\right.$$

$$\left. -\left(\sum_{\theta=-\bar{\tau}}^{-1}\sum_{s=\theta}^{-1}\left(\iota^h(i+s,j)\right)^T S_2^h(i,j)\left(\iota^h(i+s,j)\right) - \sum_{\theta=-\underline{\tau}}^{-1}\sum_{s=\theta}^{-1}\left(\iota^h(i+s,j)\right)^T S_3^h(i,j)\left(\iota^h(i+s,j)\right)\right)|\partial(i,j)\right\}$$

$$= \left(\iota^h(i,j)\right)^T\left(\bar{\tau}S_2^h(i,j) - \underline{\tau}S_3^h(i,j)\right)\iota^h(i,j) - \sum_{\theta=-\bar{\tau}}^{-1}\left(\iota^h(i+\theta,j)\right)^T S_2^h(i,j)\iota^h(i+\theta,j) + \sum_{\theta=-\underline{\tau}}^{-1}\left(\iota^h(i+\theta,j)\right)^T S_3^h(i,j)\iota^h(i+\theta,j)$$

$$\leq \left(\iota^h(i,j)\right)^T\left(\bar{\tau}S_2^h(i,j) - \underline{\tau}S_3^h(i,j)\right)\iota^h(i,j) - \sum_{\theta=-\bar{\tau}}^{-1}\left(\iota^h(i+\theta,j)\right)^T\left(S_2^h(i,j) - S_3^h(i,j)\right)\iota^h(i+\theta,j), \tag{41}$$

$$E\{\Delta V_1^v(i,j)\} = E\left\{(\iota^v(i,j+1))^T P^v(i,j)\iota^h(i,j+1) - (\iota^v(i,j))^T P^v(i,j)\iota^v(i,j)|\partial(i,j)\right\}, \tag{42}$$

$$E\{\Delta V_2^v(i,j)\}$$

$$= E\left\{\sum_{\theta=-\tau^v(i,j+1)}^{-1}(\iota^v(i,j+\theta+1))^T S_1^v(i,j)\iota^v(i,j+\theta+1) - \sum_{\theta=-\tau^v(i,j)}^{-1}(\iota^v(i,j+\theta))^T S_1^v(i,j)\iota^v(i,j+\theta)|\partial(i,j)\right\}$$

$$= (\iota^v(i,j))^T S_1^v(i,j)\iota^v(i,j) - (\iota^v(i,j-\tau^v(i,j)))^T S_1^v(i,j)\iota(i,j-\tau^v(i,j))$$

$$+ \sum_{\theta=1-\tau^v(i,j+1)}^{-1}(\iota^v(i,j+\theta))^T S_1^v(i,j)\iota^v(i,j+\theta) - \sum_{\theta=1-\tau^v(i,j)}^{-1}\iota^T(i,j+\theta)S_1^v(i,j)\iota(i,j+\theta)$$

$$\leq (\iota^v(i,j))^T S_1^v(i,j)\iota^v(i,j) - \left(\iota^v(i,j-\tau^v(i,j))^T S_1^v(i,j)\iota^v(i,j-\tau^v(i,j)) + \sum_{\theta=1-\bar{\tau}}^{-\underline{\tau}}(\iota^v(i,j+\theta))^T S_1^v(i,j)\iota^v(i,j+\theta)\right), \tag{43}$$

$$E\{\Delta V_3^v(i,j)\}$$

$$= E\left\{\sum_{\theta=1-\bar{\tau}}^{-\underline{\tau}}\sum_{s=\theta}^{-1}(\iota^v(i,j+s+1))^T S_1^v(i,j)\iota^v(i,j+s+1) - \sum_{\theta=1-\bar{\tau}}^{-\underline{\tau}}\sum_{s=\theta}^{-1}(\iota^v(i,j+s))^T S_1^v(i,j)\iota^v(i,j+s)\bigg|\partial(i,j)\right\}$$

$$= \sum_{\theta=1-\bar{\tau}}^{-\underline{\tau}}\left((\iota^v(i,j))^T S_1^v(i,j)\iota^v(i,j) - (\iota^v(i,j+\theta))^T S_1^v(i,j)\iota^v(i,j+\theta)\right)$$

$$= \left(\bar{\tau}-\underline{\tau}\right)(\iota^v(i,j))^T S_1^v(i,j)\iota^v(i,j) - \sum_{\theta=1-\bar{\tau}}^{-\underline{\tau}}(\iota^v(i,j+\theta))^T S_1^v(i,j)\iota^v(i,j+\theta), \tag{44}$$

$$E\{\Delta V_4^v(i,j)\}$$

$$
= \left\{ \sum_{\theta=-\overline{\tau}}^{-1} \sum_{s=\theta}^{-1} (\iota^v(i,j+s+1))^T S_2^v(i,j)(\iota^v(i,j+s+1)) - \sum_{\theta=-\underline{\tau}}^{-1} \sum_{s=\theta}^{-1} (\iota^v(i,j+s+1))^T S_3^v(i,j)(\iota^v(i,j+s+1)) \right.
$$

$$
\left. - \left(\sum_{\theta=-\overline{\tau}}^{-1} \sum_{s=\theta}^{-1} (\iota^v(i,j+s))^T S_2^v(i,j)(\iota^v(i,j+s)) - \sum_{\theta=-\underline{\tau}}^{-1} \sum_{s=\theta}^{-1} (\iota^v(i,j+s))^T S_3^v(i,j)(\iota^v(i,j+s)) \right) |\partial(i,j) \right\}
\tag{45}
$$

$$
= (\iota^v(i,j))^T \left(\overline{\tau} S_2^v(i,j) - \underline{\tau} S_3^v(i,j) \right) \iota^v(i,j) - \sum_{\theta=-\overline{\tau}}^{-1} (\iota^v(i+\theta,j))^T S_2^v(i,j) \iota^v(i+\theta,j) + \sum_{\theta=-\underline{\tau}}^{-1} (\iota^v(i+\theta,j))^T S_3^v(i,j) \iota^v(i+\theta,j)
$$

$$
\leq (\iota^v(i,j))^T \left(\overline{\tau} S_2^v(i,j) - \underline{\tau} S_3^v(i,j) \right) \iota^v(i,j) - \sum_{\theta=-\overline{\tau}}^{-1} (\iota^v(i+\theta,j))^T \left(S_2^v(i,j) - S_3^v(i,j) \right) \iota^v(i+\theta,j).
$$

Substituting (38)-(45) into (36), it is easy to obtain that

$$
J(i,j) = E\{V^+(i,j) - V(i,j)|\partial(i,j)\}
$$

$$
\leq E\left\{ \left(\iota^h(i+1,j) \right)^T P^h(i,j) \iota^h(i+1,j) - \left(\iota^h(i,j) \right)^T P^h(i,j) \iota^h(i,j) | \partial(i,j) \right\}
$$

$$
+ E\left\{ (\iota^v(i,j+1))^T P^v(i,j) \iota^h(i,j+1) - (\iota^v(i,j))^T P^v(i,j) \iota^v(i,j) | \partial(i,j) \right\}
$$

$$
+ \left(\iota^h(i,j) \right)^T \left(\left(1 + \overline{\tau} - \underline{\tau} \right) S_1^h(i,j) + \left(\overline{\tau} S_2^h(i,j) - \underline{\tau} S_3^h(i,j) \right) \right) \iota^h(i,j)
$$

$$
- \left(\iota^h\left(i - \tau^h(i,j),j \right) \right)^T S_1^h(i,j) \iota^h\left(i - \tau^h(i,j),j \right) - (\iota^v(i,j - \tau^v(i,j))^T S_1^v(i,j) \iota^v(i,j - \tau^v(i,j)) \tag{46}
$$

$$
+ (\iota^v(i,j))^T \left(\left(1 + \overline{\tau} - \underline{\tau} \right) S_1^v(i,j) + \left(\overline{\tau} S_2^v(i,j) - \underline{\tau} S_3^v(i,j) \right) \right) \iota^v(i,j)
$$

$$
- \sum_{\theta=-\overline{\tau}}^{-1} (\iota^v(i,j+\theta))^T \left(S_2^v(i,j) - S_3^v(i,j) \right) \iota^v(i,j+\theta) - \sum_{\theta=-\overline{\tau}}^{-1} \left(\iota^h(i+\theta,j) \right)^T \left(S_2^h(i,j) - S_3^h(i,j) \right) \iota^h(i+\theta,j)
$$

$$
= (\iota(i,j))^T P(i,j) \iota(i,j) + \iota^T(i,j)(\overline{S}(i,j) - P(i,j)) \iota(i,j)
$$

$$
- \iota_\tau^T(i,j) S_1(i,j) \iota_\tau(i,j) - \sum_{\theta=-\overline{\tau}}^{-1} (\iota_\theta(i,j))^T (S_2(i,j) - S_3(i,j)) \iota_\theta(i,j),
$$

where $\overline{S}(i,j) = \left(1 + \overline{\tau} - \underline{\tau} \right) S_1(i,j) + \left(\overline{\tau} S_2(i,j) - \underline{\tau} S_3(i,j) \right)$, $\iota_\theta(i,j) = \begin{bmatrix} \iota^h(i+\theta,j) \\ \iota^v(i,j+\theta) \end{bmatrix}$.

Next, we will further consider the impact of event-triggered scheduling mechanism, hybrid cyber-attacks and nonlinear functions on the filtering performance.

For $(i_k,j_k) \leq (i,j) < (i_{k+1},j_{k+1})$, recalling the event-triggered transmission rule (7), one has

$$
\sigma \mathscr{Y}^T(i,j) \Phi_{(i,j)} \mathscr{Y}(i,j) - r^T(i,j) \Phi_{(i,j)} r(i,j) \geq 0. \tag{47}
$$

Reconstruct the nonlinear function constraints (5) and (6), which could be further written as:

$$
(\overline{g}(\iota(i,j)))^T (\overline{g}(\iota(i,j)) - \widetilde{\mathscr{F}} \iota(i,j)) \leq 0, \tag{48}
$$

where $\widetilde{\mathscr{F}} = \Omega^T \widehat{M} \Omega$, $\widehat{M} = diag\{G^h, G^v, G^h, G^v\}$.

Subsequently, according to the norm-bounded condition $\| v(i,j) \| \leq \overline{v}$ of FDI attacks, one has

$$
v^T(i,j) v(i,j) - \overline{v}^2 I \leq 0, \tag{49}
$$

Substituting (13), (47), (48) and (49) into (46), we can further infer the following relationship holds if there exist positive scalars $\gamma_1(i,j)$ and $\gamma_2(i,j)$:

$$
\begin{aligned}
J(i,j) \leq & E\big\{(\iota(i,j))^T P(i,j)\iota(i,j) + \iota^T(i,j)(\overline{S}(i,j) - P(i,j))\iota(i,j) - \iota_\tau^T(i,j)S_1(i,j)\iota_\tau(i,j) \\
& - \sum_{\theta=-\overline{\tau}}^{-1} (\iota_\theta(i,j))^T (S_2(i,j) - S_3(i,j))\iota_\theta(i,j)\big\} - \gamma_1(i,j)\boldsymbol{r}^T(i,j)\Phi_{(i,j)}\boldsymbol{r}(i,j) - 2\big((\overline{\boldsymbol{g}}(\iota(i,j)))^T(\overline{\boldsymbol{g}}(\iota(i,j)) - \widetilde{\mathscr{F}}\iota(i,j))\big) \\
& + \gamma_2(i,j)\big(\overline{\boldsymbol{v}}^2 I - \boldsymbol{v}^T(i,j)\boldsymbol{v}(i,j)\big) + \sigma\gamma_1(\widetilde{C}(i,j)\iota(i,j) + D(i,j)\boldsymbol{\omega}(i,j))^T\Phi_{(i,j)}(\widetilde{C}(i,j)\iota(i,j) + D(i,j)\boldsymbol{\omega}(i,j)) \\
\leq & \, \iota^T(i,j)\big(\big(\widehat{\mathscr{A}}_1(i,j) + \widetilde{B}(i,j)\widetilde{M}\big)^T P(i,j)\big(\widehat{\mathscr{A}}_1(i,j) + \widetilde{B}(i,j)\widetilde{M}\big) + \sigma\gamma_1(i,j)\widetilde{C}^T(i,j)\Phi_{(i,j)}\widetilde{C}(i,j) \\
& + \overline{\varsigma}_1^2 \breve{\mathscr{A}}_1^T(i,j)P(i,j)\breve{\mathscr{A}}_1(i,j)\big)\iota(i,j) + \iota^T(i,j)(\overline{S}(i,j) - P(i,j))\iota(i,j) \\
& + \iota^T(i,j)\big(\widehat{\mathscr{A}}_1(i,j) + \widetilde{B}(i,j)\widetilde{M}\big)^T P(i,j)\widetilde{A}_2(i,j)\iota_\tau(i,j) \\
& + \iota^T(i,j)\big(\big(\widehat{\mathscr{A}}_1(i,j) + \widetilde{B}(i,j)\widetilde{M}\big)^T P(i,j)\widetilde{B}(i,j) + \widetilde{\mathscr{F}}^T\big)\overline{\boldsymbol{g}}(\iota(i,j)) \\
& + \iota^T(i,j)\big(\big(\widehat{\mathscr{A}}_1(i,j) + \widetilde{B}(i,j)\widetilde{M}\big)^T P(i,j)\widehat{\mathscr{O}}(i,j) + \overline{\varsigma}_{12}^2 \breve{\mathscr{A}}_1^T(i,j)P(i,j)\breve{\mathscr{O}}(i,j)\big)\boldsymbol{v}(i,j) \\
& + \iota^T(i,j)\big(\big(\widehat{\mathscr{A}}_1(i,j) + \widetilde{B}(i,j)\widetilde{M}\big)^T P(i,j)\widehat{\mathscr{R}}(i,j) + \overline{\varsigma}_1^2 \breve{\mathscr{A}}_1^T(i,j)P(i,j)\breve{\mathscr{R}}(i,j)\big)\boldsymbol{r}(i,j) \\
& + \iota_\tau^T(i,j)\big(\widetilde{A}_2^T(i,j)P(i,j)\widetilde{A}_2(i,j) - S_1(i,j)\big)\iota_\tau(i,j) + \iota_\tau^T(i,j)\widetilde{A}_2^T(i,j)P(i,j)\widetilde{B}(i,j)\overline{\boldsymbol{g}}(\iota(i,j)) \\
& + \iota_\tau^T(i,j)\widetilde{A}_2^T(i,j)P(i,j)\widehat{\mathscr{O}}(i,j)\boldsymbol{v}(i,j) + \iota_\tau^T(i,j)\widetilde{A}_2^T(i,j)P(i,j)\widehat{\mathscr{R}}(i,j)\boldsymbol{r}(i,j) \\
& + \overline{\boldsymbol{g}}^T(\iota(i,j))\big(\widetilde{B}^T(i,j)P(i,j)\widetilde{B}(i,j) - 2I\big)\overline{\boldsymbol{g}}(\iota(i,j)) + \overline{\boldsymbol{g}}^T(\iota(i,j))\widetilde{B}^T(i,j)P(i,j)\widehat{\mathscr{R}}(i,j)\boldsymbol{r}(i,j) \\
& + \overline{\boldsymbol{g}}^T(\iota(i,j))\widetilde{B}^T(i,j)P(i,j)\widehat{\mathscr{O}}(i,j)\boldsymbol{v}(i,j) + \boldsymbol{r}^T(i,j)\big(\widehat{\mathscr{R}}^T(i,j)P(i,j)\widehat{\mathscr{R}}(i,j) \\
& + \overline{\varsigma}_1^2 \breve{\mathscr{R}}^T(i,j)P(i,j)\breve{\mathscr{R}}(i,j) - \Phi_{(i,j)}\big)\boldsymbol{r}(i,j) + \boldsymbol{r}^T(i,j)\big(\widehat{\mathscr{R}}^T(i,j)P(i,j)\widehat{\mathscr{O}}(i,j) + \overline{\varsigma}_{12}^2 \breve{\mathscr{R}}^T(i,j)P(i,j)\breve{\mathscr{O}}(i,j)\big)\boldsymbol{v}(i,j) \\
& + \boldsymbol{v}^T(i,j)\big(\widehat{\mathscr{O}}^T(i,j)P(i,j)\widehat{\mathscr{O}}(i,j) + \overline{\varsigma}_2^2 \breve{\mathscr{O}}^T(i,j)P(i,j)\breve{\mathscr{O}}(i,j)\big)\boldsymbol{v}(i,j) - \gamma_2(i,j)\boldsymbol{v}^T(i,j)\boldsymbol{v}(i,j) \\
& + tr\big\{\mathscr{W}^T\big(\widehat{\mathscr{E}}^T(i,j)P(i,j)\widehat{\mathscr{E}}(i,j) + \overline{\varsigma}_1^2 \breve{\mathscr{E}}^T(i,j)P(i,j)\breve{\mathscr{E}}(i,j) + \sigma\gamma_1(i,j)D^T(i,j)\Phi_{(i,j)}D(i,j)\big)\mathscr{W}\big\} + \gamma_2(i,j)\overline{\boldsymbol{v}}^2 \\
& + \Big[\iota^T(i,j)\big(\widehat{\mathscr{A}}_1(i,j) + \widetilde{B}(i,j)\widetilde{M}\big)^T P(i,j)\widetilde{A}_2(i,j)\iota_\tau(i,j) \\
& + \iota^T(i,j)\big(\big(\widehat{\mathscr{A}}_1(i,j) + \widetilde{B}(i,j)\widetilde{M}\big)^T P(i,j)\widetilde{B}(i,j) + \widetilde{\mathscr{F}}^T\big)\overline{\boldsymbol{g}}(\iota(i,j)) \\
& + \iota^T(i,j)\big(\big(\widehat{\mathscr{A}}_1(i,j) + \widetilde{B}(i,j)\widetilde{M}\big)^T P(i,j)\widehat{\mathscr{O}}(i,j) + \overline{\varsigma}_{12}^2 \breve{\mathscr{A}}_1^T(i,j)P(i,j)\breve{\mathscr{O}}(i,j)\big)\boldsymbol{v}(i,j) \\
& + \iota^T(i,j)\big(\big(\widehat{\mathscr{A}}_1(i,j) + \widetilde{B}(i,j)\widetilde{M}\big)^T P(i,j)\widehat{\mathscr{R}}(i,j) + \overline{\varsigma}_1^2 \breve{\mathscr{A}}_1^T(i,j)P(i,j)\breve{\mathscr{R}}(i,j)\big)\boldsymbol{r}(i,j) \\
& + \iota_\tau^T(i,j)\widetilde{A}_2^T(i,j)P(i,j)\widetilde{B}(i,j)\overline{\boldsymbol{g}}(\iota(i,j))\big) + \iota_\tau^T(i,j)\widetilde{A}_2^T(i,j)P(i,j)\widehat{\mathscr{F}}(i,j)\boldsymbol{v}(i,j) \\
& + \iota_\tau^T(i,j)\widetilde{A}_2^T(i,j)P(i,j)\widehat{\mathscr{R}}(i,j)\boldsymbol{r}(i,j) + \overline{\boldsymbol{g}}^T(\iota(i,j))\widetilde{B}^T(i,j)P(i,j)\widehat{\mathscr{R}}(i,j)\boldsymbol{r}(i,j) \\
& + \overline{\boldsymbol{g}}^T(\iota(i,j))\widetilde{B}^T(i,j)P(i,j)\widehat{\mathscr{O}}(i,j)\boldsymbol{v}(i,j) + \boldsymbol{r}^T(i,j)\big(\widehat{\mathscr{R}}^T(i,j)P(i,j)\widehat{\mathscr{O}}(i,j) \\
& + \overline{\varsigma}_{12}^2 \breve{\mathscr{R}}^T(i,j)P(i,j)\breve{\mathscr{O}}(i,j)\big)\boldsymbol{v}(i,j)\Big]^T - \sum_{\theta=-\overline{\tau}}^{-1}(\iota_\theta(i,j))^T(S_2(i,j) - S_3(i,j))\iota_\theta(i,j).
\end{aligned}
\tag{50}
$$

Then, in virtue of the elementary inequality $a^T b + b^T a \leq a^T a + b^T b$, it is obtained that

$$
\begin{aligned}
& \overline{\varsigma}_{12}^2 \iota^T(i,j)\breve{\mathscr{A}}_1^T(i,j)P(i,j)\breve{\mathscr{O}}(i,j)\boldsymbol{v}(i,j) + \overline{\varsigma}_{12}^2 \boldsymbol{v}^T(i,j)\breve{\mathscr{O}}^T(i,j)P(i,j)\breve{\mathscr{A}}_1(i,j)\iota(i,j) \\
& \quad \leq \overline{\varsigma}_{12}^2 \iota^T(i,j)\breve{\mathscr{A}}_1^T(i,j)P(i,j)\breve{\mathscr{A}}_1(i,j)\iota(i,j) + \overline{\varsigma}_{12}^2 \boldsymbol{v}^T(i,j)\breve{\mathscr{O}}^T(i,j)P(i,j)\breve{\mathscr{O}}(i,j)\boldsymbol{v}(i,j)
\end{aligned}
\tag{51.a}
$$

$$
\begin{aligned}
& \overline{\varsigma}_{12}^2 \boldsymbol{r}^T(i,j)\breve{\mathscr{R}}^T(i,j)P(i,j)\breve{\mathscr{O}}(i,j)\boldsymbol{v}(i,j) + \overline{\varsigma}_{12}^2 \boldsymbol{v}^T(i,j)\breve{\mathscr{O}}^T(i,j)P(i,j)\breve{\mathscr{R}}(i,j)\boldsymbol{r}(i,j) \\
& \quad \leq \overline{\varsigma}_{12}^2 \boldsymbol{r}^T(i,j)\breve{\mathscr{R}}^T(i,j)P(i,j)\breve{\mathscr{R}}(i,j)\boldsymbol{r}(i,j) + \overline{\varsigma}_{12}^2 v^T(i,j)\breve{\mathscr{O}}^T(i,j)P(i,j)\breve{\mathscr{O}}(i,j)\boldsymbol{v}(i,j)
\end{aligned}
\tag{51.b}
$$

From (50) and (51), it is easy to derive the following inequality:

$$
\begin{aligned}
J(i,j) \le{}& \chi^T(i,j)\Xi\chi(i,j) - \sum_{\theta=-\bar{\tau}}^{-1}(\iota_\theta(i,j))^T(S_2(i,j)-S_3(i,j))\iota_\theta(i,j) \\
&+tr\Big\{\mathscr{W}^T\Big(\widehat{\mathscr{E}}^{\,T}(i,j)P(i,j)\widehat{\mathscr{E}}(i,j)+\bar{\varsigma}_1^2\breve{\mathscr{E}}^{\,T}(i,j)P(i,j)\breve{\mathscr{E}}(i,j)+\boldsymbol{\sigma}\gamma_1(i,j)D^T(i,j)\Phi_{(i,j)}D(i,j)\Big)\Big)\mathscr{W}\Big\}+\gamma_2(i,j)\overline{\boldsymbol{v}}^2
\end{aligned}
\tag{52}
$$

where

$$
\chi(i,j)=\begin{bmatrix}\iota^T(i,j)&\iota_\tau^T(i,j)&\bar{\boldsymbol{g}}^T(\iota(i,j))&\boldsymbol{r}^T(i,j)&\boldsymbol{v}^T(i,j)\end{bmatrix}^T,\Xi=\begin{bmatrix}\Xi_{11}&\Xi_{12}&\Xi_{13}&\Xi_{14}&\Xi_{15}\\ *&\Xi_{22}&\Xi_{23}&\Xi_{24}&\Xi_{25}\\ *&*&\Xi_{33}&\Xi_{34}&\Xi_{35}\\ *&*&*&\Xi_{44}&\Xi_{45}\\ *&*&*&*&\Xi_{55}\end{bmatrix},
$$

$$
\begin{aligned}
\Xi_{11}={}&\Big(\widehat{\mathscr{A}}_1(i,j)+\widetilde{B}(i,j)\widetilde{M}\Big)^T P(i,j)\Big(\widehat{\mathscr{A}}_1(i,j)+\widetilde{B}(i,j)\widetilde{M}\Big)+\sigma\gamma_1(i,j)\widetilde{C}^T(i,j)\Phi_{(i,j)}\widetilde{C}(i,j)\\
&+\overline{S}(i,j)-P(i,j)+\big(\bar{\varsigma}_1^2+\bar{\varsigma}_{12}^2\big)\breve{\mathscr{A}}_1^T(i,j)P(i,j)\breve{\mathscr{A}}_1(i,j),
\end{aligned}
$$

$$
\Xi_{22}=\widetilde{A}_2^T(i,j)P(i,j)\widetilde{A}_2(i,j)-S_1(i,j),\Xi_{33}=\widetilde{B}^T(i,j)P(i,j)\widetilde{B}(i,j)-2I_{2n_x+2n_v},
$$

$$
\Xi_{44}=\widehat{\mathscr{R}}^{\,T}(i,j)P(i,j)\widehat{\mathscr{R}}(i,j)+\big(\bar{\varsigma}_1^2+\bar{\varsigma}_{12}^2\big)\breve{\mathscr{R}}^{\,T}(i,j)P(i,j)\breve{\mathscr{R}}(i,j)-\gamma_1(i,j)\Phi_{(i,j)},
$$

$$
\Xi_{55}=\widehat{\mathscr{O}}^{\,T}(i,j)P(i,j)\widehat{\mathscr{O}}(i,j)+\big(\bar{\varsigma}_2^2+2\bar{\varsigma}_{12}^2\big)\breve{\mathscr{O}}^{\,T}(i,j)P(i,j)\breve{\mathscr{O}}(i,j)-\gamma_2(i,j)I_{n_y},
$$

$$
\Xi_{12}=\Big(\widehat{\mathscr{A}}_1(i,j)+\widetilde{B}(i,j)\widetilde{M}\Big)^T P(i,j)\widetilde{A}_2(i,j),\Xi_{13}=\Big(\widehat{\mathscr{A}}_1(i,j)+\widetilde{B}(i,j)\widetilde{M}\Big)^T P(i,j)\widetilde{B}(i,j)+\widetilde{\mathscr{F}}^T,
$$

$$
\Xi_{14}=\Big(\widehat{\mathscr{A}}_1(i,j)+\widetilde{B}(i,j)\widetilde{M}\Big)^T P(i,j)\widehat{\mathscr{R}}(i,j)+\bar{\varsigma}_1^2\breve{\mathscr{A}}_1^T(i,j)P(i,j)\breve{\mathscr{R}}(i,j),\Xi_{15}=\Big(\widehat{\mathscr{A}}_1(i,j)+\widetilde{B}(i,j)\widetilde{M}\Big)^T P(i,j)\widehat{\mathscr{O}}(i,j),\cdot
$$

$$
\Xi_{23}=\widetilde{A}_2^T(i,j)P(i,j)\widetilde{B}(i,j),\Xi_{24}=\widetilde{A}_2^T(i,j)P(i,j)\widehat{\mathscr{R}}(i,j),\Xi_{25}=\widetilde{A}_2^T(i,j)P(i,j)\widehat{\mathscr{O}}(i,j),\Xi_{34}=\widetilde{B}^T(i,j)P(i,j)\widehat{\mathscr{R}}(i,j),
$$

$$
\Xi_{35}=\widetilde{B}^T(i,j)P(i,j)\widehat{\mathscr{O}}(i,j),\Xi_{45}=\widehat{\mathscr{R}}^{\,T}(i,j)P(i,j)\widehat{\mathscr{O}}(i,j).
$$

Then, we perform an equivalent transformation for (52). If there exist a scalar $\rho>0$, from (52) it is straightforward to verify that the following inequality holds:

$$
\begin{aligned}
J(i,j) &\le\chi^T(i,j)\Xi\chi(i,j)+\frac{1}{\rho}V_1(i,j)-\frac{1}{\rho}V_1(i,j)-\sum_{\theta=-\bar{\tau}}^{-1}(\iota_\theta(i,j))^T(S_2(i,j)-S_3(i,j))\iota_\theta(i,j)+\delta(i,j)\\
&=\chi^T(i,j)\widehat{\Xi}\chi(i,j)-\frac{1}{\rho}V_1(i,j)-\sum_{\theta=-\bar{\tau}}^{-1}(\iota_\theta(i,j))^T(S_2(i,j)-S_3(i,j))\iota_\theta(i,j)+\delta(i,j),
\end{aligned}
\tag{53}
$$

where

$$
\widehat{\Xi}=\begin{bmatrix}\widehat{\Xi}_{11}&\widehat{\Xi}_{12}&\widehat{\Xi}_{13}&\widehat{\Xi}_{14}&\widehat{\Xi}_{15}\\ *&\widehat{\Xi}_{22}&\widehat{\Xi}_{23}&\widehat{\Xi}_{24}&\widehat{\Xi}_{25}\\ *&*&\widehat{\Xi}_{33}&\widehat{\Xi}_{34}&\widehat{\Xi}_{35}\\ *&*&*&\widehat{\Xi}_{44}&\widehat{\Xi}_{45}\\ *&*&*&*&\widehat{\Xi}_{55}\end{bmatrix},
$$

$$
\begin{aligned}
\widehat{\Xi}_{11}={}&\Big(\widehat{\mathscr{A}}_1(i,j)+\widetilde{B}(i,j)\widetilde{M}\Big)^T P(i,j)\Big(\widehat{\mathscr{A}}_1(i,j)+\widetilde{B}(i,j)\widetilde{M}\Big)+\overline{S}(i,j)-\Big(1-\frac{1}{\rho}\Big)P(i,j)\\
&+\sigma\gamma_1(i,j)\widetilde{C}^T(i,j)\Phi_{(i,j)}\widetilde{C}(i,j)+\big(\bar{\varsigma}_1^2+\bar{\varsigma}_{12}^2\big)\breve{\mathscr{A}}_1^T(i,j)P(i,j)\breve{\mathscr{A}}_1(i,j)
\end{aligned}
$$

$$
\widehat{\Xi}_{12}=\Big(\widehat{\mathscr{A}}_1(i,j)+\widetilde{B}(i,j)\widetilde{M}\Big)^T P(i,j)\widetilde{A}_2(i,j),\widehat{\Xi}_{13}=\Big(\widehat{\mathscr{A}}_1(i,j)+\widetilde{B}(i,j)\widetilde{M}\Big)^T P(i,j)\widetilde{B}(i,j)+\widetilde{\mathscr{F}}^T,
$$

$$
\widehat{\Xi}_{14}=\Big(\widehat{\mathscr{A}}_1(i,j)+\widetilde{B}(i,j)\widetilde{M}\Big)^T P(i,j)\widehat{\mathscr{R}}(i,j)+\bar{\varsigma}_1^2\breve{\mathscr{A}}_1^T(i,j)P(i,j)\breve{\mathscr{R}}(i,j),\widehat{\Xi}_{15}=\Big(\widehat{\mathscr{A}}_1(i,j)+\widetilde{B}(i,j)\widetilde{M}\Big)^T P(i,j)\widehat{\mathscr{O}}(i,j),
$$

$$\widehat{\Xi}_{22} = \widetilde{A}_2^T(i,j)P(i,j)\widetilde{A}_2(i,j) - S_1(i,j), \widehat{\Xi}_{23} = \widetilde{A}_2^T(i,j)P(i,j)\widetilde{B}(i,j), \widehat{\Xi}_{24} = \widetilde{A}_2^T(i,j)P(i,j)\widehat{\mathscr{R}}(i,j),$$

$$\widehat{\Xi}_{25} = \widetilde{A}_2^T(i,j)P(i,j)\widehat{\mathscr{O}}(i,j), \widehat{\Xi}_{33} = \widetilde{B}^T(i,j)P(i,j)\widetilde{B}(i,j) - I_{2n_h+2n_v}, \widehat{\Xi}_{34} = \widetilde{B}^T(i,j)P(i,j)\widehat{\mathscr{R}}(i,j),$$

$$\widehat{\Xi}_{35} = \widetilde{B}^T(i,j)P(i,j)\widehat{\mathscr{O}}(i,j), \widehat{\Xi}_{44} = \widehat{\mathscr{R}}^T(i,j)P(i,j)\widehat{\mathscr{R}}(i,j) + \left(\overline{\varsigma}_1^2 + \overline{\varsigma}_{12}^2\right)\widecheck{\mathscr{R}}^T(i,j)P(i,j)\widecheck{\mathscr{R}}(i,j) - \gamma_1(i,j)\Phi_{(i,j)},$$

$$\widehat{\Xi}_{45} = \widehat{\mathscr{R}}^T(i,j)P(i,j)\widehat{\mathscr{O}}(i,j), \widehat{\Xi}_{55} = \widehat{\mathscr{O}}^T(i,j)P(i,j)\widehat{\mathscr{O}}(i,j) + \left(\overline{\varsigma}_2^2 + 2\overline{\varsigma}_{12}^2\right)\widecheck{\mathscr{O}}^T(i,j)P(i,j)\widecheck{\mathscr{O}}(i,j) - \gamma_2(i,j)I_{n_y},$$

$$\delta(i,j) = tr\left\{ \mathscr{W}^T\left(\widetilde{\mathscr{E}}^T(i,j)P(i,j)\widehat{\mathscr{E}}(i,j) + \overline{\varsigma}_1^2\widetilde{\mathscr{E}}^T(i,j)P(i,j)\widecheck{\mathscr{E}}(i,j) + \boldsymbol{\sigma}\gamma_1(i,j)D^T(i,j)\Phi_{(i,j)}D(i,j)\right)\mathscr{W}\right\} + \gamma_2(i,j)\overline{\boldsymbol{v}}^2.$$

Additionally, if $\widehat{\Xi} < 0$, we apply the Schur complement lemma for (53), which yields

$$J(i,j) \leq \chi^T(i,j)\widetilde{\Xi}\chi(i,j) - \frac{1}{\rho}V_1(i,j) - \sum_{\theta=-\overline{\tau}}^{-1}(\iota_\theta(i,j))^T(S_2(i,j) - S_3(i,j))\iota_\theta(i,j) + \delta(i,j), \tag{54}$$

where

$$\widetilde{\Xi} = \begin{bmatrix} \widetilde{\Xi}_{11} & \widetilde{\Xi}_{12} \\ * & \widetilde{\Xi}_{22} \end{bmatrix}, \widetilde{\Xi}_{11} = \begin{bmatrix} \overrightarrow{S}(i,j) & 0 & \widetilde{\mathscr{F}}^T & 0 & 0 \\ * & -S_1(i,j) & 0 & 0 & 0 \\ * & * & -2I_{2n_x+2n_v} & 0 & 0 \\ * & * & * & -\gamma_1(i,j)\Phi_{(i,j)} & 0 \\ * & * & * & * & -\gamma_2(i,j)I_{n_y} \end{bmatrix},$$

$$\overrightarrow{S}(i,j) = S(i,j) - \left(1 - \frac{1}{\rho}\right)P(i,j) + \sigma\gamma_1(i,j)\widetilde{C}^T(i,j)\Phi_{(i,j)}\widetilde{C}(i,j)$$

$$\widetilde{\Xi}_{12} = \begin{bmatrix} \left(\widehat{\mathscr{A}}_1(i,j) + \widetilde{B}(i,j)\widetilde{M}\right)^T & \overline{\varsigma}_1\widecheck{\mathscr{A}}_1^T(i,j) & \overline{\varsigma}_{12}\widecheck{\mathscr{A}}_1^T(i,j) & 0 & 0 \\ \widetilde{A}_2^T(i,j) & 0 & 0 & 0 & 0 \\ \widetilde{B}^T(i,j) & 0 & 0 & 0 & 0 \\ \widehat{\mathscr{R}}(i,j) & \overline{\varsigma}_1\widecheck{\mathscr{R}}^T(i,j) & 0 & \overline{\varsigma}_{12}\widecheck{\mathscr{R}}^T(i,j) & 0 \\ \widehat{\mathscr{O}}^T(i,j) & 0 & 0 & 0 & \sqrt{(\overline{\varsigma}_2^2 + 2\overline{\varsigma}_{12}^2)}\widecheck{\mathscr{O}}^T(i,j) \end{bmatrix}, \widetilde{\Xi}_{22} = I_5 \otimes -P^{-1}(i,j).$$

Furthermore, it follows from (36) that

$$V_2^h(i,j) = \sum_{\theta=-\tau^h(i,j)}^{-1}\left(\iota^h(i+\theta,j)\right)^T S_1^h(i,j)(\iota(i+\theta,j)) \leq \sum_{\theta=-\overline{\tau}}^{-1}\left(\iota^h(i+\theta,j)\right)^T S_1^h(i,j)(\iota(i+\theta,j)), \tag{55}$$

$$V_3^h(i,j) = \sum_{\theta=1-\overline{\tau}}^{-\underline{\tau}}\sum_{s=\theta}^{-1}\left(\iota^h(i+s,j)\right)^T S_1^h(i,j)(\iota^h(i+s,j)) \leq \sum_{\theta=-\overline{\tau}}^{-1}\sum_{s=\theta}^{-1}\left(\iota^h(i+s,j)\right)^T S_1^h(i,j)\iota^h(i+s,j)$$

$$\leq \overline{\tau}\sum_{s=-\overline{\tau}}^{-1}\left(\iota^h(i+s,j)\right)^T S_1^h(i,j)\iota^h(i+s,j), \tag{56}$$

$$V_4^h(i,j) = \sum_{\theta=-\overline{\tau}}^{-1}\sum_{s=\theta}^{-1}\left(\iota^h(i+s,j)\right)^T S_2^h(i,j)\left(\iota^h(i+s,j)\right) - \sum_{\theta=-\underline{\tau}}^{-1}\sum_{s=\theta}^{-1}\left(\iota^h(i+s,j)\right)^T S_3^h(i,j)\left(\iota^h(i+s,j)\right)$$

$$= \sum_{\theta=-\overline{\tau}}^{-1}\sum_{s=\theta}^{-1}\left(\iota^h(i+s,j)\right)^T\left(S_2^h(i,j) - S_3^h(i,j)\right)\iota^h(i+s,j) + \sum_{\theta=-\overline{\tau}}^{-\underline{\tau}-1}\sum_{s=\theta}^{-1}\left(\iota^h(i+s,j)\right)^T S_3^h(i,j)\iota(i+s,j)$$

$$\leq \overline{\tau}\sum_{s=-\overline{\tau}}^{-1}\left(\iota^h(i+s,j)\right)^T\left(S_2^h(i,j) - S_3^h(i,j)\right)\iota^h(i+s,j) + \left(\overline{\tau} - \underline{\tau}\right)\sum_{s=-\overline{\tau}}^{-1}\left(\iota^h(i+s,j)\right)^T S_3^h(i,j)\iota^h(i+s,j)$$

$$= \sum_{s=-\overline{\tau}}^{-1}\left(\iota^h(i+s,j)\right)^T\left(\overline{\tau}S_2^h(i,j) - \underline{\tau}S_3^h(i,j)\right)\iota^h(i+s,j), \tag{57}$$

$$V_2^v(i,j) = \sum_{\theta=-\tau^v(i,j)}^{-1}(\iota^v(i,j+\theta))^T S_1^v(i,j)(\iota^v(i,j+\theta)) \leq \sum_{\theta=-\overline{\tau}}^{-1}(\iota^v(i,j+\theta))^T S_1^v(i,j)(\iota^v(i,j+\theta)), \tag{58}$$

$$V_3^v(i,j) = \sum_{\theta=1-\overline{\tau}}^{-\overline{\tau}} \sum_{s=\theta}^{-1} (\iota^v(i,j+s))^T S_1^v(i,j)\iota^v(i,j+s) \leq \sum_{\theta=-\overline{\tau}}^{-1} \sum_{s=\theta}^{-1} (\iota^v(i,j+s))^T S_1^v(i,j)\iota^v(i,j+s)$$

$$\leq \overline{\tau} \sum_{s=-\overline{\tau}}^{-1} (\iota^v(i,j+s))^T S_1^v(i,j)\iota^v(i,j+s), \tag{59}$$

$$V_4^v(i,j) = \sum_{\theta=-\overline{\tau}}^{-1} \sum_{s=\theta}^{-1} (\iota^v(i,j+s))^T S_2^v(i,j)\iota^v(i,j+s) - \sum_{\theta=-\underline{\tau}}^{-1} \sum_{s=\theta}^{-1} (\iota^v(i,j+s))^T S_3^v(i,j)\iota^v(i,j+s)$$

$$V_4^v(i,j) = \sum_{\theta=-\overline{\tau}}^{-1} \sum_{s=\theta}^{-1} (\iota^v(i,j+s))^T S_2^v(i,j)\iota^v(i,j+s) - \sum_{\theta=-\underline{\tau}}^{-1} \sum_{s=\theta}^{-1} (\iota^v(i,j+s))^T S_3^v(i,j)\iota^v(i,j+s)$$

$$= \sum_{\theta=-\overline{\tau}}^{-1} \sum_{s=\theta}^{-1} (\iota^v(i,j+s))^T \left(S_2^v(i,j) - S_3^v(i,j)\right)\iota^v(i,j+s) + \sum_{\theta=-\overline{\tau}}^{-\underline{\tau}-1} \sum_{s=\theta}^{-1} (\iota^v(i,j+s))^T S_3^v(i,j)\iota^v(i,j+s)$$

$$\leq \overline{\tau} \sum_{s=-\overline{\tau}}^{-1} (\iota^v(i,j+s))^T \left(S_2^v(i,j) - S_3^v(i,j)\right)\iota^v(i,j+s) + \left(\overline{\tau} - \underline{\tau}\right) \sum_{s=-\overline{\tau}}^{-1} (\iota^v(i,j+s))^T S_3^v(i,j)\iota^v(i,j+s) \tag{60}$$

$$= \sum_{s=-\overline{\tau}}^{-1} (\iota^v(i,j+s))^T \left(\overline{\tau} S_2^v(i,j) - \underline{\tau} S_3^v(i,j)\right)\iota^v(i,j+s).$$

Therefore, by considering (36.a) and (55)-(60) comprehensively, it can be further deduced that

$$\frac{1}{\rho}V(i,j) \leq \frac{1}{\rho}\Big\{ (\iota^h(i,j))^T P^h(i,j)\iota^h(i,j) + (\iota^v(i,j))^T P^v(i,j)\iota^v(i,j)$$

$$+ \sum_{s=-\overline{\tau}}^{-1} (\iota^h(i+s,j))^T \left((1+\overline{\tau})S_1^h(i,j) + \overline{\tau}S_2^h(i,j) - \underline{\tau}S_3^h(i,j)\right)\iota^h(i+s,j)$$

$$+ \sum_{s=-\overline{\tau}}^{-1} (\iota^v(i,j+s))^T \left((1+\overline{\tau})S_1^v(i,j) + \overline{\tau}S_2^v(i,j) - \underline{\tau}S_3^v(i,j)\right)\iota^v(i,j+s) \Big\} \tag{61}$$

$$= \frac{1}{\rho}\Big\{ \iota^T(i,j)P(i,j)\iota(i,j) + \sum_{\theta=-\overline{\tau}}^{-1} (\iota_\theta(i,j))^T \widetilde{S}(i,j)\iota_\theta(i,j) \Big\},$$

where $\widetilde{S}(i,j) = (1+\overline{\tau})S_1(i,j) + \overline{\tau}S_2(i,j) - \underline{\tau}S_3(i,j)$. Then, we combine (16), (54) with (61), which implies

$$\Delta V(i,j) \leq \chi^T(i,j)\widetilde{\Xi}\chi(i,j) - \frac{1}{\rho}V_1(i,j) - \sum_{\theta=-\overline{\tau}}^{-1} (\iota_\theta(i,j))^T (S_2(i,j) - S_3(i,j))\iota_\theta(i,j) + \delta(i,j)$$

$$\leq \chi^T(i,j)\widetilde{\Xi}\chi(i,j) - \frac{1}{\rho}V_1(i,j) - \frac{1}{\rho}\sum_{\theta=-\overline{\tau}}^{-1} (\iota_\theta(i,j))^T \widetilde{S}\iota_\theta(i,j) + \delta(i,j) \tag{62}$$

$$\leq \chi^T(i,j)\widetilde{\Xi}\chi(i,j) - \frac{1}{\rho}V(i,j) + \delta(i,j) \leq -\frac{1}{\rho}V(i,j) + \delta(i,j).$$

Subsequently, for arbitrary positive scalar $b > 1$, it is obtained from (62) that

$$E\{b^{k+1}V^+(i,j)|\partial(i,j)\} - E\{b^k(V(i,j)|\partial(i,j)\} = E\{b^{k+1}(V^+(i,j) - V(i,j))|\partial(i,j)\} + b^k(b-1)E\{V(i,j)|\partial(i,j)\}$$

$$= b^{k+1}E\{\Delta V(i,j)|\partial(i,j)\} + b^k(b-1)E\{V(i,j)|\partial(i,j)\}$$

$$\leq -\frac{1}{\rho}b^{k+1}V(i,j) + b^{k+1}\delta(i,j) + b^k(b-1)E\{V(i,j)|\partial(i,j)\} \tag{63}$$

$$= b^k\left(b - \frac{1}{\rho}b - 1\right)E\{V(i,j)|\partial(i,j)\} + b^{k+1}\delta(i,j).$$

Define $0 < \varrho = 1 - \frac{1}{\rho} = \frac{1}{b} < 1$, then it follows from (63) that

$$E\{V^+(i,j)|\partial(i,j)\} \leq \frac{1}{b}E\{(V(i,j)|\partial(i,j)\} + \delta(i,j). \tag{64}$$

From (34c) and (62), one has

$$E\{V^h(i+1,j) + V^v(i,j+1)|\partial(i,j)\} \leq \delta(i,j) + \frac{1}{b}E\{V^h(i,j) + V^v(i,j)|\partial(i,j)\}. \tag{65}$$

According to initial boundary constraints (2), it implies $V^h(0,K) = 0$ and $V^v(K,0) = 0$ (K is a positive integer that is larger enough, and $K > \max\{t_1, t_2\}$). Summing up both sides of (65) with respect to both i and j from 0 to K, we can obtain

$$
\begin{aligned}
E\left\{\sum_{i+j=K} V(i,j)\right\} &= E\{V^h(0,K) + V^h(1,K-1) + V^h(2,K-2) + ... + V^h(K-1,1) + V^h(K,0) \\
&\quad + V^v(0,K) + V^v(1,K-1) + V^v(2,K-2) + ... + V^v(K-1,1) + V^v(K,0)\} \\
&\leq \frac{1}{b} E\{V^h(0,K-1) + V^h(1,K-2) + V^h(2,K-3) + ... + V^h(K-2,1) + V^h(K-1,0) \\
&\quad + V^v(0,K-1) + V^v(1,K-2) + V^v(2,K-3) + ... + V^v(K-2,1) + V^v(K-1,0))\} + \delta(i,j) \\
&= \frac{1}{b} \sum_{i+j=K-1} V(i,j) + \delta(i,j) = \varrho^{K-S} \sum_{i+j=S} V(i,j) + \frac{1-\varrho^{K-S}}{1-\varrho}\delta(i,j).
\end{aligned}
\tag{66}
$$

From (36a), it is straightforward to obtain the following inequality:

$$
\varsigma_1 E\{\| \iota(i,j) \|^2\} \leq E\{V(i,j)\} \leq \varsigma_2 \| \iota(i,j) \|_{\mathscr{M}}^2,
\tag{67}
$$

where

$$
\varsigma_1 = \lambda_{\min}(P(i,j)),
$$

$$
\varsigma_2 = \lambda_{\max}(P(i,j)) + \overline{\tau}\lambda_{\max}(S_1(i,j)) + \frac{1}{2}\left(\overline{\tau} - \underline{\tau}\right)\left(\overline{\tau} + \underline{\tau} + 1\right)\lambda_{\max}(S_1(i,j)) + \frac{1}{2}\overline{\tau}(\overline{\tau}+1)\lambda_{\max}(S_2(i,j)) - \frac{1}{2}\underline{\tau}\left(\underline{\tau}+1\right)\lambda_{\max}(S_3(i,j)).
$$

Inequality (67) implies that $E\left\{\sum_{i+j=K} \| \iota(i,j) \|^2\right\} \leq \frac{1}{\varsigma_1}E\left\{\sum_{i+j=K} V(i,j)\right\}$ and $\varsigma_2 \sum_{i+j=S} \| \iota(i,j) \|_{\mathscr{M}}^2 \geq E\left\{\sum_{i+j=S} V(i,j)\right\}$, then, together with (66) and (67), we know that

$$
E\left\{\sum_{i+j=K} \| \iota(i,j) \|^2\right\} \leq \frac{1}{\varsigma_1}E\left\{\sum_{i+j=K} V(i,j)\right\} \leq \frac{\varsigma_2}{\varsigma_1}\varrho^{K-S} \sum_{i+j=S} \| \iota(i,j) \|_{\mathscr{M}}^2 + \frac{1-\varrho^{K-S}}{\varsigma_1(1-\varrho)}\delta(i,j).
$$

According to Definition 1, it is clear that the dynamic filtering error systems (13) is exponentially ultimately bounded in mean-square sense with asymptotic upper bound $\frac{\delta(i,j)}{\varsigma_1(1-\varrho)}$. The proof is thus completed.

Appendix B. The Proof of Theorem 2

Proof.   It is worth noting that (14) contains nonlinear term $P^{-1}(i,j)$, so it is necessary to process some variables and convert (14) into the linear matrix inequalities. For a positive definite symmetric matrix $P(i,j)$, consider the following permanent relationship:

$P^{-1}(i,j) + P(i,j) - 2I_{2n_h+2n_v} = (I_{2n_h+2n_v} - P(i,j))P^{-1}(i,j)(I_{2n_h+2n_v} - P(i,j))^T \geq 0.$

Then, based on $P^{-1}(i,j) - 2I_{2n_h+2n_v} \geq -P(i,j)$ and $\Omega^T\Omega = \Omega\Omega^T = I_{2n_h+2n_v}$ (Ω is an orthogonal matrix), we utilize the matrix $diag\{I_2 \otimes \Omega, I_{2n_x+2n_v}, I_{n_y}, I_{n_y}, I_5 \otimes \Omega\}$ to perform the congruent transformation on (14), and define $P^{-1}(i,j) = \Omega^T\overline{P}(i,j)\Omega, \overline{S}_1(i,j) = \Omega S_1(i,j)\Omega^T, \overline{S}_2(i,j) = \Omega S_2(i,j)\Omega^T, \overline{S}_3(i,j) = \Omega S_3(i,j)\Omega^T$, which yields

$$
\Theta = \begin{bmatrix} \Theta_{11} & \Theta_{12} \\ * & \Theta_{22} \end{bmatrix} \leq 0,
\tag{68}
$$

where $\Theta_{11} = \begin{bmatrix} \Theta_{11}^1 & 0 & \widehat{M}^T\Omega & 0 & 0 \\ * & -\overline{S}_1(i,j) & 0 & 0 & 0 \\ * & * & -2I_{2n_x+2n_v} & 0 & 0 \\ * & * & * & -\gamma_1(i,j)\Phi_{(i,j)} & 0 \\ * & * & * & * & -\gamma_2(i,j)I_{n_y} \end{bmatrix}$,

$$
\begin{aligned}
\Theta_{11}^1 = \left(1 + \overline{\tau} - \underline{\tau}\right)\overline{S}_1(i,j) + \left(\overline{\tau}\overline{S}_2(i,j) - \underline{\tau}\overline{S}_3(i,j)\right) + \sigma\gamma_1(i,j)\Omega\widetilde{C}^T(i,j)\Phi_{(i,j)}\widetilde{C}(i,j)\Omega^T \\
+ \left(1 - \frac{1}{\rho}\right)\overline{P}(i,j) - 2\left(1 - \frac{1}{\rho}\right)I_{2n_h+2n_v},
\end{aligned}
$$

$$\Theta_{12} = \begin{bmatrix} \widehat{A}_1^T(i,j) + M^T\overline{B}^T(i,j) & \overline{\varsigma}_1\widecheck{A}_1^T(i,j) & \overline{\varsigma}_{12}\widecheck{A}_1^T(i,j) & 0 & 0 \\ \overline{A}_2^T(i,j) & 0 & 0 & 0 & 0 \\ \Omega^T\overline{B}^T(i,j) & 0 & 0 & 0 & 0 \\ \widehat{\mathscr{R}}(i,j)\Omega^T & \overline{\varsigma}_1\widecheck{\mathscr{R}}^T(i,j)\Omega^T & 0 & \overline{\varsigma}_{12}\widecheck{\mathscr{R}}^T(i,j)\Omega^T & 0 \\ \widehat{\mathscr{O}}^T(i,j)\Omega^T & 0 & 0 & 0 & \sqrt{(\overline{\varsigma}_2^2 + 2\overline{\varsigma}_{12}^2)}\widecheck{\mathscr{O}}^T(i,j)\Omega^T \end{bmatrix},$$

$$\Theta_{22} = I_5 \otimes -\overline{P}(i,j).$$

Subsequently, we correspond to reconstruct the matrix Ω of (12) in the following form:

$$\Omega = \begin{bmatrix} \overline{I}_{n_h} & \overline{I}_{n_v} \\ \widetilde{I}_{n_h} & \widetilde{I}_{n_v} \end{bmatrix},$$

where $\overline{I}_{n_h} = \begin{bmatrix} I_{n_h} & 0 \\ 0 & 0 \end{bmatrix}, \widetilde{I}_{n_h} = \begin{bmatrix} 0 & I_{n_h} \\ 0 & 0 \end{bmatrix}, \overline{I}_{n_v} = \begin{bmatrix} 0 & 0 \\ I_{n_v} & 0 \end{bmatrix}, \widetilde{I}_{n_v} = \begin{bmatrix} 0 & 0 \\ 0 & I_{n_v} \end{bmatrix}$. Then, it is easy to obtain that

$$\overline{S}_1(i,j) = \begin{bmatrix} \overline{I}_{n_h}S_1^h(i,j)\overline{I}_{n_h} + \overline{I}_{n_v}S_1^v(i,j)\overline{I}_{n_v} & \overline{I}_{n_h}S_1^h(i,j)\widetilde{I}_{n_h} + \overline{I}_{n_v}S_1^v(i,j)\widetilde{I}_{n_v} \\ * & \widetilde{I}_{n_h}S_1^h(i,j)\widetilde{I}_{n_h} + \widetilde{I}_{n_v}S_1^v(i,j)\widetilde{I}_{n_v} \end{bmatrix}, \tag{69a}$$

$$\overline{S}_2(i,j) = \begin{bmatrix} \overline{I}_{n_h}S_2^h(i,j)\overline{I}_{n_h} + \overline{I}_{n_v}S_2^v(i,j)\overline{I}_{n_v} & \overline{I}_{n_h}S_2^h(i,j)\widetilde{I}_{n_h} + \overline{I}_{n_v}S_2^v(i,j)\widetilde{I}_{n_v} \\ * & \widetilde{I}_{n_h}S_2^h(i,j)\widetilde{I}_{n_h} + \widetilde{I}_{n_v}S_2^v(i,j)\widetilde{I}_{n_v} \end{bmatrix}, \tag{69b}$$

$$\overline{S}_3(i,j) = \begin{bmatrix} \overline{I}_{n_h}S_3^h(i,j)\overline{I}_{n_h} + \overline{I}_{n_v}S_3^v(i,j)\overline{I}_{n_v} & \overline{I}_{n_h}S_3^h(i,j)\widetilde{I}_{n_h} + \overline{I}_{n_v}S_3^v(i,j)\widetilde{I}_{n_v} \\ * & \widetilde{I}_{n_h}S_3^h(i,j)\widetilde{I}_{n_h} + \widetilde{I}_{n_v}S_3^v(i,j)\widetilde{I}_{n_v} \end{bmatrix}. \tag{69c}$$

Moreover, taking (20) into consideration, one has

$$\begin{aligned} \delta(i,j) &= tr\left\{ \mathscr{W}^T\left(\widehat{\mathscr{E}}^T(i,j)P(i,j)\widehat{\mathscr{E}}(i,j) + \overline{\varsigma}_1^2\widecheck{\mathscr{E}}^T(i,j)P(i,j)\widecheck{\mathscr{E}}(i,j) + \sigma\gamma_1(i,j)D^T(i,j)\Phi_{(i,j)}D(i,j)\right)\mathscr{W}\right\} + \gamma_2(i,j)\overline{\bm{v}}^2 \\ &= tr\left\{ \mathscr{W}^T\left(\widehat{\mathscr{E}}^T(i,j)\Omega^T\overline{P}^{-1}(i,j)\Omega\widehat{\mathscr{E}}(i,j) + \overline{\varsigma}_1^2\widecheck{\mathscr{E}}^T(i,j)\Omega^T\overline{P}^{-1}(i,j)\Omega\widecheck{\mathscr{E}}(i,j) + \sigma\gamma_1(i,j)\widetilde{D}^T(i,j)\Phi_{(i,j)}\widetilde{D}(i,j)\right)\mathscr{W}\right\} + \gamma_2(i,j)\overline{\bm{v}}^2 \tag{70} \\ &\le tr\left\{ \mathscr{W}^T\left(\widehat{\mathscr{E}}^T(i,j)Q(i,j)\widehat{\mathscr{E}}(i,j) + \overline{\varsigma}_1^2\widecheck{\mathscr{E}}^T(i,j)Q(i,j)\widecheck{\mathscr{E}}(i,j) + \sigma\gamma_1(i,j)\widetilde{D}^T(i,j)\Phi_{(i,j)}\widetilde{D}(i,j)\right)\mathscr{W}\right\} + \gamma_2(i,j)\overline{\bm{v}}^2 = \widehat{\delta}(i,j). \end{aligned}$$

Obviously, it can be derived from (66) and (21) that

$$\begin{aligned} \sum_{i+j=K}\|\widetilde{\mathscr{Z}}(i,j)\|^2 &= \sum_{i+j=K}\imath^T(i,j)\widetilde{H}^T(i,j)\widetilde{H}(i,j)\imath(i,j) \le \sum_{i+j=K}\imath^T(i,j)\left(2I_{2n_h+2n_v} - \Omega^T\overline{P}(i,j)\Omega\right)\imath(i,j) \\ &\le \sum_{i+j=K}\imath^T(i,j)P(i,j)\imath(i,j) = \sum_{i+j=K}E\{V_1(i,j)\} \le \varrho^{K-S}\sum_{i+j=S}V(i,j) + \frac{1-\varrho^{K-S}}{1-\varrho}\widehat{\delta}(i,j). \end{aligned} \tag{71}$$

Subsequently, by combining (68)-(71), it is easy to see that the nonlinear term of (14) is eliminated, and an upper bound $\frac{\widehat{\delta}(i,j)}{1-\varrho}$ of the controlled output error $\sum_{i+j=K}\|\widetilde{\mathscr{Z}}(i,j)\|^2$ is derived. Consequently, the desired filtering gains can be obtained by minimizing $\widehat{\delta}(i,j)$. The proof is thus completed.

References

[1] C.K. Ahn, P. Shi, H.R. Karimi, Novel results on generalized dissipativity of two-dimensional digital filters, IEEE Trans. Circuits Syst. I -Express Briefs 63 (9) (2016) 893–897.

[2] C. Du, L. Xie, Stability analysis and stabilization of uncertain two-dimensional discrete systems: an LMI approach, IEEE Trans. Circuits Syst. I-Regular Papers 46 (11) (1999), 1371-137.

[3] S. Knorn, R.H. Middleton, Stability of two-dimensional linear systems with singularities on the stability boundary using LMIs, IEEE Trans. Autom. Control 58 (10) (2013) 2579–2590.

[4] L. Wu, Z. Wang, Filtering and Control for Classes of Two-Dimensional Systems, Springer International Publishing, Cham, Switzerland, 2015.

[5] R.P. Roesser, A discrete state-space model for linear image processing, IEEE Trans. Autom. Control 20 (1) (1975) 1–10.

[6] E. Fornasini, G. Marchesini, State-space realization theory of two-dimensional filters, IEEE Trans. Autom. Control 21 (4) (2016) 484–492.

[7] E. Fornasini, G. Marchesini, Doubly indexed dynamical systems: state models and structural properties, Math. Syst. theory 12 (1) (1978) 59–72.

[8] J.E. Kurek, The general state-space model for a two-dimensional linear digital system, IEEE Trans. Autom. Control 30 (6) (1985) 600–602.

[9] P.H. Coutinho, I. Bessa, P. Pessim, R. Palhares, A switching approach to event-triggered control systems under denial-of-service attacks, Nonlinear Anal.-Hybrid 50 (2023), 101383. Article number.

[10] M. Yang, J.Y. Zhai, Observer-based dynamic event-triggered secure control for nonlinear networked control systems with false data injection attacks, Inf. Sci. 644 (2023), 119262. Article number.

[11] T. Saravanakumar, T.H. Lee, Hybrid-driven-based resilient control for networked T-S fuzzy systems with time-delay and cyber-attacks, Int. J. Robust Nonlinear Control 33 (13) (2023) 7869–7891.

[12] T.T. Jiang, Y.P. Zhang, J.H. Park, X.S. Cai, K.B. Shi, Novel dropout compensation control design for networked control systems with mixed delays, IEEE Trans. Syst. Man Cybern, DOI: 10.1109/TSMC.2023.3306317.

[13] Y.Wang H, J.C. Xu, H.T. Zhao, W. Shang, A self-triggered stochastic model predictive control for uncertain networked control system, Int. J. Control 96 (8) (2023) 2113–2123.

[14] L.V. Hien, H. Trinh, Exponential stability of two-dimensional homogeneous monotone systems with bounded directional delays, IEEE Trans. Autom. Control 63 (8) (2018) 2694–2700.

[15] D. Peng, H.M. Nie, Abel lemma-based finite-sum inequality approach to stabilization for 2-D time-varying delay systems, Asian J. Control 23 (3) (2021) 1394–1406.

[16] Y. Yan, L.L. Su, V. Gupta, Analysis of two-dimensional feedback systems over networks using dissipativity, IEEE Trans. Autom. Control 65 (8) (2020) 3241–3255.

[17] S.P. Huang, Z.Y. Xiang, Delay-dependent robust H_∞ control for 2-D discrete nonlinear systems with state delays, Multidimens. Syst. Signal Process 25 (4) (2014) 775–794.

[18] D.H. Li, J.L. Liang, F. Wang, Robust H_∞ filtering for 2D systems with RON under the stochastic communication protocol, IET Control. Theory Appl. 18 (14) (2020) 2795–2804.

[19] F. Wang, J. Liang, Z. Wang, Robust finite-horizon filtering for 2-D systems with randomly varying sensor delays, IEEE Trans. Syst. Man Cybern.: Syst 50 (1) (2020) 220–232.

[20] M.M. Fu, S. Liu, G.L. Wei, H. Li, Event-based joint estimation for unknown inputs and states: a distributed Recursive filtering method, Int. J. Robust Nonlinear Control, DOI: 10.1002/rnc.6910.

[21] Y.Q. Shen, S.L. Sun, Distributed recursive filtering for multi-rate uniform sampling systems with packet losses in sensor networks, Int. J. Syst. 54 (8) (2023) 1729–1745.

[22] H. Fu, H.L. Dong, F. Han, Outlier-resistant H_∞ filtering for a class of networked systems under Round-Robin protocol, Neurocomputing 401 (2020) 133–142.

[23] M.A. Nezar, S.M. Magdi, Distributed H_2/H_∞ filter design for discrete-time switched systems, IEEE-CAA J Autom. 7 (1) (2020) 158–168.

[24] J. Mao, X. Meng, D.R. Ding, Fuzzy set-membership filtering for discrete-time nonlinear systems, IEEE-CAA J. Autom. 9 (6) (2022) 1026–1036.

[25] C. Liu, L. Yang, J. Tao, Y. Xu, T.W. Huang, Set-membership filtering for complex networks with constraint communication channels, Neural Networks 152 (2022) 479–486.

[26] L.C. Wang, Z.D. Wang, G.L. Wei, F.E. Alsaadi, Finite-time state estimation for recurrent delayed neural networks with component-based event-triggering protocol, IEEE Trans. Neural Netw. Learn. Syst. 29 (4) (2018) 1046–1057.

[27] M.Z. Zhu, Y.K. Chen, G.C. Ya, Distributed filtering for Markov jump systems with randomly occurring one-sided Lipschitz nonlinearities under Round-Robin scheduling, Neurocomputing 417 (2020) 396–405.

[28] Y.C. Zhang, B. Chen, L. Yu, Distributed Kalman filtering for interconnected dynamic systems, IEEE Trans. Cybern. 52 (11) (2021) 11571–11580.

[29] H.Z. Fang, M.A. Haile, Y.B. Wang, Robust extended Kalman filtering for systems with measurement outliers, IEEE Trans. Control Syst. Technol. 30 (2) (2022) 795–802.

[30] S. Liu, Z.D. Wang, Y. Chen, G.L. Wei, Protocol-based unscented Kalman filtering in the presence of stochastic uncertainties, IEEE Trans. Autom. Control 65 (3) (2020) 1303–1309.

[31] Y.M. Ju, D. Liu, D.R. Ding, G.L. Wei, Distributed cubature Kalman filtering for nonlinear systems with stochastic communication protocol, Asian J. Control 24 (6) (2022) 3566–3579.

[32] H. Geng, Z.D. Wang, X.J. Yi, F.E. Alsaadi, Y.H. Cheng, Tobit Kalman filtering for fractional-order systems with stochastic nonlinearities under Round-Robin protocol, Int. J. Robust Nonlinear Control 31 (6) (2021) 2348–2370.

[33] J.Y. Guo, Z.D. Wang, L. Zou, Z.Y. Zhao, Ultimately bounded filtering for time-delayed nonlinear stochastic systems with uniform quantizations under random access protocol, Sensors 20 (15) (2020) 4134–4146.

[34] L. Zou, Z.D. Wang, J. Hu, Ultimately bounded filtering subject to impulsive measurement outliers, IEEE Trans. Autom. Control 67 (1) (2022) 304–319.

[35] S. Li, W.C. Zou, J. Guo, Consensus of switched nonlinear multiagent systems subject to cyber-attacks, IEEE Syst. J. 16 (3) (2022) 4423–4432.

[36] W.L. Duo, M.C. Zhou, A. Abusorrah, A survey of cyber-attacks on cyber physical systems: recent advances and challenges, IEEE-CAA J. Autom. 9 (5) (2022) 784–800.

[37] Z. Lian, P. Shi, C.-C. Lim, Fuzzy-model-based lateral control for networked autonomous vehicle systems under hybrid cyber-attacks, IEEE Trans. Cybern 53 (4) (2023) 2600–2609.

[38] J.M. Cao, J.F. Zhou, J. Chen, Sliding mode control for discrete-time systems with randomly occurring uncertainties and nonlinearities under hybrid cyber-attacks, Circ. Syst. Signal Pr. 40 (12) (2021) 5864–5885.

[39] M.M. Hamdan, M.S. Mahmoud, U.A. Baroudi, Event-triggering control scheme for discrete time cyberphysical systems in the presence of simultaneous hybrid stochastic attacks, ISA T 122 (2022) 1–12.

[40] J.L. Liu, N. Zhang, Y. Li, H_∞ filter design for discrete-time networked systems with adaptive event-triggered mechanism and hybrid cyber-attacks, J. Frankl. Inst 358 (17) (2021) 9325–9345.

[41] S.X. Luo, F.Q. Deng, On event-triggered control of nonlinear stochastic systems, IEEE Trans. Autom. Control 65 (1) (2020) 369–375.

[42] G.L. Zhao, C.C. Hua, A hybrid dynamic event-triggered approach to consensus of multi-agent systems with external disturbances, IEEE Trans. Autom. Control 66 (7) (2021) 3213–3220.

[43] F.Z. Li, Y.G. Liu, Adaptive event-triggered output-feedback controller for uncertain nonlinear systems, Automatica 117 (2020), 109006. Article number.

[44] Z. Gu, X.H. Zhou, T. Zhang, F. Yang, M.Q. Shen, Event-triggered filter design for nonlinear cyber-physical systems subject to deception attacks, ISA T 104 (2020) 130–137.

[45] Y.S. Tan, Y. Yuan, X.P. Xie, E.G. Tian, J.L. Liu, Observer-based event-triggered control for interval type-2 fuzzy networked system with network attacks, IEEE Trans. Fuzzy Syst. 31 (8) (2023) 2788–2798.

[46] M.L. Wang, X.S. Yang, S.Y. Mao, K.F. Yiu, J.H. Park, Consensus of multi-agent systems with one-sided lipschitz nonlinearity via nonidentical double event-triggered control subject to deception attacks, J. Frankl. Inst. 360 (9) (2023) 6275–6295.

[47] Y.H. Deng, H.Q. Lu, W.N. Zhou, Security event-triggered filtering for delayed neural networks under denial-of-service attack and randomly occurring deception attacks, Neural Process Lett. 54 (6) (2022) 5273–5298.

RESEARCH ARTICLE

WILEY

Recursive set-membership filtering for two-dimensional shift-varying systems with FlexRay protocol and hybrid cyber attacks

Pan Zhang | **Chaoqun Zhu** | **Zhiwen Wang** 🟢 | **Bin Yang**

College of Electrical and Information Engineering, Lanzhou University of Technology, Lanzhou, China

Correspondence

Zhiwen Wang, College of Electrical and Information Engineering, Lanzhou University of Technology, Lanzhou 730050, China.
Email: wwwangzhiwen@yeah.net

Abstract

The problem of recursive set-membership filter design for two-dimensional (2-D) systems subject to FlexRay communication protocol and hybrid cyber attacks (HCAs) is investigated in this article. The FlexRay protocol that integrates time-triggered and event-triggered mechanisms and involves a series of pre-defined communication cycles based on bidirectional metrics is developed to alleviate the network bandwidth load. Furthermore, the envisioned system is exposed to false data injection and denial-of-service attacks that occur in a randomized manner. Subsequently, the dynamic filtering error system (FES) subject to bidirectional evolutionary HCAs and FlexRay scheduling protocol is constructed. Then, sufficient conditions are obtained such that the dynamic FES consistently resides within an ellipsoidal set by utilizing double mathematical induction and recursive linear matrix inequalities (RLMIs). Moreover, the optimal filtering algorithm is given by minimizing the ellipsoidal constraints from the perspective of the traces of the matrix. The effectiveness of the presented recursive set-membership filter design approach is validated by a long-distance transmission line example.

KEYWORDS

FlexRay communication protocol, hybrid cyber attacks, set-membership filtering, two-dimensional systems, unknown-but-bounded noises

1 | INTRODUCTION

Recently, two-dimensional (2-D) systems have been found in many real-world systems, such as seismographic data processing, thermal processes, gas absorption, and water stream heating [1–4]. The Roesser model [5], the Fornasini and Marchesini (FM) model [6, 7], and the Kurek model [8] are widely employed 2-D state space models. With the integration of network technology and control science, networked systems have arisen. It is an uncontroversial fact that the introduction of shared

networks enables traditional control systems to be more energetic, but the dynamic evolutionary behavior of these systems becomes increasingly sophisticated. Under this background, the networked 2-D systems have been investigated owing to their great theoretical value and real-world significance [9–14].

It is worth noting that an implicit assumption in many underlying investigations of the stability analysis and control synthesis for 2-D systems is that the shared communication network has adequate communication resources, that is, all sensors can simultaneously transmit

measurement information to the filter through the communication network during each sampling shift instant. Nevertheless, it is quite unrealistic to implement such a communication scheme, as simultaneous multiple access to a limited-bandwidth network will inevitably result in data collisions. The bidirectional evolutionary behavior of 2-D systems is more susceptible to network congestion due to data redundancy than that of one-dimensional (1-D) systems. In such a circumstance, as one of the most effective means to deal with data conflict problems, communication scheduling protocols are widely employed in various types of industry control practices due to their ability to orchestrate the order of data transmission. Several prevailing communication protocols have been continuously advanced and optimized up to now, that is, the Try-Once-Discard protocol (TODP) [15, 16], the Round-Robin protocol (RRP) [17, 18], the stochastic communication protocol (SCP) [19, 20], and the FlexRay protocol (FRP) [21, 22]. Among these protocols, the SCP and RRP belong to the category of time-triggered scheduling schemes; the TODP is categorized as an event-triggered scheme; and the FRP is a hybrid communication protocol that simultaneously involves time-triggered and event-triggered rules. Due to the predetermined fixed time-triggered and event-triggered periods for scheduling high-real-time and high-priority data, the FRP provides greater flexibility and reliability in the communication network than the previous three protocols. Currently, considering the actual control practice in which the signal transmission of networked systems can be implemented via multiple communication networks with different communication protocols (hybrid communication protocols) [23] and the prospect of remarkable industrial applications (notably providing fault-tolerant communications capabilities for safety-critical mechanical and electrical systems) of FRP [24], academics have conducted preliminary discussions on the analysis and synthesis of networked systems equipped with FRP [25–27]. It is worth noting that the results obtained in the aforementioned literature are all based on the 1-D systems as a baseline. The design of high-performance scheduling protocols is increasingly necessary for 2-D systems with greater computational and transmission burdens. Very few research related to 2-D systems under the impact of FRP have been reported. A potential challenge may lie in defining static and dynamic time sequences based on bidirectional indices and designing transmission rules for the rational scheduling of measurement output. However, the current FRP strategies proposed are no longer applicable to 2-D systems, and the development of FRP for 2-D systems is the primary motivation for our current investigation.

Due to the openness of communication networks, several types of common cyber attacks have been emphasized by scholars, including but not limited to denial-of-service (DoS) attacks [28], false data injection (FDI) attacks [29, 30], and replay attacks [31]. The authors of [28] are concerned with the output consensus problem for a class of nonlinear multiagent systems where DoS attacks occur in the communication channel. The security issue against FDI attacks in the identification of finite impulse response systems with binary-valued observations is investigated in [29]. The FDI attacks detection problem for a class of continuous-time switched systems is discussed in [30], assuming a malicious attacker tampers with the binary 01 code transmitted through the network to compromise the systems. The literature [31] discusses the resilient distributed control scheme against replay attacks for multi-agent networked systems subject to input and state constraints. All of the above literature considers communication networks subject to only one type of attack. More importantly, the hybrid cyber attacks (HCAs) model is more threatening than the single attacks to be favored by the adversaries, and the security issues of systems in this context have been continuously researched [32–34]. Unfortunately, there are very few results regarding the security of 2-D systems with the occurrence of HCAs. Considering the mixed properties of data information actively discarded by protocol scheduling as well as passively discarded data information by HCAs render the evolutionary behavior of 2-D systems more complicated, reducing the burden on the systems while ensuring their security is another motivation for our current research.

The filtering problem has hitherto been a trending research topic. The Kalman filtering [35, 36], the H$_\infty$ filtering [37, 38], and the set-membership filtering [39, 40] have been extensively investigated depending on different systems noise characteristics as well as performance demands. The set-membership filtering approach has two main advantages over other filtering techniques: (1) it depends upon a strict bound limitation instead of the precise statistical property of the system noises; and (2) it can produce a set of ellipsoidal sets that contain all possible error and state vectors with 100% confidence. In the last few years, the set-membership filtering issue for 1-D systems has been widely investigated; see, for example, [41–43]. From a practical engineering perspective, due to the external environment and the systems' inherent limitations, it is common to only obtain information regarding the bounds of noise. As set-membership filtering techniques excel in 1-D systems, the extension of existing set-membership filtering methods to 2-D systems has garnered significant research attention, as documented in references [44–46]. To name a few, the authors of [44] are concerned with the set-membership filtering problem for 2-D systems under RRP and sensor saturation. The

set-membership filtering problem for 2-D systems under the dynamic event-triggered mechanism has been investigated, examining the impact of the triggered frequency on the filter performance in the 2-D setting [45]. The issue of non-fragile set-membership filtering for 2-D systems with TODP and uniform quantization is investigated in [46]. Although the aforementioned literature has discussed the problem of set-membership filtering for 2-D systems with communication scheduling strategies, the results obtained are still fragmented. In particular, most of the literature is based on a single communication protocol scenario. Therefore, developing set-membership filtering algorithms for 2-D systems based on hybrid communication protocols is worthy of in-depth study.

Inspired by the aforementioned discussions, in summary, we are committed to addressing the recursive set-membership filtering problem for 2-D systems under FRP and HCAs, and the identified challenges are as follows: (1) How to define FRP based on bidirectional evolutionary metrics that integrate time-triggered and event-triggered mechanisms within a communication cycle. (2) How to characterize the synergistic effects of FRP and HCAs on measurement outputs and design an appropriate filter structure. (3) How to develop set-membership filtering algorithms that incorporate protocol constraints, attack energies, unknown but bounded noises, and possibly state vectors simultaneously into given ellipsoidal set constraints. By addressing the above challenges, the innovations of this paper can be summarized as follows: (1) The FRP scheduling and HCAs that involve bidirectional evolutionary indexes are established, respectively, and a descriptive model of 2-D systems subject to FRP and HCAs is developed. (2) Building on the results of (1), a recursive set-membership filter structure is proposed under the constraints of FRP and HCAs. Furthermore, the filtering error system (FES) subject to scheduling parameters and attack parameters is developed. (3) The sufficient conditions for the existence of explicit filter gains are transformed into an ellipsoidal set optimization problem using the principle of double induction and the technique of recursive linear matrix inequalities (RLMIs), which is simple and suitable for online operation.

The rest of this paper is organized as follows: In Section 2, the FRP and HCAs models based on bidirectional evolutionary are proposed. In Section 3, a set-membership filtering structure is proposed for 2-D systems with the impacts of FRP and HCAs. Section 4 uses a practical example to illustrate the effectiveness of the proposed filter algorithm. Finally, Section 5 concludes with a discussion of future research directions.

Notation: The notation used throughout the paper is fairly standard. R^n denotes the n-dimensional Euclidean space and $P > 0$ means that it is real symmetric and positive definite. G^T and G^{-1} represent the transpose and the inverse of the matrix G, respectively. $diag\{\rho_1, \cdots, \rho_n\}$ stands for block diagonal matrix. $\|A\|$ refers to the norm of a matrix A defined by $\|A\| = \sqrt{A^T A}$. $\mathbb{N}$ denotes the set of natural numbers. The n-dimensional identity matrix is denoted by I_n.

2 | PROBLEM DESCRIPTION AND PRELIMINARIES

As shown in Figure 1, consider the 2-D shift-varying system [12] in a finite horizon $\mathbb{Q} \triangleq \{i, j \in [0, \kappa]\}$ as follows:

$$\begin{cases} x(i+1,j+1) = A_1(i+1,j)x(i+1,j) + A_2(i,j+1)x(i,j+1) + B_1(i+1,j)\omega(i+1,j) \\ \quad + B_2(i,j+1)\omega(i,j+1) + F_1(i+1,j)f(x(i+1,j)) + F_2(i,j+1)f(x(i,j+1)), \\ y(i,j) = C(i,j)x(i,j) + D(i,j)v(i,j) \end{cases}$$

(1)

where $x(i,j) \in R^{n_x}$ represents the system state vector. $y(i,j) \in R^{n_y}$ is the measurement output. $\omega(i,j) \in R^{n_\omega}$ and $v(i,j) \in R^{n_v}$ denote the unknown-but-bounded process and measurement noises, respectively. $A_1(i,j)$, $A_2(i,j)$, $B_1(i,j)$, $B_2(i,j)$, $C(i,j)$, $D(i,j)$, $F_1(i,j)$, and $F_2(i,j)$ are known time-varying matrices with appropriate dimensions. The indicators i and j represent generalized time variables, which can be time itself or variables with time-varying characteristics. The initial conditions $x(i,0)$ and $x(0,j)$ meet the following probability distribution and are independent of the other variables
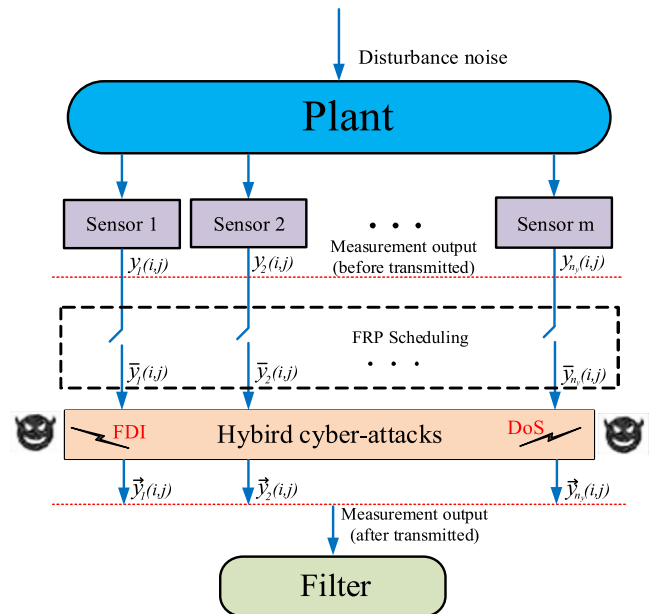

FIGURE 1 Set-membership filtering problem for two-dimensional (2-D) systems.

$$E\{x(i,0)\} = \mu_1(i), E\{x(0,j)\} = \mu_2(j),$$

where $\mu_1(i)$ and $\mu_2(j)$ are known vectors with $\mu_1(0) = \mu_2(0)$. $f(x(i,j))$ is a nonlinear function associated with a state vector that satisfies sector-bounded conditions as follows:

$$
\begin{aligned}
f(0) = 0, & \Big[f(\zeta_1(i,j)) - f(\zeta_2(i,j)) \\
& - G_1(i,j)(\zeta_1(i,j) - \zeta_2(i,j)) \Big]^T \Big[f(\zeta_1(i,j)) - f(\zeta_2(i,j)) \\
& - G_2(i,j)(\zeta_1(i,j) - \zeta_2(i,j)) \Big] \leq 0,
\end{aligned}
\tag{2}
$$

where $\zeta_1(i,j)$ and $\zeta_2(i,j)$ are arbitrary vectors belonging to R^{n_x}, $G_1(i,j)$, and $G_2(i,j)$ are known matrices with proper dimensions.

Assumption 1. The unknown-but-bounded noises are restricted to the following set ranges of ellipsoids:

$$
\begin{cases}
W(i,j) \triangleq \{\omega(i,j) : \omega^T(i,j)S^{-1}(i,j)\omega(i,j) \leq 1\} \\
V(i,j) \triangleq \{v(i,j) : v^T(i,j)R^{-1}(i,j)v(i,j) \leq 1\}
\end{cases},
$$

where $S(i,j) > 0$ and $R(i,j) > 0$ are time-varying matrices with appropriate dimensions.

2.1 | FlexRay protocol

Next, the model of 2-D systems under the FRP and HCAs will be introduced. The measured outputs of sensors are first scheduled by the FRP network. Generally speaking, the dynamic behavior of 2-D systems evolves in both vertical and horizontal evolutionary directions, which substantiates that 2-D systems are more susceptible to network traffic jams due to data redundancy. Therefore,

certain network protocols are required to be employed to protect the data transmission between sensors and filter from potential data conflicts. In what follows, we will introduce the scheduling of FRP. FRP is a type of hybrid communication protocol that integrates time-triggered and event-triggered mechanisms and involves a series of pre-defined communication cycles, which are structurally characterized as shown in Figure 2. Each of the communication cycles consists of a static segment, a dynamic segment, a symbol window, and a network ideal time, as well as the corresponding time lengths are defined as T_1, T_2, T_3, and T_4. In summary, static segments depend on Time Division Multiple Access methods to arrange network resources through static communication protocol (e.g., RRP). Dynamic segments utilize a Flexible Time Division Multiple Access technique that utilizes a dynamic communication protocol (e.g., TODP) to select sensor or controller nodes online to transmit information. The symbol window refers to the time required for the communication network to manage the transmitted data. The network idle time is the time required for the clock to be synchronized, and the communication network will not transmit data during this period. It should be emphasized that the lengths of the symbol window and network idle time are almost negligible compared to the static and dynamic segments, that is, $T_3 = 0$, $T_4 = 0$. Considering that the 2-D system has n_y sensor nodes, for the purpose of the subsequent description, we assume that the time lengths of the static segment and dynamic segment in each communication cycle are $T_1 = l_1 \leq n_y - 2$, $(l_1 \in \mathbb{N})$, and $T_2 = l_2$ with $l_1 + l_2 \leq n_y(l_2 \in \mathbb{N})$, respectively.

Without loss of generality, the time interval of a static segment can be summarized in the following sequence:

$$\Psi \triangleq \{(i,j) \mid \mathrm{mod}(i\kappa + j, l_1 + l_2) < l_1, i, j \in \mathbb{Q}\},$$

then, the time interval of the dynamic segment can be expressed as $\wp \triangleq \mathbb{Q} \backslash \Psi$. Furthermore, we assign the n_y sensor nodes to sets $\iota_1 = \{1, 2, ..., l_1\}$ and $\iota_2 = \{l_1 + 1, l_1 + 2, ..., n_y\}$. It is assumed that the nodes in set $\iota_1 = \{1, 2, ..., l_1\}$ belong to the RRP scheduling and
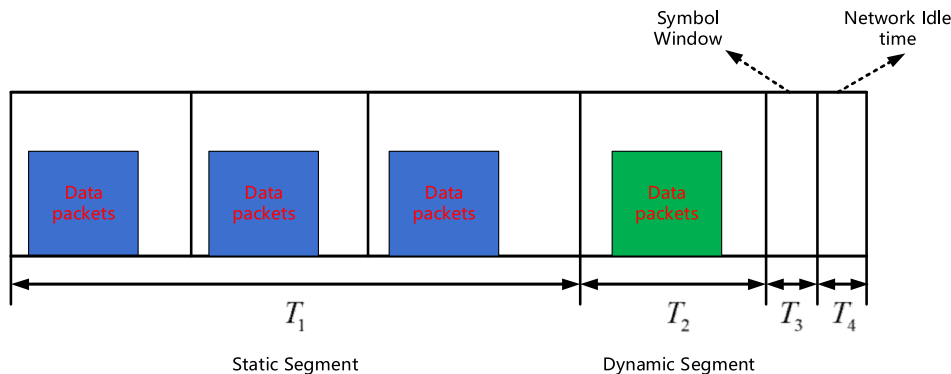
FIGURE 2 Structure diagram of FlexRay protocol for two-dimensional (2-D) systems.

the nodes in set $\iota_2 = \{l_1+1, l_1+2, ..., n_y\}$ belong to the TODP scheduling. In addition, let $\bar{y}(i,j) = \left[\bar{y}_1^T(i,j)\ \bar{y}_2^T(i,j) \cdots \bar{y}_{n_y}^T(i,j)\right]^T$ indicates the measurement output orchestrated by the FRP. Based on the above-mentioned features of the FRP, assuming that sensor nodes are authorized to obtain network access under the RRP and TODP, they are defined as $o(i,j)$ and $\pi(i,j)$ at each shift instant (i,j), respectively, and a bidirectional sequence associated with the TODP-triggered mechanism is defined as:

$$(i,j) < \left(\tilde{i},\tilde{j}\right) \Leftrightarrow \left\{(i,j) \mid i = \tilde{i}, j < \tilde{j}\right\} \cup \left\{(i,j) \mid i < \tilde{i}, j = \tilde{j}\right\}, (i_1, j_1)$$
$$= (i_2, j_2) \Leftrightarrow i = i_2 \text{ and } j = j_2,$$

then, the specific selection rules are as follows:

1. RRP:

$$o(i,j) = \begin{cases} \mathrm{mod}(i\kappa + j - 1, l_1) + 1 & (i,j) \in \Psi \\ 0 & (i,j) \in \wp \end{cases},$$

where $o(i,j) \in \iota_1$ represents which sensor is selected to communicate with the filter under the RRP at each shift instant (i,j). Then, the measurement output $\bar{y}_{m_1}(i,j)$ of the m_1-th $(1 \le m_1 \le l_1)$ sensor scheduled by RRP, which is received by the filter with a zero-order, can be expressed as:

$$\bar{y}_{m_1}(i,j) = \begin{cases} y_{m_1}(i,j) & m_1 = o(i,j), (i,j) \in \Psi \\ \bar{y}_{m_1}(i,j-1) & m_1 \ne o(i,j), (i,j) \in \Psi \\ 0 & (i,j) \in \wp \end{cases}. \quad (3)$$

2. TODP:

$$\pi(i,j) = \begin{cases} \arg\max\limits_{m_2 = l_2+1, ..., n_y} \left\{ \left(y_{m_2}(i,j) - y_{m_2}^*(i,j)\right)^T \Phi_{m_2} \left(y_{m_2}(i,j) - y_{m_2}^*(i,j)\right) \right\} & (i,j) \in \wp \\ 0 & (i,j) \in \Psi \end{cases},$$

where $\pi(i,j) \in \iota_2$ indicates which sensor is selected to communicate with the filter under the TODP at instant (i,j). $y_{m_2}^*(i,j)$ $(l_1+1 \le m_2 \le n_y)$ represents the latest transmitted measurement signal of node m_2 at shift instant (i,j). Φ_{m_2} is the known positive definite matrix. Similarly, the measurement output $\bar{y}_{m_2}(i,j)$ of the m_2-th $(l_1+1 \le m_2 \le n_y)$ sensor scheduled by TODP and zero-order hold strategy can be expressed as:

$$\bar{y}_{m_2}(i,j) = \begin{cases} y_{m_2}(i,j) & m_2 = \xi(i,j), (i,j) \in \wp \\ \bar{y}_{m_2}(i,j-1) & m_2 \ne \xi(i,j), (i,j) \in \wp \\ 0 & (i,j) \in \Psi \end{cases}. \quad (4)$$

To facilitate the subsequent derivation, the first l_1 measurement output scheduled through the RRP can be characterized as:

$$y^{[1]}(i,j) = \left[y_1^T(i,j)\ y_2^T(i,j)\ ...\ y_{l_1}^T(i,j)\right]^T, \quad (5)$$

then, the scheduling of the remaining $n_y - l_1$ measurement output by means of the TODP can be represented as:

$$y^{[2]}(i,j) = \left[y_{l_1+1}^T(i,j)\ y_{l_1+2}^T(i,j)\ ...\ y_{n_y}^T(i,j)\right]^T. \quad (6)$$

Moreover, the following augmented and partitioned matrices are defined:

$$C^{[1]}(i,j) = \left[C_1^T(i,j)\ C_2^T(i,j)\ ...\ C_{l_1}^T(i,j)\right]^T, C^{[2]}(i,j)$$
$$= \left[C_{l_1+1}^T(i,j)\ C_{l_1+2}^T(i,j)\ ...\ C_{n_y}^T(i,j)\right]^T,$$
$$D^{[1]}(i,j) = \left[D_1^T(i,j)\ D_2^T(i,j)\ ...\ D_{l_1}^T(i,j)\right]^T, D^{[2]}(i,j)$$
$$= \left[D_{l_1+1}^T(i,j)\ D_{l_1+2}^T(i,j)\ ...\ D_{n_y}^T(i,j)\right]^T,$$

$$\bar{y}(i,j) = \left[\left(\bar{y}^{[1]}(i,j)\right)^T\ \left(\bar{y}^{[2]}(i,j)\right)^T\right]^T,$$

then, according to (3)–(6), the $\bar{y}(i,j)$ can be further presented as:

$$\begin{aligned} \bar{y}(i,j) &= \mathcal{G}_1 \bar{y}^{[1]}(i,j) + \mathcal{G}_2 \bar{y}^{[2]}(i,j) \\ &= \mathcal{G}_1 \left(\Pi_{o(i,j)} y^{[1]}(i,j) + (I - \Pi_{o(i,j)}) y^{[2]}(i,j-1)\right) \\ &\quad + \mathcal{G}_2 \left(\Pi_{\pi(i,j)} y^{[1]}(i,j) + (I - \Pi_{\pi(i,j)}) y^{[2]}(i,j-1)\right) \\ &= \mathcal{G}_1 \left(\Pi_{o(i,j)} \left(C^{[1]}(i,j) x(i,j) + D^{[2]}(i,j) v(i,j)\right) + (I - \Pi_{o(i,j)}) y^{[1]}(i,j-1)\right) \\ &\quad + \mathcal{G}_2 \left(\Pi_{\pi(i,j)} \left(C^{[2]}(i,j) x(i,j) + D^{[2]}(i,j) v(i,j)\right) + (I - \Pi_{\pi(i,j)}) y^{[2]}(i,j-1)\right), \end{aligned} \quad (7)$$

where $\Pi_{o(i,j)} = diag_{1 \leq m_1 \leq l_2}\{\delta(o(i,j) - m_1)I\}$, $\Pi_{\pi(i,j)} = diag_{l_2+1 \leq m_2 \leq n_y}\{\delta(\pi(i,j) - m_2)I\}$, and $\delta(\cdot) \in \{0,1\}$ is the Kronecker delta function.

2.2 | Hybrid cyber-attacks model

First and foremost, FDI attacks are projected to degrade filtering performance by replacing correct information with damaging data. The random variable $\vartheta(i,j) \in \{0,1\}$ is employed to denote FDI attacks indicators. $\vartheta(i,j) = 1$ and $\vartheta(i,j) = 0$ indicate the FDI attacks successfully distort regular data by using false data, and the FDI attacks are unable to tamper with data, respectively. Suppose that the $\vartheta(i,j)$ is determined by the Bernoulli stochastic process, and the following occurrence probability of $\vartheta(i,j)$ is provided:

$$\Pr\{\vartheta(i,j) = 1\} = \overline{\vartheta}, \Pr\{\vartheta(i,j) = 0\} = 1 - \overline{\vartheta}.$$

Then, the $\overline{y}(i,j)$ affected by FDI attacks can be portrayed as:

$$\widetilde{y}(i,j) = \overline{y}(i,j) + \vartheta(i,j)\mathcal{M}(i,j), \tag{8}$$

where $\mathcal{M}(i,j) = \left[\mathcal{M}_1^T(i,j) \ \mathcal{M}_2^T(i,j) \ \cdots \ \mathcal{M}_{n_y}^T(i,j)\right]^T$ defined as attacker-generated false data signals, which can be produced as follows:

$$\mathcal{M}(i,j) = -\overline{y}(i,j) + v(i,j), \tag{9}$$

where $v(i,j)$ indicates the bounded energy single and satisfies $\|v(i,j)\| \leq \overline{v}$.

In what follows, the DoS attacks that disrupt the normal transmission are discussed, and suppose that the indicators of DoS attacks are determined by another random variable $\xi(i,j) \in \{0,1\}$. Analogously, $\xi(i,j) = 0$ and $\xi(i,j) = 1$ indicate that DoS attacks arise when measurement output is being transmitted, and DoS attacks do not occur, respectively. In addition, the following probability distribution is defined:

$$\Pr\{\xi(i,j) = 1\} = \overline{\xi}, \Pr\{\xi(i,j) = 0\} = 1 - \overline{\xi}.$$

Consequently, considering (7)–(9), the latest measurement output received by the filter can be expressed as:

$$\begin{aligned}
\vec{y}(i,j) &= \xi(i,j)\overline{y}(i,j) + \xi(i,j)\vartheta(i,j)(-\overline{y}(i,j) + v(i,j)) \\
&= \xi(i,j)\overline{y}(i,j) - \xi(i,j)\vartheta(i,j)\overline{y}(i,j) + \xi(i,j)\vartheta(i,j)v(i,j) \\
&= \xi(i,j)(1 - \vartheta(i,j))\overline{y}(i,j) + \xi(i,j)\vartheta(i,j)v(i,j),
\end{aligned} \tag{10}$$

where $\varpi_1(i,j) = \xi(i,j)(1 - \vartheta(i,j))$, $\varpi_2(i,j) = \xi(i,j)\vartheta(i,j)$.

2.3 | Problem formulation

In this paper, the recursive set-membership filtering problem will be addressed for the 2-D system under FRP and HCAs. Substituting (7) into (1) and defining the following augmented matrix

$$\eta(i,j) = \left[x^T(i,j) \ \left(\overline{y}^{[1]}(i,j-1)\right)^T \ \left(\overline{y}^{[2]}(i,j-1)\right)^T\right],$$

then, the 2-D system with FRP and HCAs can be reformulated as follows:

$$\begin{cases}
\eta(i+1,j+1) = \overline{A}_1(i+1,j)\eta(i+1,j) \\
\qquad + \overline{A}_2(i,j+1)\eta(i,j+1) + \overline{B}_1(i+1,j)\omega(i+1,j) \\
\qquad + \overline{B}_2(i,j+1)\omega(i,j+1) + \overline{F}_1(i+1,j)\overline{f}(P\eta(i+1,j)), \\
\qquad + \overline{F}_2(i,j+1)\overline{f}(P\eta(i,j+1)) \\
\vec{y}(i,j) = \overline{C}(i,j)\eta(i,j) + \overline{D}(i,j)v(i,j) + \varpi_2(i,j)v(i,j)
\end{cases} \tag{11}$$

where

$$\overline{A}_1(i+1,j) = \begin{bmatrix} A_1(i+1,j) & 0 & 0 \\ \Pi_{o(i,j)}C^{[1]}(i,j) & I - \Pi_{o(i,j)} & 0 \\ \Pi_{\pi(i,j)}C^{[2]}(i,j) & 0 & I - \Pi_{\pi(i,j)} \end{bmatrix},$$

$$\overline{A}_2(i,j+1) = \begin{bmatrix} A_2(i,j+1) & 0 & 0 \\ 0 & 0 & 0 \\ 0 & 0 & 0 \end{bmatrix}, \overline{B}_1(i+1,j) = \begin{bmatrix} B_1(i+1,j) \\ \Pi_{o(i,j)}D^{[1]}(i,j) \\ \Pi_{\pi(i,j)}D^{[2]}(i,j) \end{bmatrix}$$

$$\overline{B}_2(i,j+1) = \begin{bmatrix} B_2(i,j+1) \\ 0 \\ 0 \end{bmatrix}, \overline{F}_1(i+1,j) = \begin{bmatrix} F_1(i+1,j) & 0 & 0 \\ 0 & 0 & 0 \\ 0 & 0 & 0 \end{bmatrix},$$

$$\overline{F}_2(i,j+1) = \begin{bmatrix} F_2(i,j+1) & 0 & 0 \\ 0 & 0 & 0 \\ 0 & 0 & 0 \end{bmatrix}, \overline{f}(P\eta(i+1,j)) = \begin{bmatrix} f(P\eta(i+1,j)) \\ 0 \\ 0 \end{bmatrix},$$

$$\overline{f}(P\eta(i,j+1)) = \begin{bmatrix} f(P\eta(i,j+1)) \\ 0 \\ 0 \end{bmatrix},$$

$$\overline{C}(i,j) = [\varpi_1(i,j)\mathcal{G}_1\Pi_{o(i,j)}C^{[1]}(i,j) + \varpi_1(i,j)\mathcal{G}_2\Pi_{\pi(i,j)}C^{[2]}(i,j)$$
$$\times \varpi_1(i,j)\mathcal{G}_1(I - \Pi_{o(i,j)}) \varpi_1(i,j)\mathcal{G}_2(I - \Pi_{\pi(i,j)})]$$

$$\overline{D}(i,j) = \varpi_1(i,j)\mathcal{G}_1 D^{[1]}(i,j) + \varpi_1(i,j)\mathcal{G}_2 D^{[2]}(i,j), P = [I_{n_x} \ 0 \ 0].$$

Based on the 2-D system (11), the following recursive form of filter structure is proposed:

$$
\begin{aligned}
\widehat{\eta}^-(i+1,j+1) = &\overline{A}_1(i+1,j)\widehat{\eta}(i+1,j) + \overline{A}_2(i,j+1)\widehat{\eta}(i,j+1) \\
&+ \overline{F}_1(i+1,j)\overline{f}(P\widehat{\eta}(i+1,j)) \\
&+ \overline{F}_2(i,j+1)\overline{f}(P\widehat{\eta}(i,j+1)),
\end{aligned}
\tag{12}
$$

$$
\begin{aligned}
\widehat{\eta}(i+1,j+1) = &\widehat{\eta}^-(i+1,j+1) + K(i+1,j+1) \\
&\left(\vec{y}(i+1,j+1) - \overline{C}(i+1,j+1)\widehat{\eta}^-(i+1,j+1) \right),
\end{aligned}
\tag{13}
$$

where $\widehat{\eta}(i+1,j+1) \in R^{n_x+n_y}$ is the estimate of $\eta(i+1,j+1)$, $K(i+1,j+1)$ is the time-varying filter gain. The initial conditions of $\widehat{\eta}(i,j)$ are given as $\widehat{\eta}(i,0) = 0$ and $\widehat{\eta}(0,j) = 0$ for $i,j \in [0,\kappa]$.

Define the filtering error as $e(i,j) = \eta(i,j) - \widehat{\eta}(i,j)$, then, combining (11)–(13), the dynamic FES can be derived as:

$$
\begin{aligned}
e(i+1,j+1) = &\widetilde{A}_1(i+1,j)e(i+1,j) + \widetilde{A}_2(i,j+1)e(i,j+1) \\
&+ \widetilde{F}_1(i+1,j)\widetilde{f}(Pe(i+1,j)) \\
&+ \widetilde{F}_2(i,j+1)\widetilde{f}(Pe(i,j+1)) \\
&+ \widetilde{B}_1(i+1,j)\omega(i+1,j) + \widetilde{B}_2(i,j+1)\omega(i,j+1) \\
&- K(i+1,j+1)\overline{D}(i+1,j+1)v(i+1,j+1) \\
&- K(i+1,j+1)\varpi_2(i+1,j+1)v(i+1,j+1),
\end{aligned}
\tag{14}
$$

where

$$
\begin{aligned}
\widetilde{A}_1(i+1,j) &= \overline{A}_1(i+1,j) - L(i+1,j+1)\overline{C}(i+1,j+1)\overline{A}_1(i+1,j), \\
\widetilde{A}_2(i,j+1) &= \overline{A}_2(i,j+1) - L(i+1,j+1)\overline{C}(i+1,j+1)\overline{A}_2(i,j+1), \\
\widetilde{F}_1(i+1,j) &= \overline{F}_1(i+1,j) - L(i+1,j+1)\overline{C}(i+1,j+1)\overline{F}_1(i+1,j), \\
\widetilde{F}_2(i,j+1) &= \overline{F}_2(i,j+1) - L(i+1,j+1)\overline{C}(i+1,j+1)\overline{F}_2(i,j+1), \\
\widetilde{B}_1(i+1,j) &= \overline{B}_1(i+1,j) - L(i+1,j+1)\overline{C}(i+1,j+1)\overline{B}_1(i+1,j), \\
\widetilde{B}_2(i,j+1) &= \overline{B}_2(i,j+1) - L(i+1,j+1)\overline{C}(i+1,j+1)\overline{B}_2(i,j+1), \\
\widetilde{f}(Pe(i+1,j)) &= \overline{f}(P\eta(i+1,j)) - \overline{f}(P\widehat{\eta}(i+1,j)), \\
\widetilde{f}(Pe(i,j+1)) &= \overline{f}(P\eta(i,j+1)) - \overline{f}(P\widehat{\eta}(i,j+1)).
\end{aligned}
$$

Before proceeding further, let us introduce the following Definition, Assumption, and Lemmas, which will be helpful in subsequent developments.

Assumption 2. The initial states of the 2-D system (11) are located inside the given set of ellipsoids:

$$
\begin{aligned}
&(\eta(i,0) - \widehat{\eta}(i,0))^T P^{-1}(i,0)(\eta(i,0) - \widehat{\eta}(i,0)) \\
&\leq 1, (\eta(0,j) - \widehat{\eta}(0,j))^T P^{-1}(0,j)(\overline{x}(0,j) - \widehat{x}(0,j)) \leq 1,
\end{aligned}
$$

where $P(i,0)$ and $P(0,j)$ are given positive definite matrices.

Definition 1. [40]: For the 2-D system (11) and the proposed filters (12) and (13), the given sequence of constrained positive matrices $P(i,j) \in R^{(n_x+n_y) \times (n_x+n_y)}$, the dynamic filtering error $e(i,j)$ is said to satisfy the $P(i,j)$-dependent ellipsoidal constraint if the following inequality:

$$
e^T(i,j)P^{-1}(i,j)e(i,j) \leq 1
$$

holds for $i,j \in [0,\kappa]$.

Lemma 1. [47] (Suarze, 1989): (Principle of Double Induction) Let us suppose that for $i,j \in [0,\kappa]$, $\Omega(i,j)$ is a proposition. If we want to prove that each of propositions $\Omega(i,j)$ is true, it is sufficient to exhibit a generative set, with molecules $\Omega_{(i-1,j)}$, $\Omega_{(i,j-1)}$, and initial set $I = \{(i,0) : i \in [0,\kappa]\} \cup \{(0,j) : j \in [0,\kappa]\}$ for which:

1. (**initial step**) $\Omega(i,j)$ is true for all $(i,j) \in I$;
2. (**inductive step**) if $\Omega_{(i-1,j)}$ and $\Omega_{(i,j-1)}$ are true for all $\{(i-1,j),(i,j-1)\} \in \mathbb{Q}$, which yields that $\Omega(i,j)$ is true.

Then, $\Omega(i,j)$ is true for all $i,j \in [0,\kappa]$.

Lemma 2. [42]: (S-procedure) Let $\Upsilon_0, \Upsilon_1, ..., \Upsilon_n \in R^{n \times n}$ be symmetric matrices. $\Upsilon_0, \Upsilon_1, ..., \Upsilon_n$ are assumed to satisfy the following conditions: $\psi^T \Upsilon_0 \psi > 0$ for all $\psi \in R^n, (\psi \neq 0)$ such that $\psi^T \Upsilon_\mu \psi \geq 0$, $\mu = 1, 2, ..., n$. Note that if exist positive scalars $\tau_1 \geq 0, \tau_2 \geq 0, ..., \tau_n \geq 0$ such that $\Upsilon_0 - \sum_{\mu=1}^n \tau_\mu \Upsilon_\mu > 0$. Then, $\psi^T \Upsilon_0 \psi > 0$ holds.

Now, we are in the position of analyzing the dynamic FES (14) under the FRP and HCAs.

3 | MAIN RESULTS

3.1 | $P(i,j)$-dependent constraint analysis

The recursive set-membership filter design for the augmented 2-D system (11) is accomplished by solving the following problems:

1. Deduce the sufficient conditions that can guarantee the dynamic FES (14) inside the ellipsoidal set as follows:

$$\mathscr{H}(i,j) \triangleq \left\{ e(i,j) \mid e^T(i,j)P^{-1}(i,j)e(i,j) \leq 1 \right\}.$$

2. Compute the set-membership filter gains $K(i,j)$ by optimizing the trace of the matrix $P(i,j)$ to minimize the ellipsoid size for the dynamic filtering error $e(i,j)$.

Theorem 1. For the given sequence of constraint matrices $P(i,0)$, $P(0,j)$ for all $(j = 0, i \in [0,\kappa]$ or $i = 0, j \in [0,\kappa])$ and the initial conditions $x(i,0)$ and $x(0,j)$, considering 2-D system (11) under FRP (4) and HCAs (10), as well as set-membership filter (12) and (13), if there exist positive scalars $\rho_\gamma(i,j)$ $(\gamma = 1, 2, ..., 10)$, $\mu_\sigma(\pi(i+1,j))$ $(\sigma = l_2+1, l_2+2, ...n_y)$, $\mu_\sigma(\pi(i,j+1))$, $(\sigma = l_2+1, l_2+2, ..., n_y)$, and filter gains $K(i+1,j+1)$ satisfying the following RLMI:

$$\begin{bmatrix} -\overline{\Lambda}(i,j) - \widetilde{\Lambda}(i,j) & \Lambda^T(i,j) \\ * & -P(i+1,j+1) \end{bmatrix} \leq 0, i,j \in [0,\kappa], \quad (15)$$

where

$$\overline{\Lambda}(i,j) = \Gamma_0 + \sum_{\gamma=1}^{10} \rho_\gamma(i,j)\Gamma_\gamma,$$

$$\widetilde{\Lambda}(i,j) = \sum_{\sigma=l_2+1}^{n_y} \mu_\sigma(\pi(i+1,j))\overline{\Upsilon}^T(i,j)\left(\overline{\Phi}_\sigma - \overline{\Phi}_{\pi(i+1,j)}\right)\overline{\Upsilon}(i,j)$$
$$+ \sum_{\sigma=l_2+1}^{n_y} \mu_\sigma(\pi(i,j+1))\widetilde{\Upsilon}^T(i,j)\left(\overline{\Phi}_\sigma - \overline{\Phi}_{\pi(i,j+1)}\right)\widetilde{\Upsilon}(i,j),$$

$$\Gamma_0 = diag\{1,0,0,0,0,0,0,0,0,0,0,0\},$$
$$\Gamma_1(i,j) = diag\{-1,0,0,0,0,S^{-1}(i+1,j),0,0,0,0,0,0\},$$
$$\Gamma_2(i,j) = diag\{-1,0,0,0,0,0,S^{-1}(i,j+1),0,0,0,0,0\},$$
$$\Gamma_3(i,j) = diag\{-1,0,0,0,0,0,0,R^{-1}(i+1,j),0,0,0,0\},$$
$$\Gamma_4(i,j) = diag\{-1,0,0,0,0,0,0,0,R^{-1}(i,j+1),0,0\},$$
$$\Gamma_5(i,j) = diag\{-1,0,0,0,0,0,0,0,0,R^{-1}(i+1,j+1),0\},$$
$$\Gamma_6(i,j) = diag\{-1,0,0,0,0,0,0,0,0,0,\overline{\nu}^{-1}\},$$

$$\Gamma_7 = \begin{bmatrix} 0 & 0 & 0 & 0 & 0 & 0 \\ 0 & L^T(i+1,j)P^T\dfrac{\mathscr{M}_1^T\mathscr{M}_2+\mathscr{M}_2^T\mathscr{M}_1}{2}PL(i+1,j) & 0 & -L^T(i+1,j)P^T\dfrac{\mathscr{M}_1^T+\mathscr{M}_2^T}{2} & 0 & 0 \\ 0 & 0 & 0 & 0 & 0 & 0 \\ 0 & -\dfrac{\mathscr{M}_1+\mathscr{M}_2}{2}PL(i+1,j) & 0 & I & 0 & 0 \\ 0 & 0 & 0 & 0 & 0 & 0 \\ 0 & 0 & 0 & 0 & 0 & 0 \end{bmatrix},$$

$$\Gamma_8 = \begin{bmatrix} 0 & 0 & 0 & 0 & 0 & 0 \\ 0 & 0 & 0 & 0 & 0 & 0 \\ 0 & 0 & L^T(i,j+1)P^T\dfrac{\mathscr{M}_1^T\mathscr{M}_2+\mathscr{M}_2^T\mathscr{M}_1}{2}PL(i,j+1) & 0 & -L^T(i,j+1)P^T\dfrac{\mathscr{M}_1^T+\mathscr{M}_2^T}{2} & 0 \\ 0 & 0 & 0 & 0 & 0 & 0 \\ 0 & 0 & -\dfrac{\mathscr{M}_1+\mathscr{M}_2}{2}PL(i,j+1) & 0 & I & 0 \\ 0 & 0 & 0 & 0 & 0 & 0 \end{bmatrix},$$

$\mathcal{M}_1 = diag\{G_1(i,j),0,0\}, \mathcal{M}_2 = diag\{G_2(i,j),0,0\}$,

$\Gamma_9 = diag\{-1,I,0,0,0,0,0,0,0,0,0\}$,

$\Gamma_{10} = diag\{-1,0,I,0,0,0,0,0,0,0,0\}$,

$\Lambda(i,j) = [\Lambda_1(i,j) \quad \Lambda_2(i,j)], \Lambda_1(i,j) \equiv [1 \ \widetilde{A}_1(i+1,j)L(i+1,j)$

$\widetilde{A}_2(i,j+1)L(i,j+1) \quad \widetilde{F}_1(i+1,j) \quad \widetilde{F}_2(i,j+1)]^T$,

$\Lambda_2(i,j) \equiv [\widetilde{B}_1(i+1,j) \quad \widetilde{B}_2(i,j+1) \quad -K(i+1,j+1)\widetilde{D}(i+1,j+1)$

$-K(i+1,j+1)\varpi_2(i+1,j+1)]^T$,

$\widetilde{D}(i+1,j+1) = [0 \ \ 0 \ \ D(i+1,j+1)], \overline{\Phi}_{\pi(i,j)} = \widetilde{\Phi}\Pi_{\pi(i,j)}$,

$\widetilde{\Phi} = diag\{\widetilde{\Phi}_{l_2+1}, \widetilde{\Phi}_{l_2+2}, ..., \widetilde{\Phi}_{n_y}\}, \overline{\Phi}_\sigma = \widetilde{\Phi}\Pi_\sigma$,

$\overline{\Upsilon}(i,j) = [\widetilde{C}(i+1,j)\widehat{\eta}(i+1,j) \quad \widetilde{C}(i+1,j)L(i+1,j) \ \ 0 \ \ 0 \ \ \overline{\mathcal{P}}(i,j) \ \ 0]$,

$\overline{L}(i,j) = [L(i+1,j) \ \ 0], \overline{\mathcal{P}}(i,j) = [D^{[2]}(i+1,j+1) \ \ 0 \ \ 0]$,

$\widetilde{C}(i,j) = [C^{[2]}(i,j) \ \ 0 \ \ -I], \widetilde{\mathcal{P}}(i,j) = [0 \ \ D^{[2]}(i+1,j+1) \ \ 0]$,

$\widetilde{\Upsilon}(i,j) = [\widetilde{C}(i,j+1)\widehat{\eta}(i,j+1) \quad \widetilde{C}(i,j+1)\widetilde{L}(i,j) \ \ 0 \ \ 0 \ \ \widetilde{\mathcal{P}}(i,j) \ \ 0]$,

$\widetilde{L}(i,j) = [0 \ \ L(i,j+1)]$.

Then, the dynamic FES (14) satisfy $P(i,j)$-dependent ellipsoidal constraint for all $i,j \in \mathbb{Q}$:

$$e^T(i,j)P^{-1}(i,j)e(i,j) \le 1.$$

Proof. In what follows, the mathematical induction, including the initial step and induction step, is employed to prove Theorem 1.

1. ***Initial step.*** For the initial set $I = \{(i,0) : i \in [0,\kappa]\} \cup \{(0,j) : j \in [0,\kappa]\}$, based on Assumption 2, it can be immediately inferred that $e^T(i,0)P^{-1}(i,0)e(i,0) \le 1$ and $e^T(0,j)P^{-1}(0,j)e(0,j) \le 1$.

2. ***Inductive step.*** Suppose the initial states $x(i,0)$, $x(0,j)$, $\widehat{x}(i,0)$, and $\widehat{x}(0,j)$ satisfy $P(i,j)$-dependent constraint, then the immediate target would be to demonstrate that

$$e^T(i+1,j+1)P^{-1}(i+1,j+1)e(i+1,j+1) \le 1, \quad (16)$$

to be true at $(i+1,j+1)$ on the basis of the following inequality constraints hold at $(i,j+1)$ and $(i+1,j)$:

$$e^T(i,j+1)P^{-1}(i,j+1)$$

$e(i,j+1) \le 1$ and $e^T(i+1,j)P^{-1}(i+1,j) \ e(i+1,j) \le 1$. ∎

To facilitate succeeding analysis, the $e^T(i+1,j+1)P^{-1}(i+1,j+1)e(i+1,j+1) - 1 \le 0$ can be rewritten as:

$r^T(i+1,j+1)L^T(i+1,j+1)P^{-1}(i+1,j+1)$

$L(i+1,j+1)r(i+1,j+1) - 1 \le 0$,

where $e(i,j) = L(i,j)r(i,j)$, and $L(i,j)$ is a factorization of $P(i,j) = L(i,j)L^T(i,j)$, obviously, if $\|r(i,j)\| \le 1$ holds for all $i,j \in \mathbb{Q}$, the following inequality constraint holds:

$$e^T(i+1,j+1)P^{-1}(i+1,j+1)e(i+1,j+1) - 1 \le 0.$$

Subsequently, we deduce sufficient conditions for the $e^T(i+1,j+1)P^{-1}(i+1,j+1)e(i+1,j+1) \le 1$ under the impact of nonlinear function (2), FRP (4), and HCAs (10).

To simplify the derivation, let us define:

$$\xi(i,j) \equiv [1 \ \overline{r}^T(i,j) \ \overline{f}^T(Pe(i,j)) \ \overline{\omega}^T(i,j) \ \overline{v}(i,j) \ v(i+1,j+1)]^T,$$

$$\overline{r}(i,j) = \begin{bmatrix} r(i+1,j) \\ r(i,j+1) \end{bmatrix}, \widehat{f}(Pe(i,j)) = \begin{bmatrix} \widetilde{f}(Pe(i+1,j)) \\ \widetilde{f}(Pe(i,j+1)) \end{bmatrix},$$

$$\overline{\omega}(i,j) = \begin{bmatrix} \omega(i+1,j) \\ \omega(i,j+1) \end{bmatrix}, \overline{v}(i,j) = \begin{bmatrix} v(i+1,j) \\ v(i,j+1) \\ v(i+1,j+1) \end{bmatrix},$$

$$\Lambda(i,j) = [\Lambda_1(i,j) \quad \Lambda_2(i,j)],$$

$$\Lambda_1(i,j) \equiv [1 \ \widetilde{A}_1(i+1,j)L(i+1,j) \quad \widetilde{A}_2(i,j+1)L(i,j+1)$$

$$\widetilde{F}_1(i+1,j) \quad \widetilde{F}_2(i,j+1)]^T,$$

$$\Lambda_2(i,j) \equiv [\widetilde{B}_1(i+1,j) \quad \widetilde{B}_2(i,j+1) - K(i+1,j+1)\widetilde{D}(i+1,j+1)$$

$$-K(i+1,j+1)\varpi_2(i+1,j+1)]^T,$$

$$\widetilde{D}(i+1,j+1) = [0 \ \ 0 \ \ D(i+1,j+1)].$$

Furthermore, in view of the dynamic FES (14), one has

$$e(i+1,j+1) = \Lambda(i,j)\xi(i,j), \quad (17)$$

combining (16) with (17), which yields

$$e^T(i+1,j+1)P^{-1}(i+1,j+1)e(i+1,j+1) - 1$$
$$= \xi^T(i,j)\Lambda^T(i,j)P^{-1}(i+1,j+1)\Lambda(i,j)\xi(i,j) \quad (18)$$
$$- \xi^T(i,j)diag\{1,0,0,0,0,0,0,0,0,0,0\}\xi(i,j).$$

Next, we will address the unknown-but-bounded noises and FDI attacks energy limitation, from Assumption 1 and (9), it is easy to obtain

$$\begin{cases} \omega^T(i+1,j)S^{-1}(i+1,j)\omega(i+1,j) \le 1 \\ \omega^T(i,j+1)S^{-1}(i,j+1)\omega(i,j+1) \le 1 \\ v^T(i+1,j)R^{-1}(i+1,j)v(i+1,j) \le 1 \\ v^T(i,j+1)R^{-1}(i,j+1)v(i,j+1) \le 1 \\ v^T(i+1,j+1)R^{-1}(i+1,j+1)v(i+1,j+1) \le 1 \\ v^T(i+1,j+1)\overline{v}^{-1}v(i+1,j+1) \le 1 \end{cases},$$

which are further rewritten as follows:

$$\begin{cases} \xi^T(i,j)\Gamma_1(i,j)\xi(i,j) \le 1 \\ \xi^T(i,j)\Gamma_2(i,j)\xi(i,j) \le 1 \\ \xi^T(i,j)\Gamma_3(i,j)\xi(i,j) \le 1 \\ \xi^T(i,j)\Gamma_4(i,j)\xi(i,j) \le 1 \\ \xi^T(i,j)\Gamma_5(i,j)\xi(i,j) \le 1 \\ \xi^T(i,j)\Gamma_6(i,j)\xi(i,j) \le 1 \end{cases}, \qquad (19)$$

where $\Gamma_1(i,j) = diag\{-1,0,0,0,0,S^{-1}(i+1,j),0,0,0,0,0\}$,
$\Gamma_2(i,j) = diag\{-1,0,0,0,0,0,S^{-1}(i,j+1),0,0,0,0\}$,

$\Gamma_3(i,j) = diag\{-1,0,0,0,0,0,0,R^{-1}(i+1,j),0,0,0\}$,

$\Gamma_4(i,j) = diag\{-1,0,0,0,0,0,0,0,R^{-1}(i,j+1),0,0\}$,

$\Gamma_5(i,j) = diag\{-1,0,0,0,0,0,0,0,0,R^{-1}(i+1,j+1),0\}$,

$\Gamma_6(i,j) = diag\{-1,0,0,0,0,0,0,0,0,0,\overline{v}^{-1}\}$.

$$\Gamma_7 = \begin{bmatrix} 0 & 0 & 0 & 0 & 0 & 0 \\ 0 & L^T(i+1,j)P^T\dfrac{\mathcal{M}_1^T\mathcal{M}_2 + \mathcal{M}_2^T\mathcal{M}_1}{2}PL(i+1,j) & 0 & -L^T(i+1,j)P^T\dfrac{\mathcal{M}_1^T + \mathcal{M}_2^T}{2} & 0 & 0 \\ 0 & 0 & 0 & 0 & 0 & 0 \\ 0 & -\dfrac{\mathcal{M}_1 + \mathcal{M}_2}{2}PL(i+1,j) & 0 & I & 0 & 0 \\ 0 & 0 & 0 & 0 & 0 & 0 \\ 0 & 0 & 0 & 0 & 0 & 0 \end{bmatrix}.$$

Subsequently, the sector-bounded conditions of nonlinear function (2) are taken into account. From (2), which yields

$$\left(\widetilde{f}(Pe(i+1,j)) - \mathcal{M}_1Pe(i+1,j)\right)^T\left(\widetilde{f}(Pe(i+1,j)) - \mathcal{M}_2Pe(i+1,j)\right) \le 0, \qquad (20)$$

where $\mathcal{M}_1 = diag\{G_1(i,j),0,0\}$, $\mathcal{M}_2 = diag\{G_2(i,j),0,0\}$.

Obviously, (20) can be reorganized into the following inequality:

$$\frac{1}{2}\left(\widetilde{f}(Pe(i+1,j)) - \mathcal{M}_1Pe(i+1,j)\right)^T\left(\widetilde{f}(Pe(i+1,j)) - \mathcal{M}_2Pe(i+1,j)\right)$$
$$+\frac{1}{2}\left(\widetilde{f}(Pe(i+1,j)) - \mathcal{M}_2Pe(i+1,j)\right)^T\left(\widetilde{f}(Pe(i+1,j)) - \mathcal{M}_1Pe(i+1,j)\right) \le 0. \qquad (21)$$

Furthermore, one can reorganize (21) into the following inequality:

$$\widetilde{f}^T(Pe(i+1,j))\widetilde{f}(Pe(i+1,j)) - r^T(i+1,j)L^T(i+1,j)$$
$$P^T\frac{\mathcal{M}_1^T + \mathcal{M}_2^T}{2}\widetilde{f}(Pe(i+1,j)) - \widetilde{f}^T(Pe(i+1,j))\frac{\mathcal{M}_1 + \mathcal{M}_2}{2}PL(i+1,j)r(i+1,j)$$
$$+r^T(i+1,j)L^T(i+1,j)P^T\frac{\mathcal{M}_1^T\mathcal{M}_2 + \mathcal{M}_2^T\mathcal{M}_1}{2}PL(i+1,j)r(i+1,j) \le 0, \qquad (22)$$

accordingly, it can be obtained that (22) is equivalent to

$$\xi^T(i,j)\Gamma_7\xi(i,j) \le 0, \qquad (23)$$

where

Similarly, it can be readily obtained that the following inequality holds true at instant $(i,j+1)$

$$\xi^T(i,j)\Gamma_8\xi(i,j) \le 0, \qquad (24)$$

where

$$\Gamma_8 = \begin{bmatrix} 0 & 0 & 0 & 0 & 0 & 0 \\ 0 & 0 & 0 & 0 & 0 & 0 \\ 0 & 0 & L^T(i,j+1)P^T\dfrac{\mathscr{M}_1^T\mathscr{M}_2+\mathscr{M}_2^T\mathscr{M}_1}{2}PL(i,j+1) & 0 & -L^T(i,j+1)P^T\dfrac{\mathscr{M}_1^T+\mathscr{M}_2^T}{2} & 0 \\ 0 & 0 & 0 & 0 & 0 & 0 \\ 0 & 0 & -\dfrac{\mathscr{M}_1+\mathscr{M}_2}{2}PL(i,j+1) & 0 & I & 0 \\ 0 & 0 & 0 & 0 & 0 & 0 \end{bmatrix}.$$

In addition, the constraints $\|r(i+1,j)\| \le 1$ and $\|r(i,j+1)\| \le 1$ for $i,j \in \mathbb{Q}$ also need to be highlighted, which implies that the following inequalities hold:

$$\xi^T(i,j)\Gamma_9\xi(i,j) \le 1 \text{ and } \xi^T(i,j)\Gamma_{10}\xi(i,j) \le 1, \qquad (25)$$

where $\Gamma_9 = diag\{-1, I, 0, 0, 0, 0, 0, 0, 0, 0, 0\}$, $\Gamma_{10} = diag\{-1, 0, I, 0, 0, 0, 0, 0, 0, 0, 0\}$.

Moreover, noting the constraints of the TODP for arbitrary $\sigma \in \iota_2$ and shift instant $(i+1,j)$, the following inequality holds:

$$\left(y^{[2]}(i+1,j) - y^{[2]^*}(i+1,j)\right)^T \overline{\Phi}_{\pi(i+1,j)}\left(y^{[2]}(i+1,j) - y^{[2]^*}(i+1,j)\right)$$
$$\ge \left(y^{[2]}(i+1,j) - y^{[2]^*}(i+1,j)\right)^T \overline{\Phi}_\sigma\left(y^{[2]}(i+1,j) - y^{[2]^*}(i+1,j)\right). \qquad (26)$$

On the other hand, as per the scheduling rule of the TODP, it is straightforward to obtain

$$y^{[2]}(i+1,j) - y^{[2]^*}(i+1,j)$$
$$= y^{[2]}(i+1,j) - \overline{y}^{[2]}(i+1,j-1)$$
$$= C^{[2]}(i+1,j)x(i+1,j) + D^{[2]}(i+1,j)v(i+1,j)$$
$$\quad - \overline{y}^{[2]}(i+1,j-1)$$
$$= \widetilde{C}(i+1,j)\eta(i+1,j) + D^{[2]}(i+1,j)v(i+1,j)$$
$$= \widetilde{C}(i+1,j)e(i+1,j) + \widetilde{C}(i+1,j)\widehat{\eta}(i+1,j)$$
$$\quad + D^{[2]}(i+1,j)v(i+1,j), \qquad (27)$$

where $\widetilde{C}(i,j) = \begin{bmatrix} C^{[2]}(i,j) & 0 & -I \end{bmatrix}$. Then, considering (26) and (27), the constraints of the TODP can be further deduced that

$$\left(\widetilde{C}(i+1,j)e(i+1,j) + \widetilde{C}(i+1,j)\widehat{\eta}(i+1,j) + D^{[2]}(i+1,j)v(i+1,j)\right)^T$$
$$\left(\overline{\Phi}_\sigma - \overline{\Phi}_{\pi(i+1,j)}\right)$$
$$\times \left(\widetilde{C}(i+1,j)e(i+1,j) + \widetilde{C}(i+1,j)\widehat{\eta}(i+1,j) + D^{[2]}(i+1,j)v(i+1,j)\right) \le 0, \qquad (28)$$

where $\overline{\Phi}_{\pi(i,j)} = \widetilde{\Phi}\Pi_{\pi(i,j)}, \widetilde{\Phi} = diag\left\{\widetilde{\Phi}_{l_2+1}, \widetilde{\Phi}_{l_2+2}, ..., \widetilde{\Phi}_{n_y}\right\}$, $\overline{\Phi}_\sigma = \widetilde{\Phi}\Pi_\sigma$. From (28), it is easy to obtain that

$$\xi^T(i,j)\overline{\Upsilon}^T(i,j)\left(\overline{\Phi}_\sigma - \overline{\Phi}_{\pi(i+1,j)}\right)\overline{\Upsilon}(i,j)\xi(i,j) \le 0, \qquad (29)$$

where $\overline{\Upsilon}(i,j) = \begin{bmatrix} \widetilde{C}(i+1,j)\widehat{\eta}(i+1,j) & \widetilde{C}(i+1,j) & L(i+1,j) \\ 0 & 0 & \overline{\mathcal{P}}(i,j) & 0 \end{bmatrix}$, $\overline{L}(i,j) = [L(i+1,j) \quad 0]$, $\overline{\mathcal{P}}(i,j) = \begin{bmatrix} D^{[2]}(i,j+1)0 & 0 \end{bmatrix}$.

Similarly, for arbitrary $\sigma \in \iota_2$ and shift instant $(i,j+1)$, one has

$$\xi^T(i,j)\widetilde{\Upsilon}^T(i,j)\left(\overline{\Phi}_\sigma - \overline{\Phi}_{\pi(i,j+1)}\right)\widetilde{\Upsilon}(i,j)\xi(i,j) \le 0, \qquad (30)$$

where $\widetilde{\Upsilon}(i,j) = \begin{bmatrix} \widetilde{C}(i,j+1) & \widehat{\eta}(i,j+1) & \widetilde{C}(i,j+1) \\ \widetilde{L}(i,j) & 0 & 0 & \widetilde{\mathcal{P}}(i,j) & 0 \end{bmatrix}$, $\widetilde{L}(i,j) = \begin{bmatrix} 0 & L(i,j+1) \end{bmatrix}$, $\widetilde{\mathcal{P}}(i,j) = \begin{bmatrix} 0 & D^{[2]}(i+1,j+1)0 \end{bmatrix}$.

Furthermore, comprehensive consideration of (18), (19), (23)–(25), (29), and (30), if there exist the $\rho_\gamma(i,j)$ $(i = 1, 2, ..., 10)$, $\mu_\sigma(\pi(i+1,j))$ $(\sigma = l_2+1, l_2+2, ..., n_y)$, and $\mu_\sigma(\pi(i,j+1))$ $(\sigma = l_2+1, l_2+2, ..., n_y)$, such that the following inequality holds:

$$\xi^T(i,j)\Lambda^T(i,j)P^{-1}(i+1,j+1)\Lambda(i,j)\xi(i,j)$$
$$- \xi^T(i,j)\overline{\Lambda}(i,j)\xi(i,j) - \xi^T(i,j)\widetilde{\Lambda}(i,j)\xi(i,j) \le 0, \qquad (31)$$

where

$$\overline{\Lambda}(i,j) = \Gamma_0 + \sum_{\gamma=1}^{10} \rho_\gamma(i,j)\Gamma_\gamma, \Gamma_0$$
$$= diag\{1,0,0,0,0,0,0,0,0,0,0\},$$

$$\widetilde{\Lambda}(i,j) = \sum_{\sigma=l_2+1}^{n_y} \mu_\sigma(\pi(i+1,j))\overline{\Upsilon}^T(i,j)(\overline{\Phi}_\sigma - \overline{\Phi}_{\pi(i+1,j)})\overline{\Upsilon}(i,j)$$
$$+ \sum_{\sigma=l_2+1}^{n_y} \mu_\sigma(\pi(i,j+1))\widetilde{\Upsilon}^T(i,j)(\overline{\Phi}_\sigma - \overline{\Phi}_{\pi(i,j+1)})\widetilde{\Upsilon}(i,j),$$

then, according to Lemma 2, it can be derived that

$$\Lambda^T(i,j)P^{-1}(i+1,j+1)\Lambda(i,j)$$
$$- diag\{1,0,0,0,0,0,0,0,0,0,0\} \le 0. \quad (32)$$

In view of (18), the inequality (32) is a sufficient condition to guarantee that the $P(i+1,j+1)$-dependent constraint $e^T(i+1,j+1)P^{-1}(i+1,j+1)e(i+1,j+1) - 1 \le 0$ to be true. By applying the Schur complement, (31) is equivalent to

$$\begin{bmatrix} -\overline{\Lambda}(i,j) - \widetilde{\Lambda}(i,j) & \Lambda^T(i,j) \\ * & -P(i+1,j+1) \end{bmatrix} \le 0, i,j \in \mathbb{Q}.$$

The proof is thus completed.

In Theorem 1, sufficient conditions are deduced such that the FES (14) to satisfy $P(i,j)$-dependent constraints, and the filter gains $K(i,j)$ at each shift instant (i,j) have been acquired by utilizing the RLMIs technology. On account of $P(i,j)$-dependent constraint, $e^T(i,j)P^{-1}(i,j)e(i,j) - 1 \le 0$ is equivalent to $e(i,j)e^T(i,j) \le P(i,j)$; hence, the minimize dynamic filtering error $e(i,j)$ can be obtained by calculating the minimization problem of $P(i,j)$.

3.2 | Optimization problem

Corollary 1. For the given sequence of constraint matrices $P(i,0)$, $P(0,j)(j=0,i \in [0,\kappa]$ or $i=0,j \in [0,\kappa])$ and the initial conditions $x(i,0)$ and $x(0,j)$, considering 2-D system (11) under FRP (4) and HCAs (10), as well as set-membership filter (12) and (13), if there exist positive scalars $\rho_\gamma(i,j)(i=1,2,...,10)$, $\mu_\sigma(\pi(i+1,j) \quad (\sigma=l_2+1,l_2+2,...,n_y)$, $\mu_\sigma(\pi(i,j+1)) \quad (\sigma=l_2+1,l_2+2,...,n_y)$, and filter gains $K(i+1,j+1)$, we can solve the following optimization problem:

$$\mathbf{OP}: \min_{K(i+1,j+1)} tr\{P(i+1,j+1)\} \quad (33)$$

subject to (15). Then, the dynamic filtering error $e(i,j)$ will be minimized at each instant $(i,j).K(i,j)$

In terms of Theorem 1 and Corollary 1, we summarize the recursive set-membership filtering algorithm as follows:

Algorithm 1 Recursive Set-membership Filtering Algorithm for 2-D Systems under FRP and HCAs

Step 1: Set the initial conditions $x(i,0)$, $x(0,j)$, $\hat{x}(i,0)$, $\hat{x}(0,j)$, $P(i,0)$, $P(0,j)$, $S(i,j)$ and $R(i,j)$ satisfying Assumption 1 and Assumption 2 for $j=0$, $i \in [0,\kappa]$ or $i=0$, $j \in [0,\kappa]$.

Step 2: For $i=[0,\kappa]$ and $j=0$, calculate $K(i,0)$ from (15) and (33).

Step 3: For $j=[1,\kappa]$ and $i=0$, calculate $K(0,j)$ from (15) and (33).

Step 4: For $i=1:\kappa$
      For $j=1:\kappa$
        calculate $K(i,j)$, $P(i,j)$ and $\hat{x}(i,j)$
        from (15) and (33)
      end
    end

Step 5: Stop.

---

4 | NUMERICAL SIMULATION

The following equations can be utilized to represent the relationship between voltage $\mathcal{U}(x,t)$ and current $\mathcal{I}(x,t)$ in the long-distance transmission line system depicted in Figure 3.

$$\frac{\partial \mathcal{U}(x,t)}{\partial x} = -\mathscr{L}\frac{\partial \mathcal{I}(x,t)}{\partial t}, \frac{\partial \mathcal{I}(x,t)}{\partial x} = \mathcal{C}\frac{\partial \mathcal{U}(x,t)}{\partial t}, \quad (34)$$

where $x \in [0 \ X]$ and $t \in [0 \ T]$ denote the spatial dimension and the time dimension, respectively. In addition, the parameters $\mathscr{L}$ and $\mathcal{C}$ with are used to represent inductance and capacitance, respectively.

Then, let us define

FIGURE 3 The long-distance transmission line system.
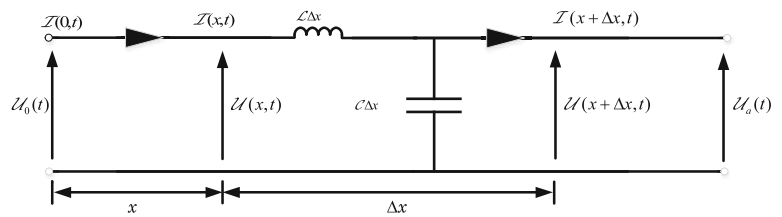
$$\begin{bmatrix} \overline{\mathcal{U}}(x,t) \\ \overline{\mathcal{I}}(x,t) \end{bmatrix} = \begin{bmatrix} 1 & \sqrt{\dfrac{\mathscr{L}}{\mathcal{C}}} \\ \sqrt{\dfrac{\mathcal{C}}{\mathscr{L}}} & -1 \end{bmatrix} \begin{bmatrix} \mathcal{U}(x,t) \\ \mathcal{I}(x,t) \end{bmatrix},$$

considering (34), one has

$$\frac{\partial}{\partial t} \begin{bmatrix} \overline{\mathcal{U}}(x,t) \\ \overline{\mathcal{I}}(x,t) \end{bmatrix} = \begin{bmatrix} \dfrac{1}{\sqrt{\mathscr{L}\mathcal{C}}} & 0 \\ 0 & -\dfrac{1}{\sqrt{\mathscr{L}\mathcal{C}}} \end{bmatrix} \frac{\partial}{\partial x} \begin{bmatrix} \overline{\mathcal{U}}(x,t) \\ \overline{\mathcal{I}}(x,t) \end{bmatrix}, \qquad (35)$$

furthermore, we define $\overline{\mathcal{U}}(x,t) \triangleq \mathcal{U}_e(i\Delta x, j\Delta t)$, $\overline{\mathcal{I}}(x,t) \triangleq \mathcal{I}_e(i\Delta x, j\Delta t)$, $\overline{\mathcal{U}}(x,t) \approx \overline{\mathcal{U}}_e(i,j)$, and $\overline{\mathcal{I}}(x,t) \approx \overline{\mathcal{I}}_e(i,j)$, one has

$$\frac{\partial \overline{\mathcal{U}}(x,t)}{\partial x} \approx \frac{\mathcal{U}_e(i\Delta x, j\Delta t) - \mathcal{U}_e((i-1)\Delta x, j\Delta t)}{\Delta x}, \qquad (36)$$

$$\frac{\partial \overline{\mathcal{U}}(x,t)}{\partial t} \approx \frac{\mathcal{U}_e(i\Delta x, (j+1)\Delta t) - \mathcal{U}_e(i\Delta x, j\Delta t)}{\Delta t},$$

$$\frac{\partial \overline{\mathcal{I}}(x,t)}{\partial x} \approx \frac{\mathcal{I}_e(i\Delta x, j\Delta t) - \mathcal{I}_e((i-1)\Delta x, j\Delta t)}{\Delta x}, \qquad (37)$$

$$\frac{\partial \overline{\mathcal{I}}(x,t)}{\partial t} \approx \frac{\mathcal{I}_e(i\Delta x, (j+1)\Delta t) - \mathcal{I}_e(i\Delta x, j\Delta t)}{\Delta t},$$

therefore, according to (35)–(37), it is easy to obtain (38) holds

$$\begin{cases} \mathcal{U}_e(i,j+1) = \left(1 + \dfrac{\Delta t}{\Delta x}\dfrac{1}{\sqrt{\mathscr{L}\mathcal{C}}}\right)\mathcal{U}_e(i,j) - \dfrac{\Delta t}{\Delta x}\dfrac{1}{\sqrt{\mathscr{L}\mathcal{C}}}\mathcal{U}_e(i-1,j) \\ \mathcal{I}_e(i,j+1) = \left(1 - \dfrac{\Delta t}{\Delta x}\dfrac{1}{\sqrt{\mathscr{L}\mathcal{C}}}\right)\mathcal{I}_e(i,j) + \dfrac{\Delta t}{\Delta x}\dfrac{1}{\sqrt{\mathscr{L}\mathcal{C}}}\mathcal{I}_e(i-1,j) \end{cases}, \qquad (38)$$

then define $x_e^h(i,j) = [\mathcal{U}_e(i-1,j)\ \ \mathcal{I}_e(i-1,j)]^T$, $x_e^v(i,j) = [\mathcal{U}_e(i,\ j)\ \mathcal{I}_e(i,j)]^T$, and $x(i,j) = [x_e^h(i-1,j)\ \ x_e^v(i-1,j)]^T$, based on (38), which yields

$$x(i+1,j+1) = A_1 x(i+1,j) + A_2 x(i,j+1),$$

where

$$A_1 = \begin{bmatrix} 0 & 0 & 0 & 0 \\ 0 & 0 & 0 & 0 \\ -\dfrac{\Delta t}{\Delta x}\dfrac{1}{\sqrt{LC}} & 0 & 1+\dfrac{\Delta t}{\Delta x}\dfrac{1}{\sqrt{LC}} & 0 \\ 0 & \dfrac{\Delta t}{\Delta x}\dfrac{1}{\sqrt{LC}} & 0 & 1-\dfrac{\Delta t}{\Delta x}\dfrac{1}{\sqrt{LC}} \end{bmatrix},$$

$$A_1 = \begin{bmatrix} 0 & 0 & 1 & 0 \\ 0 & 0 & 0 & 1 \\ 0 & 0 & 0 & 0 \\ 0 & 0 & 0 & 0 \end{bmatrix}.$$

Then, based on [48], we employ the parameters as follows:

$$\Delta t = 0.02, \Delta x = 0.02, \mathscr{L} = (10 + e^{-i})\mathbb{H}, \mathcal{C} = (40 - \sin(i)\cos(j))\mathbb{F},$$

where $\mathbb{H}$ and $\mathbb{F}$ denote henry (unit of inductance) and farad (unit of capacitance), respectively. The transmission line system can be transformed into a 2-D system (1) with the following parameters:

$$B_1(i+1,j) = \begin{bmatrix} 0.2+0.5\sin(0.3\pi(i+j)) & 0.2 & 0 & 0 \\ 0 & 0.4 & 0.1 & 0 \\ 0.1 & 0 & 0.3 & 0.1 \\ 0 & 0 & 0 & 0.3 \end{bmatrix},$$

$$B_2(i,j+1) = \begin{bmatrix} 0.1+0.4\sin(0.5\pi(i+j)) & 0 & 0.3 & 0.1 \\ 0.1 & 0.5 & 0.1 & 0.2 \\ 0.2 & 0 & 0.3 & 0.1 \\ 0.1 & 0 & 0 & 0.4 \end{bmatrix},$$

$$F_1(i+1,j) = \begin{bmatrix} 0.2 & 0.1 & 0 & 0.1 \\ 0 & 0.3 & 0 & 0.4\sin(0.4\pi(i+j)) \\ 0.2 & 0 & 0 & 0.2\sin(0.5\pi(i+j)) \\ 0 & 0.2 & 0 & 0.3 \end{bmatrix},$$

$$F_2(i,j+1) = \begin{bmatrix} 0.3\sin(0.4\pi(i+j)) & 0.1 & 0 & 0.1 \\ 0 & 0.3 & 0.2 & 0.3 \\ 0.2 & 0.5\sin(0.5\pi(i+j)) & 0 & 0.4 \\ 0 & 0.2 & 0.2 & 0.3 \end{bmatrix},$$

$$C(i,j)=I_4, D(i,j)=\begin{bmatrix} 0.5+\cos(0.3(i+j)) & 0.3 & 0 & 0.5 \\ 0.3+\sin(0.5(i+j)) & 0 & 0.3 & 0.1 \\ 0.6 & & 0.2 & 0.4 & 0.6 \\ 0 & & 0.2 & 0 & 0.5 \end{bmatrix}.$$

Moreover, we set $f(x(i,j))=0.4\sin(-x(i,j))+0.2x(i,j)$ and consider that the $\sin(\cdot)\in[-1\ 1]$, it is easy to observe that the sector-bounded conditions (2) hold with $G_1(i,j)=G_2(i,j)=0.2$. In the simulation, the initial states are taken as $x(i,j)=[3.2\sin(i)\cos(j) \ 3.3\sin(j)\cos(i-1)4.2\sin(i)\cos(j). \ 3.3\sin(j)\cos(i-1)]^T$ for $i\in[0\ 50]$ and $j=0$, $x(i,j)=[4\sin(i)\cos(j)3.5\sin(j)\cos(i)4.2\sin(j)\cos(i).3.1\sin(j)\cos(i+1)]^T$ for $i=0$ and $j\in[1\ 50]$. Moreover, let $P(i,0)=P(0,j)=16I_4$ for $i,j\in[0,50]$.

The unknown-but-bounded process noises $\omega(i,j)$ and measurement noises $\upsilon(i,j)$ are selected as:

$$\omega(i,j)=\begin{cases} [0.5\sin(0.6(i+j)) \ 0.4\cos(0.7(i+j)) \ 0.6\sin(0.9(i+j)) \ 0.6\cos(0.6(i+j))]^T \\ \quad i,j\in[1\ 30] \\ 0 \qquad\qquad\qquad\qquad\qquad otherwise \end{cases},$$

$$\upsilon(i,j)=\begin{cases} [0.3\sin(0.4(i+j)) \ 0.3\cos(0.6(i+j)) \ 0.3\cos(0.7(i+j)) \ 0.3\cos(0.3(i+j))]^T \\ \quad i,j\in[1\ 30] \\ 0 \qquad\qquad\qquad\qquad\qquad otherwise \end{cases},$$

then, the matrix $R(i,j)$ and $S(i,j)$ can be chosen be $1.5I_4$ for $i,j\in[0,50]$.

It is assumed that the first two nodes of the sensors are scheduled via RRP and the remaining nodes are scheduled by TODP, that is, $l_1=2$, $l_2=2$, and weight matrix Φ_{m_2} $(l_1+1\le m_2\le n_y)$ are set as 30.

Then, suppose that HCAs parameters satisfy $\overline{\vartheta}=0.15$ and $\overline{\xi}=0.85$. In addition, consider the HCAs occur in the interval $i,j\in[20\ 40]$ and chose the bounded energy single $v(i,j)$ as

$$v(i,j)=\begin{cases} [\ 0.3\sin(0.2(i+j)) \ 0.3\cos(0.2(i+j)) \ 0.3\cos(0.3(i+j)) \ 0.3\cos(0.3(i+j))]^T \\ \quad i,j\in[20\ 40] \\ 0 \qquad\qquad\qquad\qquad\qquad otherwise \end{cases}.$$

Finally, we take the following parameters $\rho_1(i,j)=\rho_2(i,j)=\rho_3(i,j)=\rho_4(i,j)=0.57$, $\rho_\gamma(i,j)=1.21$ $(\gamma=5,6,\dots,10), \mu_3(\pi(i+1,j))=\mu_4(\pi(i+1,j)=1.0314,$
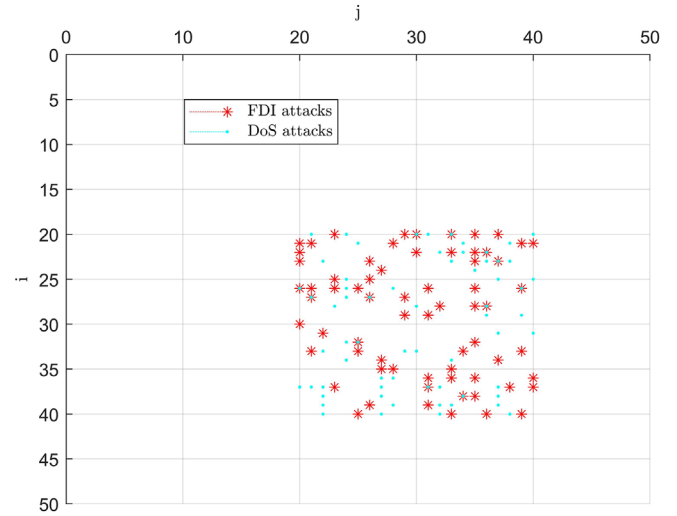
FIGURE 5 The hybrid cyber attacks (HCAs) scenarios.
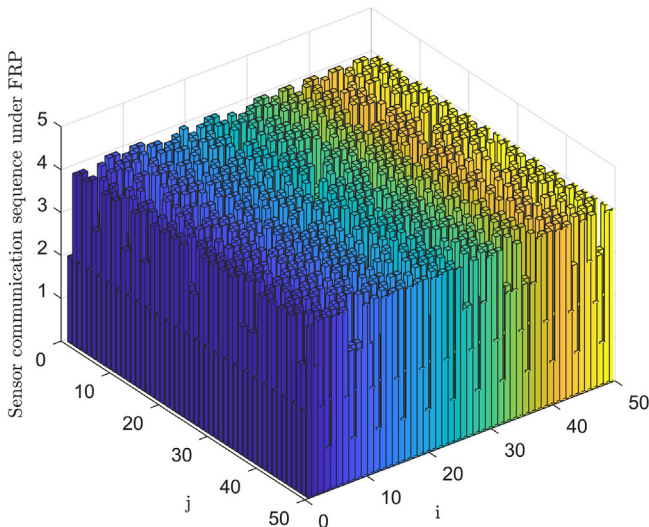
FIGURE 4 Communication sequence under the FlexRay protocol (FRP).
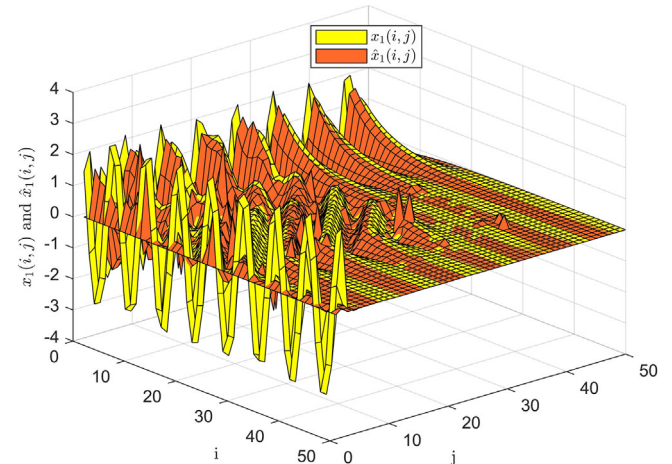
FIGURE 6 The trajectory of state $x_1(i,j)$ and its estimate $\widehat{x}_1(i,j)$.

$\mu_3(\pi(i,j+1)) = \mu_4(\pi(i,j+1)) = 1.8424$, and by applying Theorem 1 and Corollary 1, the part of the set-membership filter gains $\{K(i,j)\}$ are exhibited as follows:

$$K(1,1) = \begin{bmatrix} 0.5102 & -0.0275 & 0.0022 & 1.6321 \\ 0.0125 & 0.4332 & 1.3469 & -0.0650 \\ 1.5321 & 0.0076 & 0.0030 & 0.0011 \\ -0.0083 & 1.2846 & 0.0021 & -0.0000 \\ 0.1561 & 0.5932 & 0.2404 & -0.2101 \\ 1.5932 & 0.0000 & 0.0045 & -0.0148 \\ 0.0091 & 0.0128 & 1.0000 & 0.0000 \\ -0.0214 & -0.0005 & 0.0000 & 1.6264 \end{bmatrix},$$

$$K(1,2) = \begin{bmatrix} 0.2417 & 1.1221 & 0.0001 & -0.0001 \\ -0.0006 & -0.0004 & 0.2141 & 0.1451 \\ 0.0384 & 1.0527 & 0.0206 & 1.6321 \\ 1.2213 & -0.0013 & -0.0043 & 1.2147 \\ 0.3085 & 0.3351 & 0.0358 & -0.0021 \\ 0.0841 & 0.1376 & 0.1320 & -0.0386 \\ 0.0003 & 1.2147 & 0.0566 & 0.0002 \\ 0.0001 & -0.0002 & -0.0000 & 1.1196 \end{bmatrix},$$

$$K(1,3) = \begin{bmatrix} 0.2671 & -0.0971 & 0.0301 & -0.1045 \\ 1.3144 & 0.0787 & 0.7581 & -0.0000 \\ -0.0000 & 0.0000 & 0.0140 & 0.0000 \\ 0.4522 & 1.7674 & 0.9920 & 0.0000 \\ 0.3114 & -0.2541 & 0.0000 & -0.0001 \\ -0.4077 & 0.0000 & -0.0151 & -0.0000 \\ 0.2525 & 0.2867 & 1.0014 & 0.0000 \\ 1.4633 & -0.0000 & -0.0000 & 0.4962 \end{bmatrix},$$

$$K(1,50) = \begin{bmatrix} 0.0000 & 0.5841 & -0.0001 & -0.0000 \\ -0.0000 & 0.0000 & 0.2417 & -0.3321 \\ -0.0002 & 0.0042 & 0.0201 & 0.5414 \\ 0.0001 & -0.0201 & 0.0513 & 0.0047 \\ 0.0014 & 0.0004 & 0.1647 & -0.0132 \\ 0.0000 & 1.0125 & -0.0002 & 0.0000 \\ -0.0000 & 0.3516 & -0.0002 & -0.0000 \\ 0.0000 & -0.0104 & -0.0000 & 0.3786 \end{bmatrix}.$$

The simulation results are shown in Figures 4–18. Figures 4 and 5 depict the communication sequence subject to the FRP and the HCAs scenarios, respectively. Figures 6–9 are concerning the trajectories of the first component of state $x(i,j)$, the second component of state $x(i,j)$, the third component of state $x(i,j)$, and the fourth component of state $x(i,j)$, respectively. Figures 10–13 describe the trajectories of the first component of estimate $\widehat{x}(i,j)$, the second component of estimate
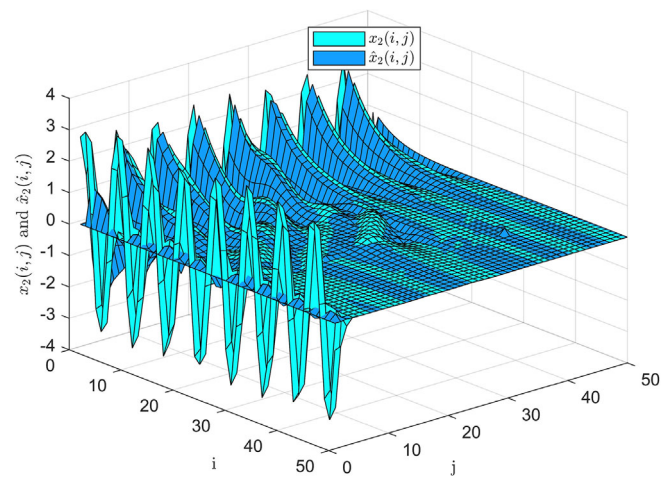
FIGURE 7 The trajectory of state $x_2(i,j)$ and its estimate $\widehat{x}_2(i,j)$.
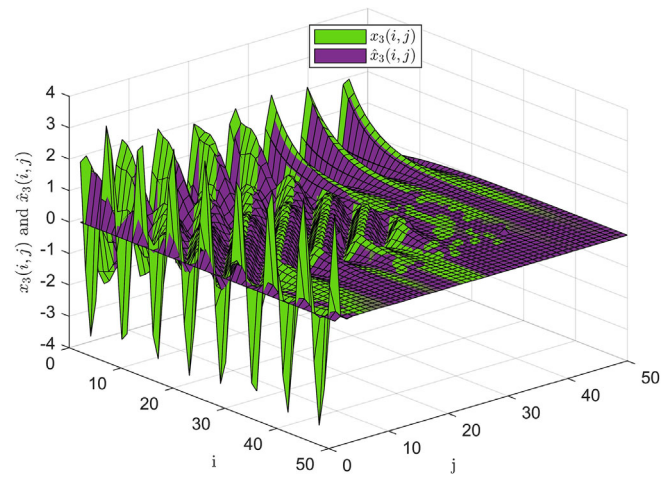
FIGURE 8 The trajectory of state $x_3(i,j)$ and its estimate $\widehat{x}_3(i,j)$.
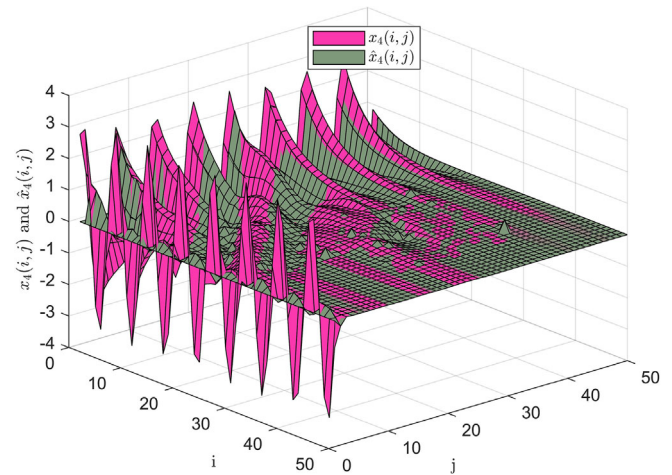
FIGURE 9 The trajectory of the $x_4(i,j)$ and its estimate $\widehat{x}_4(i,j)$.
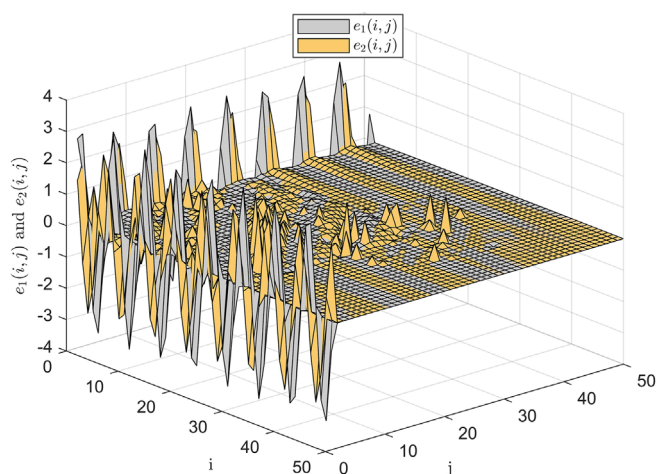
FIGURE 10 The trajectory of filtering error $e_1(i,j)$ and $e_2(i,j)$.
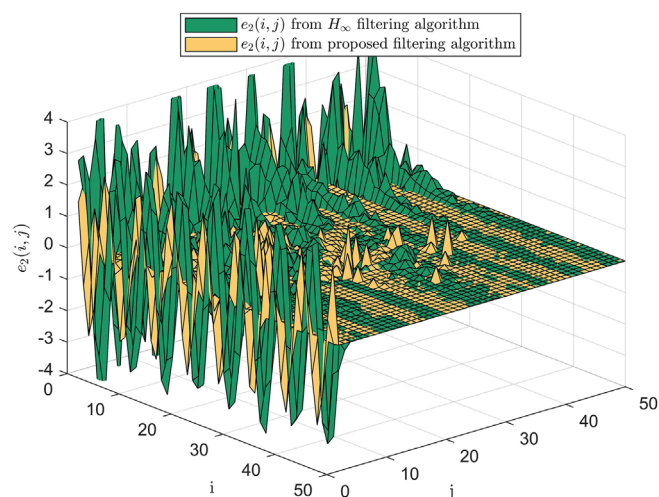
FIGURE 13 Filtering error $e_2(i,j)$ under the different filtering algorithms.
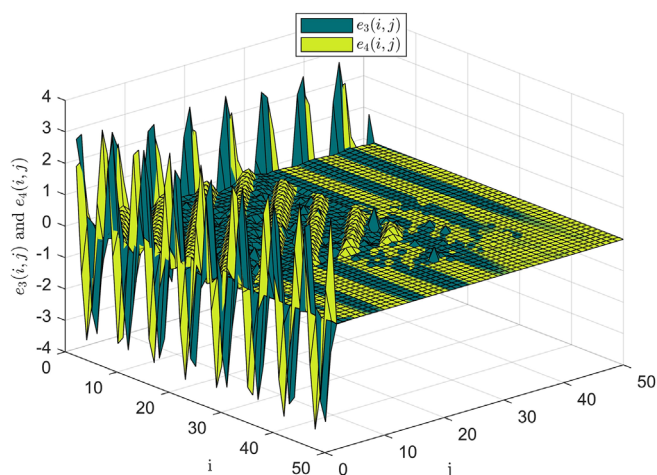
FIGURE 11 The trajectory of filtering error $e_3(i,j)$ and $e_4(i,j)$.
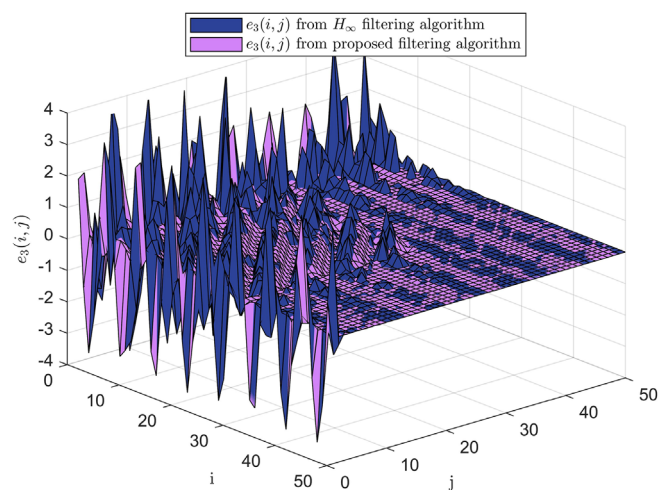
FIGURE 14 Filtering error $e_3(i,j)$ under the different filtering algorithms.
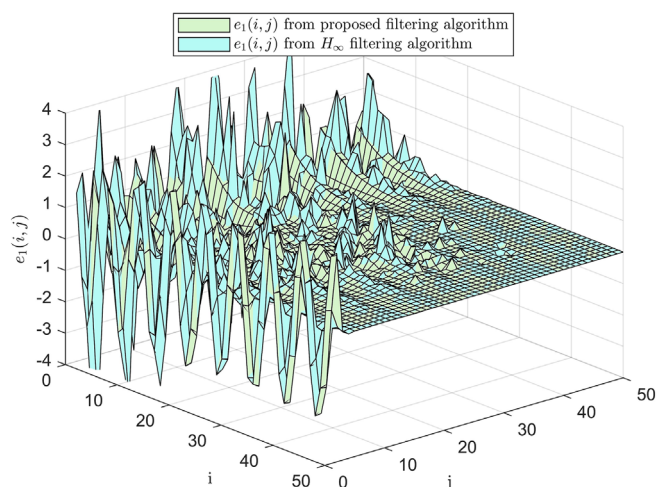
FIGURE 12 Filtering error $e_1(i,j)$ under the different filtering algorithms.
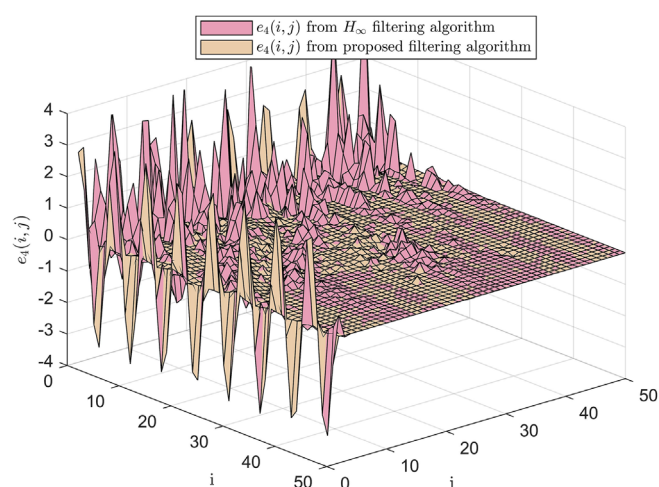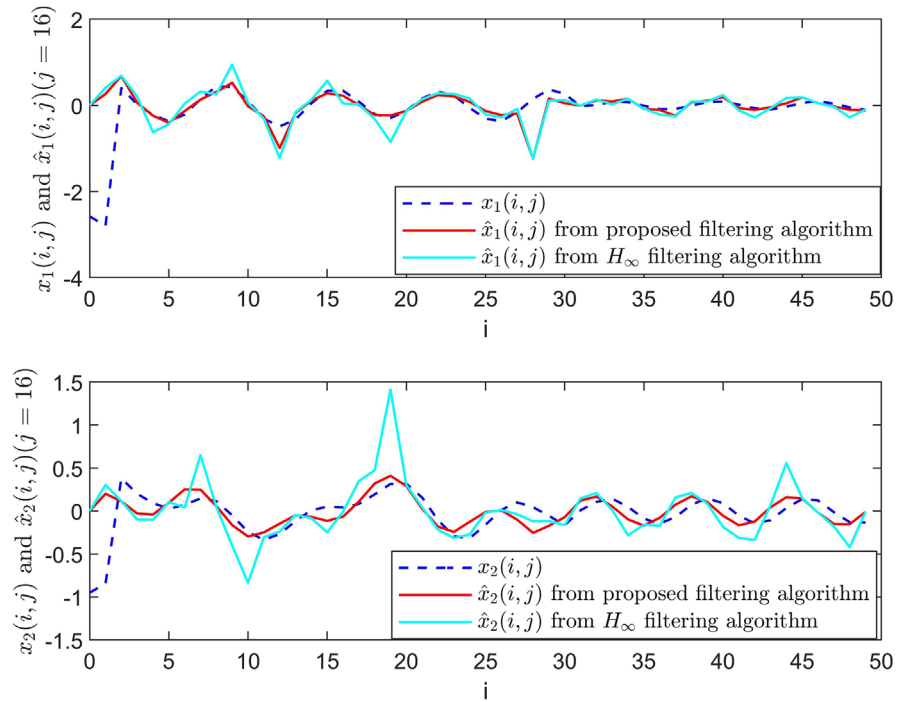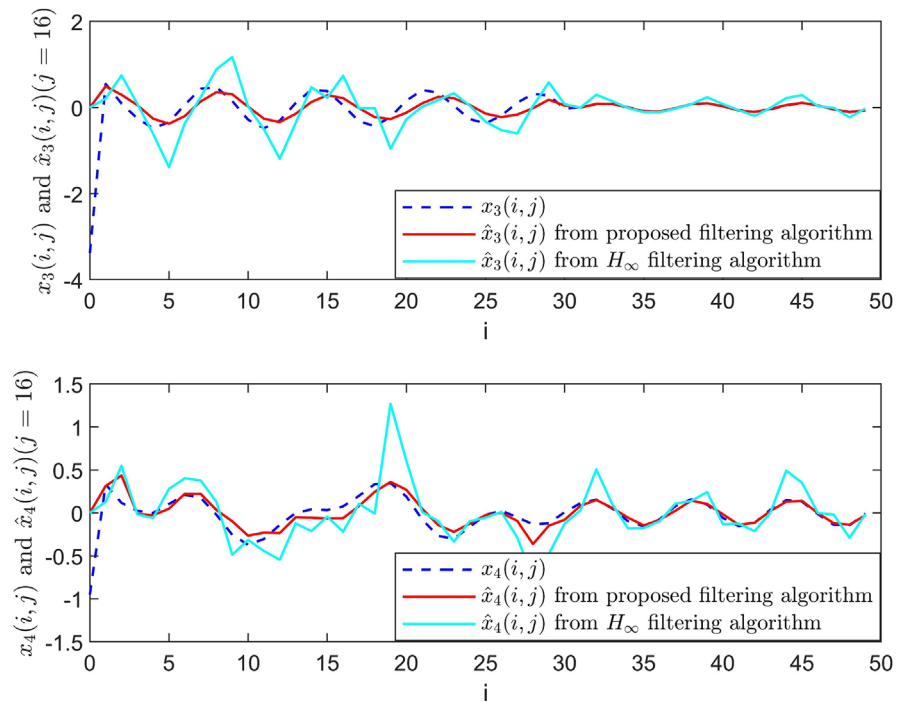

FIGURE 15 Filtering error $e_4(i,j)$ under the different filtering algorithms.

FIGURE 16 The state $x_m(i,j)m \in \{1,2\}$ and its estimate $\hat{x}_m(i,j)$ on $j = 16$.

FIGURE 17 The state $x_m(i,j)m \in \{3,4\}$ and its estimate $\hat{x}_m(i,j)$ on $j = 16$.

$\hat{x}(i,j)$, the third component of estimate $\hat{x}(i,j)$, and the fourth component of estimate $\hat{x}(i,j)$, respectively. Figures 14–17 describe the trajectories of the first component of the filtering error $e(i,j)$, the second component of the filtering error $e(i,j)$, the third component of the filtering error $e(i,j)$, and the fourth component of the filtering error $e(i,j)$, respectively. It can be seen from Figures 14–17 that the filtering error $e(i,j)$ converge rapidly after the initial horizon. In addition, it can be seen from Figures 10–17 that the systems estimation and filtering error fluctuate in horizon $i,j \in [0 \ 40]$ due to process noises, measurement noises, and HCAs. Moreover, the filtering error finally converges to 0 after the end of the external disturbance, which reflects the excellent performance of the proposed filtering algorithm.
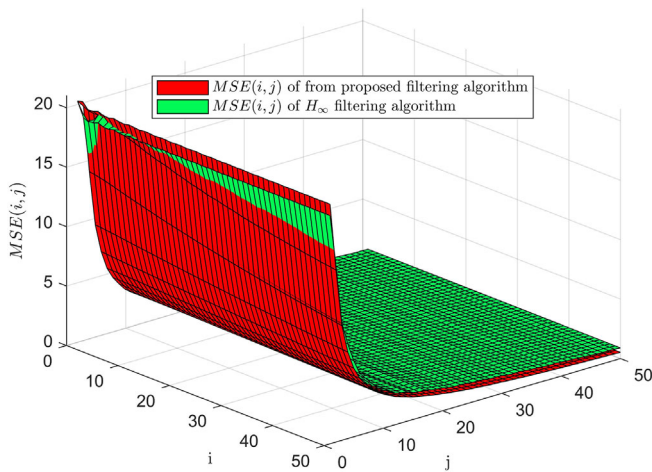
FIGURE 18 The $MSE(i,j)$ under the different filtering algorithms.

In addition, we compare the proposed set-membership filtering algorithm with the robust H_∞ filtering algorithm proposed in [49] under the same systems (1), FRP (7), and HCAs (10) conditions to demonstrate the superiority of the proposed filtering Algorithm 1. We define the mean square filtering error as $MSE(i,j) = (1/T^2)\sum_j = 1^T \sum_{i=1}^T (x(i,j) - \widehat{x}(i,j))^2$, the simulation results are displayed in Figures 12–18. Figures 12–15 describe the component of filtering error $e(i,j)$ under the different filtering algorithms. Furthermore, the comparison of systems state $x(i,j)$ and its estimate $\widehat{x}(i,j)$ with the qualification $j = 16$ are shown in Figures 16 and 17. It can be seen from Figures 12–17 that the filtering error $e(i,j)$ under the set-membership filtering algorithm is overall smaller than that under the robust H_∞ filtering algorithm. Finally, Figure 18 demonstrates the $MSE(i,j)$ under both filtering algorithms, and it can be seen that the developed set-membership filtering algorithm provides better filtering performance compared to the robust H_∞ filtering algorithm.

5 | CONCLUSIONS

In this research, the set-membership filtering problem for the 2-D systems with FRP and the HCAs has been examined. A bi-directional time-sequence hybrid communication protocol is developed to alleviate the communications burden, which is based on the idea of employing predefined time-triggered and event-triggered conditions to decide whether the current measurement output is released. In addition, considering the influence of HCAs occurring in random patterns on filtering performance, a comprehensive model of 2-D systems affected by FRP and HCAs is constructed. Sufficient

conditions are deduced to ensure that the FES always satisfies the ellipsoidal restriction. Furthermore, the optimal set-membership filter gains have been derived by minimizing the ellipsoidal constraints of filtering error. The effectiveness and superiority of the developed set-membership filter design approach are validated by a long-distance transmission line example. It is one of the future development directions to extend the presented FRP with bi-directional evolutionary indexes to various 2-D systems filtering algorithms, such as Kalman filtering and bounded filtering, based on the noise characteristics. Additionally, the HCAs considered in this paper all occur in a stochastic manner, which simplifies the analysis to some extent. Investigating security control/filtering problems for 2-D systems with queued DoS attacks and replay attacks is worth pondering.

ORCID
Zhiwen Wang https://orcid.org/0000-0002-5425-0705

REFERENCES
1. C. K. Ahn, P. Shi, and H. R. Karimi, *Novel results on generalized dissipativity of two-dimensional digital filters*, IEEE Trans. Circuits Syst. II -Express Briefs. **63** (2016), no. 9, 893–897.
2. C. Du and L. Xie, *Stability analysis and stabilization of uncertain two-dimensional discrete systems: an LMI approach*, IEEE Trans. Circuits Syst. I-Regular Papers **46** (1999), no. 11, 1371–1374.
3. S. Knorn and R. H. Middleton, *Stability of two-dimensional linear systems with singularities on the stability boundary using LMIs*, IEEE Trans. Autom. Control **58** (2013), no. 10, 2579–2590.

4. L. Wu and Z. Wang, *Filtering and control for classes of two-dimensional systems*, Springer International Publishing, Cham, Switzerland, 2015.

5. R. P. Roesser, *A discrete state-space model for linear image processing*, IEEE Trans. Autom. Control **20** (1975), no. 1, 1–10.

6. E. Fornasini and G. Marchesini, *State-space realization theory of two-dimensional filters*, IEEE Trans. Autom. Control **21** (2016), no. 4, 484–492.

7. E. Fornasini and G. Marchesini, *Doubly indexed dynamical systems: state models and structural properties*, Math Syst theory **12** (1978), no. 1, 59–72.

8. J. E. Kurek, *The general state-space model for a two-dimensional linear digital system*, IEEE Trans. Autom. Control **30** (1985), no. 6, 600–602.

9. L. V. Hien and H. Trinh, *Exponential stability of two-dimensional homogeneous monotone systems with bounded directional delays*, IEEE Trans. Autom. Control **63** (2018), no. 8, 2694–2700.

10. D. Peng and H. M. Nie, *Abel lemma-based finite-sum inequality approach to stabilization for 2-D time-varying delay systems*, Asian J. Control **23** (2021), no. 3, 1394–1406.

11. Y. Yan, L. L. Su, and V. Gupta, *Analysis of two-dimensional feedback systems over networks using dissipativity*, IEEE Trans. Autom. Control **65** (2020), no. 8, 3241–3255.

12. I. Ghous, Z. Y. Xiang, and H. R. Karimi, *State feedback H∞ control for 2-D switched delay systems with actuator saturation in the second FM model*, Circ Syst Signal Pr **34** (2015), no. 7, 2167–2192.

13. D. H. Li, J. L. Liang, and F. Wang, *Observer-based H∞ control of two-dimensional delayed networks under the random access protocol*, Neurocomputing **401** (2020), 353–363.

14. F. Wang, J. Liang, and Z. D. Wang, *Robust finite-horizon filtering for 2-D systems with randomly varying sensor delays*, IEEE Trans. Syst. Man Cybern.: Syst **50** (2020), no. 1, 220–232.

15. G. C. Walsh, H. Ye, and L. Bushnell, *Stability analysis of networked control systems*, In *Proceedings of the American Control Conference*, San Diego, California, 1999, 2875–2880.

16. G. C. Walsh and H. Ye, *Scheduling of networked control systems*, IEEE Control Syst Mag **21** (2001), no. 1, 57–65.

17. G. C. Walsh, H. Ye, and L. Bushnell, *Stability analysis of networked control systems*, IEEE Trans. Autom. Control **10** (2002), no. 3, 438–446.

18. D. Hristu-Varsakelis and K. Morgansen, *Limited communication control*, Syst. Control Lett **37** (1999), no. 4, 193–205.

19. W.-A. Zhang, L. Yu, and G. Feng, *Optimal linear estimation for networked systems with communication constraints*, Automatica **47** (2011), no. 9, 1992–2000.

20. M. Tabbara and D. Nesic, *Input-output stability of networked control systems with stochastic protocols and channels*, IEEE Trans. Autom. Control **53** (2008), no. 5, 1160–1175.

21. W. Wei, D. Nesic, and R. Postoyan, *Emulation-based stabilization of networked control systems implemented on FlexRay*, Automatica **59** (2015), 73–83.

22. W. Wei, D. Nesic, and R. Postoyan, *Observer design for networked control systems with FlexRay*, Automatica **82** (2017), 42–48.

23. L. Zou, Z. D. Wang, J. Hu, J. Y. R. Liu, and X. H. Liu, *Communication-protocol-based analysis and synthesis of networked systems: progress, prospects and challenges*, Int. J. Syst. Sci **52** (2021), no. 14, 3013–3034.

24. R. Makowitz and C. Temple, *FlexRay—a communication network for automotive control systems*, In *IEEE International Workshop on Factory Communication Systems*, Turin, Italy, 2006, 207–212.

25. Y. Z. Wang, Z. D. Wang, L. Zou, L. F. Ma, and H. L. Dong, *Ultimately bounded PID control for T-S fuzzy systems under FlexRay communication protocol*, IEEE Trans. Fuzzy Syst **31** (2023), no. 12, 4308–4320.

26. S. Liu, Z. D. Wang, L. C. Wang, and G. L. Wei, *Finite-horizon H∞ filtering via a high-rate network with the FlexRay protocol*, IEEE Trans. Autom. Control **68** (2023), no. 6, 3596–3603.

27. Y. Tang, D. D. Zhang, D. W. C. Ho, and F. Qian, *Tracking control of a class of cyber-physical systems via a FlexRay communication network*, IEEE Trans. Cybern **49** (2019), no. 4, 1186–1199.

28. S. Li, W. C. Zou, and J. Guo, *Consensus of switched nonlinear multiagent systems subject to cyber attacks*, IEEE Syst. J **16** (2022), no. 3, 4423–4432.

29. J. Guo, R. Z. Jia, R. N. Su, and Y. L. Zhao, *Identification of FIR systems with binary-valued observations against data tampering attacks*, IEEE Trans. Syst. Man Cybern.-Syst. **53** (2023), no. 9, 5861–5873.

30. J. J. Yan, Y. Q. Xia, X. L. Feng, and Y. Q. Zhang, *Deception attack detection based on bandwidth allocation for switched systems with quantization*, Automatica **154** (2023), Article 111094.

31. F. Giuseppe, T. Francesc, and F. Domenico, *Resilience against replay attacks: a distributed model predictive control scheme for networked multi-agent systems*, IEEE-CAA J. Autom. **8** (2021), no. 3, 628–640.

32. L. X. Wang, Y. Long, S. Li, H. Q. Yang, C. L. Philip, and Chen, *Asynchronous attack tolerant control for Markov jump cyber-physical systems under hybrid cyber-attacks*, Appl. Math. Comput **470** (2024), 28583.

33. L. H. Tan and X. Wang, *Sampled-based adaptive event-triggered resilient control for multiagent systems with hybrid cyber-attacks*, Neural. Netw. **172** (2024), 106090.

34. Y. H. Cui, H. B. Sun, L. L. Hou, and K. B. Shi, *Dynamic event-triggered adaptive neural network decentralized output-feedback control for nonlinear interconnected systems with hybrid cyber attacks and its application*, IEEE Trans. Syst. Man Cybern.-Syst **54** (2024), no. 4, 2149–2158.

35. Y. C. Zhang, B. Chen, and L. Yu, *Distributed Kalman filtering for interconnected dynamic systems*, IEEE Trans. Cybern **52** (2021), no. 11, 11571–11580.

36. Y. D. Qin, D. Heng, and J. D. Han, *Direct inverse hysteresis compensation of piezoelectric actuators using adaptive Kalman filter*, IEEE Trans. Ind. Electron **69** (2022), no. 9, 9385–9395.

37. H. Fu, H. L. Dong, and F. Han, *Outlier-resistant H∞ filtering for a class of networked systems under Round-Robin protocol*, Neurocomputing **401** (2020), 133–142.

38. M. A. Nezar and S. M. Magdi, *Distributed H2/H∞ filter design for discrete-time switched systems*, IEEE-CAA J Autom **7** (2020), no. 1, 158–168.

39. J. Mao, X. Meng, and D. R. Ding, *Fuzzy set-membership filtering for discrete-time nonlinear systems*, IEEE-CAA J. Autom. **9** (2022), no. 6, 1026–1036.

40. C. Liu, L. Yang, and J. Tao, *Set-membership filtering for complex networks with constraint communication channels*, Neural. Netw. **152** (2022), 479–486.

41. L. Zou, Z. D. Wang, H. Geng, and X. H. Liu, *Set-membership filtering subject to impulsive measurement outliers: a recursive algorithm*, IEEE-CAA J. Autom. **8** (2021), no. 2, 377–388.

42. L. Liu, L. F. Ma, J. Guo, J. Zhang, and Y. Bo, *Distributed set-membership filtering for time-varying systems under constrained measurements and replay attacks*, J. Frankl. Inst **357** (2020), 4983–5003.

43. L. Liu, L. F. Ma, J. Guo, J. Zhang, and Y. Bo, *Distributed set-membership filtering for time-varying systems: a coding-decoding-based approach*, Automatica **129** (2021), 109684.

44. M. Y. Li, J. L. Liang, and F. Wang, *Robust set-membership filtering for two-dimensional systems with sensor saturation under the Round-Robin protocol*, Int. J. Syst. Sci **53** (2022), no. 13, 2773–2785.

45. K. Q. Zhu, Z. D. Wang, H. L. Dong, and G. L. Wei, *Set-membership filtering for two-dimensional systems with dynamic event-triggered mechanism*, Automatica **143** (2022), 110416.

46. M. Y. Li, J. L. Liang, and J. L. Qiu, *Set-membership filtering for 2-D systems under uniform quantization and weighted Try-Once-Discard protocol*, IEEE Trans. Circuits Syst.- II Express Briefs **70** (2023), no. 9, 3474–3478.

47. R. Suarez, *Difference equations and a principle of double induction*, Math. Mag. **62** (1989), no. 5, 334–339.

48. Y. Q. Luo, Z. D. Wang, G. L. Wei, and F. E. Alsaadi, *Robust H∞ filtering for a class of two-dimensional uncertain fuzzy systems with randomly occurring mixed delays*, IEEE Trans. Fuzzy Syst **24** (2017), no. 1, 70–83.

49. D. H. Li, J. J. Liang, and F. Wang, *Robust H∞ filtering for 2-D systems with RON under the stochastic communication protocol*, IET Control Theory Appl. **14** (2021), no. 18, 2795–2804.

AUTHOR BIOGRAPHIES

Pan Zhang was born in Longnan, Gansu, China. He received the M.E. degree in control theory and control engineering from Lanzhou University of Technology, Lanzhou, in 2019. He is currently working toward the Ph.D. degree in control theory and control engineering at Lanzhou University of Technology, Lanzhou, China. His current research interests include networked control systems, two-dimensional systems, and robust filtering.

Chaoqun Zhu was born in Tacheng, Xinjiang, China, in 1977. He received the M.E. degree in control theory and control engineering from Lanzhou University of Technology, Lanzhou, in 2008 and the Ph.D. degree in control theory and control engineering from Dalian Maritime University, Dalian, in 2013. His current research interests include networked control systems and vehicular cooperative control. He has published over 10 journal papers within these areas.

Zhiwen Wang was born in Minqin, Gansu, China, in 1976. He is a senior member of the Chinese Society of Automation. He graduated from Xi'an Jiaotong University, School of Electrical Engineering, majoring in industrial automation, in 1999 and received the M.E. degree in control theory and control engineering from Lanzhou University of Technology, Lanzhou, in 2008 and the Ph.D. degree in control theory and control engineering from Dalian Maritime University, Dalian, in 2013. His current research interests include networked control systems, cyber-physical systems security, advanced control theory, and applications for industrial processes. He has published over 60 papers within these areas.

Bing Yang was born in Panjin, Liaoning, China, in 1977. She received the M.E. degree in control theory and control engineering from Lanzhou University of Technology, Lanzhou, in 2008. Her current research interests include networked control systems and autonomous vehicle control.

Encryption-Decryption-Based Bounded Filtering for 2-D Systems under Dynamic Event-Triggered Mechanism

Pan Zhang, Chaoqun Zhu, Bin Yang, Bohan Zhang and Zhiwen Wang*

Abstract—**This paper investigates the bounded filtering problem for two-dimensional (2-D) discrete systems with encryption-decryption mechanism (EDM) and dynamic event-triggered mechanism (ETM). Firstly, considering the potential information leakage, a novel EDM is designed for 2-D systems based on the quantization-based encoding-decoding mechanism. In addition, the dynamic ETM with bidirectional evolutionary characteristics is proposed to alleviate the computational and communication burdens. In such a framework, the filtering error systems (FESs) at the eavesdropper side and the user side are obtained, respectively. Subsequently, the encryption parameters are devised such that the filtering error at the eavesdropper side diverges. Additionally, the boundedness criteria are established to ensure that the client-side FESs are bounded in terms of Lyapunov stability analysis approach. Finally, it is demonstrated that the proposed bounded filtering algorithm is valid for 2-D systems in several types of industrial environments.**

Index Terms: **Two-dimensional systems, Fornasini and Marchesini model, dynamic event-triggered mechanism, encryption-decryption mechanism, filtering algorithm design**

Abbreviations and Acronyms

ETM	Event-triggered mechanism.
2-D systems	Two-dimensional systems.
EDM	Encryption-decryption mechanism.
FESs	Filtering error systems
$\mathbb{R}^n$	The n-dimensional Euclidean space.
$diag\{\cdots\}$	The block-diagonal matrix
LMI	Linear matrix inequality
$\|A\|$	$\|A\| = \sqrt{\lambda_{\max}(A^T A)}$.
G^T	The transpose of the matrix G.
G^{-1}	The inverse of the matrix G.
I_{n_y}	The n_y-dimensional identity matrix.
$\lambda_{\max}(\bullet)$	The largest eigenvalue.
$\mathbb{E}\{\bullet\}$	The mathematical expectation of the variable.

I. INTRODUCTION

2-D systems is found in many real-world systems, such as seismographic data processing, thermal processes, gas absorption, and water stream heating [1-4]. To emphasize the unique bidirectional evolutionary features of 2-D systems, the Roesser model [5], the Fornasini-Marchesini model [6], and the Kurek model [7] have been proposed and continuously refined. Based on the models developed above, the issues of stability analysis [8], control synthesis [9], filter design [10], and fault diagnosis [11] for 2-D systems have garnered substantial research interest among scholars. Meanwhile, control theory has progressed from classical control methods to network-based control methods. With this background, the investigations have contributed significantly to the accelerated development of 2-D systems, which renders them one of the most active research directions in the control field [12-18].

With the explosive growth of information, alleviating the communication and computational burdens caused by redundant data has become particularly urgent. In this context, the ETM has arisen. Its core philosophy is to reduce the frequency of data transmission or sampling while ensuring the preservation of system performance, thereby achieving a balance between system performance and network load. In general, ETM has been developed as a transmission mechanism that decides whether to release data based on preset triggering conditions. In contrast to the time-triggered mechanism, which delivers data at each sampling instant, the ETM can reduce the frequency of data transmission to conserve network resources. Up to date, the ETM can be primarily categorized into two types: static ETM and dynamic ETM. Typically, the triggering condition in static ETM is fixed. In contrast, dynamic ETM introduces an auxiliary variable based on the static ETM to further reduce the frequency of data transmission. It is worth emphasizing that, although the ETM based on 1-D systems as the research baseline has achieved fruitful results, many of these methods are difficult to directly apply to 2-D systems due to their unique bidirectional evolutionary complexity, which leads to a lag in the investigation of the dynamic ETM for 2-D systems. Moreover, most of the available results primarily focus on the static ETM [19-22]. The challenge of designing dynamic ETM for 2-D systems lies in constructing a non-incremental, bidirectional, and positive auxiliary variable. Up to now, there is limited literature on dynamic ETM for 2-D systems [23-25]. Among them, the designed dynamic auxiliary variable changes only with respect to the vertical direction and focuses on the recursive filtering theory presented in [23]. While references [24] and [25] are both based on the set-membership filtering theory, i.e., allowing all possible state vectors to satisfy a given ellipsoid set constraint, which is quite different

P. Zhang, C. Zhu, B. Yang, B. Zhang and Z. Wang are with the College of Electrical and Information Engineering, Lanzhou University of Technology, Lanzhou 730050, China (e-mail: zhangpanlut@163.com, chaoqunzhu@yeah.net; yangbin0@yeah.net; 15139352987@163.com wwwangzhiwen@yeah.net).

from the filtering theory based on Lyapunov stability. Therefore, enriching the design methodology of dynamic ETM for 2-D systems based on existing results, and analyzing its impact on filtering performance by utilizing Lyapunov stability theory, are among the motivations for this investigation.

Due to the openness and vulnerability of communication networks, the security of networked systems has garnered significant attention, and research on cyber-attacks has yielded fruitful results. Several categories of widely researched attack tactics include, but are not limited to, DoS attacks [26], deception attacks [27], and replay attacks [28]. These attack strategies generally disrupt the performance of the networked systems by maliciously interfering with the transmission of original normal data. Additionally, as another type of attack, eavesdropping is stealthier and more dangerous because it does not actively inject data into the communication network and does not change the characteristics of network traffic. Therefore, it is of theoretical value and practical significance to deal with potential eavesdropping attacks from the perspectives of security filtering and state estimation. Currently, the defense strategy against eavesdropping attacks on networked systems primarily relies on the design of encryption mechanisms, i.e., the adoption of secure protocols for data transmission, which mainly encompass encryption mechanisms based on data scheduling [29-31] and data encoding [32-35]. Considering that all the data information being encrypted would be costly, reasonably encrypting part of the data to minimize encryption costs while guaranteeing the desired estimated performance is the objective of the data scheduling-based encryption mechanism. The data encoding-based encryption mechanism involves encrypting the original data into a codeword by using a key, and the client can restore the original data to the maximum extent possible through the decryption process. Apparently, the key is unknown to the eavesdropper, which results in the eavesdropper obtaining useless information. In brief, the data encoding-based encryption mechanism encrypts data at all instants, which leads to improved security performance but requires the allocation of additional computational and communication resources. Unfortunately, the aforementioned research results are all based on 1-D systems, and the development of EDM for 2-D systems deserves intensive research. Considering the characteristics of the encryption mechanism based on data compression encoding, the challenge of collaboratively designing the dynamic ETM and EDM for 2-D systems, specifically, to alleviate the network burden while ensuring the security of the systems is an open problem that merits investigation, which is another motivation of our research.

We are committed to investigating the filtering algorithm design for 2-D systems under dynamic ETM and EDM in response to the previously demonstrated issue. The challenges encountered mainly include the following aspects:1) How to establish the ETM and EDM within the framework of 2-D systems; 2) How to evaluate the impact of the ETM nd EDM on system security; 3) How to analyze the performance of the client's filtering system under the influence of dynamic ETM and EDM. To address the aforementioned challenges, the contributions are summarized: (1) A positive definite and bounded dynamic auxiliary variable is designed using the stability criterion of 2-D systems, which serves as the foundation for proposing a bidirectional evolutionary dynamic ETM; (2) For the first time, the EDM is provided for

potential eavesdropping attacks in 2-D systems, and the encryption parameters are quantitatively analyzed to enable the divergence of the eavesdropper's filtering error dynamics; (3) Based on the developed dynamic ETM and EDM, the client's filter gains are obtained, which guarantee the controlled output error is exponentially ultimately bounded in the mean-square sense.

The rest of this paper is organized as follows: In Section 2, the dynamic ETM and EDM based on bidirectional evolutionary mechanisms are proposed. In Section 3, the effect of encryption parameters on the eavesdropper is analyzed, and boundedness criterion are deduced to ensure that the FESs of client are bounded. Section 4 illustrates the effectiveness of the proposed dynamic ETM and EDM, as well as filtering algorithms, with the help of several practical examples. Section 5 presents conclusions and discusses potential development directions.

II. PRELIMINARIES
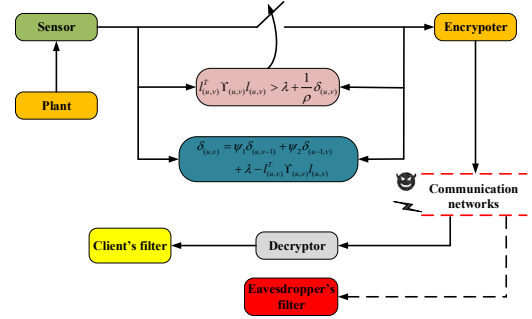
Fig. 1. Diagram of 2-D systems structure under dynamic ETM and EDM

Consider the discrete 2-D systems [18] indicated by the FM-II model in a finite horizon as follows:

$$
\begin{cases}
x_{(u+1,v+1)} = \mathcal{A}_{(u+1,v)}^{[1]} x_{(u+1,v)} + \mathcal{A}_{(u,v+1)}^{[2]} x_{(u,v+1)} \\
\qquad\qquad + \mathcal{B}_{(u+1,v)}^{[1]} w_{(u+1,v)} + \mathcal{B}_{(u,v+1)}^{[2]} w_{(u,v+1)} \\
y_{(u,v)} = \mathcal{C}_{(u,v)} x_{(u,v)} + \mathcal{D}_{(u,v)} \upsilon_{(u,v)} \\
z_{(u,v)} = \mathcal{H}_{(u,v)} x_{(u,v)}
\end{cases}, \ u,v \in \Gamma \triangleq [0,\kappa] \ (1)
$$

where κ is a given positive integer. The parameters u and v denote generalized time variables, signifying either time itself or variables that exhibit characteristics which change with time. $x_{(u,v)} \in \mathbb{R}^{n_x}$ represents the systems state vector, $y_{(u,v)} \in \mathbb{R}^{n_y}$ is the measurement output, $z_{(u,v)} \in \mathbb{R}^{n_z}$ is the controlled output, $w_{(u,v)} \in \mathbb{R}^{n_w}$ and $\upsilon_{(u,v)} \in \mathbb{R}^{n_v}$ denote the process noise and measurement noise, respectively, both of them are zero-mean Gaussian white noise sequences with variances $W = \mathcal{W}\mathcal{W}^T \geq 0$ and $V = \mathcal{V}\mathcal{V}^T \geq 0$, respectively. $\mathcal{A}_{(u,v)}^{[1]}$, $\mathcal{A}_{(u,v)}^{[2]}$, $\mathcal{B}_{(u,v)}^{[1]}$, $\mathcal{B}_{(u,v)}^{[2]}$, $\mathcal{C}_{(u,v)}$, $\mathcal{D}_{(u,v)}$ and $\mathcal{H}_{(u,v)}$ are known time-varying matrices with proper dimensions. With respect to the distinctive evolutionary properties (1) of the 2-D system, the current system state $x_{(u+1,v+1)}$ always consists of the past state $x_{(u+1,v)}$ and $x_{(u,v+1)}$. Therefore, to be concise, the generalized temporal characteristics of the 2-D systems are represented by the transversal line $\Phi_j = \{(u,v) \mid j = u + v\}$.

In addition, the initial states, $x_{(u,0)}$ and $x_{(0,v)}$ are independent of

This article has been accepted for publication in IEEE Transactions on Network Science and Engineering. This is the author's version which has not been fully edited and content may change prior to final publication. Citation information: DOI 10.1109/TNSE.2025.3542177

3

> REPLACE THIS LINE WITH YOUR MANUSCRIPT ID NUMBER (DOUBLE-CLICK HERE TO EDIT) <

other variables, and their mean values obey the following distribution:

$$\mathbb{E}\{x_{(u,0)}\} = \mu_1(u), \quad \mathbb{E}\{x_{(0,v)}\} = \mu_2(v), \quad u,v \in \Gamma,$$

where $\mu_1(u)$ and $\mu_2(v)$ are known vectors with $\mu_1(0) = \mu_2(0)$.

A. Dynamic event-triggered mechanism

Some measures are necessary to organize data transmission rationally in order to alleviate the communication burdens. The ETM is one of the most prevalent methods for allocating network resources, which prompts us to develop the dynamic ETM in the context of 2-D systems as shown in Fig. 1. Firstly, the bidirectional time series is defined as follows:

$$\begin{cases} (u,v) < (\overline{u},\overline{v}) \Leftrightarrow \{(u,v) \mid u = \overline{u}, v < \overline{v}\} \bigcup \{(u,v) \mid u < \overline{u}, v = \overline{v}\} \\ (u,v) = (\overline{u},\overline{v}) \Leftrightarrow u = \overline{u} \ and \ v = \overline{v} \end{cases}.$$

Furthermore, we present the following triggering sequence to indicate the instants that the measurement output is released:

$$(0,0) = (u_0,v_0) < (u_1,v_1) < \cdots < (u_r,v_r) < \cdots \ r \in [1 \ \infty),$$

where (u_r,v_r) stands for the r-th triggering instant. The update of the triggering sequence is determined by the rule (2). In the case that (2) holds, the measurement output of the current instant is allowed to be transmitted through the communication network, and the triggering instant is updated accordingly. Conversely, the filter follows the measurement output from the latest triggering instant.

$$(u_{r+1},v_{r+1}) = \inf\left\{(u,v) \mid (u,v) > (u_r,v_r), l_{(u,v)}^T \Upsilon_{(u,v)} l_{(u,v)} > \lambda + \frac{1}{\rho}\delta_{(u,v)}\right\}, (2)$$

where $l_{(u,v)} = y_{(u_r,v_r)} - y_{(u,v)}$. $\Upsilon_{(u,v)}$ is a positive definite matrix. $y_{(u_r,v_r)} \in \mathbb{R}^{n_y}$ represents the latest released measurement output. ρ and λ are given positive constants, in addition, the update rule of the dynamic auxiliary variable $\delta_{(u,v)}$ is characterized as follows:

$$\delta_{(u,v)} = \psi_1 \delta_{(u,v-1)} + \psi_2 \delta_{(u-1,v)} + \lambda - l_{(u,v)}^T \Upsilon_{(u,v)} l_{(u,v)}, \quad (3)$$

where $0 < \psi_1 < 1/2$, $0 < \psi_2 < 1/2$. The bounded initial conditions satisfy $\delta_{(u,0)} > 0$ and $\delta_{(0,v)} > 0$ for all $u,v \in \Gamma$.

We now propose the following lemmas and proposition, which reveal the essential property of the dynamic auxiliary variable $\delta_{(u,v)}$.

Lemma 1 [4]: Considering the FM-II model as follows:

$$x_{(u+1,v+1)} = A_1 x_{(u+1,v)} + A_2 x_{(u,v+1)} + B_1 w_{(u+1,v)} + B_2 w_{(u,v+1)}, \quad (4)$$

if there exist scalars θ_1 and θ_2 satisfying $\theta_1 + \theta_2 = 1$, as well as positive definite matrix P such that the following inequality holds:

$$A^T P A - Q < 0,$$

where $A = [A_1 \ A_2]$ and $Q = diag\{\theta_1 P, \theta_2 P\}$, then, the 2-D systems (4) is asymptotically stable.

Lemma 2 [36]: (Principle of Double Induction) Suppose that $X_{(u,v)}$ is a proposition for all $u,v \in \Gamma$. If the molecules $X_{(u-1,v)}$ and $X_{(u,v-1)}$ of $X_{(u,v)}$ as well as the initial condition $X_{(0,v)}$ and $X_{(u,0)}$ satisfy the following steps for all $u,v \in \Gamma$:

1) (**Initial step**) $X_{(0,v)}$ and $X_{(u,0)}$ are true for all $u,v \in \Gamma$;

2) (**Inductive step**) if the molecules $X_{(u-1,v)}$ and $X_{(u,v-1)}$ are true, then $X_{(u,v)}$ is true.

Then, $X_{(u,v)}$ is true for all $u,v \in \Gamma$.

Lemma 3: Let the positive scalars ρ, λ, ψ_1 and ψ_2 be given. If initial value satisfy $\delta_{(u,0)} > 0$ and $\delta_{(0,v)} > 0$ ($u,v \in \Gamma$), then, $\delta_{(u,v)} > 0$ holds for all $u,v \in \Gamma$.

Proof: Define the set of time sequence $(u,v) \in \bigcup_{u+v=0}^{\infty} \Theta_{(u,v)} = \Gamma$, where $\Theta_{(u,v)} \triangleq \{(u,v) \mid (u_r,v_r) \le (u,v) < (u_{r+1},v_{r+1})\}$. According to (2), one has

$$l_{(u,v)}^T \Upsilon_{(u,v)} l_{(u,v)} \le \lambda + (1/\rho)\delta_{(u,v)}. \quad (5)$$

Combine the (3) and (5), which yields

$$\delta_{(u,v)} \ge (\psi_1/\overline{\rho})\delta_{(u,v-1)} + (\psi_2/\overline{\rho})\delta_{(u-1,v)}, \quad (6)$$

where $\overline{\rho} = (1+(1/\rho))$. Moreover, the new variable $\zeta_{(u,v)}$ is constructed that adheres to the following evolutionary rule:

$$\zeta_{(u,v)} = (\psi_1/\overline{\rho})\zeta_{(u,v-1)} + (\psi_2/\overline{\rho})\zeta_{(u-1,v)}, \quad (7)$$

and the initial conditions satisfy $\delta_{(0,v)} = \zeta_{(0,v)} > 0$ and $\delta_{(u,0)} = \zeta_{(u,0)} > 0$. With the help of the following 2-D mathematical induction one can obtain **Lemma 3** is established. ***Initial step.*** For $u = 0$, $v \in [0,\kappa]$ or $v = 0$, $u \in [0,\kappa]$, it is straightforward to observe that $\delta_{(0,v)} \ge \zeta_{(0,v)}$ and $\delta_{(u,0)} \ge \zeta_{(u,0)}$. ***Inductive step.*** Our aim is to prove that $\delta_{(u,v)} \ge \zeta_{(u,v)}$ holds under the assumption that $\delta_{(u,v-1)} \ge \zeta_{(u,v-1)}$ and $\delta_{(u-1,v)} \ge \zeta_{(u-1,v)}$ are true. Based on (6) and (7), it is easy to obtain that $\delta_{(u,v)} \ge \zeta_{(u,v)}$. Then, assuming $\theta_1 = \theta_2 = 1/2$, it follows from **Lemma1** and (7), one can deduce $\zeta_{(u,v)}$ is asymptotically stable and $\zeta_{(u,v)} > 0$, which can be immediately infer that $\delta_{(u,v)} \ge \zeta_{(u,v)} > 0$ for all $u,v \in \Gamma$. ∎

Remark 1: According to the **Lemma 3** and the triggering rule (2), compared with the static ETM under the same conditions, the designed dynamic ETM provides a lower triggering frequency and can more effectively alleviate the burdens on the communication network. In addition, when the parameter ρ tends to infinity, the dynamic ETM will degenerate into the static one.

Proposition 1: For the update rule (3), let the parameters $\psi_1,\psi_2 \in (0,1/2)$, the bounded initial value $\delta_{(u,0)} > 0$ and $\delta_{(0,v)} > 0$ ($u,v \in \Gamma$), as well as positive integer k_0 be given, then, $\delta_{(u,v)}$ and $l_{(u,v)}$ are bounded.

Proof: According to the update rule (3) and **Lemma 3**, one has $0 < \delta_{(u,v)} \le \psi_1 \delta_{(u,v-1)} + \psi_2 \delta_{(u-1,v)} + \lambda$. It can be further concluded that $0 < \delta_{(u,v)} \le \tilde{\psi}\delta_{(u,v-1)} + \tilde{\psi}\delta_{(u-1,v)} + \lambda$, where $\tilde{\psi} \triangleq \max\{\psi_1,\psi_2\}$. For a given positive integer k_0, the following relationship is obtained by utilizing an iterative procedure:

$$\delta_{(u,v)} \le \tilde{\psi}\delta_{(u,v-1)} + \tilde{\psi}\delta_{(u-1,v)} + \lambda$$

$$\le \tilde{\psi}^2 \delta_{(u,v-2)} + 2\tilde{\psi}^2 \delta_{(u-1,v-1)} + \tilde{\psi}^2 \delta_{(u-2,v)} + 2\tilde{\psi}\lambda + \lambda$$

$$\le \tilde{\psi}^3 \delta_{(u,v-3)} + 3\tilde{\psi}^3 \delta_{(u-1,v-2)} + 3\tilde{\psi}^3 \delta_{(u-2,v-1)} + \tilde{\psi}^3 \delta_{(u-3,v)}$$
$$+ 4\tilde{\psi}^2 \lambda + 2\tilde{\psi}\lambda + \lambda$$

$$\le \tilde{\psi}^4 \delta_{(u,v-4)} + 4\tilde{\psi}^4 \delta_{(u-1,v-3)} + 4\tilde{\psi}^4 \delta_{(u-3,v-1)} + 6\tilde{\psi}^4 \delta_{(u-2,v-2)}$$
$$+ \tilde{\psi}^4 \delta_{(u-4,v)} + 8\tilde{\psi}^3 \lambda + 4\tilde{\psi}^2 \lambda + 2\tilde{\psi}\lambda + \lambda$$

$$\le \cdots \le \frac{1}{2}(2\tilde{\psi})^{k_0} \sum_{u+v-k_0} \delta_{(u,v)} + (2\tilde{\psi})^{k_0-1}\lambda + (2\tilde{\psi})^{k_0-2}\lambda + \cdots + \lambda$$

$$= \frac{1}{2}(2\tilde{\psi})^{k_0} \sum_{u+v-k_0} \delta_{(u,v)} + \lambda \frac{1-(2\tilde{\psi})^{k_0}}{1-2\tilde{\psi}}, \qquad (8)$$

it is easy to deduce $\delta_{(u,v)}$ is bounded and $\dfrac{\lambda}{\tilde{\lambda}_{\min}(\Upsilon_{(u,v)})}(1+\dfrac{1}{\rho(1-2\tilde{\psi})})$

is an asymptotic upper bound for $\|l_{(u,v)}\|$.

Remark 2: Indeed, **Lemma 3** and **Proposition 1** analyze the sufficient conditions that guarantee the boundedness of $\delta_{(u,v)}$ (i.e., $\tilde{\psi} < 1/2$), which coincides with stability criterion for 2-D systems presented in **Lemma 1**. For the given initial condition $\delta_{(u,0)} > 0$ and $\delta_{(0,v)} > 0$ for all $u, v \in \Gamma$, the parameters ψ_1 and ψ_2 render $\delta_{(u,v)}$ gradually converge to 0 if the two terms on the right side of the update rule (3) are removed. This prevents $\delta_{(u,v)}$ from diverging to avoid invalidating the triggering condition (2). Furthermore, the only relevant literature published for the investigation of dynamic ETM for 2-D systems is found in [24, 25]. Compared with the literature [24], the triggering condition (2) presented in this paper introduces a fixed parameter λ to further reduce the triggering frequency and improve flexibility. In [25], the design idea of the dynamic auxiliary variable is based on the exponential convergence, and the corresponding parameters ψ_1, ψ_2 and ρ need to meet specific conditions mutually. Our developed parameters ψ_1 and ψ_2 are simple and easy to implement, compared to the method of literature [25], thus reducing the design complexity to a certain extent.

B. Encryption-decryption Mechanism

Considering the vulnerability of communication networks and data privacy, preventing eavesdropping attacks and improving the security of networked systems are key starting points for the design of the EDM. The developed EDM is committed to enhancing the security of data transmission and the reliability of the filter, primarily through the following steps: 1) Based on the dynamic ETM, the variable $y_{(u_r,v_r)}$ is encrypted by utilizing the an encoding mechanism and transmitted through the network; 2) A decoder-based decryption mechanism is employed to maximize the restoration of $y_{(u_r,v_r)}$.

Inspired by the encoding and decoding mechanisms proposed in [32-34], the following bidirectional index-based EDM for 2-D systems is developed:

Encryption mechanism:

$$\begin{cases} \vec{y}_{(u,v)} = \wp(\varphi_{(u,v)}q_{(u,v)} + y_{(u_r,v_r)}) \\ \nabla_{(u,v)} = \varphi_{(u,v)}q_{(u,v)} + y_{(u_r,v_r)} - \vec{y}_{(u,v)} \\ q_{(u,v+1)} = \mathcal{M}_{(u,v)}q_{(u,v)} + \mathcal{N}_{(u,v)}\nabla_{(u,v)} \\ q_{(0,v)} = q_{(u,0)} = g_0 \qquad \forall u, v \in \Gamma \end{cases} \qquad (9)$$

where $q_{(u,v)} \in \mathbb{R}^{n_y}$ and $\vec{y}_{(u,v)} \in \mathbb{R}^{n_y}$ denote the internal state of the encoder and the encrypted output, respectively. $g_0 \in \mathbb{R}^{n_y}$ is the given initial state of $q_{(u,v)}$ without the element 0. $\wp_p(\bullet)$ represents the quantization function that is subsequently defined. $\mathcal{M}_{(u,v)}$ and $\mathcal{N}_{(u,v)}$ are known time-varying full rank matrices with proper dimensions. $\varphi_{(u,v)}$ is a known time-varying scaling factor, representing encryption parameters that are inaccessible to the eavesdropper. $\nabla_{(u,v)} \in \mathbb{R}^{n_y}$ represents the decoding error that will be subsequently interpreted. The encryption encoder employs a quantizer structure with the following form:

$$\wp_p(\bullet) \triangleq \{\vartheta_p^{[\gamma]}, \vartheta_p^{[\gamma]} \triangleq \gamma\mu_p, \gamma = 0, \pm 1, \pm 2, \cdots\}, p \in \{1, 2, 3, \cdots, n_y\},$$

where $\wp_p(\bullet)$ represents the p-th quantization function. The known positive scalar μ_p indicates the quantization interval and $\vartheta_p^{[\gamma]}$ denotes the quantization level. Defining $\tilde{y}_{(u,v)} = \varphi_{(u,v)}q_{(u,v)} + y_{(u_r,v_r)}$, it is easy to obtain that $\vartheta_p^{[\gamma]} \le \tilde{y}_{(u,v)} \le \vartheta_p^{[\gamma+1]}$, and the p-th quantization level satisfies the following probability distribution:

$$\begin{cases} \Pr\{\vec{y}_{p,(u,v)} = \wp_p(\tilde{y}_{p,(u,v)}) = \vartheta_p^{[\gamma]}\} = 1 - \chi_{p,(u,v)} \\ \Pr\{\vec{y}_{p,(u,v)} = \wp_p(\tilde{y}_{p,(u,v)}) = \vartheta_p^{[\gamma+1]}\} = \chi_{p,(u,v)} \end{cases},$$

where $\chi_{p,(u,v)} = (\tilde{y}_{p,(u,v)} - \vartheta_p^{[\gamma]})/\mu_p = (\tilde{y}_{p,(u,v)} - \gamma\mu_p)/\mu_p$ ($0 < \chi_{p,(u,v)} < 1$).

Furthermore, the decoding error of the p-th quantization function satisfies the following probability distribution:

$$\Pr\{\nabla_{p,(u,v)}\} = \Pr\{\tilde{y}_{p,(u,v)} - \gamma\mu_p\} = \Pr\{\mu_p\chi_{p,(u,v)}\} = 1 - \chi_{p,(u,v)}$$

and $\Pr\{\nabla_{p,(u,v)}\} = \Pr\{\tilde{y}_{p,(u,v)} - (\gamma+1)\mu_p\} = \Pr\{\mu_p(\chi_{p,(u,v)} - 1)\} = \chi_{p,(u,v)}$.

Then, we can directly calculate the mean value and variance of the $\nabla_{p,(u,v)}$ as

$$\mathbb{E}\{\nabla_{p,(u,v)}\} = \mu_p\chi_{p,(u,v)}(1 - \chi_{p,(u,v)}) + \chi_{p,(u,v)}\mu_p(\chi_{p,(u,v)} - 1) = 0$$

and

$$\mathbb{E}\{\nabla_{p,(u,v)}^2\} = (\mu_p\chi_{p,(u,v)})^2(1 - \chi_{p,(u,v)}) + (\mu_p(\chi_{p,(u,v)} - 1))^2 \chi_{p,(u,v)}$$
$$= \mu_p^2 \chi_{p,(u,v)}(1 - \chi_{p,(u,v)}) \le \mu_p^2/4,$$

therefore, it can be immediately inferred that $\mathbb{E}\{\nabla_{(u,v)}\} = 0$ and $\mathbb{E}\{\nabla_{(u,v)}\nabla_{(u,v)}^T\} \le \Psi = diag\{\mu_1^2/4, \mu_2^2/4, ..., \mu_{n_y}^2/4\}$.

Remark 3: It is assumed that the systems is maximally threatened by eavesdropping, which means that the system parameters $\mathcal{A}_{(u,v)}^{[1]}$, $\mathcal{A}_{(u,v)}^{[2]}$, $\mathcal{B}_{(u,v)}^{[1]}$, $\mathcal{B}_{(u,v)}^{[2]}$, $\mathcal{C}_{(u,v)}$ and $\mathcal{D}_{(u,v)}$, the

noise statistics characteristics W and V, as well as encrypted output $\vec{y}_{(u,v)}$ are publicly available to both the client and the eavesdropper. The encryption parameters $\mathcal{M}_{(u,v)}$ and $\mathcal{N}_{(u,v)}$, the quantization function $\wp_p(\bullet)$, and internal state of the encoder $q_{(u,v)}$ are not available to the eavesdropper, but are available to the client. In addition, the system's initial values $\mu_1(u)$ and $\mu_2(v)$ serve as internal variables of system, which are difficult to access directly for both the eavesdropper and the client.

Decryption mechanism:

Based on the encryption mechanism, the following decryption mechanism for client is designed:

$$\begin{cases} \kappa_{(u,v+1)} = \mathcal{M}_{(u,v)}\kappa_{(u,v)} + \mathcal{N}_{(u,v)}\nabla_{(u,v)} \\ \hat{y}_{(u,v)} = \vec{y}_{(u,v)} - \kappa_{(u,v)} \\ \kappa_{(0,v)} = \kappa_{(u,0)} = g_0 \qquad \forall u,v \in \Gamma \end{cases}, \qquad (10)$$

where $\kappa_{(u,v)} \in \mathbb{R}^{n_y}$ and $\hat{y}_{(u,v)} \in \mathbb{R}^{n_y}$ represent the internal state of the decoder and the decrypted output, respectively, both of them are available to the client. Suppose that the client and the eavesdropper use the identical recursive filter structure as follows:

Client：

$$\begin{cases} \hat{x}_{(u,v)}^- = \mathcal{A}_{(u,v-1)}^{[1]}\hat{x}_{(u,v-1)} + \mathcal{A}_{(u-1,v)}^{[2]}\hat{x}_{(u-1,v)} \\ \hat{x}_{(u,v)} = \hat{x}_{(u,v)}^- + \ell_{(u,v)}(\hat{y}_{(u,v)} - \mathcal{C}_{(u,v)}\hat{x}_{(u,v)}^-), \\ \hat{z}_{(u,v)} = \mathcal{H}_{(u,v)}x_{(u,v)} \end{cases} \qquad (11)$$

Eavesdropper：

$$\begin{cases} \tilde{x}_{(u,v)}^- = \mathcal{A}_{(u,v-1)}^{[1]}\tilde{x}_{(u,v-1)} + \mathcal{A}_{(u-1,v)}^{[2]}\tilde{x}_{(u-1,v)} \\ \tilde{x}_{(u,v)} = \tilde{x}_{(u,v)}^- + \mathcal{K}_{(u,v)}(\vec{y}_{(u,v)} - \mathcal{C}_{(u,v)}\tilde{x}_{(u,v)}^-) \end{cases}, \qquad (12)$$

where $\hat{x}_{(u,v)}$ and $\tilde{x}_{(u,v)}$ denote the estimates of the $x_{(u,v)}$ at the client side and the eavesdropper side, respectively. $\hat{z}_{(u,v)}$ is the estimate of the controlled output $z_{(u,v)}$ at the client side. $\ell_{(u,v)}$ and $\mathcal{K}_{(u,v)}$ represent filter gains at the client side and the eavesdropper side, respectively. It is important to emphasize that, due to the EDM, the client estimates the internal state of systems based on $\hat{y}_{(u,v)}$, while the eavesdropper uses $\vec{y}_{(u,v)}$ to estimate the actual state of systems. Then, we define the filtering error dynamics of the client and the eavesdropper as $e_{(u,v)} = x_{(u,v)} - \hat{x}_{(u,v)}$ and $\tilde{e}_{(u,v)} = x_{(u,v)} - \tilde{x}_{(u,v)}$, respectively. The controlled output error of the client is defined as $\mathcal{Z}_{(u,v)} = z_{(u,v)} - \hat{z}_{(u,v)}$. According to (1), (3), (9), (10), (11) and (12), one has

$$\begin{cases} e_{(u,v)} = \bar{\mathcal{A}}_{(u,v-1)}^{[1]}e_{(u,v-1)} + \bar{\mathcal{A}}_{(u-1,v)}^{[2]}e_{(u-1,v)} + \bar{\mathcal{B}}_{(u,v-1)}^{[1]}\omega_{(u,v-1)} \\ \quad + \bar{\mathcal{B}}_{(u-1,v)}^{[2]}\omega_{(u-1,v)} - \ell_{(u,v)}\mathcal{D}_{(u,v)}\upsilon_{(u,v)} - \ell_{(u,v)}l_{(u,v)} + \ell_{(u,v)}\nabla_{(u,v)}, (13) \\ \mathcal{Z}_{(i,j)} = \mathcal{H}_{(u,v)}e_{(u,v)} \end{cases}$$

and

$$\tilde{e}_{(u,v)} = \tilde{\mathcal{A}}_{(u,v-1)}^{[1]}\tilde{e}_{(u,v-1)} + \tilde{\mathcal{A}}_{(u-1,v)}^{[2]}\tilde{e}_{(u-1,v)} + \tilde{\mathcal{B}}_{(u,v-1)}^{[1]}\omega_{(u,v-1)} + \tilde{\mathcal{B}}_{(u-1,v)}^{[2]}\omega_{(u-1,v)}$$
$$\quad - \mathcal{K}_{(u,v)}\varphi_{(u,v)}q_{(u,v)} - \mathcal{K}_{(u,v)}l_{(u,v)} + \mathcal{K}_{(u,v)}\nabla_{(u,v)} - \mathcal{K}_{(u,v)}\mathcal{D}_{(u,v)}\upsilon_{(u,v)}, \quad (14)$$

where $\bar{\mathcal{A}}_{(u,v-1)}^{[1]} = \mathcal{A}_{(u,v-1)}^{[1]} - \ell_{(u,v)}\mathcal{C}_{(u,v)}\mathcal{A}_{(u,v-1)}^{[1]}$,

$\bar{\mathcal{A}}_{(u-1,v)}^{[2]} = \mathcal{A}_{(u-1,v)}^{[2]} - \ell_{(u,v)}\mathcal{C}_{(u,v)}\mathcal{A}_{(u-1,v)}^{[2]}$, $\bar{\mathcal{B}}_{(u,v-1)}^{[1]} = \mathcal{B}_{(u,v-1)}^{[1]} - \ell_{(u,v)}\mathcal{C}_{(u,v)}\mathcal{B}_{(u,v-1)}^{[1]}$,

$\bar{\mathcal{B}}_{(u-1,v)}^{[2]} = \mathcal{B}_{(u-1,v)}^{[2]} - \ell_{(u,v)}\mathcal{C}_{(u,v)}\mathcal{B}_{(u-1,v)}^{[2]}$, $\tilde{\mathcal{A}}_{(u,v-1)}^{[1]} = \mathcal{A}_{(u,v-1)}^{[1]} - \mathcal{K}_{(u,v)}\mathcal{C}_{(u,v)}\mathcal{A}_{(u,v-1)}^{[1]}$,

$\tilde{\mathcal{A}}_{(u-1,v)}^{[2]} = \mathcal{A}_{(u-1,v)}^{[2]} - \mathcal{K}_{(u,v)}\mathcal{C}_{(u,v)}\mathcal{A}_{(u-1,v)}^{[2]}$, $\tilde{\mathcal{B}}_{(u,v-1)}^{[1]} = \mathcal{B}_{(u,v-1)}^{[1]} - \mathcal{K}_{(u,v)}\mathcal{C}_{(u,v)}\mathcal{B}_{(u,v-1)}^{[1]}$,

$\tilde{\mathcal{B}}_{(u-1,v)}^{[2]} = \mathcal{B}_{(u-1,v)}^{[2]} - \mathcal{K}_{(u,v)}\mathcal{C}_{(u,v)}\mathcal{B}_{(u-1,v)}^{[2]}$.

Remark 4: Comparing the FESs (13) and (14), the influence of the internal state $q_{(u,v)}$ on the filtering error dynamics $e_{(u,v)}$ is avoided due to the client employs the decryption mechanism (10). In addition, the variables $\upsilon_{(u,v)}$, $l_{(u,v)}$ and $\nabla_{(u,v)}$ are bounded, which are necessary conditions for the filter gains $\ell_{(u,v)}$ to ensure convergence of the FESs (13) at the client side.

Remark 5: In this paper, we propose an encryption and decryption mechanism tailored to the characteristics of 2-D systems, which provides the following advantages: 1) The proposed EDM leverages encoding and decoding techniques to achieve data compression, facilitating digital data transmission; 2) The decoding error $\nabla_{(u,v)}$ with its stochastic properties, as well as encryption parameters $\mathcal{M}_{(u,v)}$ and $\mathcal{N}_{(u,v)}$ are introduced into the encryption mechanism (9), which further ensures the security of the system; 3) The addition of the scaling function $\varphi_{(u,v)}$ provides more flexibility.

III. Main Results

A. Encryption Parameters Design of Eavesdropper's Filter

The main purpose of this section is to design suitable encryption parameters $\mathcal{M}_{(u,v)}$ and $\mathcal{N}_{(u,v)}$ such that $q_{(u,v)}$ diverges, thereby guaranteeing that the encrypted output $\vec{y}_{(u,v)}$ at the eavesdropper is unavailable.

Assumption 1: Considering the energy constraints, the encryption matrices $\mathcal{M}_{(u,v)}$ and $\mathcal{N}_{(u,v)}$ satisfy the following inequalities relationships:

$$\underline{m}^2 I \le \left\|\mathcal{M}_{(u,v)}\right\|^2 \le \bar{m}^2 I , \ \underline{n}^2 I \le \left\|\mathcal{N}_{(u,v)}\right\|^2 \le \bar{n}^2 I , \qquad (15)$$

where $\underline{m}$, $\bar{m}$, $\underline{n}$ and $\bar{n}$ are positive scalars.

Theorem 1: Let the parameter satisfies $\underline{m} \ge \varpi + \left\|q_{(u,0)}\right\|^{-1} \bar{n}tr\{\Psi\}$ ($\varpi > 1$) and $\varphi_{(u,v)} \ne 0$ be given, where $tr\{\Psi\}$ denotes the trace of matrix Ψ. then the inequality $\left\|q_{(u,M)}\right\| \ge \varpi^M \left\|q_{(u,0)}\right\|$, $(u,v \in \Gamma)$ holds based on encryption rule (9), where M is a positive integer. Furthermore, for the eavesdropper's FESs (14), if the condition $\mathcal{K}_{(u,v)} \ne \mathbf{0}$ holds (i.e., there exists $\left\|\mathcal{K}_{(u,v)}\right\| > 0$), we can conclude that $\left\|\mathbb{E}\{\tilde{e}_{(u,v)}\}\right\|$ is divergent.

Proof: Depending on the encryption rule (9) and the property of the matrix norm, it is easy to establish the following relationship:

$$\left\|q_{(u,v+1)}\right\| = \left\|\mathcal{M}_{(u,v)}q_{(u,v)} + \mathcal{N}_{(u,v)}\nabla_{(u,v)}\right\| \ge \left\|\mathcal{M}_{(u,v)}q_{(u,v)}\right\| - \left\|\mathcal{N}_{(u,v)}\nabla_{(u,v)}\right\|$$

$$\geq \underline{m}\left\|q_{(u,v)}\right\| - \bar{n}tr\{\Psi\}. \quad (16)$$

Then, the $\left\|q_{(u,v+M)}\right\| \geq \varpi^M \left\|q_{(u,0)}\right\|$ holds for all $u,v \in \Gamma$, which can be summarized by mathematical induction as follows: **Initial step.** For $v = 0$, it follows that (16) and $\underline{m} \geq \varpi + \left\|q_{(u,0)}\right\|^{-1} \bar{n}tr\{\Psi\}$, it is straightforward to deduce that $\left\|q_{(u,1)}\right\| \geq \varpi \left\|q_{(u,0)}\right\|$ is true. **Inductive step.** Assuming $\left\|q_{(u,M-1)}\right\| > \varpi^{M-1} \left\|q_{(u,0)}\right\|$ holds for $v = M-1$, from (16) and $\underline{m} \geq \varpi + \left\|q_{(u,0)}\right\|^{-1} \bar{n}tr\{\Psi\}$, it is not difficult to calculate that

$$\left\|q_{(u,M)}\right\| \geq \underline{m}\left\|q_{(u,M-1)}\right\| - \bar{n}tr\{\Psi\} \geq \underline{m}\varpi^{M-1}\left\|q_{(u,0)}\right\| - \bar{n}tr\{\Psi\},$$

$$= (\varpi + \left\|q_{(u,0)}\right\|^{-1}\bar{n}tr\{\Psi\})\varpi^{M-1}\left\|q_{(u,0)}\right\| - \bar{n}tr\{\Psi\}$$

$$= \varpi^M \left\|q_{(u,0)}\right\| + (\varpi^{M-1}-1)\bar{n}tr\{\Psi\} \geq \varpi^M \left\|q_{(u,0)}\right\|. \quad (17)$$

It has been proven that $\left\|q_{(u,v+M)}\right\| \geq \varpi^M \left\|q_{(u,0)}\right\|$ $(u,v \in \Gamma)$, which implies that $\left\|q_{(u,v)}\right\|$ is divergent.

Subsequently, computing the mathematical expectation of (14), one has

$$\mathbb{E}\{\tilde{e}_{(u,v)}\} = \tilde{\mathcal{A}}_{(u,v-1)}^{[1]}\mathbb{E}\{\tilde{e}_{(u,v-1)}\} + \tilde{\mathcal{A}}_{(u-1,v)}^{[2]}\mathbb{E}\{\tilde{e}_{(u-1,v)}\}$$
$$-\varphi_{(u,v)}\mathcal{K}_{(u,v)}\mathbb{E}\{q_{(u,v)}\} - \mathcal{K}_{(u,v)}\mathbb{E}\{l_{(u,v)}\}. \quad (18)$$

It follows from (18) that

$$\left\|\varphi_{(u,v)}\mathcal{K}_{(u,v)}\mathbb{E}\{q_{(u,v)}\} + \mathcal{K}_{(u,v)}\mathbb{E}\{l_{(u,v)}\}\right\|$$

$$= \left\|\tilde{\mathcal{A}}_{(u,v-1)}^{[1]}\mathbb{E}\{\tilde{e}_{(u,v-1)}\} + \tilde{\mathcal{A}}_{(u-1,v)}^{[2]}\mathbb{E}\{\tilde{e}_{(u-1,v)}\} - \mathbb{E}\{\tilde{e}_{(u,v)}\}\right\|, \quad (19)$$

then we assume $\left\|E\{\tilde{e}_{(u,v)}\}\right\| \leq e^\circ$, where e° represents the existence of a positive scalar. According to the boundedness of $l_{(u,v)}$ in **Proposition 1**, it can be further concluded from (19) that

$$\lim_{u+v\to\infty}\left\|\varphi_{(u,v)}\mathcal{K}_{(u,v)}\mathbb{E}\{q_{(u,v)}\}\right\|$$

$$\leq (\left\|\tilde{\mathcal{A}}_{(u,v-1)}^{[1]}\right\| + \left\|\tilde{\mathcal{A}}_{(u-1,v)}^{[2]}\right\| + 1)e^\circ + \lambda(1 + \frac{1}{\rho(1-2\tilde{\psi})})\lim_{u+v\to\infty}\left\|\mathcal{K}_{(u,v)}\right\|, \quad (20)$$

based on (20), this conflicts with the assumption that $\left\|E\{\tilde{e}_{(u,v)}\}\right\| \leq e^\circ$ in the case of $\mathcal{K}_{(u,v)} \neq \mathbf{0}$, therefore, the $\left\|\mathbb{E}\{\tilde{e}_{(u,v)}\}\right\|$ is divergent. The proof is thus completed.

Remark 6: If $\underline{m} \geq \varpi + \left\|q_{(u,0)}\right\|^{-1} \bar{n}tr\{\Psi\}$ ($\varpi > 1$) holds, it follows that the $\left\|q_{(u,v)}\right\|$ is divergent. Therefore, the LMI obtained by the eavesdropper according to Lyapunov stability theory is unsolvable, as the difference along the FESs of the eavesdropper is positive definite. If the eavesdropper desires $\left\|\mathbb{E}\{\tilde{e}_{(u,v)}\}\right\|$ to be bounded, then the filter gains should satisfy $\mathcal{K}_{(u,v)} = \mathbf{0}$ as early as possible. Taking into account noise and the effect of unknown initial values, the estimation of the open-loop FESs becomes unavailable. In addition, we can set the parameter ϖ as large as possible to enable $\left\|q_{(u,v)}\right\|$ to diverge faster and improve the system's security. In conclusion, under

the encryption mechanism (9), the eavesdropper cannot access the actual state of the system, regardless of whether the filter gains $\mathcal{K}_{(u,v)}$ can be calculated or not.

Remark 7: In contrast to the encoding-decoding schemes developed in the literature [34] and [35], Theorem 1 presents a design method of the encryption parameters that renders eavesdropping attacks invalid and quantitatively analyzes the effects of these parameters. Moreover, for another filter structure $\tilde{x}_{(u,v)} = \mathcal{A}_{(u,v-1)}^{[1]}\tilde{x}_{(u,v-1)} + \mathcal{A}_{(u-1,v)}^{[2]}\tilde{x}_{(u-1,v)} + \mathcal{K}_{(u,v-1)}(\vec{y}_{(u,v-1)} - \mathcal{C}_{(u,v-1)}\tilde{x}_{(u,v-1)}) + \mathcal{K}_{(u-1,v)}(\vec{y}_{(u-1,v)} - \mathcal{C}_{(u-1,v)}\tilde{x}_{(u-1,v)})$, which is common in 2-D systems, following the same analytical approach as Theorem 1, the $\left\|\mathbb{E}\{\tilde{e}_{(u,v)}\}\right\|$ is also divergent when $\left\|\mathcal{K}_{(u,v)}\right\| > 0$.

Remark 8: In actual control practice, we can initially select the upper and lower bounds for $\left\|\mathfrak{N}_{(u,v)}\right\|$, non-zero elements for the initial encoder state $q_{(u,0)}$, and the scalar ϖ ($\varpi > 1$). Subsequently, according to $\underline{m} = \varpi + \left\|q_{(u,0)}\right\|^{-1} \bar{n}tr\{\Psi\}$, it is straightforward to calculate $\underline{m}$, thereby obtaining a lower bound $\underline{m}I$ for $\left\|\mathfrak{M}_{(u,v)}\right\|$.

B. Filtering Performance Analysis of Client's Filter

Theorem 2: For the client's FESs (13) subject to the dynamic ETM (2) and EDM (9)-(10), let the scalars $\psi_1, \psi_2 \in (0,1/2)$, $\hbar \in (1/2,1)$, ρ, λ as well as filter gains $\ell_{(u,v)}$ be given, if there exist positive definite symmetric matrices $\mathcal{T}_{(u+1,v+1)}$, $\mathcal{P}_{(u+1,v)}$ and $\mathcal{Q}_{(u,v+1)}$, positive scalars $\gamma_{1,(u+1,v)}$, $\gamma_{2,(u,v+1)}$ and β such that the following inequality hold:

$$\tilde{\Pi} = \begin{bmatrix} \tilde{\Pi}_{11} & \tilde{\Pi}_{12} & \tilde{\Pi}_{13} & 0 & 0 \\ * & \tilde{\Pi}_{22} & \tilde{\Pi}_{23} & 0 & 0 \\ * & * & \tilde{\Pi}_{33} & 0 & 0 \\ * & * & * & \tilde{\Pi}_{44} & 0 \\ * & * & * & * & \tilde{\Pi}_{55} \end{bmatrix} < 0, \quad (21)$$

where $\tilde{\Pi}_{11} = (\bar{\mathcal{A}}_{(u+1,v)}^{[1]})^T \mathcal{T}_{(u+1,v+1)}\bar{\mathcal{A}}_{(u+1,v)}^{[1]} - (1-\hbar)\mathcal{P}_{(u+1,v)}$,

$\tilde{\Pi}_{12} = (\bar{\mathcal{A}}_{(u+1,v)}^{[1]})^T \mathcal{T}_{(u+1,v+1)}\bar{\mathcal{A}}_{(u,v+1)}^{[2]}$, $\tilde{\Pi}_{13} = -(\bar{\mathcal{A}}_{(u+1,v)}^{[1]})^T \mathcal{T}_{(u+1,v+1)}\ell_{(u+1,v+1)}$,

$\tilde{\Pi}_{22} = (\bar{\mathcal{A}}_{(u,v+1)}^{[2]})^T \mathcal{T}_{(u+1,v+1)}\bar{\mathcal{A}}_{(u,v+1)}^{[2]} - (1-\hbar)\mathcal{Q}_{(u,v+1)}$,

$\tilde{\Pi}_{23} = -(\bar{\mathcal{A}}_{(u,v+1)}^{[2]})^T \mathcal{T}_{(u+1,v+1)}\ell_{(u+1,v+1)}$,

$\tilde{\Pi}_{33} = (1+\beta)\ell_{(u+1,v+1)}^T \mathcal{T}_{(u+1,v+1)}\ell_{(u+1,v+1)} - (\frac{2}{\rho} + \gamma_{1,(u+1,v)})\Upsilon_{(u+1,v+1)}$,

$\tilde{\Pi}_{44} = (2\psi_1 - 1 + \gamma_{1,(u+1,v)} + \hbar)/\rho$, $\tilde{\Pi}_{55} = (2\psi_2 - 1 + \gamma_{2,(u,v+1)} + \hbar)/\rho$,

$\Lambda = \lambda_{\max}\{(\bar{\mathcal{B}}_{(u+1,v)}^{[1]})^T \mathcal{T}_{(u+1,v+1)}\bar{\mathcal{B}}_{(u+1,v)}^{[1]} + (\bar{\mathcal{B}}_{(u,v+1)}^{[2]})^T \mathcal{T}_{(u+1,v+1)}\bar{\mathcal{B}}_{(u,v+1)}^{[2]}\}tr\{W\}$
$+ \lambda_{\max}\{\mathcal{D}_{(u+1,v+1)}^T \ell_{(u+1,v+1)}^T \mathcal{T}_{(u+1,v+1)}\ell_{(i+1,j+1)}\mathcal{D}_{(i+1,j+1)}\}tr\{V\}$
$+ \lambda_{\max}\{\ell_{(u+1,v+1)}^T \mathcal{T}_{(u+1,v+1)}\ell_{(i+1,j+1)}\}tr\{\Psi\} + \lambda(\gamma_{1,(u+1,v)} + \gamma_{2,(u,v+1)}) + \frac{2\lambda}{\rho}$,

then the FESs of client (13) are exponentially ultimately bounded in mean square sense.

Proof: To guarantee that the FESs of client (13) are exponentially ultimately bounded in the mean square sense, we define the Lyapunov-like function as follows

This article has been accepted for publication in IEEE Transactions on Network Science and Engineering. This is the author's version which has not been fully edited and content may change prior to final publication. Citation information: DOI 10.1109/TNSE.2025.3542177

7

> REPLACE THIS LINE WITH YOUR MANUSCRIPT ID NUMBER (DOUBLE-CLICK HERE TO EDIT) <

$$V_{(u,v)} = V_{(u,v)}^{[1]} + V_{(u,v)}^{[2]} \tag{22}$$

with $V_{(u,v)}^{[1]} = e_{(u,v)}^T \mathcal{P}_{(u,v)} e_{(u,v)} + (1/\rho)\delta_{(u,v)}$, $V_{(u,v)}^{[2]} = e_{(u,v)}^T \mathcal{Q}_{(u,v)} e_{(u,v)} + (1/\rho)\delta_{(u,v)}$.

Considering the following index:

$$\Delta V_{(u,v)} \triangleq V_{(u+1,v+1)} - V_{(u+1,v)}^{[1]} - V_{(u,v+1)}^{[2]} = V_{(u+1,v+1)}^{[1]} - V_{(u+1,v)}^{[1]} + V_{(u+1,v+1)}^{[2]} - V_{(u,v+1)}^{[2]}$$

$$= \Delta V_{(u,v)}^{[1]} + \Delta V_{(u,v)}^{[2]},$$

then the difference of (22) can be calculated as:

$$\mathbb{E}\{\Delta V_{(u,v)}^{[1]}\} = \mathbb{E}\{e_{(u+1,v+1)}^T \mathcal{P}_{(u+1,v+1)} e_{(u+1,v+1)} + (1/\rho)\delta_{(u+1,v+1)}$$
$$- e_{(u+1,v)}^T \mathcal{P}_{(u+1,v)} e_{(u+1,v)} - (1/\rho)\delta_{(u+1,v)}\}, \tag{23}$$

$$(1/\rho)(\delta_{(u+1,v+1)} - \delta_{(u+1,v)})$$
$$= (1/\rho)(\lambda + \psi_1 \delta_{(u+1,v)} + \psi_2 \delta_{(u,v+1)} - l_{(u+1,v+1)}^T \Upsilon_{(u+1,v+1)} l_{(u+1,v+1)} - \delta_{(u+1,v)}), \tag{24}$$

$$\mathbb{E}\{\Delta V_{2,(i,j)}\} = \mathbb{E}\{e_{(u+1,v+1)}^T \mathcal{Q}_{(u+1,v+1)} e_{(u+1,v+1)} + (1/\rho)\delta_{(u+1,v+1)}$$
$$- e_{(u,v+1)}^T \mathcal{Q}_{(u,v+1)} e_{(u,v+1)} - (1/\rho)\delta_{(u+1,v)}\}, \tag{25}$$

$$(1/\rho)(\delta_{(u+1,v+1)} - \delta_{(u,v+1)})$$
$$= (1/\rho)(\lambda + \psi_1 \delta_{(u+1,v)} + \psi_2 \delta_{(u,v+1)} - l_{(u,v+1)}^T \Upsilon_{(u,v+1)} l_{(u,v+1)} - \delta_{(u,v+1)}), \tag{26}$$

Moreover, by taking into account the triggering condition (2), it can be easily seen that there exist positive scalars $\gamma_{1,(u+1,v)}$ and $\gamma_{2,(u,v+1)}$ such that the following inequalities hold:

$$\gamma_{1,(u+1,v)}(\lambda + (1/\rho)\delta_{(u+1,v)} - l_{(u+1,v)}^T \Upsilon_{(u+1,v)} l_{(u+1,v)}) \geq 0, \tag{27}$$

$$\gamma_{2,(u,v+1)}(\lambda + (1/\rho)\delta_{(u,v+1)} - l_{(u,v+1)}^T \Upsilon_{(u,v+1)} l_{(u,v+1)}) \geq 0. \tag{28}$$

Subsequently, with the help of the elementary inequality $a^T b + b^T a \leq \beta a^T a + \beta^{-1} b^T b$ $(\forall \beta > 0)$, where β is a positive scalar, a and b are vectors with proper dimensions. Then, the coupling term can be rewritten in the following form:

$$\upsilon_{(u+1,v+1)}^T \mathcal{D}_{(u+1,v+1)}^T \ell_{(u+1,v+1)}^T \mathcal{T}_{(u+1,v+1)} \ell_{(u+1,v+1)} l_{(u+1,v+1)}$$
$$+ l_{(u+1,v+1)}^T \ell_{(u+1,v+1)}^T \mathcal{T}_{(u+1,v+1)} \ell_{(u+1,v+1)} \mathcal{D}_{(u+1,v+1)} \upsilon_{(u+1,v+1)}$$
$$\leq \beta^{-1} \upsilon_{(u+1,v+1)}^T \mathcal{D}_{(u+1,v+1)}^T \ell_{(u+1,v+1)}^T \mathcal{T}_{(u+1,v+1)} \ell_{(u+1,v+1)} \mathcal{D}_{(u+1,v+1)} \upsilon_{(u+1,v+1)}$$
$$+ \beta l_{(u+1,v+1)}^T \ell_{(u+1,v+1)}^T \mathcal{T}_{(u+1,v+1)} \ell_{(u+1,v+1)} l_{(u+1,v+1)}, \tag{29}$$

Then, we define $\eta_{(u,v)} = \begin{bmatrix} e_{(u+1,v)}^T & e_{(u,v+1)}^T & l_{(u+1,v+1)}^T & \sqrt{\delta_{(u+1,v)}} & \sqrt{\delta_{(u,v+1)}} \end{bmatrix}^T$, and consider (23)-(29), which yields

$$\mathbb{E}\{\Delta V_{(u,v)}\} + \mathbb{E}\{\hbar(V_{(u+1,v)}^{[1]} + V_{(u,v+1)}^{[2]})\} \leq \eta_{(u,v)}^T \tilde{\Pi} \eta_{(u,v)} + \Lambda, \tag{30}$$

where $\tilde{\Pi} = \begin{bmatrix} \tilde{\Pi}_{11} & \tilde{\Pi}_{12} & \tilde{\Pi}_{13} & 0 & 0 \\ * & \tilde{\Pi}_{22} & \tilde{\Pi}_{23} & 0 & 0 \\ * & * & \tilde{\Pi}_{33} & 0 & 0 \\ * & * & * & \tilde{\Pi}_{44} & 0 \\ * & * & * & * & \tilde{\Pi}_{55} \end{bmatrix}$,

$\tilde{\Pi}_{11} = (\bar{\mathcal{A}}_{(u+1,v)}^{[1]})^T \mathcal{T}_{(u+1,v+1)} \bar{\mathcal{A}}_{(u+1,v)}^{[1]} - (1-\hbar)\mathcal{P}_{(u+1,v)}$,

$\tilde{\Pi}_{12} = (\bar{\mathcal{A}}_{(u+1,v)}^{[1]})^T \mathcal{T}_{(u+1,v+1)} \bar{\mathcal{A}}_{(u,v+1)}^{[2]}$, $\tilde{\Pi}_{13} = -(\bar{\mathcal{A}}_{(u+1,v)}^{[1]})^T \mathcal{T}_{(u+1,v+1)} \ell_{(u+1,v+1)}$,

$\tilde{\Pi}_{22} = (\bar{\mathcal{A}}_{(u,v+1)}^{[2]})^T \mathcal{T}_{(u+1,v+1)} \bar{\mathcal{A}}_{(u,v+1)}^{[2]} - (1-\hbar)\mathcal{Q}_{(u,v+1)}$,

$\tilde{\Pi}_{23} = -(\bar{\mathcal{A}}_{(u,v+1)}^{[2]})^T \mathcal{T}_{(u+1,v+1)} \ell_{(u+1,v+1)}$,

$\tilde{\Pi}_{33} = (1+\beta)\ell_{(u+1,v+1)}^T \mathcal{T}_{(u+1,v+1)} \ell_{(u+1,v+1)} - (2/\rho)\Upsilon_{(u+1,v+1)}$,

$\tilde{\Pi}_{44} = (2\psi_1 - 1 + \gamma_{1,(u+1,v)} + \hbar)/\rho$, $\tilde{\Pi}_{55} = (2\psi_2 - 1 + \gamma_{2,(u,v+1)} + \hbar)/\rho$,

If $\tilde{\Pi} < 0$, based on (30) and (22), one has

$$\mathbb{E}\{V_{(u+1,v+1)}\}$$
$$\leq \mathbb{E}\{(1-\hbar)(V_{(u+1,v)}^{[1]} + V_{(u,v+1)}^{[2]})\} + \Lambda$$
$$\leq \mathbb{E}\{(1-\hbar)(V_{(u+1,v)}^{[1]} + V_{(u,v+1)}^{[2]}) + (1-\hbar)(V_{(u,v)}^{[2]} + V_{(u+1,v)}^{[1]})\} + \Lambda$$
$$= \mathbb{E}\{(1-\hbar)(V_{(u+1,v)} + V_{(u,v+1)})\} + \Lambda. \tag{31}$$

Similarly, by employing the identical iterative approach outlined in (8), for any sufficiently large positive integer $\mathcal{S}$, it can be further deduced that

$$\mathbb{E}\{V_{(u,v)}\}$$
$$< \frac{1}{2}(2\bar{\hbar})^{\mathcal{S}} \mathbb{E}\{\sum_{u+v-\mathcal{S}} V_{(u,v)}\} + (2\bar{\hbar})^{\mathcal{S}-1}\Lambda + (2\bar{\hbar})^{\mathcal{S}-2}\Lambda + ... + \Lambda$$
$$= \frac{1}{2}(2\bar{\hbar})^{\mathcal{S}} \mathbb{E}\{\sum_{u+v-\mathcal{S}} V_{(u,v)}\} + \Lambda\frac{1-(2\bar{\hbar})^{\mathcal{S}}}{1-2\bar{\hbar}}, \tag{32}$$

where $\bar{\hbar} = 1 - \hbar$. It follows from (32) that $\iota_1 \mathbb{E}\{\|e_{(u,v)}\|^2\} \leq \mathbb{E}\{V_{(u,v)}\}$,

where $\iota_1 = \hat{\lambda}_{\min}(\mathcal{T}_{(u,v)})$. Then, we have $\mathbb{E}\{\|e_{(u,v)}\|^2\} \leq \frac{1}{\iota_1}\mathbb{E}\{V_{(u,v)}\}$

$< \frac{1}{2\iota_1}(2\bar{\hbar})^{\mathcal{S}} \mathbb{E}\{\sum_{u+v-\mathcal{S}} V_{(u,v)}\} + \Lambda\frac{1}{\iota_1(1-2\bar{\hbar})}$. Obviously, if $\tilde{\Pi} < 0$

holds, the client's FESs (13) are exponentially ultimately bounded in the mean-square sense. The proof is thus completed.

Theorem 3: For the client's FESs (13) with the dynamic ETM (2) and EDM (9)-(10), let the scalars $\psi_1, \psi_2 \in (0, 1/2)$, $\hbar \in (1/2, 1)$, ρ, and λ be given. If there exist positive definite symmetric matrices $\mathcal{X}_{(u+1,v+1)}$, $\mathcal{T}_{(u+1,v+1)}$, $\mathcal{P}_{(u+1,v)}$ and $\mathcal{Q}_{(u,v+1)}$, positive scalars $\gamma_{1,(u+1,v)}$, $\gamma_{2,(u,v+1)}$ and β such that the following inequalities hold:

$$\Pi = \begin{bmatrix} \Pi^{[1]} & \Pi^{[2]} \\ * & \Pi^{[3]} \end{bmatrix} < 0, \tag{33}$$

$$\mathcal{H}_{(u,v)}^T \mathcal{H}_{(u,v)} \leq \mathcal{T}_{(u,v)}, \tag{34}$$

where $\Pi^{[1]} = diag\{\Pi_{11}^{[1]}, \Pi_{22}^{[1]}, \Pi_{33}^{[1]}, \Pi_{44}^{[1]}, \Pi_{55}^{[1]}\}$,

$$\Pi^{[2]} = \begin{bmatrix} \Pi_{11}^{[2]} & 0 \\ \Pi_{21}^{[2]} & 0 \\ -\mathcal{X}_{(u+1,v+1)} & -\sqrt{\beta}\mathcal{X}_{(u+1,v+1)} \\ 0 & 0 \\ 0 & 0 \end{bmatrix}, \Pi^{[3]} = diag\{-\mathcal{T}_{(u+1,v+1)}, -\mathcal{T}_{(u+1,v+1)}\},$$

$\Pi_{11}^{[1]} = -(1-\hbar)\mathcal{P}_{(u+1,v)}$, $\Pi_{22}^{[1]} = -(1-\hbar)\mathcal{Q}_{(u,v+1)}$, $\Pi_{33}^{[1]} = -(2/\rho)\Upsilon_{(u+1,v+1)}$,

$\Pi_{44}^{[1]} = (2\psi_1 - 1 + \gamma_{1,(u+1,v)} + \hbar)/\rho$, $\Pi_{55}^{[1]} = (2\psi_2 - 1 + \gamma_{2,(u,v+1)} + \hbar)/\rho$,

$\Pi_{11}^{[2]} = (\mathcal{A}_{(u+1,v)}^{[1]})^T \mathcal{T}_{(u+1,v+1)} - (\mathcal{A}_{(u+1,v)}^{[1]})^T \mathcal{C}_{(u+1,v+1)}^T \mathcal{X}_{(u+1,v+1)}$,

$\Pi_{21}^{[2]} = (\mathcal{A}_{(u,v+1)}^{[2]})^T \mathcal{T}_{(u+1,v+1)} - (\mathcal{A}_{(u,v+1)}^{[2]})^T \mathcal{C}_{(u+1,v+1)}^T \mathcal{X}_{(u+1,v+1)}$, and the other symbols are defined in **Theorem 2**. Then, $\|\mathcal{Z}_{(u,v)}\|$ is exponentially ultimately bounded in the mean square sense, and the filter gains $\ell_{(u,v)}$ can be given as:

$$\ell_{(u,v)} = (\mathcal{X}_{(u,v)} \mathcal{T}_{(u,v)}^{-1})^T. $$

Proof. By utilizing the Schur complement lemma and performing a congruent transformation on (21) with the matrix

$diag\{I,I,I,I,\mathcal{T}_{(u+1,v+1)},\mathcal{T}_{(u+1,v+1)}\}$, then defining $\ell_{(u,v)}^T \mathcal{T}_{(u,v)} = \mathcal{X}_{(u,v)}$, it is easily to shown that (33) holds. Furthermore, by combining (13) and (34), it is not difficult to obtain that

$$\mathbb{E}\{\|\mathcal{Z}_{(u,v)}\|\} = \mathbb{E}\{e_{(u,v)}^T \mathcal{H}_{(u,v)}^T \mathcal{H}_{(u,v)} e_{(u,v)}\} \le \mathbb{E}\{e_{(u,v)}^T \mathcal{T}_{(u,v)} e_{(u,v)}\}$$

$$\le \mathbb{E}\{V_{(u,v)}\} \le \frac{1}{2}(2\bar{\hbar})^{\mathcal{S}} \mathbb{E}\{\sum_{u+v-\mathcal{S}} V_{(u,v)}\} + \Lambda \frac{1-(2\bar{\hbar})^{\mathcal{S}}}{1-2\bar{\hbar}},$$

which implies that the controlled output error $\mathcal{Z}_{(u,v)}$ is exponentially ultimately bounded in the mean square sense with an asymptotic upper bound $\frac{\Lambda}{1-2\bar{\hbar}}$. The proof is thus completed.

Remark 9: The client's filter gains design method developed in this paper is accomplished with the help of LMI technology, and the algorithms based on the standard LMI systems have polynomial time complexity, e.g., the computational complexity of LMI is defined as $\mathcal{O}(\mathcal{Q}\mathcal{Y}^3 \log(\mathfrak{R}/\mathfrak{I}))$ [37], where $\mathcal{Q}$ denotes the row size, $\mathcal{Y}$ represents for the number of scalar decision variables, $\mathfrak{R}$ is a data-dependent scaling factor, and $\mathfrak{I}$ is relative accuracy set for algorithm. In addition, $\mathcal{Q}$, $\mathcal{Y}$, $\mathfrak{R}$ and $\mathfrak{I}$ are the same for each instant of the (33)-(34). Therefore, the computational complexity of Theorem 3 is easily derived by the method presented in [37]. Moreover, Theorem 3 can be solved offline since the matrices of the time-varying system are known.

In view of Theorem 2 and 3, we summarize the the design of encryption and decryption parameters, as well as the filtering algorithm as follows:

Encryption parameters design and filtering algorithm for 2-D systems

---

Step 1: Set the initial value $q_{(u,v)}$ for $u = 0$, $v \in [0,\kappa]$ or $v = 0$, $u \in [0,\kappa]$, the positive scalar $\varpi > 1$ and $\bar{n}$, as well as μ_p ($p \in \{1,2,3,\cdots,n_y\}$).

Step 2: Given ϖ, $\Psi = diag\{\mu_1^2/4, \mu_2^2/4,...,\mu_{n_y}^2/4\}$, $q_{(u,0)}$ and $\bar{n}$, then, calculate $\underline{m} = \varpi + \|q_{(u,0)}\|^{-1} \bar{n} tr\{\Psi\}$.

Step 3: Determine appropriate encryption rule (9).

Step 4: Initialization $x_{(u,0)}$, $x_{(0,v)}$, $\hat{x}_{(u,0)}$, $\hat{x}_{(0,v)}$, $\delta_{(u,0)}$ and $\delta_{(0,v)}$ for $u = 0$, $v \in [0,\kappa]$ or $v = 0$, $u \in [0,\kappa]$ as well as parameters ψ_1, ψ_2, ρ and λ.

Step 5: For $u = 1:\kappa$

  For $v = 1:\kappa$

  Calculate filter gains of client $\ell_{(u,v)}$ by applying Theorem 2, then, compute the $\hat{x}_{(u,v)}$ and $e_{(u,v)}$

  End

  End

Step 6: Stop.

IV. NUMERICAL SIMULATIONS

In this section, the effectiveness and superiority of the proposed filtering method is verified through two examples.

Example 1: A practical metal strip process example is employed to verify the effectiveness of the proposed algorithm.
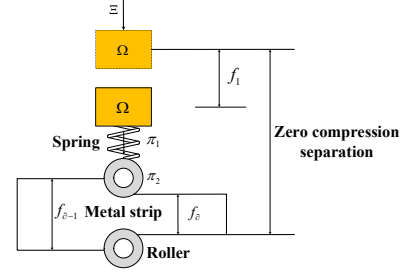
Fig.2. Physical diagram of the metal rolling process.

The metal rolling process depicted in Fig. 2 can be characterized by the following delayed differential system equation [38]:

$$f_{\partial}(t) = \frac{\pi}{\pi + \Omega\alpha^2}\left\{\left(1 + \frac{\Omega\alpha^2}{\pi_1}\right)f_{\partial-1}(t) - \frac{1}{\pi_2}\Xi\right\}, \quad (35)$$

where $f_{\partial}(t)$ denotes the ∂-th actual roll-gap thickness, α denotes the differentiation operator, Ω represents the aggregated mass of the roll-gap adjustment mechanism. Let π_1 represents the spring constant of the adjustment mechanism. π_2 is the hardness coefficient of the metal strip, and define π as the composite stiffness. Considering the effects of heterogeneous materials, the $\pi = (1+\tau_{(u,v)})\frac{\pi_1\pi_2}{\pi_1+\pi_2}$ characterizes the combined rigidity of both the metal strip and the rolling mechanism, where $\tau_{(u,v)} = 0.25\cos(0.6(u+v))$. Ξ means the force generated by the motor.

By utilizing a backward difference scheme and choosing the sampling interval T, the equation (35) can be rewritten as follows:

$$f_{\partial}(t+T) = c_1 f_{\partial}(t) + c_2 f_{\partial}(t-T) + c_3 f_{\partial-1}(t+T)$$
$$+ c_4 f_{\partial-1}(t) + c_5 f_{\partial-1}(t-T) + \bar{c}\Xi \quad (36)$$

where $c_1 = \frac{2\Omega}{\pi T^2 + \Omega}$, $c_2 = -\frac{\Omega}{\pi T^2 + \Omega}$, $c_3 = \frac{\pi}{\pi T^2 + \Omega}(T^2 + \frac{\Omega}{\pi_1})$,

$c_4 = -\frac{2\pi\Omega}{\pi_1(\pi T^2 + \Omega)}$, $c_5 = \frac{\pi\Omega}{\pi_1(\pi T^2 + \Omega)}$, $\bar{c} = \frac{\pi T^2}{\pi_2(\pi T^2 + \Omega)}$.

Define $t = vT$ and $\Xi = 0$, then, the equation (36) can be constructed as the following state-space model:

$$x_{(u+1,v+1)} = \mathcal{A}_{(u+1,v)}^{[1]} x_{(u+1,v)} + \mathcal{A}_{(u,v+1)}^{[2]} x_{(u,v+1)},$$

where $\mathcal{A}_{(u+1,v)}^{[1]} = \begin{bmatrix} c_3 & c_4 & c_1 & c_2 & c_5 \\ 0 & 0 & 1 & 0 & 0 \\ 0 & 0 & 0 & 0 & 0 \\ 0 & 0 & 0 & 0 & 0 \\ 0 & 0 & 0 & 0 & 0 \end{bmatrix}$, $\mathcal{A}_{(u,v+1)}^{[2]} = \begin{bmatrix} 0 & 0 & 0 & 0 & 0 \\ 0 & 0 & 0 & 0 & 0 \\ c_3 & c_4 & c_1 & c_2 & c_5 \\ 0 & 0 & 1 & 0 & 0 \\ 0 & 1 & 0 & 0 & 0 \end{bmatrix}$,

$x_{(u,v)} = [f_{\partial-1}((v+1)T) \quad f_{\partial-1}(vT) \quad f_{\partial}(vT) \quad f_{\partial}((v-1)T) \quad f_{\partial-1}((v-1)T)]^T$.

Considering the parameters $\Omega = 50kg$, $T = 1s$, $\pi_1 = 300N/\text{mm}$,

$\mathcal{B}_{(u,v)}^{[1]} = \begin{bmatrix} 0.2+0.5\sin(0.2(u+v)) & 0.3 & 0.4 & 0.5 & 0.4 \end{bmatrix}^T$,

$\mathcal{B}_{(u,v)}^{[2]} = \begin{bmatrix} 0.35 & 0.14 & 0.6 & 0.4 & 0.2+0.5\sin(0.2(u+v)) \end{bmatrix}^T$,

$\pi_2 = 1000 N/mm$, $\mathcal{C}_{(u,v)} = 0.64I$, $\mathcal{D}_{(u,v)} = 0.8I$, $\mathcal{H}_{(u,v)} = 1.02I$.

Setting the initial state as $x_{(u,v)} = \begin{bmatrix} 3.2\cos(u)\sin(v) & 3.4\cos(u-1)\sin(v) \end{bmatrix}$ $3.14\cos(u)\sin(v)$ $3.3\cos(u-1)\sin(v)$ $3.65\cos(u+1)\sin(v)]^T$ for $u \in [0\ \ 30]$ and $v = 0$, $x_{(u,v)} = \begin{bmatrix} 3.2\cos(u)\sin(v) & 3.3\cos(u-1)\sin(v) & 3.14\cos(u)\sin(v) \end{bmatrix}$ $3.3\cos(u-1)\sin(v)$ $3.65\cos(u+1)\sin(v)]^T$ for $u = 0$ and $v \in [1\ \ 30]$. Moreover, the initial conditions of filter are set as $\hat{x}_{(u,0)} = \hat{x}_{(0,v)} = \tilde{x}_{(u,0)} = \tilde{x}_{(0,v)} = \begin{bmatrix} 0 & 0 & 0 & 0 & 0 \end{bmatrix}^T$ for $u,v \in \Gamma$. The initial values of dynamic auxiliary variables are set as $\delta_{(u,0)} = \delta_{(0,v)} = 0.4$ for all $u,v \in \Gamma$, and the remaining parameters are selected as $\psi_1 = 0.3$, $\psi_2 = 0.2$ and $\lambda = 0.4$. It is assumed that the process noise $w_{(u,v)}$ and measurement noise $\upsilon_{(u,v)}$ with variance $W = 0.75I$ and $V = 0.82I$ for $u,v \in [0\ \ 20]$. Subsequently, suppose that $\mathcal{M}_{(u,v)} = (1.73+0.2\sin(u+v))I$, $\mathcal{N}_{(u,v)} = (0.98+0.2\cos(u+v))I$, $\mu_p = 0.2$ $(p \in \{1,2,3,\cdots,n_y\})$, $\varpi = 1.2$, and $q_{(u,0)} = q_{(0,v)} = g_0 = \begin{bmatrix} 0.2 & 0.2 & 0.2 & 0.2 & 0.2 \end{bmatrix}^T$ for all $u,v \in \Gamma$. Then, we can easily calculate that $1.53 \le \|\mathcal{M}_{(u,v)}\| \le 1.93$, $0.78 \le \|\mathcal{N}_{(u,v)}\| \le 1.12$, and the condition $\underline{m} \ge \varpi + \|q_{(u,0)}\|^{-1} \overline{n} tr\{\Psi\}$ is satisfied.
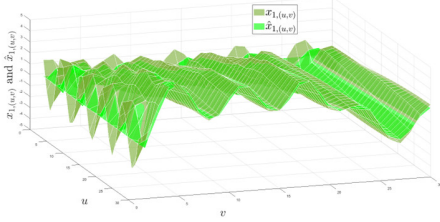
Fig.3. The trajectories of $x_{1,(u,v)}$ and $\hat{x}_{1,(u,v)}$
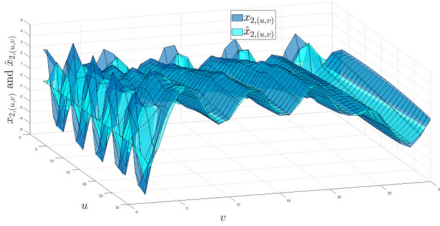
Fig.4. The trajectories of $x_{2,(u,v)}$ and $\hat{x}_{2,(u,v)}$
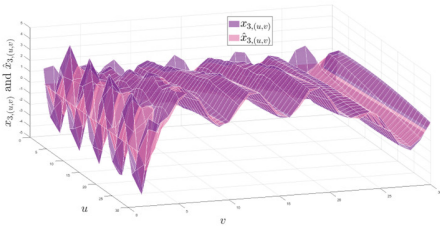
Fig.5. The trajectories of $x_{3,(u,v)}$ and $\hat{x}_{3,(u,v)}$
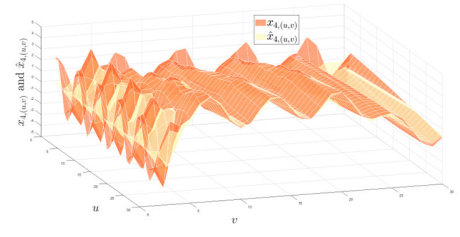
Fig.6. The trajectories of $x_{4,(u,v)}$ and $\hat{x}_{4,(u,v)}$
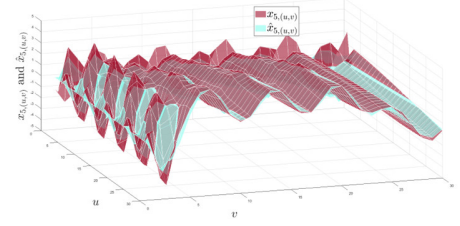
Fig.7. The trajectories of $x_{5,(u,v)}$ and $\hat{x}_{5,(u,v)}$
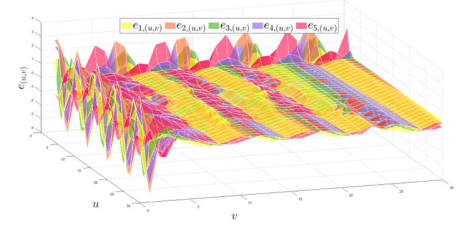
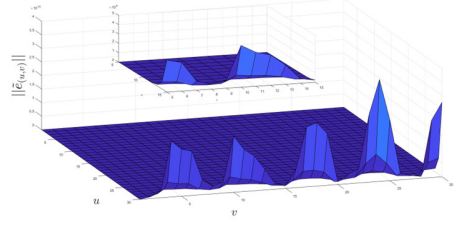**Fig.8.** The trajectory of the client's filtering error $e_{(u,v)}$

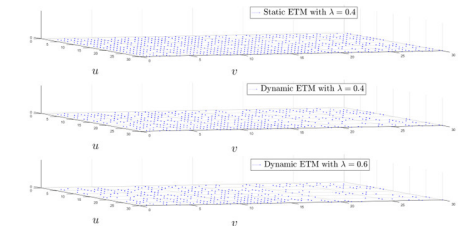**Fig.9.** The trajectory of $\|\mathbb{E}\{\tilde{e}_{(u,v)}\}\|$
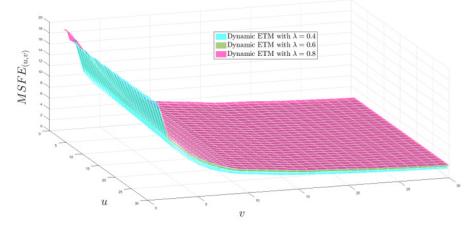

Fig.10. The event-triggered instants with different λ

Fig.11. The $MSFE_{(u,v)}$ under different triggering conditions

The simulation results are displayed in Figs.3-11. The trajectories of $x_{(u,v)}$ and $\hat{x}_{(u,v)}$ under the ETM and EDM are shown in Figs.3-7, where $x_{\varepsilon,(u,v)}$ and $\hat{x}_{\varepsilon,(u,v)}$ ($\varepsilon \in \{1,2,3,4,5\}$) represent the ε-th component of $x_{(u,v)}$ and $\hat{x}_{(u,v)}$, respectively. Fig.8 shows the trajectory of the client's filtering error $e_{(u,v)}$, where $e_{\varepsilon,(u,v)}$ ($\varepsilon \in \{1,2,3,4,5\}$) denotes the ε-th component of $e_{(u,v)}$. The above figures demonstrate that the provided bounded filtering algorithm exhibits superior performance. The eavesdropper's filtering error with $\mathcal{K}_{(u,v)} = 10^{-4}$ is plotted in Fig. 9, which shows that even if the filter gain is small enough, the $\left\| \mathbb{E}\{\tilde{e}_{(u,v)}\} \right\|$ still diverges rapidly under the effect of the encryption parameters $\mathcal{M}_{(u,v)}$ and $\mathcal{N}_{(u,v)}$. Then, the impact of different triggering conditions on the filtering performance is demonstrated. Furthermore, we introduce the mean square filtering error as $MSFE_{(u,v)} = (1/T^2)\sum_{u=1}^{T}\sum_{v=1}^{T}(x_{(u,v)} - \hat{x}_{(u,v)})^2$. Subsequently, as shown in Figs. 10-11, the dynamic ETM efficiently mitigates the communication pressure and guarantees filter performance. Moreover, the reduction of the triggering frequency leads to a degradation of the filtering performance that is within an acceptable range.

Example 2: The following partial differential equation is utilized to describe the industrial heating exchange process [39]:

$$\frac{\partial o_{(\varsigma,\sigma)}}{\partial \varsigma} + \frac{\partial o_{(\varsigma,\sigma)}}{\partial \sigma} = -h o_{(\varsigma,\sigma)} + i U_{(\varsigma,\sigma)}, \qquad (37)$$

where $o_{(\varsigma,\sigma)}$ is the temperature function connected to the time $\varsigma \in [0,\mathcal{R}]$ and the spatial $\sigma \in [0,\mathcal{T}]$, where $\mathcal{R}$ and $\mathcal{T}$ are given positive scalars. $U_{(\varsigma,\sigma)}$ represents external input. The parameters h and i denote the exchange factors. Define $o_{(\varsigma,\sigma)} = o_{(u\Delta\varsigma, v\Delta\sigma)}$, then one has $\frac{\partial o_{(\varsigma,\sigma)}}{\partial \varsigma} \approx \frac{o_{(u\Delta\varsigma, v\Delta\sigma)} - o_{((u-1)\Delta\varsigma, v\Delta\sigma)}}{\Delta\varsigma}$, $\frac{\partial o_{(\varsigma,\sigma)}}{\partial \sigma} \approx \frac{o_{(u\Delta\varsigma, v\Delta\sigma)} - o_{(u\Delta\varsigma, (v-1)\Delta\sigma)}}{\Delta\sigma}$ and $o_{(\varsigma,\sigma)} \approx o_{(u,v)}$. Additionally, the equation (37) can be approximately rewritten as follows for $i = 0$:

$$x_{(u+1,v+1)} = \begin{bmatrix} 0 & 0 \\ \dfrac{\Delta\sigma}{\Delta\varsigma} & 1 - \dfrac{\Delta\sigma}{\Delta\varsigma} + h\Delta\sigma \end{bmatrix} x_{(u+1,v)} + \begin{bmatrix} 0 & 1 \\ 0 & 0 \end{bmatrix} x_{(u,v+1)}. \quad (38)$$

Subsequently, according to the literature [39], we adopt the following parameters:

$$h = 2\sin(0.5(u+v)), \Delta\sigma = 0.1, \ \Delta\varsigma = 0.1,$$

then, we consider (38) with the following variables:

$$\mathcal{A}^{[1]}_{(u+1,v)} = \begin{bmatrix} 0 & 0 \\ 1 & 0.2\cos(0.5(u+v)) \end{bmatrix}, \mathcal{A}^{[2]}_{(u,v+1)} = \begin{bmatrix} 0 & 1 \\ 0 & 0 \end{bmatrix},$$

$$\mathcal{B}^{[1]}_{(u+1,v)} = \begin{bmatrix} 0.4\sin(0.4(u+v)) \\ 0.32 \end{bmatrix}, \mathcal{B}^{[2]}_{(u,v+1)} = \begin{bmatrix} 0.59 \\ 0.61\cos(0.3(u+v)) \end{bmatrix},$$

$$\mathcal{D}_{(u,v)} = \begin{bmatrix} 0.55 \\ 0.46 + 0.2\sin(u+v) \end{bmatrix}, \mathcal{C}_{(u,v)} = 0.6I, \mathcal{H}_{(u,v)} = 0.73I.$$

The event-triggered parameters are set as $\delta_{(u,0)} = \delta_{(0,v)} = 0.4$ ($u,v \in \Gamma$), $\psi_1 = 0.25$, $\psi_2 = 0.15$ and $\lambda = 0.8$. Setting the initial state as $x_{(u,v)} = [1.9\cos(u)\sin(v) \quad 1.3\cos(u-1)\sin(v)]^T$ for $u \in [0 \ 30]$ and $v = 0$, $x_{(u,v)} = [3.1\sin(u)\cos(v+1) \quad 2.6\cos(u+1)\sin(v)]^T$ for $u = 0$ and $v \in [1 \ 30]$. The initial states of the estimate are $\hat{x}_{(u,0)} = \hat{x}_{(0,v)} = \tilde{x}_{(u,0)} = \tilde{x}_{(0,v)} = [0 \ 0]^T$ for $u,v \in \Gamma$. In addition, it is assumed that $W = 0.5I$ and $V = 0.62I$. The encryption parameters are chosen as $\mu_p = 0.2$ ($p \in \{1,2,3,\cdots,n_y\}$), $\mathcal{M}_{(u,v)} = \begin{bmatrix} 1.73+0.2\sin(u+v) & 0.3 \\ 0.27 & 1.76 \end{bmatrix}$, $\mathcal{N}_{(u,v)} = \begin{bmatrix} 0.98+0.2\cos(u+v) & 0.59 \\ 0.27 & 0.36 \end{bmatrix}$, $\varpi = 1.36$, and $q_{(u,0)} = q_{(0,v)} = g_0 = [0.4 \ 0.4]^T$ for all $u,v \in \Gamma$. It is easy to deduce that $1.3378 \le \|\mathcal{M}_{(u,v)}\| \le 2.1425$, $1.0706 \le \|\mathcal{N}_{(u,v)}\| \le 1.2984$, and the condition $\underline{m} \ge \varpi + \|q_{(u,0)}\|^{-1} \bar{n} tr\{\Psi\}$ is satisfied.

Then, by applying Theorem 3 with the help of LMI toolbox in Matlab, the client's filter gains $\ell_{(u,v)}$ are exhibited as follows:

Table 1. Part of the filter gains $\ell_{(u,v)}$

|		
$\ell_{(1,1)} = \begin{bmatrix} 0.5351 & 0.0584 \\ 0.0647 & 0.6419 \end{bmatrix}$	$\ell_{(1,1)} = \begin{bmatrix} 0.5760 & 0.0322 \\ 0.0715 & 0.7012 \end{bmatrix}$	$\cdots$
$\ell_{(2,1)} = \begin{bmatrix} 0.5124 & 0.0640 \\ 0.0514 & 0.5951 \end{bmatrix}$	$\ell_{(3,2)} = \begin{bmatrix} 0.5786 & 0.0334 \\ 0.0726 & 0.5981 \end{bmatrix}$	$\cdots$
$\cdots$	$\cdots$	$\cdots$
$\ell_{(30,1)} = \begin{bmatrix} 0.4335 & 0.0072 \\ 0.0269 & 0.4652 \end{bmatrix}$	$\ell_{(30,2)} = \begin{bmatrix} 0.6100 & 0.1023 \\ 0.0038 & 0.5691 \end{bmatrix}$	$\cdots$

The simulation figures are exhibited in Figs.12-17. The trajectories of $x_{(u,v)}$ and $\hat{x}_{(u,v)}$ are shown in Figs.12-13, respectively. Fig.14 illustrates the client's filtering error $e_{(u,v)}$, and it is easy to observe that the estimates can track the actual system state well. To intuitively illustrate the superior performance of proposed filtering algorithm, we compare the proposed bounded filtering algorithm with the H∞ filtering algorithm developed in [17] and [40]. Figs. 15-16 show system state and its estimate of client at instants $u \in \{8,9\}$ and $v \in \{8,9\}$, respectively. Fig.17 indicates that the mean square filtering error $MSFE_{(u,v)}$ of our proposed bounded filtering algorithm is smaller, which results in superior performance compared to that of H∞ filtering algorithm. Based on Figs.15-17, the proposed bounded filtering algorithm provides better performance compared to the H∞ algorithm.
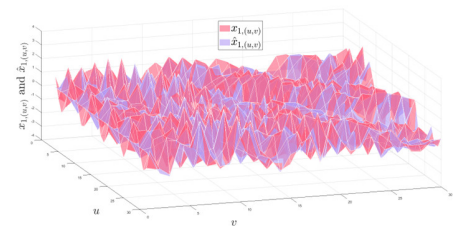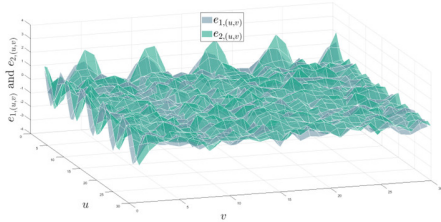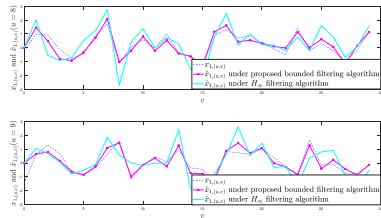
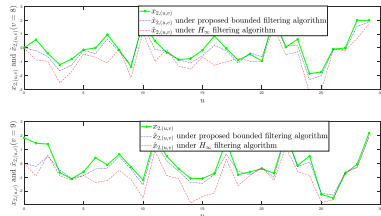**Fig. 12.** The trajectories of $x_{1,(u,v)}$ and $\hat{x}_{1,(u,v)}$
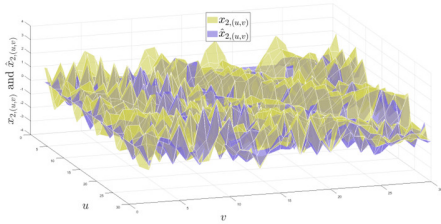
Fig. 13. The trajectories of $x_{2,(u,v)}$ and $\hat{x}_{2,(u,v)}$
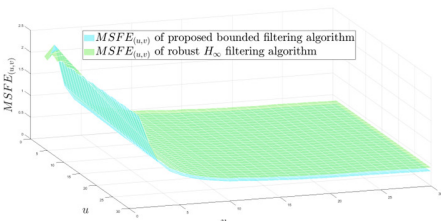

Fig. 14. The trajectory of the client's filtering error $e_{(u,v)}$

Fig.15. The $x_{1,(u,v)}$ and its estimate $\hat{x}_{1,(u,v)}$ on $u = 8,9$

Fig.16. The $x_{2,(u,v)}$ and its estimate $\hat{x}_{2,(u,v)}$ on $v = 8,9$

Fig. 17. The $MSFE_{(u,v)}$ under different filtering algorithms.

V. CONCLUSIONS

The bounded filtering issues for 2-D systems involving dynamic ETM and EDM have been addressed in this paper. To prevent eavesdroppers from stealing system-critical information, a novel EDM that depends on the encoding-decoding mechanism is designed. Furthermore, the dynamic ETM is employed to conserve network computing and communication resources. Based on the proposed dynamic ETM and EDM, the FESs at eavesdropper side

and user side are obtained, respectively. Then, the encryption parameters have been designed such that the filtering error at the eavesdropper side is divergent, and boundedness criteria are deduced to ensure that the client-side FESs are bounded. Eventually, the validity of the developed filtering strategy is confirmed by several examples. This is the first attempt to design an EDM for 2-D systems, and future research directions include improving the reliability of the EDM and generalizing additional filtering algorithms.

REFERENCES

[1] C. K. Ahn, P. Shi, and H. R. Karimi, "Novel results on generalized dissipativity of two-dimensional digital filters," *IEEE Trans. Circuits Syst.*, II -Express Briefs, vol. 63, no. 9, pp. 893-987, Sept. 2016.

[2] C. Du and L. Xie, "Stability analysis and stabilization of uncertain two-dimensional discrete systems: an LMI approach," *IEEE Trans. Circuits Syst.*, I-Regular Papers, vol. 46, no 11, pp. 1371-1374, Nov. 1999.

[3] S. Knorn and R. H. Middleton, "Stability of two-dimensional linear systems with singularities on the stability boundary using LMIs," *IEEE Trans. Autom. Control*, vol. 58, no. 10, pp. 2579-2590, Oct. 2013.

[4] L. Wu and Z. Wang, *Filtering and control for classes of two-dimensional systems*. Cham, Switzerland: Springer International Publishing, 2015, pp. 6-7.

[5] R. P. Roesser, "A discrete state-space model for linear image processing," *IEEE Trans. Autom. Control*, vol. 20, no 1, pp. 1-10, Feb. 1975.

[6] E. Fornasini and G. Marchesini, "State-space realization theory of two-dimensional filters," *IEEE Trans. Autom. Control*, vol. 21, no. 4, pp. 484-492, Aug. 2016.

[7] J. E. Kurek, "The general state-space model for a two-dimensional linear digital system," *IEEE Trans. Autom. Control*, vol. 30, no 6, pp. 600-602, Jun. 1985.

[8] P. H. Coutinho, I. Bessa, P. Pessim, and R. Palhares, "A switching approach to event-triggered control systems under denial-of-service attacks," *Nonlinear Anal-Hybrid*, vol. 50, Nov. 2023, Art. no. 101383.

[9] M. Yang and J. Y. Zhai, "Observer-based dynamic event-triggered secure control for nonlinear networked control systems with false data injection attacks," *Inf. Sci*, vol. 644, Jun. 2023, Art. no. 119262.

[10] T. Saravanakumar and T. H. Lee, "Hybrid-driven-based resilient control for networked T-S fuzzy systems with time-delay and cyber-attacks," *Int. J. Robust Nonlinear Control*, vol. 33, no. 13, pp. 7869-7891, Jun. 2023.

[11] T. T. Jiang, Y. P. Zhang, J. H. Park, X. S. Cai, and K. B. Shi, "Novel dropout compensation control design for networked control systems with mixed delays," *IEEE Trans. Syst. Man Cybern*, vol. 54, no. 1, pp. 212-224, Jan. 2024.

[12] H, Y. Wang, J. C. Xu, H. T. Zhao, and W. Shang, "A self-triggered stochastic model predictive control for uncertain networked control system," *Int. J. Control*, vol. 96, on. 8, pp. 2113-2123, Aug. 2023.

[13] L. V. Hie and H. Trinh, "Exponential stability of two-dimensional homogeneous monotone systems with bounded directional delays," *IEEE Trans. Autom. Control*, vol. 63, no. 8, pp. 2694-2700, Aug. 2018.

[14] D. Peng and H. M. Nie, "Abel lemma-based finite-sum inequality approach to stabilization for 2-D time-varying delay systems," *Asian J Control*, vol. 23, no. 3, pp. 1394-1406, May. 2021.

[15] Y. Yan, L. L. Su, and V. Gupta, "Analysis of two-dimensional feedback systems over networks using dissipativity," *IEEE Trans. Autom. Control*, vol. 65, no. 8, pp. 3241-3255, Aug. 2020.

[16] S. P. Huang and Z. Y. Xiang, "Delay-dependent robust H_∞ control for 2-D discrete nonlinear systems with state delays," *Multidimens Syst Signal Process*, vol. 25, no. 4, pp. 775-794, Oct. 2014.

[17] D. H. Li, J. L. Liang, and F. Wang, "Robust H_∞ filtering for 2D systems with RON under the stochastic communication protocol," *IET Control. Theory Appl*, vol. 18, no. 14, pp. 2795-2804, Dec. 2021.

[18] F. Wang, J. Liang, and Z. Wang, "Robust finite-horizon filtering for 2-D systems with randomly varying sensor delays," *IEEE Trans. Syst. Man Cybern.: Syst*, vol. 50, no. 1, pp. 220-232, Jan. 2020.

This article has been accepted for publication in IEEE Transactions on Network Science and Engineering. This is the author's version which has not been fully edited and content may change prior to final publication. Citation information: DOI 10.1109/TNSE.2025.3542177

12

> REPLACE THIS LINE WITH YOUR MANUSCRIPT ID NUMBER (DOUBLE-CLICK HERE TO EDIT) <

[19] L. L. Li, R. N. Yang, Z. G. Feng, and L. D. Wu, "Event-triggered dissipative control for 2-D switched systems," *Inf. Sci*, vol. 589, pp. 802-812, Jan. 2022.

[20] Y.-Y Tao and Z.-G. Wu, "Asynchronous control of two-dimensional Markov jump Roesser systems: an event-triggering strategy," *IEEE Trans. Netw. Sci. Eng*, vol. 9, no. 7, pp. 2278-2289, Aug. 2022.

[21] X. Y. Lv, Y. G. Niu, and Z. R. Cao, "Sliding mode control of uncertain FMII 2D systems under directional event-triggered schemes," *Int. J. Robust Nonlinear Control*, vol. 32, pp. 5226-5246, Oct. 2023.

[22] X. D. Wang, Z. Y. Fei, P. Shi, and J. Y. Yu, "Zonotopic fault detection for 2-D systems under event-triggered mechanism," *IEEE Trans Cybern*, vol. 52, no. 5, pp. 3510-3518, May. 2022.

[23] F. Wang, Z. D. Wang, J. L. Liang, and Steven. X. Ding, "Recursive distributed filter design for 2-D systems over sensor networks: on component-based node-wise and dynamic event-triggered scheme," *IEEE Trans. Signal Inf. Pr*, vol. 8, pp. 584-596. Jul. 2022.

[24] K. Q. Zhu, Z. D. Wang, H. L. Dong, and G. L. Wei, "Set-membership filtering for two-dimensional systems with dynamic event-triggered mechanism," *Automatica*, vol. 143, Jun. 2022, Art. no. 110416.

[25] Z. Y. Fei, L. Yang, C. X. Gu, and Y. H. Wu, "Zonotopic state bounding for 2-D systems with dynamic event-triggered mechanism," *Automatica*, vol. 154, Aug. 2023, Art. no. 111066.

[26] L. J. Zha, Y. P. Guo, J. L. Liu, X. P. Xie, and E. G. Tian, "Protocol-based distributed security fusion estimation for time-varying uncertain systems over sensor networks: tackling DoS attacks," *IEEE Trans. Signal Inf. Pr*, vol. 10, pp. 119-130, Jan. 2024.

[27] Z. Z. Pan, R. H. Chi, and Z. S. Hou, "Distributed model-free adaptive predictive control for MIMO multi-agent systems with deception attack," *IEEE Trans. Signal Inf. Pr*, vol. 10, pp. 32-47, Jan. 2024.

[28] Y. Sun, Y. M. Ju, D. R. Ding, and H. J. Liu, "Distributed H_∞ filtering of replay attacks over sensor networks," *ISA. T*, vol.141, pp. 113-120. Oct. 2023.

[29] L. Wang, X. H. Cao, H. Zhang, C. Y. Sun, and W. X. Zheng, "Transmission scheduling for privacy-optimal encryption against eavesdropping attacks on remote state estimation," *Automatica*, vol. 137, May. 2022, Art. no. 110145.

[30] L. Y. Huang, K. M. Ding, A. S. Leong, D. E. Quevedo, and L. Shi, "Encryption scheduling for remote state estimation under an operation constraint," *Automatica*, vol. 127, May. 2021, Art. no. 109537.

[31] L. Wang; X. H. Cao, B. W. Sun, H. Zhang, and C. Y. Sun, "Optimal schedule of secure transmissions for remote state estimation against eavesdropping," *IEEE Trans. Ind. Inf*, vol. 17, no. 3, pp. 1987-1997, Mar. 2021.

[32] L. Zou, Z. D. Wang, B. Shen, and H. L. Dong, "Encryption-decryption-based state estimation with multirate measurements against eavesdroppers: a recursive minimum-variance approach," *IEEE Trans. Autom. Control*, vol. 68, no. 12, pp. 8111-8118, Dec. 2023.

[33] C. Gao, Z. D. Wang, X. He, and H. L. Dong, "Fault-tolerant consensus control for multiagent systems: an encryption-decryption scheme," *IEEE Trans. Autom. Control*, vol. 67, no. 5, pp. 2560-2567, May. 2022.

[34] K. Q. Zhu, Z. D. Wang, Q.-L. Han, and G. L. Wei, "Distributed set-membership fusion filtering for nonlinear 2-D systems over sensor networks: an encoding-decoding scheme," *IEEE Trans Cybern*, vol. 53, no. 1, pp. 416-427, Jan. 2022.

[35] K. Q. Zhu, Z. D. Wang, Y. Chen, and G. L. Wei, "Neural-network-based set-membership fault estimation for 2-D systems under encoding-decoding mechanism," *IEEE Trans. Neural Netw*, vol. 34, no. 2, pp. 786-978, Feb. 2023.

[36] R. Suarez, "Difference equations and a principle of double induction," *Mathematics Magazine*, vol. 62, no. 5, pp. 334-339, Dec. 1989.

[37] B. Shen, Z. D. Wang, and X. H. Liu, "Bounded H_∞ synchronization and state estimation for discrete time-varying stochastic complex networks over a finite horizon," *IEEE Trans. Neural Netw*, vol. 22, no. 1, pp. 145-157, Jan. 2011.

[38] S. Foda and P. Agathoklls, "Control of the metal rolling process-a multidimensional system approach," *J. Frankl. Inst*, vol. 329, no. 2, pp. 317-332, Feb. 1992.

[39] I. Ghous, Z. R. Xiang, and H. R. Karimi, "State feedback H_∞ control for 2-D switched delay systems with actuator saturation in the second FM model," *Circ Syst. Signal Pr*, vol. 34, pp. 2167-2192, Jan. 2015.

[40] D. H. Li, J. L. Liang, and F. Wang, "H_∞ state estimation for two-dimensional systems with randomly occurring uncertainties and Round-Robin protocol," *Neurocomputing*, vol. 349, pp. 248-260, Apr. 2020.

PAN ZHANG received the M.E. degree in control theory and control engineering from Lanzhou University of Technology, Lanzhou, in 2019. He is currently working toward the Ph.D. degree in control theory and control engineering from Lanzhou University of Technology, Lanzhou, China. His current research interests include networked control systems, two-dimensional systems and robust filtering

CHAOQUN ZHU He received the M.E. degree in control theory and control engineering from Lanzhou University of Technology, Lanzhou, in 2008 and the Ph.D. degree in control theory and control engineering from Dalian Maritime University, Dalian, in 2013. His current research interests include networked control systems and cyber physical systems security. He has published over 30 Journal papers within these areas.
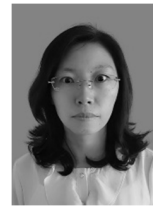
BING YANG received the M.E. degree in control theory and control engineering from Lanzhou University of Technology, Lanzhou, in 2008. Her current research interests include networked control systems and autonomous vehicle control.

BOHAN ZHANG received his Bachelor's degree in Communication Engineering from Shandong University of Science and Technology in 2022. He is currently pursuing a Master's degree at the School of Electrical Engineering and Information Engineering, Lanzhou University of Technology. His research focus is on attack detection in industrial cyber-physical systems.

ZHIWEN WANG, born in Minqin, Gansu, China in 1976, He is a senior member of the Chinese Society of Automation, a member of the Youth Working Committee of the Chinese Society of Automation, a member of the Working Committee of the Robotics Engineering Professional Union. He graduated from Xi'an Jiaotong University, School of Electrical Engineering, majoring in industrial automation in 1999, and received the Ph.D. degree in control theory and control engineering from Lanzhou University of Technology, Lanzhou, in 2008. His current research interests include networked control systems, cyber physical systems security, advanced control theory and applications for industrial processes.

ADIMPL: a dynamic, real-time and robustness attack detection model for industrial cyber-physical systems based on improved meta pseudo labels

Bohan Zhang¹ · Pan Zhang¹ · Zhiwen Wang¹ · Jiaqi Lv¹ · Wei Miao²

Abstract

While the introduction of networking has increased the efficiency of Industrial Cyber-Physical Systems (ICPS), it has also lowered the cost for attackers, significantly increasing security risks. Current research on ICPS attack detection focuses on deep learning methods. However, the dependence on large labeled datasets often hinders these systems from adapting quickly to the dynamic changes and real-time demands of the ICPS environment. To address these issues, we present an attack detection method based on improved meta pseudo label (ADIMPL). ADIMPL innovatively combines two-layer network traffic feature extraction with the compact SqueezeNet deep neural network, achieving high performance with a minimal number of labeled samples. Additionally, the method dynamically adapts to changing attack patterns, significantly increasing detection accuracy while enhancing the robustness and real-time processing capabilities of the detection system. Extensive experiments on real-world industrial CPS datasets (CIC-IDS2017, CIC-IDS2018, and the CIC-Attack Dataset 2023) demonstrate that ADIMPL can effectively, robustly, and in real-time detect network attacks against industrial CPS. Notably, ADIMPL achieves a detection accuracy of 99.13% with an average latency of 0.098 s and maintains a minimum attack detection accuracy of 91.99% even under our proposed GAN+OPSO malicious attacks.

Keywords Attack detection · Democracy co-training · Dual-level feature · Meta pseudo labels · Industrial Cyber-physical systems · Semi-supervised learning

1 Introduction

With the advent of a new industrial revolution, Industrial Cyber-Physical Systems (ICPS) utilize the characteristics of "3C" (computing, communication, and control) [1] to enhance real-time perception and dynamic control within industrial frameworks. These systems are extensively integrated into several national strategies, including "*Made in China 2025*", "*Industry 4.0*" and the "*Advanced Manufacturing National Program of the United States*" [2, 3]. On a technical level, ICPS adds a cyberspace dimension to traditional industrial systems, markedly improving information sensing capabilities and the efficiency of big data processing in industrial processes [4]. However, the integration of cyberspace also offers attackers lower-cost pathways, escalating the security risks to industrial systems. According to the "*2022 China Industrial Information Security Situation Report*" [5] a total of 312 industrial system security incidents were publicly reported globally in 2022. These attacks on ICPS not only compromise the economic and security aspects of the businesses involved but also pose threats to the safety and property of local residents.

To increase the security of ICPS, Attack Detection Systems (ADS) have become crucial. Existing research categorizes these systems based on the basis of detection principles

✉ Zhiwen Wang
  wzw@lut.edu.cn

  Bohan Zhang
  15139352987@163.com

  Pan Zhang
  zhangpanlut@163.com

  Jiaqi Lv
  lvjiaqi0507@163.com

  Wei Miao
  11302478@qq.com

¹ College of Electrical and Information Engineering, Lanzhou University of Technology, Lanzhou 730050, China

² GS-Unis Intelligent Transportation System & Control Technology Co. Ltd., Lanzhou 730050, China

into rule-based, estimation-based, and learning-based methods [6]. Rule-based attack detection employs predefined rules to identify and respond to potential malicious activities, including fixed thresholds, specific data watermarks, and authentication signatures to identify and respond to potential malicious activities [7]. For example, Ankit et al. [8] introduced a verification mechanism using Physically Unclonable Functions (PUF) for systems utilizing the MQTT protocol, which generates unique credentials to significantly reduce the risks associated with traditional password vulnerabilities such as dictionary attacks. However, rule-based methods face two main disadvantages when applied to ICPS: (1) limited applicability: as they may fail to detect previously undefined attack patterns, and (2) high maintenance costs: due to the continual need to update rule sets to address new security threats. Estimation-based methods leverage control theory to establish state observers for estimating system states in industrial processes to detect attacks. For example, Zhang et al. [9] proposed the use of the consistency and stationarity features of the system data to construct state observers for direct current microgrid systems, distinguishing genuine state changes from those induced by attacks. However, this approach increases the communication overhead as industrial devices communicate via low-speed sensor links, and state observers may not simultaneously process the extensive network data in ICPS, thus occupying the network bandwidth and causing detection delays.

To address the processing challenges associated with large-scale network traffic data in networked environments, Machine Learning (ML) [10] is extensively employed in ICPS for attack detection. These systems leverage advanced algorithms to manage substantial data volumes and iteratively recognize emerging threats. Various detection models have been developed to suit different ICPS contexts. For example, Alper et al. [11] proposed the RAIDS system, which uses autoencoders to reconstruct and analyze network traffic data. This method helps the model recognize standard traffic patterns and detect significant anomalies. Rana et al. [12] proposed the FTG-Net-E model, which is a sophisticated framework employing a hierarchical ensemble of Graph Neural Networks (GNN) to scrutinize traffic across multiple granularity levels, thus enhancing the detection of complex attack patterns. This model integrates the strengths of multiple GNNs through ensemble learning, significantly increasing the prediction accuracy. The efficacy of such an ADS heavily depends on the quantity of labeled data available [13]. However, acquiring labeled network traffic data in real-world settings involves considerable human and temporal resources, which hampers the deployment of ADS in practical ICPS scenarios. Furthermore, the prevalent issue of data imbalance in existing datasets necessitates intricate feature engineering to achieve precise detection, presenting substantial challenges in developing a well-balanced ADS.

In response to the limitations of the existing research, this paper proposes an ADS termed ADIMPL, which balances effectiveness, real-time performance, and robustness. This model first attempts to apply the proposed Improved Meta Pseudo Labels (IMPL) [14] method to attack detection in ICPS. The IMPL method merges meta-learning concepts with the principles of Deep Semi-Supervised Learning (DSSL) [15], enabling the ADS to dynamically adjust its optimal detection parameters. This adjustment minimizes the impact of insufficient labeled samples on the detection precision. Furthermore, the introduction of frequency domain feature analysis simplifies feature engineering, enhancing the real-time performance of the detection system. The main contributions of this paper are outlined as follows:

(1) We propose an attack detection model based on IMPL for ICPS. This model integrates meta-learning with deep semi-supervised learning, achieving high detection accuracy (98.61%) even with extremely few labeled samples and dynamically updates the optimal parameters based the basis of system status.

(2) We improve the meta pseudo labels method through democratic co-training. The improved method shows increased sensitivity to attack traffic and significantly reduces the impact of dataset imbalances on the system performance.

(3) We propose a dual-level network traffic feature extraction method that extracts both the time-domain and frequency-domain features from network traffic data, effectively reducing the granularity of detection. This significantly lowers the detection overhead and enhances the system's real-time performance and robustness.

Extensive experiments demonstrate the following: (1) On three real datasets for ICPS, ADIMPL outperforms the most advanced semi-supervised detection models in terms of accuracy, recall, F1 score, and AUC values; (2) Under various network load conditions, ADIMPL exhibits excellent real-time performance with average latencies of 0.098 s and 0.314 s; (3) Compared with other models, ADIMPL shows superior robustness under our proposed GAN+OPSO attack algorithm, with less than 10% performance degradation even under high attack costs.

The remainder of this paper is organized as follows: Sect. 2 introduces related work on attack detection. Section 3 describes the proposed method. Section 4 details the experimental process and analysis of results. Section 5 presents conclusions and future discussions.

2 Related work

The most extensively researched attack types currently include Denial-of-Service (DoS) attacks, Deception attacks and False Data Injection (FDI) attacks. Various other attack types are derived from these three categories. For example, the Stuxnet [16, 17] virus, which extensively damaged Iran's nuclear facilities in 2010, evolved from deception attacks [18]. As the stealth and variety of attacks have increased, deep learning-based detection methods have diversified according to the type of attack. In this section, we briefly introduce the work on attack detection via three deep learning approaches, with a focus on explaining the MPL method.

2.1 Deep learning-based attack detection methods for ICPS

With the emergence of neural networks [19], deep learning models have increasingly been deployed in clustering tasks because of their robust learning capabilities. These models are categorized into supervised, unsupervised, and semi-supervised learning, depending on the required labeled data volume [20]. In attack detection research, unsupervised deep learning-based ADS have been extensively explored due to the scarcity of labeled data. For example, Lan et al. [21] proposed HAT-UDA, an attack detection method that employs a hierarchical attention triple network with unsupervised domain adaptation, enhancing model generalizability across new network environments. This method uses a variant of the One-Class Support Vector Machine (OCSVM) and Support Vector Data Description (SVDD) for threshold setting. Liu et al. [22] combined deep autoencoders with Gaussian Mixture Models to develop MemAe-gmm-ma, an ADS that produces data's low-dimensional representations and reconstruction errors through autoencoders. This system optimizes the parameters of both the autoencoder and Gaussian Mixture Models end-to-end, effectively balancing reconstruction and density estimation to avoid local optima and improves the attack detection accuracy to 98.54%. To address data imbalance in unsupervised learning, Yang et al. [23] proposed the ADUL method, which extracts and converts network packet payloads into characters. ADUL integrates a one-dimensional Convolutional Neural Network (1D-CNN) with Bidirectional Encoder Representations from Transformers (BERT), and analyzes the payload data's short-term and long-term dependencies to detect anomalies.

Although unsupervised deep learning-based ADS can effectively reduce detection costs, their performance significantly decreases or even collapses when facing specific attacks that target detection models, such as generative adversarial attacks. Consequently, more accurate supervised deep learning-based ADS have been extensively studied. For example, Fathima et al. [24] compared three classic supervised learning algorithms-Random Forest, K-Nearest Neighbors (KNN), and Logistic Regression-in detecting DDoS attacks. Their experiments demonstrated that the random forest method achieved the highest detection accuracy. Altunay et al. [25] compared a standalone CNN model, a standalone LSTM model, and a hybrid model (CNN+LSTM). The results indicate that the hybrid model effectively detects various types of attacks in the dataset, demonstrating superior classification and detection capabilities. To handle high-dimensional data, Xu et al. [26] introduced an edge-based self-attention mechanism, establishing a self-supervised graph representation learning framework named NetFlow-Edge Generative Subgraph Contrast (NEGSC). This system generates subgraphs of central nodes and their immediate neighbors, uses graph contrastive learning to differentiate between normal and anomalous network traffic, accurately detects high-dimensional data with significant computational costs. With the widespread adoption of attention mechanisms, Sikder et al. [27] proposed the Deep H2O system to detect cyberattacks in urban water supply systems. Deep H2O utilizes a Temporal Graph Convolutional Network (TGCN) combined with an attention mechanism and robust Mahalanobis distance to increase classification accuracy and robustness. This model achieves an accuracy of 98.78% in detecting data poisoning samples processed by GANs. Compared with unsupervised methods, supervised learning-based ADS generally exhibit superior effectiveness in detection; however, they often lack generalizability due to data limitations, and both supervised and unsupervised methods struggle to adjust dynamically to changes in industrial processes.

Considering the above limitations, semi-supervised learning-based ADS excels in achieving high accuracy with minimal labeled data. Most current systems utilize pseudo-labeling methods [28]. For example, Zhang et al. [29] proposed a detection model called FS-DL, which is based on Mutual Adversarial Networks (MAN). This system outputs residual network traffic data to detect attacks and achieves 99.60% accuracy with only 5% labeled samples. Liu et al. [30] proposed a system for ICPS that relies on a bias network and feature selection called SFAD, which uses minimal labeled data to create a bias loss function and effectively distinguishes between positive and negative samples. To address data imbalances in semi-supervised learning, Niu et al. [31] proposed ADESSA. This system combines margin sampling with democratic co-learning to build a balanced training set of manually labeled high-information samples and high-confidence auto labeled samples. Li et al. [32] proposed an enhanced model named EseT, which incorporates a confidence selection module to remove low-confidence pseudo-labels and achieves 98.59% detection accuracy.

Table 1 briefly summarizes the existing work on deep learning-based attack detection, highlighting the unique

Table 1 Summary of part of the existing work

ADS	Type	Efficiency	Robustness	Generalizability	Limitations
HAT-UDA [21]	Unsupervised	●	○	●	Inability to detect traffic quickly; Poor ability to detect new attack traffic
MemAe-gmm-ma [22]	Unsupervised	●	◐	○	More complex feature engineering and higher detection overhead
ADUL [23]	Unsupervised	◐	○	●	Larger coarse-graining of detection may cause attacks to escape
CNN+LSTM [25]	Supervised	◐	○	◐	Lack of attention to spatial characterization of network traffic
NetFlow-Edge [26]	Supervised	●	●	○	Requires specific modeling based on specific ICPS
FS-DL [27]	Semi-supervised	●	◐	●	Detection thresholds cannot be changed dynamically
SFAD [29]	Semi-supervised	●	●	◐	High computational overhead
ADESSA [31]	Semi-supervised	●	●	○	High modeling cost; Not applicable to attack detection in industrial scenarios
Eset [32]	Semi-supervised	●	●	◐	Detection thresholds cannot be changed dynamically

The symbol ● indicates that the features are supported, ○ indicates that the features are not supported, ◐ indicates that the features are partially supported

shortcomings in each study. Moving forward, we aim to refine semi-supervised deep learning algorithms to support high-accuracy and real-time detection with very few labeled samples. Additionally, we optimize the meta pseudo-label algorithm for dynamic updates in response to changes in the ICPS environment.

2.2 Meta pseudo labels

In reference [14], the authors introduced the MPL method to make the detection model dynamic. This method employs teacher and student networks, adding feedback and loops to the pseudo label (PL) method to identify optimal model parameters at any given time. The MPL framework is depicted in Fig. 1. The pseudo label method is fundamentally an optimization problem. We define the teacher network as T and the student network as S, with θ_T and θ_S representing their respective parameters. The PL method trains the student model to minimize cross-entropy loss on unlabeled samples,

and the optimization process is described in (1).

$$\theta_S^{PL} = \arg\min_{\theta_s} \underbrace{\mathbb{E}_{x_u}\left[CE\left(T\left(x_u; \theta_T\right), S\left(x_u; \theta_S\right)\right)\right]}_{:=\mathcal{L}(\theta_T, \theta_s)}, \quad (1)$$

where x_u denotes a set of unlabeled samples. $T(x_u; \theta_T)$ denotes the prediction results of T for x_u under certain parameters, $S(x_u; \theta_S)$ denotes the prediction of T for x_u under certain parameters, and $\mathbb{E}_{x_u}\left[CE\left(T\left(x_u; \theta_T\right), S\left(x_u; \theta_S\right)\right)\right]$ denotes the average cross-entropy loss between the two under x_u, which can be simplified as $\mathcal{L}_u(\theta_T, \theta_S)$. θ_S^{PL} denotes the optimal student network parameters that minimize the cross-entropy loss.

In MPL, in addition to the dependency of the student network on the teacher network $\theta_S^{PL}(\theta_T)$, a reverse dependency $\theta_T^{MPL}(\theta_S)$ is added. Taking $\theta_S^{PL}(\theta_T)$ as an example, directly computing the dependency between the two requires understanding the gradient $\nabla_{\theta_T}\theta_S^{PL}(\theta_T)$, which is a complex process involving the calculation of the gradient of the gradi-
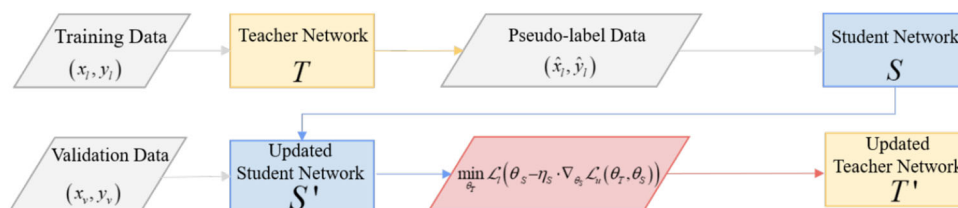
Fig. 1 The MPL method utilizes the teacher network to generate pseudo-labeled data and employs feedback based on the student network's performance in the validation set, continuously optimizing the interaction between the two

ent. Therefore, using relevant concepts from meta-learning, we approximate this process as the one-step gradient update of θ_S. The entire process is represented by (2).

$$\theta_S^{PL}(\theta_T) \approx \theta_S - \eta_S \cdot \nabla_{\theta_S}\mathcal{L}_u(\theta_T, \theta_S), \tag{2}$$

where η_S is the learning rate; by incorporating this (2) into the above (1), we can obtain the objective function of the MPL method in (3).

$$\min_{\theta_T} \mathcal{L}_l \left(\theta_S - \eta_S \cdot \nabla_{\theta_S}\mathcal{L}_u(\theta_T, \theta_S)\right). \tag{3}$$

The continuous optimization process of teacher and student network parameters in the MPL can be described as a repeated cycle of the following two steps:

Student network By receiving the prediction results (pseudo labeled samples) of the teacher network $T(x_u; \theta_T)$ for the unlabeled data x_u, the updated parameters of the student network are

$$\theta_S' = \theta_S - \eta_S \nabla_{\theta_S}\mathcal{L}_u(\theta_T, \theta_S). \tag{4}$$

Teacher network This network transforms unlabeled data into pseudo-labeled samples and updates its parameters according to the performance of the student network on the validation set. The updated parameters of the teacher network are

$$\theta_T' = \theta_T - \eta_T \nabla_{\theta_T}\mathcal{L}_l \left(\theta_S - \nabla_{\theta_S}\mathcal{L}_u(\theta_T, \theta_S)\right). \tag{5}$$

3 Methodology

In this chapter, we first introduce the overall framework of the proposed ADIMPL model. We propose a dual-level feature extraction method and analyze how to extract the vector features of packet-level traffic and the frequency domain features of flow-level traffic. Finally, we present an improved MPL detection model based on democracy co-training, tailored to address practical issues in ICPS.

3.1 Model framework

Figure 2 shows the overall structure of the ADIMPL system, which includes two main parts: dual-level feature extraction and semi-supervised learning via the IMPL method. In ICPS, the system extracts two types of features: packet-level vector features and flow-level frequency domain features. These features are then fed into the semi-supervised learning module, which consists of teacher and student networks developed through co-training. Both networks use the lightweight SqueezeNet [33] neural network to improve the model's ability to generalize. Initially, both the teacher and student networks start from the same pre-trained model. The teacher network processes the input data first, creating "pseudo-labels" that help enhance the dataset for training the student network. The student network then uses this enriched dataset to update its parameters and shares these updates with the teacher network. This cycle of mutual teaching allows both networks to gradually become better at understanding and processing the data, improving the overall performance of the system.
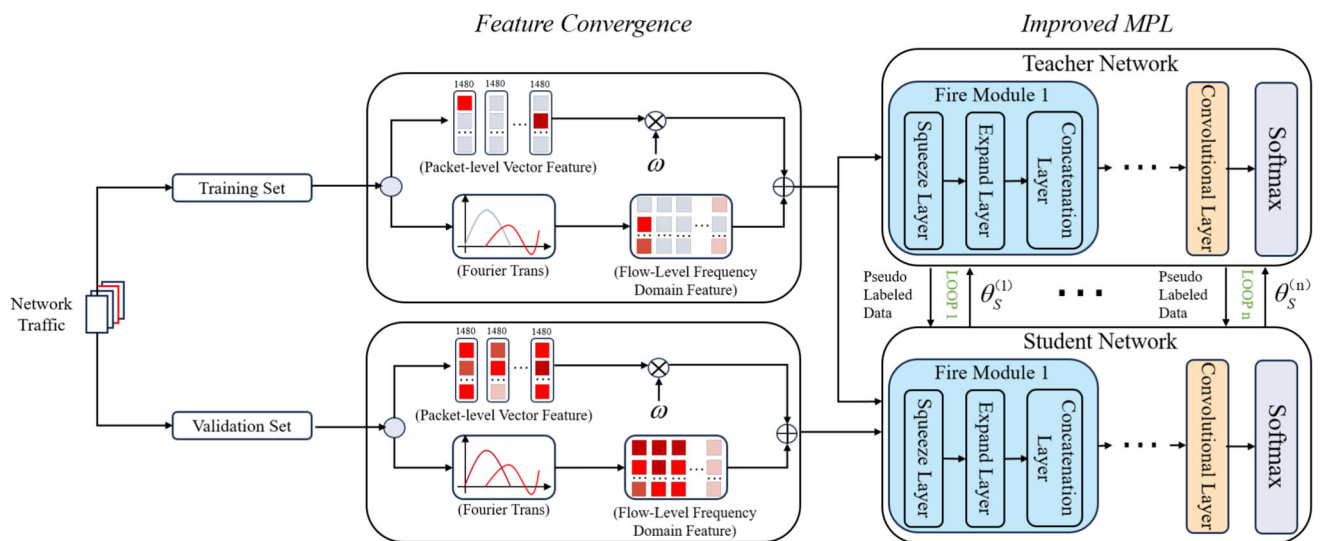

Fig. 2 The ADIMPL framework

3.2 Dual-level feature extraction

(1) Packet-level vector feature extraction

Input normalization: Based on the analysis of the dataset, we select 1480 bytes as the length for each data packet. If this length is not sufficient, the packet is padded at the end at 0x00. Each truncated packet is then encoded into an 8-bit number within the [0-255] range. For data requiring detokenization, IP addresses, MAC addresses, and attack type information within the packets are replaced with zeros.

Vector encoding: With a fixed packet length of 1480 bytes, packets from the same dataset are obtained and encoded, along with their features, via (6). We represent the ith data packet and the total of features within the packet using for the packet and for features [34].

$$S = \left[s^{(1)}, ..., s^{(M)} \right] = \begin{bmatrix} s_{11} & \cdots & s_{1M} \\ \vdots & \ddots & \vdots \\ s_{N1} & \cdots & s_{NM} \end{bmatrix}. \qquad (6)$$

We obtain the packet-level vector feature υ by multiplying the packet vector encoding S with the feature vector matrix, as shown in (7). The feature vector matrix ω represents the weight of each feature in the packet. The initialization and updating of the matrix are detailed in 3.3.

$$\upsilon = S\omega = [\upsilon_1 \dots \upsilon_i \dots \upsilon_N]^T, \upsilon_i = \sum_{l=1}^{M} s_{ik}\omega_k, \qquad (7)$$

where υ_i denotes the real number representation of the vector, and where S_{ik} denotes the kth feature in the ith packet.

(2) Flow-level frequency domain feature extraction

Vector segmentation: We convert packet-level data to flow-level data by setting a stride, resulting in (8), where represents the ith frame after segmentation, and where N_f denotes the number of frames after segmentation [34].

$$N_f = \left[\frac{N}{L_{seg}} \right], \qquad (8)$$
$$f_i = \upsilon \left[\!\left[(i-1) \times L_{seg} : i \times L_{seg} \right]\!\right]. (1 \leqslant i \leqslant N_f)$$

Discrete fourier transform (DFT): Due to the complexity of the network traffic features in the time domain and the difficulty in capturing correlations between features, we apply the Discrete Fourier Transform (DFT) to each frame to convert time-domain features into frequency-domain features. Frequency domain features are characterized by low overhead and fine granularity,

which can further enhance the accuracy and robustness of the detection model while also shortening the detection time. We obtain (9) and (10), where F_i represents the frequency domain features of the ith frame and where F_{ik} represents the various frequency components in the ith frame.

$$F_i = \mathcal{F}(f_i)(1 \leqslant i \leqslant N_f), \qquad (9)$$

$$F_{ik} = \sum_{n=1}^{L_{seg}} f_{in} e^{-j \frac{2\pi(n-1)(k-1)}{L_{seg}}} (1 \leqslant k \leqslant L_{seg}). \qquad (10)$$

Numerical conversion: Since deep neural networks cannot process complex number inputs, converting the complex number F_{ik} into a real number J_{jk} is necessary. Then, the real number J_{jk} is transformed into R_{jk} through logarithmic conversion to prevent a floating-point overflow in the detection model due to excessively large input ranges. The entire conversion process is demonstrated in (11)-(13).

$$F_{ik} = a_{ik} + jb_{ik}(1 \leqslant i \leqslant N_f, 1 \leqslant k \leqslant L_{seg}), \qquad (11)$$

$$J_{ik} = a_{ik}^2 + b_{ik}^2(1 \leqslant i \leqslant N_f, 1 \leqslant k \leqslant L_{seg}), \qquad (12)$$

$$R_{ik} = \frac{\ln(J_{ik} + 1)}{C}(1 \leqslant i \leqslant N_f, 1 \leqslant k \leqslant L_{seg}), \qquad (13)$$

where J_{ik} represents the modulus of the complex number and is also the real number representation after conversion. C denotes a constant that controls the numerical range, and R_{ik} represents the real number after logarithmic transformation.

To demonstrate the low overhead and detailed granularity of the frequency domain features, we examined and displayed these features via 600 randomly chosen packets from the CIC-IDS2017 dataset. With a stride $L_{seg} = 10$, resulting in the number of frames $N_f = 60$, we extracted seven key features ($M = 7$) from each packet: size, transmission frequency, TTL, numerical protocol type, average delay, packet loss rate, and port number. Finally we map the extracted frequency domain features to RGB space for visualization and the results are shown in Fig. 3.

As shown in Fig. 3, we can clearly observe significant differences between benign and attack traffic in the frequency domain. Therefore, using frequency domain feature analysis to extract the temporal information of network traffic can significantly reduce the overhead of the detection model while also enhancing the model's robustness against adversarial attacks.
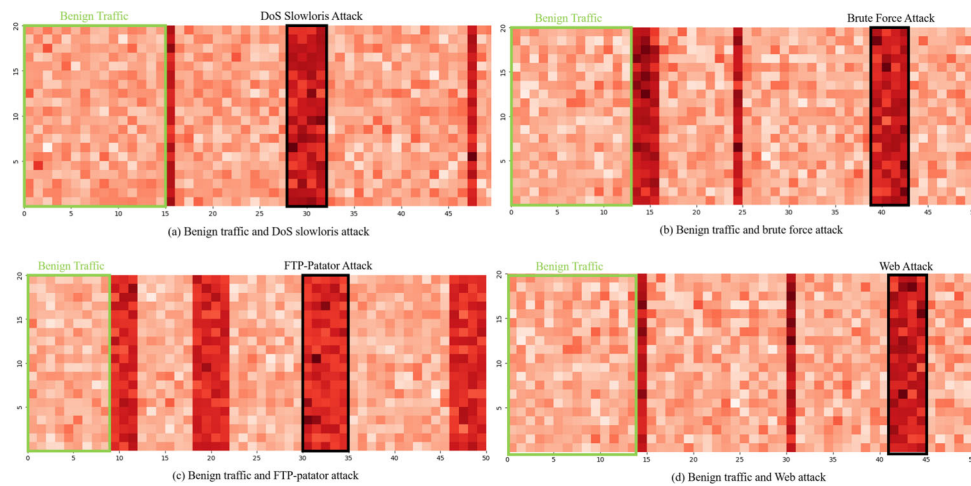
Fig. 3 The RGB pseudo-spectrogram of benign traffic and four types of malicious attack traffic under frequency domain features. (a) is DoS slowloris attack and benign traffic; (b) is brute force attack and benign; (c) is FTP-patator attack and benign traffic

3.3 Improved MPL

In industrial processes, assembly line labor division inspires collaborative training methods for models. Different data feature descriptions enhance model performance through mutual learning. We propose a democracy co-training approach for class collaboration to refine the MPL method. Specifically, we train the teacher network with a real-world traffic dataset (mostly benign traffic) and the student network with a balanced artificial traffic dataset (equal parts benign and attack traffic). We use a validation set consisting only of anomalous traffic. The student network checks the pseudo-label samples generated by the teacher network, enhancing the sensitivity to the attack traffic and mitigating dataset imbalance effects. Using deep semi-supervised learning, we require fewer labeled samples and lower the cost of manually designing the training and validation sets.

We define the total set of unlabeled samples as D_u and the total set of labeled samples as D_L, where D_{Lt} is used for training the teacher network, D_{Ls} is used for training the student network, and D_{Lv} serves as the validation set for updating the student network's parameters. In the labeled samples, attack traffic is defined as $A_L = \{(x_1, y_1), \ldots, (x_N, y_N)\}$, and benign traffic is defined as $B_L = \{(x_1, y_1), \ldots, (x_N, y_N)\}$. The pseudo-label sample set generated by the teacher network is D_{MPL}, which includes pseudo-anomalous samples $\hat{A}_L = \{(\hat{x}_1, \hat{y}_1), \ldots, (\hat{x}_N, \hat{y}_N)\}$ and pseudo-benign samples $\hat{B}_L = \{(\hat{x}_1, \hat{y}_1), \ldots, (\hat{x}_N, \hat{y}_N)\}$ The initial parameters of the trained teacher and student networks are θ_T and θ_S, respectively, which include the feature vector matrix ω.

To assess the confidence level of pseudo-label samples, we introduce a concept called the margin. The teacher network generates pseudo-labels and a probability $p(\hat{y}_1|x)$ for unlabeled data, which are then processed and input into the student network, which also generates a probability $p(\hat{y}_2|x)$. The margin between these two probabilities is calculated via (14). A smaller margin indicates greater confidence, whereas a larger margin suggests lower confidence. On the basis of reference [35], we establish a threshold $P = 6$. Samples below this threshold are classified as high-confidence pseudo-labels and added to the dataset D_L, whereas those above the threshold are considered low-confidence pseudo-labels and returned to the dataset D_U.

$$x_{m\arg in} = \arg \left| p(\hat{y}_1|x) - p(\hat{y}_2|x) \right|. \tag{14}$$

To ensure that teacher network generates more accurate pseudo-attack samples, we use a fixed validation set D_p to assess the performance of the student network. Simultaneously, we introduce an indicator that reflects the overall network performance without increasing the model latency. We choose the area under the precision-recall curve (AUC-PR) metric, as it emphasizes the model's ability to classify minority classes (attack traffic) in imbalanced datasets, thereby enhancing the student network's sensitivity to attack data.

We update the parameters of the two networks alternately to approximate the calculation known as "gradient of the gradient." According to meta-learning principles, each parameter optimization moves only one step in the direction of the gradient, indicating that the current optimal parameters are locally optimal. The proposed IMPL method is detailed in Algorithm 1.

At the start of Algorithm 1, lines 1 to 5 cover the initial training of the teacher and student networks. As shown in lines 6 and 7, the teacher network generates pseudo-labels for unlabeled samples. Then, from lines 8 to 12, the algorithm filters pseudo-labels basis of the confidence level P

and assigns samples to different sets according to their confidence levels. Lines 14 to 16 create new parameters for the student network and determine if the update leads to positive behavior using the AUC-PR metric. Line 19 concludes this epoch with the teacher network updating its parameters the basis of feedback from the student network.

Algorithm 1 learning algorithm of ADIMPL.

Input: (1) Teacher network training data set D_{Lt};(2) Student network training data set D_{Ls};(3) Unlabled data set D_U;(4) Validation set D_{Lv};(5) Threshold for pseudo-label data P;(6) Epochs E, batch size B and the number of batches every epoch Q

Output: (1) Current optimal parameters of the student network θ'_S;(2) Current optimal parameters of the teacher network θ'_T

1: **while** e<E,q<Q **do**
2:   **if** e=1 **then**
3:     $\theta_T^{(0)} \leftarrow$ Train teacher network T using D_{Lt};
4:     $\theta_S^{(0)} \leftarrow$ Train student network S using D_{Ls};
5:   **else**
6:     Randomly sample B data from D_U to comprise a batch and send to teacher network and student network;
7:   **end if**
8:   Applying $x_{m\arg in} = \arg \left| p\left(\hat{y}_1|x\right) - p\left(\hat{y}_2|x\right)\right|$ to determine the confidence level of pseudo-labeled data;
9:   **if** $x_{m\arg in}$>p **then**
10:     This data is sent to set D_{MPL} as high-confidence data;
11:   **else**
12:     This data is sent back set D_U as low-confidence data;
13:   **end if**
14:   Update the $\theta_S^{(t)}$ using the $\hat{A}_L$: $\theta_S^{(t+1)} = \theta_S^{(t)} - \eta_s \nabla_{\theta_S} \mathcal{L}\left(y_l, \theta_S\left(x_l\right)\right)|_{\theta_S=\theta_S^{(t)}}$;
15:   Input the validation set D_{Lv} into $\theta_S^{(t)}$ to obtain the AUC-PR value $AUC-PR_S^{(t)}$ at time t;
16:   **if** $AUC-PR_S^{(t)}$>$AUC-PR_S^{(t-1)}$ **then**
17:     Update the $\theta_T^{(t+1)}$ using $\theta_S^{(t)}$:$\theta_T^{(t+1)} = \theta_T^{(t)} - \eta_T \nabla_{\theta_T} \mathcal{L}\left(\theta_S - \nabla_{\theta_S}\mathcal{L}\left(y_l, \theta_S\left(x_l\right)\right)\right)$;
18:   **else**
19:     Teacher network still retains its original parameters $\theta_T^{(t)}$;
20:   **end if**
21: **end while**
22: **return** θ'_T,θ'_S

---

4 Experiment and analysis

4.1 Experimental setups

This section primarily introduces the public datasets used in the experiments, comparison models, deep neural network choices, experimental settings, and all the evaluation metrics employed in the experiments (Table 2).

(1) Datasets

In our experiments, three benchmark datasets were used: CIC-IDS2017 and CIC-IDS2018, which include real-world network traffic and various types of network attacks. In order to avoid the dependence of our proposed method on a single dataset, we mix the CIC-IDS2017 and CIC-IDS2018, then divide them into two new training sets D_U and D_L, based on the presence or absence of labels. The third dataset, CIC-Attack dataset 2023, contains only attack network traffic. The main role of this dataset is to validate the model's ability to generalize over ICPS in the real world by obtaining the performance of the model's attack recognition. Hence the data for set D_{Lv} originate from this dataset. The detailed information for each dataset is as follows:

CIC-IDS2017 [36]: Provided by the Canadian Institute for Cybersecurity. It utilizes the CICFlowMeter tool for traffic labeling, which is based on timestamps, source and destination IPs, ports, protocols, and types of attacks.

CIC-IDS2018 [36]: Building upon CIC-IDS2017, the CIC-IDS2018 dataset offers more updated and diverse attack scenarios. It includes a wider variety of attack types and benign traffic.

CIC-Attack Dataset 2023 [37]: CIC-Attack Dataset 2023 is a real-time dataset provided by the Canadian Institute for cybersecurity. It comprises 33 attacks, divided into seven categories: DDoS, DoS, Recon, Web Attack, Brute Force, Spoofing and Mirai.

(2) Comparative models

To demonstrate the superiority of the ADIMPL method, we selected six advanced deep learning models for comparison. The characteristics of each model are introduced as follows:

MemAe-gmm-ma [22]: This model optimizes the parameters of both the autoencoder and Gaussian mixture models end-to-end, effectively balancing the reconstruction and density estimation to avoid local optima.

NetFlow-edge [26]: This model uses graph contrastive learning to differentiate between normal and anomalous network traffic, accurately detecting high-dimensional data with significant computational costs.

SFAD [29]: This model uses minimal labeled data to create a bias loss function and effectively distinguishes between positive and negative samples.

ADESSA [31]: This model combines margin sampling with democratic co-learning to build a balanced training set of manually labeled high-information samples and high-confidence auto-labeled samples.

ESeT [32]: Based on the Transformer neural network, ESeT extracts the byte encoding and frequency domain features of the network traffic and introduces a confidence selector to enhance semi-supervised learning performance.

MPL [14]: MPL improves the traditional pseudo-label method with a regularization strategy, using cycles

Table 2 Statistics of CIC-IDS2017, CIC-IDS2018 and CIC-Attack Dataset 2023

Attack Types	CIC-IDS2017	CIC-IDS2018	CIC-Attack Dataset 2023	Total Used
benign	2,223,072	12,523,951	14,567	14,761,590
bot	1,847	265,089	1,089,417	1,356,353
dos	355,527	574,968	1,529,071	2,459,566
ddos	38,761	25,487	1,631,730	1,695,978
infiltration	34	148,260	794	149,088
portscan	148,531	1,179,251	1,572,997	2,900,779
web attack	2,164	180,206	951,034	1,133,404
brute force	13,083	175,240	867,314	1,055,637

between two networks to prevent premature convergence, significantly enhancing the model's ability to adapt to environmental changes.

(3) Deep neural network

SqueezeNet is a compact deep neural network that performs comparably to larger networks. It features two convolutional layers, multiple Fire modules, and a Softmax layer. Each Fire module includes a "squeeze layer" with 1x1 convolutional kernels and an "expand layer" with both 1x1 and 3x3 kernels [33]. We have replaced the network's first convolutional layer with a level feature extraction module, effectively reducing the model's size and parameter count. The primary advantage of SqueezeNet is its lightweight design, which facilitates rapid data transfer and real-time processing without sacrificing performance. This makes it ideal for classification tasks. Consequently, we chose SqueezeNet to build both the teacher network T and the student network S.

(4) Experimental settings

All the experiments were conducted on a computer equipped with an Intel Core i7-11800 H CPU @ 2.30GHz and 16 GB of RAM. The NVIDIA GeForce RTX 3050 Ti Laptop GPU was used for training acceleration. The development framework is PyTorch 1.12.1, with an initial learning rate set to 0.001 and an optimizer set to Adam. The training epochs E are set to 30, the batch size B is set to 256, and the number of batches per epoch Q is set to 5. The loss function is CrossEntropyLoss. The kaiming_normal function is used to initialize the weight parameters in the feature vector matrix ω, as well as the initial parameters $\theta_T^{(0)}$ and $\theta_S^{(0)}$ for the student and teacher networks.

Accuracy: Proportion of correct predictions (TP+TN) in the total samples.

Recall: This metric measures the proportion of actual positive class samples (attack traffic) correctly identified (TP) out of the total positive class samples (TP+FN). A high recall rate means that fewer positive class samples are missed.

F1 score: This metric is the harmonic mean of the accuracy and recall, and is used to evaluate the precision and robustness of the model. The closer the value is to 1, the better.

AUC (Area Under The ROC Curve): This metric reflects the balance between the false positive rate and true positive rate (recall) at different thresholds. A higher AUC, closer to 1, indicates a better model classification performance.

MER (Malicious traffic Evasion Rate): This metric measures the ratio of undetected malicious traffic. A higher MER indicates more effective evasion and lower model robustness. The calculation (15) is as follows:

$$MER = (1 - TrueAttack/TotalNumber of Samples) \times 100\%. \tag{15}$$

ADR (Accuracy Decline Rate): This metric calculates the decrease in model accuracy after an post-attack. A higher ADR signifies reduced robustness. The calculation (16) is as follows:

$$ADR = \frac{PreAttackAccuracy - PostAttackAccuracy}{PostAttackAccuracy} \times 100\%. \tag{16}$$

RDR (Recall Decline Rate): This metric quantifies the reduction in the recall rate following an attack. Greater values indicate less sensitivity to attacks and diminished robustness. The calculation (17) is as follows:

$$RDR = \frac{PreAttackRecall - PostAttackRecall}{PostAttackRecall} \times 100\%. \tag{17}$$

Fig. 4 CPU throughput at runtime between MPL and ADIMPL models
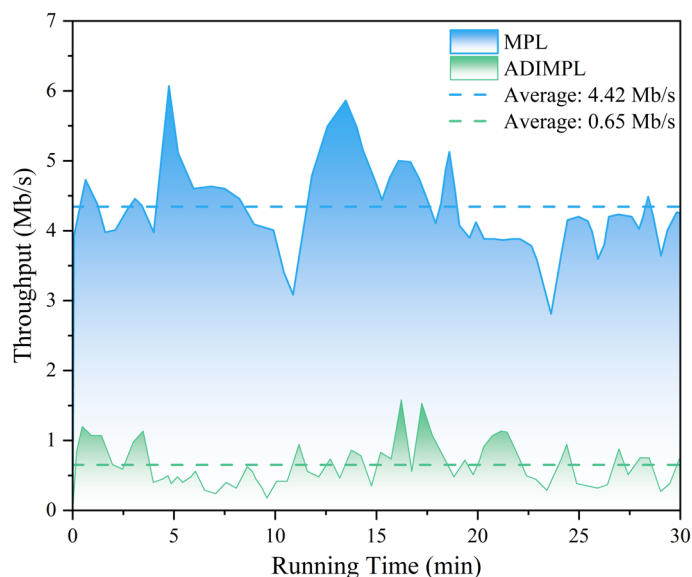
4.2 Effectiveness experiment

Experimental preparation To prevent the model from learning solely from a single dataset, we combined the CIC-IDS2017 and CIC-IDS2018 datasets. In accordance with our experimental design, we introduce the N-way and K-shot concepts, where N-way represents the type of network traffic. This experiment includes nine types: benign, bot, dos, ddos, infiltration, portscan, web attack, brute force, and other attacks; thus, N=9. We also set up three groups with extremely few, moderately few, and few labeled samples, with K values of 100, 500, and 1000, respectively. Labeled samples were randomly selected, with the remaining data forming the unlabeled dataset D_U. Additionally, we randomly drew 5000 network traffic instances from the CIC-Attack Dataset 2023 to create a validation set D_{Lv}. To ensure fairness in the experiment, all the supervised models were trained with only the same number of labeled samples,

whereas unsupervised models were trained with an equal number of unlabeled samples.

Experimental results We measured the throughput of traditional MPL model and ADIMPL on 11th Gen Intel(R) Core(TM) i7-11800H chip. As shown in Fig. 4, we find that ADIMPL achieves an average throughput of 0.65 Mb/s, while MPL achieves 4.42 Mb/s. ADIMPL obtains a lower computational overhead due to the significant reduction in feature engineering complexity. The average throughput of 0.65Mb/s also proves that our proposed ADIMPL model can be deployed in resource-constrained real ICPS. Table 3 displays the performance of seven systems under different labeled sample size groups (extremely few, moderately few, and few) during pre-training. The results show that ADIMPL outperforms the other seven models across all four evaluation metrics. As shown in Fig. 5, 6 and 7, the performance of each model varies an increasing number of detection epochs.

Table 3 The accuracy, recall, F1 score, and AUC results of each model with extremely few, moderately few, and few labeled samples

Dreege		Extremely few labeled samples (Total 700 samples)				Moderately few labeled samples (Total 3,500 samples)				Few labeled samples (Total 7,000 samples)			
Setup		N-way 7		K-shot 100		N-way 7		K-shot 500		N-way 7		K-shot 1000	
Metrics		Acc	Rec	F1	AUC	Acc	Rec	F1	AUC	Acc	Rec	F1	AUC
Supervised	MemAe-gmm-ma	0.8153	0.7863	0.8041	0.7985	0.8468	0.8369	0.8399	0.8316	0.9317	0.9472	0.9371	0.9346
Unsupervised	NetFlow-Edge	0.9567	0.9542	0.9557	0.9431	0.9611	0.9608	0.9609	0.9589	0.9635	0.9625	0.9631	0.9543
Semi-Supervised	SFAD	0.9545	0.9367	0.9431	0.9411	0.9677	0.9653	0.9662	0.9579	0.9701	0.9687	0.9695	0.9651
	ADESSA	0.9675	0.9348	0.9572	0.9341	0.9764	0.9683	0.9724	0.9652	0.9811	0.9798	0.9802	0.9805
	EseT	0.9735	0.9689	0.9713	0.9735	0.9826	0.9811	0.9817	0.9804	0.9857	0.9843	0.9850	0.9836
	MPL	0.9296	0.9176	0.9215	0.9258	0.9317	0.9256	0.9259	0.9211	0.9357	0.9356	0.9356	0.9298
	ADIMPL	**0.9862**	**0.9901**	**0.9881**	**0.9844**	**0.9911**	**0.9906**	**0.9908**	**0.9905**	**0.9913**	**0.9911**	**0.9912**	**0.9912**

The best results are boldfaced
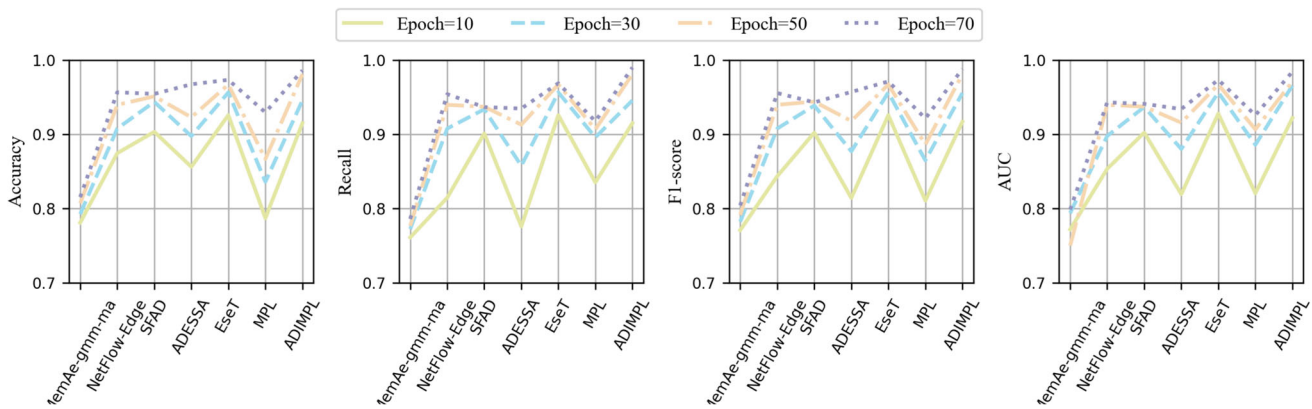
Fig. 5 The accuracy, recall rate, F1 score, and AUC results of each model under the pre-training with extremely few labeled samples

Specifically, as shown in Fig. 5, the ADIMPL model initially performs worse than EseT at lower epochs, however, after surpassing 50 epochs, due to continuous optimization and adaptation to data changes, the performance of ADIMPL significantly improves. The experimental results demonstrate that even with an extremely small number of labeled samples, ADIMPL can adapt to the detection task based on the basis of its learning capabilities, showing excellent effectiveness.

4.3 Real-time experiment

To objectively assess the real-time performance of the model, we used overall latency as the benchmark. This measures the time from data packet input to detection completion, including transmission, queuing, and detection latency.

Experimental preparation We set up two network traffic groups with different loads to test the latency across seven

models. The low-load group used traffic from "Tues-20-02-2018" (short-duration DDoS attacks) in the CIC-IDS 2018 dataset. The high-load group used traffic from "Wed-14-02-2018" (long-duration Bruteforce attacks) and "Thurs-15-02-2018" (long-duration DDoS Attacks). We ran the experiment with Ostinato software, using 1000 packets for each group, which was evenly split between benign and attack traffic to reduce randomness.

Experimental results To visualize latency, we introduced the cumulative distribution function (CDF) [38]. Figure 8 shows a latency box plot for seven methods under low-load conditions. The overall latency of ADIMPL ranged from 0.062 to 0.182 s, with a median of 0.098 s, outperforming those of the other methods. Figure 9 illustrates ADIMPL's overall latency and includes CDF curves for transmission, queuing, and detection latencies. The average detection latency was 0.108 s, which was the largest component. Under high-load conditions, as shown in Fig. 10, the overall latency of
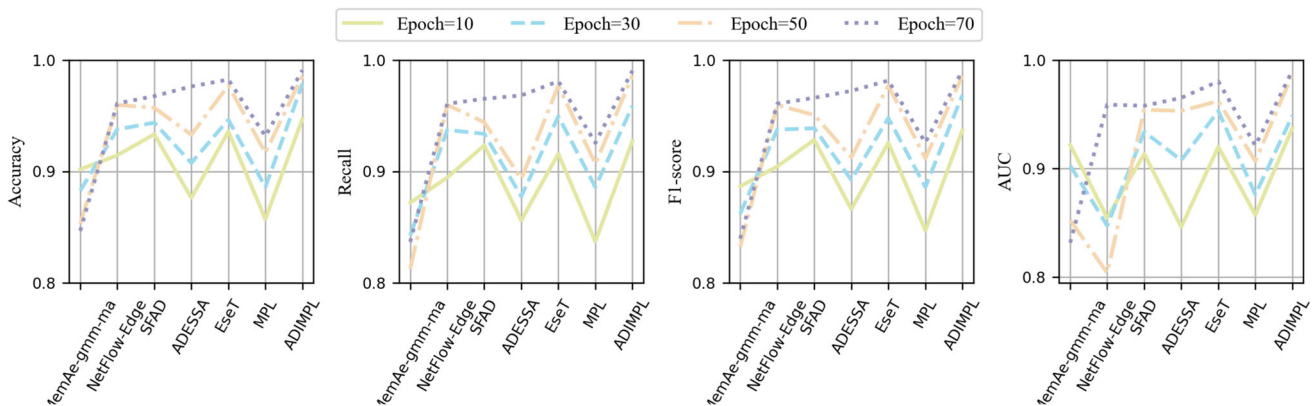
Fig. 6 The accuracy, recall rate, F1 score, and AUC results of each model under the pre-training with moderately few labeled samples
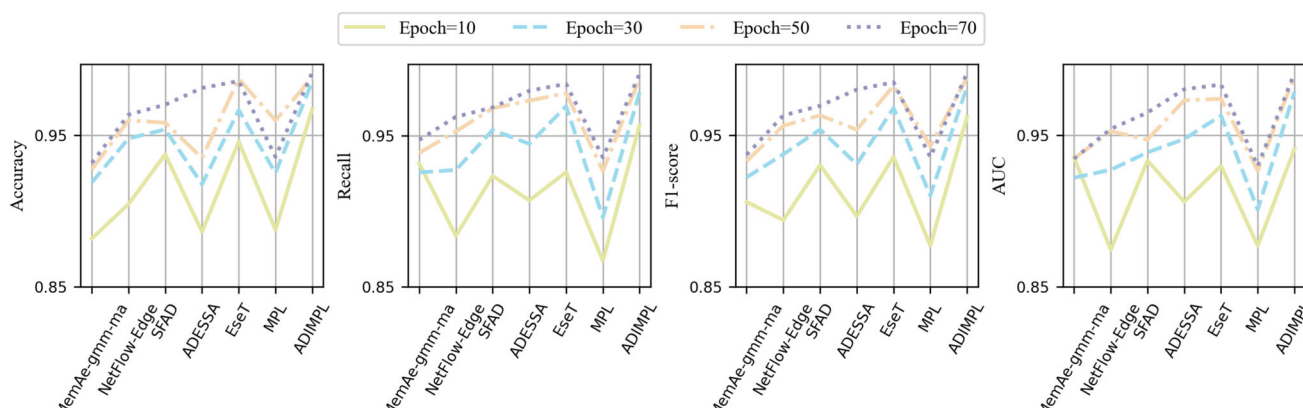
Fig. 7 The accuracy, recall rate, F1 score, and AUC results of each model under the pre-training with few labeled samples

ADIMPL varied from 0.267 to 0.385 s, with a median of 0.314 s. This ranked second among the seven methods, just behind NetFlow-Edge, which uses a simpler classification algorithm instead of deep neural networks. Figure 11 indicates that the queuing and detection latencies account for 99.5% of total latency under high load, highlighting that increased detection overhead leads to congestion. To enhance real-time detection, models need improved processing capabilities. Among the models employing deep neural networks, ADIMPL had the lowest detection time overhead, indicating a strong real-time performance.

4.4 Robustness experiment

On the basis of the results of increased overall latency of ADIMPL in high-load environments, we observed that the performance of the detection model is somewhat affected when attackers send a large volume of attack traffic to the ICPS in a short period. Consequently, we focus more on the robustness of the model and verify the robustness of ADIMPL through experiments.

Adversarial attacks can be divided into three types based on the basis of the attacker's knowledge of the model. White-box attacks occur when the attacker has complete knowledge of the target model, including its internal mechanisms, parameters, architecture, and training data. Black-box attacks occur when the attacker has a limited understanding of the model. Gray-box attacks are intermediate, combining elements of both white-box and black-box attacks. Owing to their nature, black-box attacks are more common seen in real-world scenarios.

In [39], the authors introduced a black-box attack method that combines the GAN+PSO algorithms. This approach uses GANs to generate adversarial examples and PSO to mimic benign traffic, enhancing the sample's disguise. However, PSO struggles with large traffic volumes because to oversized search spaces and local optima. We refine the PSO objective function to better adapt to the network traffic environment in our experiment.

In the standard PSO algorithm, particles find the optimal particle by learning from their own historical experience p_best and collective experience b_best. To solve the vari-
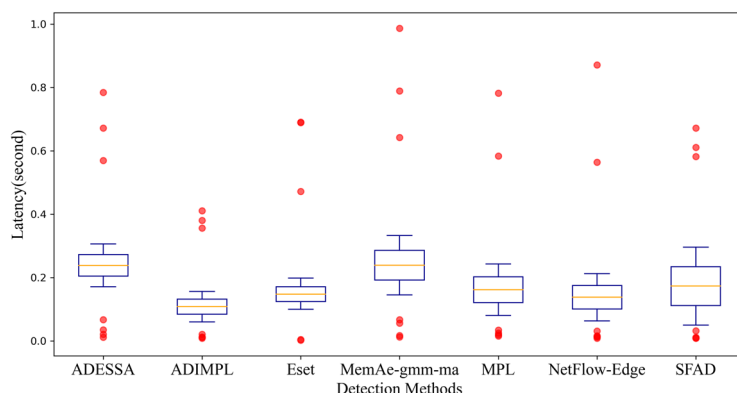
Fig. 8 The box plot based on the overall latency results of each method in low-load environments
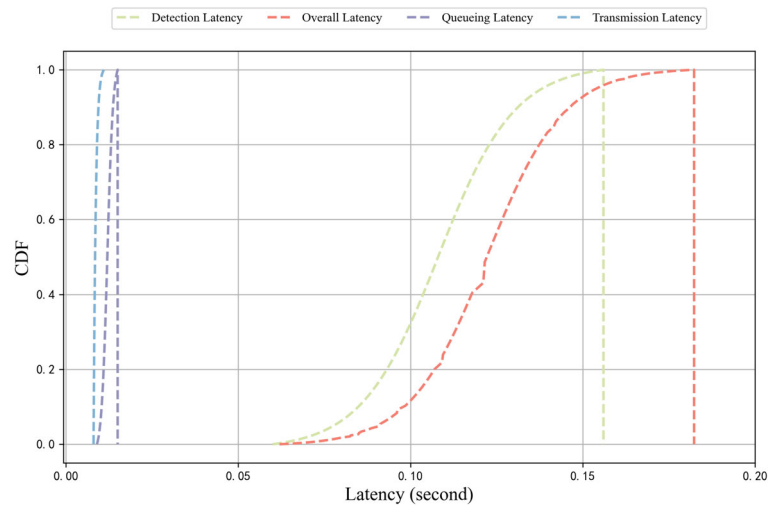
Fig. 9 We plotted the corresponding CDF curves based on the latency results of different stages in low-load environments

able $X = \{x_1, x_2, \cdots, x_i\}\}$, with the objective function being $\min \{f(x)\}$, the particle update formulas in the standard PSO algorithm are expressed as (18) and (19).

$$
\begin{aligned}
v_i(t + 1) =& wv_i(t) + c_1 r_1 (p\_best_i - x_i(t)) \\
& + c_2 r_2 (g\_best_i - x_i(t))
\end{aligned}
\tag{18}
$$

$$
x_i(t + 1) = x_i(t) + v_i(t + 1),
\tag{19}
$$

where $v_i(t + 1)$ and $x_i(t + 1)$ represent the velocity and position of particle i at the $t + 1$ generation, respectively; w is the inertia weight, which linearly decreases with the number of iterations in the standard PSO algorithm; c_1 and c_2 are learning factors, typically set to 2; and r_1 and r_1 are random numbers uniformly distributed in the range [0,1].

By linearly combining the individual best and the group best, and replacing $\left(\frac{p\_best_i + g\_best_i}{2}\right)$ and $\left(\frac{p\_best_i - g\_best_i}{2}\right)$

with p_best and b_best respectively in the above formula, we obtain the new particle velocity update equation as follows.

$$
\begin{aligned}
v_i(t + 1) =& wv_i(t) + c_1 r_1 \left\{ \frac{p\_best_i + g\_best_i}{2} - x_i(t) \right\} \\
& + c_2 r_2 \left\{ \frac{p\_best_i - g\_best_i}{2} - x_i(t) \right\}.
\end{aligned}
\tag{20}
$$

The Optimized PSO algorithm has a wider search range and faster search speed, enhancing the likelihood of finding the global optimum during the mutation process. To test the effectiveness of the GAN+OPSO attack algorithm (black-box attack), we incorporated the GAN+OPSO algorithm and FGSM (white-box attack) based on the Ref. [39] experimental setup. As shown in Fig. 12, when MER is used as
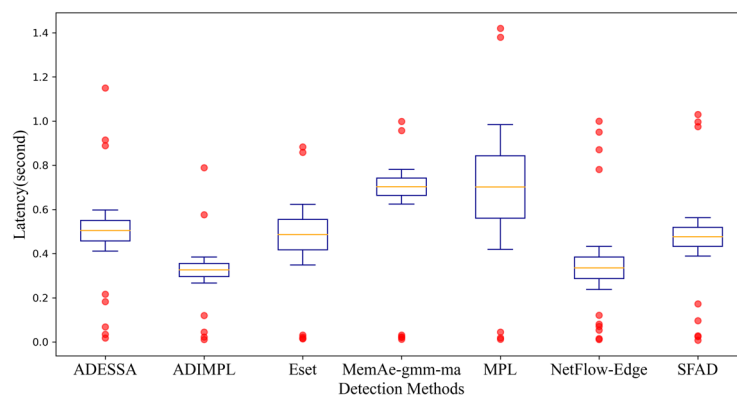
Fig. 10 The box plot based on the overall latency results of each method in high-load environments
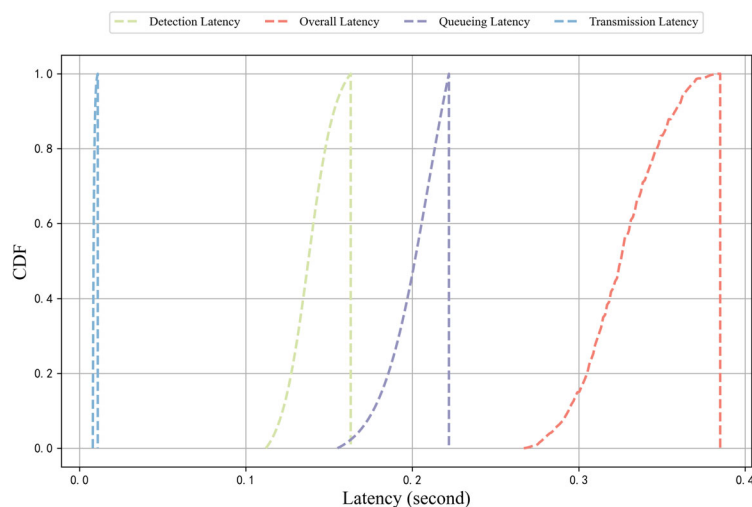
Fig. 11 We plotted the corresponding CDF curves based on the latency results of different stages in high-load environments

the evaluation metric, our GAN+OPSO algorithm slightly outperforms the original GAN+PSO and surpasses the white-box attack FGSM, demonstrating its effectiveness.

We attacked the detection model via the GAN+OPSO approach. First, we generated black-box adversarial attack

samples with the GAN model. We then mutate these samples via the optimized PSO algorithm. To validate the robustness of the model, two metrics (l_c, l_t) were used to quantify the attack cost, where l_c is the ratio of adversarial attack packets to original packets, and where l_t is
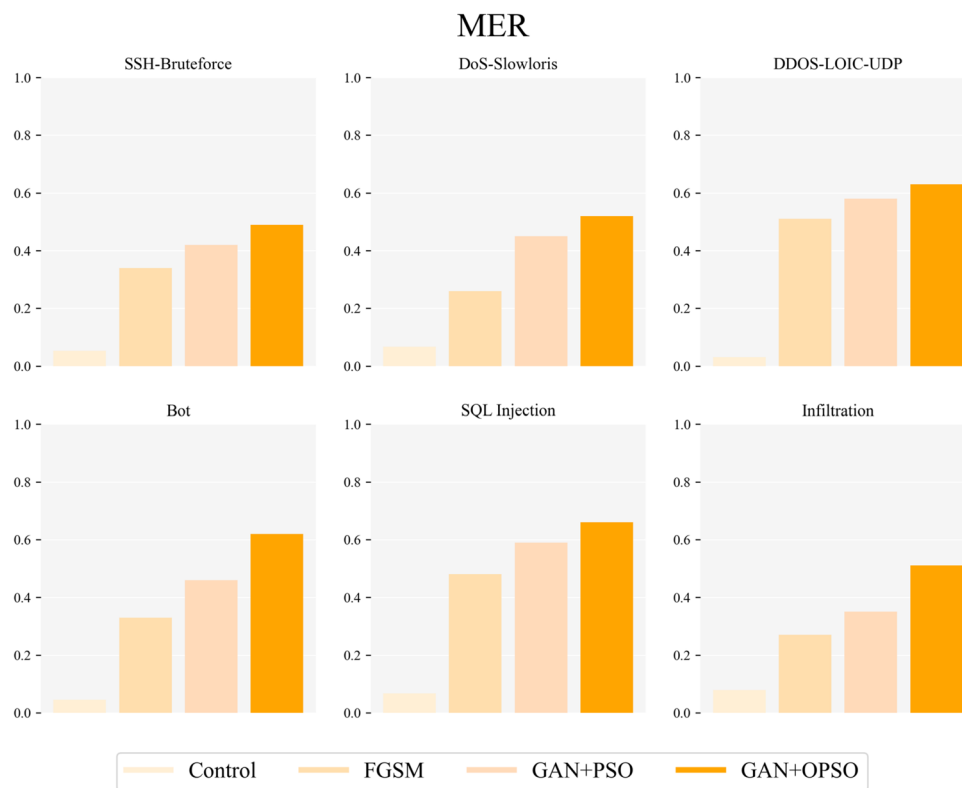
Fig. 12 Comparison of different attack algorithms across six types of attacks with the control group (higher values indicate better attack effectiveness)

the ratio of mutated traffic in the packets to the original traffic. We define ($l_c = 0.2, l_t = 0.5$) as a low attack cost, ($l_c = 0.35, l_t = 0.75$) as a medium attack cost, and ($l_c = 0.35, l_t = 0.75$) as a high attack cost. The performance of each model under these three cost scenarios is shown in the following Table 4.

Table 4 shows that NetFlow-Edge's performance decreases with increasing attack costs. This is due to its basic packet-level detection which allows altered adversarial samples to escape detection. SFAD and EseT, which use frequency domain features, are more robust. After attacks via low and medium-cost GAN+OPSO, their Attack Detection Rate (ADR) and Recovery Detection Rate (RDR) remain below 10%. ADIMPL extracts features at two levels and updates them cyclically with the IMPL method. It adapts continuously to attack environment changes. Even under high-cost GAN+PSO attacks, ADIMPL maintains its ADR and RDR under 10%. These results show ADIMPL's strong robustness against black-box attacks.

4.5 Analysis

In the ICPS environment, three key performance indicators are critical for detection models: effectiveness, real-time performance, and robustness. Effectiveness ensures accurate identification and response to attacks, real-time performance maintains system security without delays in detection, and robustness allows the model to perform reliably, even under attack. These indicators are vital for any detection model. We normalized the performance data for seven models under various scenarios and calculated the arithmetic mean of these three metrics to evaluate the overall performance. Figure 13 shows that our method significantly outperforms the other

Table 4 The accuracy, recall rate, F1 score, and AUC results of each model under the pre-training with moderately few labeled samples

Attack Cost	Models	ACC	Recall	F1	AUC	MER	ADR	RDR
Non-attack	MemAe-gmm-ma	0.8468	0.8369	0.8399	0.8316	0	0	0
	NetFlow-Edge	0.9611	0.9608	0.9609	0.9589	0	0	0
	SFAD	0.9677	0.9653	0.9662	0.9579	0	0	0
	ADESSA	0.9764	0.9683	0.9724	0.9652	0	0	0
	EseT	0.9826	0.9811	0.9817	0.9804	0	0	0
	MPL	0.9317	0.9256	0.9259	0.9211	0	0	0
	ADIMPL	0.9911	0.9906	0.9908	0.9905	0	0	0
Low-attack	MemAe-gmm-ma	0.8015	0.7761	0.7886	0.7831	6.13%	5.35%	7.26%
	NetFlow-Edge	0.7514	0.7377	0.7445	0.7431	28.25%	21.82%	23.22%
	SFAD	0.9425	0.9274	0.9349	0.9289	4.56%	2.60%	3.93%
	ADESSA	0.8863	0.8490	0.8672	0.8522	15.66%	9.23%	12.32%
	EseT	0.9664	0.9571	0.9617	0.9579	3.72%	1.62%	2.09%
	MPL	0.9025	0.8621	0.8818	0.8728	11.78%	2.16%	5.53%
	ADIMPL	0.9865	0.9832	0.9848	0.9815	**0.86%**	**0.45%**	**0.72%**
Medium-attack	MemAe-gmm-ma	0.6933	0.6519	0.6720	0.6523	23.51%	18.13%	18.50%
	NetFlow-Edge	0.6278	0.5589	0.5913	0.5734	53.92%	34.68%	41.83%
	SFAD	0.8871	0.8954	0.8912	0.8896	10.65%	8.33%	6.78%
	ADESSA	0.7439	0.7028	0.7228	0.7125	30.29%	23.81%	27.42%
	EseT	0.9468	0.9531	0.9499	0.9502	4.37%	3.62%	2.50%
	MPL	0.8325	0.8421	0.8372	0.8397	15.71%	9.75%	7.72%
	ADIMPL	0.9623	0.9845	0.9732	0.9798	**0.73%**	**2.89%**	**0.59%**
High-attack	MemAe-gmm-ma	0.4322	0.3598	0.3927	0.3643	69.02%	48.84%	57.01%
	NetFlow-Edge	0.3219	0.2015	0.2479	0.2265	79.85%	66.51%	79.03%
	SFAD	0.7359	0.7856	0.7599	0.7664	21.44%	23.95%	18.62%
	ADESSA	0.5523	0.6015	0.5758	0.5871	39.85%	43.44%	37.88%
	EseT	0.8541	0.8961	0.8745	0.8872	10.39%	13.05%	8.33%
	MPL	0.7015	0.7860	0.7413	0.7739	21.41%	23.95%	13.87%
	ADIMPL	0.9199	0.9445	0.9320	0.9438	**5.06%**	**7.17%**	**4.63%**

The best results are boldfaced
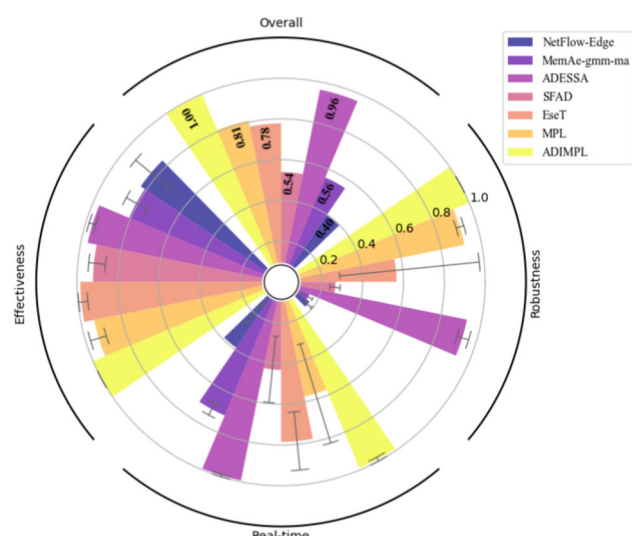
Fig. 13 We normalized the effectiveness, real-time performance, and robustness of each model, plotting the average values in the graph (the closer to 1, the better). Additionally, we calculated the overall performance of each model and illustrated it at the top

methods, demonstrating its exceptional capabilities in ICPS attack detection.

5 Conclusion

Within the framework of industrial control systems, this paper introduces ADIMPL, an advanced deep semi-supervised learning method for attack detection. This model employs the IMPL method, which is based on democratic co-training and incorporates dual-level network traffic feature extraction. Applying the IMPL algorithm between teacher and student networks enhances the sensitivity to attack traffic. This makes it suitable for ICPS attack detection scenarios. ADIMPL adapts to dynamic attack changes, improving detection performance and significantly increasing the robustness and real-time capabilities of the deep semi-supervised learning models. Experiments show that ADIMPL outperforms other models in terms of effectiveness and robustness under the same conditions. Considering its effectiveness, real-time performance, and robustness, ADIMPL demonstrates significant superiority. However, this study did not fully address the security and privacy of industrial process data. In future work, we plan to apply the proposed algorithm within a federated learning framework. This will create independent industrial information silos, isolating each industrial process to ensure data privacy and security.

Declarations

Conflict of interest The authors declare that they have no known competing financial interests or personal relationships that could have appeared to influence the work reported in this paper.

References

1. Zhang J, Pan L, Han QL et al (2021) Deep learning based attack detection for cyber-physical system cybersecurity: a survey. J Automatic Sincia 9(3):377–391. https://doi.org/10.1109/JAS.2021.1004261
2. Ghobakhloo M (2020) Industry 4.0, digitization, and opportunities for sustainability. J Clean Prod 252:119869. https://doi.org/10.1016/j.jclepro.2019.119869
3. Wübbeke J, Meissner M, J M, et al (2016) Made in china 2025. Mercator Institute for China Studies Papers on China 2(74):4
4. Kocabay A, Javadi H (2023) Cyber-Physical Systems—Manufacturing Applications, Springer Nature Singapore, Singapore, pp 35–56. https://doi.org/10.1007/978-981-19-2012-7_2
5. Industrial Internet Industry Alliance C (2023) 2022 industrial information security situation report. Figshare. http://221.179.172.81/images/20230720/62491689823058354.pdf
6. Woodard M, Sarvestani SS, Hurson AR (2015) A survey of research on data corruption in cyber-physical critical infrastructure systems. Adv Comput 98:59–87. https://doi.org/10.1016/bs.adcom.2015.03.002
7. Pinto R, Gonçalves G, Delsing J et al (2022) Enabling data-driven anomaly detection by design in cyber-physical production systems. Cybersecurity 5(1):9. https://doi.org/10.1186/s42400-022-00114-z
8. Sharma A, Bhushan K (2024) A hybrid approach based on puf and ml to protect mqtt based iot system from ddos attacks. Cluster Comput 5(9):1–26. https://doi.org/10.1007/s10586-024-04638-6
9. Zhang X, Zhang Z, Zhang R et al (2024) Event-triggered resilient recovery learning control protocol for interconnected dc microgrids with distributed attack detection. Sustain Energy, Grids 38:101364. https://doi.org/10.1016/j.segan.2024.101364
10. Fraccaroli M, Bizzarri A, Casellati P et al (2024) Exploiting cnn's visual explanations to drive anomaly detection. Appl Intell 54(1):414–427. https://doi.org/10.1007/s10489-023-05177-0
11. Bakar RA, De Marinis L, Cugini F et al (2024) Ftg-net-e: a hierarchical ensemble graph neural network for ddos attack detection. Computer Netw 250:110508. https://doi.org/10.1016/j.comnet.2024.110508
12. Sarıkaya A, Kılıç BG, Demirci M (2023) Raids: robust autoencoder-based intrusion detection system model against adversarial attacks. Comput & Secur 135:103483. https://doi.org/10.1016/j.cose.2023.103483
13. Farhat S, Abdelkader M, Meddeb-Makhlouf A et al (2023) Cadsml/dl: efficient cloud-based multi-attack detection system. Int J

Inf Secur 22(6):1989–2013. https://doi.org/10.1007/s10207-023-00729-4

14. Pham H, Dai Z, Xie Q, et al (2022) Meta pseudo labels. pp 11557–11568, https://doi.org/10.1109/CVPR46437.2022.01139, paper presented at the 2021 IEEE/CVF conference on computer vision and pattern recognition, Nashville, TN, USA, 20-25 June 2021

15. Yang X, Song Z, King I et al (2023) A survey on deep semi-supervised learning. IEEE T Knowl Data En 35(9):8934–8954. https://doi.org/10.1109/TKDE.2022.3220219

16. Hu S, Chen X, Li J et al (2023) Observer-based resilient controller design for networked stochastic systems under coordinated dos and fdi attacks. IEEE T Control Netw Syst 11(2):890–901. https://doi.org/10.1109/TCNS.2023.3314578

17. Zhang H, Chen Z, Yu C et al (2024) Event-trigger-based resilient distributed energy management against fdi and dos attack of cyber–physical system of smart grid. IEEE T on Syst Cy 54(5):3220–3230. https://doi.org/10.1109/TSMC.2024.3357497

18. Kumar P, Govindaraj V, Erturk VS et al (2023) Fractional mathematical modeling of the stuxnet virus along with an optimal control problem. Ain Shams Eng J 14(7):102004. https://doi.org/10.1016/j.asej.2022.102004

19. Taye MM (2023) Theoretical understanding of convolutional neural network: Concepts, architectures, applications, future directions. Computation 11(3):52. https://doi.org/10.3390/computation11030052

20. Zhang L, Liu K, Xie X et al (2023) A data-driven network intrusion detection system using feature selection and deep learning. J Inform Secur Appl 78:103606. https://doi.org/10.1016/j.jisa.2023.103606

21. Lan J, Liu X, Li B et al (2023) A novel hierarchical attention-based triplet network with unsupervised domain adaptation for network intrusion detection. Appl Intell 53(10):11705–11726. https://doi.org/10.1007/s10489-022-04076-0

22. Liu X, Zhu S, Yang F et al (2023) Research on unsupervised anomaly data detection method based on improved automatic encoder and gaussian mixture model. J Cloud Comp 11(58):155–172. https://doi.org/10.1186/s13677-023-00328-z

23. Tao Y, Zhen J, Pei L et al (2023) A traffic anomaly detection approach based on unsupervised learning for industrial cyber–physical system. Knowl-Based Syst 279:110949. https://doi.org/10.1016/j.knosys.2023.110949

24. Fathima A, Devi GS, Faizaanuddin M (2023) Improving distributed denial of service attack detection using supervised machine learning. Measurement: Sensors 30:100911. https://doi.org/10.1016/j.measen.2023.100911

25. Altunay HC, Albayrak Z (2023) A hybrid cnn+ lstm-based intrusion detection system for industrial iot networks. Eng Sci Technol 38:101322. https://doi.org/10.1016/j.jestch.2022.101322

26. Xu R, Wu G, Wang W et al (2024) Applying self-supervised learning to network intrusion detection for network flows with graph neural network. Comput Netw 248:110495

27. Sikder MNK, Nguyen MB, Elliott ED et al (2023) Deep h2o: Cyber attacks detection in water distribution systems using deep learning. J Water Process Eng 52:103568. https://doi.org/10.1016/j.jwpe.2023.103568

28. Xie MK, Xiao J, Liu HZ, et al (2023) Class-distribution-aware pseudo-labeling for semi-supervised multi-label learning. In:

29. He Q, Shah P, Zhao X (2023) Resilient operation of dc microgrid against fdi attack: a gru based framework. Inter J Elect Power & Energy Syst 145:108586. https://doi.org/10.1016/j.ijepes.2022.108586

30. Liu Y, Deng W, Liu Z et al (2024) Semi-supervised attack detection in industrial control systems with deviation networks and feature selection. J Supercomputing 80:1–22. https://doi.org/10.1007/s11227-024-06018-8

31. Niu Z, Guo W, Xue J et al (2023) A novel anomaly detection approach based on ensemble semi-supervised active learning (adessa). Comput & Secur 129:103190. https://doi.org/10.1016/j.cose.2023.103190

32. Li Y, Yuan X, Li W (2022) An extreme semi-supervised framework based on transformer for network intrusion detection. In: Proceedings of the 31st ACM International Conference on Information & Knowledge Management, pp 4204–4208

33. Ms M, SS SR, et al (2022) Optimal squeeze net with deep neural network-based arial image classification model in unmanned aerial vehicles. Trait Signal 39(1). https://doi.org/10.18280/ts.390128

34. Fu C, Li Q, Shen M, et al (2021) Realtime robust malicious traffic detection via frequency domain analysis. pp 3431–3446, https://doi.org/10.1145/3460120.3484585, paper presented at the 2021 ACM SIGSAC conference on computer and communications Security

35. Zhao S, Yu Z, Li S et al (2023) Meta pseudo labels for anomaly detection via partially observed anomalies. En Appl Arti Intell 126:106955. https://doi.org/10.1016/j.engappai.2023.106955

36. Rosay A, Cheval E, Carlier F, et al (2022) Network intrusion detection: A comprehensive analysis of CIC-IDS2017. pp 25–36, https://doi.org/10.5220/0000157000003120, pape presented at the 8th international conference on information systems security and privacy, Online Streaming, France, 9-11 February 2022

37. Leevy JL, Khoshgoftaar TM (2020) A survey and analysis of intrusion detection models based on cse-cic-ids 2018 big data. J Big Data 7:1–19. https://doi.org/10.1186/s40537-020-00382-x

38. Drew JH, Glen AG, Leemis LM (2000) Computing the cumulative distribution function of the kolmogorov-smirnov statistic. Comput Stat Data An 34(1):1–15. https://doi.org/10.1016/S0167-9473(99)00069-9

39. Han D, Wang Z, Zhong Y et al (2021) Evaluating and improving adversarial robustness of machine learning-based network intrusion detectors. IEEE J Sele Areas Commun 39(8):2632–2647. https://doi.org/10.1109/JSAC.2021.3087242

Advances in Neural Information Processing Systems, vol 36. Curran Associates, Inc., pp 25731–25747

Bohan Zhang was born in 2000, received his Bachelor's degree in Communication Engineering from Shandong University of Science and Technology in 2022. He is currently pursuing a Master's degree at the School of Electrical Engineering and Information Engineering, Lanzhou University of Technology. His research focus is on attack detection in industrial cyber-physical systems.

Jiaqi Lv was born in 1999, received his Bachelor's degree in Automatization Engineering from Lanzhou University of Technology in 2020. He is currently pursuing a Master's degree at the School of Electrical Engineering and Information Engineering, Lanzhou University of Technology. His research focus is on security of networked control systems.

Pan Zhang was born in 1995, received his Master's degree in Control Theory and Control Engineering from Lanzhou University of Technology in 2022. He is currently pursuing a Ph.D. degree at the School of Electrical Engineering and Information Engineering, Lanzhou University of Technology. His research focus is on security of networked control systems.

Wei Miao serves as a senior engineer and senior manager of Gansu Ziguang Intelligent Transportation and Control Technology Co.

Zhiwen Wang was born in 1976, received his Ph.D. in Control Theory and Control Engineering from Lanzhou University of Technology in 2007. He currently serves as a professor and doctoral supervisor at the School of Electrical Engineering and Information Engineering at Lanzhou University of Technology. His research interests include analysis and processing of networked control systems, security of cyber-physical systems, and advanced control theory and application in industrial processes.

Asynchronous filtering for two-dimensional Markovian jump systems with time delays under stochastic communication protocol and hybrid cyber attacks

Pan Zhang, Chaoqun Zhu, Bin Yang, Zhiwen Wang⬤ and Jiaqi Lv

Abstract

The asynchronous filtering problem for two-dimensional (2D) Markovian jump systems (MJSs) under hybrid cyber attacks and stochastic communication protocol (SCP) is the focus of this investigation. To avoid data transmission collisions, only a single sensor can send measurement data through the communication network at each sample shift moment, and the sensor chosen is decided by the SCP mechanism. Besides, the impact of stochastic hybrid cyber attacks on filtering performance is also considered. In the background of hybrid cyber attacks and SCP, an augmented model of 2D MJSs is constructed. Then, a novel asynchronous filter structure is proposed that can simultaneously characterize the MJSs and filter pattern mismatch as well as the mismatch between the actual SCP pattern information and the available SCP pattern information. Then, sufficient criteria conditions are established to ensure that dynamic filtering error systems meet robust H_∞ mean-square stability with a certain level of disturbance attenuation. Moreover, the conservativeness of the stability criterion is further reduced by the 2D summation inequality lemma. Finally, an industrial heating exchange process is employed to illustrate the effectiveness of the developed asynchronous filtering algorithm.

Introduction

The ability of two-dimensional (2D) systems to precisely characterize many practical systems, such as multi-variable network implementation, seismic detection data processing, power transmission lines, and X-ray image enhancement, has drawn growing interest (Duan et al., 2020; Men and Sun, 2023; Yang et al., 2020, 2024). Consequently, one of the most interesting fields in systems control has emerged: 2D systems theory. In summary, the Roesser model (Roesser, 1975), the Fornasini and Marchesini (FM) model (Fornasini and Marchesini, 1978), and the Kurek model (Kurek, 1985) are the three most popular categories of state space models. Furthermore, the time-delay phenomenon commonly exists in 2D systems, which is one of the main causes of system performance degradation or even instability. As a result, analyzing the properties of time-delay systems is a fundamental concern for practical applications and has attracted considerable attention in recent years. The stability analysis and control synthesis of the time-delay systems have been extensively explored and developed, especially in the utilization of time-delay correlation conditions to obtain stability criteria and less conservative results (Chelliq et al., 2023; Ghous et al., 2019; Hien and Trinh, 2018; Peng and Nie, 2021; Tandon et al., 2019).

With the rapid advancement of computer science and cybernetics, the structure of the controlled system has evolved from classical point-to-point to networked, and networked-based control theory is gradually established. In this scenario, the investigation results of networked 2D systems are frequently published owing to their deep significance in real-world engineering (Li et al., 2020; Song et al., 2023; Wang et al., 2020; Yan et al., 2020; Zhu et al., 2023). Meanwhile, the vulnerability of shared communication network has brought information security to the forefront. Generally speaking, there are several different types of cyber attacks that are comprehensively investigated: denial-of-service (DoS), false data injection (FDI), and replay attacks (Duo et al., 2022; He et al., 2022; Hu et al., 2022; Li et al., 2022a, 2023; Li and Ye, 2023; Liu et al., 2023; Sun et al., 2023; Tan et al., 2022; Xing et al., 2023; Yang and Zhai, 2023; Zhang et al., 2023; Zhao et al., 2022). It is important to notice that adversaries tend to

College of Electrical and Information Engineering, Lanzhou University of Technology, China

Corresponding author:
Zhiwen Wang, College of Electrical and Information Engineering, Lanzhou University of Technology, Lanzhou 730050, China.
Email: wwwangzhiwen@yeah.net

maximize the effectiveness of attacks by using collaborative hybrid cyber attacks on networked systems. Recently, a lot of research attention has been focused on the security issues of hybrid cyber attacks. (Ali et al., 2023; Cao et al., 2021; Cheng and Liu, 2023; Hamdan et al., 2022; Hu et al., 2023; Lian et al., 2023; Liu et al., 2021; Mao et al., 2024). Unfortunately, the abovementioned results are all obtained on the basis of one-dimensional (1D) systems, and there are very few results concerning the analysis of evolutionary behavior for 2D systems subject to hybrid cyber attacks, which is the main motivation for our current investigation.

It is important to highlight that much fundamental research for 2D systems generates the implicit assumption that the network has enough bandwidths, which means that all sensors are able to transmit data to the filter through the network at each sampling shift instant. Nevertheless, it is quite unfeasible to apply such an idealized communication scheme due to the limited-bandwidth network and the complexity of the network structure. The try-once-discard protocol (TODP) (Niu et al., 2023), the round-robin protocol (RRP) (Xu et al., 2022), and the stochastic communication protocol (SCP) (Li et al., 2022b; Lv et al., 2023) are a few well-known communication scheduling mechanisms that have been developed to rationally arrange data transmission. Among these protocols, the SCP and RRP are classified as time-triggered scheduling schemes, and the TODP is classified as an event-triggered scheme. Numerous industrial control networks, such as Ethernet's CSMA (carrier sense multiple access) protocol and the wireless local area network's ALOHA protocol, can widely employ SCP (Tobagi, 1980). Consequently, a great deal of attention has been paid to the control/filtering issues under SCP. However, to the author's knowledge, considerable research achievements have been obtained for the filter design problem of 1D systems affected by SCP, whereas available results for 2D systems under SCP are still relatively scattered, which may be due to the distinctive evolutionary regulations of 2D systems, and this is another motivation for our current investigation.

On the contrary, the dynamic behavior of many practical systems can change abruptly during operation due to exogenous disturbances and component faults. As a kind of stochastic hybrid system, Markovian jump systems (MJSs) can well characterize such variations, and the analysis and synthesis of MJSs have also gradually attracted research interests. More significantly, mode switching is one of the most important features for MJSs, and it is vital to fully utilize the mode jump information for the design of the controller and filter. Nevertheless, due to various uncertainties of the system itself and the communication network (e.g. switching device failures, randomly occurring packet dropouts, and time delays) in practice, it is almost impossible for the controller/filtering mode and system mode to achieve synchronous matching at each sampling instant, which is also referred to as the asynchronous phenomenon. To explore an effective stability analysis strategy in the case of pattern mismatch, scholars have conducted preliminary research on asynchronous control/filtering of 2D systems in recent years (Cheng et al., 2023; Hien

and Trinh, 2017; Tao and Wu, 2022; Wu and Tao, 2022; Wu et al., 2019). The Roesser model is the basis for all of the above-reported results, even though some have been obtained for asynchronous filtering of 2D systems. In contrast to the more general Fornasini and Marchesini II (FM-II) model, the asynchronous filtering of 2D systems remains unaddressed. In addition, considering the network-induced problems, the communication scheduling mechanism, and the jump pattern that remains asynchronous with the 2D MJSs, designing a reasonable filter structure to obtain the desired filtering performance is a more practical issue.

In conclusion, there are few research results on the 2D MJSs asynchronous filtering problem subject to SCP and hybrid cyber attacks, and the potential challenges may be as follows: (1) How to analyze the influence of hybrid cyber attacks and SCP on 2D systems? (2) How to characterize the asynchronous interactions between stochastic communication mode, MJS mode, and filter mode in the context of 2D MJSs? (3) How to design an asynchronous filtering algorithm to obtain filtering gain matrices that guarantee the filtering error systems satisfy the desired H_∞ performance? The main purpose of this article is to cope with the aforementioned challenges and develop an asynchronous filtering algorithm for 2D MJSs.

In this paper, we are dedicated to the investigation of asynchronous filtering design for a class of 2D MJSs under the SCP and hybrid cyber attacks. The following summarizes this paper's innovations: (1) A bidirectional index model for determining SCP and hybrid cyber attacks is presented; (2) on the basis of (1), a novel asynchronous filter structure is proposed that can simultaneously characterize the pattern information mismatch of MJSs and filter as well as the pattern information mismatch between the actual SCP and the available SCP; (3) with the help of the Lyapunov theory, the 2D summation inequality lemma, and the linear matrix inequality (LMI) technology, the filter gains with explicit parameters are derived to guarantee the delay-dependent low-conservative stability of the filtering error systems.

Notation: The notation used throughout the paper is fairly standard. R^n denotes the n-dimensional Euclidean space, and $P > 0 (P \geqslant 0)$ means that it is real symmetric and positive definite (semi-definite). G^T and G^{-1} represent the transpose and the inverse of the matrix G, respectively. $diag\{\rho_1, \cdots, \rho_n\}$ stands for a diagonal matrix with the indicated elements on the diagonal, and zeros are located elsewhere. $\Pr\{\xi\}$ means the occurrence probability of the event ξ. $E\{\zeta\}$ indicates the expectation of the stochastic variable ζ. $\|A\|$ refers to the norm of a matrix A defined by $\|A\| = \sqrt{A^T A}$. $\mathbb{N}$ denotes the set of natural numbers. The Kronecker delta function $\delta(\psi)$ is a binary function that equals 1 if $\psi = 0$ and equals 0 otherwise.

Problem Description and Preliminaries

As shown in Figure 1, we consider a class of 2D MJSs with time delays under hybrid cyber attacks and SCP, which is described by the FM-II model as follows

$$\begin{cases} x(i+1,j+1) = A_1(r(i+1,j))x(i+1,j) \\ \quad + A_2(r(i,j+1))x(i,j+1) \\ \quad + A_{d1}(r(i+1,j))x(i+1,j-\tau(j)) + A_{d2}(r(i,j+1)) \\ \quad\quad x(i-d(i),j+1) \\ \quad + E_1(r(i+1,j))\omega(i+1,j) + E_2(r(i,j+1))\omega(i,j+1) \\ y(i,j) = C(r(i,j))x(i,j) + D(r(i,j))\omega(i,j) \\ z(i,j) = H(r(i,j))x(i,j) \end{cases} \quad (1)$$

where $x(i,j) \in R^{n_x}$ represents the system state vector, $y(i,j) \in R^{n_y}$ and $z(i,j) \in R^{n_z}$ are the measurement output and the controlled output, respectively. $\omega(i,j) \in R^{n_\omega}$ denotes the external disturbance with bounded energy. $A_1(r(i+1,j))$, $A_2(r(i,j+1))$, $A_{d1}(r(i+1,j))$, $A_{d2}(r(i,j+1))$, $E_1(r(i+1,j))$, $E_2(r(i,j+1))$, $C(r(i,j))$, $D(r(i,j))$, and $H(r(i,j))$ are known time-varying matrices with proper dimensions, which depend on a specific Markov chain $r(i,j)$. Furthermore, $r(i,j)$ indicates the mode of the systems at shift instant (i,j), and its value belongs to a finite set $\mathrm{M}_s = \{1, 2, ..., s\}$ with the following transition probabilities

$$\begin{aligned} \Pr\{r(i+1,j+1) &= n|r(i,j+1) = m\} \\ &= \Pr\{r(i+1,j+1) = n|r(i+1,j) = m\} \quad (2) \\ &= \pi_{mn}, \forall m, n \in \mathrm{M}_s \end{aligned}$$

where $\pi_{mn} \geqslant 0 (\forall m, n \in \mathrm{M}_s)$ represents the transition probability from mode m to mode n, and satisfying $\sum_{n=1}^s \pi_{mn} = 1$ for all $m \in \mathrm{M}_s$, $\chi = [\pi_{mn}]$ is defined as the transition probability matrix. In addition, the positive integers $d(i)$ and $\tau(j)$ satisfy the following limited constraints and represent time-varying delays

$$1 \leqslant \underline{d} \leqslant d(i) \leqslant \bar{d}, \ 1 \leqslant \underline{\tau} \leqslant \tau(j) \leqslant \bar{\tau}$$

where $\underline{d}, \bar{d}, \underline{\tau}$, and $\bar{\tau}$ are known positive scalars. Assume that the following the initial conditions hold

$$\begin{cases} x(i,j) = \psi(i,j), & \forall 0 \leqslant j \leqslant t_1, i = -\bar{d}, -\bar{d}+1, ..., 0. \\ x(i,j) = \Gamma(i,j), & \forall 0 \leqslant i \leqslant t_2, j = -\bar{\tau}, -\bar{\tau}+1, ..., 0. \\ \psi(0,0) = \Gamma(0,0), \\ x(i,j) = 0, & \forall j > t_1, i = -\bar{d}, -\bar{d}+1, ..., 0. \\ x(i,j) = 0, & \forall i > t_2, j = -\bar{\tau}, -\bar{\tau}+1, ..., 0 \end{cases} \quad (3)$$

where $\psi(i,j)$ and $\Gamma(i,j)$ are known vectors, and t_1 and t_2 are two sufficiently large positive integers.

SCP

To prevent data conflicts, specific network protocols arrange the network resources for the 2D MJSs (equation (1)) that have a large number of sensors. The SCP scheme based on the concept of 2D systems is presented. Assuming that the SCP allows only a single sensor node to gain access to the communication network, let $\xi(i,j) \in \{1, 2, \cdots, n_y\}$ indicate which sensor is chosen to transmit data information at each shift instant, and its value is taken in a finite set $\mathcal{M}_s = \{1, 2, ..., n_y\}$ with the following transition probabilities

$$\begin{aligned} \Pr\{\xi(i+1,j+1) &= \epsilon|\xi(i,j+1) = \varrho\} \\ &= \Pr\{\xi(i+1,j+1) = \epsilon|\xi(i+1,j) = \varrho\} = \jmath_{\varrho\epsilon}, \forall \varrho, \epsilon \in \mathcal{M}_s \end{aligned}$$

where $\jmath_{\varrho\epsilon} \geqslant 0 (\forall \varrho, \epsilon \in \mathcal{M}_s)$ represents the transition probability from mode ϱ to mode ϵ, and satisfies $\sum_{\epsilon=1}^{n_y} \jmath_{\varrho\epsilon} = 1$. $\mathfrak{s} = [\jmath_{\varrho\epsilon}]$ is defined as the transition probability matrix for the decision of which sensor to communicate with filter according to the SCP. The measurement output can be reconstructed in the following form

$$y(i,j) = \begin{bmatrix} y_1^T(i,j) & y_2^T(i,j) & \cdots & y_{n_y}^T(i,j) \end{bmatrix}^T$$

where $y_l(i,j)(1 \leqslant l \leqslant n_y)$ represents measured output of the lth sensor at the shift instant (i,j). Furthermore, the update rule of signal transmission is introduced. Define $\bar{y}_l(i,j)$ represents the latest measurement output of the lth sensor, then $\bar{y}_l(i,j)$ can be expressed as

$$\bar{y}_l(i,j) = \begin{cases} y_l(i,j) & if \ l = \xi(i,j) \\ 0 & otherwise \end{cases}$$

The following composite form of $\bar{y}(i,j)$ can be derived in accordance with the update rule

$$\bar{y}(i,j) = \Phi_{\xi(i,j)} y(i,j) \quad (4)$$

where $\Phi_{\xi(i,j)} = diag\{\delta(\xi(i,j) - 1), \cdots, \delta(\xi(i,j) - l), \cdots, \delta(\xi(i,j) - n_y)\}$ $(1 \leqslant l \leqslant n_y)$, and $\delta(\cdot)$ is the Kronecker delta function.

Hybrid cyber-attack model

First of all, it is thought that FDI attacks usually result in a degradation in filtering performance by altering correct information with harmful data. We employ the random variable $\vartheta(i,j) \in \{0, 1\}$ to represent FDI attack indicators. $\vartheta(i,j) = 1$ represents that the FDI attacks successfully distort regular data by using false data, and $\vartheta(i,j) = 0$ represents that the FDI attacks are unable to tamper with normal data. Assuming that the random variable $\vartheta(i,j)$ is determined by Bernoulli distribution, and the occurrence probability of $\vartheta(i,j)$ is provided as follows

$$\Pr\{\vartheta(i,j) = 1\} = \bar{\vartheta}, \ \Pr\{\vartheta(i,j) = 0\} = 1 - \bar{\vartheta}$$

Subsequently, the following measured output subject to FDI attacks can be described

$$\tilde{y}(i,j) = \bar{y}(i,j) + \vartheta(i,j)\gamma(i,j) \quad (5)$$

where $\gamma(i,j) = \begin{bmatrix} \gamma_1^T(i,j) & \gamma_2^T(i,j) & \cdots & \gamma_{n_y}^T(i,j) \end{bmatrix}^T$ defined as attacker-generated false data signals, which can be produced as follows

$$\gamma(i,j) = -\bar{y}(i,j) + \upsilon(i,j)$$

where $\upsilon(i,j)$ indicates the bounded energy single and satisfies $\|\upsilon(i,j)\| \leqslant \bar{\upsilon}$.

In what follows, we discuss the DoS attacks that disrupt the information transmission of the communication network. Besides, suppose that the $\sigma(i,j) \in \{0, 1\}$ represents DoS attack indicators. Analogously, $\sigma(i,j) = 0$ indicates that DoS attacks arise when measurement output is being transmitted,
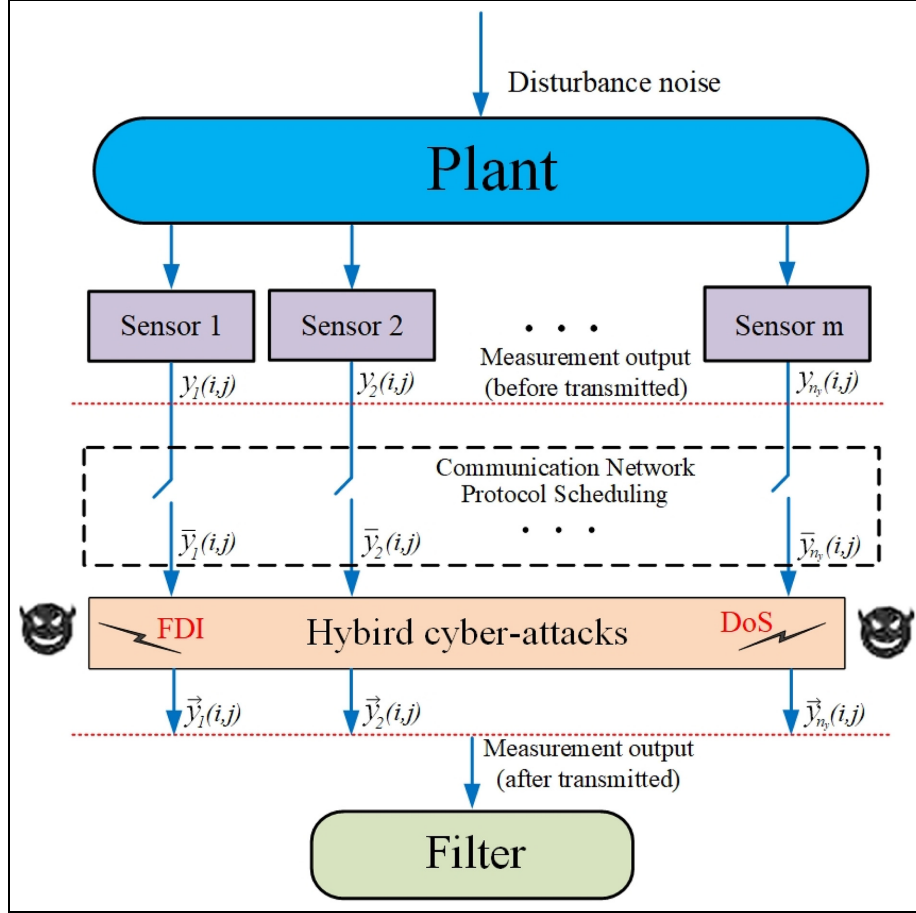
Figure 1. Asynchronous filtering problem for 2D MJSs with time-varying delays.

whereas $\sigma(i,j) = 1$ indicates that DoS attacks do not occur. In addition, the following probability distribution is defined

$$\Pr\{\sigma(i,j) = 1\} = \bar{\sigma}, \ \Pr\{\sigma(i,j) = 0\} = 1 - \bar{\sigma}$$

In addition, the zero-order hold strategy is employed to guarantee the latest measurement data transmission. Consequently, the latest measurement output after the communication network can be expressed as

$$\vec{y}(i,j) = \sigma(i,j)\tilde{y}(i,j) + (1 - \sigma(i,j))\vec{y}(i,j-1) \quad (6)$$

Remark 1. DoS attacks are a kind of cyber-attack strategy that is often utilized for occupying the communication resources to discourage the transmission of measurement and signals. The deception attacks also known as FDI attacks are defined as the tampering of normal data with false data to disrupt system operation. Based on the proposed principle of measured output under hybrid cyber attacks, when $\vartheta(i,j) = 0$ and $\sigma(i,j) = 0$, the shared network is impacted only by DoS attacks; when $\vartheta(i,j) = 1$ and $\sigma(i,j) = 0$, the shared network is impacted by both DoS and FDI attacks; when $\vartheta(i,j) = 0$ and $\sigma(i,j) = 1$, the shared network is not impacted by cyber attacks; when $\vartheta(i,j) = 1$ and $\sigma(i,j) = 1$, the shared network is only impacted by FDI attacks.

Problem formulation

The asynchronous filtering problem for 2D MJSs (equation (1)) under the SCP and hybrid cyber attacks will be discussed in this paper. Considering the possibility that the filter mode remains in an asynchronous state with the system mode and the SCP mode simultaneously, the following asynchronous filter structure is proposed

$$\begin{cases} \hat{x}(i+1,j+1) = A_1(r(i+1,j))\hat{x}(i+1,j) \\ \qquad + A_2(r(i,j+1))\hat{x}(i,j+1) \\ \qquad + A_{d1}(r(i+1,j))\hat{x}(i+1,j-\tau(j)) + A_{d2}(r(i,j+1)) \\ \qquad \hat{x}(i-d(i),j+1) \\ \qquad + K_{1,\zeta(i+1,j)}^{\delta(i+1,j)}(\vec{y}(i+1,j) - C(r(i+1,j))\hat{x}(i+1,j)) \\ \qquad + K_{2,\zeta(i,j+1)}^{\delta(i,j+1)}(\vec{y}(i,j+1) - C(r(i,j+1))\hat{x}(i,j+1)) \\ \hat{z}(i,j) = H(r(i,j))\hat{x}(i,j) \end{cases} \quad (7)$$

where $\hat{x}(i,j) \in R^{n_x}$ is the estimation of state vector $x(i,j)$, and $\hat{z}(i,j)$ is the estimation of controlled output $z(i,j)$. $K_{1,\zeta(i+1,j)}^{\delta(i+1,j)}$ and $K_{2,\zeta(i,j+1)}^{\delta(i,j+1)}$ are parameters $\delta(i,j)$ and $\zeta(i,j)$-dependent asynchronous H_∞ filter gain matrices, in which $\delta(i,j)$ denotes a Markov chain with transition probability different from χ

to described the non-synchronous connections between the mode of filter and 2D discrete MJSs (equation (1)), and takes the value in a finite set $M_g = \{1, 2, ..., g\}$ with the transition probability matrix $\phi^{r(i+1,j+1)} = \left[\mu_{\hbar\eth}^{r(i+1,j+1)}\right]$ as follows

$$\Pr(\delta(i+1,j+1) = \eth|\delta(i+1,j) = \hbar) = \Pr(\delta(i+1,j+1) = \eth|\delta(i,j+1) = \hbar) = \mu_{\hbar\eth}^{r(i+1,j+1)}, \forall \hbar, \eth \in M_g$$

The SCP usually regulates sensors to access the network medium according to some specific stochastic process, which is essentially a scheduling strategy with uncertainty. In control engineering practice, it is often difficult to attain the real situation of data exchange between the sensor and the filter due to the limitations of the system and network. Hence, the asynchronous attribute is more consistent with the actual scheduling situation. To reflect the asynchronous characteristics of sensor nodes' access to the communication network, we reintroduce another Markov stochastic process $\zeta(i,j)$, which is closely related to $\xi(i,j)$, and assume that $\zeta(i,j)$ denotes a Markov chain whose value belongs to a finite set $\mathcal{M}_g = \{1, 2, ..., n_y\}$ with the following transition probabilities

$$\Pr\{\zeta(i+1,j+1) = \mathfrak{y}|\zeta(i+1,j) = \mathfrak{w}\} = \Pr\{\zeta(i+1,j+1) = \mathfrak{y}|\zeta(i,j+1) = \mathfrak{w}\} = o_{\mathfrak{w}\mathfrak{y}}^{\xi(i+1,j+1)}, \forall \mathfrak{w}, \mathfrak{y} \in \mathcal{M}_g$$

and satisfying $\sum_{\mathfrak{y}=1}^{n_y} o_{\mathfrak{w}\mathfrak{y}}^{\xi(i+1,j+1)} = 1$ for all $\mathfrak{y} \in \mathcal{M}_g$. Similarly, $\bar{o}^{\xi(i+1,j+1)} = \left[o_{\mathfrak{w}\mathfrak{y}}^{\xi(i+1,j+1)}\right]$ is denoted as the transition probability matrix of $\zeta(i,j)$. Besides, the values of state estimation are set as $\hat{x}(i,0) = \hat{x}(0,j) = 0$.

Then, we define $e(i,j), x(i,j) - \hat{x}(i,j)$ and $\tilde{z}(i,j), z(i,j) - \hat{z}(i,j)$. By considering equations (7) and (8), the dynamic filtering error $e(i,j)$ of 2D MJSs (equation (1)) can be described as

$$
\begin{aligned}
&e(i+1,j+1)\\
&= (A_1(r(i+1,j)) - K_{1,\zeta(i+1,j)}^{\delta(i+1,j)}C(r(i+1,j)))e(i+1,j) + (A_2(r(i,j+1)) - K_{2,\zeta(i,j+1)}^{\delta(i,j+1)}C(r(i,j+1)))e(i,j+1)\\
&\quad + A_{d1}(r(i+1,j))e(i+1,j-\tau(j)) + A_{d2}(r(i,j+1))e(i-d(i),j+1)\\
&\quad + (E_1(r(i+1,j)) - K_{1,\zeta(i+1,j)}^{\delta(i+1,j)}\sigma(i+1,j)\bar{\vartheta}(i+1,j)\Phi_{\xi(i+1,j)}D(r(i+1,j))\omega(i+1,j)\\
&\quad + (E_2(r(i,j+1)) - K_{2,\zeta(i,j+1)}^{\delta(i,j+1)}\sigma(i,j+1)\bar{\vartheta}(i,j+1)\Phi_{\xi(i,j+1)}D(r(i,j+1))\omega(i,j+1)\\
&\quad + K_{1,\zeta(i+1,j)}^{\delta(i+1,j)}(I - \sigma(i+1,j)\bar{\vartheta}(i+1,j)\Phi_{\xi(i+1,j)})C(r(i+1,j))x(i+1,j)\\
&\quad - K_{1,\zeta(i+1,j)}^{\delta(i+1,j)}\sigma(i+1,j)\vartheta(i+1,j)v(i+1,j) - K_{1,\zeta(i+1,j)}^{\delta(i+1,j)}\bar{\sigma}(i+1,j)\vec{y}(i+1,j-1)\\
&\quad + K_{2,\zeta(i,j+1)}^{\delta(i,j+1)}(I - \sigma(i,j+1)\bar{\vartheta}(i,j+1)\Phi_{\xi(i,j+1)})C(r(i,j+1))x(i,j+1)\\
&\quad - K_{2,\zeta(i,j+1)}^{\delta(i,j+1)}\sigma(i,j+1)\vartheta(i,j+1)v(i,j+1) - K_{2,\zeta(i,j+1)}^{\delta(i,j+1)}\bar{\sigma}(i,j+1)\vec{y}(i,j)
\end{aligned}
\tag{8}
$$

In virtue of the following augmented matrices

$$\eta(i,j) = \left[e^T(i,j) \quad x^T(i,j) \quad \vec{y}^T(i,j-1)\right]^T, \tilde{\omega}(i,j) = \left[\omega^T(i+1,j) \quad \omega^T(i,j+1) \quad v^T(i+1,j) \quad v^T(i,j+1)\right]^T$$

Moreover, the following structure can be implemented to regenerate the dynamic filtering error systems (equation (8))

$$
: \begin{cases}
\eta(i+1,j+1) = (\tilde{\Pi}_1 + \varpi_1(i,j)\hat{\Pi}_1 + \varpi_2(i,j)\widehat{\Pi}_1)\eta(i+1,j) + (\tilde{\Pi}_2 + \varpi_1(i,j+1)\hat{\Pi}_2 + \varpi_2(i,j+1)\widehat{\Pi}_2)\eta(i,j+1)\\
\quad + \Pi_3(i+1,j-\tau(j))\eta(i+1,j-\tau(j)) + \Pi_4(r(i-d(i),j+1))\eta(r(i-d(i),j+1))\\
\quad + (\bar{\Theta} + \varpi_1(i+1,j)\tilde{\Theta} + \varpi_1(i,j+1)\hat{\Theta} + \varpi_3(i+1,j)\widehat{\Theta} + \varpi_3(i,j+1)\breve{\Theta})\tilde{\omega}(i,j)\\
\tilde{z}(i,j) = \tilde{H}(r(i,j))\eta(i,j)
\end{cases}
\tag{9}
$$

where

$$
\tilde{\Pi}_1 = \begin{bmatrix}
A_1(r(i+1,j)) - K_{1,\zeta(i+1,j)}^{\delta(i+1,j)}C(r(i+1,j)) & \tilde{\Pi}_1^{12} & -K_{1,\zeta(i+1,j)}^{\delta(i+1,j)}(1-\bar{\sigma})\\
0 & A_1(r(i+1,j)) & 0\\
0 & \bar{\sigma}(1-\bar{\vartheta})\Phi_{\xi(i+1,j)}C(r(i+1,j)) & 1-\bar{\sigma}
\end{bmatrix},
$$

$$\tilde{\Pi}_1^{12} = K_{1,\zeta(i+1,j)}^{\delta(i+1,j)}C(r(i+1,j)) - \bar{\sigma}(1-\bar{\vartheta})K_{1,\zeta(i+1,j)}^{\delta(i+1,j)}\Phi_{\xi(i+1,j)}C(r(i+1,j)),$$

$$
\hat{\Pi}_1 = \begin{bmatrix}
0 & -K_{1,\zeta(i+1,j)}^{\delta(i+1,j)}\Phi_{\xi(i+1,j)}C(r(i+1,j)) & 0\\
0 & 0 & 0\\
0 & \Phi_{\xi(i+1,j)}C(r(i+1,j)) & 0
\end{bmatrix}, \widehat{\Pi}_1 = \begin{bmatrix}
0 & 0 & -K_{1,\zeta(i+1,j)}^{\delta(i+1,j)}\\
0 & 0 & 0\\
0 & 0 & I
\end{bmatrix},
$$

$$\tilde{\Pi}_2 = \begin{bmatrix} A_2(r(i,j+1)) - K_{2,\zeta(i,j+1)}^{\delta(i,j+1)}C(r(i,j+1)) & \tilde{\Pi}_2^{12} & -K_{2,\zeta(i,j+1)}^{\delta(i,j+1)}(1-\bar{\sigma}) \\ 0 & A_2(r(i,j+1)) & 0 \\ 0 & 0 & 0 \end{bmatrix}, \quad \hat{\Pi}_2 = \begin{bmatrix} 0 & 0 & -K_{2,\zeta(i,j+1)}^{\delta(i,j+1)} \\ 0 & 0 & 0 \\ 0 & 0 & 0 \end{bmatrix},$$

$$\tilde{\Pi}_2^{12} = K_{2,\zeta(i,j+1)}^{\delta(i,j+1)}C(r(i,j+1)) - \bar{\sigma}(1-\bar{\vartheta})K_{2,\zeta(i,j+1)}^{\delta(i,j+1)}\Phi_{\xi(i,j+1)}C(r(i,j+1)), \quad \hat{\Pi}_2 = \begin{bmatrix} 0 & -K_{2,\zeta(i,j+1)}^{\delta(i,j+1)}\Phi_{\xi(i,j+1)}C(r(i,j+1)) & 0 \\ 0 & 0 & 0 \\ 0 & 0 & 0 \end{bmatrix},$$

$$\Pi_3(i+1,j-\tau(j)) = \begin{bmatrix} 0 & A_{d1}(r(i+1,j)) & 0 \\ 0 & A_{d1}(r(i+1,j)) & 0 \\ 0 & 0 & 0 \end{bmatrix}, \quad \Pi_4(r(i-d(i),j+1)) = \begin{bmatrix} 0 & A_{d2}(r(i,j+1)) & 0 \\ 0 & A_{d2}(r(i,j+1)) & 0 \\ 0 & 0 & 0 \end{bmatrix},$$

$$\bar{\Theta} = \begin{bmatrix} \bar{\Theta}_{11} & \bar{\Theta}_{12} & -K_{1,\zeta(i+1,j)}^{\delta(i+1,j)}\bar{\sigma}\bar{\vartheta} & -K_{2,\zeta(i,j+1)}^{\delta(i,j+1)}\bar{\sigma}\bar{\vartheta} \\ E_1(r(i+1,j)) & E_2(r(i,j+1)) & 0 & 0 \\ \bar{\sigma}(1-\bar{\vartheta})\Phi_{\xi(i+1,j)}D(r(i+1,j)) & 0 & \bar{\sigma}\bar{\vartheta} & 0 \end{bmatrix},$$

$$\bar{\Theta}_{11} = E_1(r(i+1,j) - K_{1,\zeta(i+1,j)}^{\delta(i+1,j)}\bar{\sigma}(1-\bar{\vartheta})\Phi_{\xi(i+1,j)}D(r(i+1,j)), \quad \bar{\Theta}_{12} = E_2(r(i,j+1) - K_{2,\zeta(i,j+1)}^{\delta(i,j+1)}\bar{\sigma}(1-\bar{\vartheta})\Phi_{\xi(i,j+1)}D(r(i,j+1)),$$

$$\tilde{\Theta} = \begin{bmatrix} -K_{1,\zeta(i+1,j)}^{\delta(i+1,j)}\Phi_{\xi(i+1,j)}D(r(i+1,j)) & 0 & 0 & 0 \\ 0 & 0 & 0 & 0 \\ \Phi_{\xi(i+1,j)}D(r(i+1,j)) & 0 & 0 & 0 \end{bmatrix}, \quad \hat{\Theta} = \begin{bmatrix} 0 & -K_{2,\zeta(i,j+1)}^{\delta(i,j+1)}\Phi_{\xi(i,j+1)}D(r(i,j+1)) & 0 & 0 \\ 0 & 0 & 0 & 0 \\ 0 & 0 & 0 & 0 \end{bmatrix},$$

$$\widehat{\Theta} = \begin{bmatrix} 0 & 0 & -K_{1,\zeta(i+1,j)}^{\delta(i+1,j)} & 0 \\ 0 & 0 & 0 & 0 \\ 0 & 0 & I & 0 \end{bmatrix}, \quad \breve{\Theta} = \begin{bmatrix} 0 & 0 & 0 & -K_{2,\zeta(i,j+1)}^{\delta(i,j+1)} \\ 0 & 0 & 0 & 0 \\ 0 & 0 & 0 & 0 \end{bmatrix}, \quad \tilde{H}(r(i,j)) = \begin{bmatrix} H(r(i,j)) & 0 & 0 \end{bmatrix},$$

$$\varpi_1(i,j) = \sigma(i,j)(1-\vartheta(i,j)) - \bar{\sigma}(1-\bar{\vartheta}), \quad \varpi_2(i,j) = (1-\sigma(i,j)) - (1-\bar{\sigma}), \quad \varpi_3(i,j) = \sigma(i,j)\vartheta(i,j) - \bar{\sigma}\bar{\vartheta}$$

In addition, the following statistical characteristics of the random sequences of DoS and FDI attacks are provided in order facilitate the presentation of the subsequent results

$$E\{\varpi_1^2(i,j)\} = \bar{\sigma}(1-\bar{\vartheta})(1-\bar{\sigma}(1-\bar{\vartheta})) = \bar{\varsigma}_1^2, \quad E\{\varpi_2^2(i,j)\} = (1-\bar{\sigma})(1-(1-\bar{\sigma})) = \bar{\varsigma}_2^2,$$

$$E\{\varpi_3^2(i,j)\} = \bar{\sigma}\bar{\vartheta}(1-\bar{\sigma}\bar{\vartheta}) = \bar{\varsigma}_3^2, \quad E\{\varpi_1(i,j)\varpi_2(i,j)\} = -\bar{\sigma}(1-\bar{\vartheta})(1-\bar{\sigma}) = \bar{\varsigma}_{12}^2,$$

$$E\{\varpi_1(i,j)\varpi_3(i,j)\} = -\bar{\sigma}\bar{\vartheta}(1-\bar{\vartheta}) = \bar{\varsigma}_{13}^2, \quad E\{\varpi_2(i,j)\varpi_3(i,j)\} = -\bar{\sigma}\bar{\vartheta}(1-\bar{\sigma}) = \bar{\varsigma}_{23}^2$$

Remark 2. From the control practice viewpoint, it is difficult to accurately obtain all of system information at each instant due to network limitations and its own component limitations, and it is impractical to investigate control/filtering algorithm design based on the assumption that all information is available. According to filter structure (equation (7)), it is easy to see the filter gain matrices $K_{1,\zeta(i+1,j)}^{\delta(i+1,j)}$ and $K_{2,\zeta(i,j+1)}^{\delta(i,j+1)}$ are parameters $\delta(i,j)$ and $\zeta(i,j)$-dependent. By establishing Markov stochastic processes $\delta(i,j)$ and $\zeta(i,j)$ to allow the filter (equation (7)) simultaneously reflect that the MJSs and filter pattern communication mismatch as well as the pattern information mismatch between the actual SCP and the available SCP. The above investigation better tackles the challenges imposed by the complexity of 2D MJSs in the real world.

Definition 1 (Ghous et al., 2015). For arbitrary given initial bounded conditions (equation (3)) and external disturbance satisfying $\omega(i,j)\equiv 0$, the dynamic filtering error systems (equation (9)) based on 2D MJSs (equation (1)) is globally asymptotically stable in the mean-square sense if the following relationship holds

$$\lim_{i+j\to\infty} E\{\|\eta(i,j)\|^2\} = 0$$

Definition 2 (Ghous et al., 2015). The dynamic filtering error systems (equation (9)) satisfy the robust H_∞ stability with disturbance attenuation level γ if the following conditions hold:

1. Dynamic filtering error systems (equation (9)) with $\omega(i,j)\equiv 0$ is globally asymptotically stable in the mean-square sense.
2. For a given scalar $\gamma > 0$ and under zero initial conditions, the following inequality is satisfied for any bounded disturbance $\omega(i,j) \neq 0$

$$\sum_{i=0}^{\infty}\sum_{j=0}^{\infty}E\{\|\hat{z}(i,j)\|^2\} \leqslant \gamma^2\left(\sum_{i=0}^{\infty}\sum_{j=0}^{\infty}\right)E\{\|\tilde{\omega}(i,j)\|^2\}$$

where $\|\hat{z}(i,j)\|^2 = \left\|\begin{bmatrix}\tilde{z}(i+1,j)\\ \tilde{z}(i,j+1)\end{bmatrix}\right\|^2$, $\|\tilde{\omega}(i,j)\|^2 = \|[\ \omega^T(i+1,j)$ $\omega^T(i,j+1)v^T(i+1,j)v^T(i,j+1)]^T\|^2$.

Moreover, to reduce the conservatism of the stability criterion, we introduce an inequality relation based on the 2D Abel lemma.

Lemma 1 (Peng and Nie, 2021). In the vertical direction, for a positive definite symmetric matrix R, integers r_1 and r_2 satisfying $r_2 - r_1 > 1$, the following inequality holds

$$\varphi_2(r_1,r_2) \geqslant \frac{1}{Q_1}v_1^T R v_1 + \frac{3Q_2}{Q_1 Q_3}v_2^T R v_2$$

where $\varphi_2(r_1,r_2) = \sum_{j=r_1}^{r_2-1}y_{1,j}^T R y_{1,j}$, $Q_1 = r_2 - r_1$, $Q_2 = r_2 - r_1 - 1$, $Q_3 = r_2 - r_1 + 1$, $y_{1,j} = x_{1,j+1} - x_{1,j}$, $v_1 = x_{1,r_2} - x_{1,r_1}$, $v_2 = x_{1,r_2} + x_{1,r_1} - \frac{2}{r_2-r_1-1}\sum_{j=r_1+1}^{r_2-1}x_{1,j}$.

In the horizontal direction, it is obtained that

$$\varphi_1(r_1,r_2) \geqslant \frac{1}{Q_1}v_1^T R v_1 + \frac{3Q_2}{Q_1 Q_3}v_2^T R v_2$$

where $\varphi_1(r_1,r_2) = \sum_{i=r_1}^{r_2-1}y_{i,1}^T R y_{i,1}$, $y_{i,1} = x_{i+1,1} - x_{i,1}$, $v_1 = x_{r_2,1} - x_{r_1,1}$, $v_2 = x_{r_2,1} + x_{r_1,1} - \frac{2}{r_2-r_1-1}\sum_{i=r_1+1}^{r_2-1}x_{i,1}$.

Remark 3. According to Peng and Nie (2021), for the finite-sum term $\varphi_1(r_1,r_2)$ and $\varphi_2(r_1,r_2)$, the Lemma 1 can obtain time-delay boundary conditions with smaller conservatism than that of Jensen inequality, which is crucial for subsequently obtaining conclusions on the stability of the low conservativeness with respect to the time-delay boundary.

Heretofore, the dynamic filtering error systems (equation (9)) with asynchronous characteristics are obtained for the 2D MJSs (equation (1)) limited by SCP and hybrid cyber attacks. Next, we will endeavor to establish sufficient criteria for the dynamic filtering error system (equation (9)) with an H_∞ disturbance attenuation performance γ. In addition, for the convenience of subsequent derivation, $P_{\xi(i+1,j),\zeta(i+1,j)}^{r(i+1,j),\delta(i+1,j)}(i+1,j)$, $Q_{\xi(i,j+1),\zeta(i,j+1)}^{r(i,j+1),\delta(i,j+1)}(i,j+1)$, $P_{\xi(i+1,j+1),\zeta(i+1,j+1)}^{r(i+1,j+1),\delta(i+1,j+1)}(i+1,j+1)$, $Q_{\xi(i+1,j+1),\zeta(i+1,j+1)}^{r(i+1,j+1),\delta(i+1,j+1)}(i+1,j+1)$, $\Pi_1(i+1,j)$, $\Pi_2(i,j+1)$, $\Pi_3(i+1,j-\tau(j))$ and $\Pi_4(i-d(i),j+1)$ are, respectively, abbreviated as $P_{\varrho,\mathfrak{w}}^{m,\hbar}$, $Q_{\varrho,\mathfrak{w}}^{m,\hbar}$, $P_{\epsilon,\mathfrak{y}}^{n,\eth}$, $Q_{\epsilon,\mathfrak{y}}^{n,\eth}$, Π_1, Π_2, Π_3, and Π_4.

Main Results

Theorem 1: For given scalars $\bar{\tau}$, $\underline{\tau}$, $\bar{d}$, and $\underline{d}$, the dynamic filtering error systems (equation (9)) with $\omega(i,j) \equiv 0$ is asymptotically stable in the mean-square sense if there exist positive definite symmetric matrices $P_{\varrho,\mathfrak{w}}^{m,\hbar}$, $Q_{\varrho,\mathfrak{w}}^{m,\hbar}$, $\bar{P}_{\epsilon,\mathfrak{y}}^{n,\eth}$, $\bar{Q}_{\epsilon,\mathfrak{y}}^{n,\eth}$, S_1, S_2, S_3, and S_4, such that the following inequality holds

$$\begin{bmatrix}\tilde{\Phi} & \tilde{\Psi}\\ * & \hat{\Xi}\end{bmatrix} \leq 0 \tag{10}$$

where

$$\tilde{\Phi} = \begin{bmatrix}\tilde{\Phi}_{11} & \tilde{\Phi}_{12} & \tilde{\Phi}_{13}\\ * & \tilde{\Phi}_{22} & \tilde{\Phi}_{23}\\ * & * & \tilde{\Phi}_{33}\end{bmatrix}, \tilde{\Phi}_{11} = \begin{bmatrix}\tilde{S} & -S_2\tilde{\Pi}_2 - \tilde{\Pi}_1^T S_4 & -S_2\Pi_3 & -S_2\Pi_4\\ * & \bar{S} & -S_4\Pi_3 & -S_4\Pi_4\\ * & * & -S_1 & 0\\ * & * & * & -S_3\end{bmatrix}, \bar{P}_{\epsilon,\mathfrak{y}}^{n,\eth} = \sum_{\mathfrak{y}=1}^{\mathcal{M}_g}\sum_{\epsilon=1}^{\mathcal{M}_s}\sum_{n=1}^{M_s}\sum_{\eth=1}^{M_g}\pi_{mn}\mu_{\hbar\eth}^n \jmath_{\varrho\epsilon}o_{\mathfrak{w}\mathfrak{y}}^\epsilon P_{\epsilon,\mathfrak{y}}^{n,\eth},$$

$$\bar{Q}_{\epsilon,\mathfrak{y}}^{n,\eth} = \sum_{\mathfrak{y}=1}^{\mathcal{M}_g}\sum_{\epsilon=1}^{\mathcal{M}_s}\sum_{n=1}^{M_s}\sum_{\eth=1}^{M_g}\pi_{mn}\mu_{\hbar\eth}^n \jmath_{\varrho\epsilon}o_{\mathfrak{w}\mathfrak{y}}^\epsilon Q_{\epsilon,\mathfrak{y}}^{n,\eth}, \tilde{S} = (1+\bar{\tau}-\underline{\tau})S_1 + \frac{-4\underline{\tau}+2}{\underline{\tau}+1}S_2 - P_{\varrho,\mathfrak{w}}^{m,\hbar} + (\underline{\tau}^2 + (\bar{\tau}-\underline{\tau})^2)(I - \tilde{\Pi}_1^T S_2 - S_2\tilde{\Pi}_1),$$

$$\bar{S} = (1+\bar{d}-\underline{d})S_1 + \frac{-4\underline{d}+2}{\underline{d}+1}S_4 - Q_{\varrho,\mathfrak{w}}^{m,\hbar} + (\underline{d}^2 + (\bar{d}-\underline{d})^2)(I - \tilde{\Pi}_2^T S_4 - S_4\tilde{\Pi}_2), \tilde{\Phi}_{12} = diag\left\{\frac{-2\underline{\tau}+4}{\underline{\tau}+1}S_2, \frac{-2\underline{d}+4}{\underline{d}+1}S_4, 0, 0\right\},$$

$$\tilde{\Phi}_{13} = \begin{bmatrix}0 & \frac{6(\underline{\tau}-1)}{\underline{\tau}+1}S_2 & 0 & 0\\ 0 & 0 & \frac{3(\underline{d}-1)}{\underline{d}+1}S_4 & 0\\ 0 & 0 & 0 & 0\\ 0 & 0 & 0 & 0\end{bmatrix}, \tilde{\Phi}_{22} = \begin{bmatrix}(\tilde{\tau}+\hat{\tau})S_2 & 0 & \hat{\tau}S_2 & 0\\ 0 & (\tilde{d}+\hat{d})S_4 & 0 & \hat{d}S_4\\ 0 & 0 & \hat{\tau}S_2 & 0\\ 0 & 0 & 0 & \hat{d}S_4\end{bmatrix},$$

$$\tilde{\Phi}_{23} = \begin{bmatrix}6\vec{\tau}S_2 & 0 & \frac{6(\underline{\tau}-1)}{\underline{\tau}+1}S_2 & 0\\ 0 & 6\vec{d}S_4 & 0 & \frac{6(\underline{d}-1)}{\underline{d}+1}S_4\\ 6\vec{\tau}S_2 & 0 & 0 & 0\\ 0 & 6\vec{d}S_4 & 0 & 0\end{bmatrix}, \tilde{\Phi}_{33} = diag\left\{-12\vec{\tau}S_2, -12\vec{d}S_4, -\frac{12(\underline{\tau}-1)}{\underline{\tau}+1}S_2, -\frac{12(\underline{d}-1)}{\underline{d}+1}S_4\right\},$$

$$\tilde{\Psi} = [\Psi_{12}\ \Psi_{13}\ \Psi_{14}\ \Psi_{15}\ \Psi_{16}], \hat{\Xi} = I_5\otimes -\Xi, \tilde{\tau} = \frac{-4\underline{\tau}+2}{\underline{\tau}+1}, \tilde{d} = \frac{-4\underline{d}+2}{\underline{d}+1}, \hat{\tau} = \frac{-4\bar{\tau}+4\underline{\tau}+2}{\bar{\tau}-\underline{\tau}+1}, \hat{d} = \frac{-4\bar{d}+4\underline{d}+2}{\bar{d}-\underline{d}+1},$$

$$\hat{\tau} = \frac{-2\bar{\tau}+2\underline{\tau}+4}{\bar{\tau}-\underline{\tau}+1}, \hat{d} = \frac{-2\bar{d}+2\underline{d}+4}{\bar{d}-\underline{d}+1}, \vec{\tau} = \frac{(\bar{\tau}-\underline{\tau}-1)}{\bar{\tau}-\underline{\tau}+1}, \vec{d} = \frac{(\bar{d}-\underline{d}-1)}{\bar{d}-\underline{d}+1}, \Xi = (\bar{P}_\epsilon^{n,f} + \bar{Q}_\epsilon^{n,f} + (\underline{\tau}^2 + (\bar{\tau}-\underline{\tau})^2)S_2 + (\underline{d}^2 + (\bar{d}-\underline{d})^2)S_4),$$

$$\Psi_{12} = \begin{bmatrix} \Xi\tilde{\Pi}_1 & \Xi\tilde{\Pi}_2 & \Xi\Pi_3 & \Xi\Pi_4 & 0 & 0 & 0 & 0 & 0 & 0 & 0 & 0 \end{bmatrix}^T, \Psi_{13} = \begin{bmatrix} \bar{\varsigma}_1\Xi\hat{\Pi}_1 & \bar{\varsigma}_1\Xi\hat{\Pi}_2 & 0 & 0 & 0 & 0 & 0 & 0 & 0 & 0 & 0 & 0 \end{bmatrix}^T,$$

$$\Psi_{14} = \begin{bmatrix} \bar{\varsigma}_{12}\Xi\hat{\Pi}_1 & \bar{\varsigma}_{12}\Xi\hat{\Pi}_2 & 0 & 0 & 0 & 0 & 0 & 0 & 0 & 0 & 0 & 0 \end{bmatrix}^T, \Psi_{15} = \begin{bmatrix} \bar{\varsigma}_{12}\Xi\hat{\Pi}_1 & \bar{\varsigma}_{12}\Xi\hat{\Pi}_2 & 0 & 0 & 0 & 0 & 0 & 0 & 0 & 0 & 0 & 0 \end{bmatrix}^T,$$

$$\Psi_{16} = \begin{bmatrix} \bar{\varsigma}_2\Xi\hat{\Pi}_1 & \bar{\varsigma}_2\Xi\hat{\Pi}_2 & 0 & 0 & 0 & 0 & 0 & 0 & 0 & 0 & 0 & 0 \end{bmatrix}^T, e_i^T = \begin{bmatrix} 0_{n_x \times (i-1)n_x} & I_{n_x \times n_x} & 0_{n_x \times (12-i)n_x} \end{bmatrix}, i = 1, 2, ..., 12.$$

Proof: First of all, we consider the globally asymptotically mean-square stability of the dynamic filtering error systems (equation (9)) under external disturbance $\omega(i,j) \equiv 0$. Choose the following Lyapunov energy-like function

$$V(i,j) = V_1(i,j) + V_2(i,j) = \sum_{q=1}^{5} V_{1,q}(i,j) + \sum_{q=1}^{5} V_{2,q}(i,j) \tag{11}$$

with $V_{1,1}(i,j) = \eta^T(i,j)P_{\xi(i,j)}^{r(i,j),\delta(i,j)}(i,j)\eta(i,j), V_{1,2}(i,j) = \sum_{\theta=-\tau(j)}^{-1} \eta^T(i,j+\theta)S_1\eta(i,j+\theta),$

$$V_{1,3}(i,j) = \sum_{\theta=1-\bar{\tau}}^{-\underline{\tau}} \sum_{s=\theta}^{-1} \eta^T(i,j+s)S_1\eta(i,j+s), V_{1,4}(i,j) = \underline{\tau}\sum_{\theta=-\underline{\tau}}^{-1} \sum_{s=\theta}^{-1} \wp_1^T(i,j+s)S_2\wp_1(i,j+s)$$

$$\wp_1(i,j+s) = \eta(i,j+s+1) - \eta(i,j+s), V_{1,5}(i,j) = (\bar{\tau}-\underline{\tau})\sum_{\theta=-\bar{\tau}}^{-\underline{\tau}-1} \sum_{s=\theta}^{-1} \wp_1^T(i,j+s)S_2\wp_1(i,j+s),$$

$$V_{2,1}(i,j) = \eta^T(i,j)Q_{\xi(i,j)}^{r(i,j),\delta(i,j)}\eta(i,j), V_{2,2}(i,j) = \sum_{\theta=-d(i)}^{-1} \eta^T(i+\theta,j)S_3\eta(i+\theta,j),$$

$$V_{2,3}(i,j) = \sum_{\theta=1-\bar{d}}^{-\underline{d}} \sum_{s=\theta}^{-1} \eta^T(i+s,j)S_3\eta(i+s,j), \wp_2(i+s,j) = \eta(i+s+1,j) - \eta(i+s,j),$$

$$V_{2,4}(i,j) = \underline{d}\sum_{\theta=-\underline{d}}^{-1} \sum_{s=\theta}^{-1} \wp_2^T(i+s,j)S_4\wp_2^T(i+s,j), V_{2,5}(i,j) = (\bar{d}-\underline{d})\sum_{\theta=-\bar{d}}^{-\underline{d}-1} \sum_{s=\theta}^{-1} \wp_2^T(i+s,j)S_4\wp_2(i+s,j)$$

Based on the relationship between $r(i,j)$, $\delta(i,j)$, $\xi(i,j)$, and $\zeta(i,j)$, the following probability transition relationship can be obtained

$$\Pr\left\{ \begin{matrix} r(i+1,j+1)=n, \delta(i+1,j+1)=\eth, \zeta(i+1,j+1)=\mathfrak{y}, \xi(i+1,j+1)=\epsilon \\ |r(i,j+1)=m, \delta(i,j+1)=\hbar, \zeta(i,j+1)=\mathfrak{w}, \xi(i,j+1)=\varrho \end{matrix} \right\}$$

$$= \Pr\left\{ r(i+1,j+1)=n \left| \begin{matrix} r(i,j+1)=m, \delta(i,j+1)=\hbar, \zeta(i,j+1)=\mathfrak{w}, \xi(i,j+1)=\varrho, \\ \delta(i+1,j+1)=\eth, \zeta(i+1,j+1)=\mathfrak{y}, \xi(i+1,j+1)=\epsilon \end{matrix} \right. \right\}$$

$$\times \Pr\left\{ \delta(i+1,j+1)=\eth \left| \begin{matrix} r(i,j+1)=m, \delta(i,j+1)=\hbar, \zeta(i,j+1)=\mathfrak{w}, \xi(i,j+1)=\varrho, \\ r(i+1,j+1)=n, \zeta(i+1,j+1)=\mathfrak{y}, \xi(i+1,j+1)=\epsilon \end{matrix} \right. \right\}$$

$$\times \Pr\left\{ \xi(i+1,j+1)=\epsilon \left| \begin{matrix} r(i,j+1)=m, \delta(i,j+1)=\hbar, \zeta(i,j+1)=\mathfrak{w}, \xi(i,j+1)=\varrho, \\ r(i+1,j+1)=n, \delta(i+1,j+1)=\eth, \zeta(i+1,j+1)=\mathfrak{y} \end{matrix} \right. \right\}$$

$$\times \Pr\left\{ \zeta(i+1,j+1)=\mathfrak{y} \left| \begin{matrix} r(i,j+1)=m, \delta(i,j+1)=\hbar, \zeta(i,j+1)=\mathfrak{w}, \xi(i,j+1)=\varrho, \\ r(i+1,j+1)=n, \delta(i+1,j+1)=\eth, \xi(i+1,j+1)=\epsilon \end{matrix} \right. \right\}$$

$$= \pi_{mn}\mu_{\hbar\eth}^n \jmath_{\varrho\epsilon} o_{\mathfrak{w}\mathfrak{y}}^\epsilon$$

Similarly, it is easy to deduce that

$$\Pr\left\{ \begin{matrix} r(i+1,j+1)=n, \delta(i+1,j+1)=\eth, \zeta(i+1,j+1)=\mathfrak{y}, \xi(i+1,j+1)=\epsilon \\ |r(i+1,j)=m, \delta(i+1,j)=\hbar, \zeta(i+1,j)=\mathfrak{w}, \xi(i+1,j)=\varrho \end{matrix} \right\} = \pi_{mn}\mu_{\hbar\eth}^n \jmath_{\varrho\epsilon} o_{\mathfrak{w}\mathfrak{y}}^\epsilon \tag{12}$$

Furthermore, the mathematical expectation of matrix $P_\varepsilon^{n,f}$ can be derived from the relation of equation (12) as follows

$$E\left\{P_{\epsilon,\mathfrak{y}}^{n,\eth}\right\} = \sum_{\mathfrak{y}=1}^{\mathcal{M}_g}\sum_{\epsilon=1}^{\mathcal{M}_s}\sum_{n=1}^{\mathcal{M}_s}\sum_{\eth=1}^{\mathcal{M}_g} \pi_{mn}\mu_{\hbar\eth}^n \jmath_{\varrho\epsilon} o_{\mathfrak{w}\mathfrak{y}}^\epsilon P_{\epsilon,\mathfrak{y}}^{n,\eth} = \bar{P}_{\epsilon,\mathfrak{y}}^{n,\eth} \quad (13)$$

similarly, one has

$$E\left\{Q_{\epsilon,\mathfrak{y}}^{n}\right\} = \sum_{\mathfrak{y}=1}^{\mathcal{M}_g}\sum_{\epsilon=1}^{\mathcal{M}_s}\sum_{n=1}^{\mathcal{M}_s}\sum_{\eth=1}^{\mathcal{M}_g} \pi_{mn}\mu_{\hbar\eth}^n \jmath_{\varrho\epsilon} o_{\mathfrak{w}\mathfrak{y}}^\epsilon Q_{\epsilon,\mathfrak{y}}^{n,\eth} = \bar{Q}_{\epsilon,\mathfrak{y}}^{n,\eth} \quad (14)$$

Considering the following index

$$J(i,j) \triangleq E\{(V(i+1,j+1) - V_1(i+1,j) - V_2(i,j+1)|\partial(i,j)\} = E\left\{\sum_{q=1}^5 \Delta V_{1,q}(i,j) + \sum_{q=1}^5 \Delta V_{2,q}(i,j)|\partial(i,j)\right\} \quad (15)$$

where $\partial(i,j) \triangleq \{\eta(i+1,j), \eta(i+1,j-1), ..., \eta(i+1,j-\bar{\tau}), \eta(i,j+1), \eta(i-1,j+1), ..., \eta(i-\bar{d},j+1)\},$

$$\Delta V_{1,q}(i,j) = V_{1,q}(i+1,j+1) - V_{1,q}(i+1,j), \Delta V_{2,q}(i,j) = V_{2,q}(i+1,j+1) - V_{2,q}(i,j+1).$$

Define the following augmented matrices

$$\Im^T(i,j) = \left[\eta^T(i+1,j)., \eta^T(i,j+1), \eta^T(i+1,j-\tau(j)), \eta^T(i-d(i),j+1), \eta^T(i+1,j-\underline{\tau}),. \right.$$

$$\eta^T(i-\underline{d},j+1), \eta^T(i+1,j-\bar{\tau}), \eta^T(i-\bar{d},j+1), \frac{1}{\bar{\tau}-\underline{\tau}-1}\sum_{\theta=-\bar{\tau}+1}^{-\underline{\tau}-1}\eta^T(i+1,j+\theta),$$

$$\left.\frac{1}{\bar{d}-\underline{d}-1}\sum_{\theta=-\bar{d}+1}^{-\underline{d}-1}\eta^T(i+\theta,j+1), \frac{1}{\underline{\tau}-1}\sum_{\theta=-\underline{\tau}+1}^{-1}\eta^T(i+1,j+\theta), \frac{1}{\underline{d}-1}\sum_{\theta=-\underline{d}+1}^{-1}\eta^T(i+\theta,j+1)\right],$$

$$A(i,j) = \left[\tilde{\Pi}_1 + \varpi_1(i+1,j)\hat{\Pi}_1 + \varpi_2(i+1,j)\widehat{\Pi}_1, \tilde{\Pi}_2 + \varpi_1(i,j+1)\hat{\Pi}_2 + \varpi_2(i,j+1)\widehat{\Pi}_2, \Pi_3, \Pi_4, 0, 0, 0, 0, 0, 0, 0, 0\right]$$

the dynamic filtering error system (equation (9)) with $\omega(i,j)\equiv 0$ can be rewritten as

$$\eta(i+1,j+1) = A(i,j)\Im(i,j) \quad (16)$$

Combine equations (11), (13), (14), and (15) with equation (16), which yields

$$E\{\Delta V_{1,1}(i,j)\} = E\{\eta^T(i+1,j+1)P_\varepsilon^{n,f}\eta(i+1,j+1) - \eta^T(i+1,j)P_\alpha^{m,l}\eta(i+1,j)|\partial(i,j)\} \quad (17)$$

$$E\{\Delta V_{1,2}(i,j)\}$$

$$= E\{\sum_{\theta=-\tau(j+1)}^{-1}\eta^T(i+1,j+1+\theta)S_1\eta(i+1,j+1+\theta) - \sum_{\theta=-\tau(j)}^{-1}\eta^T(i+1,j+\theta)S_1\eta(i+1,j+\theta)|\partial(i,j)\}$$

$$= \eta^T(i+1,j)S_1\eta(i+1,j) - \eta^T(i+1,j-\tau(j))S_1\eta(i+1,j-\tau(j)) + \sum_{\theta=1-\tau(j+1)}^{-1}\eta^T(i+1,j+\theta)S_1\eta(i+1,j+\theta)$$

$$- \sum_{\theta=1-\tau(j)}^{-1}\eta^T(i+1,j+\theta)S_1\eta(i+1,j+\theta) \quad (18)$$

$$\leqslant \eta^T(i+1,j)S_1\eta(i+1,j) - \eta^T(i+1,j-\tau(j))S_1\eta(i+1,j-\tau(j)) + \sum_{\theta=1-\bar{\tau}}^{-\underline{\tau}}\eta^T(i+1,j+\theta)S_1\eta(i+1,j+\theta),$$

$$\leqslant \Im^T(i,j)(e_1^T S_1 e_1 - e_3^T S_1 e_3)\Im^T(i,j) + \sum_{\theta=1-\bar{\tau}}^{-\underline{\tau}}\eta^T(i+1,j+\theta)S_1\eta(i+1,j+\theta)$$

$$E\{\Delta V_{1,3}(i,j)\}$$

$$= E\{\sum_{\theta=1-\bar{\tau}}^{-\underline{\tau}}\sum_{s=\theta}^{-1}\eta^T(i+1,j+1+s)S_1\eta(i+1,j+1+s) - \sum_{\theta=1-\bar{\tau}}^{-\underline{\tau}}\sum_{s=\theta}^{-1}\eta^T(i+1,j+s)S_1\eta(i+1,j+s)|\partial(i,j)\}$$

$$= E\{\sum_{\theta=1-\bar{\tau}}^{-\underline{\tau}}(\eta^T(i+1,j)S_1\eta(i+1,j) - \eta^T(i+1,j+\theta)S_1\eta(i+1,j+\theta))|\partial(i,j)\} \quad (19)$$

$$= (\bar{\tau}-\underline{\tau})\Im^T(i,j)e_1^T S_1 e_1 \Im^T(i,j) - \sum_{\theta=1-\bar{\tau}}^{-\underline{\tau}}\eta^T(i+1,j+\theta)S_1\eta(i+1,j+\theta)$$

$$E\{\Delta V_{1,4}(i,j)\}$$

$$= E\{\underline{\tau}\sum_{\theta=-\underline{\tau}}^{-1}\sum_{s=\theta}^{-1}\wp_1^T(i+1,j+s+1)S_2\wp_1(i+1,j+s+1) - \underline{\tau}\sum_{\theta=-\underline{\tau}}^{-1}\sum_{s=\theta}^{-1}\wp_1^T(i+1,j+s)S_2\wp_1(i+1,j+s)|\partial(i,j)\} \tag{20}$$

$$= \underline{\tau}^2 E\{\wp_1^T(i+1,j)S_2\wp(i+1,j)\} - \underline{\tau}E\{\sum_{\theta=-\underline{\tau}}^{-1}\wp_1^T(i+1,j+\theta)S_2\wp_1(i+1,j+\theta)\}$$

$$E\{\Delta V_{1,5}(i,j)\}$$

$$= E\{(\bar{\tau}-\underline{\tau})\sum_{\theta=-\bar{\tau}}^{-\underline{\tau}-1}\sum_{s=\theta}^{-1}\wp_1^T(i+1,j+s+1)S_2\wp(i+1,j+s+1) - (\bar{\tau}-\underline{\tau})\sum_{\theta=-\bar{\tau}}^{-\underline{\tau}-1}\sum_{s=\theta}^{-1}\wp_1(i+1,j+s)S_2\wp(i+1,j+s)|\partial(i,j)\} \tag{21}$$

$$= (\bar{\tau}-\underline{\tau})^2\wp_1^T(i+1,j)S_2\wp_1(i+1,j) - (\bar{\tau}-\underline{\tau})\sum_{\theta=-\bar{\tau}}^{-\underline{\tau}-1}\wp_1^T(i+1,j+\theta)S_2\wp_1(i+1,j+\theta)$$

Similarly, by applying the same procedure, one has

$$E\{\Delta V_{2,1}(i,j)\} = E\{\eta^T(i,j+1)Q_\varepsilon^{n,f}\eta(i,j+1) - \eta^T(i,j+1)$$
$$Q_\alpha^{m,l}\eta(i,j+1)|\partial(i,j)\} \tag{22}$$

$$E\{\Delta V_{2,2}(i,j)\} \leqslant \Im^T(i,j)(e_2^T S_3 e_2 - e_4^T S_3 e_4)\Im(i,j) +$$
$$\sum_{\theta=1-\bar{d}}^{-\underline{d}}\eta^T(i+\theta,j+1)S_3\eta(i+\theta,j+1) \tag{23}$$

$$E\{\Delta V_{2,3}(i,j)\} = (\bar{d}-\underline{d})\Im^T(i,j)e_2^T S_3 e_2\Im(i,j) -$$
$$\sum_{\theta=1-\bar{d}}^{-\underline{d}}\eta^T(i+\theta,j+1)S_3\eta(i+\theta,j+1)) \tag{24}$$

$$E\{\Delta V_{2,4}(i,j)\} = \underline{d}^2\wp_2^T(i,j+1)S_4\wp_2(i,j+1) - \underline{d}$$
$$\sum_{\theta=-\underline{d}}^{-1}\wp_2^T(i+\theta,j+1)S_4\wp_2(i+\theta,j+1) \tag{25}$$

$$E\{\Delta V_{2,5}(i,j)\} = (\bar{d}-\underline{d})^2 E\{\wp_2^T(i,j+1)S_4\wp_2(i,j+1)\} - (\bar{d}-\underline{d})$$
$$\sum_{\theta=-\bar{d}}^{-\underline{d}-1}\wp_2^T(i+\theta,j+1)S_4\wp_2(i+\theta,j+1) \tag{26}$$

In addition, consider equation (11), which yields

$$\wp_1^T(i+1,j)S_2\wp(i+1,j) = \Im^T(i,j)\bar{\Xi}_{11}^T S_2\bar{\Xi}_{11}\Im(i,j) \tag{27}$$

$$\wp_2^T(i,j+1)S_4\wp_2(i,j+1) = \Im^T(i,j)\bar{\Xi}_{22}^T S_4\bar{\Xi}_{22}\Im(i,j) \tag{28}$$

where

$$\Xi_{11} = \begin{bmatrix}\tilde{\Pi}_1 + \varpi_1(i+1,j)\hat{\Pi}_1 + \varpi_2(i+1,j)\hat{\Pi}_1 - I & \tilde{\Pi}_2 + \varpi_1(i,j+1)\end{bmatrix}$$

$$\hat{\Pi}_2 + \varpi_2(i,j+1)\hat{\Pi}_2 \quad \Pi_3 \quad \Pi_4 \quad 0 \quad 0 \quad 0 \quad 0 \quad 0 \quad 0 \quad 0 \quad 0],$$

$$\Xi_{22} = \begin{bmatrix}\tilde{\Pi}_1 + \varpi_1(i+1,j)\hat{\Pi}_1 + \varpi_2(i+1,j)\widehat{\Pi}_1 & \tilde{\Pi}_2 + \varpi_1(i,j+1)\end{bmatrix}$$

$$\hat{\Pi}_2 + \varpi_2(i,j+1)\widehat{\Pi}_2 - I \quad \Pi_3 \quad \Pi_4 \quad 0 \quad 0 \quad 0 \quad 0 \quad 0 \quad 0 \quad 0 \quad 0].$$

Then, according to the Lemma 1, one has

$$-\underline{\tau}\sum_{\theta=-\underline{\tau}}^{-1}\wp_1^T(i+1,j+\theta)S_2\wp_1(i+1,j+\theta)$$

$$\leqslant \Im^T(i,j)(-(e_1-e_5)^T S_2(e_1-e_5) - \frac{3(\underline{\tau}-1)}{\underline{\tau}+1}(e_1+e_5-2e_{11})^T$$

$$S_2(e_1+e_5-2e_{11}))\Im(i,j) \tag{29}$$

$$-\underline{d}\sum_{\theta=-\underline{d}}^{-1}\wp_2^T(i+\theta,j+1)S_4\wp_2(i+\theta,j+1)$$

$$\leqslant \Im^T(i,j)(-(e_2-e_6)^T S_4(e_2-e_6) - \frac{3(\underline{d}-1)}{\underline{d}+1}(e_2+e_6-2e_{12})^T$$

$$S_4(e_2+e_6-2e_{12}))\Im(i,j) \tag{30}$$

$$-(\bar{\tau}-\underline{\tau})\sum_{\theta=-\bar{\tau}}^{-\underline{\tau}-1}\wp_1^T(i+1,j+\theta)S_2\wp_1(i+1,j+\theta)$$

$$\leqslant \Im^T(i,j)(-(e_5-e_7)^T S_2(e_5-e_7) - \frac{3(\bar{\tau}-\underline{\tau}-1)}{\bar{\tau}-\underline{\tau}+1} \tag{31}$$

$$(e_5+e_7-2e_9)^T S_2(e_5+e_7-2e_9))\Im(i,j)$$

$$-(\bar{d}-\underline{d})\sum_{\theta=-\bar{d}}^{-\underline{d}-1}\wp_2^T(i+\theta,j+1)S_4\wp_2(i+\theta,j+1)$$

$$\leqslant \Im^T(i,j)(-(e_6-e_8)^T S_4(e_6-e_8) - \frac{3(\bar{d}-\underline{d}-1)}{\bar{d}-\underline{d}+1} \tag{32}$$

$$(e_6+e_8-2e_{10})^T S_4(e_6+e_8-2e_{10}))\Im(i,j)$$

Consider equations (17)–(32), which yields

$$J(i,j) = E\left\{\sum_{q=1}^5\Delta V_{1,q}(i,j) + \sum_{q=1}^5\Delta V_{2,q}(i,j)|\partial(i,j)\right\} \leqslant$$
$$\Im^T(i,j)(\tilde{\Phi}+\bar{\Phi})\Im(i,j),$$

where

$$\tilde{\Phi} = \begin{bmatrix} \tilde{\Phi}_{11} & \tilde{\Phi}_{12} & \tilde{\Phi}_{13} \\ * & \tilde{\Phi}_{22} & \tilde{\Phi}_{23} \\ * & * & \tilde{\Phi}_{33} \end{bmatrix}, \bar{\Phi} = \sum_i^5 \mathrm{H}_i^T \Xi \mathrm{H}_i, \tilde{\Phi}_{11} = \begin{bmatrix} \tilde{S} & -S_2\tilde{\Pi}_2 - \tilde{\Pi}_1^T S_4 & -S_2\Pi_3 & -S_2\Pi_4 \\ * & \bar{S} & -S_4\Pi_3 & -S_4\Pi_4 \\ * & * & -S_1 & 0 \\ * & * & * & -S_3 \end{bmatrix},$$

$$\tilde{S} = (1 + \bar{\tau} - \underline{\tau})S_1 + \frac{-4\underline{\tau} + 2}{\underline{\tau} + 1}S_2 - P_{\varrho,\mathfrak{w}}^{m,\hbar} + (\underline{\tau}^2 + (\bar{\tau} - \underline{\tau})^2)(I - \tilde{\Pi}_1^T S_2 - S_2\tilde{\Pi}_1),$$

$$\bar{S} = (1 + \bar{d} - \underline{d})S_1 + \frac{-4\underline{d} + 2}{\underline{d} + 1}S_4 - Q_{\varrho,\mathfrak{w}}^{m,\hbar} + (\underline{d}^2 + (\bar{d} - \underline{d})^2)(I - \tilde{\Pi}_2^T S_4 - S_4\tilde{\Pi}_2), \tilde{\Phi}_{12} = diag\left\{\frac{-2\underline{\tau} + 4}{\underline{\tau} + 1}S_2, \frac{-2\underline{d} + 4}{\underline{d} + 1}S_4, 0, 0\right\},$$

$$\tilde{\Phi}_{13} = \begin{bmatrix} 0 & \frac{6(\underline{\tau}-1)}{\underline{\tau}+1}S_2 & 0 & 0 \\ 0 & 0 & \frac{3(\underline{d}-1)}{\underline{d}+1}S_4 & 0 \\ 0 & 0 & 0 & 0 \\ 0 & 0 & 0 & 0 \end{bmatrix}, \tilde{\Phi}_{22} = \begin{bmatrix} (\tilde{\tau}+\hat{\tau})S_2 & 0 & \hat{\tau}S_2 & 0 \\ 0 & (\tilde{d}+\hat{d})S_4 & 0 & \hat{d}S_4 \\ 0 & 0 & \hat{\tau}S_2 & 0 \\ 0 & 0 & 0 & \widehat{d}S_4 \end{bmatrix}$$

$$\tilde{\Phi}_{23} = \begin{bmatrix} 6\vec{\tau}S_2 & 0 & \frac{6(\underline{\tau}-1)}{\underline{\tau}+1}S_2 & 0 \\ 0 & 6\vec{d}S_4 & 0 & \frac{6(\underline{d}-1)}{\underline{d}+1}S_4 \\ 6\vec{\tau}S_2 & 0 & 0 & 0 \\ 0 & 6\vec{d}S_4 & 0 & 0 \end{bmatrix}, \tilde{\Phi}_{33} = diag\left\{-12\vec{\tau}S_2, -12\vec{d}S_4, -\frac{12(\underline{\tau}-1)}{\underline{\tau}+1}S_2, -\frac{12(\underline{d}-1)}{\underline{d}+1}S_4\right\}, \tilde{\tau} = \frac{-4\underline{\tau}+2}{\underline{\tau}+1},$$

$$\tilde{d} = \frac{-4\underline{d}+2}{\underline{d}+1}, \hat{\tau} = \frac{-4\bar{\tau}+4\underline{\tau}+2}{\bar{\tau}-\underline{\tau}+1}, \hat{d} = \frac{-4\bar{d}+4\underline{d}+2}{\bar{d}-\underline{d}+1}, \widehat{\tau} = \frac{-2\bar{\tau}+2\underline{\tau}+4}{\bar{\tau}-\underline{\tau}+1}, \widehat{d} = \frac{-2\bar{d}+2\underline{d}+4}{\bar{d}-\underline{d}+1}, \vec{\tau} = \frac{(\bar{\tau}-\underline{\tau}-1)}{\bar{\tau}-\underline{\tau}+1},$$

$$\vec{d} = \frac{(\bar{d}-\underline{d}-1)}{\bar{d}-\underline{d}+1}, \Xi = \bar{P}_{\epsilon,\mathfrak{y}}^{n,\eth} + \bar{Q}_{\epsilon,\mathfrak{y}}^{n,\eth} + (\underline{\tau}^2 + (\bar{\tau} - \underline{\tau})^2)S_2 + (\underline{d}^2 + (\bar{d} - \underline{d})^2)S_4,$$

$$\mathrm{H}_1 = \begin{bmatrix} \tilde{\Pi}_1 & \tilde{\Pi}_2 & \Pi_3 & \Pi_4 & 0 & 0 & 0 & 0 & 0 & 0 & 0 & 0 \end{bmatrix}, \mathrm{H}_2 = \begin{bmatrix} \bar{\varsigma}_1\hat{\Pi}_1 & \bar{\varsigma}_1\hat{\Pi}_2 & 0 & 0 & 0 & 0 & 0 & 0 & 0 & 0 & 0 & 0 \end{bmatrix},$$

$$\mathrm{H}_3 = \begin{bmatrix} \bar{\varsigma}_{12}\hat{\Pi}_1 & \bar{\varsigma}_{12}\hat{\Pi}_2 & 0 & 0 & 0 & 0 & 0 & 0 & 0 & 0 & 0 & 0 \end{bmatrix}, \mathrm{H}_4 = \begin{bmatrix} \bar{\varsigma}_{12}\hat{\Pi}_1 & \bar{\varsigma}_{12}\hat{\Pi}_2 & 0 & 0 & 0 & 0 & 0 & 0 & 0 & 0 & 0 & 0 \end{bmatrix},$$

$$\mathrm{H}_5 = \begin{bmatrix} \bar{\varsigma}_2\hat{\Pi}_1 & \bar{\varsigma}_2\hat{\Pi}_2 & 0 & 0 & 0 & 0 & 0 & 0 & 0 & 0 & 0 & 0 \end{bmatrix}.$$

It is straightforward to verify that the index function $J(i,j) \leqslant 0$ if $\tilde{\Phi} + \bar{\Phi} \leqslant 0$ holds. In virtue of Schur Complement Lemma, we can obtain the following inequality

$$\tilde{\Phi} + \bar{\Phi} \leqslant 0 \Leftrightarrow \Psi = \begin{bmatrix} \tilde{\Phi} & \tilde{\mathrm{H}} \\ * & \widehat{\Xi} \end{bmatrix} \leqslant 0 \tag{33}$$

where

$$\tilde{\mathrm{H}} = \begin{bmatrix} \mathrm{H}_1^T \Xi & \mathrm{H}_2^T \Xi & \mathrm{H}_3^T \Xi & \mathrm{H}_4^T \Xi & \mathrm{H}_5^T \Xi \end{bmatrix}, \widehat{\Xi} = I_5 \otimes -\Xi.$$

Furthermore, the inequality (equation (33)) implies there is a scalar $\rho > 0$ such that

$$\Psi < diag\{\ell_{11}I, \ell_{22}I, \ell_{33}I, \ell_{44}I, \ell_{44}I, \ell_{44}I, \ell_{44}I, \ell_{44}I\} < diag\{\Gamma, 0, 0, 0, 0, 0\} \tag{34}$$

where $\ell_{11} = \lambda_{\max}\{\tilde{S}, \bar{S}, -S_1, -S_2\}$, $\ell_{22} = \lambda_{\max}\{(\tilde{\tau} + \hat{\tau})S_2, (\tilde{d} + \hat{d})S_4, \hat{\tau}S_2, \widehat{d}S_4\}$, $\ell_{33} = \lambda_{\max}\left\{-12\vec{\tau}S_2, -12\vec{d}S_4, -\frac{12(\underline{\tau}-1)}{\underline{\tau}+1}S_2, -\frac{12(\underline{d}-1)}{\underline{d}+1}S_4\right\}$, $\ell_{44} = \lambda_{\max}(-\Xi)$, $\Gamma = diag\{-\rho I, 0, 0, 0\}$.

Moreover, it is easy to derive that equation (34) is equivalent to

$$E\{(V(i+1, j+1) - V_1(i+1, j) - V_2(i, j+1)|\partial(i,j)\} \leqslant -\rho E\{\|\eta(i+1, j)\|^2\} \tag{35}$$

Summing up both sides of equation (35) with respect to both i and j from 0 to λ (λ is a positive integer that is larger enough, and $\lambda > \max\{t_1, t_2\}$), one has

$$J(i,j) = \sum_{i=0}^{\lambda} \sum_{j=0}^{\lambda} E\{(V(i+1,j+1) - V_1(i+1,j) - V_2(i,j+1)|\partial(i,j)\}$$

$$= \sum_{i=0}^{\lambda} \sum_{j=0}^{\lambda} E\{(V_1(i+1,j+1) - V_1(i+1,j) + V_2(i+1,j+1) - V_2(i,j+1)|\partial(i,j)\} \tag{36}$$

$$\leqslant -\rho \sum_{i=0}^{\lambda} \sum_{j=0}^{\lambda} \|\eta(i+1,j)\|^2$$

It follows from equation (36) that

$$J(i,j) = \sum_{i=0}^{\lambda} E\{(V_1(i+1,1) + V_1(i+1,2) + \ldots + V_1(i+1,\hbar) + V_1(i+1,\hbar+1) - V_1(i+1,0)$$

$$- V_1(i+1,1) - V_1(i+1,2) - \ldots - V_1(i+1,\hbar-1) - V_1(i+1,\hbar)\}$$

$$+ \sum_{j=0}^{\lambda} E\{(V_2(1,j+1) + V_2(2,j+1) + \ldots + V_2(\hbar,j+1) + V_2(\hbar+1,j+1) \tag{37}$$

$$- V_2(0,j+1) - V_2(1,j+1) - \ldots - V_2(\hbar-1,j+1) - V_2(\hbar,j+1)\}$$

$$= \sum_{i=0}^{\lambda} E\{(V_1(i+1,\hbar+1) - V_1(i+1,0)\} + \sum_{j=0}^{\hbar} E\{(V_2(\hbar+1,j+1) - V_2(0,j+1)\} \leqslant -\rho \sum_{i=0}^{\lambda} \sum_{j=0}^{\lambda} E\{\|\eta(i+1,j)\|^2\}$$

According to equation (37), we can further infer

$$\sum_{i=0}^{\lambda} \sum_{j=0}^{\lambda} \|\eta(i+1,j)\|^2 \leqslant \rho^{-1} \sum_{i=0}^{\lambda} E\{(V_1(i+1,0) - V_1(i+1,\hbar+1)\} + \rho^{-1} \sum_{i=0}^{\lambda} E\{V_2(0,j+1) - V_2(i+1,\hbar+1)\}$$

$$\leqslant \rho^{-1} \sum_{i=0}^{\lambda} E\{(V_1(i+1,0)\} + \rho^{-1} \sum_{i=0}^{\lambda} E\{V_2(0,j+1)\} < \infty \tag{38}$$

According to the bounded initial conditions (3) and equation (38), which yields $\lim\limits_{i+j\to\infty} \sum\limits_{i=0}^{\lambda} \sum\limits_{j=0}^{\lambda} \|\eta(i+1,j)\|^2 = 0$, which

implies $\lim\limits_{i+j\to\infty} \sum\limits_{i=0}^{\lambda} \sum\limits_{j=0}^{\lambda} \|e(i,j)\|^2 = 0$. Based on Definition 1, it can be said that the filtering error systems (equation (9)) with $\omega(i,j) \equiv 0$ are asymptotically stable in the mean-square sense. The proof is thus completed.

In what follows, based on the sufficient conditions obtained in Theorem 1, we aim to further guarantee the dynamic filtering error systems (equation (9)) to be robust H$_\infty$ stability with disturbance attenuation level γ in the presence of external disturbance $\omega(i,j) \neq 0$.

Theorem 2: Consider the filtering error systems (equation (9)) with zero initial condition, for given scalars $\bar{\tau}$, $\underline{\tau}$, $\bar{d}$, and $\underline{d}$, if there exists positive scalars γ, positive definite symmetric matrices $P_{\varrho,\mathfrak{w}}^{m,\hbar}$, $Q_{\varrho,\mathfrak{w}}^{m,\hbar}$, $\bar{P}_{\epsilon,\mathfrak{y}}^{n,\eth}$, $\bar{Q}_{\epsilon,\mathfrak{y}}^{n,\eth}$, S_1, S_2, S_3, and S_4, such that the following inequality holds

$$\Omega = \begin{bmatrix} \sum_{11} & \sum_{12} & \Omega_{13} & \Omega_{14} \\ 0 & -\gamma^2 I & 0 & 0 \\ 0 & 0 & \Delta_1 & 0 \\ 0 & 0 & 0 & \Delta_2 \end{bmatrix} \leqslant 0 \tag{39}$$

where

$$\sum_{11} = \begin{bmatrix} \hat{\Phi}_{11} & \tilde{\Phi}_{12} & \tilde{\Phi}_{13} \\ * & \tilde{\Phi}_{22} & \tilde{\Phi}_{23} \\ * & * & \tilde{\Phi}_{33} \end{bmatrix}, \quad \hat{\Phi}_{11} = \begin{bmatrix} \tilde{S} & -(\underline{\tau}^2 + (\bar{\tau}-\underline{\tau})^2)S_2\tilde{\Pi}_2 - (\underline{d}^2 + (\bar{d}-\underline{d})^2)\tilde{\Pi}_1^T S_4 & -S_2\Pi_3 & -S_2\Pi_4 \\ * & \bar{S} & -S_4\Pi_3 & -S_4\Pi_4 \\ * & * & -S_1 & 0 \\ * & * & * & -S_3 \end{bmatrix},$$

$$\tilde{S} = (1 + \bar{\tau} - \underline{\tau})S_1 + \frac{-4\underline{\tau}+2}{\underline{\tau}+1}S_2 - P_{\varrho,\mathfrak{w}}^{m,\hbar} + (\underline{\tau}^2 + (\bar{\tau}-\underline{\tau})^2)(I - \tilde{\Pi}_1^T S_2 - S_2\tilde{\Pi}_1) + \tilde{H}^T(r(i+1,j))\tilde{H}(r(i+1,j)),$$

$$\bar{S} = (1 + \bar{d} - \underline{d})S_1 + \frac{-4\underline{d}+2}{\underline{d}+1}S_4 - Q_{\varrho,\mathfrak{w}}^{m,\hbar} + (\underline{d}^2 + (\bar{d}-\underline{d})^2)(I - \tilde{\Pi}_2^T S_4 - S_4\tilde{\Pi}_2) + \tilde{H}^T(r(i,j+1))\tilde{H}(r(i,j+1)),$$

$$\sum{}^2 = \left[-(\underline{\tau}^2 + (\bar{\tau} - \underline{\tau})^2)\bar{\Theta}^T S_2 \quad -(\underline{d}^2 + (\bar{d} - \underline{d})^2)\bar{\Theta}^T S_4 \quad 0 \quad 0\right]^T,$$

$$\Omega_{13}^2 = \left[\Psi_1 \quad \Psi_2 \quad \Psi_3 \quad \Psi_4 \quad \Psi_5 \quad \Psi_6\right], \Omega_{14} = \left[\Psi_7 \quad \Psi_8 \quad \Psi_9 \quad \Psi_{10} \quad \Psi_{11} \quad \Psi_{12} \quad \Psi_{13}\right],$$

$$\Psi_1 = \left[\Xi\tilde{\Pi}_1 \quad \Xi\tilde{\Pi}_2 \quad \Xi\Pi_3 \quad \Xi\Pi_4 \quad 0 \quad 0 \quad 0 \quad 0 \quad 0 \quad 0 \quad 0 \quad 0 \quad \Xi\bar{\Theta}\right]^T,$$

$$\Psi_2 = \left[\bar{\varsigma}_1\Xi\hat{\Pi}_1 \quad \bar{\varsigma}_1\Xi\hat{\Pi}_2 \quad 0 \quad 0 \quad 0 \quad 0 \quad 0 \quad 0 \quad 0 \quad 0 \quad 0 \quad 0 \quad \bar{\varsigma}_1\Xi\tilde{\Theta} + \bar{\varsigma}_1\Xi\hat{\Theta}\right]^T,$$

$$\Psi_3 = \left[\bar{\varsigma}_{12}\Xi\hat{\Pi}_1 \quad \bar{\varsigma}_{12}\Xi\hat{\Pi}_2 \quad 0 \quad 0 \quad 0 \quad 0 \quad 0 \quad 0 \quad 0 \quad 0 \quad 0 \quad 0 \quad 0\right]^T, \Psi_4 = \left[\bar{\varsigma}_{12}\Xi\hat{\Pi}_1 \quad \bar{\varsigma}_{12}\Xi\hat{\Pi}_2 \quad 0 \quad 0 \quad 0 \quad 0 \quad 0 \quad 0 \quad 0 \quad 0 \quad 0 \quad 0 \quad 0\right]^T,$$

$$\Psi_5 = \left[\bar{\varsigma}_2\Xi\hat{\Pi}_1 \quad \bar{\varsigma}_2\Xi\hat{\Pi}_2 \quad 0 \quad 0 \quad 0 \quad 0 \quad 0 \quad 0 \quad 0 \quad 0 \quad 0 \quad 0 \quad 0\right]^T, \Psi_6 = \left[\sqrt{2}\bar{\varsigma}_{13}\Xi\hat{\Pi}_1 \quad 0 \quad 0 \quad 0 \quad 0 \quad 0 \quad 0 \quad 0 \quad 0 \quad 0 \quad 0 \quad 0 \quad 0\right]^T,$$

$$\Psi_7 = \left[\sqrt{2\bar{\varsigma}_{21}^2 + 2\bar{\varsigma}_{23}^2}\Xi\hat{\Pi}_1 \quad 0 \quad 0 \quad 0 \quad 0 \quad 0 \quad 0 \quad 0 \quad 0 \quad 0 \quad 0 \quad 0 \quad 0\right]^T, \Psi_8 = \left[0 \quad \sqrt{2}\bar{\varsigma}_{13}\Xi\hat{\Pi}_2 \quad 0 \quad 0 \quad 0 \quad 0 \quad 0 \quad 0 \quad 0 \quad 0 \quad 0 \quad 0 \quad 0\right]^T,$$

$$\Psi_9 = \left[0 \quad \sqrt{2\bar{\varsigma}_{12}^2 + 2\bar{\varsigma}_{23}^2}\Xi\hat{\Pi}_2 \quad 0 \quad 0 \quad 0 \quad 0 \quad 0 \quad 0 \quad 0 \quad 0 \quad 0 \quad 0 \quad 0\right]^T, \Psi_{10} = \left[0 \quad 0 \quad 0 \quad 0 \quad 0 \quad 0 \quad 0 \quad 0 \quad 0 \quad 0 \quad 0 \quad 0 \quad \sqrt{(2\bar{\varsigma}_{21}^2 + 2\bar{\varsigma}_1^2 + 2\bar{\varsigma}_{13}^2)}\Xi\tilde{\Theta}\right]^T,$$

$$\Psi_{11} = \left[0 \quad 0 \quad 0 \quad 0 \quad 0 \quad 0 \quad 0 \quad 0 \quad 0 \quad 0 \quad 0 \quad 0 \quad \sqrt{(2\bar{\varsigma}_{21}^2 + 2\bar{\varsigma}_1^2 + 2\bar{\varsigma}_{13}^2)}\Xi\hat{\Theta}\right]^T,$$

$$\Psi_{12} = \left[0 \quad 0 \quad 0 \quad 0 \quad 0 \quad 0 \quad 0 \quad 0 \quad 0 \quad 0 \quad 0 \quad 0 \quad \sqrt{(4\bar{\varsigma}_{13}^2 + 2\bar{\varsigma}_{23}^2 + 2\bar{\varsigma}_3^2)}\Xi\hat{\Theta}\right]^T,$$

$$\Psi_{13} = \left[0 \quad 0 \quad 0 \quad 0 \quad 0 \quad 0 \quad 0 \quad 0 \quad 0 \quad 0 \quad 0 \quad 0 \quad \sqrt{(4\bar{\varsigma}_{13}^2 + 2\bar{\varsigma}_{23}^2 + 2\bar{\varsigma}_3^2)}\Xi\check{\Theta}\right]^T,$$

$$\Delta_1 = diag\{-\Xi, -\Xi, -\Xi, -\Xi, -\Xi, -\Xi\}, \Delta_2 = diag\{-\Xi, -\Xi, -\Xi, -\Xi, -\Xi, -\Xi, -\Xi\}$$

the filtering error systems (equation (9)) satisfy the robust H_∞ stability with disturbance attenuation level γ.

Proof: Define new augmented matrices

$$\tilde{\Im}(i,j) = \left[\Im^T(i,j) \quad \tilde{\omega}^T(i,j)\right]^T, \tilde{A}(i,j) = \left[A(i,j) \quad \Theta(i,j)\right]$$

then the dynamic filtering error systems (equation (9)) can be reconstructed in the following form with external disturbance $\omega(i,j) \neq 0$

$$\eta(i + 1, j + 1) = A(i,j)\Im(i,j) + (\bar{\Theta} + \varpi_1(i + 1, j)\tilde{\Theta} + \varpi_1(i, j + 1)\hat{\Theta} + \varpi_3(i + 1, j)\widehat{\Theta} + \varpi_3(i, j + 1)\check{\Theta})\tilde{\omega}(i,j)$$

Furthermore, consider the following robust H_∞ stability performance index

$$\Upsilon(i,j) \overset{\Delta}{=} E\{\tilde{z}^T(i,j)\tilde{z}(i,j) - \gamma^2\tilde{\omega}^T(i,j)\tilde{\omega}(i,j) + J(i,j)|\partial(i,j)\} \tag{40}$$

It is easy to deduce

$$\Upsilon(i,j) = \eta^T(i + 1, j)\tilde{H}^T(r(i + 1, j))\tilde{H}(r(i + 1, j))\eta(i + 1, j) + \eta^T(i, j + 1)\tilde{H}^T(r(i, j + 1))\tilde{H}(r(i, j + 1))\eta(i, j + 1)$$

$$- \gamma^2\tilde{\omega}^T(i,j)\tilde{\omega}(i,j) + E\left\{\sum_{q=1}^{5}\Delta V_{1,q}(i,j) + \sum_{q=1}^{5}\Delta V_{2,q}(i,j)|\partial(i,j)\right\}$$

Similarly, based on the derivation process and result of Theorem 1, one has

$$\Upsilon(i,j) \leq \tilde{\Im}^T(i,j)\sum\tilde{\Im}(i,j) + \sum_{i=1}^{13}\tilde{\Im}^T(i,j)\Psi_i^T\Xi\Psi_i\tilde{\Im}(i,j) = \tilde{\Im}^T(i,j)\Omega\tilde{\Im}(i,j) \tag{41}$$

where

$$\sum = \begin{bmatrix}\sum_{11} & \sum_{12} \\ * & -\gamma^2 I\end{bmatrix}, \Omega = \begin{bmatrix}\sum_{11} & \sum_{12} & \Omega_{13} & \Omega_{14} \\ 0 & -\gamma^2 I & 0 & 0 \\ 0 & 0 & \Delta_1 & 0 \\ 0 & 0 & 0 & \Delta_2\end{bmatrix} \leq 0, \sum_{11} = \begin{bmatrix}\widehat{\Phi}_{11} & \tilde{\Phi}_{12} & \tilde{\Phi}_{13} \\ * & \tilde{\Phi}_{22} & \tilde{\Phi}_{23} \\ * & * & \tilde{\Phi}_{33}\end{bmatrix}, \Omega_{13} = \left[\Psi_1 \quad \Psi_2 \quad \Psi_3 \quad \Psi_4 \quad \Psi_5 \quad \Psi_6\right]$$

$$\sum_{12} = \left[-(\underline{\tau}^2 + (\bar{\tau} - \underline{\tau})^2)\bar{\Theta}^T S_2 \quad -(\underline{d}^2 + (\bar{d} - \underline{d})^2)\bar{\Theta}^T S_4 \quad 0 \quad 0\right]^T, \Omega_{14} = \left[\Psi_7 \quad \Psi_8 \quad \Psi_9 \quad \Psi_{10} \quad \Psi_{11} \quad \Psi_{12} \quad \Psi_{13}\right],$$

$$\Delta_1 = diag\{-\Xi, -\Xi, -\Xi, -\Xi, -\Xi, -\Xi\}, \Delta_2 = diag\{-\Xi, -\Xi, -\Xi, -\Xi, -\Xi, -\Xi, -\Xi\},$$

specifically, other symbols are defined in equations (10) and (39), which are not provided.

If $\Omega < 0$ holds, we sum up both sides of performance index $\Upsilon(i,j)$ with respect to both i and j from 0 to λ, which yields

$$\sum_{i=0}^{\lambda}\sum_{j=0}^{\lambda} E\{\hat{z}^T(i,j)\hat{z}(i,j)\} \leq \sum_{i=0}^{\lambda}\sum_{j=0}^{\lambda} E\{\gamma^2\tilde{\omega}^T(i,j)\tilde{\omega}(i,j)\} -$$

$$\sum_{i=0}^{\lambda}\sum_{j=0}^{\lambda} E\{J(i,j)|\partial(i,j)\} \qquad (42)$$

Based on equation (15) and the zero initial condition, we can easily calculate that

$$\sum_{i=0}^{\lambda}\sum_{j=0}^{\lambda} J(i,j) = \sum_{i=0}^{\lambda} E\{(V_1(i+1,\hbar+1) - V_1(i+1,0)\} +$$

$$\sum_{j=0}^{\lambda} E\{(V_2(\hbar+1,j+1) - V_2(0,j+1)\}$$

$$= \sum_{i=0}^{\lambda} E\{(V_1(i+1,\hbar+1)\} + \sum_{j=0}^{\lambda} E\{(V_2(\hbar+1,j+1)\} \geq 0$$

obviously, $\sum_{i=0}^{\infty}\sum_{j=0}^{\infty} E\{\|\hat{z}(i,j)\|^2\} \leq \gamma^2(\sum_{i=0}^{\infty}\sum_{j=0}^{\infty} E\{\|\tilde{\omega}(i,j)\|^2\}$.

According to Definition 2, the dynamic filtering error systems (equation (9)) satisfies the condition of robust H_∞ stability with disturbance attenuation level γ. The proof is thus completed.

Theorem 3: Consider the dynamic filtering error systems (equation (9)) under zero initial condition, for given scalars $\bar{\tau}$, $\underline{\tau}$, $\bar{d}$, $\underline{d}$, λ_1, and λ_2, if there exists positive scalars γ, positive definite symmetric matrices $P_{\varrho,\mathfrak{w}}^{m,\hbar}$, $Q_{\varrho,\mathfrak{w}}^{m,\hbar}$, $\bar{P}_{\epsilon,\mathfrak{y},i}^{n,\eth}$, $\bar{Q}_{\epsilon,\mathfrak{y},i}^{n,\eth}$ ($i \in \{1,2,3\}$), S_1 and S_3, such that the following inequality holds

$$\tilde{\Omega} = \begin{bmatrix} \tilde{\Omega}_{11} & \tilde{\Omega}_{12} & \Omega_{13} & \Omega_{14} \\ 0 & -\gamma^2 I & 0 & 0 \\ 0 & 0 & \tilde{\Omega}_{33} & 0 \\ 0 & 0 & 0 & \tilde{\Omega}_{44} \end{bmatrix} \leq 0 \qquad (43)$$

where

$$\tilde{\Omega}_{11} = \begin{bmatrix} \hat{\Omega}_{11} & \hat{\Omega}_{12} & \hat{\Omega}_{13} \\ * & \hat{\Omega}_{22} & \hat{\Omega}_{23} \\ * & * & \hat{\Omega}_{33} \end{bmatrix}, \tilde{\Omega}_{12} = \begin{bmatrix} -\lambda_1(\underline{\tau}^2 + (\bar{\tau}-\underline{\tau})^2)\bar{\Lambda}^T & -\lambda_2(\underline{d}^2 + (\bar{d}-\underline{d})^2)\bar{\Lambda}^T & 0 & 0 & 0 & 0 & 0 & 0 & 0 & 0 & 0 & 0 \end{bmatrix}^T,$$

$$\tilde{\Omega}_{33} = diag\{-\tilde{\Xi}, -\tilde{\Xi}, -\tilde{\Xi}, -\tilde{\Xi}, -\tilde{\Xi}, -\tilde{\Xi}\}, \tilde{\Omega}_{44} = diag\{-\tilde{\Xi}, -\tilde{\Xi}, -\tilde{\Xi}, -\tilde{\Xi}, -\tilde{\Xi}, -\tilde{\Xi}, -\tilde{\Xi}\},$$

$$\hat{\Omega}_{11} = \begin{bmatrix} \tilde{S} & -\lambda_1(\underline{\tau}^2 + (\bar{\tau}-\underline{\tau})^2)\tilde{X}_2 - \lambda_2(\underline{d}^2 + (\bar{d}-\underline{d})^2)\tilde{X}_1^T & -\lambda_1(\underline{\tau}^2 + (\bar{\tau}-\underline{\tau})^2)X_3 & -\lambda_1(\underline{\tau}^2 + (\bar{\tau}-\underline{\tau})^2)X_4 \\ * & \bar{S} & -\lambda_2(\underline{d}^2 + (\bar{d}-\underline{d})^2)X_3 & -\lambda_2(\underline{d}^2 + (\bar{d}-\underline{d})^2)X_4 \\ * & * & -S_1 & 0 \\ * & * & * & -S_3 \end{bmatrix},$$

$$\hat{\Omega}_{12} = diag\left\{\frac{-2\underline{\tau}+4}{\underline{\tau}+1}S_2, \frac{-2\underline{d}+4}{\underline{d}+1}S_4, 0, 0\right\}, \hat{\Omega}_{13} = \begin{bmatrix} 0 & \frac{6(\underline{\tau}-1)}{\underline{\tau}+1}S_2 & 0 & 0 \\ 0 & 0 & \frac{3(\underline{d}-1)}{\underline{d}+1}S_4 & 0 \\ 0 & 0 & 0 & 0 \\ 0 & 0 & 0 & 0 \end{bmatrix},$$

$$\hat{\Omega}_{22} = \begin{bmatrix} (\tilde{\tau}+\hat{\tau})S_2 & 0 & \hat{\tau}S_2 & 0 \\ 0 & (\tilde{d}+\hat{d})S_4 & 0 & \hat{d}S_4 \\ 0 & 0 & \hat{\tau}S_2 & 0 \\ 0 & 0 & 0 & \hat{d}S_4 \end{bmatrix}, \hat{\Omega}_{23} = \begin{bmatrix} 6\vec{\tau}S_2 & 0 & \frac{6(\underline{\tau}-1)}{\underline{\tau}+1}S_2 & 0 \\ 0 & 6\vec{d}S_4 & 0 & \frac{6(\underline{d}-1)}{\underline{d}+1}S_4 \\ 6\vec{\tau}S_2 & 0 & 0 & 0 \\ 0 & 6\vec{d}S_4 & 0 & 0 \end{bmatrix},$$

$$\hat{\Omega}_{33} = diag\left\{-12\vec{\tau}S_2, -12\vec{d}S_4, -\frac{12(\underline{\tau}-1)}{\underline{\tau}+1}S_2, -\frac{12(\underline{d}-1)}{\underline{d}+1}S_4\right\},$$

$$S_2 = \lambda_1(\bar{P}_{\epsilon,\mathfrak{y}}^{n,\eth} + \bar{Q}_{\epsilon,\mathfrak{y}}^{n,\eth}), S_4 = \lambda_2(\bar{P}_{\epsilon,\mathfrak{y}}^{n,\eth} + \bar{Q}_{\epsilon,\mathfrak{y}}^{n,\eth}), \bar{P}_{\epsilon,\mathfrak{y}}^{n,\eth} = diag\left\{\bar{P}_{\epsilon,\mathfrak{y},1}^{n,\eth}, \bar{P}_{\epsilon,\mathfrak{y},2}^{n,\eth}, \bar{P}_{\epsilon,\mathfrak{y},3}^{n,\eth}\right\}, \bar{Q}_{\epsilon,\mathfrak{y}}^{n,\eth} = diag\left\{\bar{Q}_{\epsilon,\mathfrak{y},1}^{n,\eth}, \bar{Q}_{\epsilon,\mathfrak{y},2}^{n,\eth}, \bar{Q}_{\epsilon,\mathfrak{y},3}^{n,\eth}\right\},$$

$$\Psi_1 = \begin{bmatrix} \tilde{X}_1 & \tilde{X}_2 & X_3 & X_4 & 0 & 0 & 0 & 0 & 0 & 0 & 0 & \bar{\Lambda} \end{bmatrix}^T, \Psi_2 = \begin{bmatrix} \bar{\varsigma}_1\hat{X}_1 & \bar{\varsigma}_1\hat{X}_2 & 0 & 0 & 0 & 0 & 0 & 0 & 0 & 0 & 0 & \bar{\varsigma}_1\bar{\Lambda} \end{bmatrix}^T,$$

$$\Psi_3 = \begin{bmatrix} \bar{\varsigma}_{12}\hat{X}_1 & \bar{\varsigma}_{12}\hat{X}_2 & 0 & 0 & 0 & 0 & 0 & 0 & 0 & 0 & 0 & 0 \end{bmatrix}^T, \Psi_4 = \begin{bmatrix} \bar{\varsigma}_{12}\hat{X}_1 & \bar{\varsigma}_{12}\hat{X}_2 & 0 & 0 & 0 & 0 & 0 & 0 & 0 & 0 & 0 & 0 \end{bmatrix}^T,$$

$$\Psi_5 = \begin{bmatrix} \bar{\varsigma}_2\widehat{X}_1 & \bar{\varsigma}_2\widehat{X}_2 & 0 & 0 & 0 & 0 & 0 & 0 & 0 & 0 & 0 & 0 & 0 \end{bmatrix}^T, \Psi_6 = \begin{bmatrix} \sqrt{2}\bar{\varsigma}_{13}\widehat{X}_1 & 0 & 0 & 0 & 0 & 0 & 0 & 0 & 0 & 0 & 0 & 0 & 0 \end{bmatrix}^T,$$

$$\Psi_7 = \begin{bmatrix} \sqrt{2\bar{\varsigma}_{21}^2 + 2\bar{\varsigma}_{23}^2}\widehat{X}_1 & 0 & 0 & 0 & 0 & 0 & 0 & 0 & 0 & 0 & 0 & 0 & 0 \end{bmatrix}^T, \Psi_8 = \begin{bmatrix} 0 & \sqrt{2}\bar{\varsigma}_{13}\widehat{X}_2 & 0 & 0 & 0 & 0 & 0 & 0 & 0 & 0 & 0 & 0 & 0 \end{bmatrix}^T,$$

$$\Psi_9 = \begin{bmatrix} 0 & \sqrt{2\bar{\varsigma}_{12}^2 + 2\bar{\varsigma}_{23}^2}\widehat{X}_2 & 0 & 0 & 0 & 0 & 0 & 0 & 0 & 0 & 0 & 0 & 0 \end{bmatrix}^T, \Psi_{10} = \begin{bmatrix} 0 & 0 & 0 & 0 & 0 & 0 & 0 & 0 & 0 & 0 & 0 & 0 & \sqrt{(2\bar{\varsigma}_{21}^2 + 2\bar{\varsigma}_1^2 + 2\bar{\varsigma}_{13}^2)}\tilde{\Lambda} \end{bmatrix}^T,$$

$$\Psi_{11} = \begin{bmatrix} 0 & 0 & 0 & 0 & 0 & 0 & 0 & 0 & 0 & 0 & 0 & 0 & \sqrt{(2\bar{\varsigma}_{21}^2 + 2\bar{\varsigma}_1^2 + 2\bar{\varsigma}_{13}^2)}\widehat{\Lambda} \end{bmatrix}^T,$$

$$\Psi_{12} = \begin{bmatrix} 0 & 0 & 0 & 0 & 0 & 0 & 0 & 0 & 0 & 0 & 0 & 0 & \sqrt{(4\bar{\varsigma}_{13}^2 + 2\bar{\varsigma}_{23}^2 + 2\bar{\varsigma}_3^2)}\widehat{\Lambda} \end{bmatrix}^T,$$

$$\Psi_{13} = \begin{bmatrix} 0 & 0 & 0 & 0 & 0 & 0 & 0 & 0 & 0 & 0 & 0 & 0 & \sqrt{(4\bar{\varsigma}_{13}^2 + 2\bar{\varsigma}_{23}^2 + 2\bar{\varsigma}_3^2)}\breve{\Lambda} \end{bmatrix}^T,$$

$$\tilde{\Xi} = (1 + \lambda_1\underline{\tau}^2 + \lambda_1(\bar{\tau} - \underline{\tau})^2 + \lambda_2\underline{d}^2 + \lambda_2(\bar{d} - \underline{d})^2)(\bar{P}_\varepsilon^{n,f} + \bar{Q}_\varepsilon^{n,f}),$$

$$\tilde{S} = (1 + \bar{\tau} - \underline{\tau})S_1 + \frac{-4\underline{\tau} + 2}{\underline{\tau} + 1}S_2 - P_{\varrho,\mathfrak{w}}^{m,\hbar} + (\underline{\tau}^2 + (\bar{\tau} - \underline{\tau})^2)(I - \lambda_1\tilde{X}_1^T - \lambda_1\tilde{X}_1) + \tilde{H}^T(r(i+1,j))\tilde{H}(r(i+1,j)),$$

$$\bar{S} = (1 + \bar{d} - \underline{d})S_1 + \frac{-4\underline{d} + 2}{\underline{d} + 1}S_4 - Q_{\varrho,\mathfrak{w}}^{m,\hbar} + (\underline{d}^2 + (\bar{d} - \underline{d})^2)(I - \lambda_2\tilde{X}_2^T - \lambda_2\tilde{X}_2) + \tilde{H}^T(r(i,j+1))\tilde{H}(r(i,j+1)),$$

$$\tilde{X}_1 = \begin{bmatrix} \tilde{X}_1^{11} & \tilde{X}_1^{12} & \tilde{X}_1^{13} \\ 0 & \tilde{X}_1^{22} & 0 \\ 0 & \tilde{X}_1^{32} & \tilde{X}_1^{33} \end{bmatrix}, \tilde{X}_1^{11} = (\bar{P}_{\epsilon,\mathfrak{y},1}^{n,\eth} + \bar{Q}_{\epsilon,\mathfrak{y},1}^{n,\eth})A_1(r(i+1,j)) - W_{1,\zeta(i+1,j)}^{\delta(i+1,j)}C(r(i+1,j)),$$

$$\tilde{X}_1^{12} = W_{1,\zeta(i+1,j)}^{\delta(i+1,j)}(1 - \bar{\sigma}(1 - \bar{\vartheta})\Phi_{\xi(i+1,j)})C(r(i+1,j)),$$

$$\tilde{X}_1^{13} = -W_{1,\zeta(i+1,j)}^{\delta(i+1,j)}(1 - \bar{\sigma}), \tilde{X}_1^{22} = (\bar{P}_{\epsilon,\mathfrak{y},2}^{n,\eth} + \bar{Q}_{\epsilon,\mathfrak{y},2}^{n,\eth})A_1(r(i+1,j)), \tilde{X}_1^{32} = (\bar{P}_{\epsilon,\mathfrak{y},3}^{n,\eth} + \bar{Q}_{\epsilon,\mathfrak{y},3}^{n,\eth})\bar{\sigma}(1 - \bar{\vartheta})\Phi_{\xi(i+1,j)}C(r(i+1,j)),$$

$$\tilde{X}_1^{33} = (\bar{P}_{\epsilon,\mathfrak{y},3}^{n,\eth} + \bar{Q}_{\epsilon,\mathfrak{y},3}^{n,\eth})(1 - \bar{\sigma}), \tilde{X}_1^{12} = -W_{1,\zeta(i+1,j)}^{\delta(i+1,j)}\Phi_{\xi(i+1,j)}C(r(i+1,j)), \tilde{X}_1^{32} = (\bar{P}_{\epsilon,\mathfrak{y},3}^{n,\eth} + \bar{Q}_{\epsilon,\mathfrak{y},3}^{n,\eth})\Phi_{\xi(i+1,j)}C(r(i+1,j)),$$

$$\tilde{X}_2 = \begin{bmatrix} \tilde{X}_2^{11} & \tilde{X}_2^{12} & \tilde{X}_2^{13} \\ 0 & \tilde{X}_2^{22} & 0 \\ 0 & 0 & 0 \end{bmatrix}, \tilde{X}_2^{11} = (\bar{P}_{\epsilon,\mathfrak{y},1}^{n,\eth} + \bar{Q}_{\epsilon,\mathfrak{y},1}^{n,\eth})A_2(r(i,j+1)) - W_{2,\zeta(i,j+1)}^{\delta(i,j+1)}C(r(i,j+1)),$$

$$\tilde{X}_2^{12} = W_{2,\zeta(i,j+1)}^{\delta(i,j+1)}(1 - \bar{\sigma}(1 - \bar{\vartheta})\Phi_{\xi(i,j+1)})C(r(i,j+1)), \tilde{X}_2^{13} = -W_{2,\zeta(i,j+1)}^{\delta(i,j+1)}(1 - \bar{\sigma}), \tilde{X}_2^{22} = (\bar{P}_{\epsilon,\mathfrak{y},2}^{n,\eth} + \bar{Q}_{\epsilon,\mathfrak{y},2}^{n,\eth})A_2(r(i,j+1)),$$

$$X_3 = \begin{bmatrix} 0 & (\bar{P}_{\epsilon,\mathfrak{y},1}^{n,\eth} + \bar{Q}_{\epsilon,\mathfrak{y},1}^{n,\eth})A_{d1}(r(i+1,j)) & 0 \\ 0 & (\bar{P}_{\epsilon,\mathfrak{y},2}^{n,} + \bar{Q}_{\epsilon,\mathfrak{y},2}^{n,\eth})A_{d1}(r(i+1,j)) & 0 \\ 0 & 0 & 0 \end{bmatrix}, X_4 = \begin{bmatrix} 0 & (\bar{P}_{\epsilon,\mathfrak{y},1}^{n,\eth} + \bar{Q}_{\epsilon,\mathfrak{y},1}^{n,\eth})A_{d2}(r(i,j+1)) & 0 \\ 0 & (\bar{P}_{\epsilon,\mathfrak{y},2}^{n,} + \bar{Q}_{\epsilon,\mathfrak{y},2}^{n,\eth})A_{d2}(r(i,j+1)) & 0 \\ 0 & 0 & 0 \end{bmatrix}, \bar{\Lambda} = \begin{bmatrix} \bar{\Lambda}_{11} & \bar{\Lambda}_{12} & \bar{\Lambda}_{13} & \bar{\Lambda}_{14} \\ \bar{\Lambda}_{21} & \bar{\Lambda}_{22} & 0 & 0 \\ \bar{\Lambda}_{31} & 0 & \bar{\Lambda}_{33} & 0 \end{bmatrix},$$

$$\bar{\Lambda}_{11} = (\bar{P}_{\epsilon,\mathfrak{y},1}^{n,\eth} + \bar{Q}_{\epsilon,\mathfrak{y},1}^{n,\eth})E_1(r(i+1,j)) - W_{1,\zeta(i+1,j)}^{\delta(i+1,j)}\bar{\sigma}(1 - \bar{\vartheta})\Phi_{\xi(i+1,j)}D(r(i+1,j)),$$

$$\bar{\Lambda}_{12} = (\bar{P}_{\epsilon,\mathfrak{y},1}^{n,} + \bar{Q}_{\epsilon,\mathfrak{y},1}^{n,\eth})E_2(r(i,j+1)) - W_{2,\zeta(i,j+1)}^{\delta(i,j+1)}\bar{\sigma}(1 - \bar{\vartheta})\Phi_{\xi(i,j+1)}D(r(i,j+1)), \bar{\Lambda}_{13} = -W_{1,\zeta(i+1,j)}^{\delta(i+1,j)}\bar{\sigma}\bar{\vartheta}, \bar{\Lambda}_{14} = -W_{2,\zeta(i,j+1)}^{\delta(i,j+1)}\bar{\sigma}\bar{\vartheta},$$

$$\bar{\Lambda}_{21} = (\bar{P}_{\epsilon,\mathfrak{y},2}^{n,} + \bar{Q}_{\epsilon,\mathfrak{y},2}^{n,\eth})E_1(r(i+1,j)), \bar{\Lambda}_{22} = (\bar{P}_{2,\varepsilon}^{n,f} + \bar{Q}_{2,\varepsilon}^{n,f})E_2(r(i,j+1)), \bar{\Lambda}_{31} = (\bar{P}_{\epsilon,\mathfrak{y},3}^{n,} + \bar{Q}_{\epsilon,\mathfrak{y},3}^{n,\eth})\bar{\sigma}(1 - \bar{\vartheta})\Phi_{\xi(i+1,j)}D(r(i+1,j)),$$

$$\bar{\Lambda}_{33} = (\bar{P}_{\epsilon,\mathfrak{y},3}^{n,} + \bar{Q}_{\epsilon,\mathfrak{y},3}^{n,\eth})\bar{\sigma}\bar{\vartheta}, \widehat{X}_1 = \begin{bmatrix} 0 & -W_{1,\zeta(i+1,j)}^{\delta(i+1,j)}\Phi_{\xi(i+1,j)}C(r(i+1,j)) & 0 \\ 0 & 0 & 0 \\ 0 & (\bar{P}_{\epsilon,\mathfrak{y},3}^{n,} + \bar{Q}_{\epsilon,\mathfrak{y},3}^{n,\eth})\Phi_{\xi(i+1,j)}C(r(i+1,j)) & 0 \end{bmatrix}, \widehat{X}_2 = \begin{bmatrix} 0 & -W_{2,\zeta(i,j+1)}^{\delta(i,j+1)}\Phi_{\xi(i,j+1)}C(r(i,j+1)) & 0 \\ 0 & 0 & 0 \\ 0 & 0 & 0 \end{bmatrix},$$

$$\vec{\Lambda} = \begin{bmatrix} \vec{\Lambda}_{11} & \vec{\Lambda}_{12} & 0 & 0 \\ 0 & 0 & 0 & 0 \\ \vec{\Lambda}_{31} & 0 & 0 & 0 \end{bmatrix}, \vec{\Lambda}_{11} = -W_{1,\zeta(i+1,j)}^{\delta(i+1,j)}\Phi_{\xi(i+1,j)}D(r(i+1,j)), \vec{\Lambda}_{12} = -W_{2,\zeta(i,j+1)}^{\delta(i,j+1)}\Phi_{\xi(i,j+1)}D(r(i,j+1)),$$

$$\vec{\Lambda}_{31} = (\bar{P}^n_{\epsilon,\mathfrak{y},3} + \bar{Q}^{n,\eth}_{\epsilon,\mathfrak{y},3})\Phi_{\xi(i+1,j)}D(r(i+1,j)), \quad \widehat{X}_1 = \begin{bmatrix} 0 & 0 & -W^{\delta(i+1,j)}_{1,\zeta(i+1,j)} \\ 0 & 0 & 0 \\ 0 & 0 & \bar{P}^n_{\epsilon,\mathfrak{y},3} + \bar{Q}^{n,\eth}_{\epsilon,\mathfrak{y},3} \end{bmatrix}, \quad \widehat{X}_2 = \begin{bmatrix} 0 & 0 & -W^{\delta(i,j+1)}_{2,\zeta(i,j+1)} \\ 0 & 0 & 0 \\ 0 & 0 & \bar{P}^n_{\epsilon,\mathfrak{y},3} + \bar{Q}^{n,\eth}_{\epsilon,\mathfrak{y},3} \end{bmatrix},$$

$$\tilde{\Lambda} = \begin{bmatrix} -W^{\delta(i+1,j)}_{1,\zeta(i+1,j)}\Phi_{\xi(i+1,j)}D(r(i+1,j)) & 0 & 0 & 0 \\ 0 & 0 & 0 & 0 \\ (\bar{P}^n_{\epsilon,\mathfrak{y},3} + \bar{Q}^{n,\eth}_{\epsilon,\mathfrak{y},3})\Phi_{\xi(i+1,j)}D(r(i+1,j)) & 0 & 0 & 0 \end{bmatrix}, \quad \hat{\Lambda} = \begin{bmatrix} 0 & -W^{\delta(i,j+1)}_{2,\zeta(i,j+1)}\Phi_{\xi(i,j+1)}D(r(i,j+1)) & 0 & 0 \\ 0 & 0 & 0 & 0 \\ 0 & 0 & 0 & 0 \end{bmatrix},$$

$$\widehat{\Lambda} = \begin{bmatrix} 0 & 0 & -W^{\delta(i+1,j)}_{1,\zeta(i+1,j)} & 0 \\ 0 & 0 & 0 & 0 \\ 0 & 0 & (\bar{P}^n_{\epsilon,\mathfrak{y},3} + \bar{Q}^{n,\eth}_{\epsilon,\mathfrak{y},3}) & 0 \end{bmatrix}, \quad \check{\Lambda} = \begin{bmatrix} 0 & 0 & 0 & -W^{\delta(i,j+1)}_{2,\zeta(i,j+1)} \\ 0 & 0 & 0 & 0 \\ 0 & 0 & 0 & 0 \end{bmatrix},$$

then the dynamic filtering error systems (equation (9)) are asymptotically mean-square stability with a disturbance attenuation level γ. Furthermore, the asynchronous filtering gain matrices are given by

$$K^{\delta(i+1,j)}_{1,\zeta(i+1,j)} = (\bar{P}^n_{\epsilon,\mathfrak{y},1} + \bar{Q}^{n,\eth}_{\epsilon,\mathfrak{y},1})^{-1}W^{\delta(i+1,j)}_{1,\zeta(i+1,j)}, \quad K^{\delta(i,j+1)}_{2,\zeta(i+1,j)} = (\bar{P}^n_{\epsilon,\mathfrak{y},1} + \bar{Q}^{n,\eth}_{\epsilon,\mathfrak{y},1})^{-1}W^{\delta(i,j+1)}_{2,\zeta(i+1,j)}$$

Proof: It should be noted that due to the large number of nonlinear elements in equation (39), it is required to separate certain variables and transform equation (39) into LMIs. Therefore, we define the matrices with the following structure

$$\bar{P}^{n,\eth}_{\epsilon,\mathfrak{y}} = diag\left\{\bar{P}^{n,\eth}_{\epsilon,\mathfrak{y},1}, \bar{P}^{n,\eth}_{\epsilon,\mathfrak{y},2}, \bar{P}^{n,\eth}_{\epsilon,\mathfrak{y},3}\right\},$$

$$\bar{Q}^{n,\eth}_{\epsilon,\mathfrak{y}} = diag\left\{\bar{Q}^{n,\eth}_{\epsilon,\mathfrak{y},1}, \bar{Q}^{n,\eth}_{\epsilon,\mathfrak{y},2}, \bar{Q}^{n,\eth}_{\epsilon,\mathfrak{y},3}\right\} \tag{44}$$

where $\bar{P}^{n,\eth}_{\epsilon,\mathfrak{y},i}, \bar{Q}^{n,\eth}_{\epsilon,\mathfrak{y},i}, (\in \{1,2,3\})$ are the positive definite symmetric matrices with appropriate dimensions. In addition, according to equations (13) and (14), it is not difficult to deduce the following relationship holds

$$\bar{P}^{n,\eth}_{\epsilon,\mathfrak{y},i} = \sum_{\mathfrak{y}=1}^{\mathcal{M}_g}\sum_{\epsilon=1}^{\mathcal{M}_s}\sum_{n=1}^{\mathcal{M}_s}\sum_{\eth=1}^{\mathcal{M}_g} \pi_{mn}\mu^n_{\hbar\eth}\jmath_{\varrho\epsilon}o^\epsilon_{\mathfrak{w}\mathfrak{y}}P^{n,\eth}_{\epsilon,\mathfrak{y},i},$$

$$\bar{Q}^{n,\eth}_{\epsilon,\mathfrak{y},i} = \sum_{\mathfrak{y}=1}^{\mathcal{M}_g}\sum_{\epsilon=1}^{\mathcal{M}_s}\sum_{n=1}^{\mathcal{M}_s}\sum_{\eth=1}^{\mathcal{M}_g} \pi_{mn}\mu^n_{\hbar\eth}\jmath_{\varrho\epsilon}o^\epsilon_{\mathfrak{w}\mathfrak{y}}Q^{n,\eth}_{\epsilon,\mathfrak{y},i}, \quad i \in \{1,2,3\}$$

$$\tag{45}$$

In what follows, we set $S_2 = \lambda_1(\bar{P}^{n,\eth}_{\epsilon,\mathfrak{y}} + \bar{Q}^{n,\eth}_{\epsilon,\mathfrak{y}})$ and $S_4 = \lambda_2(\bar{P}^{n,\eth}_{\epsilon,\mathfrak{y}} + \bar{Q}^{n,\eth}_{\epsilon,\mathfrak{y}})$, substitute equation (45) into equation (39), and select $W^{\delta(i+1,j)}_{1,\zeta(i+1,j)} = (\bar{P}^{n,\eth}_{\epsilon,\mathfrak{y},1} + \bar{Q}^{n,\eth}_{\epsilon,\mathfrak{y},1})K^{\delta(i+1,j)}_{1,\zeta(i+1,j)}$ and $W^{\delta(i,j+1)}_{2,\zeta(i,j+1)} = (\bar{P}^{n,\eth}_{\epsilon,\mathfrak{y},1} + \bar{Q}^{n,\eth}_{\epsilon,\mathfrak{y},1})K^{\delta(i,j+1)}_{2,\zeta(i,j+1)}$, then the following asynchronous filter gain can be calculated

$$K^{\delta(i+1,j)}_{1,\zeta(i+1,j)} = (\bar{P}^{n,\eth}_{\epsilon,\mathfrak{y},1} + \bar{Q}^{n,\eth}_{\epsilon,\mathfrak{y},1})^{-1}W^{\delta(i+1,j)}_{1,\zeta(i+1,j)}, \quad K^{\delta(i,j+1)}_{2,\zeta(i,j+1)} = (\bar{P}^{n,\eth}_{\epsilon,\mathfrak{y},1} + \bar{Q}^{n,\eth}_{\epsilon,\mathfrak{y},1})^{-1}W^{\delta(i,j+1)}_{2,\zeta(i,j+1)}$$

The proof is thus completed.

Numerical Simulations

Taking into account the partial differential equation for an industrial heating exchange process as follows

$$\frac{\partial \hbar(x,t)}{\partial x} + \frac{\partial \hbar(x,t)}{\partial t} = -a^{r(x,t)}_0\hbar(x,t) - a^{r(x,t)}_1\hbar(x,t-\tau(t)) \tag{46}$$

where $\hbar(x,t)$ is the temperature function related to the space $x \in [0 \quad X]$ and the time $t \in [0 \quad T]$, and $\tau(t) > 0$ indicates the time delays. Besides, on account of the failure and recovery of chemical reactor components and the impact of subsystem connection changes, the system structure often appears the switching process subject to Markov stochastic process. Thus, the real number $a^{r(i,j)}_0$ and $a^{r(i,j)}_1$ with Markov jumping properties is utilized to indicate the exchange coefficients.

Define $\hbar(i,j) = \hbar(i\Delta x, j\Delta t), r(i,j) = r(i\Delta x, j\Delta t)$, which yields

$$\frac{\partial \hbar(x,t)}{\partial x} \approx \frac{\hbar(i\Delta x, j\Delta t) - \hbar((i-1)\Delta x, j\Delta t)}{\Delta x}, \quad \frac{\partial \hbar(x,t)}{\partial t} \approx$$

$$\frac{\hbar(i\Delta x, j\Delta t) - \hbar(i\Delta x, (j-1)\Delta t)}{\Delta t}, \quad \hbar(x,t) \approx \hbar(i,j)$$

Moreover, equation (46) can be reformulated as follows

$$\hbar(i,j+1) = (1 - \frac{\Delta t}{\Delta x} - a^{r(i,j)}_0\Delta t)\hbar(i,j) + \frac{\Delta t}{\Delta x}\hbar(i-1,j) - a^{r(i,j)}_1\Delta t\hbar(i,j-\tau(j))$$

Therefore, the following FM-II model can be generated by developing the initial partial differential equation

$$x(i+1,j+1) = A_1(r(i+1,j))x(i+1,j) + A_2(r(i,j+1))x(i,j+1) + A_{d1}(r(i+1,j))x(i+1,j-\tau(j)) + A_{d2}(r(i,j+1))x(i-d(i),j+1)$$

where

$$A_1(r(i,j)) = \begin{bmatrix} 0 & 1 \\ 0 & 0 \end{bmatrix}, A_2(r(i,j)) = \begin{bmatrix} 0 & 0 \\ \frac{\Delta t}{\Delta x} & 1 - \frac{\Delta t}{\Delta x} - a^{r(i,j)}_0\Delta t \end{bmatrix},$$

$$A_{d1}(r(i,j)) = \begin{bmatrix} 0 & 0 \\ 0 & -a^{r(i,j)}_1\Delta t \end{bmatrix}, \text{ and } A_{d2}(r(i,j)) = 0.$$

Consider the following parameters according to the literature (Ghous et al., 2015)

$$\Delta t = 0.1, \Delta x = 0.33, a^1_0 = 3, a^2_0 = 3.5, a^1_1 = 1.2, a^2_1 = 1.4$$

consequently, the subsystems 1 and 2 can be defined utilizing the following parameters:

Subsystem 1:

$$A_11 = \begin{bmatrix} 0 & 1 \\ 0 & 0 \end{bmatrix}, A_21 = \begin{bmatrix} 0 & 0 \\ 0.3 & 0.4 \end{bmatrix}, A_{d1}1 = \begin{bmatrix} 0 & 0 \\ 0 & -0.12 \end{bmatrix},$$

$$A_{d2}1 = 0, E_11 = \begin{bmatrix} -0.4 \\ 0.2 \end{bmatrix}, \text{ and } E_21 = \begin{bmatrix} 0.65 \\ -0.2 \end{bmatrix}.$$

Subsystem 2

$$A_12 = \begin{bmatrix} 0 & 1 \\ 0 & 0 \end{bmatrix}, A_22 = \begin{bmatrix} 0 & 0 \\ 0.3 & 0.35 \end{bmatrix}, A_{d1}2 = \begin{bmatrix} 0 & 0 \\ 0 & -0.14 \end{bmatrix},$$

$$A_{d2}2 = 0, E_12 = \begin{bmatrix} 0.1 \\ -0.4 \end{bmatrix}, \text{ and } E_22 = \begin{bmatrix} 0.3 \\ 0.2 \end{bmatrix}.$$

Subsequently, we choose the transition probability matrices of system mode and filter mode as follows

$$\chi = \begin{bmatrix} 0.7 & 0.3 \\ 0.4 & 0.6 \end{bmatrix}, \phi^1 = \begin{bmatrix} 0.6 & 0.4 \\ 0.5 & 0.5 \end{bmatrix}, \phi^2 = \begin{bmatrix} 0.4 & 0.6 \\ 0.6 & 0.4 \end{bmatrix}.$$

We assume that the transition probability matrix of SCP is $\mathfrak{s} = \begin{bmatrix} 0.5 & 0.5 \\ 0.5 & 0.5 \end{bmatrix}$. Besides, we set $\bar{o}^1 = \begin{bmatrix} 0.35 & 0.65 \\ 0.4 & 0.6 \end{bmatrix}$ and $\bar{o}^2 = \begin{bmatrix} 0.6 & 0.4 \\ 0.55 & 0.45 \end{bmatrix}$. Moreover, we set the initial conditions of state as $x(i,j) = [1.9 \cos(j) \sin(i) \quad 2.1 \cos(i-1) \sin(j)]^T$ for $i \in [0 \quad 40]$ and $j = 0$, $x(i,j) = [2.3 \sin(i) \cos(j+1) \quad 1.8 \cos(i+1) \sin(j)]^T$ for $i = 0$ and $j \in [1 \quad 50]$, and the initial conditions of filter as $\hat{x}(i,0) = \hat{x}(0,j) = [0 \quad 0]^T$ for $i, j \in [0, 50]$.

The external disturbance with bounded energy is chosen as follows

$$\omega(i,j) = \begin{cases} 0.3 \cos(0.6(i+j)) & i,j \in [1 \quad 30] \\ 0 & otherwise \end{cases}$$

Besides, assume the hybrid cyber attacks occur at instant $i,j \in [20 \quad 40]$, and $\bar{\vartheta} = 0.2$ and $\bar{\sigma} = 0.85$, and the following false data signal is selected

$$\upsilon(i,j) =$$
$$\begin{cases} [0.4 \sin(0.45(i+j)) \quad 0.3 \cos(0.3(i+j))]^T i,j \in [20 \quad 40] \\ 0 & otherwise \end{cases}$$

Then, by using the LMI toolbox in MATLAB, the corresponding filtering gain matrices can be obtained as follows

$$K_{1,1}^1 = \begin{bmatrix} 1.3824 & -0.0270 \\ -0.0429 & 0.3905 \end{bmatrix}, K_{2,1}^1 = \begin{bmatrix} 0.4955 & -0.0270 \\ -0.0154 & 0.3913 \end{bmatrix},$$

$$K_{1,2}^1 = \begin{bmatrix} 1.5926 & -0.0032 \\ -0.0053 & 0.3139 \end{bmatrix}, K_{2,2}^1 = \begin{bmatrix} 0.4245 & -0.0034 \\ -0.0016 & 0.3335 \end{bmatrix},$$
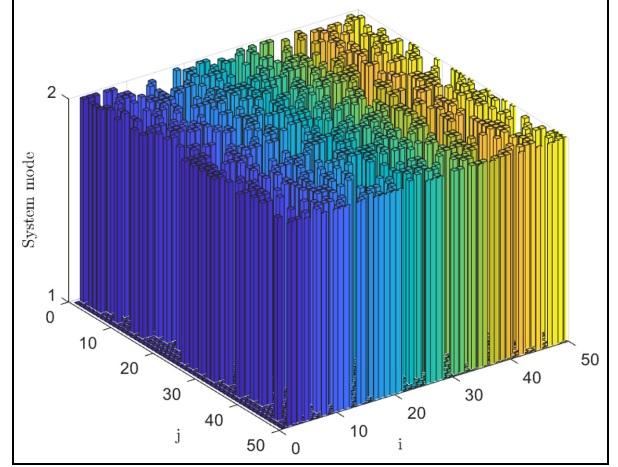
Figure 2. System mode evolution.
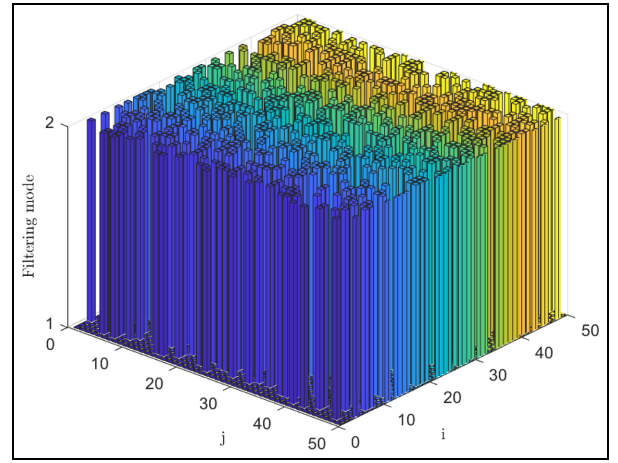
Figure 3. Filter mode evolution.

$$K_{1,1}^2 = \begin{bmatrix} 1.1764 & -0.0031 \\ -0.0073 & 0.5116 \end{bmatrix}, K_{2,1}^2 = \begin{bmatrix} 0.6214 & -0.0054 \\ -0.0073 & 0.8879 \end{bmatrix},$$

$$K_{1,2}^2 = \begin{bmatrix} 1.5108 & 0.0014 \\ -0.0066 & -0.1167 \end{bmatrix}, K_{2,2}^2 = \begin{bmatrix} 0.4832 & -0.0038 \\ -0.0066 & -0.3091 \end{bmatrix}.$$

Figures 2 and 3 show the system and filter mode evolution subject to the transition probability matrix χ and $\phi^{r(i+1,j+1)}$, respectively. It is easy to see the mode jumps of systems and filter are not always consistent from Figures 2 and 3. Figures 4 and 5, respectively, describe the sensor scheduling sequence under the SCP and the estimated sensor communication sequence, where the "1" denotes sensor 1 obtains the access permission, and the "2" denotes sensor 2 obtains the access permission. Figure 6 displays the occurrence of hybrid attacks at instant $i,j \in [20 \quad 40]$. Figures 7 and 8 show the $x(i,j)$ and $\hat{x}(i,j)$. Figures 9 and 10 display the first component of $e(i,j)$ and the second component of $e(i,j)$, respectively. It is easy to see from Figures 7 to 10 that the estimation and filtering error fluctuate at instant $i,j \in [1 \quad 40]$ owing to disturbance and
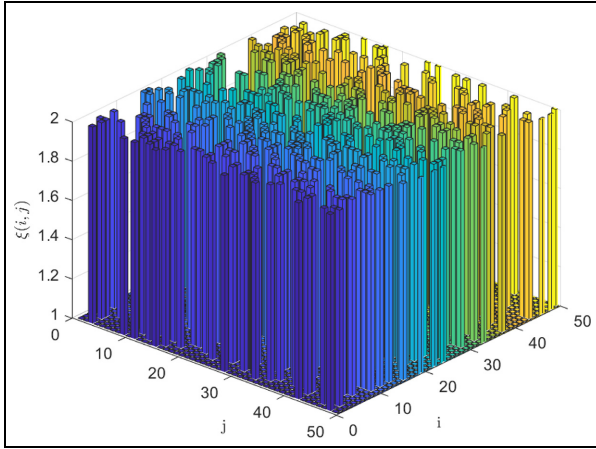
Figure 4. Sensor communication sequence under the SCP.

Figure 5. The estimated sensor communication sequence.

Figure 6. The hybrid cyber-attack case.

Figure 7. The trajectory of the states $x_1(i,j)$ and $\hat{x}_1(i,j)$.

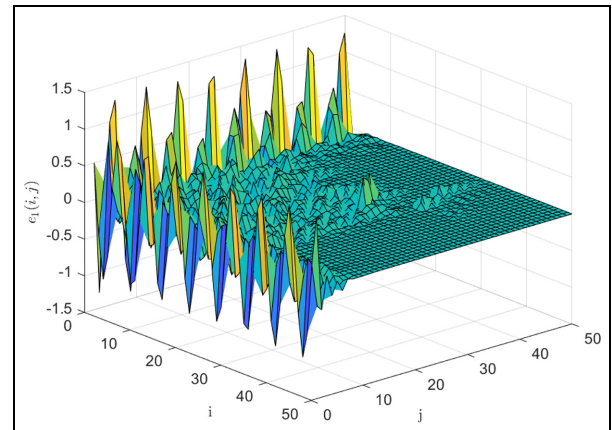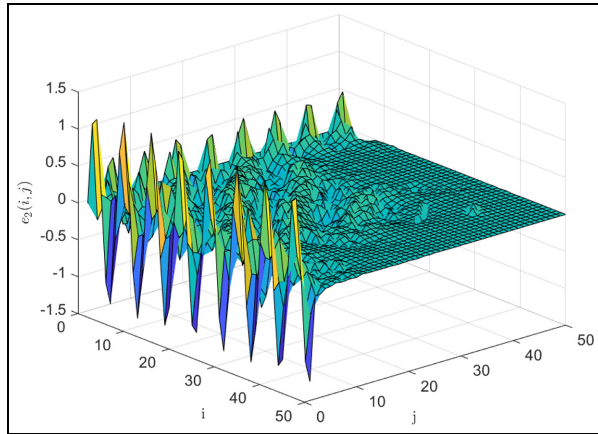**Figure 8.** The trajectory of the states $x_2(i,j)$ and $\hat{x}_2(i,j)$.

Figure 9. The trajectory of the first component of dynamic filtering error $e_1(i,j)$.

Figure 10. The trajectory of the second component of dynamic filtering error $e_2(i, j)$.

Table 1. The disturbance attenuation performance γ^* comparison between the synchronous H_∞ filtering algorithm and asynchronous H_∞ filtering algorithm

Performance	Synchronous H_∞ filtering algorithm	Asynchronous H_∞ filtering algorithms
γ^*	2.6221	3.1547

Table 2. The filtering gain matrices solving time of synchronous H_∞ filtering algorithm.

$l...j$	1 (seconds)	2 (seconds)	...	50 (seconds)
1	0.462	0.0501	...	0.0334
2	0.0417	0.0482	...	0.0319
...	...	...	...	...
50	0.0284	0.0261	...	0.0201

hybrid cyber attacks. Furthermore, Figures 7 to 10 exhibit that estimated state can commendably track the evolution of the actual state, and the developed asynchronous filter design method shows excellent track performance.

Finally, the influence of the synchronous H_∞ filtering algorithm and the asynchronous H_∞ filtering algorithm on filtering performance is further investigated. Table 1 depicts the optimal disturbance attenuation performance of synchronous and asynchronous H_∞ filtering algorithm. It is worth noting that the synchronous H_∞ filtering algorithm tends to produce better filtering performance compared with the asynchronous one under the same conditions, mainly due to the underlying prerequisite that the synchronous algorithm has a priori knowledge about the system operation (including the mode switching of the subsystem and communication sensor nodes). In this paper, Theorem 3 is solved with a Core i5 CPU 2.50 GHz computer by virtue of the MATLAB LMI toolbox. The computation time of the synchronous H_∞ filtering algorithm at each sampling shift instant (i, j) is displayed in Table 2, and the total computation time is 52.7431 seconds. In addition, the total computation time of the asynchronous H_∞ filtering algorithm to obtain filtering gain matrices is approximately 0.40 seconds, which conserves a lot of computing time and resources compared with the synchronous H_∞ filtering algorithm.

Conclusion

The asynchronous filtering problem for 2D MJSs under hybrid cyber attacks and the SCP has been addressed in this research. Due to the communication network's restricted bandwidth, only one sensor can transmit measurement information through the communication network at each shift instant, and the SCP strategy determines which sensor is chosen. Besides, the impact of stochastic hybrid cyber attacks on filtering performance is also considered. Then, a comprehensive 2D MJSs incorporating SCP and hybrid cyber attacks are developed, and the asynchronous filter with a special structure is proposed to satisfy the operating mode that remains asynchronization with both the system mode and the communication scheduling mode. Subsequently, the sufficient criteria conditions are obtained to ensure the robust H_∞ mean-square stability with the H_∞ disturbance attenuation level γ. Moreover, the conservativeness of the obtained criterion is reduced with the help of the 2D summation inequality approach. Finally, a simulation example is provided to demonstrate the validity of the presented asynchronous filtering algorithm. The developed asynchronous filtering algorithm has certain application potential for long-distance transmission and industrial heat exchange processes described by networked 2D systems. In addition, another queuing DoS attack model based on the 2D systems framework deserves further investigation.

Declaration of conflicting interests

The author(s) declared no potential conflicts of interest with respect to the research, authorship, and/or publication of this article.

ORCID iD

Zhiwen Wang https://orcid.org/0000-0002-5425-0705

Data availability statement

Data sharing is not applicable to this article as no data sets were generated or analyzed during this study.

References

Ali MS, Tajudeen MM, Rajchakit GP, et al. (2023) Adaptive event-triggered pinning synchronization control for complex networks with random saturation subject to hybrid cyber-attacks. *International Journal of Adaptive Control and Signal Processing* 37(8): 2041–2062.

Cao JM, Zhou JF, Chen J, et al. (2021) Sliding mode control for discrete-time systems with randomly occurring uncertainties and nonlinearities under hybrid cyber attacks. *Circuits, Systems, and Signal Processing* 40(12): 5864–5885.

Chelliq EH, Alfidi M and Chalh Z (2023) Admissibility and robust $H\infty$ controller design for uncertain 2D singular discrete systems with interval time-varying delays. *Optimal Control Applications and Methods* 44(5): 2476–2503.

Cheng GF and Liu H (2023) Asynchronous finite-time $H\infty$ filtering for linear neutral semi-Markovian jumping systems under hybrid cyber attacks. *Journal of the Franklin Institute* 360(3): 1495–1522.

Cheng P, Wu D, He SP, et al. (2023) Asynchronous control for 2D Markov jump cyber-physical systems against aperiodic denial-of-service attacks. *Science China Information Sciences* 66(7): 195–209.

Duan ZX, Ghous I, Xia YQ, et al. (2020) H-infinity control problem of discrete 2D switched mixed delayed systems using the improved Lyapunov–Krasovskii functional. *International Journal of Control Automation and Systems* 18(8): 2075–2087.

Duo WL, Zhou MC and Abusorrah A (2022) A survey of cyber attacks on Cyber Physical Systems: Recent advances and challenges. *IEEE/CAA Journal of Automatica Sinica* 9(5): 784–800.

Fornasini E and Marchesini G (1978) Doubly indexed dynamical systems: State models and structural properties. *Mathematics of Control, Signals, and Systems* 12(1): 59–72.

Ghous I, Duan ZX, Akhtar J, et al. (2019) Robust stabilization of uncertain 2D discrete-time delayed systems using sliding mode control. *Journal of the Franklin Institute* 356(16): 9407–9731.

Ghous I, Xiang ZY and Karimi HR (2015) State feedback $H\infty$ control for 2D switched delay systems with actuator saturation in the second FM model. *Circuits, Systems, and Signal Processing* 34(7): 2167–2192.

Hamdan MM, Mahmoud MS and Baroudi UA (2022) Event-triggering control scheme for discrete time Cyberphysical Systems in the presence of simultaneous hybrid stochastic attacks. *ISA Transactions* 122: 1–12.

He WM, Li S, Ahn CK, et al. (2022) Sampled-data stabilization of stochastic interconnected cyber-physical systems under DoS attacks. *IEEE Systems Journal* 16(3): 3844–3854.

Hien LV and Trinh H (2017) Observer-based control of 2D Markov jump systems. *IEEE Transactions on Circuits and Systems II: Express Briefs* 64(11): 1322–1326.

Hien LV and Trinh H (2018) On reachable set estimation of two-dimensional systems described by the Roesser model with time-varying delays. *International Journal of Robust and Nonlinear Control* 28(1): 227–246.

Hu M-J, Park JH, Cheng J, et al. (2023) Security fuzzy control of nonlinear Semi-Markov switching systems with event-based mechanism and hybrid cyber-attacks. *IEEE Transactions on Systems, Man, and Cybernetics: Systems* 53(9): 1–12.

Hu ZJ, Liu Shi C, Luo WS, et al. (2022) Resilient distributed fuzzy load frequency regulation for power systems under cross-layer random Denial-of-Service attacks. *IEEE Transactions on Cybernetics* 52(4): 2396–2406.

Kurek JE (1985) The general state-space model for a two-dimensional linear digital system. *IEEE Transactions on Automatic Control* 30(6): 600–602.

Li DH, Liang JL and Wang F (2020) Robust $H\infty$ filtering for 2D systems with RON under the stochastic communication protocol. *IET Control Theory & Applications* 18(14): 2795–2804.

Li S, Zou WC, Guo J, et al. (2022a) Consensus of switched nonlinear multiagent systems subject to cyber attacks. *IEEE Systems Journal* 16(3): 4423–4432.

Li W, Niu YG, Cao ZR, et al. (2022b) Sliding mode control for multi-agent systems under stochastic communication protocol. *International Journal of Robust and Nonlinear Control* 32(13): 7522–7535.

Li XH and Ye D (2023) Security-based event-triggered fuzzy control for multiarea power systems under cross-layer DoS attacks. *IEEE Transactions on Circuits and Systems I: Regular Papers* 70(7): 2995–3004.

Li ZC, Xu HL, Lin ZP, et al. (2023) Event-triggered robust distributed output feedback model predictive control for nonlinear MASs against false data injection attacks. *ISA Transactions* 141: 197–211.

Lian Z, Shi P, Lim C-C, et al. (2023) Fuzzy-model-based lateral control for networked autonomous vehicle systems under hybrid cyber-attacks. *IEEE Transactions on Cybernetics* 53(4): 2600–2609.

Liu JL, Zhang N, Li Y, et al. (2021) $H\infty$ filter design for discrete-time networked systems with adaptive event-triggered mechanism and hybrid cyber attacks. *Journal of the Franklin Institute* 358(17): 9325–9345.

Liu XH, Deng FQ, Zeng PY, et al. (2023) Sampled-data resilient control for stochastic nonlinear CPSs under DoS attacks. *International Journal of Systems Science* 51(5): 1165–1170.

Lv XY, Niu YG and Cao ZR (2023) Sliding mode control for uncertain 2D FM-II systems under stochastic scheduling. *IEEE Transactions on Cybernetics*. Epub ahead of print 26 April. DOI: 10.1109/TCYB.2023.3267406

Mao DC, Niu YG, Li JR, et al. (2024) Security sliding mode control for networked control system under multi-channel Markovian hybrid cyber-attacks. *International Journal of Robust and Nonlinear Control* 34: 773–792.

Men YZ and Sun J (2023) Asynchronous control of 2D Semi-Markov jump systems under actuator saturation. *IEEE Transactions on Circuits and Systems II: Express Briefs* 70(11): 4118–4122.

Niu Y, Song Y, Zhang B, et al. (2023) Dynamic output feedback model predictive control for asynchronous Markovian jump systems under try-once-discard protocol. *International Journal of Robust and Nonlinear Control* 33(17): 10789–10823.

Peng D and Nie HM (2021) Abel lemma-based finite-sum inequality approach to stabilization for 2D time-varying delay systems. *Asian Journal of Control* 23(3): 1394–1406.

Roesser RP (1975) A discrete state-space model for linear image processing. *IEEE Transactions on Automatic Control* 20(1): 1–10.

Song J, Wang Z, Niu YG, et al. (2023) Co-design of dissipative deconvolution filter and round-robin protocol for networked 2D digital systems: Optimization and application. *IEEE Transactions on Systems, Man, and Cybernetics: Systems* 53(10): 1–13.

Sun Y, Ju YM, Ding DR, et al. (2023) Distributed $H\infty$ filtering of replay attacks over sensor networks. *ISA Transactions* 141: 113–120.

Tan MC, Song ZQ and Zhang XM (2022) Robust leader-following consensus of cyber-physical systems with cyber attack via sampled-data control. *ISA Transactions* 109: 61–71.

Tandon A, Dhawan A and Tiwari M (2019) Optimal guaranteed cost control of uncertain 2D discrete state-delayed systems described by the Roesser model via memory state feedback. *Transactions of the Institute of Measurement and Control* 41(1): 285–294.

Tao Y-Y and Wu ZG (2022) Asynchronous control of two-dimensional dimensional Markov jump Roesser systems: An event-triggering strategy. *IEEE Transactions on Network Science and Engineering* 9(4): 2278–2289.

Tobagi FA (1980) Multiaccess protocols in packet communication systems. *IEEE Transactions on Communications* 28(4): 468–488.

Wang F, Liang JL and Wang ZD (2020) Robust finite-horizon filtering for 2D systems with randomly varying sensor delays. *IEEE Transactions on Systems, Man, and Cybernetics: Systems* 50(1): 220–232.

Wu ZG and Tao Y-Y (2022) Asynchronous guaranteed cost control of 2D Markov jump Roesser system. *IEEE Transactions on Cybernetics* 52(12): 13063–13072.

Wu ZG, Shen Y, Shi P, et al. (2019) H∞ control for 2D Markov jump systems in Roesser model. *IEEE Transactions on Automatic Control* 64(1): 427–432.

Xing W, Zhao XD, Zhao N, et al. (2023) Denial-of-service attacks on cyber-physical systems with two-hop networks under round-robin protocol. *Systems & Control Letters* 180: 105589.

Xu Y, Lv WJ, Lin WQ, et al. (2022) Quevedo DE. On extended state estimation for nonlinear uncertain systems with round-robin protocol. *Automatica* 138: 110154.

Yan Y, Su LL and Gupta V (2020) Analysis of two-dimensional feedback systems over networks using dissipativity. *IEEE Transactions on Automatic Control* 65(8): 3241–3255.

Yang M and Zhai JY (2023) Observer-based dynamic event-triggered secure control for nonlinear networked control systems with false data injection attacks. *Information Sciences* 644: 119262.

Yang RN, Ding SH and Zheng WX (2024) Event-triggered sliding mode control for 2D Roesser model with mismatched disturbance. *Automatica* 159: 111355.

Yang RN, Li LL and Su XJ (2020) Finite-region dissipative dynamic output feedback control for 2D FM systems with missing measurements. *Information Sciences* 514: 1–14.

Zhang YJ, Hu J, Zhang HX, et al. (2023) Adaptive sliding mode control for uncertain nonlinear switched system under probabilistic replay attacks: The output feedback approach. *International Journal of Adaptive Control and Signal Processing* 37(8): 2216–2232.

Zhao R, Zuo ZQ and Wang YJ (2022) Event-triggered control for switched systems with Denial-of-Service attack. *IEEE Transactions on Automatic Control* 67(8): 4077–4090.

Zhu KQ, Wang Z, Han Q-L, et al. (2023) Distributed set-membership fusion filtering for nonlinear 2D systems over sensor networks: An encoding-decoding scheme. *IEEE Transactions on Cybernetics* 53(1): 416–427.

Recursive filtering for time-varying systems with mixed time-delays subject to stochastic communication protocol and dynamic quantization effects

Chaoqun Zhu[1], Pan Zhang[1], Zibao Lu[2], Bin Yang[1] and Zhiwen Wang[1] (iD)

Abstract
The recursive filtering problem for a class of time-varying systems with mixed time-delays subject to stochastic communication protocol and dynamic quantization effects is discussed in this article. It is assumed that only one sensor can transmit the measured information to the filter at each sampling period, and the selected sensor is determined by the scheduling strategy of the stochastic communication protocol. Based on this assumption, the dynamic upper bound of the filtering error covariance is derived for time-varying systems with mixed time-delays and an underlying scheduling protocol by solving two Riccati difference equations in each sampling period. Then, the trace of the upper bound is minimized to obtain the filter gain with the desired filtering performance. Subsequently, the boundedness issue of the filtering error covariance is investigated. Sufficient conditions are given to ensure that the filtering error covariance is exponentially bounded in the mean square. Finally, numerical examples are given to demonstrate the effectiveness and superiority of the proposed algorithm.

Introduction

Filtering problems have received much attention in the control and signal processing communities for several decades.[1–4] The main purpose of filtering is to estimate the internal state of the system according to the measurement output contaminated by noise signals. At present, filtering has been widely used in aircraft tracking, smart grids, and bioprocess monitoring. Based on these applications, several filtering methods are proposed according to different noise characteristics and performance indices, such as recursive filtering,[5,6] H_∞ filtering,[7,8] and set-membership filtering.[9,10] Among them, the recursive filtering method has the advantages of easy implementation and high estimation accuracy,[11,12] which has garnered increasing research interest. In general, three recursive schemes are commonly used to solve the state estimation problem, namely, classical Kalman filtering, extended Kalman filtering, and unscented Kalman filtering. Recursive filtering is essentially a state estimation method based on

optimizations. Specifically, the main idea of recursive filtering algorithms is to obtain the upper bound of the filtering error covariance and provide a filter to minimize the upper bound at each sampling period.[13,14]

In networked systems, the design of recursive filtering is challenged due to network-induced communication limitations, such as time-delays, quantization effects, and medium access constraints. Applying the traditional recursive filtering algorithm directly to the networked systems will inevitably deteriorate the filtering performance and even lead to the divergence of filtering errors. Therefore, it is very significant to

[1]College of Electrical and Information Engineering, Lanzhou University of Technology, Lanzhou, China
[2]School of Physics and Electronic Information, Anhui Normal University, Wuhu, China

Corresponding author:
Zhiwen Wang, College of Electrical and Information Engineering, Lanzhou University of Technology, Lanzhou 730050, China.
Email: wwwangzhiwen@yeah.net

investigate the recursive filtering design problem under various communication limitations. In the practical control processes, the system information must be quantized before being transferred through the network. Due to the influence of network bandwidth and calculation accuracies, quantization errors will inevitably occur and be one of the main network-induced constraints that degrade the performance of networked systems. In recent years, several methods have been proposed to address the signal quantization of networked systems. Such methods include but are not limited to uniform quantizer,[15] logarithmic quantizer,[16] and dynamic quantizer.[17] Essentially, both uniform quantizer and logarithmic quantizer can be classified as static quantization technologies. Compared with them, the dynamic quantification mechanism has proven to be the most effective in mitigating performance degradation, and some control problems concerning dynamic quantization have been deeply investigated; more information and references are provided in the literature.[18,19] However, according to the results obtained by consulting the literature, the recursive filtering design problem of networked systems affected by the dynamic quantization has not attracted enough attention, which motivates us to fill this gap.

It is worth noting that in many underlying investigations on the filtering problem of networked systems, an implicit assumption is that there are adequate communication channels between the sensors and the filter, and all the sensors can simultaneously access the communication network to transmit the measured information to the filter during each sampling period. In many practical systems, however, it is quite unrealistic to implement such a communication scheme because simultaneous multiple access over a limited-bandwidth network would result in unavoidable data collisions. One important aspect to take into account in such a situation is implementing communication scheduling. To date, three communication protocols have been employed to arrange the network access sequence of sensors to effectively prevent data conflict, namely, the weighted try-once-discard (WTOD) protocol,[20,21] the round-robin (RR) protocol,[22,23] and the stochastic communication (SC) protocol.[24,25] Among the above communication protocols, the WTOD and RR communication protocols belong to the category of deterministic scheduling schemes, while the SC protocol is a communication scheduling scheme in a stochastic manner. Under the scheduling of the SC protocol, the network nodes can access the network channels randomly for data transmission. The SC protocol can be widely used in many industrial control networks, such as the carrier sense multiple access (CSMA) protocol for Ethernet and the ALOHA protocol for wireless local area networks.

Compared with the filtering methods without protocol scheduling, the introduction of communication protocols, especially SC protocols, would certainly increase the difficulties of filtering design and performance analysis. In such a situation, it is necessary to adopt effective measures to reduce the adverse effect of SC protocol on recursive filtering performance. To date, some preliminary results concerning the recursive filtering problem for networked systems with SC protocols have been presented in Wang and colleagues.[26–28] The recursive filtering problem is discussed in Alsaadia et al.[26] for complex networks under SC protocol. The upper bound of the estimation error covariance is derived by solving two sets of matrix difference equations, and then the performance analysis of the developed state estimator is provided in terms of the boundedness. In Zou et al.,[28] the recursive filtering algorithm is proposed for networked time-varying systems with a scheduling protocol governed by the Bernoulli process, and the boundedness issue of the corresponding filtering error covariance is investigated.

On the contrary, the time-delay phenomenon commonly exists in various practical control systems, which is one of the main causes of system performance degradation or even instability. In recent years, the recursive filtering design problem of time-delayed systems has attracted much attention from researchers; more information and references are provided in the literature.[29–32] Although the above studies have performed a great deal of useful exploration, there are still many problems that have not been fully investigated for the recursive filtering issue of time-delayed systems. In most existing literature, a fundamental assumption is that time-delays always occur simply in a fixed manner. However, with the rapid development of information technology, the complexity of the system structure and time-delay mechanism is gradually increasing. In this context, various time-delay models have been proposed to better characterize different system properties. Among various categories of time-delays, mixed time-delays have recently drawn growing research interest due to their practical insights into characterizing the spatial nature of signal transmission delays in some complex systems. It is worth noting that a popular general rule is that the systems with mixed time-delays have more difficulty obtaining the desired filtering performance than the dynamical systems with fixed delays under the same conditions, which has generated preliminary results; more information and references are provided in Wang and colleagues.[33–35] Unfortunately, for the filtering design problem of systems with mixed time-delays, the available results mostly employ H_∞ filtering and set-membership filtering methods. To the best of the author's knowledge, considering both dynamic quantization mechanism and SC protocol to schedule network resources has not been reported for the recursive filtering design of time-delayed networked systems, in addition to the analysis of the influence of time-delay intervals and weight coefficients on the filtering performance. Therefore, the main motivation of this article is to investigate the recursive filtering problem for

networked systems with mixed time-delays subject to the SC scheduling protocol and dynamic quantization effects.

In response to the aforementioned discussion, the recursive filtering problem for a class of time-varying systems with mixed time-delays subject to SC protocol and dynamic quantization effects is investigated in this article. The main contributions of this article can be summarized as follows: (1) a description model of networked systems with mixed time-delays limited by the SC protocol and dynamic quantization effects is obtained, and a recursive structure filter is proposed based on this model; (2) for the established augmented system with mixed time-delays, the dynamic upper bound of filtering error covariance is obtained by solving two Riccati equations, and the filter gain is derived by minimizing the upper bound; and (3) based on the results of (2), the issue of boundedness for the filtering error dynamics is further discussed, and the influence of the delay interval and weight coefficients on the filtering performance is investigated.

The rest of this article is organized as follows. In section "Problem formulation and preliminaries," the problem description and preliminaries are presented. In section "Main results," a recursive filtering algorithm is proposed for time-delayed networked systems with the impacts of the SC protocol and network-induced constraints. Illustrative examples are provided in section "Main results" to demonstrate the effectiveness and superiority of the proposed results. Finally, this article is concluded, and future research directions are discussed in section "Conclusion."

Notation

The notation used throughout this article is fairly standard. R^n denotes the n-dimensional Euclidean space, and $P > 0 (P \geqslant 0)$ indicates that it is real symmetric and positive definite (semidefinite). G^T, G^{-1}, and tr$\{G\}$ represent the transpose, the inverse, and the trace of the matrix G, respectively. $diag\{\rho_1, \ldots, \rho_n\}$ stands for a diagonal matrix with the indicated elements on the diagonal and zeros elsewhere. Pr$\{\xi\}$ is the occurrence probability of event ξ. E$\{\zeta\}$ indicates the expectation of the stochastic variable ζ. $\|A\|$ refers to the norm of a matrix A defined by $\|A\| = \sqrt{trace(A^T A)}$. The Kronecker delta function $\delta(\psi)$ takes the value 1 for $\psi = 0$ and 0 otherwise.

Problem formulation and preliminaries

Model description

In this section, we present the model of a networked system subject to the SC protocol and dynamic quantization effects, whose structure is depicted in Figure 1.
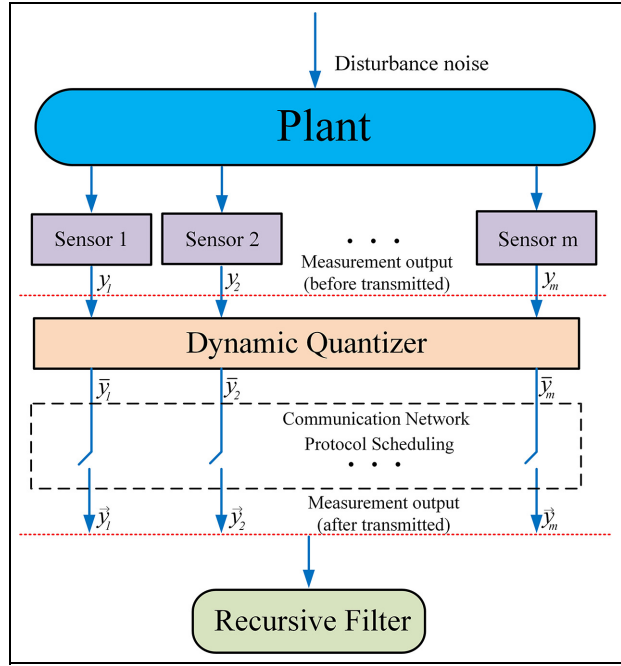
Figure 1. State estimation problem for NCSs.

We consider the discrete networked system with mixed time-delays described by

$$\begin{cases} x_{k+1} = A_k x_k + B_k x_{k-\tau_1} + F_k \sum_i^{\tau_2} \mu_i x_{k-i} + D_k \omega_k \\ y_k = C_k x_k + \nu_k \\ x(i) = \phi(i) \qquad\qquad -\max\{\tau_1, \tau_2\} \leqslant i \leqslant 0 \end{cases}$$

$$(1)$$

where $x_k \in R^n$ represents the state vector that cannot be directly observed, and $y_k \in R^m$ is the measured output before transmission through the communication network. $\omega_k \in R^p$ and $\nu_k \in R^q$ are the process noises and measurement noises, which are zero-mean Gaussian white noise processes with the covariances $Q_k > 0$ and $R_k > 0$, respectively. The positive integers τ_1 and τ_2 are the known constant time-delays, μ_i $(1 \leqslant i \leqslant \tau_2)$ represents the weight coefficients, and $\phi(i)$ is the initial conditions of the system. A_k, B_k, C_k, D_k, and F_k are the known time-varying matrices with appropriate dimensions, respectively.

Dynamic quantizer

Now, we can consider the effects of the signal quantization. In this article, we adopt the following dynamic quantizer[17]

$$\begin{cases} \varepsilon_{k+1} = A_d \varepsilon_k + B_{d1} y_k + B_{d2} \bar{y}_k \\ \bar{y}_k = \rho(C_d \varepsilon_k + D_d y_k) \end{cases}$$

$$(2)$$

where A_d, B_{d1}, B_{d2} C_d, and D_d are the constant matrices with appropriate dimensions. $\varepsilon_k \in R^n$ and $\bar{y}_k \in V^m$ are

the state vector and output vector of the dynamic quantizer, respectively, and $V \subset R$ is the discrete set on which each output takes values (V^m is the direct product of the m sets). The function $\rho : R^m \to V^m$ is the nearest-neighbor static quantizer. The initial state is given as $\varepsilon_0 = 0$. We let γ be the considered quantization level, and the following relationship holds

$$\| \rho(\zeta) - \zeta \|^2 \leqslant \frac{m\gamma^2}{4}, \ (\forall \zeta \in R^m) \tag{3}$$

Remark 1. Due to the necessity that the measurement output is transmitted through the digital channel, signal quantization inevitably occurs in network-based control systems. The selection of a quantizer is very important to reduce the impact of quantization errors on the system performance. In this article, we employ the dynamic quantizer with the structure equation (2), which is composed of a time-invariant filter and a static quantization function. Consequently, the selected dynamic quantizer is more flexible and can effectively mitigate performance degradation compared with static quantizers (e.g. uniform quantizer and logarithmic quantizer). To date, the dynamic quantizer has been successfully used in many industrial control fields; more information and references are provided in Takahashi et al.[19] and Maity and Tsiotras[36] and references therein.

The SC protocol

For networked systems with a large number of sensors, the communication between the sensors and the filter is scheduled by a certain network protocol to avoid data collisions. Moreover, we will introduce the scheduling protocol of SC. Without loss of generality, we assume that only one sensor is allowed to access the network channel according to the underlying scheduling protocol and let $\sigma(k) \in \{1, 2, \ldots, m\}$ denote which sensor is selected to communicate with the filter at each transmission period.

Under the scheduling of the SC protocol, it is assumed that $\sigma(k) \in \{1, 2, \ldots, m\}$ can be modeled by a discrete-time Markov process and corresponding transition probability is given as follows

$$\Pr\{\sigma(k) = i\} = \pi_i(k), \ \Pr\{\sigma(k+1) = j | \sigma(k) = i\} = \pi_{ij}(k)$$

where $\pi_i(k)$ is the probability that the ith sensor is selected to access the communication network at the time instant k, and $\pi_{ij}(k)$, $i, j \in \{1, 2, \ldots, m\}$, which denotes the transition probability from sensor i to sensor j, satisfying $\sum_{j=1}^{m} \pi_{ij}(k) = 1$.

Problem formulation

Next, we aim to address the recursive filtering design problem for networked systems with mixed time-delays, signal quantization, and SC protocol. Furthermore, we will consider the measurement signal received by the filter. As shown in Figure 1, the measurement output before quantizing can be characterized as

$$y_k = \begin{bmatrix} y_{1,k}^T & y_{2,k}^T & \cdots & y_{m,k}^T \end{bmatrix}^T$$

where $y_{i,k}$ denotes the measurement output of the ith sensor at the time instant k. We let

$$\bar{y}_k = \begin{bmatrix} \bar{y}_{1,k}^T & \bar{y}_{2,k}^T & \cdots & \bar{y}_{m,k}^T \end{bmatrix}^T, \vec{y}_k = \begin{bmatrix} \vec{y}_{1,k}^T & \vec{y}_{2,k}^T & \cdots & \vec{y}_{m,k}^T \end{bmatrix}^T$$

denote the output of the dynamic quantizer and the measurement output after transmission through the network, respectively. Then, the eventual measured output $\vec{y}_{i,k}$ of the ith sensor, which is received by the filter with a zero-order holder, can be formulated as

$$\vec{y}_{i,k} = \begin{cases} \bar{y}_{i,k} & \textit{if } i = \sigma(k) \\ \vec{y}_{i,k-1} & \textit{otherwise} \end{cases} \tag{4}$$

According to the updating rule of the measurement output equation (4), the following equation is obtained

$$\vec{y}_k = \Phi_{\sigma(k)} \bar{y}_k + (I - \Phi_{\sigma(k)}) \vec{y}_{k-1} \tag{5}$$

with the initial state $\vec{y}_s = Y(s)$ for $s < 0$, where $Y(s)$ is a known vector, and

$$\Phi_i = diag\{ \delta(i-1) \quad \delta(i-2) \quad \cdots \quad \delta(i-m) \} \tag{6}$$

where $\delta(\cdot) \in \{0, 1\}$ is the Kronecker delta function.

The model of time-delayed networked systems with dynamic quantization and SC scheduling protocol can be attained by substituting equations (2) and (5) into equation (1) and introducing an augmented state variable

$$\tilde{x}_k = \begin{bmatrix} x_k^T & \varepsilon_k^T & \vec{y}_{k-1}^T \end{bmatrix}^T$$

which results the augmented system model as follows

$$\begin{cases} \tilde{x}_{k+1} = \tilde{A}_k \tilde{x}_k + \tilde{B}_k \tilde{x}_{k-\tau_1} + \tilde{F}_k \sum_{i=1}^{\tau_2} \mu_i \tilde{x}_{k-i} + \tilde{D}_k w_k \\ \vec{y}_k = \tilde{C}_k \tilde{x}_k + \tilde{E}_k w_k \end{cases} \tag{7}$$

where $\varphi_k = \rho(C_d \varepsilon_k + D_d y_k) - C_d \varepsilon_k - D_d y_k$, and

$$\tilde{A}_k = \begin{bmatrix} A_k & 0 & 0 \\ (B_{d1} + B_{d2}D_d)C_k & A_k + B_{d2}C_d & 0 \\ \Phi_{\sigma(k)}D_dC_k & \Phi_{\sigma(k)}C_d & I - \Phi_{\sigma(k)} \end{bmatrix},$$

$$\tilde{B}_k = \begin{bmatrix} B_k & 0 & 0 \\ 0 & 0 & 0 \\ 0 & 0 & 0 \end{bmatrix} \tilde{F}_k = \begin{bmatrix} F_k & 0 & 0 \\ 0 & 0 & 0 \\ 0 & 0 & 0 \end{bmatrix}, w_k = \begin{bmatrix} \omega_k \\ \nu_k \\ \varphi_k \end{bmatrix}$$

$$\tilde{C}_k = [\Phi_{\sigma(k)}D_dC_k \quad \Phi_{\sigma(k)}C_d \quad I - \Phi_{\sigma(k)}],$$

$$\tilde{D}_k = \begin{bmatrix} D_k & 0 & 0 \\ 0 & B_{d1} + B_{d2}D_d & B_{d2} \\ 0 & \Phi_{\sigma(k)}D_d & \Phi_{\sigma(k)} \end{bmatrix}$$

$$\tilde{E}_k = [0 \quad \Phi_{\sigma(k)}D_d \quad \Phi_{\sigma(k)}]$$

It is obvious that the quantization error φ_k satisfies

$$\|\varphi_k\|^2 \le \frac{m\gamma^2}{4}$$

which yields

$$Q_k = E\{w_k w_k^T\} \le diag\left\{Q_k, R_k, \frac{\gamma^2 I}{4}\right\} = \tilde{Q}_k$$

For networked systems with mixed time-delays, the following recursive filter is employed

$$\begin{cases} \hat{x}_{k+1|k} = \tilde{A}_k\hat{x}_{k|k} + \tilde{B}_k\hat{x}_{k-\tau_1|k-\tau_1} + \tilde{F}_k\sum_{i=1}^{\tau_2}\mu_i\hat{x}_{k-i|k-i} \\ \hat{x}_{k+1|k+1} = \hat{x}_{k+1|k} + K_{k+1}(\vec{y}_{k+1} - \tilde{C}_{k+1}\hat{x}_{k+1|k}) \end{cases}$$

$$(8)$$

where $\hat{x}_{k+1|k}$ is the one-step prediction of $\tilde{x}_k$ at the instant time k, $\hat{x}_{k|k}$ is the estimate of $\tilde{x}_k$ at the instant time k, and K_{k+1} is the filter gain to be determined.

We define the one-step prediction error $e_{k+1|k} \stackrel{\Delta}{=} \tilde{x}_{k+1} - \hat{x}_{k+1|k}$ and one-step prediction error covariance $P_{k+1|k} = E\{e_{k+1|k}e_{k+1|k}^T\}$. Similarly, we define the filtering error $e_{k+1|k+1} \stackrel{\Delta}{=} \tilde{x}_{k+1} - \hat{x}_{k+1|k+1}$, and the filtering error covariance $P_{k+1|k+1} = E\{e_{k+1|k+1}e_{k+1|k+1}^T\}$. Based on equations (7) and (8), the following equations are developed

$$e_{k+1|k} = \tilde{A}_k e_{k|k} + \tilde{B}_k e_{k-\tau_1|k-\tau_1} + \tilde{F}_k\sum_{i=1}^{\tau_2}\mu_i e_{k-i|k-i} + \tilde{D}_k w_k$$

$$(9)$$

$$e_{k+1|k+1} = (I - K_{k+1}\tilde{C}_{k+1})e_{k+1|k} - K_{k+1}\tilde{E}_{k+1}w_{k+1}$$

$$(10)$$

Main results

In this section, we aim to develop a unified framework to deal with the recursive filtering design problem for

networked systems with mixed time-delays. Before proceeding further, we introduce the following lemmas, which will be helpful in subsequent developments.

Lemma 1. We assume there is a stochastic process $V(\xi_k)$ as well as real numbers $\underline{v}, \bar{v}, \varpi > 0$ and $0 < \alpha \le 1$ such that[31]

$$\underline{v}\|\xi_k\|^2 \le V(\xi_k) \le \bar{v}\|\xi_k\|^2$$

and

$$E\{V(\xi_{k+1})|\xi_k\} - V(\xi_k) \le -\alpha V(\xi_k) + \varpi$$

Then, the stochastic process is exponentially bounded in the mean square.

Lemma 2. For $0 \le k \le N$, we assume $X = X^T \ge 0$, $Y = Y^T \ge 0$, and $h_k(X) = h_k^T(X)$, if[32]

$$h_k(X) \le h_k(Y), \forall X \le Y$$

then the solutions W_k and M_k to

$$W_{k+1} = h_k(W_k), \quad M_{k+1} \le h_k(M_k), \quad M_0 \le W_0$$

satisfy $W_{k+1} \ge M_{k+1}$.

Lemma 3. Given the appropriate dimension matrices M, N, X, and P, the following equations hold[32]

$$\frac{\partial tr(MXN)}{\partial X} = M^T N^T, \quad \frac{\partial tr(MX^T N)}{\partial X} = NM$$

$$\frac{\partial tr\left((MXN)P(MXN)^T\right)}{\partial X} = 2MM^T XNPN^T$$

Now, we are in the position of deriving the dynamic upper bound of prediction error covariance and filtering error covariance.

Upper bound of filtering error covariance

Theorem 1. For the networked system with mixed time-delays equation (7), we provide the positive scalars η_i ($i = 1, 2, \ldots, 8$). For $k \ge 0$, there exists a positive definite symmetric matrix $\vartheta_{k|k}$ that satisfies the following two difference equations

$$\vartheta_{k+1|k} = (1 + \eta_1 + \eta_2 + \eta_3)\tilde{A}_k\vartheta_{k|k}\tilde{A}_k^T$$
$$+ (1 + \eta_2^{-1} + \eta_4^{-1} + \eta_6) \times \frac{1}{2}(\eta_7 + \eta_7^{-1})\sum_{i=1}^{\tau_2}\mu_i\sum_{i=1}^{\tau_2}$$
$$\mu_i\tilde{F}_k\vartheta_{k-i|k-i}\tilde{F}_k^T + (1 + \eta_1^{-1} + \eta_4 + \eta_5)\tilde{B}_k\vartheta_{k-\tau_1|k-\tau_1}\tilde{B}_k^T$$
$$+ (1 + \eta_3^{-1} + \eta_5^{-1} + \eta_6^{-1})\tilde{D}_k\tilde{Q}_k\tilde{D}_k^T + (1 + \eta_1^{-1} + \eta_4 + \eta_5)$$
$$\tilde{B}_k\vartheta_{k-\tau_1|k-\tau_1}\tilde{B}_k^T + (1 + \eta_3^{-1} + \eta_5^{-1} + \eta_6^{-1})\tilde{D}_k\tilde{Q}_k\tilde{D}_k^T$$

$$(11)$$

and

$$\vartheta_{k+1|k+1} = (1 + \eta_8)(I - K_{k+1}\tilde{C}_{k+1})\vartheta_{k+1|k}$$
$$\times (I - K_{k+1}\tilde{C}_{k+1})^T + (1 + \eta_8^{-1})K_{k+1}\tilde{E}_{k+1}\tilde{Q}_{k+1}\tilde{E}_{k+1}^T K_{k+1}^T \tag{12}$$

if the initial state satisfies $\vartheta_{0|0} \geqslant P_{0|0}$. Then, the $\vartheta_{k+1|k+1}$ is an upper bound of $P_{k+1|k+1}$.

Proof. The proof is provided in Appendix 1.

In Theorem 1, we have obtained dynamic upper bounds of the prediction error and filtering error covariance. Subsequently, we derive the filtering gain matrix by minimizing the proposed upper bounds.

Theorem 2. For the networked system with mixed time-delays equation (7), we provide the positive scalars η_i ($i = 1, 2, \ldots, 8$). For $k \geqslant 0$, the filter gain K_{k+1} that minimizes the upper bound of the filtering error covariance is given by

$$K_{k+1} = (1 + \eta_8)\vartheta_{k+1|k}\tilde{C}_{k+1}^T \Omega^{-1} \tag{13}$$

where $\vartheta_{k+1|k}$ is determined by equation (11), and

$$\Omega = \tilde{C}_{k+1}\vartheta_{k+1|k}\tilde{C}_{k+1}^T + (1 + \eta_8^{-1})\tilde{E}_{k+1}\tilde{Q}_{k+1}\tilde{E}_{k+1}^T$$

Proof. The proof is provided in Appendix 2.

Boundedness analysis of filtering error dynamics

In engineering practice, the norm of the system matrix, measurement noises, and process noises are usually bounded due to energy constraints, which indicates that the following assumption is reasonable.

Assumption 1. The following matrix relationships hold for every $k \geqslant 0$ and $i \in \{1, 2, \ldots, m\}$

$$\underline{a}^2 I \leqslant \tilde{A}_k \tilde{A}_k^T \leqslant \bar{a}^2 I, \quad \underline{b}^2 I \leqslant \tilde{B}_k \tilde{B}_k^T \leqslant \bar{b}^2 I, \quad \underline{c}^2 I \leqslant \tilde{C}_k \tilde{C}_k^T \leqslant \bar{c}^2 I$$
$$\underline{d}^2 I \leqslant \tilde{D}_k \tilde{D}_k^T \leqslant \bar{d}^2 I, \quad \underline{e}^2 I \leqslant \tilde{E}_k \tilde{E}_k^T \leqslant \bar{e}^2 I, \quad \underline{f}^2 I \leqslant \tilde{F}_k \tilde{F}_k^T \leqslant \bar{f}^2 I$$
$$\underline{q}^2 I \leqslant \tilde{Q}_k \tilde{Q}_k^T \leqslant \bar{q}^2 I, \quad \underline{w} I \leqslant w_k^T w_k \leqslant \bar{w} I, \quad \underline{p} I \leqslant \text{tr}\{\vartheta_{k|k}\} \leqslant \bar{p} I$$

where $\underline{a}$, $\bar{a}$, $\underline{b}$, $\bar{b}$, $\underline{c}$, $\bar{c}$, $\underline{d}$, $\bar{d}$, $\underline{e}$, $\bar{e}$, $\underline{f}$, $\bar{f}$, $\underline{q}$, $\bar{q}$, $\underline{w}$, $\bar{w}$, $\underline{p}$, and $\bar{p}$ are the positive real numbers.

According to the above assumptions, we further investigate the boundedness of the filtering error dynamics obtained by Theorems 1 and 2.

Theorem 3. For the networked system with mixed time-delays equation (7), we provide the positive scalars η_i ($i = 1, 2, \ldots, 9$). If Assumption 1 holds, the filter gain K_{k+1} equation (13) can guarantee that the filtering error dynamics is exponentially bounded in the mean square.

Proof. The proof is provided in Appendix 3.

Remark 2. In Theorem 3, we have discussed the exponentially mean-square boundedness of the filtering error covariance, which shows that the boundedness is closely related to the matrix norm of networked systems and the upper bound of the filtering error covariance. According to Theorem 3, if the system matrix norm and filtering error covariance have upper bounds, the filtering error dynamics will eventually guarantee the exponentially bounded in the mean square.

In terms of Theorems 1 and 2, we summarize the structure diagram of the recursive filtering algorithm as follows.

Remark 3. The aim of the proposed recursive filtering algorithm is to obtain the upper bounds of the one-step error covariance and filtering error covariance by solving two Riccati difference equations in each sampling period and then minimize the trace of $\vartheta_{k|k}$ to derive optimal time-varying filtering gain matrix. According to the summarized structure diagram of the recursive filtering algorithm, utilizing MATLAB to obtain the filtering gain at each sampling time is simple. Of course, if the variation range of the mixed delay (τ_1 and τ_2) is large, it will increase the difficulty of the equation derivation to a certain extent, but it will not increase the computational complexity for solving the filtering gain matrix in MATLAB.

Remark 4. The recursive filtering problem for a class of time-varying systems with mixed time-delays subject to SC protocol and dynamic quantization effects is discussed in this article. In virtue of equation (7), it is easy to understand in what manner the SC protocol and the dynamic quantizer influence the dynamic behavior of the system. For example, $\Phi_{\sigma(k)}$ and φ_k represent the influence of the SC protocol and the dynamic quantization effect, respectively. All the above-obtained conclusions are influenced by the parameters $\Phi_{\sigma(k)}$ and φ_k. Similarly, we can generalize the treatment processing in this article to the investigation of recursive filtering algorithms with other network-induced constraints. First, the parameters characterizing the network-induced constraints are incorporated into the augmentated system matrix $\tilde{A}_k$ by the modeling approach similar to the one used in this article. Then, the corresponding system control theory and Kalman filtering technology are utilized to construct the filtering error system, and subsequently, the recursive filtering gains can be obtained by the similar derivation steps of Theorems 1 and 2 (Figure 2).
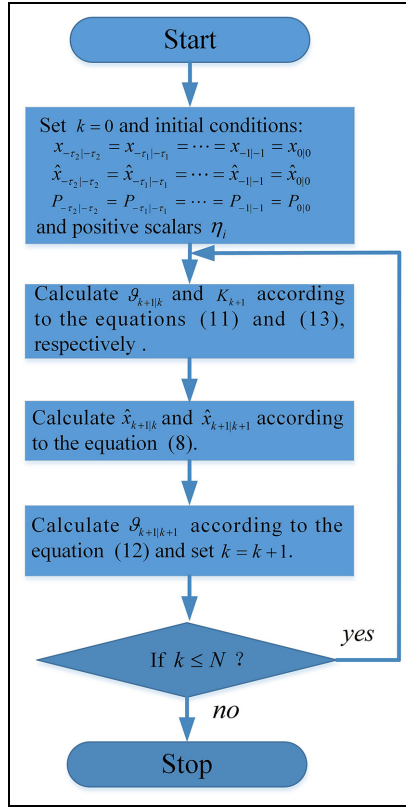
Figure 2. Structure diagram of the recursive filtering algorithm.

Numerical simulation

In this section, two simulation examples are provided to illustrate the effectiveness and superiority of the presented recursive filtering algorithm for networked systems with mixed time-delays. In Example 1, the effectiveness of the proposed filtering algorithm is demonstrated, and the influence of the time-delay interval and weight coefficients μ_i on the filtering performance is analyzed. Then, we compare the developed filtering algorithm with the H_∞ robust filtering algorithm of Zou et al.[37] for the networked direct current (DC) servo system in Example 2, which shows that our recursive filtering algorithm has better filtering performance.

Example 1. We consider a class of networked systems with mixed time-delays in the form of equation (1), and the following parameter matrices are given

$$A_k = \begin{bmatrix} 0.65 + 0.1\sin(0.4\pi k) & -0.8 + 0.1\cos(0.2\pi k) \\ 0.23 & 0.62 \end{bmatrix},$$

$$B_k = \begin{bmatrix} 0.08 & -0.4\sin(0.2\pi k) \\ 0.06 & 0.05 \end{bmatrix}$$

$$C_k = \begin{bmatrix} 0.90 & -0.25\sin(0.4\pi k) \\ 0.20 & 0.44 \end{bmatrix}, \quad D_k = \begin{bmatrix} 0.70 & 0.18 \\ 0.20 & 0.32 \end{bmatrix}$$

$$F_k = \begin{bmatrix} -1.00 & 0.00 \\ 0.00 & -1.00 \end{bmatrix}, \quad \tau_1 = 1, \ \tau_2 = 5$$

$$A_d = \begin{bmatrix} 0.5 & 0 \\ -0.2 & -0.5 \end{bmatrix}, \quad B_{d1} = \begin{bmatrix} -0.3 & -0.2 \\ -0.2 & -0.3 \end{bmatrix}$$

$$B_{d2} = \begin{bmatrix} 0.3 & 0.2 \\ 0.2 & 0.3 \end{bmatrix}, \quad C_d = \begin{bmatrix} 1.2 & 0 \\ 1.2 & 0 \end{bmatrix}, \quad D_d = \begin{bmatrix} 1 & 0 \\ 1 & 0 \end{bmatrix}$$

$$\mu_1 = \mu_2 = \mu_3 = \mu_4 = \mu_5 = 0.1$$

In the simulation, we take the initial state of the system as $x_0 = \begin{bmatrix} 4.2 & -4.3 \end{bmatrix}^T$, $\phi(-1) = \phi(-2) = \phi(-3) = \phi(-4) = \phi(-5) = \begin{bmatrix} 4.2 & -4.3 \end{bmatrix}^T$, and initial estimation as $\hat{x}_{-5|-5} = \hat{x}_{-4|-4} = \hat{x}_{-3|-3} = \hat{x}_{-2|-2} = \hat{x}_{-1|-1} = \hat{x}_{0|0} = \begin{bmatrix} 3.4 & -3.4 \end{bmatrix}^T$. The upper bounds of the initial covariance are set as $\vartheta_{0|0} = \vartheta_{-1|-1} = \vartheta_{-2|-2} = \vartheta_{-3|-3} = \vartheta_{-4|-4} = \vartheta_{-5|-5} = 3.4I$, and positive scalars η_i $(i = 1, 2, \ldots, 8)$ are set as $\eta_1 = \eta_2 = \eta_3 = \eta_6 = \eta_7 = 0.2 = 0.2$, $\eta_4 = \eta_8 = 0.1$, and $\eta_5 = 0.3$. In addition, we assume that $Q_k = 0.5I$, $R_k = 0.5I$. The quantization level γ is set to 0.8; thus

$$\tilde{Q}_k = diag\{0.5, 0.5, 0.5, 0.5, 0.32, 0.32\}$$

The transition probability of the SC protocol is set to

$$\pi = \begin{bmatrix} 0.5 & 0.5 \\ 0.4 & 0.6 \end{bmatrix}$$

Then, according to Theorem 2, the time-varying filtering gain $\{K_{k+1}\}$ under the SC protocol is obtained in Table 1.

The simulation results are shown in Figures 3–9. Figure 3 depicts the communication sequence subject to the SC scheduling protocol, where "1" represents that sensor 1 obtains the access authority to the communication network; similarly, "2" represents that sensor 2 obtains the access authority to the communication network. In such a communication protocol, which sensor obtains the network channel is determined by a Markov chain with the given transition probability. State trajectories of $x_1(k)$ and its estimate $\hat{x}_1(k)$, and state trajectories $x_2(k)$ and its estimate $\hat{x}_2(k)$ are given in Figures 4 and 5, respectively. It can be found from Figures 4 and 5 that the recursive filtering algorithm proposed in this article can effectively track the state trajectories of the system.

To analyze the influence of the delay interval and parameter μ_i on the filtering performance, we introduce the mean square error (MSE) of the state estimation, which is defined as follows

$$\text{MSE}(k) = \left(\frac{1}{k}\right) \sum_{j=1}^{k} \sum_{i=1}^{2} \left(x_i^j(k) - \hat{x}_i^j(k)\right)^2$$

Table 1. Values of K_{k+1} under the SC protocol.

k	1		2		...	49	
K_{k+1}	$\begin{bmatrix} 0.115 & 0 \\ -0.029 & 0 \\ 0.349 & 0 \\ 0.161 & 0 \\ 0.406 & 0 \\ 0 & 1.05 \end{bmatrix}$		$\begin{bmatrix} -0.048 & 0.099 \\ 0.067 & -0.032 \\ 0.134 & 0.346 \\ 0.459 & 0.173 \\ 1.05 & 0 \\ 0.388 & 0.352 \end{bmatrix}$		...	$\begin{bmatrix} -0.002 & 0.001 \\ -0.001 & 0 \\ -0.326 & -0.02 \\ -0.085 & 0.70 \\ -0.079 & 1.05 \\ 1.05 & 0.41 \end{bmatrix}$	
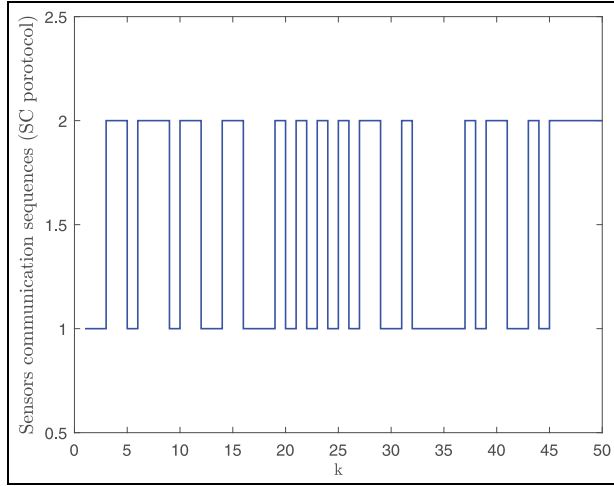
Figure 3. Sensors communication sequence under the SC protocol.
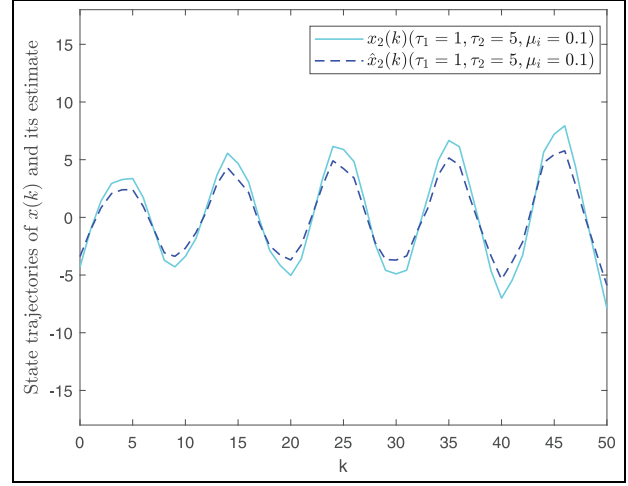
Figure 5. State trajectories of $x_2(k)$ and its estimate $\hat{x}_2(k)$.
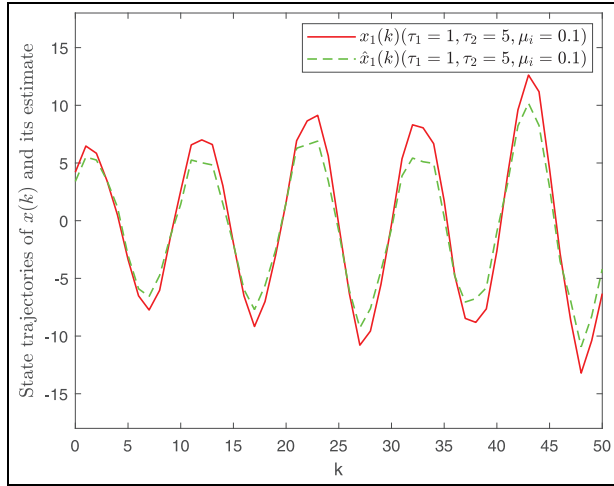
Figure 4. State trajectories of $x_1(k)$ and its estimate $\hat{x}_1(k)$.
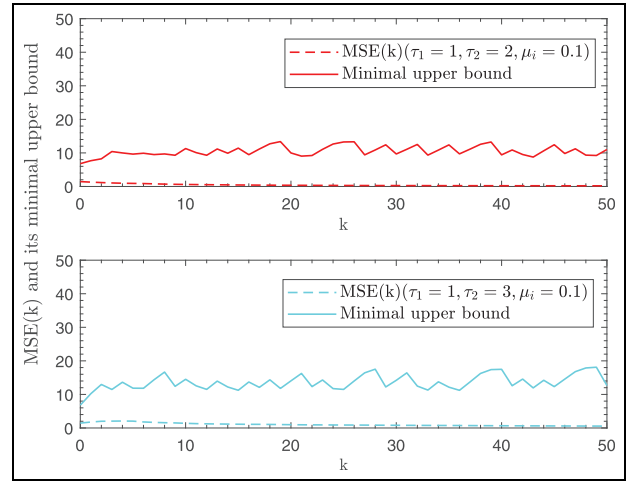
Figure 6. MSE(k) and the trace of the minimal upper bound with delay intervals ($\tau_1 = 1, \tau_2 = 2$) and ($\tau_1 = 1, \tau_2 = 3$).

where i represents the dimension of the state vector, and k represents the number of samples. Then, we let the weight coefficients be $\mu_i = 0.1$ and increase the delay interval to analyze the influence of its amplitude on the filtering performance. Similarly, the impact of the weight coefficients μ_i on the filtering performance is investigated by setting the delay interval as $\tau_1 = 1$

and $\tau_2 = 3$. The obtained results are shown in Figures 6–9 and Tables 2–5. Figures 6 and 7 and Tables 2 and 3 show the relationship of the delay interval and the filtering performance. It can be seen that when limiting $\mu_i = 0.1$, MSE(k) will increase as the delay interval gradually increases, and the trace of its upper bound has the same varying tendency. Then,
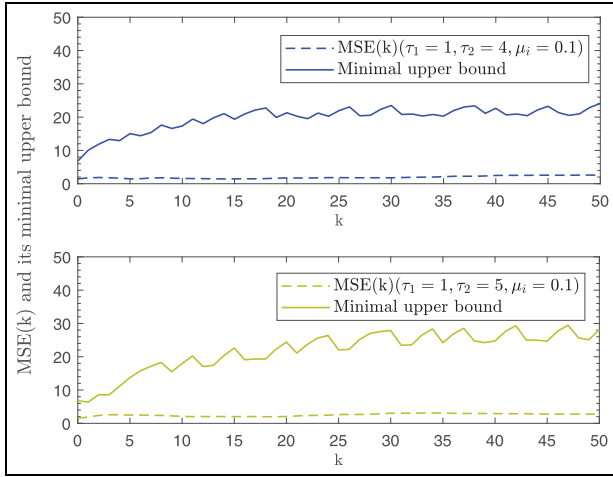
Figure 7. MSE(k) and the trace of the minimal upper bound with delay intervals ($\tau_1 = 1, \tau_2 = 4$) and ($\tau_1 = 1, \tau_2 = 5$).
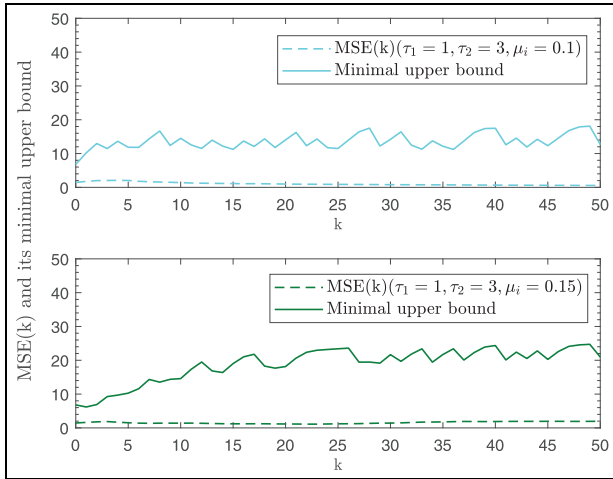
Figure 8. MSE(k) and the trace of the minimal upper bound with the weight coefficients $\mu_i = 0.1$ and $\mu_i = 0.15$.

Figures 8 and 9 and Tables 4 and 5 depict the relationship of the weight coefficients μ_i and the filtering performance, which indicate that if the delay interval is invariant ($\tau_1 = 1, \tau_2 = 3$) and μ_i is increased, MSE(k) and the trace of its minimal upper bound will increase simultaneously. We can also infer from Figures 6–9 that MSE(k) is always constrained by the trace of its upper bound. The simulation results confirm that MSE(k) converges by minimizing the trace of $\vartheta_{k|k}$ and finally achieves the desired filtering performance.

Example 2. We consider the networked DC servo system proposed in Zou et al.,[34] and the controlled plant and remote filter are connected by a shared communication network. Referring to Zou et al.,[34] the system parameters of the DC servo system are given as follows
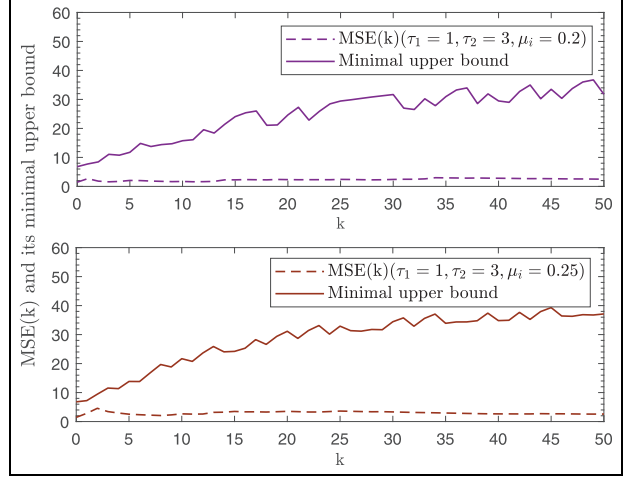
Figure 9. MSE(k) and the trace of minimal upper bound with weight coefficients $\mu_i = 0.2$ and $\mu_i = 0.25$.

$$x(k + 1) = \begin{bmatrix} 1.12 & 0.213 & -0.333 \\ 1 & 0 & 0 \\ 0 & 1 & 0 \end{bmatrix} x(k)$$

$$+ \begin{bmatrix} 0.8 \\ 0 \\ 0 \end{bmatrix} \omega(k) + \begin{bmatrix} -0.2193 & 0.0219 & 0.0844 \\ 0.2177 & -0.0032 & -0.0662 \\ 0.1298 & -0.0087 & -0.0381 \end{bmatrix} x(k - 3)$$

$$y(k) = \begin{bmatrix} 1 & 0 & 0 \\ 0 & 1 & 0 \end{bmatrix} x(k) + \begin{bmatrix} 0 \\ 0.8 \end{bmatrix} v(k)$$

In the simulation, we take the initial state of the system as $x_0 = \begin{bmatrix} 2 & 2 & 2 \end{bmatrix}^T$, $\phi(-1) = \phi(-2) = \phi(-3) = \begin{bmatrix} 2 & 2 & 2 \end{bmatrix}^T$, and the initial estimate as $\hat{x}_{-3|-3} = \hat{x}_{-2|-2} = \hat{x}_{-1|-1} = \hat{x}_{0|0} = \begin{bmatrix} 1 & 1 & 1 \end{bmatrix}^T$. The upper bound of the initial covariance is set as $\vartheta_{0|0} = \vartheta_{-1|-1} = \vartheta_{-2|-2} = \vartheta_{-3|-3} = 6I$, and positive scalars η_i ($i = 1, 2, \ldots, 8$) are set as $\eta_1 = \eta_2 = \eta_3 = \eta_6 = \eta_7 = 0.2$, $\eta_4 = \eta_8 = 0.1$, and $\eta_5 = 0.3$. We assume that $Q_k = 0.5I$ and $R_k = 0.6I$, respectively. The quantization level γ is set to 0.8, and the transition probability of the SC protocol is set to

$$\pi = \begin{bmatrix} 0.4 & 0.2 & 0.4 \\ 0.3 & 0.3 & 0.4 \\ 0.5 & 0.2 & 0.3 \end{bmatrix}$$

For a comparison with the existing results, we utilize the H_∞ robust filtering algorithm of Zou et al.[37] under the same initial conditions. The simulation results are shown in Figures 10–14. Figure 10 depicts the communication sequence subject to the SC scheduling protocol. For the proposed recursive filtering algorithm and H_∞ robust filtering algorithm of Zou et al.,[37] state trajectories of $x_1(k)$ and its estimate $\hat{x}_1(k)$, state trajectories $x_2(k)$ and its estimate $\hat{x}_2(k)$, and state trajectories $x_3(k)$ and its estimate $\hat{x}_3(k)$ are given in Figures 11–13, respectively. The trajectories of MSE(k) under the above two filter design strategies are shown in

Table 2. MSE(k) at different delay intervals ($\mu_i = 0.1$).

k	0	10	20	30	40	50
$\tau_1 = 1, \tau_2 = 2$	1.45	0.59	0.35	0.26	0.21	0.19
$\tau_1 = 1, \tau_2 = 3$	1.45	1.39	0.98	0.79	0.66	0.54
$\tau_1 = 1, \tau_2 = 4$	1.45	1.57	1.73	1.78	2.48	2.57
$\tau_1 = 1, \tau_2 = 5$	1.45	2.09	2.05	3.04	2.92	2.75

**Table 3.** Trace of minimal upper bound at different delay intervals ($\mu_i = 0.1$).

k	0	10	20	30	40	50
$\tau_1 = 1, \tau_2 = 2$	6.8	11.3	10.0	9.7	9.4	11.1
$\tau_1 = 1, \tau_2 = 3$	6.8	14.5	14.0	14.2	17.5	12.6
$\tau_1 = 1, \tau_2 = 4$	6.8	17.3	21.3	23.4	22.6	24.1
$\tau_1 = 1, \tau_2 = 5$	6.8	17.9	24.4	27.3	24.7	28.2

Table 4. MSE(k) with different weight coefficients μ_i ($\tau_1 = 1, \tau_2 = 3$).

k	0	10	20	30	40	50
$\mu_i = 0.10$	1.45	1.39	0.98	0.79	0.66	0.54
$\mu_i = 0.15$	1.45	1.45	1.16	1.41	1.88	1.95
$\mu_i = 0.20$	1.45	1.70	2.33	2.40	2.81	2.48
$\mu_i = 0.25$	1.45	2.66	3.50	3.32	2.65	2.59

Table 5. Trace of minimal upper bound with different weight coefficients μ_i ($\tau_1 = 1, \tau_2 = 3$).

k	0	10	20	30	40	50
$\mu_i = 0.10$	6.8	14.5	14.0	14.2	17.5	12.6
$\mu_i = 0.15$	6.8	15.1	18.0	21.6	24.3	20.9
$\mu_i = 0.20$	6.8	15.8	24.6	31.7	29.5	31.8
$\mu_i = 0.25$	6.8	21.6	31.2	34.4	34.8	37.1
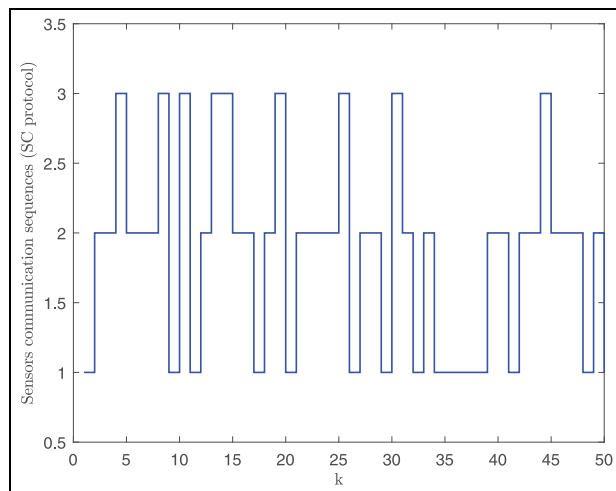
Figure 10. Sensors communication sequence under the SC protocol.
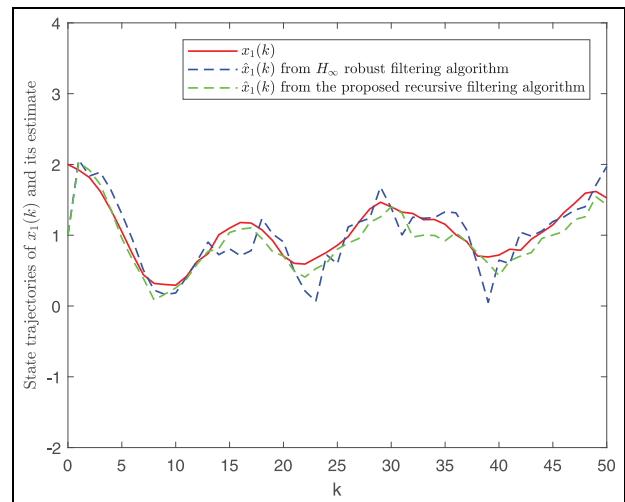
Figure 11. State trajectories of $x_1(k)$ and $\hat{x}_1(k)$ under the recursive filtering and H_∞ robust filtering algorithm.
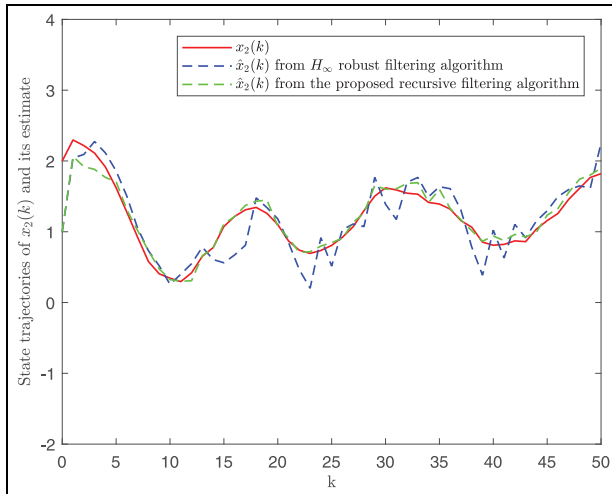
Figure 12. State trajectories of $x_2(k)$ and $\hat{x}_2(k)$ under the recursive filtering and H_∞ robust filtering algorithm.
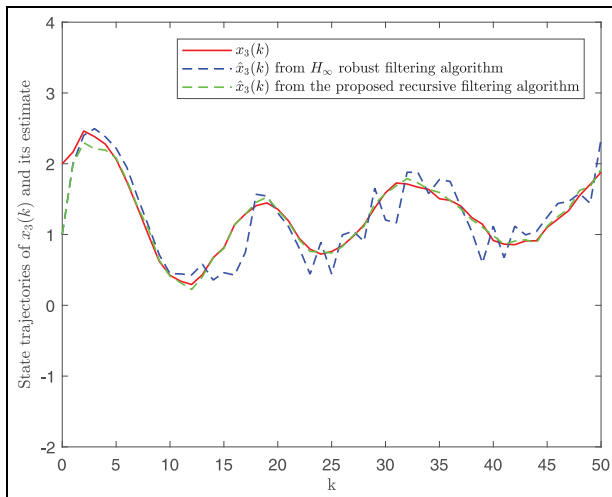
Figure 13. State trajectories of $x_3(k)$ and $\hat{x}_3(k)$ under the recursive filtering and H_∞ robust filtering algorithm.

Figure 14. Figures 11–14 show that the recursive filtering algorithm proposed in this article not only effectively tracks the state trajectories of the DC servo system but also has better filtering performance than that of the H_∞ robust filtering algorithm in Zou et al.[37]

Conclusion

The recursive filtering design problem for networked systems with mixed time-delays subject to the SC protocol and dynamic quantization effects is investigated in this article. Due to the presence of a limited-bandwidth network, it is assumed that only one sensor can transmit the measurement information to the filter at each sampling period, and the selected sensor is determined by the scheduling strategy of the corresponding communication protocol. Another fundamental issue is to mitigate the influence of the
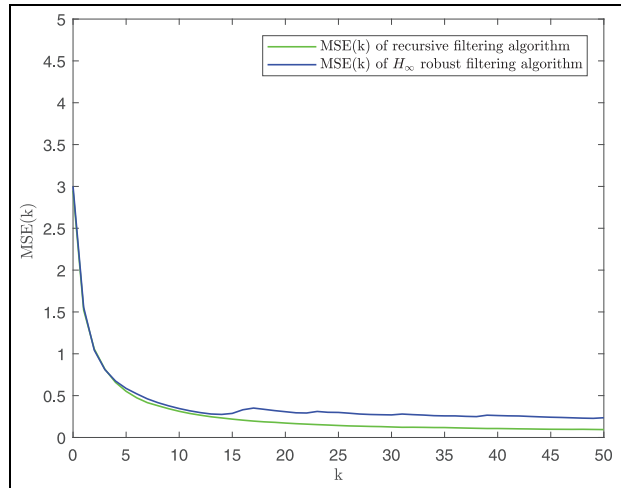
Figure 14. MSE(k) under the proposed recursive filtering algorithm and H_∞ robust filtering algorithm.

quantization errors on the filtering performance by employing the dynamic quantization mechanism. In such a framework, the recursive filter has been proposed to obtain the estimate of the system state under the influence of the SC protocol and dynamic quantization error. The upper bound of the filtering error covariance is addressed by solving two Riccati difference equations, and sufficient conditions have been derived for the presented recursive filter to guarantee the exponentially mean-square boundedness of the filtering error dynamics. Simulation examples have demonstrated the effectiveness and superiority of the developed recursive filtering algorithm by comparing the filtering effect with the H_∞ robust filtering algorithm. Moreover, a future research topic is to explore the Bayesian scheme to improve the filtering performance.

ORCID iD

Zhiwen Wang https://orcid.org/0000-0002-5425-0705

Data availability statement

All data included in this study are available upon request by contact with the corresponding author.

References

1. Mao JY, Sun Y, Yi XJ, et al. Recursive filtering of networked nonlinear systems: a survey. *Int J Syst Sci* 2021; 52(6): 1110–1128.
2. Chen B, Hu GQ, Ho DW, et al. Distributed Kalman filtering for time-varying discrete sequential systems. *Automatica* 2019; 99: 228–236.
3. Li WM, Jia YM and Du JP. State estimation for stochastic complex networks with switching topology. *IEEE T Autom Control* 2017; 62(12): 6377–6384.
4. Ding DR, Han QL, Wang ZD, et al. A survey on model-based distributed control and filtering for industrial cyber-physical systems. *IEEE T Ind Informat* 2019; 15(5): 2483–2499.
5. Gao HY, Han F, Jiang B, et al. Recursive filtering for time-varying systems under duty cycle scheduling based on collaborative prediction. *J Franklin Inst* 2020; 357(17): 13189–13204.
6. Liang JL, Wang F, Wang ZD, et al. Minimum-variance recursive filtering for two-dimensional systems with degraded measurements: boundedness and monotonicity. *IEEE T Autom Control* 2019; 64(10): 4153–4166.
7. Yan HC, Zhang H, Yang F, et al. Distributed H∞ filtering for switched repeated scalar nonlinear systems with randomly occurred sensor nonlinearities and asynchronous switching. *IEEE T Syst Man Cybern Syst* 2018; 48(12): 2263–2270.
8. Liu YR, Alsaadi FE, Yin XZ, et al. Robust H∞ filtering for discrete nonlinear delayed stochastic systems with missing measurements and randomly occurring nonlinearities. *Int J Gen Syst* 2015; 44(2): 169–181.
9. Nan X, Yang FW and Han QL. Distributed event-triggered networked set-membership filtering with partial information transmission. *IET Control Theory Appl* 2016; 11(2): 155–163.
10. Wei GL, Liu S, Song Y, et al. Probability-guaranteed set-membership filtering for systems with incomplete measurements. *Automatica* 2015; 60: 12–16.
11. Wang GL, Li N and Zhang YG. Diffusion distributed Kalman filter over sensor networks without exchanging raw measurements. *Signal Pr* 2017; 132: 1–7.
12. Chen J, Li JH, Yang SH, et al. Weighted optimization-based filter for nonlinear target tracking in collaborative sensor networks distributed Kalman filter for nonlinear target tracking in collaborative sensors networks. *IEEE T Cybern* 2017; 47(11): 3892–3905.
13. Liu D, Wang ZD, Liu YR, et al. Recursive resilient filtering for nonlinear stochastic systems with packet disorders. *J Franklin Inst* 2020; 357(8): 4817–4833.
14. Hu H, Wang ZD, Gao HJ, et al. Extended Kalman filtering with stochastic nonlinearities and multiple missing measurements. *Automatica* 2012; 48(9): 2007–2015.
15. Liu S, Wei GL, Song Y, et al. Set-membership state estimation subject to uniform quantization effects and communication constraints. *J Franklin Inst* 2017; 354: 7012–7027.
16. Zhang GH, Hu H, Lin JK, et al. Adaptive control with quantized inputs processed by Lipschitz logarithmic quantizer. *Int J Control Autom* 2021; 19(2): 921–930.
17. Azuma S and Sugie T. Optimal dynamic quantizers for discrete-valued input control. *Automatica* 2008; 44(2): 396–406.
18. Okajima H, Sawada K and Matsunaga N. Dynamic quantizer design under communication rate constraints. *IEEE T Autom Control* 2016; 61(10): 3190–3196.
19. Takahashi R, Azuma S and Hikihara T. Power regulation with predictive dynamic quantizer in power packet dispatching system. *IEEE T Ind Electron* 2016; 63(12): 7653–7661.
20. Walsh GC and Ye H. Scheduling of networked control systems. *IEEE Contr Syst Mag* 2001; 21(1): 57–65.
21. Li X, Wei GL, Ding DR, et al. Recursive filtering for time-varying discrete sequential systems subject to deception attacks: weighted try-once-discard protocol. *IEEE T Syst Man Cybern Syst* 2021; 52(6): 3704–3713.
22. Liu K, Fridman E, Johansson KH, et al. Quantized control under round-Robin communication protocol. *IEEE T Ind Electron* 2016; 63(7): 4461–4471.
23. Walsh GH, Ye H and Bushnell L. Stability analysis of networked control systems. *IEEE T Autom Control* 2002; 10(3): 438–446.
24. Zhang WA, Yu L and Feng G. Optimal linear estimation for networked systems with communication constraints. *Automatica* 2011; 47(9): 1992–2000.
25. Tabbara M and Nesic D. Input-output stability of networked control systems with stochastic protocols and channels. *IEEE T Autom Control* 2008; 53(5): 1160–1175.
26. Alsaadia FE, Wang ZD, Wang D, et al. Recursive fusion estimation for stochastic discrete time-varying complex networks under stochastic communication protocol: the state-saturated case. *Informat Fusion* 2010; 60: 11–19.
27. Wang F, Wang ZD, Liang JL, et al. Recursive distributed filtering for two-dimensional shift-varying systems over sensor networks under stochastic communication protocols. *Automatica* 2020; 115: Article No 1088.
28. Zou L, Wang ZD, Han QL, et al. Recursive filtering for time-varying systems with random access protocol. *IEEE T Autom Control* 2019; 64(2): 720–727.
29. Mao JY, Ding DR, Song Y, et al. Event-based recursive filtering for time-delayed stochastic nonlinear systems with missing measurements. *Signal Pr* 2017; 134: 158–165.
30. Mao JY, Ding DR, Wei GL, et al. Networked recursive filtering for time-delayed nonlinear stochastic systems with uniform quantisation under Round-Robin protocol. *Int J Syst Sci* 2019; 50(4): 871–884.
31. Sun Y, Mao JY, Liu H, et al. Distributed recursive filtering for discrete time-delayed stochastic nonlinear systems based on fuzzy rules. *Neurocomputing* 2019; 400: 412–419.
32. Sun J, Shen B, Liu YF, et al. A resilient outlier-resistant recursive filtering approach to time-delayed spatial-temporal systems with energy harvesting sensors. *ISA Trans* 2022; 127: 41–49.
33. Li X, Dong HL, Wang ZD, et al. Set-membership filtering for state-saturated systems with mixed time-delays under weighted try-once-discard protocol. *IEEE T Circuits Syst I: Reg Papers* 2018; 66(2): 312–316.
34. Zou L, Wang ZD and Gao HJ. Set-membership filtering for time-varying systems with mixed time-delays under Round-Robin and weighted try-once-discard protocols. *Automatica* 2016; 74: 341–348.
35. Li J, Wang ZD, Dong HL, et al. Outlier-resistant remote state estimation for recurrent neural networks with mixed time-delays. *IEEE T Neur Net Lear* 2020; 32(5): 2266–2273.
36. Maity D and Tsiotras P. Optimal controller synthesis and dynamic quantizer switching for linear-quadratic-Gaussian systems. *IEEE T Autom Control* 2022; 67(1): 382–389.
37. Zou L, Wang ZD, Hu J, et al. On H∞ finite-horizon filtering under stochastic protocol: dealing with high-rate communication networks. *IEEE T Autom Control* 2017; 62(9): 4884–4890.

Appendix I

Proof of Theorem 1

Proof. According to equation (9), the one-step error covariance can be obtained as follows

$$
\begin{aligned}
&P_{k+1|k}\\
&= \mathrm{E}\Big\{(\tilde{A}_k e_{k|k} + \tilde{B}_k e_{k-\tau_1|k-\tau_1} + \tilde{F}_k \textstyle\sum_{i=1}^{\tau_2} \mu_i e_{k-i|k-i} + \tilde{D}_k w_k)(\tilde{A}_k e_{k|k} + \tilde{B}_k e_{k-\tau_1|k-\tau_1} + \tilde{F}_k \textstyle\sum_{i=1}^{\tau_2} \mu_i e_{k-i|k-i} + \tilde{D}_k w_k)^T\Big\}\\
&= \tilde{A}_k P_{k|k} \tilde{A}_k^T + \tilde{B}_k P_{k-\tau_1|k-\tau_1} \tilde{B}_k^T + \mathrm{E}\big\{\tilde{D}_k w_k w_k^T \tilde{D}_k^T\big\} + \textstyle\sum_{i=1}^{\tau_2} \mu_i \sum_{j=1}^{\tau_2} \mu_j \mathrm{E}\big\{\tilde{F}_k e_{k-i|k-i} e_{k-j|k-j}^T \tilde{F}_k^T\big\}\\
&\quad + \mathrm{E}\Big\{\tilde{A}_k e_{k|k} e_{k-\tau_1|k-\tau_1}^T \tilde{B}_k^T + \tilde{A}_k e_{k|k} \textstyle\sum_{i=1}^{\tau_2} \mu_i e_{k-i|k-i}^T \tilde{F}_k^T + \tilde{A}_k e_{k|k} w_k^T \tilde{D}_k^T + \tilde{B}_k e_{k-\tau_1|k-\tau_1} e_{k|k}^T \tilde{A}_k^T\\
&\quad + \tilde{B}_k e_{k-\tau_1|k-\tau_1} \textstyle\sum_{i=1}^{\tau_2} \mu_i e_{k-\tau_1|k-\tau_1}^T \tilde{F}_k^T + \tilde{B}_k e_{k-\tau_1|k-\tau_1} w_k^T \tilde{D}_k^T + \tilde{F}_k \textstyle\sum_{i=1}^{\tau_2} \mu_i e_{k-i|k-i} e_{k|k}^T \tilde{A}_k^T + \tilde{D}_k w_k e_{k|k}^T \tilde{A}_k^T\\
&\quad + \tilde{F}_k \textstyle\sum_{i=1}^{\tau_2} \mu_i e_{k-i|k-i} w_k^T \tilde{D}_k^T + \tilde{F}_k \textstyle\sum_{i=1}^{\tau_2} \mu_i e_{k-i|k-i} e_{k-\tau_1|k-\tau_1}^T \tilde{B}_k^T + \tilde{D}_k w_k e_{k-\tau_1|k-\tau_1}^T \tilde{B}_k^T + \tilde{D}_k w_k \textstyle\sum_{i=1}^{\tau_2} \mu_i e_{k-\tau_1|k-\tau_1}^T \tilde{F}_k^T\Big\}
\end{aligned}
\tag{14}
$$

Obviously, the inequality $(\beta^{\frac{1}{2}}a - \beta^{-\frac{1}{2}}b)(\beta^{\frac{1}{2}}a - \beta^{-\frac{1}{2}}b)^T \geq 0$ holds and is equivalent to $ab^T + ba^T \leq \beta aa^T + \beta^{-1}bb^T$, where $\beta > 0$, and a and b are the vectors of appropriate dimensions. Then, with the help of elementary inequality

$$
ab^T + ba^T \leq \beta aa^T + \beta^{-1}bb^T \quad \forall \beta > 0
\tag{15}
$$

it is straightforward to see that

$$
\tilde{A}_k e_{k|k} e_{k-\tau_1|k-\tau_1}^T \tilde{B}_k^T + \tilde{B}_k e_{k-\tau_1|k-\tau_1} e_{k|k}^T \tilde{A}_k^T \leq \eta_1 \tilde{A}_k e_{k|k} e_{k|k}^T \tilde{A}_k^T + \eta_1^{-1} \tilde{B}_k e_{k-\tau_1|k-\tau_1} e_{k-\tau_1|k-\tau_1}^T \tilde{B}_k^T
\tag{16}
$$

$$
\tilde{A}_k e_{k|k} \textstyle\sum_{i=1}^{\tau_2} \mu_i e_{k-i|k-i}^T \tilde{F}_k^T + \tilde{F}_k \textstyle\sum_{i=1}^{\tau_2} \mu_i e_{k-i|k-i} e_{k|k}^T \tilde{A}_k^T \leq \eta_2 \tilde{A}_k e_{k|k} e_{k|k}^T \tilde{A}_k^T + \eta_2^{-1} \textstyle\sum_{i=1}^{\tau_2} \mu_i \sum_{j=1}^{\tau_2} \mu_j \tilde{F}_k e_{k-i|k-i} e_{k-j|k-j}^T \tilde{F}_k^T
\tag{17}
$$

$$
\tilde{A}_k e_{k|k} w_k^T \tilde{D}_k^T + \tilde{D}_k w_k e_{k|k}^T \tilde{A}_k^T \leq \eta_3 \tilde{A}_k e_{k|k} e_{k|k}^T \tilde{A}_k^T + \eta_3^{-1} \tilde{D}_k w_k w_k^T \tilde{D}_k^T
\tag{18}
$$

$$
\begin{aligned}
&\tilde{B}_k e_{k-\tau_1|k-\tau_1} \textstyle\sum_{i=1}^{\tau_2} \mu_i e_{k-i|k-i}^T \tilde{F}_k^T + \tilde{F}_k \textstyle\sum_{i=1}^{\tau_2} \mu_i e_{k-i|k-i} e_{k-\tau_1|k-\tau_1}^T \tilde{B}_k^T \leq \eta_4 \tilde{B}_k e_{k-\tau_1|k-\tau_1} e_{k-\tau_1|k-\tau_1}^T \tilde{B}_k^T\\
&\quad + \eta_4^{-1} \textstyle\sum_{i=1}^{\tau_2} \mu_i \sum_{j=1}^{\tau_2} \mu_j \tilde{F}_k e_{k-i|k-i} e_{k-j|k-j}^T \tilde{F}_k^T
\end{aligned}
\tag{19}
$$

$$
\tilde{B}_k e_{k-\tau_1|k-\tau_1} w_k^T \tilde{D}_k^T + \tilde{D}_k w_k e_{k-\tau_1|k-\tau_1}^T \tilde{B}_k^T \leq \eta_5 \tilde{B}_k e_{k-\tau_1|k-\tau_1} e_{k-\tau_1|k-\tau_1}^T \tilde{B}_k^T + \eta_5^{-1} \tilde{D}_k w_k w_k^T \tilde{D}_k^T
\tag{20}
$$

$$
\tilde{F}_k \textstyle\sum_{i=1}^{\tau_2} \mu_i e_{k-i|k-i} w_k^T \tilde{D}_k^T + \tilde{D}_k w_k \textstyle\sum_{i=1}^{\tau_2} \mu_i e_{k-i|k-i}^T \tilde{F}_k^T \leq \eta_6 \textstyle\sum_{i=1}^{\tau_2} \mu_i \sum_{j=1}^{\tau_2} \mu_j \tilde{F}_k e_{k-i|k-i} e_{k-j|k-j}^T \tilde{F}_k^T + \eta_6^{-1} \tilde{D}_k w_k w_k^T \tilde{D}_k^T
\tag{21}
$$

$$
\begin{aligned}
&\textstyle\sum_{i=1}^{\tau_2} \mu_i \sum_{j=1}^{\tau_2} \mu_j E\big\{\tilde{F}_k e_{k-i|k-i} e_{k-j|k-j}^T \tilde{F}_k^T\big\}\\
&= \frac{1}{2} \textstyle\sum_{i=1}^{\tau_2} \mu_i \sum_{j=1}^{\tau_2} \mu_j E\big\{\tilde{F}_k e_{k-i|k-i} e_{k-j|k-j}^T \tilde{F}_k^T + \tilde{F}_k e_{k-j|k-j} e_{k-i|k-i}^T \tilde{F}_k^T\big\}\\
&\leq \frac{1}{2} \textstyle\sum_{i=1}^{\tau_2} \mu_i \sum_{j=1}^{\tau_2} \mu_j E\big\{\eta_7 \tilde{F}_k e_{k-i|k-i} e_{k-i|k-i}^T \tilde{F}_k^T + \eta_7^{-1} \tilde{F}_k e_{k-j|k-j} e_{k-j|k-j}^T \tilde{F}_k^T\big\}\\
&= \frac{1}{2} \textstyle\sum_{i=1}^{\tau_2} \mu_i \sum_{j=1}^{\tau_2} \mu_j (\eta_7 \tilde{F}_k P_{k-i|k-i} \tilde{F}_k^T + \eta_7^{-1} \tilde{F}_k P_{k-j|k-j} \tilde{F}_k^T)\\
&= \frac{1}{2}(\eta_7 + \eta_7^{-1}) \textstyle\sum_{i=1}^{\tau_2} \mu_i \sum_{i=1}^{\tau_2} \mu_i \tilde{F}_k P_{k-i|k-i} \tilde{F}_k^T
\end{aligned}
\tag{22}
$$

By substituting equations (16)–(22) into equation (14), we can obtain

$P_{k+1|k}$

$$\leqslant (1 + \eta_1 + \eta_2 + \eta_3)\tilde{A}_k P_{k|k}\tilde{A}_k^T + \frac{1}{2}(1 + \eta_2^{-1} + \eta_4^{-1} + \eta_6)(\eta_7 + \eta_7^{-1})\sum_{i=1}^{\tau_2}\mu_i\sum_{i=1}^{\tau_2}\mu_i\tilde{F}_k P_{k-i|k-i}\tilde{F}_k^T \quad (23)$$

$$+ (1 + \eta_1^{-1} + \eta_4 + \eta_5)\tilde{B}_k P_{k-\tau_1|k-\tau_1}\tilde{B}_k^T + (1 + \eta_3^{-1} + \eta_5^{-1} + \eta_6^{-1})\tilde{D}_k\tilde{Q}_k\tilde{D}_k^T$$

Then, the filtering error covariance can be recursively calculated as

$P_{k+1|k+1}$

$$= \mathrm{E}\left\{e_{k+1|k+1}e_{k+1|k+1}^T\right\}$$

$$= \mathrm{E}\left\{((I-K_{k+1}\tilde{C}_{k+1})e_{k+1|k} - K_{k+1}\tilde{E}_{k+1}w_{k+1})((I-K_{k+1}\tilde{C}_{k+1})e_{k+1|k} - K_{k+1}\tilde{E}_{k+1}w_{k+1})^T\right\}$$

$$= \mathrm{E}\left\{((I-K_{k+1}\tilde{C}_{k+1})e_{k+1|k}e_{k+1|k}^T(I-K_{k+1}\tilde{C}_{k+1})^T - (I-K_{k+1}\tilde{C}_{k+1})e_{k+1|k}w_{k+1}^T\tilde{E}_{k+1}^T K_{k+1}^T\right.$$

$$\left. - K_{k+1}\tilde{E}_{k+1}w_{k+1}e_{k+1|k}^T(I-K_{k+1}\tilde{C}_{k+1})^T + K_{k+1}\tilde{E}_{k+1}w_{k+1}w_{k+1}^T\tilde{E}_{k+1}^T K_{k+1}^T\right\}$$

$$= (I-K_{k+1}\tilde{C}_{k+1})P_{k+1|k}(I-K_{k+1}\tilde{C}_{k+1})^T - \mathrm{E}\left\{(I-K_{k+1}\tilde{C}_{k+1})e_{k+1|k}w_{k+1}^T\tilde{E}_{k+1}^T K_{k+1}^T - K_{k+1}\tilde{E}_{k+1}w_{k+1}e_{k+1|k}^T(I-K_{k+1}\tilde{C}_{k+1})^T\right\}$$

$$+ K_{k+1}\tilde{E}_{k+1}Q_{k+1}\tilde{E}_{k+1}^T K_{k+1}^T$$

$$(24)$$

By applying the elementary inequality equation (15), we can obtain

$$\mathrm{E}\left\{\left(-(I-K_{k+1}\tilde{C}_{k+1})\right)e_{k+1|k}w_{k+1}^T\tilde{E}_{k+1}^T K_{k+1}^T + K_{k+1}\tilde{E}_{k+1}w_{k+1}e_{k+1|k}^T\left(-(I-K_{k+1}\tilde{C}_{k+1})\right)^T\right\}$$

$$\leqslant \mathrm{E}\left\{\eta_8(I-K_{k+1}\tilde{C}_{k+1})e_{k+1|k}e_{k+1|k}^T(I-K_{k+1}\tilde{C}_{k+1})^T + \eta_8^{-1}K_{k+1}\tilde{E}_{k+1}w_{k+1}w_{k+1}^T\tilde{E}_{k+1}^T K_{k+1}^T\right\} \quad (25)$$

$$\leqslant \eta_8(I-K_{k+1}\tilde{C}_{k+1})P_{k+1|k}(I-K_{k+1}\tilde{C}_{k+1})^T + \eta_8^{-1}K_{k+1}\tilde{E}_{k+1}\tilde{Q}_{k+1}\tilde{E}_{k+1}^T K_{k+1}^T$$

Considering equations (24) and (25), it is obvious that

$$P_{k+1|k+1} \leqslant (1+\eta_8)(I-K_{k+1}\tilde{C}_{k+1})P_{k+1|k}(I-K_{k+1}\tilde{C}_{k+1})^T + (1+\eta_8^{-1})K_{k+1}\tilde{E}_{k+1}Q_{k+1}\tilde{E}_{k+1}^T K_{k+1}^T \quad (26)$$

Then, we define the functions $\upsilon(\vartheta_{k+1|k})$ and $\vartheta_{k+1|k}$ as follows

$\upsilon(\vartheta_{k+1|k})$

$$= (1 + \eta_1 + \eta_2 + \eta_3)\tilde{A}_k\vartheta_{k|k}\tilde{A}_k^T + (1 + \eta_2^{-1} + \eta_4^{-1} + \eta_6)\frac{1}{2}(\eta_7 + \eta_7^{-1})\sum_{i=1}^{\tau_2}\mu_i\sum_{i=1}^{\tau_2}\mu_i\tilde{F}_k\vartheta_{k-i|k-i}\tilde{F}_k^T\frac{1}{2}(\eta_7 + \eta_7^{-1})$$

$$\sum_{i=1}^{\tau_2}\mu_i\sum_{i=1}^{\tau_2}\mu_i\tilde{F}_k\vartheta_{k-i|k-i}\tilde{F}_k^T$$

$$+ (1 + \eta_1^{-1} + \eta_4 + \eta_5)\times\tilde{B}_k\vartheta_{k-\tau_1|k-\tau_1}\tilde{B}_k^T + (1 + \eta_3^{-1} + \eta_5^{-1} + \eta_6^{-1})\tilde{D}_k\tilde{Q}_k\tilde{D}_k^T \quad (27)$$

$\vartheta_{k+1|k}$

$$= (1 + \eta_1 + \eta_2 + \eta_3)\tilde{A}_k\vartheta_{k|k}\tilde{A}_k^T + (1 + \eta_2^{-1} + \eta_4^{-1} + \eta_6)\frac{1}{2}(\eta_7 + \eta_7^{-1})\sum_{i=1}^{\tau_2}\mu_i\sum_{i=1}^{\tau_2}\mu_i\tilde{F}_k\vartheta_{k-i|k-i}\tilde{F}_k^T \quad (28)$$

$$+ (1 + \eta_1^{-1} + \eta_4 + \eta_5)\tilde{B}_k\vartheta_{k-\tau_1|k-\tau_1}\tilde{B}_k^T + (1 + \eta_3^{-1} + \eta_5^{-1} + \eta_6^{-1})\tilde{D}_k\tilde{Q}_k\tilde{D}_k^T$$

When $\vartheta_{k|k} \geqslant P_{k|k}$, by applying Lemma 2, according to equation (27) and (28), it is straightforward to see $\upsilon(\vartheta_{k|k}) \geqslant \upsilon(P_{k|k})$. By combining equation (23) and (26), we can obtain

$\upsilon(P_{k|k})$

$$= (1 + \eta_1 + \eta_2 + \eta_3)\tilde{A}_k P_{k|k}\tilde{A}_k^T + (1 + \eta_2^{-1} + \eta_4^{-1} + \eta_6) + \frac{1}{2}(1 + \eta_1^{-1} + \eta_4 + \eta_5)(\eta_7 + \eta_7^{-1})\sum_{i=1}^{\tau_2}\mu_i$$

$$\sum_{i=1}^{\tau_2}\mu_i\tilde{F}_k P_{k-i|k-i}\tilde{F}_k^T\tilde{B}_k P_{k-\tau_1|k-\tau_1}\tilde{B}_k^T$$

$$+ (1 + \eta_3^{-1} + \eta_5^{-1} + \eta_6^{-1})\tilde{D}_k\tilde{Q}_k\tilde{D}_k^T \geqslant P_{k+1|k}$$

With the initial condition $P_{0|0} \triangleq \vartheta_{0|0}$, it is obvious that $\vartheta_{k+1|k} \geqslant P_{k+1|k}$. Then, $\vartheta_{k+1|k}$ is an upper bound for $P_{k+1|k}$ at the time instant k. We define $\tilde{K}_{k+1} \triangleq I - K_{k+1}\tilde{C}_{k+1}$, one has

$$\vartheta_{k+1|k+1} = (1 + \eta_8)\tilde{K}_{k+1}\vartheta_{k+1|k}\tilde{K}_{k+1}^T + (1 + \eta_8^{-1})K_{k+1}\tilde{E}_{k+1}\tilde{Q}_{k+1}\tilde{E}_{k+1}^T K_{k+1}^T$$

In the similar lines and using Lemma 2 again, it is easy to obtain $\vartheta_{k+1|k+1} \geqslant P_{k+1|k+1}$. The proof is completed.

Appendix 2

Proof of Theorem 2

Proof. It follows from equation (12) that the trace of the upper bound can be expressed as

$$
\begin{aligned}
&\mathrm{tr}\{\vartheta_{k+1|k+1}\} \\
&= \mathrm{tr}\{(1 + \eta_8)\tilde{K}_{k+1}\vartheta_{k+1|k}\tilde{K}_{k+1}^T + (1 + \eta_8^{-1})K_{k+1}\tilde{E}_{k+1}\tilde{Q}_{k+1}\tilde{E}_{k+1}^T K_{k+1}^T\} \\
&= \mathrm{tr}\{(1 + \eta_8)(\vartheta_{k+1|k} - \vartheta_{k+1|k}\tilde{C}_{k+1}^T K_{k+1}^T - K_{k+1}\tilde{C}_{k+1}\vartheta_{k+1|k} + K_{k+1}\tilde{C}_{k+1}\vartheta_{k+1|k}\tilde{C}_{k+1}^T K_{k+1}^T) \\
&\quad + (1 + \eta_8^{-1})K_{k+1}\tilde{E}_{k+1}\tilde{Q}_{k+1}\tilde{E}_{k+1}^T K_{k+1}^T\}
\end{aligned}
$$

Through Lemma 3, we can obtain

$$\frac{\partial \mathrm{tr}\{\vartheta_{k+1|k+1}\}}{\partial K_{k+1}} = -2(1 + \eta_8)\vartheta_{k+1|k}\tilde{C}_{k+1}^T + 2K_{k+1}C_{k+1}\vartheta_{k+1|k}\tilde{C}_{k+1}^T + 2(1 + \eta_8^{-1})K_{k+1}\tilde{E}_{k+1}\tilde{Q}_{k+1}\tilde{E}_{k+1}^T$$

We let

$$\frac{\partial \mathrm{tr}\{\vartheta_{k+1|k+1}\}}{\partial K_{k+1}} = 0$$

which yields

$$2K_{k+1}C_{k+1}\vartheta_{k+1|k}\tilde{C}_{k+1}^T + 2(1 + \eta_8^{-1})K_{k+1}\tilde{E}_{k+1}\tilde{Q}_{k+1}\tilde{E}_{k+1}^T - 2(1 + \eta_8)\vartheta_{k+1|k}\tilde{C}_{k+1}^T = 0$$

Then, we can obtain

$$K_{k+1}\left(C_{k+1}\vartheta_{k+1|k}\tilde{C}_{k+1}^T + (1 + \eta_8^{-1})\tilde{E}_{k+1}\tilde{Q}_{k+1}\tilde{E}_{k+1}^T\right) = (1 + \eta_8)\vartheta_{k+1|k}\tilde{C}_{k+1}^T$$

Obviously, $C_{k+1}\vartheta_{k+1|k}\tilde{C}_{k+1}^T + (1 + \eta_8^{-1})\tilde{E}_{k+1}\tilde{Q}_{k+1}\tilde{E}_{k+1}^T > 0$, so we can obtain the filtering gain K_{k+1} in equation (13). The proof is completed.

Appendix 3

Proof of Theorem 3

Proof. We define

$$V(e_{k+1|k+1}) = e_{k+1|k+1}^T \vartheta_{k+1|k+1}^{-1} e_{k+1|k+1} \tag{29}$$

Substituting equation (10) into equation (29), we have

$V(e_{k+1|k+1})$

$= (\tilde{K}_{k+1}e_{k+1|k} - K_{k+1}\tilde{E}_{k+1}w_{k+1})^T \vartheta_{k+1|k+1}^{-1} (\tilde{K}_{k+1}e_{k+1|k} - K_{k+1}\tilde{E}_{k+1}w_{k+1})$

$= e_{k+1|k}^T \tilde{K}_{k+1}^T \vartheta_{k+1|k+1}^{-1} \tilde{K}_{k+1}e_{k+1|k} - e_{k+1|k}^T \tilde{K}_{k+1}^T \vartheta_{k+1|k+1}^{-1} K_{k+1}\tilde{E}_{k+1}w_{k+1} - w_{k+1}^T \tilde{E}_{k+1}^T K_{k+1}^T \vartheta_{k+1|k+1}^{-1} \tilde{K}_{k+1}e_{k+1|k}$

$\quad + w_{k+1}^T \tilde{E}_{k+1}^T K_{k+1}^T K_{k+1}\tilde{E}_{k+1}w_{k+1}$

$= (\tilde{A}_k e_{k|k} + \tilde{B}_k e_{k-\tau_1|k-\tau_1} + \tilde{F}_k \sum_{i=1}^{\tau_2} \mu_i e_{k-i|k-i} + \tilde{D}_k w_k)^T \tilde{K}_{k+1}^T \vartheta_{k+1|k+1}^{-1} \tilde{K}_{k+1}(\tilde{A}_k e_{k|k} + \tilde{B}_k e_{k-\tau_1|k-\tau_1} + \tilde{F}_k \sum_{i=1}^{\tau_2} \mu_i e_{k-i|k-i} + \tilde{D}_k w_k)$

$\quad - (\tilde{A}_k e_{k|k} + \tilde{B}_k e_{k-\tau_1|k-\tau_1} + \tilde{F}_k \sum_{i=1}^{\tau_2} \mu_i e_{k-i|k-i} + \tilde{D}_k w_k)^T \tilde{K}_{k+1}^T \vartheta_{k+1|k+1}^{-1} K_{k+1}\tilde{E}_{k+1}w_{k+1}$

$\quad - w_{k+1}^T \tilde{E}_{k+1}^T K_{k+1}^T \vartheta_{k+1|k+1}^{-1} \tilde{K}_{k+1}(\tilde{A}_k e_{k|k} + \tilde{B}_k e_{k-\tau_1|k-\tau_1} + \tilde{F}_k \sum_{i=1}^{\tau_2} \mu_i e_{k-i|k-i} + \tilde{D}_k w_k) + w_{k+1}^T \tilde{E}_{k+1}^T K_{k+1}^T K_{k+1}\tilde{E}_{k+1}w_{k+1}$

$$(30)$$

Subsequently, we expand equation (30) completely as follows

$V(e_{k+1|k+1})$

$= e_{k|k}^T \tilde{A}_k^T \tilde{K}_{k+1}^T \vartheta_{k+1|k+1}^{-1} \tilde{K}_{k+1} \tilde{A}_k e_{k|k} + e_{k|k}^T \tilde{A}_k^T \tilde{K}_{k+1}^T \vartheta_{k+1|k+1}^{-1} \tilde{K}_{k+1} \tilde{B}_k e_{k-\tau_1|k-\tau_1} + e_{k|k}^T \tilde{A}_k^T \tilde{K}_{k+1}^T \vartheta_{k+1|k+1}^{-1} \tilde{K}_{k+1} \tilde{F}_k$

$\quad \sum_{i=1}^{\tau_2} \mu_i e_{k-i|k-i}$

$\quad + e_{k|k}^T \tilde{A}_k^T \tilde{K}_{k+1}^T \vartheta_{k+1|k+1}^{-1} \tilde{K}_{k+1} \tilde{D}_k w_k + e_{k-\tau_1|k-\tau_1}^T \tilde{B}_k^T \tilde{K}_{k+1}^T \vartheta_{k+1|k+1}^{-1} \tilde{K}_{k+1} \tilde{A}_k e_{k|k} + e_{k-\tau_1|k-\tau_1}^T \tilde{B}_k^T \tilde{K}_{k+1}^T \vartheta_{k+1|k+1}^{-1} \tilde{K}_{k+1} \tilde{B}_k e_{k-\tau_1|k-\tau_1}$

$\quad + e_{k-\tau_1|k-\tau_1}^T \tilde{B}_k^T \tilde{K}_{k+1}^T \vartheta_{k+1|k+1}^{-1} \tilde{K}_{k+1} \tilde{F}_k \sum_{i=1}^{\tau_2} \mu_i e_{k-i|k-i} + e_{k-\tau_1|k-\tau_1}^T \tilde{B}_k^T \tilde{K}_{k+1}^T \vartheta_{k+1|k+1}^{-1} \tilde{K}_{k+1} \tilde{D}_k w_k$

$\quad + (\tilde{F}_k \sum_{i=1}^{\tau_2} \mu_i e_{k-i|k-i})^T \tilde{K}_{k+1}^T \vartheta_{k+1|k+1}^{-1} \tilde{K}_{k+1} \tilde{A}_k e_{k|k}$

$\quad + (\tilde{F}_k \sum_{i=1}^{\tau_2} \mu_i e_{k-i|k-i})^T \tilde{K}_{k+1}^T \vartheta_{k+1|k+1}^{-1} \tilde{K}_{k+1} \tilde{B}_k e_{k-\tau_1|k-\tau_1} + (\tilde{F}_k \sum_{i=1}^{\tau_2} \mu_i e_{k-i|k-i})^T \tilde{K}_{k+1}^T \vartheta_{k+1|k+1}^{-1} \tilde{K}_{k+1} \tilde{F}_k \sum_{i=1}^{\tau_2} \mu_i e_{k-i|k-i}$

$\quad + (\tilde{F}_k \sum_{i=1}^{\tau_2} \mu_i e_{k-i|k-i})^T \tilde{K}_{k+1}^T \vartheta_{k+1|k+1}^{-1} \tilde{K}_{k+1} \tilde{D}_k w_k + w_k^T \tilde{D}_k^T \tilde{K}_{k+1}^T \vartheta_{k+1|k+1}^{-1} \tilde{K}_{k+1} \tilde{A}_k e_{k|k} + w_k^T \tilde{D}_k^T \tilde{K}_{k+1}^T \vartheta_{k+1|k+1}^{-1} \tilde{K}_{k+1} \tilde{B}_k e_{k-\tau_1|k-\tau_1}$

$\quad + w_k^T \tilde{D}_k^T \tilde{K}_{k+1}^T \vartheta_{k+1|k+1}^{-1} \tilde{K}_{k+1} \tilde{F}_k \sum_{i=1}^{\tau_2} \mu_i e_{k-i|k-i} + w_k^T \tilde{D}_k^T \tilde{K}_{k+1}^T \vartheta_{k+1|k+1}^{-1} \tilde{K}_{k+1} \tilde{D}_k w_k$

$\quad - (\tilde{A}_k e_{k|k} + \tilde{B}_k e_{k-\tau_1|k-\tau_1} + \tilde{F}_k \sum_{i=1}^{\tau_2} \mu_i e_{k-i|k-i} + \tilde{D}_k w_k)^T \tilde{K}_{k+1}^T \vartheta_{k+1|k+1}^{-1} K_{k+1}\tilde{E}_{k+1}w_{k+1}$

$\quad - w_{k+1}^T \tilde{E}_{k+1}^T K_{k+1}^T \vartheta_{k+1|k+1}^{-1} \tilde{K}_{k+1}(\tilde{A}_k e_{k|k} + \tilde{B}_k e_{k-\tau_1|k-\tau_1} + \tilde{F}_k \sum_{i=1}^{\tau_2} \mu_i e_{k-i|k-i} + \tilde{D}_k w_k) + w_{k+1}^T \tilde{E}_{k+1}^T K_{k+1}^T K_{k+1}\tilde{E}_{k+1}w_{k+1}$

$$(31)$$

Similarly, considering the elementary inequality equation (15) and using the same processing method as equations (16)–(22), then, it is easy to obtain that equation (31) is equivalent to the following relationship

$\mathrm{E}\{V(e_{k+1|k+1})\}$

$\leqslant \mathrm{E}\{\chi_1 e_{k|k}^T \tilde{A}_k^T \tilde{K}_{k+1}^T \vartheta_{k+1|k+1}^{-1} \tilde{K}_{k+1} \tilde{A}_k e_{k|k} + \chi_2 e_{k-\tau_1|k-\tau_1}^T \tilde{B}_k^T \tilde{K}_{k+1}^T \vartheta_{k+1|k+1}^{-1} \tilde{K}_{k+1} \tilde{B}_k e_{k-\tau_1|k-\tau_1}$

$\quad + \chi_3 (\tilde{F}_k \sum_{i=1}^{\tau_2} \mu_i e_{k-i|k-i})^T \tilde{K}_{k+1}^T \vartheta_{k+1|k+1}^{-1} \tilde{K}_{k+1} \tilde{F}_k \sum_{i=1}^{\tau_2} \mu_i e_{k-i|k-i}$

$\quad + \chi_4 w_k^T \tilde{D}_k^T \tilde{K}_{k+1}^T \vartheta_{k+1|k+1}^{-1} \tilde{K}_{k+1} \tilde{D}_k w_k + \chi_5 w_{k+1}^T \tilde{E}_{k+1}^T K_{k+1}^T \vartheta_{k+1|k+1}^{-1} K_{k+1}\tilde{E}_{k+1}w_{k+1}\}$

$$(32)$$

where $\chi_1 = (1 + \eta_1 + \eta_2 + \eta_3)$, $\chi_2 = 1 + \eta_1^{-1} + \eta_4 + \eta_6 + \eta_7$, $\chi_3 = 1 + \eta_5 + \eta_7^{-1} + \eta_8$, $\chi_4 = 1 + \eta_2^{-1} + \eta_4^{-1} + \eta_5^{-1} + \eta_9$, and $\chi_5 = 1 + \eta_3^{-1} + \eta_6^{-1} + \eta_8^{-1} + \eta_9^{-1}$.

According to the proposed results in Theorem 1, we can obtain

$$\vartheta_{k+1|k+1} = (1 + \eta_8)\tilde{K}_{k+1}\vartheta_{k+1|k}\tilde{K}_{k+1}^T + (1 + \eta_8^{-1})K_{k+1}\tilde{E}_{k+1}\tilde{Q}_{k+1}\tilde{E}_{k+1}^T K_{k+1}^T \geqslant (1 + \eta_8)\tilde{K}_{k+1}\vartheta_{k+1|k}\tilde{K}_{k+1}^T \tag{33}$$

In light of Assumption 1, it can be obtained from equation (28) that

$$\vartheta_{k+1|k}$$

$$= (1 + \eta_1 + \eta_2 + \eta_3)\tilde{A}_k \vartheta_{k|k} \tilde{A}_k^T + \frac{1}{2}(1 + \eta_2^{-1} + \eta_4^{-1} + \eta_6)(\eta_7 + \eta_7^{-1}) \sum_{i=1}^{\tau_2} \mu_i \sum_{i=1}^{\tau_2} \mu_i \tilde{F}_k \vartheta_{k-i|k-i} \tilde{F}_k^T$$

$$+ (1 + \eta_1^{-1} + \eta_4 + \eta_5)\tilde{B}_k \vartheta_{k-\tau_1|k-\tau_1} \tilde{B}_k^T + (1 + \eta_3^{-1} + \eta_5^{-1} + \eta_6^{-1})\tilde{D}_k \tilde{Q}_k \tilde{D}_k^T \tag{34}$$

$$\geqslant (1 + \eta_1 + \eta_2 + \eta_3)\tilde{A}_k \vartheta_{k|k} \tilde{A}_k^T + \frac{1}{2}(1 + \eta_2^{-1} + \eta_4^{-1} + \eta_6)(\eta_7 + \eta_7^{-1})(\mu_1 + \mu_2 + \cdots + \mu_{\tau_2})^2 \underline{f}^2 \underline{p}^2 I$$

$$+ (1 + \eta_1^{-1} + \eta_4 + \eta_5)\underline{b}^2 \underline{p}^2 I + (1 + \eta_3^{-1} + \eta_5^{-1} + \eta_6^{-1})\underline{d}^2 \underline{q}^2 I$$

Substituting equation (34) into equation (33) yields

$$\vartheta_{k+1|k+1} \geqslant (1 + \eta_8)\tilde{K}_{k+1}\{\zeta_1 \tilde{A}_k \vartheta_{k|k} \tilde{A}_k^T + \zeta I\}\tilde{K}_{k+1}^T \tag{35}$$

where

$$\zeta = \frac{1}{2}(1 + \eta_2^{-1} + \eta_4^{-1} + \eta_6)(\eta_7 + \eta_7^{-1})(\mu_1 + \mu_2 + \cdots + \mu_{\tau_2})^2 \underline{f}^2 \underline{p}^2$$

$$+ (1 + \eta_1^{-1} + \eta_4 + \eta_5)\underline{b}^2 \underline{p}^2 I + (1 + \eta_3^{-1} + \eta_5^{-1} + \eta_6^{-1})\underline{d}^2 \underline{q}^2$$

$$\zeta_1 = 1 + \eta_1 + \eta_2 + \eta_3$$

It is obvious that the relationship between $\vartheta_{k+1|k+1}$ and $\vartheta_{k|k}$ is addressed by equation (35). Moreover, we derive the exponential mean-square boundedness for the filtering error dynamics.

From equation (35), we can obtain the inequality and the relationship of $\vartheta_{k+1|k+1}^{-1}$ and $\vartheta_{k|k}^{-1}$ as follows

$$\tilde{K}_{k+1}^T \vartheta_{k+1|k+1}^{-1} \tilde{K}_{k+1} \leqslant (1 + \eta_8)^{-1}(\zeta_1 \underline{p} \underline{a}^2 I + \zeta I)^{-1}$$

which yields

$$\tilde{A}_k^T \tilde{K}_{k+1}^T \vartheta_{k+1|k+1}^{-1} \tilde{K}_{k+1} \tilde{A}_k \leqslant (1 + \eta_8)^{-1}\zeta_1^{-1}(1 + \zeta\zeta_1^{-1}(\tilde{A}_k^T)^{-1}\vartheta_{k+1|k+1}^{-1}\tilde{A}_k^{-1})^{-1}\vartheta_{k|k}^{-1} \leqslant (1 + \eta_8)^{-1}\zeta_1^{-1}(1 + \zeta\zeta_1^{-1}\underline{a}^{-2}\underline{p}^{-1})^{-1}\vartheta_{k|k}^{-1} = \zeta_2 \vartheta_{k|k}^{-1} \tag{36}$$

where $\zeta_2 = (1 + \eta_8)^{-1}\zeta_1^{-1}(1 + \zeta\zeta_1^{-1}\underline{a}^{-2}\underline{p}^{-1})^{-1}$. Then, it follows from equation (36) and Assumption 1 that

$$E\left\{\chi_1 e_{k|k}^T \tilde{A}_k^T \tilde{K}_{k+1}^T \vartheta_{k+1|k+1}^{-1} \tilde{K}_{k+1} \tilde{A}_k e_{k|k}\right\} \leqslant \chi_1 \zeta_2 e_{k|k}^T \vartheta_{k|k}^{-1} e_{k|k} \tag{37}$$

$$E\left\{\chi_2 e_{k-\tau_1|k-\tau_1}^T \tilde{B}_k^T \tilde{K}_{k+1}^T \vartheta_{k+1|k+1}^{-1} \tilde{K}_{k+1} \tilde{B}_k e_{k-\tau_1|k-\tau_1}\right\} \leqslant \chi_2(1 + \eta_8)^{-1}(\zeta_1 \underline{p} \underline{a}^2 I + \zeta I)^{-1}\bar{b}^2 \bar{p} \tag{38}$$

$$E\left\{\chi_3(\tilde{F}_k \sum_{i=1}^{\tau_2} \mu_i e_{k-i|k-i})^T \tilde{K}_{k+1}^T \vartheta_{k+1|k+1}^{-1} \tilde{K}_{k+1} \tilde{F}_k \sum_{i=1}^{\tau_2} \mu_i e_{k-i|k-i}\right\}$$

$$\leqslant E\left\{\chi_3(1 + \eta_8)^{-1}(\zeta_1 \underline{p} \underline{a}^2 I + \zeta I)^{-1}\bar{f}^2 \sum_{i=1}^{\tau_2} \mu_i \sum_{i=1}^{\tau_2} \mu_i \tilde{F}_k \vartheta_{k-i|k-i} \tilde{F}_k^T\right\} \tag{39}$$

$$\leqslant \chi_3(1 + \eta_8)^{-1}(\zeta_1 \underline{p} \underline{a}^2 I + \zeta I)^{-1}\bar{f}^2(\mu_1 + \mu_2 + \cdots + \mu_{\tau_2})^2 \bar{p}$$

$$E\left\{\chi_4 w_{k|k}^T \tilde{D}_k^T \tilde{K}_{k+1}^T \vartheta_{k+1|k+1}^{-1} \tilde{K}_{k+1} \tilde{D}_k w_k\right\} \leqslant \chi_4(1 + \eta_8)^{-1}(\zeta_1 \underline{p} \underline{a}^2 I + \zeta I)^{-1}\bar{d}^2 \bar{q}^2 \tag{40}$$

From equation (13) and the properties of the matrix norm, it is easy to obtain

$$\|K_{k+1}\| \leqslant (1 + \eta_8)\|\vartheta_{k+1|k}\|\|\Omega^{-1}\| \leqslant (1 + \eta_8)\bar{p}\left\|\left((1 + \eta_8^{-1})\tilde{E}_{k+1}\tilde{Q}_{k+1}\tilde{E}_{k+1}^T\right)^{-1}\right\| \leqslant (1 + \eta_8)(1 + \eta_8^{-1})^{-1}\bar{p}\underline{e}^2 \underline{q} = \bar{k}$$

Then

$$\chi_5 w_{k+1}^T \tilde{E}_{k+1}^T K_{k+1}^T \vartheta_{k+1|k+1}^{-1} K_{k+1} \tilde{E}_{k+1} w_{k+1} \leqslant \chi_5(1 + \eta_8)^{-1}(\zeta_1 \underline{p} \underline{a}^2 I + \zeta I)^{-1}\bar{e}^2 \hat{q} \bar{k}^2 \tag{41}$$

By substituting equations (37)–(41) into equation (32), it is easy to derive that

$$\mathrm{E}\{V(e_{k+1|k+1})\} \leqslant \chi_1 \zeta_2 e_{k|k}^T \vartheta_{k|k}^{-1} e_{k|k} + \Theta$$

and

$$\mathrm{E}\{V(e_{k+1|k+1})\} - V(e_{k|k}) \leqslant -\alpha V(e_{k|k}) + \Theta$$

where

$$\alpha = 1 - (1 + \eta_8)^{-1}(1 + \zeta\zeta_1^{-1}\underline{a}^{-2}\underline{p}^{-1})^{-1}$$

$$\Theta = \chi_2(1 + \eta_8)^{-1}(\zeta_1\underline{p}\underline{a}^2 I + \zeta I)^{-1}\bar{b}^2\bar{p} + \chi_3(1 + \eta_8)^{-1}(\zeta_1\underline{p}\underline{a}^2 I + \zeta I)^{-1}\bar{f}^2(\mu_1 + \mu_2 + \cdots + \mu_{\tau_2})^2\bar{p}$$

$$+ \chi_4(1 + \eta_8)^{-1}(\zeta_1\underline{p}\underline{a}^2 I + \zeta I)^{-1}\bar{d}^2\bar{q}^2 + \chi_5(1 + \eta_8)^{-1}(\zeta_1\underline{p}\underline{a}^2 I + \zeta I)^{-1}\hat{e}^2\hat{q}\bar{k}^2$$

It is obvious that $0 < \alpha < 1$ and $\Theta > 0$; hence, the filtering error dynamics is exponentially bounded in the mean square by employing Lemma 1. The proof is completed.

Set-membership filtering for two-dimensional shift-varying systems with stochastic communication protocol and uniform quantization

Chaoqun Zhu, Pan Zhang and Zhiwen Wang(iD)

Abstract

This paper is concerned with the set-membership filtering problem for the two-dimensional shift-varying systems subject to the stochastic communication protocol and uniform quantization effects. To prevent the data transmission from collisions, only one sensor can transmit the measured information to the filter at each sampling shift instant, and the selected sensor is determined by the scheduling strategy of the stochastic communication protocol. On the contrary, the uniform quantization mechanism has been employed to mitigate the influence of quantization error on filtering performance. Incorporating the stochastic communication protocol and uniform quantization mechanism, this paper proposes a set-membership filter design framework for the two-dimensional shift-varying systems with unknown-but-bounded noises. Sufficient conditions are derived for the existence of desired set-membership filter by utilizing double mathematical induction, such that the estimation error resides within the ellipsoidal set. Moreover, the optimal filtering algorithm is given by minimizing the ellipsoidal constraints. Finally, several examples are provided to illustrate the effectiveness of the proposed filter design algorithm.

Introduction

In recent decades, two-dimensional (2D) systems have attracted increasing attention because of their ability to accurately characterize many practical systems, which are extensively used in various fields, such as multivariable network implementation, seismic detection data processing, power transmission lines, and X-ray image enhancement (Ahn et al., 2016; Du and Xie, 1999; Knorn and Middleton, 2013; Wu and Wang, 2015). Due to these wide applications, the 2D system theory becomes one of the most promising branches in control science. Generally speaking, there are three main mathematical models for 2D systems, including Roesser model (Roesser, 1975), Fornasini and Marchesini (FM) model (Fornasini and Marchesini, 1978; Fornasini and Marchesini, 2016), and Kurek model (Kurek, 1985). Among them, FM model is the most commonly used 2D system model, and a number of research results have been proposed based on this model (Chesi and Middleton, 2016; Wang et al., 2019; Wu et al., 2015), which has established and enriched the 2D system theory. Furthermore, owing to mathematical complexities induced by the evolution of 2D systems in two independent directions, the analysis and synthesis of 2D systems are more challenging than that of one-dimensional (1D) systems, and this fact has gained an ever-growing research interest (see Wang et al., 2017a; Wei et al., 2014) and the references therein.

The filtering problems are another research hotspot in control and signal processing communities (Ding et al., 2019; Li et al., 2017). With the rapid development of filtering technology, several well-known filtering methods have been developed according to different noises' characteristics and performance requirements, including but not limited to the Kalman filtering (Qin et al., 2022; Zhang et al., 2021b), the H_∞ filtering (Alyazidi and Mahmoud, 2020; Fu et al., 2020), and the set-membership filtering (Liu et al., 2022; Mao et al., 2022). The Kalman filtering method is always recognized as the most reliable approach for systems with Gaussian noises. However, the Kalman filtering method is difficult to obtain a satisfactory filtering effect when dealing with non-Gaussian noises. The H_∞ filtering approach usually guarantees a given disturbance attenuation level on the estimation error subject to bounded noises; nevertheless, this method tends to ignore the convergence degree of filtering error, which poses many difficulties in ensuring that the filtering error variance is within a satisfactory range. In view of the limitations of the

College of Electrical and Information Engineering, Lanzhou University of Technology, China

Corresponding author:
Zhiwen Wang, College of Electrical and Information Engineering, Lanzhou University of Technology, Lanzhou 730050, China.
Email: wwwangzhiwen@yeah.net

above filtering methods, the set-membership filtering method has been developed by limiting all the error vectors and unknown-but-bounded noises that fall into a given set of ellipsoids, and the best advantage of the set-membership filtering method is to replace the precise mathematical statistical model of noises with a hard constraint of noises. In the past few years, the set-membership filtering issue for 1D systems has been widely investigated (see Gao et al., 2022; Li et al., 2021; Liu et al., 2020, 2021; Zhao et al., 2020; Zou et al., 2021) and other representative works. Along with a variety of filtering techniques being investigated in depth, how to extend the existing filtering methods to 2D systems has attracted a great deal of research attention, and a wealth of literature has appeared on these topics. For example, the H_∞ filtering problem for 2D systems has been discussed by Li et al. (2019); Liang et al. (2016); Wang et al. (2020). In addition, the Kalman filtering methods are presented for 2D systems in Liang et al. (2018) and Wang et al. (2017). However, most of the above results are based on known prior conditions of the statistical model of noises to investigate the design of Kalman and H_∞ filtering algorithms. Since the external environment is difficult to predict in control engineering, it is more practical to obtain the bounded information of noises than the precise mathematical statistics of noises. It is widely known that the set-membership filtering method can obtain well-filtering performance for systems with unknown-but-bounded noises. Unfortunately, the results of set-membership filtering for 2D systems are still scattered compared with 1D systems, which may be due to the uniqueness of the evolving form of 2D systems. Designing a set-membership filter for 2D systems with unknown-but-bounded noises is still a challenging issue, which partially motivates our current investigation.

Besides, due to the influence of network bandwidth and calculation accuracy, signal quantization inevitably occurs and has been one of the main network-induced constraints that degrade the performance of the control systems. In recent years, the analysis and synthesis of networked systems with quantization effects have attracted an ongoing research interest, and several mechanisms have been put forward to deal with the effect of signal quantization, for example, uniform quantizer (Liu et al., 2017), logarithmic quantizer (Zhang et al.,2021a), and dynamic quantizer (Maity and Tsiotras, 2021). Generally speaking, uniform quantizer belongs to fixed-point quantization, while logarithmic quantizer and dynamic quantizer belong to floating-point quantization. Since many on-site hardware and software facilities most utilize fixed-point programming, the uniform quantization technology is widely used in control practice (see Wang et al., 2015; Zou et al., 2017) and the references therein. However, available results concerning the quantization problem of 2D systems are relatively rare. How to investigate the filtering problem based on 2D systems subject to uniform quantization effects deserves further discussion.

It is worth noting that, in many underlying investigations on the filtering problem of networked systems, an implicit assumption is that there are adequate communication channels between the sensors and the filters, and all of the sensors can simultaneously access the communication network for transmitting the measured information to the filters during each sampling period. In many practical systems, nonetheless,

it is quite unrealistic to implement such a communication scheme because that simultaneous multiple access to a limited-bandwidth network would result in data collisions inevitably. One method to handle such a situation is implementing a communication protocol schedule. By now, three communication protocols are employed to arrange the network access sequence of sensors for preventing data conflict effectively, that is, the try-once-discard protocol (Walsh et al., 1999; Walsh and Ye, 2001), the Round-Robin protocol (Walsh et al., 2002), and the stochastic communication protocol (Hristu-Varsakelis and Morgansen, 1999; Zhang et al., 2011). Among these protocols, the try-once-discard and Round-Robin protocol belong to the category of deterministic scheduling schemes, while the stochastic communication protocol is categorized as a stochastic scheduling scheme. Due to the stochastic communication, protocol can be widely used in many industrial control networks, such as Carrier Sense Multiple Access (CSMA) protocol for the Ethernet and ALOHA protocol for the wireless local area network. Therefore, the control and filtering problems under stochastic communication protocol have gained considerable attention (see Tabbara and Nesic, 2008; Zou et al., 2019). However, to the best of the author's knowledge, there is much literature on the filtering problem for the 1D systems subject to stochastic communication protocol so far, while very few results have been available for the corresponding filtering issue of 2D systems under the influence of stochastic communication protocol and uniform quantization. Consequently, it is another research motivation for us to shorten this gap.

To give the response to the above statement, this paper focuses on the set-membership filtering issue for 2D shift-varying systems whose sensors' access to the channels is subject to the stochastic communication protocol and uniform quantitation effects. The main contributions of this paper can be summarized as follows: (a) Based on the FM-II model, the 2D shift-varying systems' framework with the stochastic communication protocol and uniform quantization mechanism is established. (b) For the established model of 2D shift-varying systems, a set-membership filtering algorithm is proposed under the assumption of unknown-but-bounded noises, which can guarantee that the filtering error always resides within the $P(i, j)$-dependent ellipsoidal set. (c) In virtue of the double induction principle, sufficient conditions for the set-membership filter are derived, which is simple and suitable for online operation. Furthermore, the recursive linear matrix inequality (RLMI) technique is used to solve the optimization problem subject to ellipsoidal constraint to attain the optimal filtering gains.

The rest of this paper is organized as follows. "Problem description and preliminaries" section gives the problem description and preliminaries. In "Main results" section, the design procedure of the set-membership filter is proposed for 2D shift-varying systems with stochastic communication protocol and uniform quantization. Several illustrative examples are provided in "Numerical simulations" section to demonstrate the effectiveness of the proposed results. Finally, "Conclusion" section concludes the paper and discusses future research directions.

Notation: The notation used throughout the paper is fairly standard. R^{n_x} denotes the n_x-dimensional Euclidean space and

$P > 0 (P \geq 0)$ means that it is real symmetric and positive definite (semidefinite). G^T, G^{-1}, and $\text{tr}\{G\}$ represent the transpose, the inverse, and the trace of the matrix G, respectively. $diag\{\rho_1, \ldots, \rho_n\}$ stands for a diagonal matrix with the indicated elements on the diagonal, and zeros are located elsewhere. $\text{Pr}\{\xi\}$ means the occurrence probability of the event ξ. $\text{E}\{\zeta\}$ indicates the expectation of the stochastic variable ζ. $\|A\|$ refers to the norm of a matrix A defined by $\|A\| = \sqrt{A^T A}$. $\mathbb{N}$ denotes the set of natural numbers. The Kronecker delta function $\delta(\psi)$ is a binary function that equals 1 if $\psi = 0$ and equals 0 otherwise.

Problem description and preliminaries

Consider 2D shift-varying systems with stochastic nonlinearities described by FM-II model [32] in a finite horizon $i, j \in [0, K]$ as follows

$$
\begin{cases}
x(i+1, j+1) = A_1(i+1, j)x(i+1, j) + A_2(i, j+1) \\
\quad x(i, j+1) + B_1(i+1, j)\omega(i+1, j) \\
\quad + B_2(i, j+1)\omega(i, j+1) + \alpha_1(i+1, j)f(x(i+1, j)) \\
\quad + \alpha_2(i, j+1)f(x(i, j+1)) \\
y(i, j) = C(i, j)x(i, j) + \alpha_3(i, j)f(x(i, j)) + v(i, j)
\end{cases} \quad (1)
$$

where $x(i, j) \in R^{n_x}$ represents the system state vector. $y(i, j) \in R^{n_y}$ is the measurement output before transmitted through the communication network. $\omega(i, j) \in R^{n_p}$ and $v(i, j) \in R^{n_q}$ denote the unknown-but-bounded external disturbances and measurement noises, respectively. The initial states $x(i, 0)$ and $x(0, j)$ are independent of other variables and satisfy the following conditions

$$\text{E}\{x(i, 0)\} = \mu_1(i), \ \text{E}\{x(0, j)\} = \mu_2(j)$$

where $\mu_1(i)$ and $\mu_2(j)$ are known vector for $i, j \in [0, K]$ with $\mu_1(0) = \mu_2(0)$. $f(x(i, j))$ is known smooth nonlinear functions $f : R^{n_x} \to R^{n_x}$ and satisfies the following conditions

$$f(0) = 0, \ \|f(b(i, j)) - f(z(i, j))\| \leq F\|(b(i, j) - z(i, j))\| \quad (2)$$

where $b(i, j)$ and $z(i, j)$ are arbitrary vector belonging to R^{n_x}, and F is known real matrix with appropriate dimensions. $A_1(i, j)$, $A_2(i, j)$, $B_1(i, j)$, $B_2(i, j)$, $C(i, j)$, $\alpha_1(i, j)$, $\alpha_2(i, j)$, and $\alpha_3(i, j)$ are known time-varying matrices with appropriate dimensions, respectively. The variables i and j represent generalized time variables, which can be time itself or variables with time-varying characteristics.

Remark 1: Considered 2D time-varying systems with the FM-II model include stochastic nonlinear functions, unknown-but-bounded external disturbances, and measurement noises. As mentioned above, several significant 2D systems' models have been developed for the actual application environment. Among them, the Roesser model is a special modality of the FM-II state space model; the Attasi model is a special case of the FM-I state space model; and FM-I state space model is a special form of the FM-II state space model. Therefore, the FM-II state space model is more universal as a research framework. In addition, as shown in Figure 1, the evolution of 2D systems depends on the changes in horizontal and
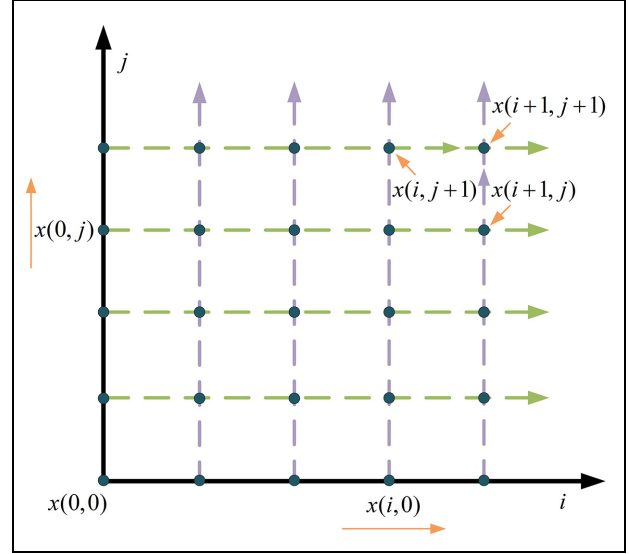
Figure 1. Structure diagram of 2D systems' evolution.

vertical components; in other words, the priority of horizontal or vertical components is crucial for 2D systems. More specifically, the state information of the 1D systems contains all the information of the past moment (global information), while 2D systems only contain local information, which is the main difference between these two types of systems. In addition, compared with the 1D systems, 2D systems can better describe the systems' model in engineering practice and have more general significance to reveal the evolution law of nature (see Li et al., 2019; Liang et al., 2016; Wang et al., 2020). For example, the gas absorption, air drying, and thermal processes can all be characterized by the mathematical model of 2D systems, which can be described by some unknown functions varying with time and space.

For the unknown-but-bounded external disturbances and measurement noises, the following assumption is made in this paper.

Assumption 1: The unknown-but-bounded external disturbances and measurement noises' sequences are confined to the following set of ellipsoids

$$W(i, j) \triangleq \left\{ \omega(i, j) : \omega^T(i, j)S^{-1}(i, j)\omega(i, j) \leq 1 \right\} \quad (3)$$

$$V(i, j) \triangleq \left\{ v(i, j) : v^T(i, j)R^{-1}(i, j)v(i, j) \leq 1 \right\} \quad (4)$$

where $S(i, j)$ and $R(i, j)$ are known positive time-varying real matrices with appropriate dimensions.

Remark 2: In this paper, we assume that both external disturbances and measurement noises are unknown but bounded. $S(i, j)$ and $R(i, j)$ are variables that measure the magnitude of disturbances and noises. When the norm of $S(i, j)$ and $R(i, j)$ is large, it means that the disturbances and noises in the engineering practice are also large. For arbitrarily bounded disturbances and noises' signals, there always exist suitable

$S(i,j)$ and $R(i,j)$ such that the constraints of equations (3) and (4) are satisfied.

Remark 3: It is well known that there are various external disturbances in the process of control practice. In general, external disturbances can be classified as natural disturbances and man-made disturbances. Most natural disturbances can be described by Gaussian noises, but some man-made disturbances (such as electromagnetic disturbances) are difficult to accurately establish their mathematical models due to their non-Gaussian characteristics. As a result, some traditional filtering methods, such as the Kalman filter and the H_∞ filter, may not be well suitable for control systems with man-made disturbances. Consequently, the process noises are assumed to satisfy the condition of bounded energy, and the ellipsoidal set is utilized to describe the unpredictability and boundedness of noises in this paper, which overcomes the difficulty that mathematical statistical characteristics of noises are not always available.

Signal quantization

Next, the model of 2D systems subject to the stochastic communication protocol and uniform quantization effects will be introduced. As shown in Figure 2, the measured signal of sensors is first quantized by the quantizer and then transmitted to the filter through the shared communication network. In this paper, the uniform quantization mechanism is employed, and its saturation level is supposed to be sufficiently large. The following $q(\cdot)$ is the quantization operator, which is defined by a function $round(\cdot)$ that rounds a number to the nearest integer

$$q(y_l(i,j)) = \kappa \, round(y_l(i,j)/\kappa)$$

where $y_l(i,j)$ is the output signal of the lth $(1 \leq l \leq n_y)$ sensor node, and κ indicates the quantizing level and can be adjusted according to the practical control process. Then, the quantization error can be expressed as

$$\Delta_l(i,j) = \tilde{y}_l(i,j) - y_l(i,j) \tag{5}$$

where $\tilde{y}_l(i,j) = q(y_l(i,j))$. It is easy to obtain

$$\|\Delta_l(i,j)\|^2 \leq \frac{\kappa^2}{4} \tag{6}$$

Stochastic communication protocol

For 2D systems with a large number of sensors, the communication between the sensors and the filter is scheduled by certain network protocols to avoid data collisions. In what follows, we will introduce the scheduling protocol of stochastic communication. Without loss of generality, we assume that only one sensor is allowed to access the network channel according to the underlying scheduling protocol, and let $\xi(i,j) \in \{1, 2, \ldots, n_y\}$ denote which sensor is selected to communicate with the filter at each shift instant.

Under the scheduling of stochastic communication protocol, it is assumed that $\xi(i,j) \in \{1, 2, \ldots, n_y\}$ satisfies Bernoulli
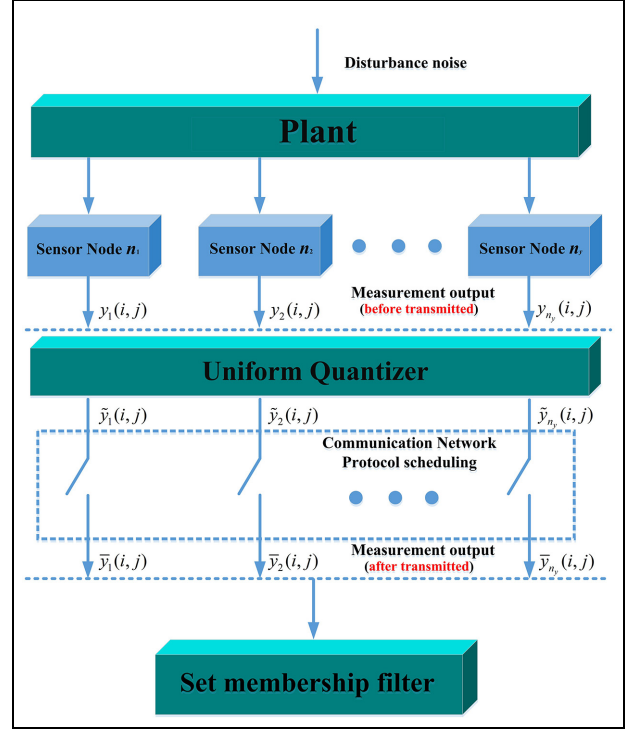
Figure 2. Set-membership filtering problem for 2D shift-varying systems.

stochastic process and mutually independent at sampling shift instant (i,j). The occurrence probability of $\xi(i,j) = m$, $m \in \{1, 2, 3, \ldots, n_y\}$, is given by

$$\Pr\{\xi(i,j) = m\} = p_m$$

where $0 \leq p_m \leq 1$ is the occurrence probability for the sensor node m to be selected to transmit data via the communication network and satisfies $\sum_{m=1}^{n_y} p_m = 1$.

Problem formulation

In this paper, the set-membership filtering problem will be addressed for 2D shift-varying systems subject to signal quantization and stochastic scheduling protocol. In what follows, the signal transmission process is introduced. As shown in Figure 2, the measurement output before quantizing can be characterized as

$$y(i,j) = \begin{bmatrix} y_1^T(i,j) & y_2^T(i,j) & \cdots & y_{n_y}^T(i,j) \end{bmatrix}^T$$

where $y_m(i,j)(1 \leq m \leq n_y)$ denotes measurement output of the mth sensor at shift instant (i,j). As previously mentioned, let

$$\tilde{y}(i,j) = \begin{bmatrix} \tilde{y}_1^T(i,j) & \tilde{y}_2^T(i,j) & \cdots & \tilde{y}_{n_y}^T(i,j) \end{bmatrix}^T \tag{7}$$

$$\bar{y}(i,j) = \begin{bmatrix} \bar{y}_1^T(i,j) & \bar{y}_2^T(i,j) & \cdots & \bar{y}_{n_y}^T(i,j) \end{bmatrix}^T \tag{8}$$

denote the output of uniform quantizer and measurement output after transmitted through the communication network, respectively. Then, the latest measured output $\bar{y}_m(i,j)$ of the mth ($1 \leq m \leq n_y$) sensor, which is received by the filter with a zero order, can be expressed as

$$\bar{y}_m(i,j) = \begin{cases} \tilde{y}_m(i,j) & if \quad \mathrm{m} = \xi(i,j) \\ \bar{y}_m(i,j-1) & otherwise \end{cases} \quad (9)$$

According to equations (7) and (8) and the updating rule of measurement output equation (9), the composite form of $\bar{y}(i,j)$ can be obtained as follows

$$\bar{y}(i,j) = \Phi_{\xi(i,j)}\tilde{y}(i,j) + \left(I - \Phi_{\xi(i,j)}\right)\bar{y}(i,j-1) \quad (10)$$

where $\Phi_{\xi(i,j)} = diag_{1 \leq m \leq n_y}\{\delta(\xi(i,j) - m)I\}$, and $\delta(\cdot)$ is the Kronecker delta function.

Substituting equations (10) and (5) into equation (1), and defining the following augmented variables

$$\bar{x}(i,j) = \begin{bmatrix} x^T(i,j) & \bar{y}^T(i,j-1) \end{bmatrix}^T, \bar{\omega}(i,j)$$
$$= \begin{bmatrix} \omega^T(i,j) & v^T(i,j) \end{bmatrix}^T, \bar{f}(x(i,j)) = \begin{bmatrix} f^T(x(i,j)) & \Delta^T(i,j) \end{bmatrix}^T,$$

the model of 2D shift-varying systems with uniform quantization and stochastic communication protocol can be reformulated as follows

$$\begin{cases} \bar{x}(i+1,j+1) = \bar{A}_1(i+1,j)\bar{x}(i+1,j) + \bar{A}_2(i,j+1) \\ \bar{x}(i,j+1) + \bar{B}_1(i+1,j)\bar{\omega}(i+1,j) \\ \quad + \bar{B}_2(i,j+1)\bar{\omega}(i,j+1) + \bar{\alpha}_1(i+1,j)\bar{f}(x(i+1,j)) \\ \quad + \bar{\alpha}_2(i,j+1)\bar{f}(x(i,j+1)) \\ \bar{y}(i,j) = \bar{C}(i,j)\bar{x}(i,j) + \bar{\alpha}_3(i,j)\bar{f}(x(i,j)) + D(i,j)\bar{\omega}(i,j) \end{cases} \quad (11)$$

where

$$\bar{A}_1(i+1,j) = \begin{bmatrix} A_1(i+1,j) & 0 \\ \Phi_{\xi(i+1,j)}C(i+1,j) & I - \Phi_{\xi(i+1,j)} \end{bmatrix},$$

$$\bar{A}_2(i,j+1) = \begin{bmatrix} A_2(i,j+1) & 0 \\ 0 & 0 \end{bmatrix},$$

$$\bar{B}_1(i+1,j) = \begin{bmatrix} B_1(i+1,j) & 0 \\ 0 & \Phi_{\xi(i+1,j)} \end{bmatrix},$$

$$\bar{B}_2(i,j+1) = \begin{bmatrix} B_2(i,j+1) & 0 \\ 0 & 0 \end{bmatrix},$$

$$\bar{C}(i,j) = \begin{bmatrix} \Phi_{\xi(i,j)}C(i,j) & I - \Phi_{\xi(i,j)} \end{bmatrix},$$

$$D(i,j) = \begin{bmatrix} 0 & \Phi_{\xi(i,j)} \end{bmatrix},$$

$$\bar{\alpha}_1(i+1,j) = \begin{bmatrix} \alpha_1(i+1,j) & 0 \\ \Phi_{\xi(i+1,j)}\alpha_3(i+1,j) & \Phi_{\xi(i+1,j)} \end{bmatrix},$$

$$\bar{\alpha}_2(i,j+1) = \begin{bmatrix} \alpha_2(i,j+1) & 0 \\ 0 & 0 \end{bmatrix},$$

$$\bar{\alpha}_3(i,j) = \begin{bmatrix} \Phi_{\xi(i,j)}\alpha_3(i,j) & \Phi_{\xi(i,j)} \end{bmatrix}.$$

Based on the augmented model of 2D system (equation (11)), a set-membership filter is proposed in the following form

$$\hat{x}(i+1,j+1)$$
$$= \bar{A}_1(i+1,j)\hat{x}(i+1,j) + \bar{A}_2(i,j+1)\hat{x}(i,j+1)$$
$$+ K_{1,\xi(i+1,j)}(\bar{y}(i+1,j) - \bar{C}(i+1,j)\hat{x}(i+1,j)) \quad (12)$$
$$+ K_{2,\xi(i,j+1)}(\bar{y}(i,j+1) - \bar{C}(i,j+1)\hat{x}(i,j+1))$$
$$+ \bar{\alpha}_1(i+1,j)\bar{f}(\hat{x}(i+1,j)) + \bar{\alpha}_2(i,j+1)\bar{f}(\hat{x}(i,j+1))$$

where $\hat{x}(i,j) \in R^{n_x + n_y}$ is the estimation of $\bar{x}(i,j)$, $K_{1,\xi(i+1,j)}$ and $K_{2,\xi(i,j+1)}$ are the filtering gains to be determined later, which are closely related to the stochastic communication protocol. The initial state of filter is set as $\hat{x}(i,0) = 0$ and $\hat{x}(0,j) = 0$ for $i,j \in [0,K]$.

Define the filtering error as $e(i,j) = \bar{x}(i,j) - \hat{x}(i,j)$. Then, the dynamics filtering error of the augmented 2D system (equation (11)) can be derived as

$$e(i+1,j+1) = \Xi_1(i+1,j)e(i+1,j) + \Xi_1(i,j+1)e(i,j+1)$$
$$+ \Xi_2(i+1,j)\bar{\omega}(i+1,j) + \Xi_2(i,j+1)\bar{\omega}$$
$$(i,j+1)$$
$$+ \bar{\alpha}_1(i+1,j)\Psi(f(x(i+1,j))) - \Xi_3$$
$$(i+1,j)\bar{f}(x(i+1,j)) + \bar{\alpha}_2(i,j+1)$$
$$\Psi(f(x(i,j+1))) - \Xi_3(i,j+1)\bar{f}(x(i,j+1))$$
$$(13)$$

where

$$\Xi_1(i+1,j) = \bar{A}_1(i+1,j) - K_{1,\xi(i+1,j)}\bar{C}(i+1,j),$$
$$\Xi_1(i,j+1) = \bar{A}_2(i,j+1) - K_{2,\xi(i,j+1)}\bar{C}(i,j+1),$$
$$\Xi_2(i+1,j) = \bar{B}_1(i+1,j) - K_{1,\xi(i+1,j)}D(i+1,j),$$
$$\Xi_2(i,j+1) = \bar{B}_2(i,j+1) - K_{2,\xi(i,j+1)}D(i,j+1),$$
$$\Psi(f(x(i+1,j))) = \bar{f}(x(i+1,j)) - \bar{f}(\hat{x}(i+1,j)),$$
$$\Psi(f(x(i,j+1))) = \bar{f}(x(i,j+1)) - \bar{f}(\hat{x}(i,j+1)),$$
$$\Xi_3(i+1,j) = K_{1,\xi(i+1,j)}\bar{\alpha}_3(i+1,j),$$
$$\Xi_3(i,j+1) = K_{2,\xi(i,j+1)}\bar{\alpha}_3(i,j+1)$$

Before proceeding further, let us introduce the following Definition, Assumption, and Lemmas, which will be helpful in ensuing developments.

Definition 1: For the augmented 2D system (equation (11)) and the proposed filter (equation (12)), the given sequence of constrained positive matrices $P(i,j) \in R^{(n_x + n_y) \times (n_x + n_y)}$, the filtering error $e(i,j)$ is said to satisfy the $P(i,j)$-dependent ellipsoidal constraint if the following inequality

$$e^T(i,j)P^{-1}(i,j)e(i,j) \leq 1$$

holds for $i,j \in [0,K]$.

Assumption 2: The initial states $x(i,0)$, $x(0,j)$, $\hat{x}(i,0)$, and $\hat{x}(0,j)$ are located inside the given set of ellipsoids:

$$(\bar{x}(i,0) - \hat{x}(i,0))^T P^{-1}(i,0)(\bar{x}(i,0) - \hat{x}(i,0)) \leq 1,$$
$$(\bar{x}(0,j) - \hat{x}(0,j))^T P^{-1}(0,j)(\bar{x}(0,j) - \hat{x}(0,j)) \leq 1$$

where $P(i,0)$ and $P(0,j)$ are given positive definite matrices.

Remark 4: For a given initial filtering error (the difference between the initial value of the systems and the initial value

of the filter) on the vertical and horizontal components, it is easy to obtain the corresponding $P(i, 0)$ and $P(0, j)$ satisfying the above ellipsoidal set constraints in practical application.

Lemma 1 (Suarez, 1989): **(Principle of Double Induction)** Let us suppose that for every $(i, j) \in \mathbb{N}$, $\Omega(i, j)$ is a proposition. If we want to prove that each of propositions $\Omega(i, j)$ is true, it is sufficient to exhibit a generative set, with molecules $\Omega(i - 1, j)$ and $\Omega(i, j - 1)$, and initial set $I = \{(i, 0) : i \in \mathbb{N}\} \cup \{(0, j) : j \in \mathbb{N}\}$ for which:

1. (*initial step*) $\Omega(i, j)$ is true for all $(i, j) \in I$;
2. (*inductive step*) if $\Omega(i - 1, j)$ and $\Omega(i, j - 1)$ are true for all $\{(i - 1, j), (i, j - 1)\} \in \mathbb{N}$, then $\Omega(i, j)$ is true.

Then, $\Omega(i, j)$ is true for all $(i, j) \in \mathbb{N}$.

Lemma 2 (Zou et al., 2016): **(S-procedure)** Let $Y_0, Y_1, \ldots, Y_n \in R^{n \times n}$ be symmetric matrices. $Y_0, Y_1, \ldots, Y_n$ are assumed to satisfy the following conditions:

$\psi^T Y_0 \psi > 0$ for all $\psi \neq 0$ such that $\psi^T Y_\mu \psi \geq 0$, $\mu = 1, 2, \ldots, n$. Note that if exist $\tau_1 \geq 0$, $\tau_2 \geq 0$, $\ldots$, $\tau_n \geq 0$ such that $Y_0 - \sum_{\mu = 1}^n \tau_\mu Y_\mu > 0$. Then, $\psi^T Y_0 \psi > 0$ holds.

Now, we are in the position of analyzing the dynamics filtering error of the set-membership filter for 2D shift-varying systems under the influence of stochastic communication protocol and uniform quantization.

Main results

In this section, the design procedure of set-membership filtering is addressed for the augmented 2D system (equation (11)) by utilizing the RLMI technology.

$P(i, j)$-dependent constraint analysis

The main purpose of this paper is to design a set-membership filter for the augmented 2D system (equation (11)) under the influence of stochastic communication protocol and quantization error. More specifically, the filter design is accomplished by solving the following two problems:

1. Deduce the sufficient conditions which can ensure the filtering error dynamics of the augmented system inside the following ellipsoidal constraint set:

$$\partial(i, j) \triangleq \left\{ e(i, j) | e^T(i, j) P^{-1}(i, j) e(i, j) \leq 1 \right\}$$

where $P(i, j)$ is a positive definite matrix.

2. Calculate the set-membership filtering gains $K_{1, \xi(i + 1, j)}$ and $K_{2, \xi(i, j + 1)}$ by optimizing $P(i, j)$ to minimize the ellipsoid size for the filtering error $e(i, j)$.

Theorem 1: For the given sequence of constraint matrices $P(i, 0)$, $P(0, j)$ ($j = 0$, $i \in [0, K]$ or $i = 0$, $j \in [0, K]$) and the initial states $x(i, 0)$ and $x(0, j)$, considering 2D shift-varying

systems with stochastic nonlinearity (equation (1)), uniform quantization effect (equation 5)), Bernoulli stochastic communication protocol (equation (10)), and set-membership filter (equation (12)), if there exist positive scalars $\lambda_{1, (i, j)}$, $\lambda_{2, (i, j)}$, $\lambda_{3, (i, j)}$, $\lambda_{4, (i, j)}$, and $\gamma(i, j)$, as well as filtering gain matrices $K_{1, \xi(i + 1, j)}$ and $K_{2, \xi(i, j + 1)}$ satisfying the following recursive matrix inequality

$$\begin{bmatrix} -\Lambda(i, j) & \Theta^T(i + 1, j) \\ \Theta(i + 1, j) & \Delta^{-1}(i + 1, j + 1) \end{bmatrix} \leq 0, \quad i, j \in [0, K] \quad (14)$$

where

$$\Lambda(i, j) = \Lambda_0 + \Lambda_1(i, j) + \Lambda_2(i, j) + \Lambda_3(i, j) + \Lambda_4(i, j),$$
$$\Lambda_0 = diag\{1, 0, 0, 0, 0, 0, 0, 0, 0, 0\},$$

$$\Lambda_1(i, j) = \lambda_{1, (i, j)} diag$$
$$\{-2, 0, \Omega^{-1}(i + 1, j), 0, 0, -2, 0, \Omega^{-1}(i, j + 1), 0, 0\},$$

$$\Omega(i + 1, j) = diag\{S(i + 1, j), R(i + 1, j)\},$$
$$\Omega(i, j + 1) = diag\{S(i, j + 1), R(i, j + 1)\},$$

$$\Lambda_2(i, j) = \lambda_{2, (i, j)} diag\{-x^T(i + 1, j) F^T F x(i + 1, j) - n_y \frac{\kappa^2}{4},$$
$$0, 0, 0, 1, -x^T(i, j + 1) F^T F x(i, j + 1) - n_y \frac{\kappa^2}{4}, 0, 0, 0, 1\},$$

$$\Lambda_3(i, j) = \lambda_{3, (i, j)} diag\{-e^T(i + 1, j) F^T F e(i + 1, j), 1, 0, 0, 0, -e^T$$
$$(i, j + 1) F^T F e(i, j + 1), 1, 0, 0, 0\},$$

$$\Lambda_4(i, j) = \lambda_{4, (i, j)} diag\{-1, 0, 0, I, 0, -1, 0, 0, I, 0\},$$
$$\Theta(i + 1, j) = \begin{bmatrix} \Pi(i + 1, j) & 0 \\ 0 & \Pi(i + 1, j) \end{bmatrix},$$

$$\Pi(i + 1, j) = [0 \quad \bar{\alpha}_1(i + 1, j) \quad \Xi_2(i + 1, j) \quad \Xi_1(i + 1, j)$$
$$L(i + 1, j) \quad -\Xi_3(i + 1, j)],$$

$$\Pi(i, j + 1) = [0 \quad \bar{\alpha}_2(i, j + 1) \quad \Xi_2(i, j + 1) \quad \Xi_1(i, j + 1)$$
$$L(i, j + 1) \quad -\Xi_3(i, j + 1)],$$

$$P(i + 1, j + 1) = L(i + 1, j + 1) L^T(i + 1, j + 1), \Delta(i + 1, j + 1)$$
$$= \begin{bmatrix} (1 + \gamma(i, j)) P^{-1}(i + 1, j + 1) & 0 \\ 0 & (1 + \gamma(i, j)^{-1}) P^{-1}(i + 1, j + 1) \end{bmatrix}$$

then, the dynamics filtering error of the augmented system (equation (13)) satisfies $P(i + 1, j + 1)$-dependent ellipsoidal constraint

$$e^T(i + 1, j + 1) P^{-1}(i + 1, j + 1) e(i + 1, j + 1) \leq 1$$

Proof: In what follows, the mathematical induction including the initial step and induction step is employed to prove Theorem 1.

Initial step. For $j = 0$, $i \in [0, K]$ or $i = 0$, $j \in [0, K]$, based on Assumption 2, it can be immediately inferred that $e^T(i, 0) P^{-1}(i, 0) e(i, 0) \leq 1$ and $e^T(0, j) P^{-1}(0, j) e(0, j) \leq 1$.

Inductive step. Suppose the initial states $x(i, 0)$, $x(0, j)$, $\hat{x}(i, 0)$, and $\hat{x}(0, j)$ satisfy $P(i, j)$-dependent constraint, then our objective is to assume that the following inequality constraints

$$e^T(i, j+1)P^{-1}(i, j+1)e(i, j+1) \leq 1 \text{ and } e^T(i+1, j)$$
$$P^{-1}(i+1, j)e(i+1, j) \leq 1$$

are true at shift instant $(i, j+1)$ and $(i+1, j)$, and prove inequality constraint

$$e^T(i+1, j+1)P^{-1}(i+1, j+1)e(i+1, j+1) \leq 1$$

to be true at shift instant $(i+1, j+1)$.

$$e^T(i+1, j+1)P^{-1}(i+1, j+1)e(i+1, j+1) - 1$$
$$= (\Pi(i+1, j)\xi(i+1, j) + \Pi(i, j+1)\xi(i, j+1))^T P^{-1}$$
$$(i+1, j+1)(\Pi(i+1, j)\xi(i+1, j) + \Pi(i, j+1)\xi(i, j+1)) - 1$$
$$= \xi^T(i+1, j)\Pi^T(i+1, j)P^{-1}(i+1, j+1)\Pi(i+1, j)\xi(i+1, j) + \xi^T(i+1, j)\Pi^T(i+1, j)P^{-1}(i+1, j+1) \quad (15)$$
$$\Pi(i, j+1)\xi(i, j+1)$$
$$+ \xi^T(i, j+1)\Pi^T(i, j+1)P^{-1}(i+1, j+1)\Pi(i+1, j)\xi(i+1, j) + \xi^T(i, j+1)\Pi^T(i, j+1)P^{-1}(i+1, j+1)$$
$$\Pi(i, j+1)\xi(i, j+1) - 1$$

For the sake of facilitating succeeding analysis, the $P(i+1, j+1)$-dependent constraint $e^T(i+1, j+1)P^{-1}(i+, j+1)e(i+1, j+1) - 1 \leq 0$ can be rewritten as

$$r^T(i+1, j+1)L^T(i+1, j+1)P^{-1}(i+1, j+1)L(i+1, j+1)$$
$$r(i+1, j+1) - 1 \leq 0$$

where $e(i+1, j+1) = L(i+1, j+1)r(i+1, j+1)$, and $L(i+1, j+1)$ is a factorization of $P(i+1, j+1) = L(i+1, j+1)L^T(i+1, j+1)$

obviously, if $\|r(i+1, j+1)\| \leq 1$, the following inequality constraint holds

$$e^T(i+1, j+1)P^{-1}(i+1, j+1)e(i+1, j+1) - 1 \leq 0$$

Subsequently, we deduce sufficient conditions for the establishment of $e^T(i+1, j+1)P^{-1}(i+1, j+1)e(i+1, j+1) \leq 1$ under the impact of stochastic nonlinearity (equation (1)), uniform quantization effect (equation (5)), and stochastic communication protocol (equation (10)). In addition, the constraints $\|r(i+1, j)\| \leq 1$ and $\|r(i, j+1)\| \leq 1$ for $i, j \in [0, K]$ also need to be highlighted.

To simplify the derivation, let us define

$$\xi(i+1, j) = [1 \quad \Psi^T(f(x(i+1, j))) \quad \bar{\omega}^T(i+1, j)$$
$$r^T(i+1, j) \quad \bar{f}^T(x(i+1, j))]^T,$$

$$\xi(i, j+1) = [1 \quad \Psi^T((f(x(i, j+1)))) \quad \bar{\omega}^T(i, j+1)$$
$$r^T(i, j+1) \quad \bar{f}^T(x(i, j+1))]^T,$$

$$\Pi(i+1, j) = [0 \quad \bar{\alpha}_1(i+1, j) \quad \Xi_2(i+1, j) \quad \Xi_1(i+1, j)L(i+1, j)$$
$$-\Xi_3(i+1, j)],$$

$$\Pi(i, j+1) = [0 \quad \bar{\alpha}_2(i, j+1) \quad \Xi_2(i, j+1) \quad \Xi_1(i, j+1)L(i, j+1),$$
$$-\Xi_3(i, j+1)]$$

Furthermore, in view of the filtering error dynamics (equation (13)), one has

$$e(i+1, j+1) = \Pi(i+1, j)\xi(i+1, j) + \Pi(i, j+1)\xi(i, j+1)$$

then, it is easy to obtain that

To deal with coupling terms and simplify equation (15), we consider the following elementary inequality

$$ab^T + ba^T \leq \rho aa^T + \rho^{-1}bb^T, \forall \rho > 0$$

where a and b are vectors of appropriate dimensions. In virtue of the above elementary inequality, it is not difficult to verify existing $\gamma(i, j) > 0$ such that

$$\xi^T(i+1, j)\Pi^T(i+1, j)P^{-1}(i+1, j+1)\Pi(i, j+1)\xi(i, j+1)$$
$$+ \xi^T(i, j+1)\Pi^T(i, j+1)P^{-1}(i+1, j+1)\Pi(i+1, j)$$
$$\xi(i+1, j)$$
$$\leq \gamma(i, j)\xi^T(i+1, j)\Pi^T(i+1, j)P^{-1}(i+1, j+1)\Pi(i+1, j)$$
$$\xi(i+1, j) + \gamma^{-1}(i, j)\xi^T(i, j+1)\Pi^T(i, j+1)$$
$$P^{-1}(i+1, j+1)\Pi(i, j+1)\xi(i, j+1)$$

$$(16)$$

Combining equations (15) with (16), which yields

$$e^T(i+1, j+1)P^{-1}(i+1, j+1)e(i+1, j+1) - 1$$
$$\leq (1 + \gamma(i, j))\xi^T(i+1, j)\Pi^T(i+1, j)P^{-1}(i+1, j+1)\Pi$$
$$(i+1, j)\xi(i+1, j)$$
$$+ (1 + \gamma^{-1}(i, j))\xi^T(i, j+1)\Pi^T(i, j+1)P^{-1}(i+1, j+1)\Pi$$
$$(i, j+1)\xi(i, j+1) - 1$$

$$(17)$$

Furthermore, let us define

$$\Gamma(i,j) = \begin{bmatrix} \xi^T(i+1,j) & \xi^T(i,j+1) \end{bmatrix}^T, \Theta(i+1,j)$$
$$= \begin{bmatrix} \Pi(i+1,j) & 0 \\ 0 & \Pi(i+1,j) \end{bmatrix}$$

$$\Delta(i+1,j+1)$$
$$= \begin{bmatrix} (1+\gamma(i,j))P^{-1}(i+1,j+1) & 0 \\ 0 & (1+\gamma^{-1}(i,j))P^{-1}(i+1,j+1) \end{bmatrix}$$

then, it is straightforward to obtain that

$$e^T(i+1,j+1)P^{-1}(i+1,j+1)e(i+1,j+1) - 1$$
$$\leqslant (1+\gamma(i,j))\xi^T(i+1,j)\Pi^T(i+1,j)P^{-1}(i+1,j+1)$$
$$\Pi(i+1,j)\xi(i+1,j)$$
$$+ \left(1+\gamma^{-1}(i,j)\right)\xi^T(i,j+1)\Pi^T(i,j+1)P^{-1}(i+1,j+1)$$
$$\Pi(i,j+1)\xi(i,j+1) - 1$$
$$= \Gamma^T(i,j)\Theta^T(i+1,j)\Delta(i+1,j+1)\Theta(i+1,j)\Gamma(i,j)$$
$$- \Gamma^T(i,j)diag\{1,0,0,0,0,0,0,0,0,0\}\Gamma(i,j) \tag{18}$$

Next, we will deal with the unknown-but-bounded external disturbances and measurement noises. From equations (3) and (4), it is easy to obtain

$$\bar{\omega}^T(i+1,j)\Omega^{-1}(i+1,j)\bar{\omega}(i+1,j) \leqslant 2 \tag{19}$$

$$\bar{\omega}^T(i,j+1)\Omega^{-1}(i,j+1)\bar{\omega}(i,j+1) \leqslant 2 \tag{20}$$

where $\Omega^{-1}(i+1,j) = diag\{S^{-1}(i+1,j), R^{-1}(i+1,j)\}$, and $\Omega^{-1}(i,j+1) = diag\{S^{-1}(i,j+1), R^{-1}(i,j+1)\}$

Considering equations (19) and (20), one has

$$\Gamma^T(i,j)diag\{-2,0,\Omega^{-1}(i+1,j),0,0,-2,0,\Omega^{-1}(i,j+1),0,0\}$$
$$\Gamma(i,j) \leqslant 0$$
$$\tag{21}$$

Subsequently, the quantization error and smooth nonlinear function in 2D system (equation (1)) are taken into account. From quantization error equation (6), which yields

$$\|\Delta(i,j)\|^2 = \left\| \begin{bmatrix} \Delta_1(i,j) \\ \Delta_2(i,j) \\ \cdots \\ \Delta_{n_y}(i,j) \end{bmatrix} \right\|^2 \leqslant n_y \frac{\kappa^2}{4}$$

From equation (2), we can obtain

$$\|f(x) - f(z)\| \leqslant \|F(x-z)\|$$

then,

$$\|\bar{f}(x(i+1,j))\|^2 = \begin{bmatrix} f(x(i+1,j)) \\ \Delta(i+1,j) \end{bmatrix}^T \begin{bmatrix} f(x(i+1,j)) \\ \Delta(i+1,j) \end{bmatrix}$$
$$= \|f(x(i+1,j))\|^2 + \|\Delta(i+1,j)\|^2 \tag{22}$$
$$\leqslant x^T(i+1,j)F^TFx(i+1,j) + n_y\frac{\kappa^2}{4}$$

$$\|\bar{f}(x(i,j+1))\|^2 = \begin{bmatrix} f(x(i,j+1)) \\ \Delta(i,j+1) \end{bmatrix}^T \begin{bmatrix} f(x(i,j+1)) \\ \Delta(i,j+1) \end{bmatrix}$$
$$= \|f(x(i,j+1))\|^2 + \|\Delta(i,j+1)\|^2 \tag{23}$$
$$\leqslant x^T(i,j+1)F^TFx(i,j+1) + n_y\frac{\kappa^2}{4}$$

Similarly, it follows from equations (22) and (23) that

$$\Gamma^T(i,j)diag\Big\{ -x^T(i+1,j)F^TFx(i+1,j) - n_y\frac{\kappa^2}{4}, 0, 0, 0, 1,$$
$$-x^T(i,j+1)F^TFx(i,j+1) - n_y\frac{\kappa^2}{4}, 0, 0, 0, 1 \Big\}\Gamma(i,j) \leqslant 0$$
$$\tag{24}$$

from equation (13), we can obtain

$$\|\Psi(f(x(i+1,j)))\|^2 = \|\bar{f}(x(i+1,j)) - \bar{f}(\hat{x}(i+1,j))\|^2$$
$$= \left\| \begin{bmatrix} f(x(i+1,j)) - f(\hat{x}(i+1,j)) \\ 0 \end{bmatrix} \right\|^2$$
$$= \|f(x(i+1,j)) - f(\hat{x}(i+1,j))\|^2 \leqslant e^T(i+1,j)F^TFe(i+1,j)$$
$$\tag{25}$$

similarly, one has

$$\|\Psi(f(x(i,j+1)))\|^2 \leqslant e^T(i,j+1)F^TFe(i,j+1) \tag{26}$$

From equations (25) and (26), it can be obtained that

$$\Gamma^T(i,j)diag\{-e^T(i+1,j)F^TFe(i+1,j),1,0,0,0,.$$
$$-e^T(i,j+1)F^TFe(i,j+1),1,0,0,0\}\Gamma(i,j) \leqslant 0 \tag{27}$$

Finally, according to the conditions $\|r(i+1,j)\| \leqslant 1$ and $\|r(i,j+1)\| \leqslant 1$, it can be rearranged by means of $\Gamma(i,j)$ as follows

$$\Gamma^T(i,j)diag\{-1,0,0,I,0,-1,0,0,I,0\}\Gamma(i,j) \leqslant 0 \tag{28}$$

According to Lemma 2, considering equations (18), (21), (23), (27), and (28), if the following inequality holds

$$\Theta^T(i+1,j)\Delta(i+1,j+1)\Theta(i+1,j)$$
$$- diag\{1,0,0,0,0,0,0,0,0,0\} - \lambda_{1,(i,j)}$$
$$diag\{-2,0,\Omega^{-1}(i+1,j),0,0,-2,0,\Omega^{-1}(i,j+1),0,0\}$$
$$- \lambda_{2,(i,j)}diag\Big\{ -x^T(i+1,j)F^TFx(i+1,j) - n_y\frac{\kappa^2}{4}, 0, 0, 0, 1,$$
$$-x^T(i,j+1)F^TFx(i,j+1) - n_y\frac{\kappa^2}{4}, 0, 0, 0, 1 \Big\}$$
$$- \lambda_{3,(i,j)}diag\Big\{ -e^T(i+1,j)F^TFe(i+1,j),1,0,0,0, -e^T$$
$$(i,j+1)F^TFe(i,j+1),1,0,0,0 \Big\}$$
$$- \lambda_{4,(i,j)}diag\{-1,0,0,I,0,-1,0,0,I,0\} \leqslant 0$$
$$\tag{29}$$

where $\lambda_{1,(i,j)}$, $\lambda_{2,(i,j)}$, $\lambda_{3,(i,j)}$, and $\lambda_{4,(i,j)}$ are positive scalars, then, one has

$$\Theta^T(i+1,j)\Delta(i+1,j+1)\Theta(i+1,j) \\ - diag\{1,0,0,0,0,0,0,0,0,0\} \leqslant 0 \tag{30}$$

in view of equation (18), it is easy to obtain that

$$e^T(i+1,j+1)P^{-1}(i+1,j+1)e(i+1,j+1) - 1 \leqslant 0$$

Obviously, inequality equation (29) is a sufficient condition for the $P(i+1,j+1)$-dependent constraint $e^T(i+1,j+1)P^{-1}(i+1,j+1)e(i+1,j+1) - 1 \leqslant 0$ to be true. In this regard, we have proved that the designed set-membership filter renders the filtering error $e(i,j)$ to fall into the given ellipsoidal set through the initial step and induction step. In what follows, to facilitate the solution of the corresponding filtering gain matrices, we convert equation (29) into the form of linear matrix inequality.

It is obvious that equation (29) is equivalent to

$$\Theta^T(i+1,j)\Delta(i+1,j+1)\Theta(i+1,j) - \Lambda(i,j) \leqslant 0 \tag{31}$$

where

$$\Lambda(i,j) = diag\{1,0,0,0,0,0,0,0,0,0\} + \lambda_{1,(i,j)}$$
$$diag\{-2,0,\Omega^{-1}(i+1,j),0,0,-2,0,\Omega^{-1}(i,j+1),0,0\}$$

$$+ \lambda_{2,(i,j)}diag\left\{-x^T(i+1,j)F^TFx(i+1,j) - n_y\frac{\kappa^2}{4},0,0,0,1,-x^T(i,j+1)F^TFx(i,j+1) - n_y\frac{\kappa^2}{4},0,0,0,1\right\}$$

$$+ \lambda_{3,(i,j)}diag\{-e^T(i+1,j)F^TFe(i+1,j),1,0,0,0,-e^T(i,j+1)F^TFe(i,j+1),1,0,0,0\}$$

$$+ \lambda_{4,(i,j)}diag\{-1,0,0,I,0,-1,0,0,I,0\}$$

By applying the Schur complement, equation (31) is equivalent to

$$\begin{bmatrix} -\Lambda(i,j) & \Theta^T(i+1,j) \\ \Theta(i+1,j) & \Delta^{-1}(i+1,j+1) \end{bmatrix} \leqslant 0.$$

The proof is thus completed.

In Theorem 1, sufficient conditions are derived for the existence of desired set-membership filter that renders the estimation error to satisfy $P(i,j)$-dependent constraints, and the filtering gain matrices at each shift instant (i,j) have been acquired by utilizing the RLMI technology. On account of $P(i,j)$-dependent constraint, $e^T(i,j)P^{-1}(i,j)e(i,j) - 1 \leqslant 0$ is equivalent to $e(i,j)e^T(i,j) \leqslant P(i,j)$, therefore, the minimize the dynamics filtering error $e(i,j)$ at each shift instant (i,j) by solving the optimization problem of $P(i,j)$.

Optimization problem

Corollary 1: For the given sequence of constraint matrices $P(i,0)$, $P(0,j)$ ($j = 0$, $i \in [0,K]$ or $i = 0$, $j \in [0,K]$), the initial states $x(i,0)$ and $x(0,j)$, considering 2D shift-varying systems with stochastic nonlinearity (equation (1)), uniform

quantization effect (equation (5)), Bernoulli stochastic communication protocol (equation (10)), and set-membership filter (equation (12)), if there exist positive scalars $\lambda_{1,(i,j)}$, $\lambda_{2,(i,j)}$, $\lambda_{3,(i,j)}$, $\lambda_{4,(i,j)}$, and $\gamma(i,j)$, as well as optimal filtering gain matrices $K_{1,\xi(i+1,j)}$ and $K_{2,\xi(i,j+1)}$, we can solve the following optimization problem

$$\min_{K_{1,\xi(i+1,j)},K_{2,\xi(i,j+1)},\tilde{\lambda}_{(i,j)},P(i+1,j+1)} tr\{P(i+1,j+1)\} \tag{32}$$

subject to equation (14), where $\tilde{\lambda}_{(i,j)} = \{\lambda_{\beta,(i,j)}\}_{\beta \in \{1,2,3,4\}}$. Then, the dynamic filtering error $e(i,j)$ of set-membership filter will be minimized.

In terms of Theorem 1 and Corollary 1, we summarize the set-membership filtering algorithm as follows:

Remark 5: It should be pointed out that there are some differences between the set-membership filter and the Kalman filter as well as the H_∞ filter. The Kalman filter usually obtains the filtering error covariance by solving two difference equations in Riccati form and then minimizes the filtering error covariance to obtain the optimal filtering gain. The H_∞ filtering method first reconstructs the state-space model of original systems and the filtering error into a new augmented system, then obtains the filtering gain that renders the augmented sys-

tem to be stable with the given disturbance attenuation level through Linear Matrix Inequality (LMI) technology. Different from the above filtering methods, the designed set-membership filter with the form of equation (12) guarantees that the filtering error always satisfies the constraint of an ellipsoidal set. To be more specific, the proposed filtering algorithm is utilized to derive the appropriate filter gains $K_{1,\xi(i+1,j)}$ and $K_{2,\xi(i,j+1)}$, and regulate the filtering error to satisfy the $P(i,j)$-dependent constraint condition. Furthermore, the minimum trace of $P(i,j)$ is acquired by using the convex optimization method to ensure the filtering error is minimal.

Numerical simulations

In this section, three examples are provided to illustrate the effectiveness of the presented set-membership filtering algorithm for 2D systems subject to the stochastic communication protocol and uniform quantization effects. It includes a numerical example of convergent 2D systems, a practical industrial heating exchange processes, and a numerical example of divergent 2D systems.

Example 1: Consider 2D systems (equation (1)) with the following parameters:

Algorithm 1. Set-membership Filtering Algorithm for 2D Systems with Stochastic Communication Protocol and Uniform Quantization:

Step 1: Set the initial conditions $x(i, 0)$, $x(0, j)$, $\hat{x}(i, 0)$, $\hat{x}(0, j)$, $P(i, 0)$, $P(0, j)$, $S(i, j)$, and $R(i, j)$ satisfying Assumption 1 and Assumption 2 for $i, j \in [0, K]$.
Step 2: For $i = [0, K]$ and $j = 0$, calculate $K_{1, \xi(i + 1, j)}$, $K_{2, \xi(i, j + 1)}$, and $P(i, j)$ from equations (14) and (32).
Step 3: For $j = [1, K]$ and $i = 0$, calculate $K_{1, \xi(i + 1, j)}$, $K_{2, \xi(i, j + 1)}$, and $P(i, j)$ from equations (14) and (32).
Step 4: For $i = 1 : K$
For $j = 1 : K$
calculate $K_{1, \xi(i + 1, j)}$, $K_{2, \xi(i, j + 1)}$, $P(i, j)$, and $\hat{x}(i, j)$ from equations (14) and (32)
end
end
Step 5: Stop.

Table 1. Values of $K_{1, \xi(i + 1, j)}$.

$$K_{1, \xi(1, 0)} = \begin{bmatrix} 0.9119 & 0 \\ -1.5755 & 0 \\ 3.4341 & 0 \\ 0 & 1 \end{bmatrix} \qquad K_{1, \xi(1, 1)} = \begin{bmatrix} 0.1164 & 0 \\ -0.3700 & 0 \\ 0.0084 & 0 \\ 0 & 1 \end{bmatrix} \quad \cdots \quad K_{1, \xi(1, 40)} = \begin{bmatrix} 0.1920 & -0.2000 \\ 0.2411 & 0 \\ 1 & 0 \\ 0 & -4.7713 \end{bmatrix}$$

$$K_{1, \xi(2, 0)} = \begin{bmatrix} 0.8654 & 0.2311 \\ 0 & 0 \\ 1 & 0 \\ 0 & -1.2827 \end{bmatrix} \qquad K_{1, \xi(2, 1)} = \begin{bmatrix} -0.0214 & 0 \\ -0.3900 & 0 \\ -1.5481 & 0 \\ 0 & 1 \end{bmatrix} \quad \cdots \quad K_{1, \xi(2, 40)} = \begin{bmatrix} -0.0609 & 0 \\ 0.0130 & 0 \\ -2.2700 & 0 \\ 0 & 1 \end{bmatrix}$$

$\cdots$ $\cdots$ $\cdots$ $\cdots$

$$K_{1, \xi(40, 0)} = \begin{bmatrix} -0.6375 & 0 \\ 0.1615 & 0 \\ -1.9330 & 0 \\ 0 & 1 \end{bmatrix} \qquad K_{1, \xi(40, 1)} = \begin{bmatrix} 0.6440 & 0 \\ -0.2870 & 0 \\ 0.0559 & 0 \\ 0 & 1 \end{bmatrix} \quad \cdots \quad K_{1, \xi(40, 40)} = \begin{bmatrix} 0.0355 & 0 \\ -0.0060 & 0 \\ -0.1059 & 0 \\ 0 & 1 \end{bmatrix}$$

$$A_1(i, j) = \begin{bmatrix} 0.2 + 0.1 \sin((i + j)/10) & 0.6 \\ -0.6 & 0.01 \end{bmatrix},$$

$$A_2(i, j) = \begin{bmatrix} 0.1 + 0.1 \sin((i + j)/10) & 0 \\ -0.6 & -0.1 \end{bmatrix},$$

$$B_1(i, j) = \begin{bmatrix} 0.05 \sin(0.1\pi(i + j)/3) & 0.12 \\ -0.3 & 0.04 \sin(0.4\pi(i + j)) \end{bmatrix},$$

$$B_2(i, j) = \begin{bmatrix} 0.02 & 0.13 \\ -0.2 \sin(0.4\pi(i + j)) & 0.1 \end{bmatrix}, \quad C(i, j) = \begin{bmatrix} 1 & 0 \\ 0 & 1 \end{bmatrix},$$

$$\alpha_1(i, j) = \begin{bmatrix} -0.2 & 0.15 \\ 0.4 \sin(0.1\pi(i + j)) & 0.4 \sin(0.12\pi(i + j)) \end{bmatrix},$$

$$\alpha_2(i, j) = \begin{bmatrix} -0.2 & 0.15 \\ 0.2 \sin(0.1\pi(i + j)) & 0.1 \sin(0.12\pi(i + j)) \end{bmatrix},$$

$$\alpha_3(i, j) = \begin{bmatrix} -0.2 & 0.15 \\ 0.4 \sin(0.1\pi(i + j)) & 0.4 \sin(0.12\pi(i + j)) \end{bmatrix}.$$

In the simulation, we take the initial state of systems as $x(i, j) = [1.2 \cos(j) \sin(i) \ 1.3 \cos(i - 1) \sin(j)]^T$ for $i \in [0 \ 40]$ and $j = 0$, $x(i, j) = [3.3 \sin(i) \cos(j + 1) \ 2.9 \cos(i + 1) \sin(j - 1)]^T$ for $i = 0$ and $j \in [1 \ 40]$, the initial estimation as $\hat{x}(i, 0) = \hat{x}(0, j) = [0 \ 0]^T$ for $i, j \in [0, 40]$. Moreover, let $P(i, 0) = P(0, j) = 0.5I, R(i, j) = S(i, j) = 0.2I$ for $i, j \in [0, 40], F = 0.2I$, respectively. The quantizing level could be selected as $\kappa = 0.2$.

The unknown-but-bounded external disturbances $\omega(i, j)$ and measurement noises $v(i, j)$ are selected as

$$\omega(i, j) = \begin{cases} [0.2 \sin(0.6(i + j)) \ 0.3 \cos(0.3(i + j))]^T & i, j \in [1 \ 25] \\ 0 & otherwise \end{cases}$$

$$v(i, j) = \begin{cases} [0.2 \sin(0.6(i + j)) \ 0.2 \cos(0.3(i + j))]^T & i, j \in [1 \ 25] \\ 0 & otherwise \end{cases}$$

It is assumed that the probability of sensor 1 obtaining access to the communication network is $\Pr\{\xi(i, j) = 1\} = p_1 = 0.7$, and the probability of sensor 2 obtaining access to the communication network is $\Pr\{\xi(i, j) = 2\} = p_2 = 0.3$.

Then, by applying Theorem 1 and Algorithm 1, the set-membership filtering gain matrices $\{K_{1, \xi(i + 1, j)}\}$ and $\{K_{2, \xi(i, j + 1)}\}$ are exhibited in Tables 1 and 2, respectively.

The simulation results are shown in Figures 3–13. Figure 3 depicts the communication sequence subject to the stochastic communication protocol. The "blue square" represents sensor 1 obtaining the access authority to communication network. Similarly, the "yellow square" represents sensor 2 obtaining the access authority to communication network. Figures 4 and 5 are concerning the trajectories of the first component of state $x_1(i, j)$ and the second component of state $x_2(i, j)$, respectively. Figures 6 and 7 describe the trajectories of the first component of dynamic filtering error $e_1(i, j)$ and the second component of dynamic filtering error $e_2(i, j)$, respectively. It can be seen from Figures 6 and 7 that the dynamic filtering error converges rapidly after the initial horizon. In addition, the filtering error fluctuates in the finite horizon $i, j \in [1 \ 25]$

Table 2. Values of $K_{2,\xi(i,j+1)}$.

$$K_{2,\xi(0,1)} = \begin{bmatrix} 5.2334 & 0 \\ -0.8018 & 0 \\ 3.4057 & 0 \\ 0 & 1 \end{bmatrix} \qquad K_{2,\xi(1,1)} = \begin{bmatrix} 0.6100 & 0 \\ -0.0380 & 0 \\ -0.2070 & 0 \\ 0 & 1 \end{bmatrix} \qquad \cdots \qquad K_{2,\xi(40,1)} = \begin{bmatrix} 0.3000 & 0.6330 \\ 0.0012 & -0.0015 \\ 1 & 0.0058 \\ 0 & 0.0424 \end{bmatrix}$$

$$K_{2,\xi(0,2)} = \begin{bmatrix} 1.1260 & 0.2311 \\ -0.2300 & 0 \\ -0.0186 & 0 \\ 0 & 1 \end{bmatrix} \qquad K_{2,\xi(1,2)} = \begin{bmatrix} 0.4340 & 0 \\ -0.2060 & 0 \\ -0.0429 & 0 \\ 0 & 1 \end{bmatrix} \qquad \cdots \qquad K_{2,\xi(40,2)} = \begin{bmatrix} 0.2362 & 0.0110 \\ -0.1430 & 0 \\ -0.0015 & 0 \\ 0 & 1 \end{bmatrix}$$

$$\cdots \qquad\qquad \cdots \qquad\qquad \cdots \qquad\qquad \cdots$$

$$K_{2,\xi(0,40)} = \begin{bmatrix} 0.7917 & 0 \\ -0.1663 & 0 \\ -0.1578 & 0 \\ 0 & 1 \end{bmatrix} \qquad K_{2,\xi(1,40)} = \begin{bmatrix} 0.6442 & 0 \\ -0.2871 & 0 \\ 0.0559 & 0 \\ 0 & 1 \end{bmatrix} \qquad \cdots \qquad K_{2,\xi(40,40)} = \begin{bmatrix} 0.0355 & 0 \\ -0.0060 & 0 \\ -0.1059 & 0 \\ 0 & 1 \end{bmatrix}$$
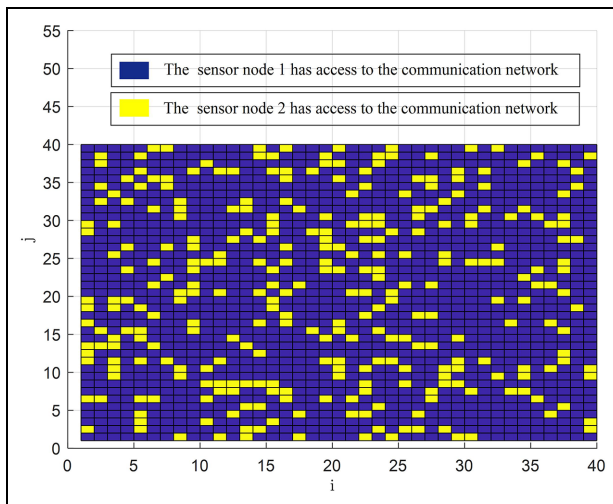
Figure 3. Sensors' communication sequence under the stochastic communication protocol.
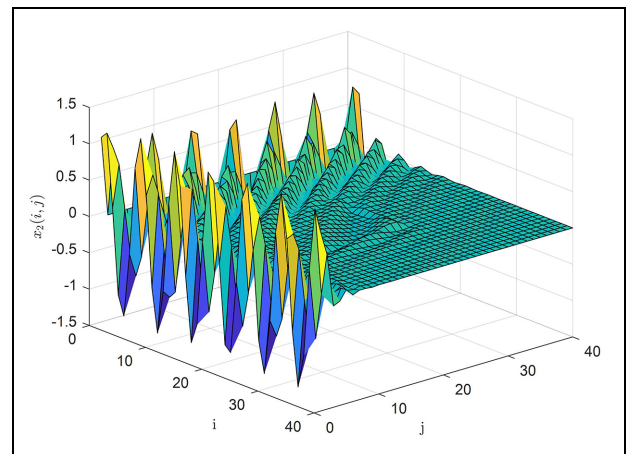
Figure 5. Trajectory of the second component of state $x_2(i,j)$ in example 1.
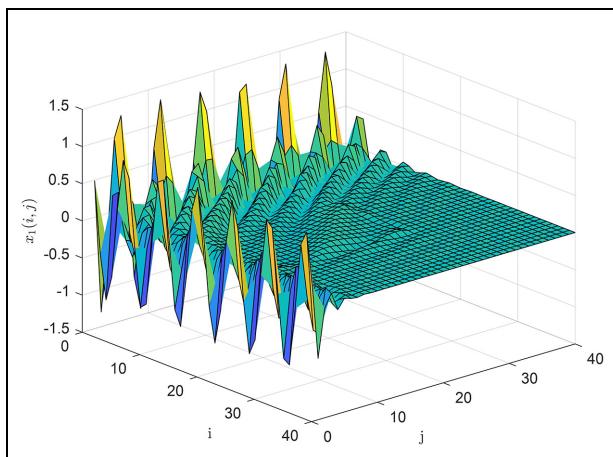
Figure 4. Trajectory of the first component of state $x_1(i,j)$ in example 1.
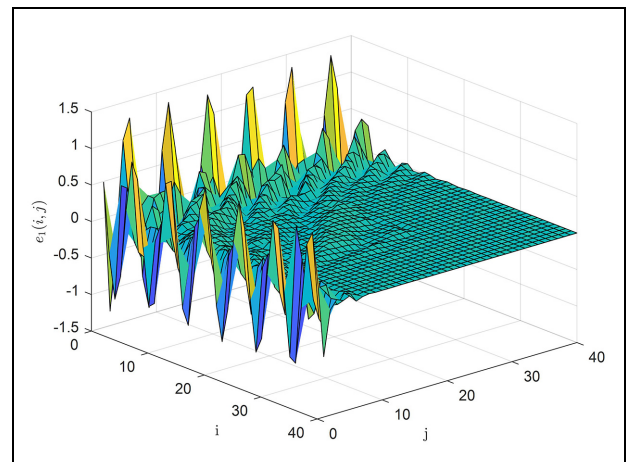
Figure 6. Trajectory of the first component of dynamic filtering error $e_1(i,j)$ in example 1.
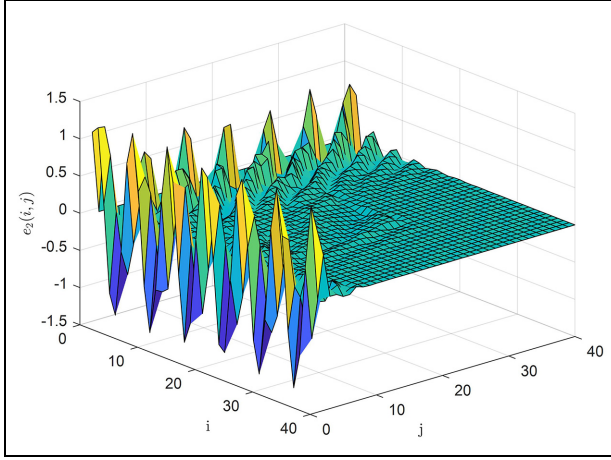
Figure 7. Trajectory of the second component of dynamic filtering error $e_2(i, j)$ in example 1.
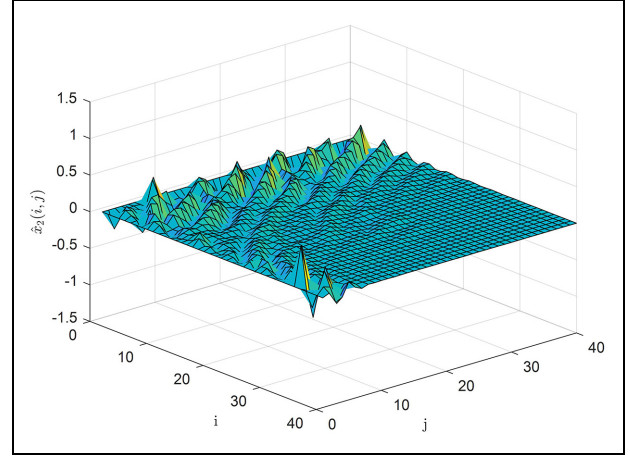
Figure 9. Trajectory of the second component of set-membership filtering estimation $\hat{x}_2(i, j)$ in example 1.
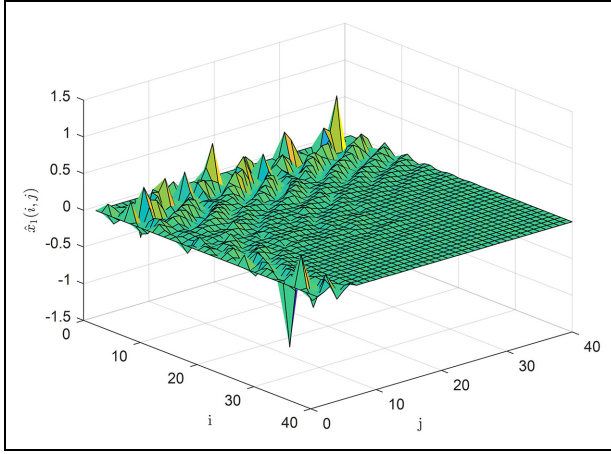
Figure 8. Trajectory of the first component of set-membership filtering estimation $\hat{x}_1(i, j)$ in example 1.

due to external disturbance, and the dynamic filtering error finally converges to 0 after the end of the external disturbance, which reflects the excellent performance of the proposed filtering algorithm. Figures 8 and 9 describe the trajectories of the first component of filtering estimation $\hat{x}_1(i, j)$ and the second component of filtering estimation $\hat{x}_2(i, j)$, respectively. To more intuitively illustrate the superior performance of designed filter, we limit the vertical component j and horizontal component i to evolve independently from 8 to 11. The comparison of the true systems' state with the estimation state is shown in Figures 10–13. It can be seen that the estimated state of proposed filtering algorithm can effectively follow the real state of the systems.

Example 2: Consider an industrial heating exchange processes satisfying the following partial differential equation (Wang et al., 2020), which structure diagram is shown in Figure 14

$$\frac{\partial \hbar(x, t)}{\partial x} + \frac{\partial \hbar(x, t)}{\partial t} = a(i, j)\hbar(x, t) - b(i, j)u(x, t)$$

where $\hbar(x, t)$ is the temperature function associated with both the space dimension $x \in \begin{bmatrix} 0 & X \end{bmatrix}$ and the time dimension $t \in \begin{bmatrix} 0 & T \end{bmatrix}$. The real numbers $a(i, j)$ and $b(i, j)$ are used to represent the exchange coefficients in the working processes.

Define $\hbar(i, j) = \hbar(i\Delta x, j\Delta t)$, then the corresponding partial derivative process can be approximated as follows

$$\frac{\partial \hbar(x, t)}{\partial x} \approx \frac{\hbar(i\Delta x, j\Delta t) - \hbar((i - 1)\Delta x, j\Delta t)}{\Delta x}, \frac{\partial \hbar(x, t)}{\partial t}$$
$$\approx \frac{\hbar(i\Delta x, j\Delta t) - \hbar(i\Delta x, (j - 1)\Delta t)}{\Delta t}, \hbar(x, t) \approx \hbar(i, j),$$

then, when $b(i, j) = 0$, the original partial differential equation can be approximately rewritten in the following form

$$\hbar(i, j + 1) = \left(1 - \frac{\Delta t}{\Delta x} + a(i, j)\Delta t\right)\hbar(i, j) + \frac{\Delta t}{\Delta x}\hbar(i - 1, j)$$

furthermore, the original partial differential equation can be transformed into the following FM-II model

$$x(i + 1, j + 1) = A_1(i + 1, j)x(i + 1, j) + A_2(i, j + 1)x(i, j + 1)$$

where

$$A_1(i + 1, j) = \begin{bmatrix} 0 & 0 \\ \frac{\Delta t}{\Delta x} & 1 - \frac{\Delta t}{\Delta x} + a(i, j)\Delta t \end{bmatrix}, A_2(i, j + 1) = \begin{bmatrix} 0 & 1 \\ 0 & 0 \end{bmatrix}.$$

From the perspective of engineering practice, the real state of 2D systems will inevitably suffer from noise pollution. In addition, there are some unpredictable changes in the processes of heating exchange, which leads the parameters of 2D systems to drift with timelapse. Furthermore, some nonlinear factors in the working processes also need to be emphasized. The partial differential equation has the following parameters:
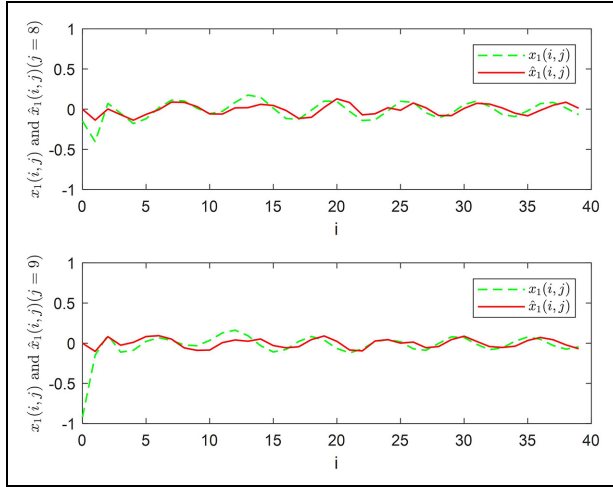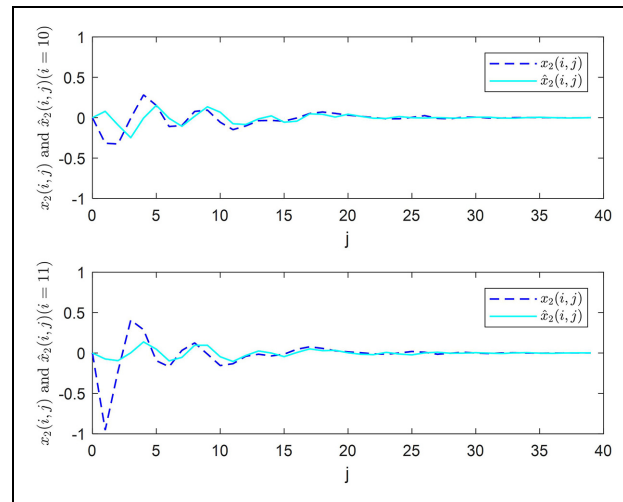
Figure 10. First component of system state $x_1(i,j)$ and its estimation $\hat{x}_1(i,j)$ on $j = 8, 9$ in example 1.
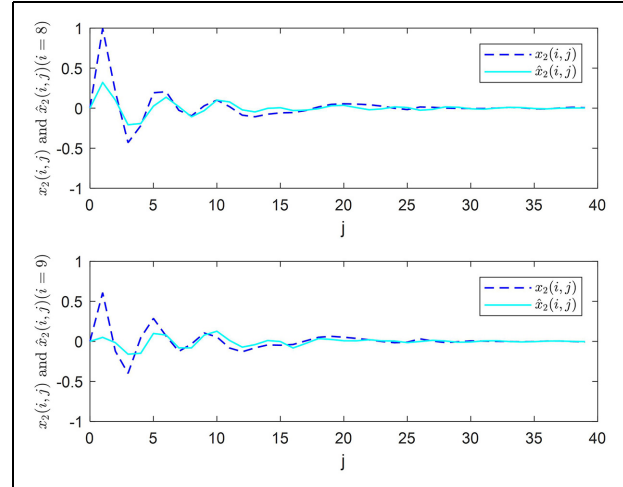
Figure 12. Second component of system state $x_2(i,j)$ and its estimation $\hat{x}_2(i,j)$ on $i = 8, 9$ in example 1.
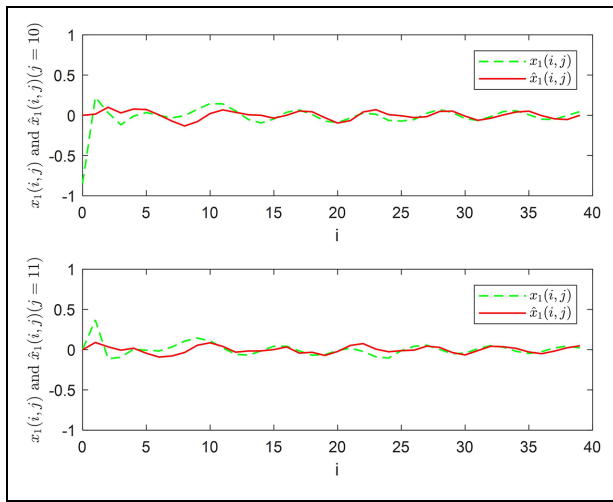
Figure 11. First component of system state $x_1(i,j)$ and its estimation $\hat{x}_1(i,j)$ on $j = 10, 11$ in example 1.


Figure 13. Second component of system state $x_2(i,j)$ and its estimation $\hat{x}_2(i,j)$ on $i = 10, 11$ in example 1.

$$\Delta t = 0.1, \ \Delta x = 0.33, \ a(i,j) = \cos(0.2(i+j)) - 3, A_1(i+1,j)$$
$$= \begin{bmatrix} 0 & 0 \\ 0.33 & 0.36 + \cos(0.2(i+j)) \end{bmatrix}, A_2(i,j+1) = \begin{bmatrix} 0 & 1 \\ 0 & 0 \end{bmatrix},$$
$$B_1(i,j) = \begin{bmatrix} -0.65 + 0.05\sin(0.1\pi(i+j)/3) & 0.12 \\ 0.2 & 0.04\sin(0.4\pi(i+j)) \end{bmatrix},$$
$$B_2(i,j) = \begin{bmatrix} 0.1 & 0.2 \\ -0.02\sin(0.4\pi(i+j)) & -0.85 \end{bmatrix}, C(i,j) = \begin{bmatrix} 1 & 0 \\ 0 & 1 \end{bmatrix},$$

and the remaining parameters are the same as example 1.

The simulation results are shown in Figures 15–20. Figures 15 and 16 are concerning the trajectories of the first component of state $x_1(i,j)$ and the second component of state $x_2(i,j)$, respectively. Figures 17 and 18 present the trajectories of the first component of filtering estimation $\hat{x}_1(i,j)$ and the second component of filtering estimation $\hat{x}_2(i,j)$, respectively.
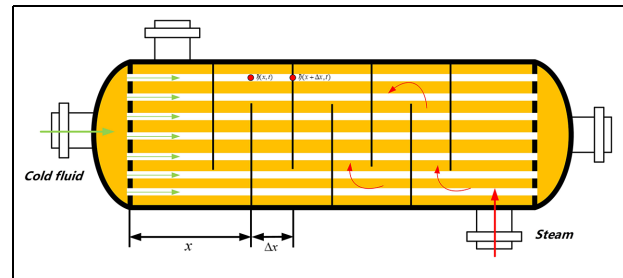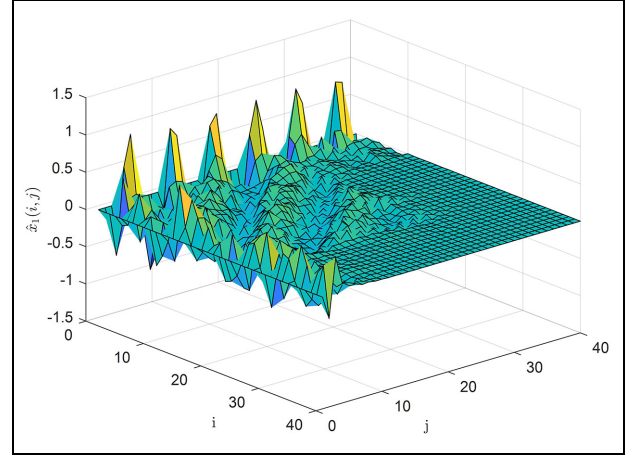

**Figure 14.** Schematic diagram of industrial heating exchange processes.

Similarly, we prescribe a limit to the vertical component j and horizontal component i to evolve independently from 10 to 11, and provide the evolution trajectory of the systems' state
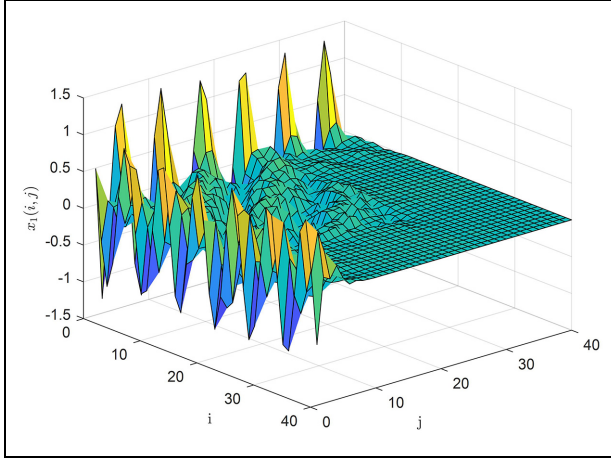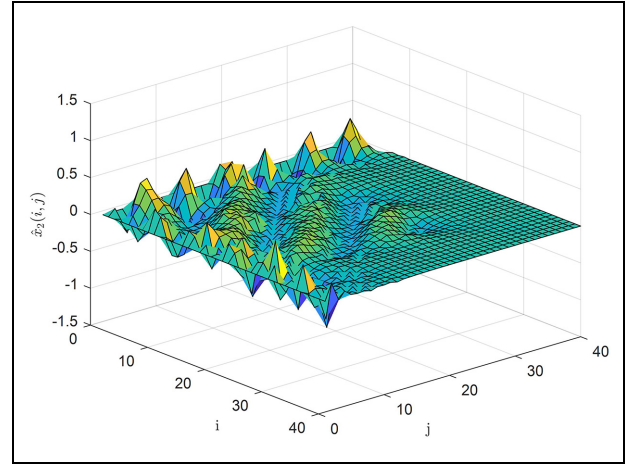
Figure 15. Trajectory of the first component of state $x_1(i,j)$ in example 2.

Figure 17. Trajectory of the first component of set-membership filtering estimation $\hat{x}_1(i,j)$ in example 2.
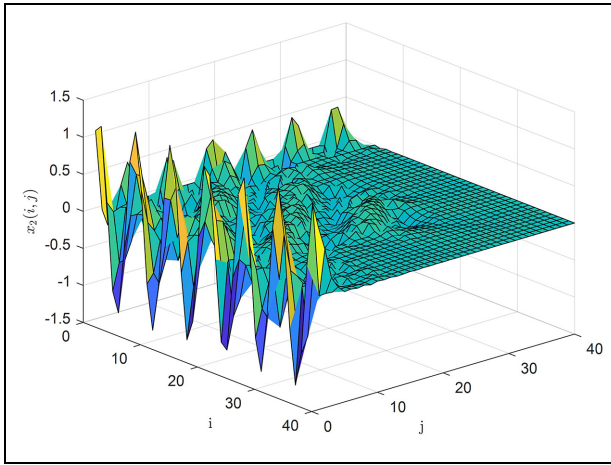
Figure 16. Trajectory of the second component of state $x_2(i,j)$ in example 2.

Figure 18. Trajectory of the second component of set-membership filtering estimation $\hat{x}_2(i,j)$ in example 2.

and estimated state in Figures 19 and 20. The comparison of systems' state with the estimated state is shown in Figures 19–20. It can be seen from Figures 15–20 that the proposed set-membership filtering algorithm has superb filtering performance, and the estimated state can effectively track the system state of 2D systems under the interference of noises.

Example 3: Consider 2D systems (equation (1)) with the following parameters:

$$A_1(i,j) = \begin{bmatrix} 0.7 + 0.1\sin\left((i+j)/10\right) & 0.38 \\ 0.24 & 0.2 \end{bmatrix},$$

$$A_2(i,j) = \begin{bmatrix} 0.65 + 0.1\sin\left((i+j)/10\right) & 0.44 \\ 0.3 & 0.35 \end{bmatrix},$$

and the remaining parameters are the same as example 1.

Simulation results are shown in Figures 21–24. Figures 21 and 22 are concerning the trajectories of the first component of state $x_1(i,j)$ and the second component of state $x_2(i,j)$,
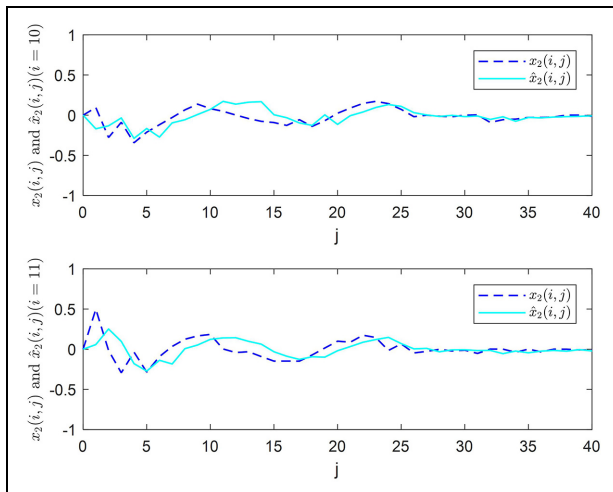
respectively. Figures 23 and 24 exhibit the trajectories of the first component of filtering estimation $\hat{x}_1(i,j)$ and the second component of filtering estimation $\hat{x}_2(i,j)$. It can be clearly seen that when the systems' state diverges, the set-membership filtering algorithm developed in this paper is still valid and has prominent filtering performance.
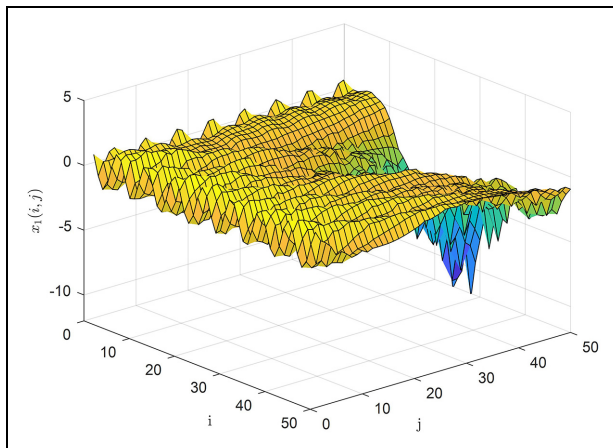
Conclusion

This paper has investigated the set-membership filtering design problem for 2D shift-varying systems subject to the stochastic communication protocol and uniform quantization effects. On account of the limited bandwidth of the communication network, only one sensor can transmit the measured information to the filter at each sampling shift instant (i,j), and the selected sensor is determined by the stochastic scheduling strategy. The uniform quantization mechanism has been employed to mitigate the influence of quantization error on filtering performance. In such a framework, the model of
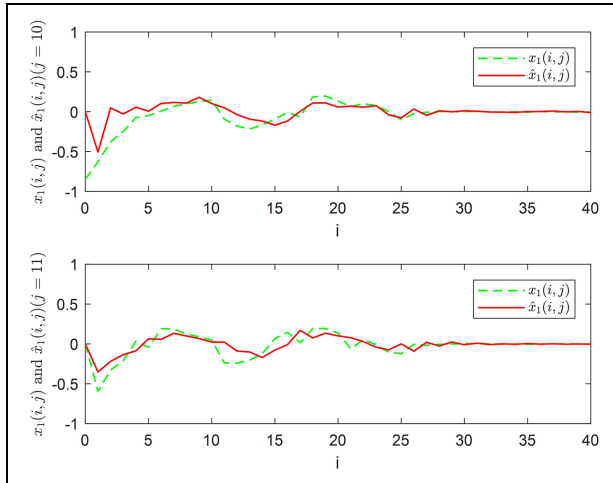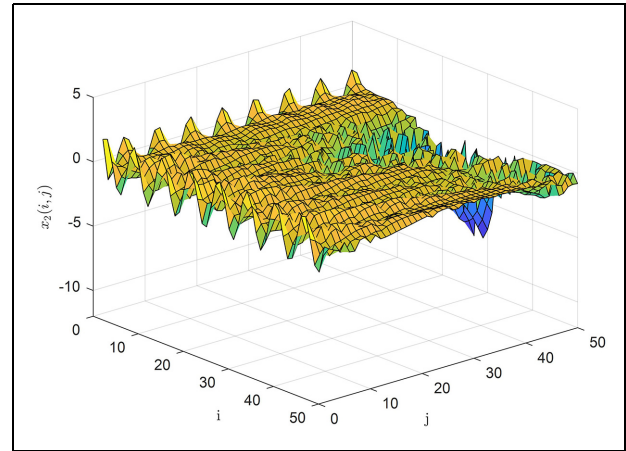
Figure 19. First component of system state $x_1(i,j)$ and its estimation $\hat{x}_1(i,j)$ on $j = 10, 11$ in example 2.
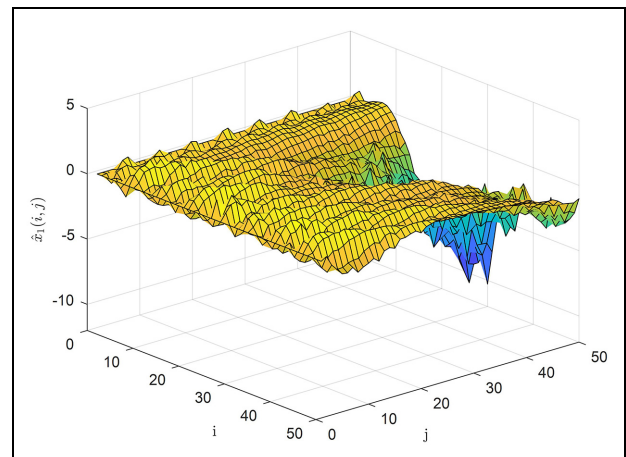

Figure 22. Trajectory of the first component of state $x_2(i,j)$ in example 3.

Figure 20. Second component of system state $x_2(i,j)$ and its estimation $\hat{x}_2(i,j)$ on $i = 10, 11$ in example 2.
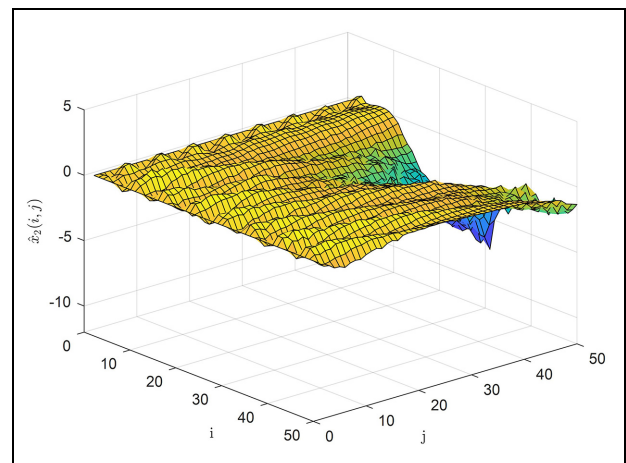

Figure 23. Trajectory of the first component of set-membership filtering estimation $\hat{x}_1(i,j)$ in example 3.

Figure 21. Trajectory of the first component of state $x_1(i,j)$ in example 3.

Figure 24. Trajectory of the first component of set-membership filtering estimation $\hat{x}_2(i,j)$ in example 3.

augmented 2D time-varying systems is established under the impact of stochastic communication protocol and signal quantization, and the set-membership filtering algorithm has been designed to obtain the estimation of system state. Sufficient conditions have been derived to guarantee that the filtering error satisfies the $P(i, j)$-dependent constraints. Then, optimal set-membership filtering gains have been obtained by minimizing the ellipsoidal constraints of filtering error. Finally, simulation examples have demonstrated the effectiveness of the developed set-membership filtering algorithm.

Declaration of conflicting interests

The author(s) declared no potential conflicts of interest with respect to the research, authorship, and/or publication of this article.

Funding

ORCID iD

Zhiwen Wang https://orcid.org/0000-0002-5425-0705

References

Ahn CK, Shi P and Karimi HR (2016) Novel results on generalized dissipativity of two-dimensional digital filters. *IEEE Transactions Circuits Systems I—Express Briefs* 63(9): 893–897.

Alyazidi N and Mahmoud M (2020) Distributed H2/H∞ filter design for discrete-time switched systems. *IEEE/CAA Journal of Automatica Sinica* 7(1): 158–168.

Chesi G and Middleton RH (2016) Robust stability and performance analysis of 2D mixed continuous-discrete-time systems with uncertainty. *Automatica* 67: 233–243.

Ding D, Han Q-L, Wang Z, et al. (2019) A survey on model-based distributed control and filtering for industrial Cyber-Physical Systems. *IEEE Transactions on Industrial Informatics* 15(5): 2483–2499.

Du C and Xie L (1999) Stability analysis and stabilization of uncertain two-dimensional discrete systems: An LMI approach. *IEEE Transactions on Circuits and Systems I: Fundamental Theory and Applications* 46(11): 1371–1374.

Fornasini E and Marchesini G (1978) Doubly indexed dynamical systems: State models and structural properties. *Mathematics of Control, Signals, and Systems* 12(1): 59–72.

Fornasini E and Marchesini G (2016) State-space realization theory of two-dimensional filters. *IEEE Transactions on Automatic Control* 21(4): 484–492.

Fu H, Dong H and Han F (2020) Outlier-resistant H∞ filtering for a class of networked systems under Round-Robin protocol. *Neurocomputing* 403: 133–142.

Gao Y, Ma L, Zhang M, et al. (2022) Distributed set-membership filtering for nonlinear time-varying systems with dynamic coding-decoding communication protocol. *IEEE Systems Journal* 16(2): 2958–2967.

Hristu-Varsakelis D and Morgansen K (1999) Limited communication control. *Systems and Control Letters* 37(4): 193–205.

Knorn S and Middleton RH (2013) Stability of two-dimensional linear systems with singularities on the stability boundary using LMIs. *IEEE Transactions on Automatic Control* 58(10): 2579–2590.

Kurek JE (1985) The general state-space model for a two-dimensional linear digital system. *IEEE Transactions on Automatic Control* 30(6): 600–602.

Li DH, Liang J and Wang F (2019) H∞ state estimation for two-dimensional systems with randomly occurring uncertainties and Round-Robin protocol. *Neurocomputing* 34: 248–260.

Li W, Jia Y and Du J (2017) State estimation for stochastic complex networks with switching topology. *IEEE Transactions on Automatic Control* 62(12): 6377–6384.

Li X, Wei G and Wang L (2021) Distributed set-membership filtering for discrete-time systems subject to denial-of-service attacks and fading measurements: A zonotopic approach. *Information Science* 547: 49–67.

Liang J, Wang F, Wang Z, et al. (2018) Robust Kalman filtering for two-dimensional systems with multiplicative noises and measurement degradations: The finite-horizon case. *Automatica* 96: 166–177.

Liang J, Wang Z, Hayat T, et al. (2016) Distributed H∞ state estimation for stochastic delayed 2-D systems with randomly varying nonlinearities over saturated sensor networks. *Information Science* 370–371: 708–724.

Liu C, Yang L, Tao J, et al. (2022) Set-membership filtering for complex networks with constraint communication channels. *Neural Networks* 152: 479–486.

Liu L, Ma L, Guo J, et al. (2020) Distributed set-membership filtering for time-varying systems under constrained measurements and replay attacks. *Journal of the Franklin Institute* 357: 4983–5003.

Liu L, Ma L, Guo J, et al. (2021) Distributed set-membership filtering for time-varying systems: A coding-decoding-based approach. *Automatica* 129: Article 109684.

Liu S, Wei L, Song Y, et al. (2017) Set-membership state estimation subject to uniform quantization effects and communication constraints. *Journal of the Franklin Institute* 354: 7012–7027.

Maity D and Tsiotras P (2021) Optimal controller synthesis and dynamic quantizer switching for Linear-Quadratic-Gaussian systems. *IEEE Transactions on Automatic Control* 67: 382–389.

Mao J, Meng X and Ding D (2022) Fuzzy set-membership filtering for discrete-time nonlinear systems. *IEEE/CAA Journal of Automatica Sinica* 9(6): 1026–1036.

Qin Y, Heng D and Han J (2022) Direct inverse hysteresis compensation of piezoelectric actuators using adaptive Kalman filter. *IEEE Transactions on Industrial Electronics* 69(9): 9385–9395.

Roesser RP (1975) A discrete state-space model for linear image processing. *IEEE Transactions on Automatic Control* 20(1): 1–10.

Suarez R (1989) Difference equations and a principle of double induction. *Mathematics Magazine* 62(5): 334–339.

Tabbara M and Nesic D (2008) Input-output stability of networked control systems with stochastic protocols and channels. *IEEE Transactions on Automatic Control* 53(5): 1160–1175.

Walsh GC and Ye H (2001) Scheduling of networked control systems. *IEEE Control System Magazine* 21(1): 57–65.

Walsh GC, Ye H and Bushnell L (1999) Stability analysis of networked control systems. In: *Proceedings of the American Control Conference*, San Diego, CA, 2–4 June 1999, pp. 2875–2880.

Walsh GC, Ye H and Bushnell L (2002) Stability analysis of networked control systems. *IEEE Transactions on Automatic Control* 10(3): 438–446.

Wang F, Liang J, Wang Z, et al. (2017a) A variance-constrained approach to recursive filtering for nonlinear 2-D systems with measurement degradations. *IEEE Transactions on Cybernetics* 47(6): 1877–1887.

Wang F, Liang J, Wang Z, et al. (2019) Resilient state estimation for 2-D shift-varying systems with redundant channels: A variance-constrained approach. *IEEE Transactions on Cybernetics* 49(7): 2479–2489.

Wang F, Liang J, Wang Z, et al. (2020) Robust finite-horizon filtering for 2-D systems with randomly varying sensor delays. *IEEE Transactions on Systems, Man, and Cybernetics: Systems* 50(1): 220–232.

Wang Y, Bian T, Xiao J, et al. (2015) Global synchronization of complex dynamical networks through digital communication with limited data rate. *IEEE Transactions on Neural Networks and Learning Systems* 26(10): 2487–2499.

Wang Y, Zhao D, Li Y, et al. (2017b) Unbiased minimum variance fault and state estimation for linear discrete shift-varying two-dimensional systems. *IEEE Transactions on Automatic Control* 62(10): 5463–5469.

Wei Y, Qiu J, Karimi H, et al. (2014) Filtering design for two-dimensional Markovian jump systems with state-delays and deficient mode information. *Information Science* 269: 316–331.

Wu L and Wang Z (2015) *Filtering and Control for Classes of Two-dimensional Systems*. Cham: Springer.

Wu L, Yang R, Shi P, et al. (2015) Stability analysis and stabilization of 2-D switched systems under arbitrary and restricted switchings. *Automatica* 59: 206–215.

Zhang H, Hu X, Lin K, et al. (2021a) Adaptive control with quantized inputs processed by Lipschitz logarithmic quantizer. *International Journal of Control, Automation and Systems* 19(2): 921–930.

Zhang WA, Yu L and Feng G (2011) Optimal linear estimation for networked systems with communication constraints. *Automatica* 47(9): 1992–2000.

Zhang Y, Bo S and Yu Y (2021b) Distributed Kalman filtering for interconnected dynamic systems. *IEEE Transactions on Cybernetics* 52: 11571–11580.

Zhao Z, Wang Z, Zou L, et al. (2020) Set-membership filtering for time-varying complex networks with uniform quantisations over randomly delayed redundant channels. *International Journal of Systems Science* 51(16): 3364–3377.

Zou L, Wang Z and Gao H (2016) Set-membership filtering for time-varying systems with mixed time-delays under Round-Robin and weighted try-once-discard protocols. *Automatica* 74: 341–348.

Zou L, Wang Z, Geng H, et al. (2021) Set-membership filtering subject to impulsive measurement outliers: A recursive algorithm. *IEEE/CAA Journal of Automatica Sinica* 8(2): 377–388.

Zou L, Wang Z, Han Q-L, et al. (2017) Ultimate boundedness control for networked systems with try-once-discard protocol and uniform quantization effects. *IEEE Transactions on Automatic Control* 62(12): 6582–6588.

Zou L, Wang Z, Han Q-L, et al. (2019) Recursive filtering for time-varying systems with random access protocol. *IEEE Transactions on Automatic Control* 64(2): 720–727.

证书号第7642611号

发明专利证书

发 明 名 称：混合网络攻击下信息物理系统事件触发自适应滑模控制方法及装置

专 利 权 人：兰州理工大学

地 址：730050 甘肃省兰州市兰工坪287号

发 明 人：张磐;祝超群;李天成;王志文;杨彬;吴义春;刘淑慧;祖文博

专 利 号：ZL 2024 1 0715639.1

授权公告号：CN 118483912 B

专利申请日：2024年06月04日

授权公告日：2025年01月03日

申请日时申请人：兰州理工大学

申请日时发明人：张磐;祝超群;李天成;王志文;杨彬;吴义春;刘淑慧;祖文博

国家知识产权局依照中华人民共和国专利法进行审查，决定授予专利权，并予以公告。
专利权自授权公告之日起生效。专利权有效性及专利权人变更等法律信息以专利登记簿记载为准。

局长
申长雨

2025年01月03日

证书号第7387144号

发明专利证书

发 明 名 称：面向混合网络攻击的信息物理系统安全预测控制方法及装置

专 利 权 人：兰州理工大学

地　　　　址：730050 甘肃省兰州市兰工坪287号

发 明 人：祝超群;张磐;吴义春;杨彬;王志文;李天成;刘淑慧;祖文博

专 利 号：ZL 2024 1 0456155.X　　　授权公告号：CN 118138367 B

专利申请日：2024年04月16日　　　授权公告日：2024年09月20日

申请日时申请人：兰州理工大学

申请日时发明人：祝超群;张磐;吴义春;杨彬;王志文;李天成;刘淑慧;祖文博

国家知识产权局依照中华人民共和国专利法进行审查，决定授予专利权，并予以公告。
专利权自授权公告之日起生效。专利权有效性及专利权人变更等法律信息以专利登记簿记载为准。

局长
申长雨

2024年09月20日

第 1 页 (共 1 页)

证书号第7597637号

发明专利证书

发 明 名 称：多源攻击下复杂信息物理系统间歇控制方法、装置及存储介质

专 利 权 人：兰州理工大学

地　　　　址：730050 甘肃省兰州市兰工坪287号

发 明 人：祝超群;张磐;刘淑慧;吴奕衡;王志文;杨彬;李天成;吴义春
祖文博

专 利 号：ZL 2024 1 0750598.X　　　　授权公告号：CN 118713874 B

专利申请日：2024年06月12日　　　　授权公告日：2024年12月13日

申请日时申请人：兰州理工大学

申请日时发明人：祝超群;张磐;刘淑慧;吴奕衡;王志文;杨彬;李天成;吴义春
祖文博

国家知识产权局依照中华人民共和国专利法进行审查，决定授予专利权，并予以公告。
专利权自授权公告之日起生效。专利权有效性及专利权人变更等法律信息以专利登记簿记载为准。

局长
申长雨

2024年12月13日